

**Novel Multivalent Hexaarylbenzene  
Derivatives and Cyclomers for Potential  
Molecular Recognition Applications**

Thesis submitted to AcSIR for the award of the

Degree of

**Doctor of Philosophy**

in

Chemical Sciences



By

**SURESH M**

10CC11J26070

Under the guidance of

**Dr. G. J. Sanjayan**

Division of Organic Chemistry  
CSIR-National Chemical Laboratory,  
Pune-411008





# सीएसआईआर - राष्ट्रीय रासायनिक प्रयोगशाला

(वैज्ञानिक तथा औद्योगिक अनुसंधान परिषद)

डॉ. होमी भाभा मार्ग, पुणे - 411 008. भारत



## CSIR - NATIONAL CHEMICAL LABORATORY

(Council of Scientific & Industrial Research)

Dr. Homi Bhabha Road, Pune - 411 008, India

### Certificate

This is to certify that the work incorporated in this Ph.D. thesis entitled "**Novel Multivalent Hexaarylbenzene Derivatives and Cyclomers for Potential Molecular Recognition Applications**" submitted by **Mr. Suresh M.** to Academy of Scientific and Innovative Research (AcsIR) in fulfillment of the requirements for the award of the Degree of Doctor of Philosophy, embodies original research work under my supervision. I further certify that this work has not been submitted to any other university or institution in part or full for the award of any degree or diploma. Research material obtained from other sources has been duly acknowledged in the thesis. Any text, illustration, table etc., used in the thesis from other sources, have been duly cited and acknowledged.

Suresh M  
(Research Student)

Dr. G. J. Sanjayan  
(Research Supervisor)

#### Communication Channels

NCL Level DID : 2590  
NCL Board No. : +91-20-2590 2000  
EPABX : +91-20-2589 3300  
: +91-20-2589 3400



#### FAX

Director's Office : +91-20-2590 2601  
COA's Office : +91-20-2590 2660  
COS&P's Office : +91-20-2590 2664

#### WEBSITE

[www.ncl-india.org](http://www.ncl-india.org)





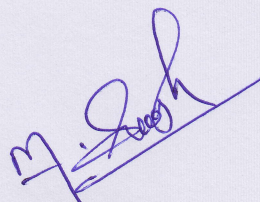
## Declaration by the Candidate

I hereby declare that the original research work embodied in this thesis entitled, "**Novel Multivalent Hexaarylbenzene Derivatives and Cyclomers for Potential Molecular Recognition Applications**" submitted to Academy of Scientific and Innovative Research for the award of degree of Doctor of Philosophy (Ph.D.) is the outcome of experimental investigations carried out by me under the supervision of Dr. G. J. Sanjayan, Senior Principal Scientist, Organic Chemistry Division, CSIR-National Chemical Laboratory, Pune. I affirm that the work incorporated is original and has not been submitted to any other academy, university or institute for the award of any degree or diploma.

December 2017

CSIR-National Chemical Laboratory

Pune-411 008



Suresh M

(Research student)



*Dedicated to my beloved  
Soulmate Brother*





## **Acknowledgements**

*During the journey of my research work, I have been acquainted, accompanied and supported by many people. Here comes the pleasant opportunity for me to express my gratitude to all of them.*

*I am inexpressible to describe how much indebted to my research supervisor **Dr. G J Sanjayan** for his invaluable guidance, never ending support and constant motivation during the entire course of my Ph.D. work. His guidance in each and every aspect of research, from working table to formulation of ideas to presentation of results has helped me to become a complete researcher today. I'm deeply thankful to him for introducing me to this fascinating area of science, which I have enjoyed by learning profoundly. Besides, he has given full freedom for independent thinking, planning and execution of research work in our research group.*

*My sincere thanks to our collaborator Dr. Rajesh Gonnade, who has inspired me with his enthusiasm and determination. He helped me to learn and explore the single crystal technique in supramolecular chemistry. I would like to thank Dr. Sreekumar, for his invaluable discussions, suggestions and perform Proton conductivity studies*

*I owe deep sense of gratitude to Dr. P R Rajamohanan for his useful suggestions and timely advice on my research work.*

*I am very much grateful to the past and present doctoral advisory committee members: Drs. Anil Kumar, Sudalai, Biju, Balaraman and Santhosh Babu Sukumaran for their appraising in my research progress, continuous support and suggestions.*

*I greatly acknowledge the insightful discussions with Drs. C P Vinod, R Vaidhyanathan, C S Gopinath, M MuthuKrishnan, T Raja, Rahul Banerjee and Santhakumari.*

*I am thankful to Dr. S P Chavan, Head, organic chemistry division and Prof. Ashwini Kumar Nangia, Director, CSIR-NCL for providing necessary infrastructure for carrying out this work. Thanks are due to University Grants Commission, New Delhi for providing the research fellowship.*

*I thank Rashmi E.V (M.Sc, project trainee colleague) who had done initial exploration of macrocyclisation and her sincere efforts are acknowledged. I also thank Mr. Rajith Kumar from Physical & Materials Chemistry Division for helping me in proton conductivity studies.*



*I would like to thank my past and present labmates: Dr. Arup, Dr. Ramesh, Dr. Gowri, Dr. Sangram, Dr. Roshna, Dr. Vijayadas, Dr. Tukaram, Dr. Ganesh, Dr. Krishna Chaithanya and Dr. Sanjeev, Dr. Sachin, Dr. Suresh R, Dr. Amol, Dr. Shiva Kumar K I, Krishna, Rashid, Kasthuri, Vinotha, Aditi, Rashmi, Mahendra, Bhibhishan, Mrudul, Ananjana, and all other who have worked alongside me. I also extend my sincere gratitude to Rupesh Gowade, Shridhar thorat, Ekta and Samir for their kind help in single crystal X-ray experiments.*

*During my stay in NCL, I had strong brotherly affection and help in particular from Jambu S and Pandi which has helped me to overcome the tough phases of my life at NCL. Special thanks to my beloved friends Abdullah, Agatheeswaran, Devanandhan, Raja M, Elavarasan, Dhanasekaran and Muthu Kumar for their moral support and encouragements. I would like to thank my dearest friends: Ramsunder, Vasudevan, Lenin, Perumal, Kubandiran, Velayutham, Edwin, Mohan, Mohanrai, Brij Bhushan, Ashok, Arulkashmir, Deva Raj, Venket, Sridhar, Loganathan, Kumar, Manikandan, Subhadip Das, Subramani, Sudhakar and Prabhu for their help at different stages of my work.*

*No words are available to explain love, relentless hard work and sacrifice from my soulmate brother Mr. **Kannan M** (A.E, TNEB) in bringing up in each and every stage of my life. Without his support, my ambition to pursue my research at NCL could have been very hard to realize.*

*I owe my deepest gratitude and love to my parents, sister-mama: Kavitha-Paramasivam, and nephews: Sathish Kumar and Santhosh Kumar for their care, encouragement and well wishes. I am very lucky to have Sowmiya as my life partner. Her unconditional love and affection are immense in keeping cheerful environment in home which has helped me to successfully complete this endeavor.*

*Finally, I would like to thank all those who have contributed to the successful realization of this dissertation. I express my apologies if I failed to thank personally one by one.*

*This chain of my gratitude could only be completed if I thank the Almighty. My deepest and sincere gratitude for inspiration and guidance to be a humble being on this planet.*

**Suresh M**

## Table of Contents

Abbreviations	VII
Abstract	IX
General Remarks	XV
List of Publications	XVII

### CHAPTER-1

#### Introduction

1	Supramolecular chemistry: A historical over view	3
1.1	Non-covalent Interactions	4
1.1.1	Hydrogen Bonding	4
1.1.2	Ion-Dipole Interactions	5
1.1.3	Cation- $\pi$ interactions	6
1.1.4	XH- $\pi$ interactions	6
1.1.5	$\pi$ - $\pi$ stacking	7
1.2	Basic Concepts of Supramolecular chemistry	8
1.2.1	Molecular self-assembly	8
1.2.2	Molecular recognition	9
1.2.2.1	The parametric effects of molecular recognition events	10
1.2.3	Multivalency	13
1.2.4	Host-guest chemistry	15
1.2.4.1	Clathrate compounds	17

1.2.4.2	Cyclodextrins	18
1.2.4.3	Cucurbit[ <i>n</i> ]urils	19
1.2.4.4	Calixarenes	20
1.3	Imine-based macrocycles	21
1.4	Metal-organic framework (MOF) in host-guest chemistry	23
1.5	Proton-conductivity	24
1.6	Hexaphenylbenzene (HPB)	25
1.7	References	28

## CHAPTER-2

### **Multivalent Hexaphenylbenzene-based Supramolecular Sponges for Molecular Entrapping**

2.1	Introduction	39
2.2	Objective of the present work	40
2.3	Structural features of supramolecular sponge	40
2.4	Results and discussions	41
2.4.1	Synthesis	41
2.4.2	Crystal growth methods used for preparation of inclusion crystals	42
2.4.3	Investigations of Crystal structures	43
2.4.3.1	Inclusion of guest molecules in HPB(COOMe) <sub>12</sub>	43
2.4.3.2	Inclusion of guest molecules in HPB(CONHMe) <sub>12</sub>	46
2.4.3.3	Entrapping of guest molecules in HPB(CONH <sub>2</sub> ) <sub>12</sub>	47

2.4.4	Channelization of guest molecules in the crystal lattice	49
2.4.5	Ammonia inclusion studies of HPB(CONH) <sub>12</sub>	50
2.4.6	Evidences for the presence of ammonia as a guest in the crystal of MeOH.Dioxane.NH <sub>3</sub> @HPB(CONH <sub>2</sub> ) <sub>12</sub>	53
2.4.6.1	Thermogravimetric Analysis (TGA)	53
2.4.6.2	Infrared analysis (IR)	54
2.4.6.3	Surface Characterization of HPB(CONH <sub>2</sub> ) <sub>12</sub>	55
2.4.7	Trapping of reaction intermediates: Mechanistical investigation of urotropine decomposition	56
2.4.8	DFT Optimization of MeOH.Dioxane.NH <sub>3</sub> @HPB(CONH <sub>2</sub> ) <sub>12</sub> and MeOH.Urotropine.NH <sub>3</sub> .2-azaallenium.Cl <sup>-</sup> @ HPB(CONH <sub>2</sub> ) <sub>12</sub>	58
2.4.9	An attempt to discriminate the chiral molecules using multivalent supramolecular sponges	61
2.5	Conclusion	63
2.6	Experimental section	64
2.7	X-ray Crystallography	103
2.8	References	105

## CHAPTER-3

### Section-A

#### **High Proton Conductivity Exhibited by a Twelve-Armed Hexaphenylbenzene-based Supramolecular Sponge**

3.1	Proton (H <sup>+</sup> ) conductivity	111
3.2	Objective of the present work	112
3.3	Synthesis and characterization	113
3.4	Proton conductivity studies	115

3.4.1	The role of supramolecular sponge nature in the proton conduction of HPB(COOH) <sub>12</sub> .	121
3.4.2	Reversal of temperature in proton conductivity of HPB(COOH) <sub>12</sub>	123
3.5	An attempt for the synthesis, characterizations and proton conductivity applications of amino acid coupled extended systems.	124
3.6	Conclusion	125
3.7	Experimental section	126
3.8	References	138

### **CHAPTER-3**

#### **Section-B**

#### **Three Dimensional Metal-Organic Polymers of Multivalent Hexaphenylbenzene**

3.9	Introduction	143
3.10	Objective of the present work	145
3.11	Synthesis and characterization	146
3.12	Single crystal X-ray studies	149
3.13	Conclusion	152
3.14	Experimental section	153
3.15	X-ray Crystallography	155
3.16	References	156



## CHAPTER-3

### Section-C

#### Synthesis of HPB-based Template Assembled Synthetic Proteins

3.17	Introduction	161
3.18	Objective of the present work	163
3.19	Result and discussion	164
3.20	Conclusion	169
3.21	Experimental procedures	170
3.22	References	182

## CHAPTER-4

#### Effect of *Gem*-Dimethyl Groups in the Formation of Imine-Based Macrocycles and Cages

4.1	Introduction: Imine-based macrocycles	187
4.1.1	Requirements of novel-strategies for the synthesis of imine-based organic macrocycles	187
4.2	<i>Gem</i> -dimethyl effect and its advantages in macrocyclization chemistry	188
4.3	Objective of our present work	194
4.4	Synthesis, results and discussion	195
4.4.1	Synthesis and characterization of [2+2] macrocycles using <i>gem</i> -dimethyl effect	195
4.4.2	Synthesis and characterization of elongated macrocycles using <i>gem</i> -dimethyl effect	202
4.4.3	Synthesis and characterization of macrobicycles/cages using <i>gem</i> -	204

	dimethyl effect	
4.4.4	Effect of <i>gem</i> -dimethyl groups in reaction equilibrium of the imine-based macrocyclization (studied by using $^1\text{H}$ NMR)	206
4.4.5	Effect of <i>gem</i> -dimethyl groups in the stability of macrocycle.	208
4.4.6	Thermogravimetric analysis of macrocycles/cages	209
4.4.7	Single crystal X-ray studies and structural features of the cages	211
4.4.8	Powder X-ray diffraction (PXRD) studies of the macrocycles	216
4.5	Conclusion	219
4.6	Experimental section	220
4.7	X-ray Crystallography	246
4.8	References	251

## ABBREVIATIONS

<b>A</b>		<b>K</b>	
Å	Ångström	$K_{dim}$	Dimerization constant
$\alpha$	Alpha	K	Kelvin
ACN	Acetonitrile	$K_{taut}$	Tautomeric constant
AcOH	Acetic acid	<b>L</b>	
AcOEt	Ethyl acetate	Leu	Leucine
Aib	$\alpha$ -aminoisobutyric acid	LCMS	Liquid chromatography–mass spectrometry
Ala	Alanine		
Ant	Anthranilic acid	<b>M</b>	
Ar	Aryl	MALDI	Matrix-Assisted Laser Desorption Ionization
<b>B</b>		m	Multiplet (NMR)
$\beta$	beta	Me	Methyl
Boc	tert-Butyloxycarbonyl	MHz	Megahertz
<b>C</b>		mp	Melting point
Calcd	Calculated	MS	Mass spectrometry
°C	Degree Celcius	ms	Millisecond
CDCl <sub>3</sub>	Chloroform- <i>d</i>	m/z	Mass to charge ratio
<b>D</b>			
D	doublet (NMR)	<b>P</b>	
$\delta$	Chemical shift (NMR)	Pd/C	palladium 10 % on activated carbon
DCM	Dichloromethane	Pro	Proline
DMF	Dimethylformamide	Pet ether	Petroleum ether
DIPEA	N,N-Diisopropylethyl amine	ppm	Parts per million
DMSO	Dimethyl sulfoxide	<b>R</b>	
<b>E</b>		r.f.	Radio frequency
EDC	1-Ethyl-3-(3-dimethylamino Propyl) carbodiimide	R <sub>f</sub>	Retention factor
		rt	Room temperature
eV	Electronvolt	<b>S</b>	
<b>G</b>		s	Singlet (NMR)
$\gamma$	Gamma	S	Second
Gly	Glycine	SEM	Scanning electron microscopy
g	Gram	<b>T</b>	
<b>H</b>		t	Triplet (NMR)
H-bond	Hydrogen bond	TFA	Trifluoroacetic acid
HBTU	O-benzotriazol-1-yl-N,N,N',N'-tetramethyluronium hexafluorophosphate	TEA	Triethyl amine
		THF	Tetrahydrofuran
HOBt	1-Hydroxybenzotriazole	$\tau$	Tau
HRMS	High Resolution Mass Spectrometry	TEM	Transmission Microscopy
HPLC	High-Pressure Liquid Chromatography	TLC	Thin layer chromatography
h	Hour	<b>V</b>	
Hz	Hertz	Val	Valine
		$\omega$	Omega
		<b>X</b>	
		XRD	X-ray diffraction



---

---

## Abstract

<b>Name of the Candidate</b>	Mr. Suresh M
<b>Title of the Thesis</b>	Novel Multivalent Hexaarylbenzene Derivatives and Cyclomers for Potential Molecular Recognition Applications
<b>Research Supervisor</b>	Dr. Gangadhar J. Sanjayan (AcSIR, CSIR-NCL, Pune)

Molecular recognition is an important and specific process which is occurring in the functional living species and nonliving things. Most often, these processes are governed by the non-covalent interactions and geometrical complementarity of the interacting partners. Molecular recognition has been observed in several biological processes such as DNA-DNA, DNA-RNA, RNA-amino acid, DNA-protein, RNA-ribosome, receptor-ligand, protein-protein, antigen-antibody, sugar-lectin interactions, etc. By mimicking these biological processes, many synthetic systems have been developed to show interesting properties and applications such as selective cation binding of crown-ethers, xylylenediammonium binding of cucurbituril, drug delivery of hydrophobic molecules using cyclodextrins, selective sodium binding of calixarenes (ionomers), xenon-cryptophane complexes, porphyrin-based molecular photovoltaics, molecular machines, etc. Notably, novel synthetic architectures having interesting properties and potential applications as a consequence of molecular recognition have always been welcomed to the realm of supramolecular chemistry. In this connection, thesis entitled “**Novel Multivalent Hexaarylbenzene Derivatives and Cyclomers for Potential Molecular Recognition Applications**” attempts at synthesis of 12-armed hexaphenylbenzene (HPB) and its derivatives to uptake diverse guest molecules. Besides, an endeavor to understand the role played by multivalency and back bone rigidity of HPB in eliciting properties such as molecular entrapping and proton conductivity is undertaken. Further, it also attempts in the synthesis of imine-based macrocycles and cages using *gem*-dimethyl amines for potential molecular recognition applications. This thesis consists of four chapters. The first is an introductory chapter. The second chapter describes the design, synthesis and supramolecular spongy nature of 12-armed hexaphenylbenzene (HPB) derivatives, which shows entrapping of a variety of guest molecules including ammonia and reaction intermediate. The third chapter deals with (i) synthesis and proton conductivity studies of novel multivalent hexaarylbenzene derivatives, (ii) synthesis and characterization of



potassium and sodium metal-organic frameworks of multi-armed HPB and (iii) synthesis and characterization of HPB-based template assembled synthetic proteins. The chapter four describes the synthesis of macrocycles and cages using *gem*-dimethyl effect as a platform for potential molecular recognition applications. The brief description of the thesis chapters are described below.

## CHAPTER 1

This chapter gives a short preface about historical over view of supramolecular chemistry and its important basic concepts such as molecular recognition, multivalency and host-guest chemistry with illustrative examples. Further, it includes a brief introduction about imine-based macrocycles/cages and metal organic frameworks. It also mentions about historical view of proton conductivity and hexaphenylbenzenes.

## CHAPTER 2

This chapter deals with rationally designed, giant multi-armed hexaphenylbenzene (HPB)-based supramolecular sponges which can encapsulate a variety of guest molecules in their voids of crystal lattice through the co-operative interplay of multivalency, noncovalent forces and backbone rigidity (Fig. 1a). In this connection, *pseudo* axially substituted twelve-armed hexaphenylbenzene has been synthesized and its spongy action (inclusion) was studied by varying number of H-bond donor-acceptor sites in the arms using single crystal X-ray diffraction.<sup>1</sup> When the arms feature ester group, the host system was acting as cavitand (intramolecular inclusion) to include nonpolar and polar aprotic guests in its crystal structure *via* CH $\cdots$  $\pi$ , CH $\cdots$ O, CH $\cdots$ N interactions with C-H of the HPB (Fig 1b). This ester functionalized supramolecular sponge (HPB(COOMe)<sub>12</sub>) was able to trap guest molecules such as benzene, toluene, salicylaldehyde, [12]-crown ether, dimethyl sulphoxide, dimethyl formamide, aniline, N-methyl aniline, *p*-chlorobenzene and pyridine. However, upon increasing the H-bond donor number from zero (-COOMe) to one (-CONHMe), 2D-sheets were formed through intermolecular aggregation without loss of intramolecular inclusion cavities. Further, increase in H-bond donors to two in the arms (CONH<sub>2</sub>) led to the inclusion of guests in the resultant intra, extramolecular cavities with the assistance of directionality of the H-bond and backbone rigidity of HPB.

Intriguingly, this system has shown an unprecedented inclusion of ammonia and segregation of the guest molecules according to their polarity in the lattice (Fig. 1c & 1d). Further, utilizing this system, we have observed the rare 2-azaallenium intermediate which is generally involved in the aminomethylation of activated arenes such as tannin<sup>2-4</sup> (Fig 1e & 1f). In addition, this primary amide was found to entrap a variety of guest molecules such as dimethyl sulfoxide, dimethylformamide, N-methyl pyrrolidone, HBr.dimethylformamide complex. On the contrary, the increase in the H-bond donor number to three (CONH<sub>2</sub>, in each arm), has switched back the ability of the HPB to undertake an intrinsic encapsulation of guests. The structural characterization of host molecules has been done using IR, <sup>1</sup>H-NMR, <sup>13</sup>C-NMR, mass spectrometry and single crystal X-ray diffraction.

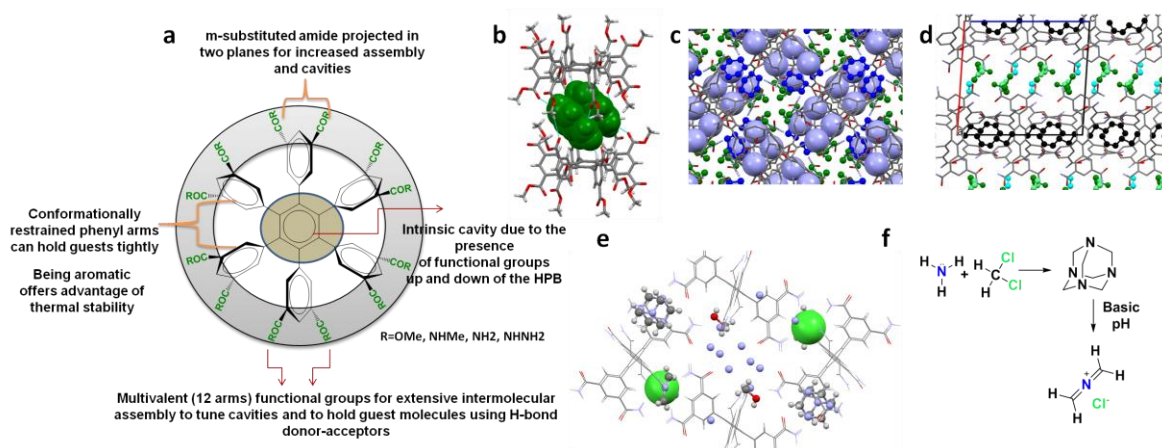


**Fig. 1:** a) Structural characteristics of multivalent hexaphenylbenzene-based supramolecular sponge; b) HPB(COOMe)<sub>12</sub> showing intrinsic inclusion of salicylaldehyde (green coloured space-fill) *via* CH $\cdots$  $\pi$  and CH $\cdots$ O interactions; c) Trapped ammonia (violet colored space fill), dioxane (blue colored ball&stick) and methanol (green colored ball&stick) in the crystal lattice of compound HPB(CONH<sub>2</sub>)<sub>12</sub>; d) Polarity-dependent channelization of guest molecules such as methanol (light blue), ethanol (light green), DMSO (green), hexane (black) in compound HPB(CONH<sub>2</sub>)<sub>12</sub>; e) Trapped ammonia, methanol, urotropine, reaction equilibrium intermediate 2-azaallenium with counter ion chloride (green space-fill) in the crystal lattice of compound HPB(CONH<sub>2</sub>)<sub>12</sub>; f) Possible mechanism for the formation of 2-azaallenium intermediate.

### CHAPTER 3

This chapter is divided into three sections, namely A, B and C. Section A of the chapter describes the synthesis and proton conductivity studies of 12-armed hexaphenylbenzene carboxylic acids. The proton conductivity of one of the derivatives HPB(COOH)<sub>12</sub> was found to be  $3.2 \times 10^{-2} \text{ Scm}^{-1}$  at 60 °C, 95% RH with the lowest

activation energy of 0.138 eV (Fig. 2b & 2c). This conductivity is about three-fold lesser than that of the state-of-the-art material Nafion<sup>5</sup> and comparable with many of the recently reported materials.<sup>6</sup> From the activity of this material under different conditions, activation energy and other characteristic of the materials suggests that the mechanism of the proton conduction is Grotthuss type.<sup>7</sup>

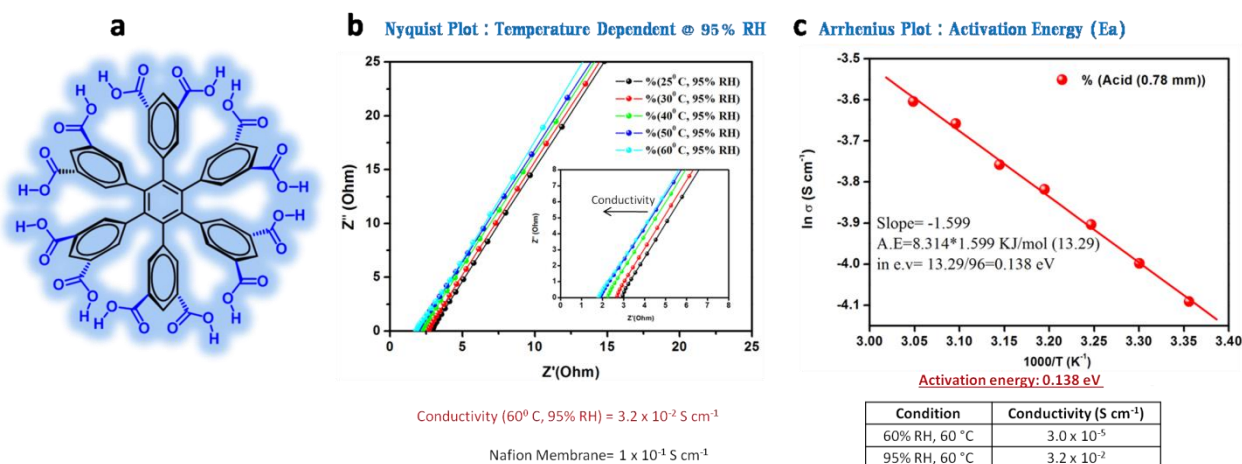


**Fig. 2:** a) Chemical structure of HPB(COOH)<sub>12</sub> showing the up and down axially substituted carboxylic acids functional groups. b) Temperature-dependent proton conductivity, Nyquist plot of HPB(COOH)<sub>12</sub> @ 95% RH showing highest conductivity  $3.2 \times 10^{-2} \text{ cm}^{-1}$  @ 60°C. c) Activation energy of HPB(COOH)<sub>12</sub> @ 95% RH, 60°C was found to be 0.138 eV.

Section B of the chapter describes the synthesis and characterization of novel sodium and potassium-containing metal-organic frameworks.<sup>8</sup> The last section C deals with the design, synthesis, and characterization of novel template-assembled synthetic proteins (TASP). The peptide sequences used in this study are H<sub>2</sub>N-Leu-Aib-Val-OMe and H<sub>2</sub>N-Aib-<sup>1</sup>Pro-<sup>S</sup>Ant-NH-iBu. The mini-proteins have been synthesized in one-pot, using peptide coupling strategy. The synthesized macromolecules were characterized using <sup>1</sup>H-NMR, <sup>13</sup>C-NMR and mass spectrometry.<sup>9</sup>

## CHAPTER 4

The chapter four deals with the high yield synthesis of a variety of organic [2+2] macrocycles and propeller shaped [2+3] cofacial organic cages by using *gem*-dimethyl effect as a platform. All these macrocycles/cages were synthesized by utilizing two *gem*-

dimethylamines as the amine building blocks (Fig 3a & 3b).<sup>10</sup> The *gem*-dimethylamines were able to react with a variety of aldehydes including conformationally flexible ones to form co-facial cages. Strikingly, following this versatile concept, four of the imine-based macrocycles/cages formations have been showed even under high concentrations (0.5 to 1 M) by instant mixing of aldehydes and *gem*-dimethyl substituted amines, at ambient conditions. The stabilities of the *gem*-dimethyl containing macrocycles are better than unsubstituted ones. Most of these macrocycles and cages exhibit high thermal stability (about 400 °C). The solid-state structural features of the macrocycles have been discussed.

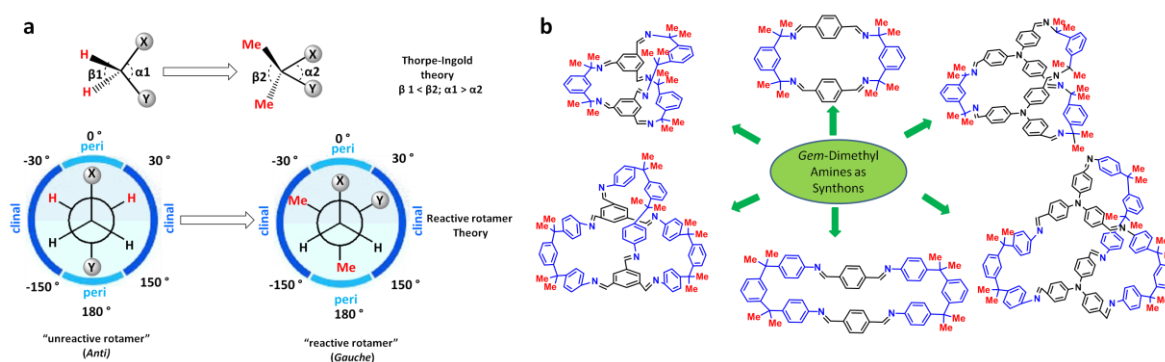


**Fig. 3:** a) Schematic representation of *gem*-dimethyl (GDM) effect explained by Thorpe-Ingold (top) and reactive rotameric (bottom) theories on cyclisation reactions. *Note:* X and Y are reactive end groups. b) Synthesis of various macrocycles and cages using *gem*-dimethyl effect as a platform.

## References:

1. Madhu, S.; Sanjayan, G. J. IN201611033413, WOPCT/IN2017/050437. *Patent filed*.
2. Arbenz, A.; Averous, L. *Green Chem.* **2015**, *17*, 2626.
3. Kamoun, C.; Pizzi, A.; Zanetti, M. *J. Appl. Polym. Sci.* **2003**, *90*, 203.
4. Madhu, S.; Gonnade, R. G.; Das, T.; Vanka, K.; Sanjayan, G. J. *Manuscript under preparation*.
5. Sone, Y.; Ekdunge, P.; Simonsson, D. *J. Electrochem. Soc.* **1996**, *143*, 1254.
6. Karmakar, A.; Illathvalappil, R.; Anothumakkool, B.; Sen, A.; Samanta, P.; Desai, A. V.; Kurungot, S.; Ghosh, S. K. *Angew. Chem. Int. Ed.* **2016**, *128*, 10825.
7. Madhu, S.; Rajith, I.; Sreekumar, K.; Sanjayan, G. J. *Manuscript under preparation*.
8. Madhu, S.; Gonnade, R. G.; Sanjayan, G. J. *Manuscript under preparation*.
9. Madhu, S.; Madica, K.; Sanjayan, G. J. *Manuscript under preparation*.
10. Madhu, S.; Rashmi, E. V.; Gonnade, R. G.; Sanjayan, G. J. *New J. Chem.* **2017**, (17), 8721-8724.





---

## GENERAL REMARKS

- Unless otherwise stated, all the chemicals and reagents were obtained commercially.
- Required dry solvents and reagents were prepared using the standard procedures.
- All the reactions were monitored by thin layer chromatography (TLC) on precoated silica gel plates (Kieselgel 60F<sub>254</sub>, Merck) with UV, I<sub>2</sub>, bromo-cresol, or ninhydrin solution as the developing reagents in the concerned cases.
- Column chromatographic purifications were done with 100-200 Mesh Silica gel or with flash silica gel (230-400 mesh) in special cases.
- Melting points were determined on a Buchi Melting Point B-540 and are uncorrected.
- IR spectra were recorded in nujol or CHCl<sub>3</sub> using Bruker-FTIR spectrophotometer.
- NMR spectra were recorded in CDCl<sub>3</sub> on Ac 200 MHz, AV 400 MHz, DRX-500 MHz Bruker and 700 MHz NMR spectrometers. All chemical shifts are reported in  $\delta$  ppm downfield to TMS and peak multiplicities as singlet (s), doublet (d), quartet (q), broad (br), broad singlet (bs) and multiplet (m).
- Elemental analyses were performed on a Elementar-Vario-EL (Heraeus Company Ltd.; Germany).
- ElectroSpray Ionization (ESI) Mass Spectrometric measurements were done with API
- HRMS data were recorded on a Thermo Scientific Q-Exactive, Accela 1250 pump. MALDI-TOF/TOF mass spectra were obtained from ABSCIEX TOF/TOFTM 5800 mass spectrometer.
- Powder X-ray diffraction (XRD) patterns were recorded on a PANalytical X'Pert PRO Xray diffractometer, using Cu K $\alpha$  radiation.
- Thermogravimetric analysis was carried out on NETSZCH TGA-DSC or METTLER TOLEDO, TGA/SDTA851e. The routine TGAs were done under N<sub>2</sub> gas flow (20ml or 50 ml/min) (purge + protective).



## LIST OF PUBLICATIONS

**(1) Exploring the *Gem*-Dimethyl Effect in the Formation of Imine-Based Macrocycles and Cages.**

Suresh Madhu, Rashmi, E. V., Rajesh Gonnade and Gangadhar J. Sanjayan  
*New J. Chem.*, 2017, 41, 17, 8721-8724.

**(2) Hexaphenylbenzene-Based Supra-Molecular Sponges for Absorbing Guest Molecules in Their Molecular Cavities.**

Suresh Madhu and Gangadhar J. Sanjayan  
*Patent filed*, IN201611033413, WOPCT/IN2017/050437.

**(3) Twelve-Armed Hexaphenylbenzene-Based Supramolecular Sponges for Molecular Entrapping.**

Suresh Madhu, Rajesh Gonnade, Tamal Das, Kumar Vanka and Gangadhar J. Sanjayan  
*Manuscript under preparation*

**(4) High Proton Conductivity in Twelve-Armed Hexaphenylbenzene-Based Supramolecular Sponge.**

Suresh Madhu, Rajith Illathvalappil, Sreekumar Kurungot and Gangadhar J. Sanjayan.  
*Manuscript under preparation*

**(5) Synthesis and Characterization of Three Dimensional Metal-Organic Polymers using Hexaphenylbenzene-Based Dodecatopic Ligand.**

Suresh Madhu, Rajesh Gonnade and Gangadhar J. Sanjayan.  
*Manuscript under preparation*

**(6) Synthesis of Double Basket-Shaped Template Assembled Synthetic Proteins**

Suresh Madhu, Krishna Prasad. M, Rajesh Gonnade and Gangadhar J. Sanjayan.  
*Manuscript under preparation*

## POSTERS, SEMINAR & CONFERENCES

**(1) A Novel class of Hexaphenylbenzene-based porous organicframework with Multiple H-bonding Networks: Crystallographic characterization of solvent-inclusion complexes:Poster**

Venue: CSIR-National Chemical Laboratory, Event: National Science Day, 2014

**(2) Supramolecular Engineering of Guest -Adaptable Porous Organic Frame Work for Ammonia and Reaction Intermediates Trapping: Poster**

Venue: CSIR-National Chemical Laboratory, Event: National Science Day, 2015

**(3) Supramolecular Engineering of Guest -Adaptable Porous Organic Frame Work for Ammonia and Reaction Intermediates Trapping**

*Venue:* Indian Institute of Science Education and Research, Pune, *Event:* 44th National Seminar on Crystallography (NSC 2016) jointly conducted by CSIR-NCL, Pune, IISER Pune, NCCS and SP Pune University, 2016.

**AWARDS AND FELLOWSHIPS**

**(1) GRADUATE APTITUDE TEST in ENGINEERING (GATE-2009)** for Chemistry: by Ministry of Human Resource Development, Government of India.

**(2) JUNIOR RESEARCH FELLOWSHIP (JRF-2011):** by Joint CSIR-UGC

**(3) SENIOR RESEARCH FELLOWSHIP (SRF-2013):** by Joint CSIR-UGC

**(4) NCL-RF AGNIMITRA MEMORIAL BEST POSTER AWARD- 2014:** For Poster Presented in Organic Chemistry.

**(5) NCL-RF AGNIMITRA MEMORIAL BEST POSTER AWARD- 2015:** For Poster Presented in Organic Chemistry.



***Chapter 1***  
***Introduction***



## Chapter-1: Introduction

### 1.0 Supramolecular chemistry: A historical over view

One of the novel branches of chemistry that deals with the construction of functional molecules using inter molecular non-covalent forces is termed as *supramolecular chemistry*.<sup>1</sup> The roots of the supramolecular chemistry are linked with many important discoveries in the history of science. In 1774, Benjamin Franklin first observed the self-assembly of oil in water.<sup>2</sup> Later in 1778, Priestley discovered '*anomalous ice*' compound  $(\text{SO}_2) \cdot (\text{H}_2\text{O})_X$  which is the first material in the family of *clathrate hydrates*.<sup>3</sup> In 1893, Werner explained the structure of coordination compounds having a central transition metal atom surrounded by neutral or anionic ligands.<sup>4</sup> Emil Fischer (1894) hypothesized the interactions between the proteins and their substrates analogous to the act of a key in a lock wherein the guest molecules with the size and shape are complementary to that of hosts. Later, this proposal has turned to become the origin of term known as '*molecular recognition*'.<sup>5</sup> In 1906, Paul Ehrlich stated that "*the molecules do not act if they do not bind*" wherein he proposed the concept of biological receptor.<sup>6</sup> In the early 20th-century, non-covalent bonds were gradually understood in more detail. Latimer and Rodebush (1920) described about the hydrogen bond and its importance.<sup>7</sup> In 1928, James Watson and Francis Crick explained the structure of molecules (*i.e.* DNA double helix structure) responsible for life using above mentioned concepts.<sup>8</sup>

The origin of modern supramolecular chemistry has begun when Charles Pedersen (1962) isolated an unusual material. It showed unexpected solubilizing effects on alkali metal cation<sup>9</sup> which was later known to be *crown ethers*. Jean-Marie Lehn (1969) synthesized first *cryptands* and coined the term '*supramolecular chemistry*'. He referred it more colloquially as "*chemistry beyond the molecule*".<sup>10</sup> Later, Donald Cram (1973) showed the effect of preorganization by the synthesis of spherand hosts from monomeric aromatic units.<sup>11</sup> The noble prize in chemistry for the year 1987 was conferred jointly to Jean-Marie Lehn, Donald J. Cram, and Charles J. Pedersen for their work on initiation and development of modern supramolecular chemistry.<sup>12</sup>

In early 1980's, Professor Jean-Pierre Sauvage made his first step towards molecular machines and succeeded in linking two ring-shaped cyclic molecules together in an interlocked manner. Later, showed that one ring structure could rotate freely in

relative to the other.<sup>13</sup> During 1990s, Stoddart *et al.* built the first molecular wheel - a free moving ring structure on an axle (molecular rotaxane) that was applied to develop molecular muscles and an abacus that could act as a computer chip.<sup>14</sup> In 1999, Ben Feringa synthesized the first molecular motor using plenty of ingenious tricks to get it to spin in one direction<sup>15</sup>. For the developments and applications in the field of molecular nano-machines, the Nobel Prize in chemistry 2016 was awarded jointly to J. F. Stoddart, B. L. Feringa and Jean-Pierre Sauvage.<sup>16</sup>

## 1.1 Non-covalent Interactions

In contrast with molecular chemistry, supramolecular chemistry deals with intermolecular noncovalent bonds. These bonds are much weaker than the conventional covalent bonds. For instance, the bond energies of the C-C or C-H are in the range of 80-100 kcal/mol<sup>17</sup>. In noncovalent forces, the bond energies are in the range of 5-40 kcal/mol (with in crystal >100 kcal/mol).<sup>18</sup> Therefore, non-covalent interactions are reversible in nature and play an important role in many of the chemical and biological systems. The properties of some non-covalent forces which are important in the supramolecular chemistry are outlined below with examples.

### 1.1.1 Hydrogen Bonding

One of the most important non-covalent interactions is hydrogen bonding.<sup>19</sup> The strength of hydrogen bonds varies from very strong ( $\Delta H(g) = \sim 40$  kcal/mol, e.g. [F...HF]-) to weak ( $\Delta H(g) = 1 - 5$  kcal/mol, e.g. [HOH...OH<sub>2</sub>]) bond energies. These energies vary depending upon the system (Fig 1.01a)<sup>20-21</sup>. Such hydrogen bonds are most prevalent in chemistry and biology due to reversible electrostatic attractive forces that arise from differences in atomic electronegativities ( $\delta^+ \dots \delta^-$ ). Nature constructs complex systems for biological process by extensive use of hydrogen bonding. A well-known example is hydrogen bonding between the nucleotide base pairs in DNA, in which H-bond is very much responsible for the stability and function of the DNA (Fig 1.01b).<sup>8, 22</sup>



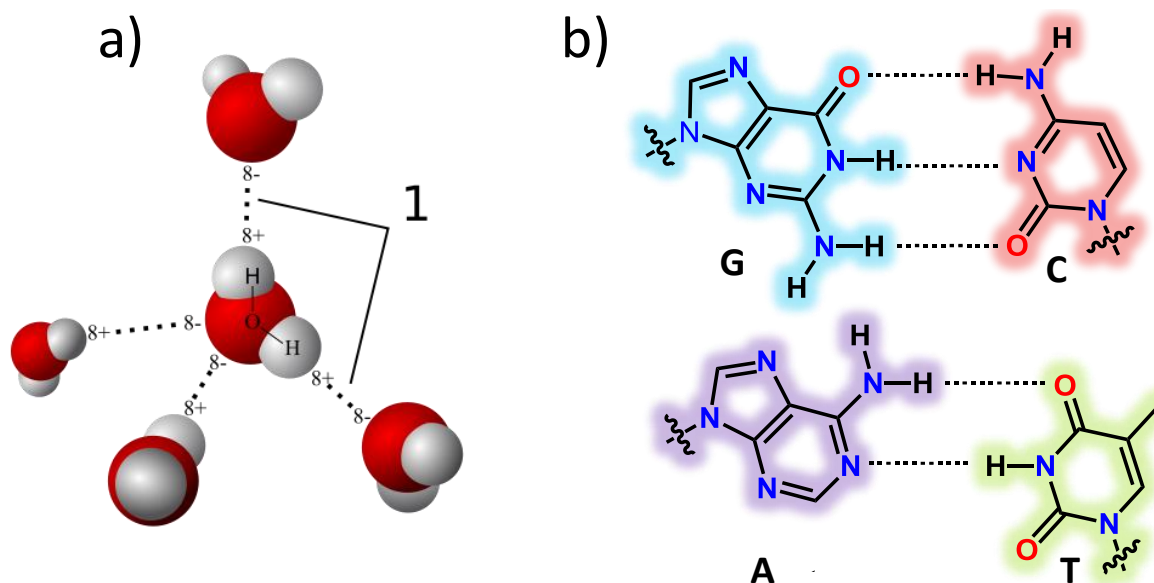


**Fig. 1.01:** a) Model of hydrogen bonding between water molecules. b) Hydrogen bonding interactions between the DNA-base pairs G-C and A-T. Image courtesy: ref. 21 (Fig 1.01a).

### 1.1.2 Ion-Dipole Interactions

The intermolecular forces dealing with interaction between ion and polar part of the molecules are known as *Ion-dipole interactions*. Alkali metals-crown ether complex is the best example for ion-dipole interactions (Fig.1.02).<sup>23</sup> The bond energies of ion-dipole interactions varies from 50 to 200 kJ mol<sup>-1</sup> in the gas phase.<sup>18</sup> Apparently, the strength of these interactions decreases in polar solvents than the non-polar solvents. Ion-dipole interactions are directional bonds since they are depending upon the orientation of dipole.

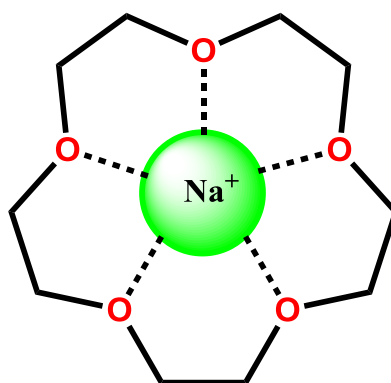


**Fig.1.02:** Ion-dipole interactions of 15-crown-5 with sodium ion.

### 1.1.3 Cation- $\pi$ interactions

The cation- $\pi$  interactions are electrostatic non-bonding attractions resulting from the cation and quadrupole of an aromatic system (Fig.1.03a).<sup>24-26</sup> The gas phase binding energies of this interaction is  $\sim 40$  kcal/mol, which is quite stronger than the analogous  $\text{H}_2\text{O}\dots\text{cation}$  interaction. In natural systems, cation- $\pi$  interactions are found between the aromatic amino acids phenylalanine, tyrosine, and tryptophan with cationic ligands or substrates. Few examples are (i) an extended series of cation- $\pi$  interactions found in the extracellular domain of human growth hormone receptor (Fig.1.03b)<sup>27</sup> (ii) the binding of positively charged acetylcholine to the enzyme acetylcholine esterase (Fig.1.03c).<sup>28</sup>

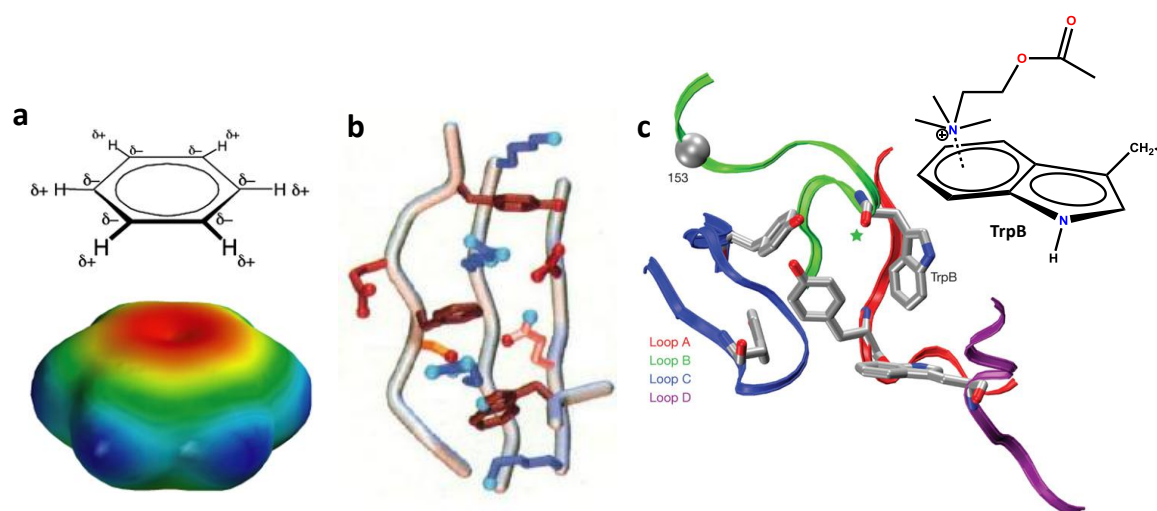


**Fig. 1.03:** a) Structure of benzene showing partial positive ( $\delta^+$ ) and negative charges ( $\delta^-$ ) in the benzene ring (top). Electrostatic potential map of benzene, red is negative and blue is positive (adapted from ref. 26). b) presence of extended cation- $\pi$  interactions in human growth hormone (adapted from ref. 27). c) cation- $\pi$  interaction between positively charged acetylcholine and enzyme acetylcholine with pocket residue TrpB (adapted from ref. 28).

### 1.1.4 XH- $\pi$ interactions

The quadrupole of aromatic  $\pi$ -systems can also interact with polarized X-H bonds, similar to H-bonded donor-acceptor pair. The XH- $\pi$  interactions are often termed as polar- $\pi$ -interaction (Fig.1.04a). The polar OH- $\pi$  and NH- $\pi$  interactions are commonly observed in proteins. Their gas phase bond energies vary from 2-5 kcal/mol.<sup>29</sup> CH- $\pi$  interactions are related to polar- $\pi$  interactions.<sup>30</sup> The electrostatic contribution of overall attractive energy of CH- $\pi$  interaction is much lower than polar- $\pi$  interactions. This is presumably due to the

electronegativity difference between C and H which is lesser than O and H, and makes the C-H much less polar than the O-H. Further, CH- $\pi$  interactions caused by the electron delocalization effect have stabilization energies that typically vary from 0.5 to 2.5 kcal/mol (Fig.1.04b).<sup>31</sup> They are also some of the commonly observed noncovalent interactions in the solid state of organic molecules.

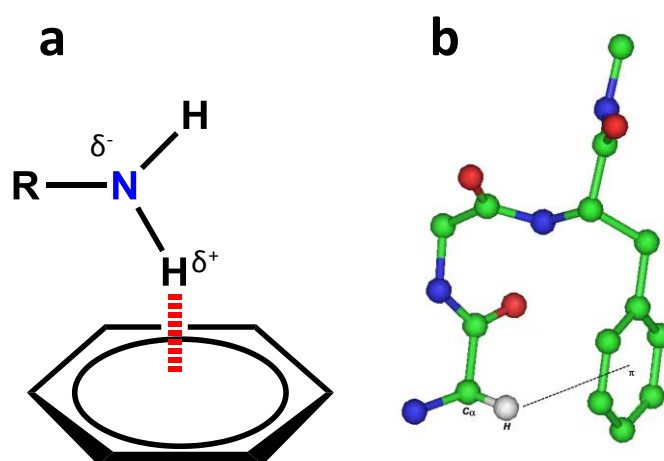


**Fig. 1.04:** a) NH- $\pi$  interaction between amine and arene showing polar partial positive ( $\delta^+$ ) and negative ( $\delta^-$ ) charges in the amine counterpart b) presence of extended cation- $\pi$  interactions in human growth hormone. Image courtesy: Imtech (Fig. 1.4b).<sup>32</sup>

### 1.1.5 $\pi$ - $\pi$ stacking

The noncovalent interactions between arene systems is known as  $\pi$ -stacking.<sup>33</sup> The  $\pi$ -interactions are believed to be arising from the overlapping of arenes  $\pi$ -orbitals of different molecules. The term stacking refers to the stacked arrangement of aromatic systems. The strength of the interactions lies in the range of 0 – 50 kJ mol<sup>-1</sup>.<sup>18</sup> These  $\pi$ -interactions were useful to stabilize the helical structures of DNA and its quadruplex (between the base pairs) found in the natural systems (Fig.1.05a).<sup>34</sup> One of the best synthetic example for stacking interaction is buckycatcher, in which the association constant of the interaction between concave buckyballs and convex fullerene molecule in solution is 8600 M<sup>-1</sup> (Fig.1.05b).<sup>35</sup>

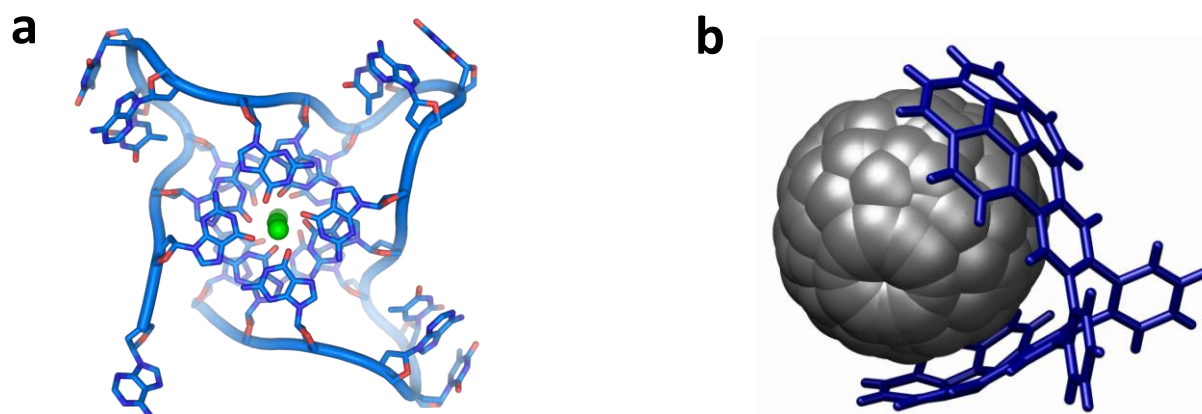


**Fig. 1.05:** a) Extended  $\pi$ - $\pi$  interaction between base pairs in the G- quadruplex structure. b) aromatic stacking interaction between bucky catcher and fullerene. Fig.1.05a is reproduced, with permission, from ref 34. Copyright © 2002 Nature Publishing Group. Fig.1.05b is reproduced, with permission, from ref 35. Copyright © 2007 American Chemical Society.

## 1.2.0 Basic Concepts of Supramolecular chemistry

For the better understanding and development of supramolecular chemistry, the following concepts are very crucial and discussed with examples.

### 1.2.1 Molecular self-assembly

It is an important spontaneous process by which molecules are arranged in a defined manner without any external guidance. Molecular self-assembly is classified into two types, *i.e.* (i) inter and (ii) intramolecular self-assembly.<sup>36-37</sup> The term self-assembly usually refers to the intermolecular self-assembly whereas the intramolecular self-assembly is commonly known as folding.<sup>38</sup> The best known cases of classical intermolecular self-assembling systems are *micelles* and *vesicles*. Micelle forms results from molecular self-assembly of surfactants in the liquid colloid.<sup>39</sup> It is typically formed by hydrophilic-heads contacting with surrounding solvents molecules and thereby segregating the hydrophobic tails inside the micelle center (Fig.1.06a). On the other hand, vesicles are small structures existing in the cells, which are ubiquitous in many of the biological processes. In contrast to the micelle, vesicles are multilayered structures; in which groups containing similar polarity (hydrophobic/hydrophilic) self-assembles on the same side to form layered spherical shaped structures as shown in the Fig.1.06b.<sup>40</sup>

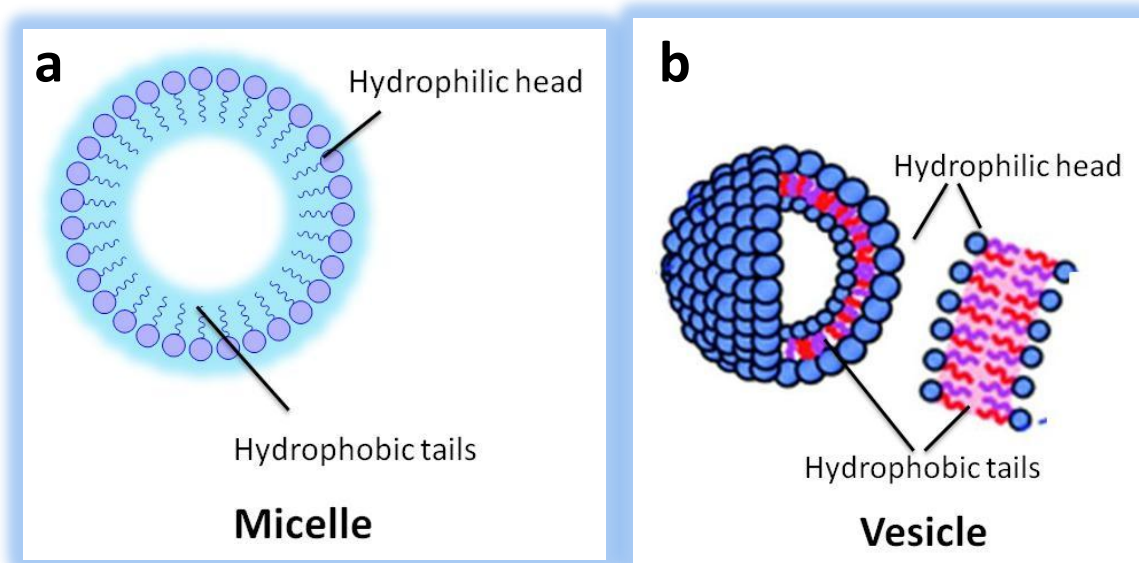


**Fig. 1.06:** a) Structure of micelle by the aggregation (self-assembly) of hydrophobic and hydrophilic surfactants b) self-assembly of hydrophobic and hydrophilic molecules forming layered vesicle. Adapted from ref: 40.

### 1.2.2 Molecular recognition

Molecular recognition is a process of specific interaction between the molecules through non-covalent forces namely hydrogen bonds,  $\pi$ - $\pi$  interactions, etc.<sup>41-42</sup> The complementarity of shape and interacting functional groups are some of the very important criterion for molecular recognition events.<sup>43</sup> The term molecular recognition is thought to be first introduced from the *lock-and-key* principle of Emil Fischer (Fig.1.07a).<sup>44</sup> In that, he mentioned the specificity of the enzymes *invertin* and *emulsin* for  $\alpha$  or  $\beta$  form of glucosides, respectively.<sup>45</sup> The illustrative evaluation of complementarity of a key to a lock is used to explain how a small molecule binds to an enzyme. Although, essentiality of shape complementarity was satisfactorily covered by this comparison, the need for functional group interaction complementarity is not considered. After many years, the isolated host molecule found to be not necessary for complementing the shape of the guest (Koshland). During binding, it undergoes an induced fit and adapts to the conformation leading to an ideal shape (Fig.1.07b).<sup>46</sup> Based on the perspective of supramolecular chemistry, the molecular recognition is considered to be information storage system.<sup>43</sup> This information is stored in the steric and shape arrangement of the complex, *i.e.* the architecture of the complex.

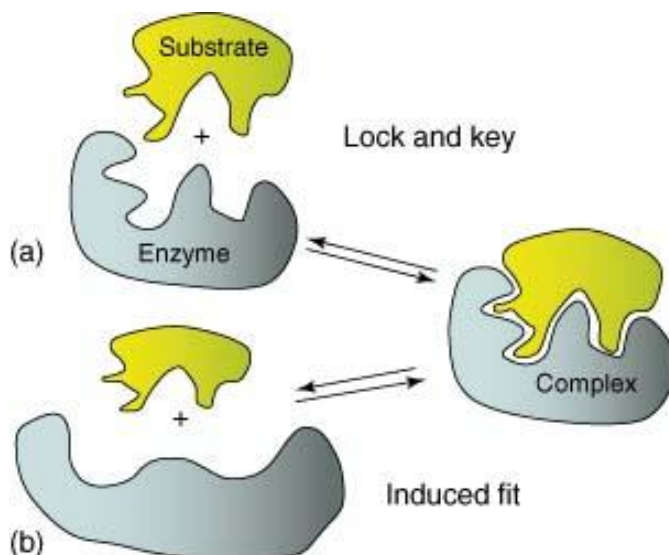


**Fig. 1.07:** a) Emil Fischer's illustration of rigid lock and key (b) Koshland's induced fit model of enzyme–substrate interaction.<sup>44</sup> Reproduced with permission from ref. 44. Copyright 2009 John Wiley and Sons.

### 1.2.2.1 The parametric effects of molecular recognition events

In 1975, Graf & Lehn synthesized extremely unusual macrotricycles-based artificial receptors<sup>47</sup> capable of selectively binding with guest molecules containing spherical and tetrahedral geometries.<sup>43</sup> Alkali metal cations, ammonium ion and water have better interactions than the other geometrical guests (Fig.1.08a). Harada & Kataoka (1999) synthesized various chain lengths containing polyanionic and polycationic block copolymers separately to study the effect of length in the molecular recognition events (Fig.1.08b).<sup>48</sup> They mixed both the ionic block co-polymers in an aqueous solution, which in turn surprisingly resulted in the exclusive formation of new co-polymer pairs with same length and having opposite charges. Subsequently, these pairs formed into larger core-shell-type assemblies with narrow size distribution.



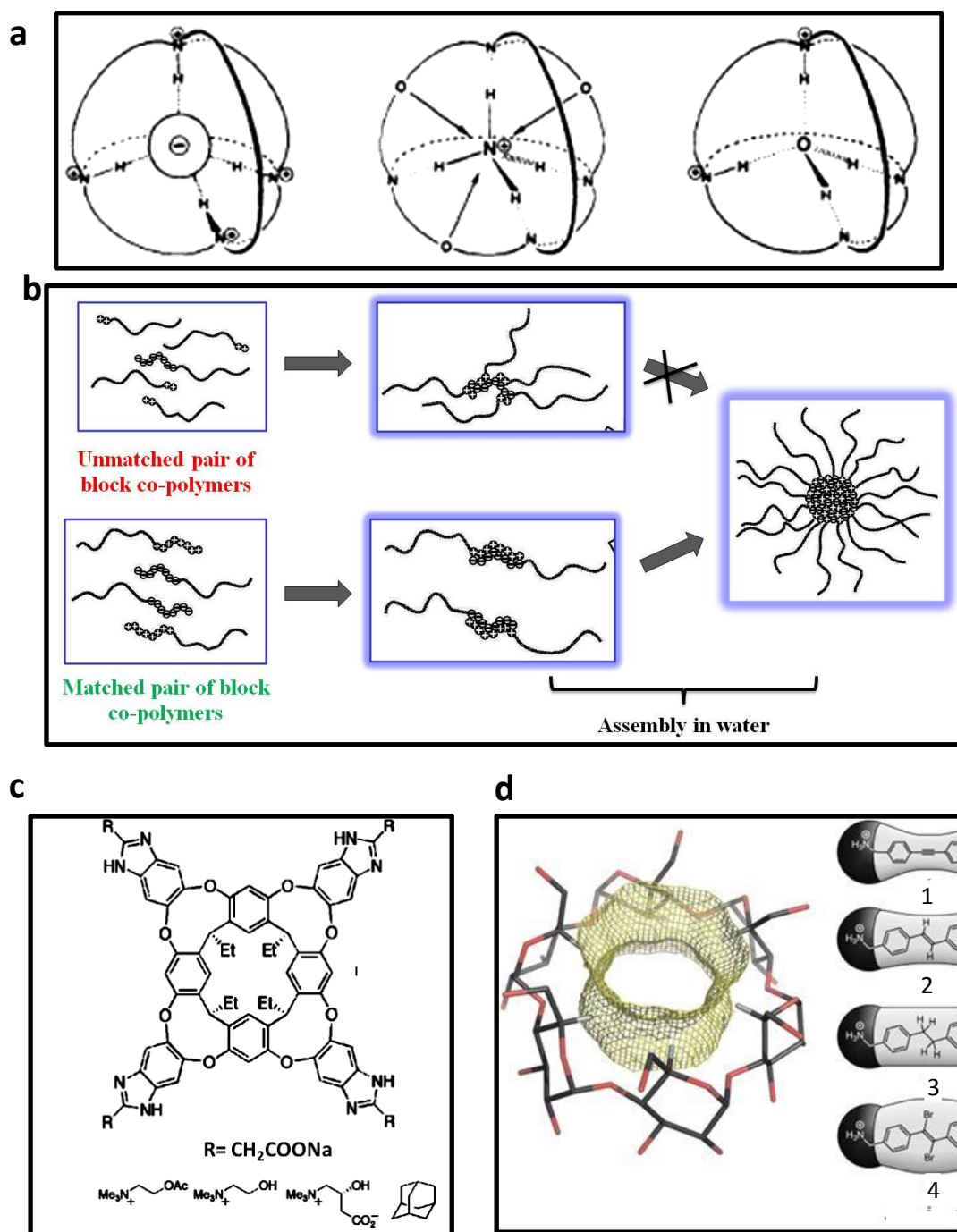


**Fig. 1.08:** a) Synthetic receptor binds with guest molecules containing spherical and tetrahedral geometries (adapted from ref: 43). b) the supramolecular (ionic polymer) system recognizes molecular length of oppositely charged species and pairs in water. As a result, poly-ion complex (PIC) micelles are formed (adapted from ref: 48). c) the artificial receptor showing high binding affinity with the cationic cholines (charge recognition)) and adamantane (shape selectivity) (Adapted from ref: 49). d)  $\alpha$ -cyclodextrin showing discrimination against various guests based on their thickness. Guest molecules 1,2 and 3 form complex with  $\alpha$ -cyclodextrin, but 4 doesn't form any complex owing to its larger thickness than the threshold thickness (adapted from ref: 50).

Hof *et al.* (2003) showed discrimination of choline type species such as tetramethylammonium cation complex from tetrapropyl- and tetrabutylammonium using a biomimetic receptor containing four negatively charged carboxylate groups.<sup>49</sup> This discrimination could be presumably due to steric barriers (Fig.1.08c). Though most of the positively charged cholines and their derivatives are able to show a good affinity towards the receptor, the structurally related *zwitterionic* molecule L-carnitine showed weak binding affinity. In addition, adamantane forms a 1:1 complex with receptor suggesting the shape complementarity between receptor and ligand. In 2007, Muller and Wenz investigated the interaction between cyclodextrins and guests having various thickness (Fig.1.08d).<sup>50</sup> For this purpose, they have synthesized a series of *bolaamphiphiles* with increasing central thickness and found thickness dependent affinity with cyclodextrins. Liu *et al.* in 2015 studied the selective binding affinity between quaternary ammonium cations and water-soluble calix[4]resorcinarene.<sup>51</sup> In 2016, Jing-Xin Liu and co-workers reported the encapsulation of aniline-containing guests using MeQ[6] and Q[7] receptors (Fig.1.09).<sup>52</sup> Though both the receptors have shown strong complexation towards the guests, it was found that TMeQ[6] exhibited more complementary in size and shape than Q[7].

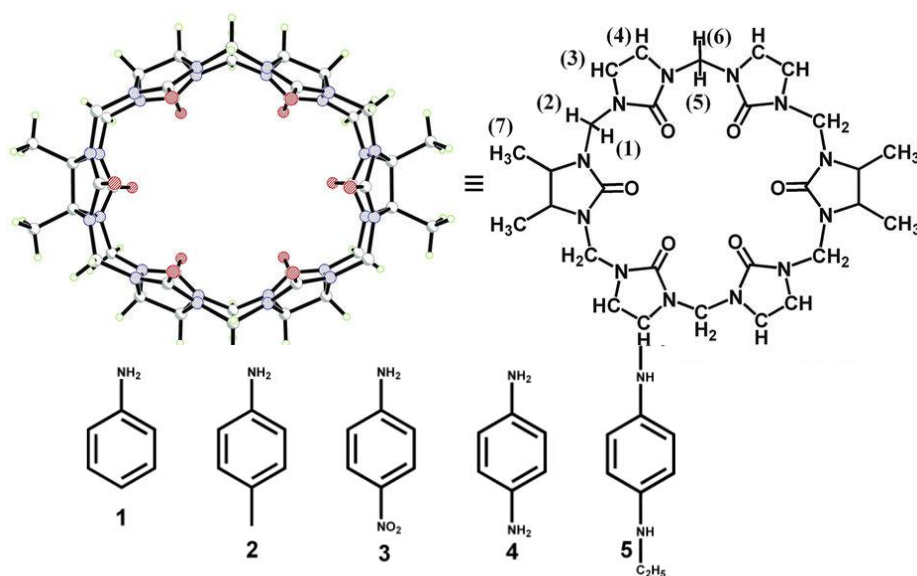


**Fig. 1.09:** X-ray crystal structure of TMeQ[6] in top view (top-left) and its aniline group containing guests (bottom) for molecular recognition. Reproduced, with permission, from ref 52. Copyright © 2016 Nature Publishing Group.



### 1.2.3 Multivalency

Multivalency refers to the synchronized binding of multiple functionalities of one entity with multiple complementary functionalities of two or more entities.<sup>53-55</sup> The two functionalities involving in the multivalent interactions are biochemically referred to as receptor and ligand.<sup>56-57</sup> In supramolecular chemistry, these terms are generally used as host and guest. The multivalent interactions between the host and guest resulted in the formation of host-guest complex. The number valency of the entity is counted by its number of individual interactions with other entities of complementary functionalities. The number of valency of the complex is defined as the number of mutual interactions between the two entities (Fig. 1.10). In general, the participation of more than one host-guest interaction is considered to be multivalent.

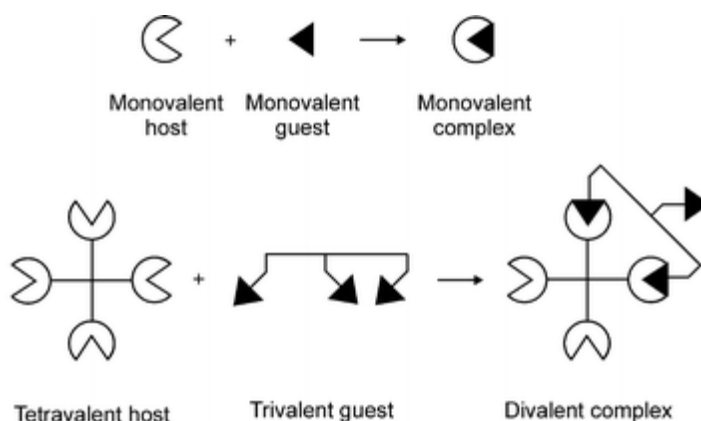


**Fig. 1.10:** Terminology of valencies. Reproduced with permission from ref 55. Copyright 2004 Royal Society of Chemistry.

The combined overall strength of multiple interactions between the two non-covalently interacting species is stronger than the monovalent *i.e* single, interaction.<sup>58-59</sup> Multivalent interactions are ubiquitous in biological processes and play an important role in the determination of events such as microbial virulence,<sup>60</sup> inflammation,<sup>57</sup> and host immune responses etc., .<sup>61-62</sup>

Further, multivalency concept was also utilized to mimic the biological process such as antagonism and agonism. These biological mimickings were performed mostly involving the combination of multivalent guest with naturally occurring multivalent hosts. The guest moieties in these studies are typically saccharide units, which are specifically recognized by naturally occurring multivalent hosts, *i.e.*, proteins.

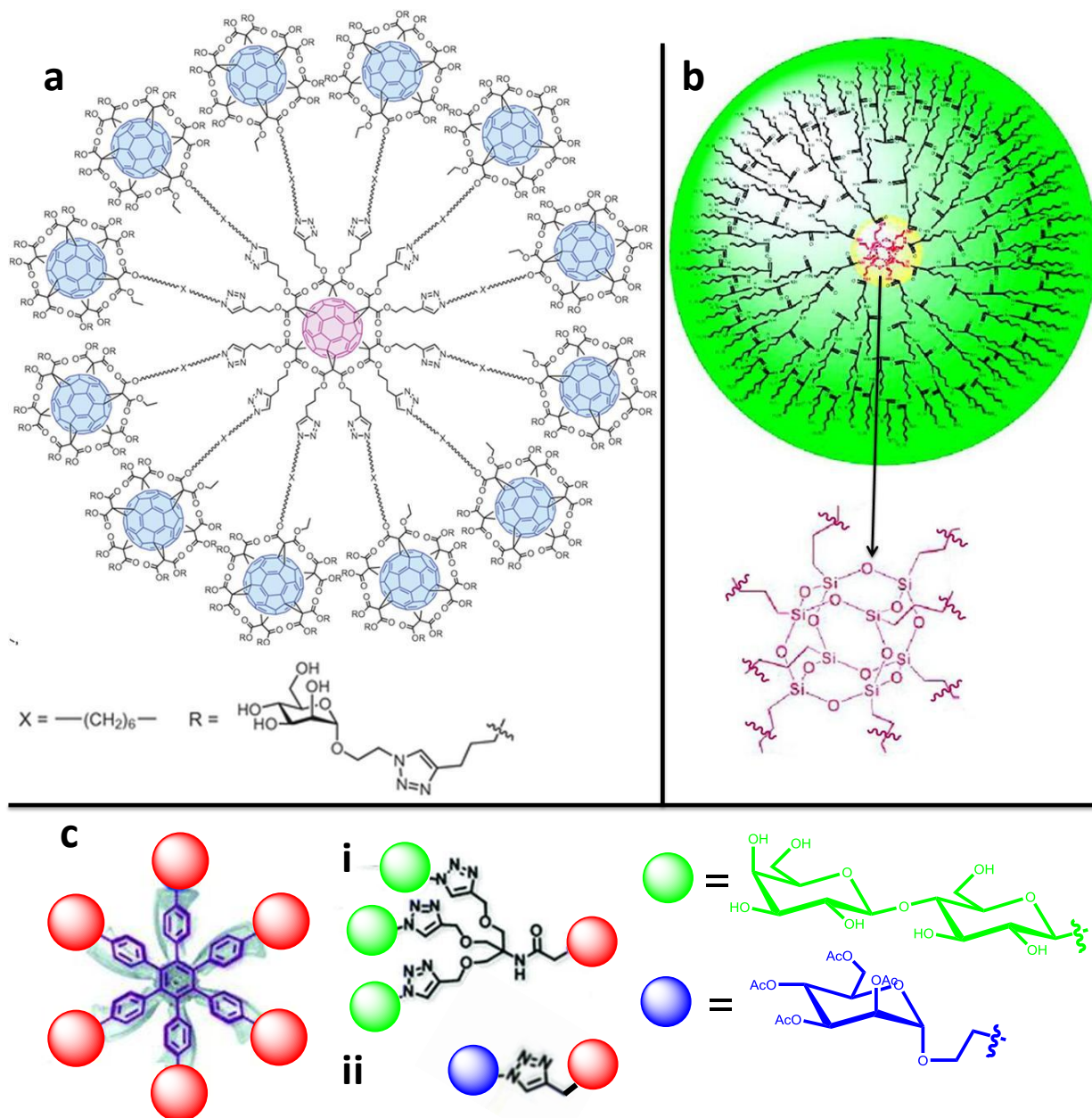


**Fig. 1.11:** Structure of various multivalent supramolecular models. a) The super ball structure artificial Ebola virus inhibiting Fullerene based glycolconjugate. b) dendrimeric structure of nanoglobular drug carrier poly-l-lysine attached cubic octa(3-aminopropyl)silsesquioxane (oas). c) the structure of hexaphenylbenzene-based glycoconjugates (i) and (ii) showing promising inhibition against galectin-3 binding to mucins (adapted from ref: 63).<sup>63</sup> Fig.1.11a is reproduced, with permission, from ref 73. Copyright © 2016 Nature Publishing Group. Fig.1.11b is reproduced, with permission, from ref 35. Copyright © 2007 American Chemical Society.

A diverse number of multivalent inhibitors have been prepared for various viruses and lectins including influenza virus,<sup>64-67</sup> cholera,<sup>68-69</sup> lectins<sup>70-71</sup> and anthrax toxin.<sup>72</sup> In

addition, many of these multivalent supramolecular models have also been reported to have various interesting properties. Some of the recent examples and their importances are discussed here. Martín and co-workers synthesized giant globular multivalent glycofullerenes or super balls (Fig 1.11a), which showed inhibition against artificial Ebola virus in the subnanomolar range concentrations.<sup>73</sup> Rong *et al.* synthesized a series of peptide attached with multivalent POSS (Fig. 1.11b) scaffolds for nano drug delivery.<sup>74</sup> Cytotoxicity studies revealed that the toxicities of nanoglobules-scaffolds were size-dependent. However, it was much lesser than its corresponding linear polypeptides. Rene Roy and co-workers have synthesized a series of hexaphenyl benzene (HPB) based multivalent-glycoconjugates by using click chemistry.<sup>75</sup> Interestingly, the hydrophobic nature of the hexaphenyl benzene (HPB) was counterbalanced by lactoside derivatives, owing to which the multivalent scaffolds were readily soluble in water. Further, the glycoconjugates such as (i) and (ii) shown in Fig. 1.11c had shown promising inhibition against galectin-3 binding to mucins.<sup>63</sup>

#### 1.2.4 Host-guest chemistry

Host-guest chemistry is one of the main branches of supramolecular chemistry that investigates complexes consisting of two or more molecules or ions formed through molecular recognition with the assistance of non-covalent interactions. Hence, the host-guest complexation is one of the molecular recognition events that involves different sizes of chemical species. Hosts are chemical species larger in size with internal cavities or external cavities which can accommodate small molecules. The small guest molecules without any interaction of their own species are accommodated or surrounded by host molecules known.<sup>76</sup>

The host-guest systems can be classified into two major types<sup>77</sup> according to their topologies (Fig. 1.12):

1. Extramolecular host-guest systems (*clathrates*)
2. Intramolecular host-guest systems (*cavitates*)

Extramolecular inclusions (*clathrates*) occur purely based on aggregation of molecules through non-covalent interactions such as charge transfer, directional H-bond, van der

Waals forces etc., They are not inherent to the isolated molecular geometry of the hosts. Clathrate-hosts are stable in solid state only; for example: gas hydrates and urea clathrates.

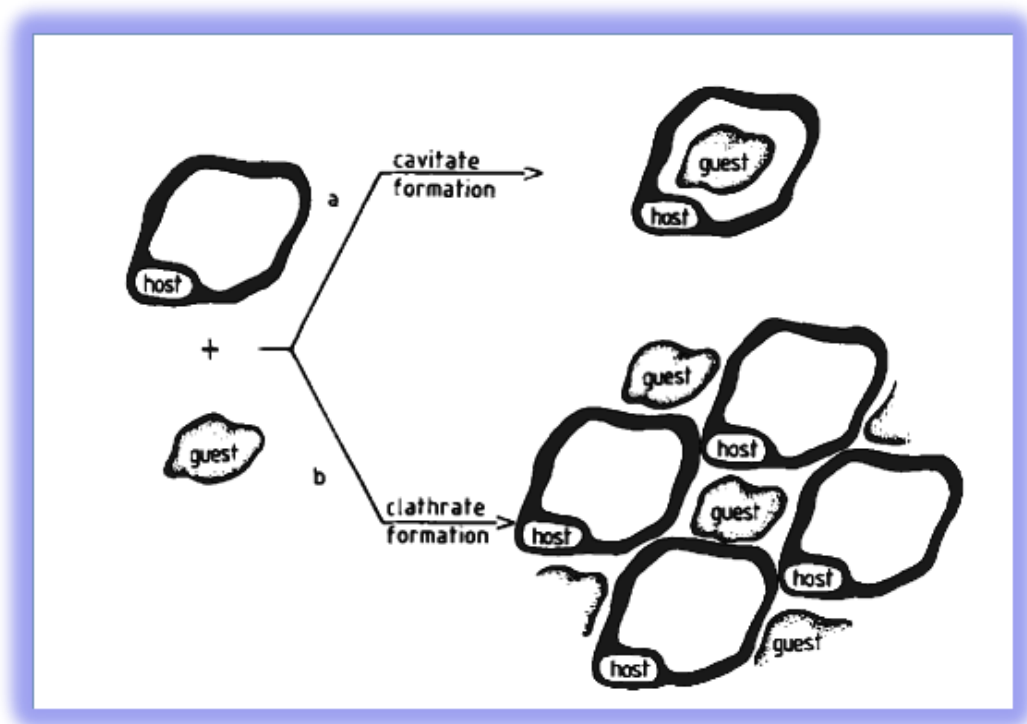


**Fig. 1.12:** Classification of host-guest systems. Schematic representation of formation of a) cavitates and b) clathrates. Adapted from ref. 72.

In intramolecular systems (cavitate), the cavity is already inherent in their molecular structure as in calixarenes, pillararenes, cucurbiturils, and shape-persistent organic cage compounds.<sup>18</sup> Representative host compounds containing intramolecular cavities are crown ethers, cyclodextrins, calixarenes, cryptand, pillar arenes and cyclophanes. Another subdivision could be made on the basis of forces between the host and guest molecules; if host-guest interactions are primarily built through electrostatic forces, the term *complex* is used and for less specific and non-directional interactions, the term “*cavitand*” or “*clathrate*” is used. These inclusion complexes are composed of two or more components without conventional chemical union. Some of the selected host-supramolecular entities related to this thesis are discussed below.

### 1.2.4.1 Clathrate compounds

Clathrate hydrates were discovered by Humphry Davy in 1810.<sup>78</sup> Later in 1927, Pfeiffer studied the properties of clathrates extensively.<sup>79</sup> The term "*molecular compounds*" was coined by E. Hertel (1930), wherein the substances are decomposed into individual components following mass action law in solutions or in gas state.<sup>80</sup> H. M. Powell analyzed their X-crystal structures and named them as clathrates in 1945.<sup>81</sup> There are also several clathrates obtained from organic hydrogen-bonded frameworks.<sup>82-84</sup> Most of these networks are adapted from molecules that "*self-associate*" by directional multiple hydrogen-bonding interactions. The most prominent and well known naturally frozen methane clathrate is one of the best examples (Fig. 1.13a). It is basically formed from surroundings of methane through H-bonding network of water molecules.<sup>85-86</sup> Few important H-bonded clathrates forming hosts are hydroquinone,<sup>87</sup> urea and thiourea.<sup>88</sup> There are also plenty of artificial host molecules reported to form clathrates. Among them, Dianin's and tris-(*o*-phenylenedioxy) cyclotriphosphazene (TPP) was studied extensively in the literature (Fig. 1.13b).<sup>89-91</sup> Some of the H-bond assisted clathrate frameworks are found to be stable even after removal/exchange of guest molecules. They have been used for gas adsorption studies.<sup>92</sup>

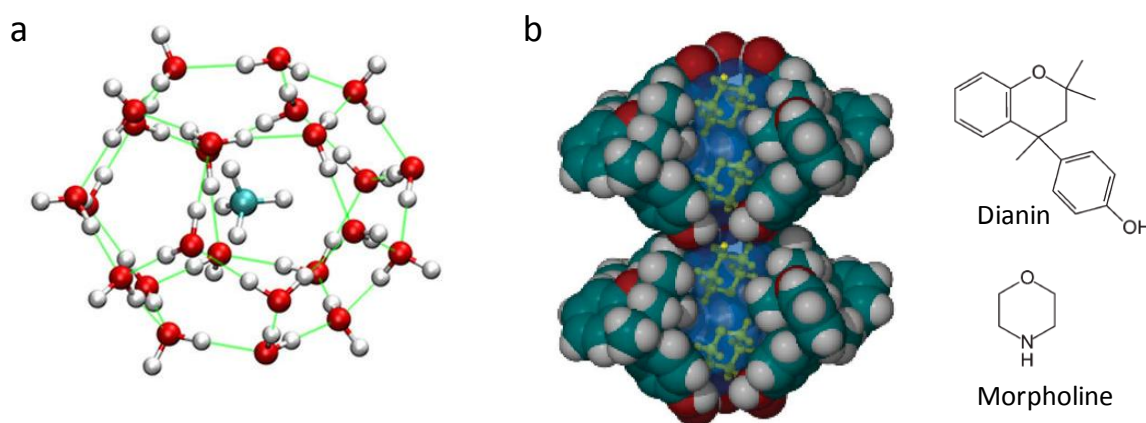


**Fig. 1.13:** a) Structure of methane hydrate cage<sup>86</sup> (adapted from ref: 81). b) protonated morpholine encapsulated Dianin's crystal structure and molecular structures of Dianin and morpholine (adapted from ref: 90). Fig.1.13a is reproduced, with permission, from ref 86. Copyright © 2016 Nature Publishing Group.



### 1.2.4.2 Cyclodextrins

Cyclodextrins (CDs) are the cyclic oligosaccharides consisting of  $\alpha$ -D-glucopyranose units and connected by 1, 4 linkages. The macrocycles called as cellulose were first discovered by A. Villiers in 1891. Now, they are known as cyclodextrins.<sup>93</sup> Soon after the discovery of cellulose, the homologous of CDs - $\alpha$ -, - $\beta$ -, and - $\gamma$  were identified by F. Schardinger from natural resources and are referred as "Schardinger sugars". The - $\alpha$ -, - $\beta$ -, and - $\gamma$  CDs contain 6, 7, and 8 membered rings, respectively (Fig.1.14).<sup>94</sup> They are cone-shaped with a large ring at one end and narrow at the other. Both faces of CD containing hydroxyl groups make it a perfect candidate for easy functionalization. Without functionalization, CDs possess inner hydrophobic and outer hydrophilic environment, making them water soluble. CDs are able to form host-guest complexes with various guest molecules owing to the presence of varied cavity size (based on the ring size) with the range of 4.9-8.0 Å.<sup>95</sup> Therefore,  $\alpha$ -CD encapsulates linear alkanes and small aromatic compounds (cavity size 4.9 Å).  $\beta$ -CD traps relatively bigger guests like bulky hydrocarbons- adamantane and cyclohexane derivatives, and polyaromatic compounds such as naphthalene and anthracene derivative.<sup>96</sup>  $\gamma$ -CD encapsulates larger guest due to the presence of large cavity size formed by eight glucopyranose units. The advantages like accessibility, non-toxicity and the ability to form host-guest complexation in aqueous media with diverse hydrophobic guests like fats, foods, medicines and coenzyme-Q10 make CDs very useful in biomedical applications.<sup>97</sup> Nevertheless, the poor solubility of CDs in non-polar solvents made organic chemists to derivatize the hydroxyl groups to increase the solubility, and thereby develop the scope of utilizing CDs efficiently.

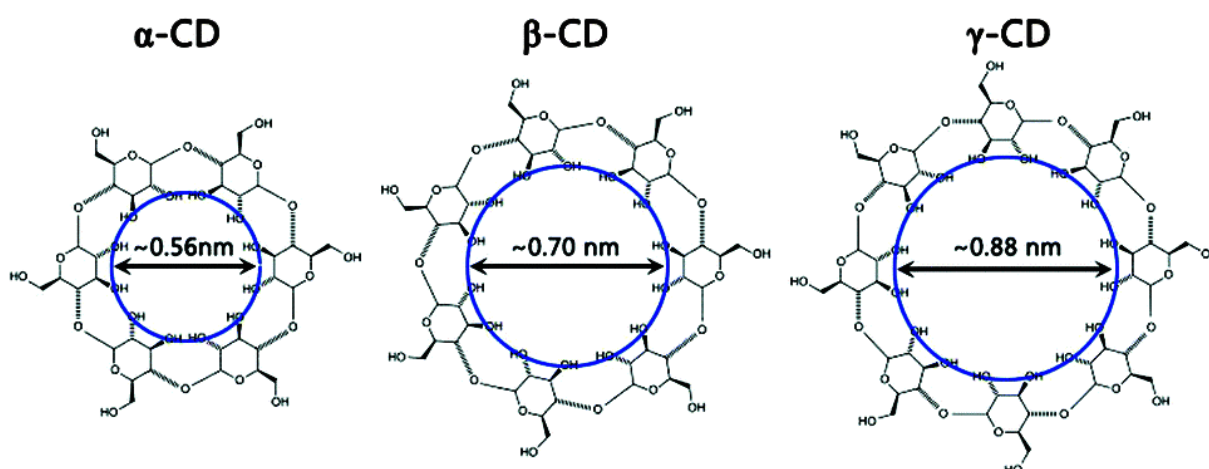


**Fig. 1.14:** Chemical structures and molecular sizes of  $\alpha$ -,  $\beta$ -,  $\gamma$ -CD.<sup>94</sup> Reproduced with permission from ref 94. Copyright 2016 Royal Society of Chemistry.

### 1.2.4.3 Cucurbit[n]urils

Cucurbit[n]urils (CB[n], n = 5-11) are symmetrical macrocycles that consist of glycouril repeating units connected by two methylene bridges. Their structure resembles the shape of pumpkin. Though the synthesis of CB[6] emerged in literature during 1905,<sup>98</sup> its complete structural characterization and host-guest properties were summarized only in 1981 by Freeman-Mock.<sup>99</sup> Until the year 2000, CB[6] did not receive much attention due to the poor solubility which led to its poor development. Then, Kim and coworkers succeeded in synthesizing CB[n] (n = 5-11) in moderate yields by lowering the reaction temperature from >110 °C to 75-90 °C which strengthened the CB[n] chemistry.<sup>100</sup> The moderate water solubility of CB[5] and CB[7] in conjunction with their symmetrical hydrophobic cavities favor the inclusion complexes of these macrocycles with water soluble guests like neutral diamines, gases and cations. The two methylene bridges between the glycouril units provide rigidity to the CB[n]s and afford no conformational flexibility. Thus, it forms inclusion complexes with outstanding selectivity and affinity. The cavity sizes are CB[6]=5.8 Å, CB[7]=7.3 Å and CB[8]=8.8 Å. The cavity sizes and inclusion properties of CB[6], CB[7] and CB[8] are typically comparable with that of  $\alpha$ -CD,  $\beta$ -CD and  $\gamma$ -CD, respectively. Miyahara and co-workers studied the decamethyl substituted CB[5] which could encapsulate small molecules including gases (Fig.1.15a).<sup>101</sup> Freeman studied the inclusion of *p*-xylylenediammonium chloride (Fig.1.15b)<sup>102</sup> and found CB[8] showing 1:1:1 ternary complexes with electron donor and acceptor. The electron acceptor failed to complex with CB[8] alone in the absence of electron donor, thus requiring the presence of CB[8] to form charge transfer complex (Fig. 1.15c).<sup>103</sup> There are two obstacles which hindered the growth of CB[n] chemistry; namely poor solubility in common organic solvents and problem in functionalization. Kim *et al.* addressed the issue of solubility of CB[5] and CB[6] by appending cyclohexyl moiety in each glycouril unit, upon which these cavitands could become water soluble despite having hydrophobic cyclohexyl groups.<sup>104</sup> Further, the same group investigated the problem of functionality by oxidizing CB[n] using K<sub>2</sub>S<sub>2</sub>O<sub>8</sub> in water to yield per-hydroxylated CB[n].<sup>105</sup> Later, Sherman's and Isaac's groups derived monohydroxylated<sup>106</sup> and monofunctionalized cucurbit[6]urils,<sup>107</sup> respectively. Afterwards, there have been number of derivatives of cucurbiturils synthesized with impressive structures and properties.<sup>108</sup>

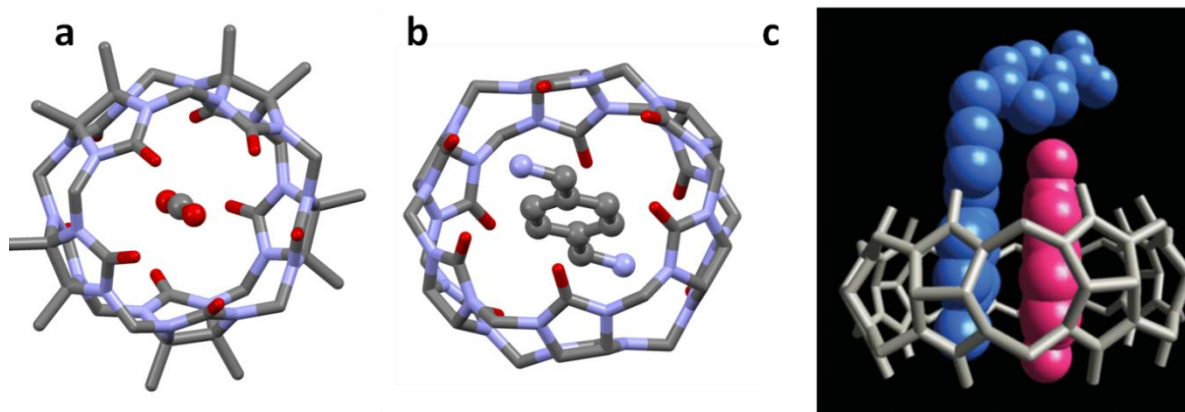


**Fig. 1.15:** Crystal structure of CB[5], CB[6] and CB[8] with guest molecules: (a) CO<sub>2</sub> included CB[5], (b) *p*-xylylenediammonium included CB[6]. (c) 1:1:1 charge transfer complex of CB[8] with viologen and 2,6-dihydroxynaphthalene (adapted from ref:103). Crystal structures courtesy of CCDC.

#### 1.2.4.4 Calixarenes

Adolf von Baeyer first reported the phenol-formaldehyde condensation in the 1870s.<sup>109</sup> Subsequently, many people have studied the synthesis and structural characterizations of calixarenes.<sup>110</sup> Calixarenes became more popular in 1978 by the work of Gutsche.<sup>111</sup> Calixarenes are vase-shaped macrocycles based on hydroxyalkylation product of phenols and aldehydes.<sup>112</sup> These [n]metacyclophanes are found with even number of repeating units ( $n = 4, 6, 8$ ) in general. The odd-numbered ( $n = 3, 5, 7$ ) calix[n]arenes and large calixarenes are rare due to low yields.<sup>113</sup> Multiple intramolecular hydrogen bonds between the hydroxyl groups of phenolic units of metacyclophanes are responsible for their vase-shape Fig 1.16a. The existence of electron rich phenolic unit aides calixarenes to encapsulate electron deficient species, especially the cations. For instance, calix[8]arenes could selectively entrap C60 and was used to isolate C60 from the fullerene mixture (Fig. 1.16b).<sup>114</sup> Sulfonated calixarenes are soluble in water (Fig. 1. 16c), and were showed to form host-guest complexation in aqueous media with cationic as well as neutral molecules.<sup>115-116</sup> Calix[n]arenes can have various conformations due to the rotation of phenolic units.<sup>117</sup> They are found in four conformations *i.e* cone, partial cone, 1,2-alternate and 1,3-alternate. The formation of modified calix[n]arenes such as thiacalix[n]arenes<sup>118</sup> involves the replacement of methylene bridges by sulfide, sulfinyl and sulfonyl units. It is important to note that thiacalix[n]arenes are capable to bind metal ions, selectively. Some of the thiacalixarenes which encapsulate lanthanide ions are used



as fluorescent markers and MRI sensitizers.<sup>119</sup> Over the years, several other calixarene analogues such as bowl-shaped resorcin[n]arenes,<sup>120</sup> pyrogallol[n]arenes<sup>121</sup> and calix[n]pyrroles,<sup>122</sup> have been found in the host-guest chemistry of calix[n]arenes.

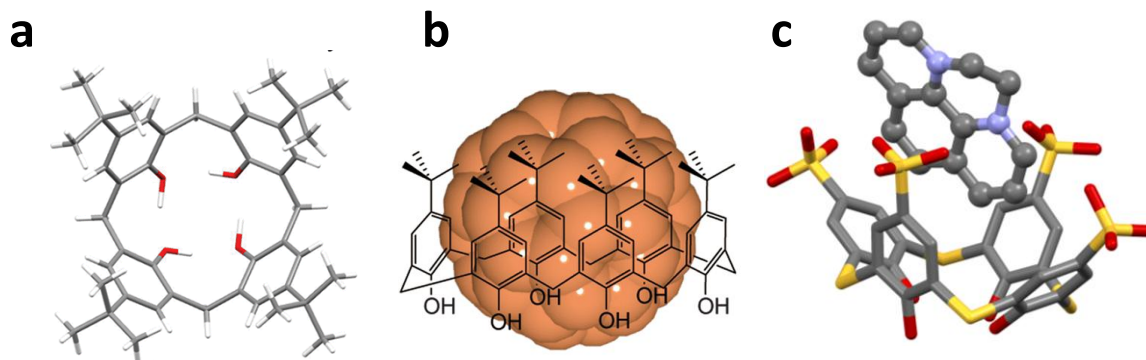


**Fig. 1.16:** (a) Top view of the crystal structure of *t*-butyl calix[4]arene (b) host-guest complex of calix[8]arene and C60 (c) crystal structure of *p*-sulfonatocalix[4]arene and phenanthroline-dium complex. Image courtesy: CCDC (Fig. 1.16a and 1.16c), ref.114 (Fig. 1.16b).

### 1.3 Imine-based macrocycles

Organic cages are an exceptional class of porous materials composed of discrete molecules with intrinsic, guest accessible cavities. To maintain their porous nature in the solid state, the cavities of the cages are connected by 1D, 2D, or 3D porous networks.<sup>123-124</sup> In the absence of connectivity between the intrinsic cavities, it would become inaccessible for guest molecules and get isolated from each other.<sup>125</sup> Usually, these cages should show shape-persistency even after addition and removal of solvents/guests. Thus, they should not lose their porous nature by the disruption of porous network. Considering the above mentioned requirements, it appears very simple to design cage molecules. However, in terms of practical synthesis, they are highly challenging. The recent works made in the preparation of cage molecules involve the dynamic covalent chemistry. In particular, majority of POCs synthesized till date rely on the formation of imine bond through the reaction between primary amine and aldehyde.<sup>126</sup> The pioneering report of this study was reported by Cram and Quan in 1991. They have synthesized a hemicarcerand by a four 1,3-diaminobenzene and two tetraformylcavitand molecules in a [2+4] condensation reaction.<sup>127</sup> Following this work, a variety of cage compounds have

been constructed using their approach. The first series of imine-based POC molecules was reported by Cooper *et al.* in 2009.<sup>128</sup> The 1,3,5-triformylbenzene (TFB) was treated with three different vicinal diamines to yield [4+6] cages. Since cages structurally adopted a tetrahedral geometry, majority of the cages were found to be thermodynamically stable (Fig. 1.17a). Bojdys *et al.* showed extrinsic cavities in cages by introducing bulky aryl groups onto the cage vertices.<sup>129</sup> Jelfs *et al.* observed that, an increase in chain length of alkane diamine results an odd-even effect on the formation of either [2+3] or [4+6] cages.<sup>130</sup> In addition, these cages displayed inclusion of various guest molecules in their intrinsic as well as extrinsic cavities. Hasell *et al.* showed that iodine and osmium tetroxide guest molecules can be sublimed into the pores of the cage structure.<sup>131</sup> Mitra *et al.* studied the facilitation of isolation of mesitylene from its C<sub>9</sub> structural isomer 4-ethyltoluene with 100 % specificity.<sup>132</sup> Porous organic cages have unique performance in the solid state for the isolation of rare gases, such as *xenon* and *krypton* (Fig. 1.17b). It is believed that the selectivity of the cages arises by a size match between the rare gases and cage cavity. Cooper and co-workers have demonstrated the practical separation of *krypton*, *xenon* and *radon* from air at concentrations of a few *ppm*.<sup>133</sup> Chiral imine-based cages also can be used for the selective binding of chiral organic molecules such as 1-phenylethanol (Fig. 1.17c).<sup>133</sup>

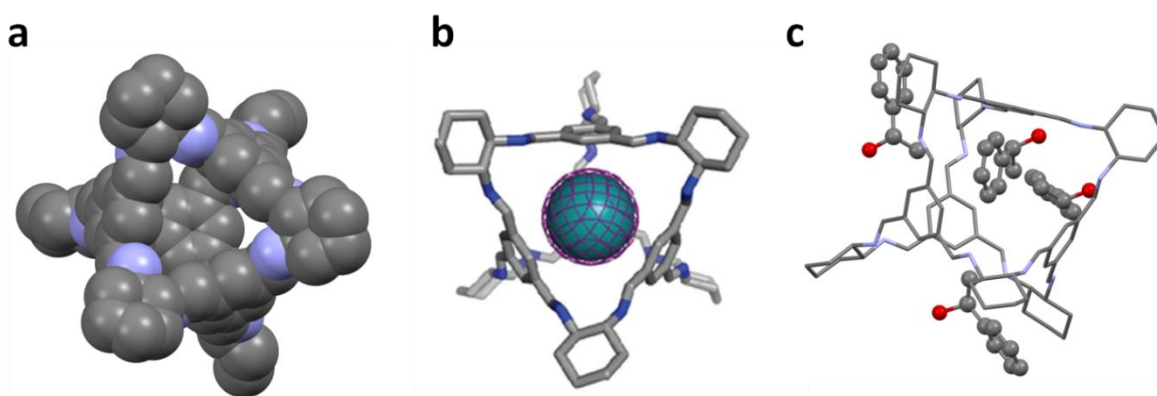


**Fig. 1.17:** (a) Crystal structure (space fill model) of [4+6] cage-CC3 showing intrinsic cavity. (b) Schematic representation of host-guest complex of xenon and cage-CC3 (c) Phenylethanol included crystal structure cage CC3. Image courtesy: CCDC (Fig. 1.17a and 1.17c), ref.128 (Fig. 1.17b).

#### 1.4 Metal-organic framework (MOF) in host-guest chemistry

Metal-Organic Frameworks (MOFs) which are also known as porous coordination polymers (PCPs) are crystalline porous materials. They have been the subject of research interest for over decades and fast growing. MOFs are constructed from metals and multi-dentate organic linkers.<sup>134</sup> Most of these materials possess three dimensional structures involving uniform pores and a network of channels. The variance of metals and organic linkers provides a tremendous degree of structural and functional tunability to design MOFs with many interesting properties. Their permanent well-defined pores and low densities have identified MOFs as excellent candidates for a wide range of applications such as gas storage, separations, catalysis and molecular inclusion.<sup>135-136</sup> Zhang and co-workers tried to capture specific organic species by molecular-recognition using designed MOF. In their attempt, they have introduced molecular-recognition sites as a domain in MOFs in order to maneuver and dock the incoming guests in a selective manner using stereochemistry and electronic interactions.<sup>137</sup> Replacing classical methods, Makoto Fujita and coworkers have reported a revolutionary crystallographic technique which could determine the stereochemistry properties of chemical species with axial and planar chiralities<sup>138</sup>. They have paid much attention in this field by reporting the chemical structure of compounds which are not needed to be crystallized.<sup>139-140</sup> X-ray crystallography is a unique technique that determines the molecular structure of compounds. However, it often requires the arduous growth of high-quality single crystals of the compound of interest. In contrary, Fujita's *et al.* prepared a crystalline host metal-organic framework (MOF) that could absorb target molecules within its pores and thus helping to order the guests within the framework lattice (Fig. 1.18a-b). Analysis of these crystals using X-ray diffraction revealed the structure of compound without ambiguity. Some of the metal phosphonates<sup>141</sup> and carboxylates<sup>142</sup> and sulphonates<sup>142-143</sup> networks are prone to trap water molecules. As a result, these materials tend to show exceptional proton conductivities ( $>10^{-2}$  S cm<sup>-1</sup>). Kitagawa and co-workers have studied the proton-conductivity area with respect to traditional coordination polymers (temperature region 20° to 75°C).<sup>142</sup>

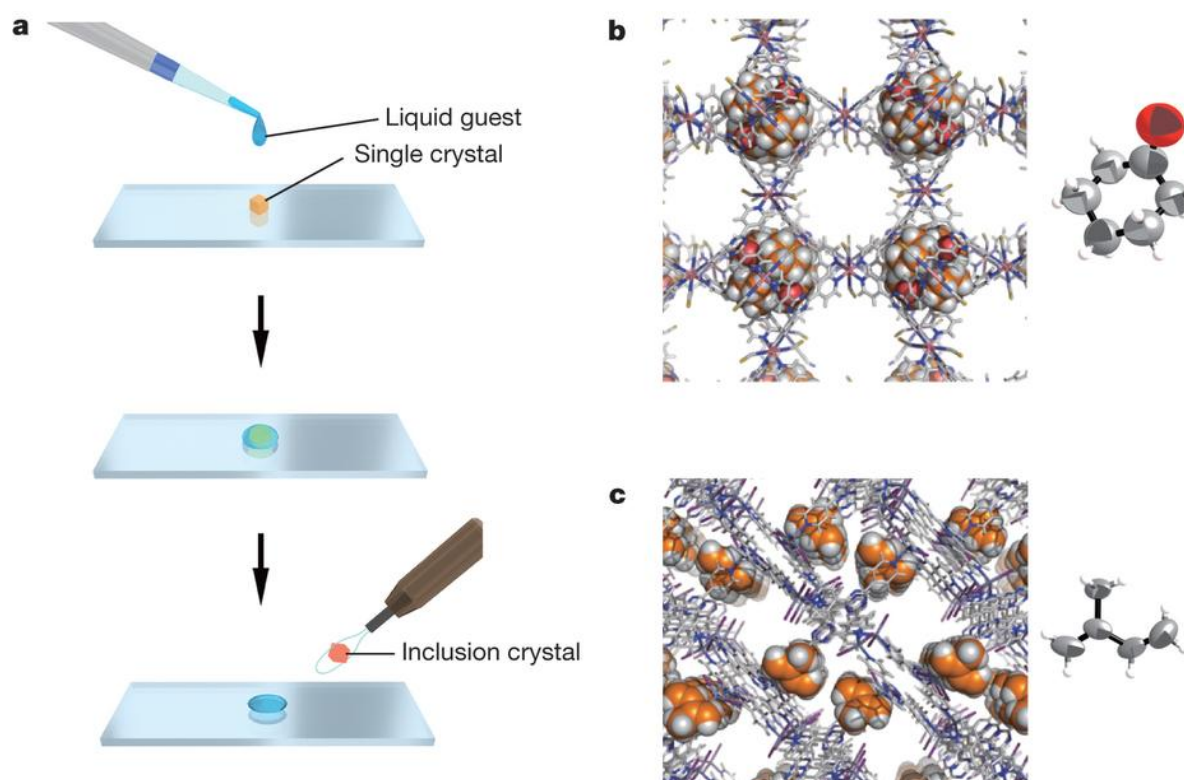


**Fig. 1.18:** a) Schematic representation of preparation of guest-included network complex MOF. b) X-ray crystal structure of cyclohexanone observed in the cavities of MOF. c) Structure of isoprene observed in the pores of MOF. Reproduced, with permission, from ref 138. Copyright © 2013 Nature Publishing Group.

## 1.5 Proton-conductivity

The proton conductors are electrolytes and usually they are solids, in which  $H^+$  are charge carriers. Proton conducting phenomena is also referred as proton conductivity which plays a key role in processes of photosynthesis in plants and in the production of electricity in hydrogen fuel cells.<sup>144</sup> Consequently, proton-transport and transfer events have been studied extensively by scientific communities. The major aim of their study is to introduce and develop proton-conducting materials which are suitable for applications in electrochemical cells. In real applications, proton conductors are typically solid materials. Usually, these materials are polymers or ceramic. Tiny pores in these materials help protons to dominate and prevent the direct current and transport of bulk solvent. Ice is a very good example for such a proton conductor, though it is relatively a poor one. Way back in 1950, proton conduction was first suggested by Alfred Rene Jean Paul and S. E. Rogers.<sup>145</sup> There are two types of proton conduction mechanisms are possible namely,

Grotthuss mechanism and vehicles mechanism (Fig 1.19).<sup>146</sup> In Grotthuss mechanism, 'excess' proton or proton-defect diffuses through the hydrogen bonding network of water molecules or other combined hydrogen-bonding networks.<sup>147</sup> In contrast, the conduction in vehicle mechanism occurs by the diffusion of protonated molecules ( $\text{H}_3\text{O}^+$ ). The polymeric material Nafion and its derivatives have been used widely as typical proton conductors in fuel cell applications. Recently, jelly-like substance comparable to that of Nafion has been discovered in certain sharks. Their proton conductivities were found to be 40-fold lesser than nafion.<sup>148</sup> It is well-known that high proton conductivities are observed in inorganic materials like cerates and zirconate-based perovskite materials.<sup>149</sup> Recently, several other organic proton conducting materials have emerged with high proton conductivities in addition to high thermal and mechanical stabilities. More details about proton conductivity of host-guest complexes which are very important in proton conducting materials are discussed in the chapter 3.

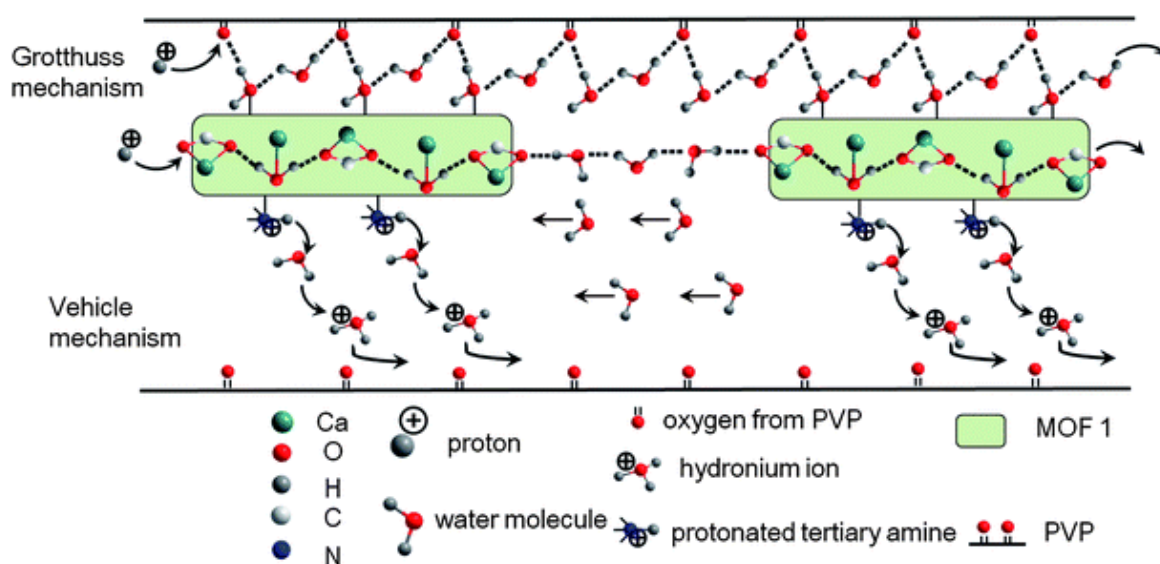


**Fig. 1.19:** (a) The possible mechanisms of proton transport in proton conducting materials. Copy rights.<sup>146</sup> Reproduced with permission from ref 146. Copyright 2013 Royal Society of Chemistry.

## 1.6 Hexaphenylbenzene (HPB)

Hexaphenylbenzene (HPB) has a unique feature for the formation of organic materials. It is due to the rigidity and wheel-shaped structural architecture, which arise from the mutual adjustment of phenyl groups. Thus, HPB and its derivatives have been used in wide variety of applications in materials chemistry.<sup>150-151</sup> In 1933, the first



synthesis of HPB was published by Trosken and co-workers using Diels–Alder reaction between stilbene and 1,2,3,4- tetraphenylcyclopentadienone.<sup>152</sup> Later, Hoeschen and co-workers have repeated the same reaction using diphenylacetylene instead of stilbene to obtain the same product.<sup>153</sup> In 1939, there have been claims that HPB was prepared by the reaction of PhMgBr with hexabromobenzene. Soon after it was found to be as 1,2,4,5-tetraphenylbenzene.<sup>154</sup> In 1950, Grummitt and Fick have performed the synthesis of HPB by a Diels–Alder reaction between 1,2,3,4 tetraphenylcyclopentadienone and stilbene at 250 °C and subsequently followed by dehydrogenation of the hexaphenyldihydrobenzene with bromine.<sup>155</sup> Presently, unsymmetrical HPB is synthesized using Diels–Alder reactions.<sup>156</sup> However, in the case of C<sub>3</sub> and C<sub>6</sub>-symmetric, HPB's are often synthesized by cyclotrimerization of corresponding substituted alkynes in the presence of transition metal complexes under inert atmosphere.<sup>157-158</sup> During 20th century, the application of hexaarylbenzenes and their derivatives (HAB) were not much explored in detail. But in recent years, there have been growing interests on these synthetic modules due to their non-planar structure and their ability to exhibit interesting properties.<sup>155, 159-160</sup> Klaus Mullen and co-workers have prepared a large number of derivatives of graphene segments using HAB templates by subjecting Scholl cyclisation of HAB's.<sup>161</sup> All these HAB templates and their corresponding graphene segments have shown drastic changes in the optoelectronic materials.<sup>162</sup> Although star-shaped HAB derivatives are generally resistive to undergo a  $\pi$ - $\pi$  interfacial self-assembly owing to their nonplanar architecture, their supramolecular assembly between HAB units can be encouraged by other intermolecular noncovalent forces between its functional groups.<sup>163</sup> During self-assembling process, HPBs leaves out voids in their solid state due to imperfect packing of the molecules. These voids are usually filled by guest molecules which make scaffolds as best platform for the inclusion complexes in crystal engineering. James D. Wuest and coworkers have reported HPB-based potential acetylene sponges in which CH- $\pi$  interactions played a vital role in capturing the acetylenes (Fig. 1.20a).<sup>164</sup> They have also accessed the diamino triazine self assembling motif in the peripherals of the HPB which showed very high guest accessible voids in its crystal structure.<sup>165</sup> Kobayshi *et al.* have reported a series of various functional groups substituted in the radial position of hexaphenylbenzenes. Each derivative of the radial HPB showed completely different properties in their solid state. Carboxylic acid substituted HPB shows two dimensional hexagonal hydrogen-bonded network with triangle-like large cavities with the inclusion of methanol and 2,7-dimethoxynaphthalene (Fig. 1.20b).<sup>166</sup> Hexakis(4-hydroxyphenyl)benzene showed two

types of H-bonded networks in diethyl ether and DMF, respectively (Fig. 1.20c & 1.20d).<sup>167</sup> Carboxamide substituted derivative exhibited solvent induced polymorphism with formation of three dimensional H-bonded network in its solid state.<sup>168</sup> Though the properties of radially substituted hexaphenylbenzenes with various functional groups have been reported to have wide range of applications, much of axially substituted hexaphenyl benzenes with various functional groups have not been explored so far. Such axially substituted HPB and their properties and applications based on molecular recognition are the main focus of this thesis and discussed in detail in the following chapters.

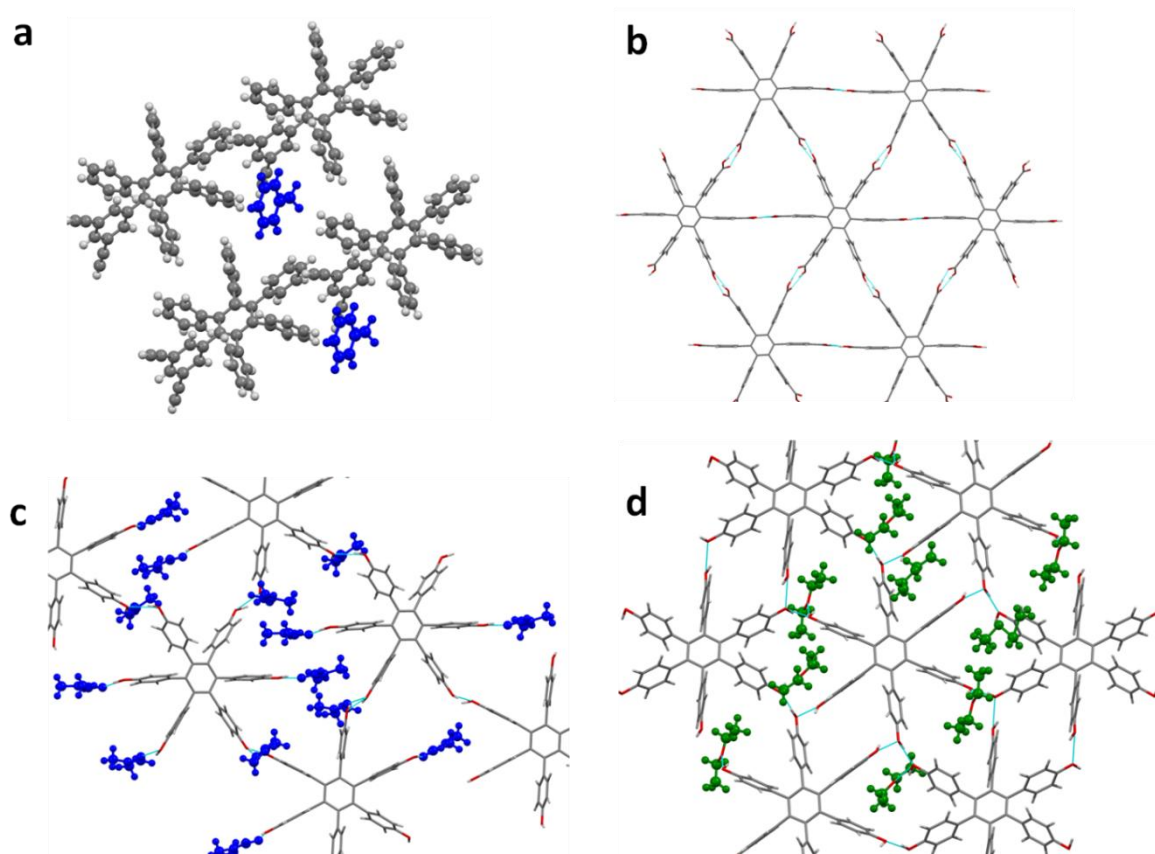


**Fig. 1.20:** (a) Crystal structure (ball and stick model) of toluene trapped HPB-based acetylene sponge. (b) crystal packing of carboxylic acid radially substituted HPB derivative showing 2D network with trigonal voids (c) DMF (blue color ball and stick) included crystal structure of hexakis(4-hydroxyphenyl)benzene. d) diethyl ether (green color ball and stick) included crystal structure of hexakis(4-hydroxyphenyl)benzene. Crystal structures courtesy of CCDC.

---

**1.7 References**

1. Gale, P. A.; Steed, J. W., *Supramolecular chemistry : from molecules to nanomaterials*. Wiley-Blackwell: [Oxford], **2012**.
2. Franklin, B.; Brownrigg, W.; Farish, M. *Phil. Trans.* **1774**, *64*, 445-460.
3. Dyadin, Y. A.; Terekhova, I. S.; Rodionova, T. V.; Soldatov, D. V. *J. Struct. Chem.* **1999**, *40* (5), 645-653.
4. Keller, R. N. *J. Chem. Educ.* **1941**, *18* (3), 134.
5. Fischer, E. *Berichte der deutschen chemischen Gesellschaft* **1894**, *27* (3), 2985-2993.
6. Silverstein, A. M. *Nat. Immunol.* **2004**, *5* (12), 1211-1217.
7. Latimer, W. M.; Rodebush, W. H. *J. Am. Chem. Soc.* **1920**, *42* (7), 1419-1433.
8. Watson, J. D.; Crick, F. H. C. *Nature* **1953**, *171* (4356), 737-738.
9. Pedersen, C. J. *J. Am. Chem. Soc.* **1967**, *89* (26), 7017-7036.
10. Lehn, J.-M.; Sanders, J. *Angew. Chem. Int. Ed.* **1995**, *34* (22), 2563.
11. Cram, D. J. *Angew. Chem. Int. Ed.* **1988**, *27* (8), 1009-1020.
12. "The Nobel Prize in Chemistry 1987". Nobelprize.org. Nobel Media AB 2014. Web. 4 Jun **2017**.  
<[http://www.nobelprize.org/nobel\\_prizes/chemistry/laureates/1987/](http://www.nobelprize.org/nobel_prizes/chemistry/laureates/1987/)>.
13. Sauvage, J.-P.; Duplan, V.; Niess, F., Contractile and Extensile Molecular Systems. In *Macrocyclic and Supramolecular Chemistry*, John Wiley & Sons, Ltd: **2016**; pp 444-464.
14. Stoddart, J. F. *Chem. Soc. Rev.* **2009**, *38* (6), 1521-1529.
15. Feringa, B. L. *Angew. Chem. Int. Ed. Engl.* **2011**, *50* (7), 1470-1472.
16. "The Nobel Prize in Chemistry 2016". Nobelprize.org. Nobel Media AB 2014. Web. 4 Jun **2017**.  
<[http://www.nobelprize.org/nobel\\_prizes/chemistry/laureates/2016/](http://www.nobelprize.org/nobel_prizes/chemistry/laureates/2016/)>.
17. Sanderson, R. T. *Chemical Bonds and Bond Energy*; 2nd ed.; Academic Press: New York, NY, **1976**.
18. Steed, J.; Atwood, J., *Supramolecular Chemistry*. John Wiley & Sons: **2000**.
19. Jeffrey, G. A. *An Introduction to Hydrogen Bonding*; Oxford University Press: Oxford, **1997**.



20. Sweetman, A. M.; Jarvis, S. P.; Sang, H.; Lekkas, I.; Rahe, P.; Wang, Y.; Wang, J.; Champness, N. R.; Kantorovich, L.; Moriarty, P. *Nat. Commun.* **2014**, *5*, 3931.
21. [https://en.wikipedia.org/wiki/Hydrogen\\_bond](https://en.wikipedia.org/wiki/Hydrogen_bond).
22. Zhurkin, V. B.; Tolstorukov, M. Y.; Xu, F.; Colasanti, A. V.; Olson, W. K. *DNA conformation and transcription* **2005**, 18-34.
23. Pedersen, C. J. *Angew. Chem. Int. Ed. Engl.* **1988**, *27* (8), 1021-1027.
24. Ma, J. C.; Dougherty, D. A. *Chem. Rev.* **1997**, *97* (5), 1303-1324.
25. Mecozzi, S.; West, A. P.; Dougherty, D. A. *J. Am. Chem. Soc.* **1996**, *118* (9), 2307-2308.
26. Dougherty, D. A. *J. Nutr.* **2007**, *137* (6), 1504S-1508S.
27. Livnah, O.; Stura, E. A.; Johnson, D. L.; Middleton, S. A.; Mulcahy, L. S.; Wrighton, N. C.; Dower, W. J.; Jolliffe, L. K.; Wilson, I. A. *Science* **1996**, *273* (5274), 464-471.
28. Xiu, X.; Puskar, N. L.; Shanata, J. A. P.; Lester, H. A.; Dougherty, D. A. *Nature* **2009**, *458* (7237), 534-537.
29. Kim, K. S.; Tarakeshwar, P.; Lee, J. Y. *Chem. Rev.* **2000**, *100* (11), 4145-4186.
30. Brandl, M.; Weiss, M. S.; Jabs, A.; Sühnel, J.; Hilgenfeld, R. *J. Mol. Biol.* **2001**, *307* (1), 357-377.
31. Nishio, M.; Umezawa, Y.; Hirota, M.; Takeuchi, Y. *Tetrahedron* **1995**, *51* (32), 8665-8701.
32. <http://www.imtech.res.in/raghava/chpredict/cho.html#ref5>.
33. Hunter, C. A.; Sanders, J. K. M. *J. Am. Chem. Soc.* **1990**, *112* (14), 5525-5534.
34. Parkinson, G. N.; Lee, M. P. H.; Neidle, S. *Nature* **2002**, *417* (6891), 876-880.
35. Sygula, A.; Fronczek, F. R.; Sygula, R.; Rabideau, P. W.; Olmstead, M. M. *J. Am. Chem. Soc.* **2007**, *129* (13), 3842-3843.
36. Menger, F. M. *Proc. Natl. Acad. Sci. U. S. A.* **2002**, *99* (8), 4818.
37. Lehn, J.-M., *Supramolecular chemistry*. Vch, Weinheim: **1995**; Vol. 1.
38. Hecht, S.; Huc, I., *Foldamers: structure, properties and applications*. John Wiley & Sons: **2007**.
39. Rawicz, W.; Olbrich, K.; McIntosh, T.; Needham, D.; Evans, E. *Biophys. J.* **2000**, *79* (1), 328-339.
40. Oh, H.; Javvaji, V.; Yaraghi, N. A.; Abezgauz, L.; Danino, D.; Raghavan, S. R. *Soft Matter*. **2013**, *9* (48), 11576-11584.

41. Lockett, M. R.; Lange, H.; Breiten, B.; Heroux, A.; Sherman, W.; Rappoport, D.; Yau, P. O.; Snyder, P. W.; Whitesides, G. M. *Angew. Chem. Int. Ed. Engl.* **2013**, *52* (30), 7714-7717.
42. Breiten, B.; Lockett, M. R.; Sherman, W.; Fujita, S.; Al-Sayah, M.; Lange, H.; Bowers, C. M.; Heroux, A.; Krilov, G.; Whitesides, G. M. *J. Am. Chem. Soc.* **2013**, *135* (41), 15579-15584.
43. Lehn, J. M. *Angew. Chem. Int. Ed. Engl.* **1988**, *27* (1), 89-112.
44. Steed, J. W.; Atwood, J. L. *Supramolecular Chemistry, Second Edition* **2009**, 105-222.
45. Fischer, E. *Eur. J. Inorg. Chem.* **1894**, *27* (3), 2985-2993.
46. Koshland, D. E. *Angew. Chem. Int. Ed. Engl.* **1995**, *33* (23-24), 2375-2378.
47. Graf, E.; Lehn, J. M. *J. Am. Chem. Soc.* **1975**, *97* (17), 5022-5024.
48. Harada, A.; Kataoka, K. *Science* **1999**, *283* (5398), 65-67.
49. Hof, F.; Trembleau, L.; Ullrich, E. C.; Rebek, J. J. *Angew. Chem. Int. Ed. Engl.* **2003**, *42* (27), 3150-3153.
50. Müller, A.; Wenz, G. *Chem. Eur. J.* **2007**, *13* (8), 2218-2223.
51. Hong, M.; Zhang, Y.-M.; Liu, Y. *J. Org. Chem.* **2015**, *80* (3), 1849-1855.
52. Lin, R.-L.; Fang, G.-S.; Sun, W.-Q.; Liu, J.-X. *Nat. Commun.* **2016**, *6*, 39057.
53. Mammen, M.; Choi, S.-K.; Whitesides, G. M. *Angew. Chem. Int. Ed. Engl.* **1998**, *37* (20), 2754-2794.
54. Fasting, C.; Schalley, C. A.; Weber, M.; Seitz, O.; Hecht, S.; Kokschi, B.; Dornedde, J.; Graf, C.; Knapp, E. W.; Haag, R. *Angew. Chem. Int. Ed. Engl.* **2012**, *51* (42), 10472-10498.
55. Mulder, A.; Huskens, J.; Reinhoudt, D. N. *Org. Biomol. Chem.* **2004**, *2* (23), 3409-3424.
56. Varki, A. *Glycobiology* **1993**, *3* (2), 97-130.
57. Lasky, L. A. *Annu. Rev. Biochem.* **1995**, *64* (1), 113-140.
58. Kitov, P. I.; Sadowska, J. M.; Mulvey, G.; Armstrong, G. D.; Ling, H.; Pannu, N. S.; Read, R. J.; Bundle, D. R. *Nature* **2000**, *403* (6770), 669-672.
59. Balzani, V.; Clemente-León, M.; Credi, A.; Lowe, J. N.; Badjić, J. D.; Stoddart, J. F.; Williams, D. J. *Chem. Eur. J.* **2003**, *9* (21), 5348-5360.
60. Lehn, J.-M., Bibliography and Notes. In *Supramolecular Chemistry*, Wiley-VCH Verlag GmbH & Co. KGaA: **2006**; pp 207-258.

61. Dwek, R. A. *Chem. Rev.* **1996**, *96* (2), 683-720.
62. Rudd, P. M.; Elliott, T.; Cresswell, P.; Wilson, I. A.; Dwek, R. A. *Science* **2001**, *291* (5512), 2370-2376.
63. Chabre, Y. M.; Roy, R. *Chem. Soc. Rev.* **2013**, *42* (11), 4657-4708.
64. Unverzagt, C.; Kelm, S.; Paulson, J. C. *Carbohydr. Res.* **1994**, *251*, 285-301.
65. Kamitakahara, H.; Suzuki, T.; Nishigori, N.; Suzuki, Y.; Kanie, O.; Wong, C. H. *Angew. Chem. Int. Ed.* **1998**, *110* (11), 1607-1611.
66. Kamitakahara, H.; Suzuki, T.; Nishigori, N.; Suzuki, Y.; Kanie, O.; Wong, C. H. *Angew. Chem. Int. Ed.* **1998**, *37* (11), 1524-1528.
67. Totani, K.; Kubota, T.; Kuroda, T.; Murata, T.; Kazuya, I.-P.; Suzuki, T.; Suzuki, Y.; Kobayashi, K.; Ashida, H.; Yamamoto, K. *Glycobiology.* **2003**, *13* (5), 315-326.
68. Shi, J.; Yang, T.; Kataoka, S.; Zhang, Y.; Diaz, A. J.; Cremer, P. S. *J. Am. Chem. Soc.* **2007**, *129* (18), 5954-5961.
69. Liu, S.; Kiick, K. L. *Macromolecules.* **2008**, *41* (3), 764-772.
70. Robinson, A.; Fang, J. M.; Chou, P. T.; Liao, K. W.; Chu, R. M.; Lee, S. J. *ChemBioChem.* **2005**, *6* (10), 1899-1905.
71. Yu, L.; Huang, M.; Wang, P. G.; Zeng, X. *Anal. Chem.* **2007**, *79* (23), 8979-8986.
72. Mourez, M.; Kane, R. S.; Mogridge, J.; Metallo, S.; Deschatelets, P.; Sellman, B. R.; Whitesides, G. M.; Collier, R. J. *Nat. Biotechnol.* **2001**, *19* (10), 958-961.
73. Muñoz, A.; Sigwalt, D.; Illescas, B. M.; Luczkowiak, J.; Rodríguez-Pérez, L.; Nierengarten, I.; Holler, M.; Remy, J.-S.; Buffet, K.; Vincent, S. P.; Rojo, J.; Delgado, R.; Nierengarten, J.-F.; Martín, N. *Nat. Chem.* **2016**, *8* (1), 50-57.
74. Kaneshiro, T. L.; Wang, X.; Lu, Z.-R. *Mol. Pharm.* **2007**, *4* (5), 759-768.
75. Chabre, Y. M.; Brisebois, P. P.; Abbassi, L.; Kerr, S. C.; Fahy, J. V.; Marcotte, I.; Roy, R. *J. Org. Chem.* **2011**, *76* (2), 724-727.
76. <http://goldbook.iupac.org/html/C/C01097.html>.
77. Vögtle, F.; Löhr, H.-G.; Franke, J.; Worsch, D. *Angew. Chem. Int. Ed. Engl.* **1985**, *24* (9), 727-742.
78. Alavi, S.; Udachin, K.; Ratcliffe, C. I.; Ripmeester, J. A., Clathrate Hydrates. In *Supramolecular Chemistry*, John Wiley & Sons, Ltd: **2012**.
79. Sloan Jr, E. D.; Koh, C., *Clathrate hydrates of natural gases*. CRC press: **2007**.
80. Thomas, E. *Wesleyan University, available online as of* **2007**, *4* (28), 02.
81. Hagan, M. M. *J. Chem. Educ.* **1963**, *40* (12), 643.

82. Buch, V.; Devlin, J. P.; Monreal, I. A.; Jagoda-Cwiklik, B.; Uras-Aytemiz, N.; Cwiklik, L. *Phys. Chem. Chem. Phys.* **2009**, *11* (44), 10245-10265.
83. Shin, K.; Moudrakovski, I. L.; Ratcliffe, C. I.; Ripmeester, J. A. *Angew. Chem. Int. Ed. Engl.* **2017**, *56* (22), 6171-6175.
84. Alavi, S.; Shin, K.; Ripmeester, J. A. *J. Chem. Eng. Data.* **2015**, *60* (2), 389-397.
85. Makogon, I. U. r. F., *Hydrates of natural gas*. PennWell Books Tulsa, Oklahoma: **1981**.
86. Jia, J.; Liang, Y.; Tsuji, T.; Murata, S.; Matsuoka, T. *Sci Rep.* **2016**, *6*, 23548.
87. Belosludov, V. R.; Dyadin, Y. A.; Chekhova, G. N.; Kolesov, B. A.; Fadeev, S. I. *J. Incl. Phenom. Macrocycl. Chem.* **1985**, *3* (3), 243-260.
88. Bhatnagar, V. *J. Struct. Chem.* **1968**, *8* (3), 513-529.
89. Bishop, R. *Supramolecular Chemistry: From Molecules to Nanomaterials* **2012**.
90. Lloyd, G. O.; Bredenkamp, M. W.; Barbour, L. J. *Chem. Commun.* **2005**, (32), 4053-4055.
91. Tian, J.; Thallapally, P. K.; McGrail, B. P. *Cryst,Eng,Comm*, **2012**, *14* (6), 1909-1919.
92. Holst, J. R.; Trewin, A.; Cooper, A. I. *Nat. Chem.* **2010**, *2* (11), 915-920.
93. Villiers, A. *Compt. Rend. Fr. Acad. Sci.* **1891**, *112*, 435-438.
94. Ren, B.; Zhang, M.; Gao, H.; Zheng, J.; Jia, L. *Phys. Chem. Chem. Phys.* **2016**, *18* (26), 17380-17388.
95. Rekharsky, M. V.; Inoue, Y. *Chem. Rev.* **1998**, *98* (5), 1875-1918.
96. Harada, A.; Hashidzume, A.; Yamaguchi, H.; Takashima, Y. *Chem. Rev.* **2009**, *109* (11), 5974-6023.
97. Uekama, K.; Hirayama, F.; Irie, T. *Chem. Rev.* **1998**, *98* (5), 2045-2076.
98. Behrend, R.; Meyer, E.; Rusche, F. *Eur. J. Org. Chem.* **1905**, *339* (1), 1-37.
99. Freeman, W.; Mock, W.; Shih, N. *J. Am. Chem. Soc.* **1981**, *103* (24), 7367-7368.
100. Kim, J.; Jung, I.-S.; Kim, S.-Y.; Lee, E.; Kang, J.-K.; Sakamoto, S.; Yamaguchi, K.; Kim, K. *J. Am. Chem. Soc.* **2000**, *122* (3), 540-541.
101. Miyahara, Y.; Abe, K.; Inazu, T. *Angew. Chem. Int. Ed. Engl.* **2002**, *41* (16), 3020-3023.
102. Freeman, W. A. *Acta Crystallogr. B: Structural Science.* **1984**, *40* (4), 382-387.
103. Ko, Y. H.; Kim, E.; Hwang, I.; Kim, K. *Chem. Commun.* **2007**, (13), 1305-1315.
104. Zhao, J.; Kim, H. J.; Oh, J.; Kim, S. Y.; Lee, J. W.; Sakamoto, S.; Yamaguchi, K.; Kim, K. *Angew. Chem. Int. Ed. Engl.* **2001**, *40* (22), 4233-4235.

105. Jon, S. Y.; Selvapalam, N.; Oh, D. H.; Kang, J.-K.; Kim, S.-Y.; Jeon, Y. J.; Lee, J. W.; Kim, K. *J. Am. Chem. Soc.* **2003**, *125* (34), 10186-10187.
106. Zhao, N.; Lloyd, G. O.; Scherman, O. A. *Chem. Commun.* **2012**, *48* (25), 3070-3072.
107. Lucas, D.; Minami, T.; Iannuzzi, G.; Cao, L.; Wittenberg, J. B.; Anzenbacher Jr, P.; Isaacs, L. *J. Am. Chem. Soc.* **2011**, *133* (44), 17966-17976.
108. Svec, J.; Necas, M.; Sindelar, V. *Angew. Chem. Int. Ed.* **2010**, *122* (13), 2428-2431.
109. Baeyer, A. *Ber Dtsch. Chem. Ges.* **1872**, *5*, 280.
110. Vicens, J.; Böhmer, V., *Calixarenes: a versatile class of macrocyclic compounds*. Springer Science & Business Media: **2012**; Vol. 3.
111. Gutsche, C. D.; Muthukrishnan, R. *J. Org. Chem.* **1978**, *43* (25), 4905-4906.
112. Gutsche, C. D., *Calixarenes: an introduction*. Royal Society of Chemistry: **2008**.
113. Stewart, D. R.; Gutsche, C. D. *J. Am. Chem. Soc.* **1999**, *121* (17), 4136-4146.
114. Atwood, J. L.; Koutsantonis, G. A.; Raston, C. L. *Nature.* **1994**, *368* (6468), 229-231.
115. Shinkai, S.; Mori, S.; Koreishi, H.; Tsubaki, T.; Manabe, O. *J. Am. Chem. Soc.* **1986**, *108* (9), 2409-2416.
116. Wang, K.; Yang, E.-C.; Zhao, X.-J.; Dou, H.-X.; Liu, Y. *Cryst. Growth Des.* **2014**, *14* (9), 4631-4639.
117. Ikeda, A.; Shinkai, S. *Chem. Rev.* **1997**, *97* (5), 1713-1734.
118. Morohashi, N.; Narumi, F.; Iki, N.; Hattori, T.; Miyano, S. *Chem. Rev.* **2006**, *106* (12), 5291-5316.
119. Schühle, D. T.; Schatz, J.; Laurent, S.; Vander Elst, L.; Muller, R. N.; Stuart, M. C.; Peters, J. A. *Chem. Eur. J.* **2009**, *15* (13), 3290-3296.
120. MacGillivray, L. R.; Atwood, J. L. *Nature.* **1997**, *389* (6650), 469-472.
121. Cram, D. J.; Karbach, S.; Kim, Y. H.; Baczynskyj, L.; Kallemeyn, G. W. *J. Am. Chem. Soc.* **1985**, *107* (8), 2575-2576.
122. Kim, S. K.; Sessler, J. L. *Acc. Chem. Res.* **2014**, *47* (8), 2525-2536.
123. Briggs, M. E.; Cooper, A. I. *Chem. Mater.* **2016**, *29* (1), 149-157.
124. Barbour, L. J. *Chem. Commun.* **2006**, (11), 1163-1168.
125. Jelfs, K. E.; Wu, X.; Schmidtman, M.; Jones, J. T.; Warren, J. E.; Adams, D. J.; Cooper, A. I. *Angew. Chem. Int. Ed. Engl.* **2011**, *50* (45), 10653-10656.
126. Jin, Y.; Zhu, Y.; Zhang, W. *CrystEngComm.* **2013**, *15* (8), 1484-1499.

127. Quan, M. L.; Cram, D. J. *J. Am. Chem. Soc.* **1991**, *113* (7), 2754-2755.
128. Tozawa, T.; Jones, J. T.; Swamy, S. I.; Jiang, S.; Adams, D. J.; Shakespeare, S.; Clowes, R.; Bradshaw, D.; Hasell, T.; Chong, S. Y. *Nat. Mater.* **2009**, *8* (12), 973-978.
129. Bojdys, M. J.; Briggs, M. E.; Jones, J. T.; Adams, D. J.; Chong, S. Y.; Schmidtmann, M.; Cooper, A. I. *J. Am. Chem. Soc.* **2011**, *133* (41), 16566-16571.
130. Jelfs, K. E.; Eden, E. G.; Culshaw, J. L.; Shakespeare, S.; Pyzer-Knapp, E. O.; Thompson, H. P.; Bacsa, J.; Day, G. M.; Adams, D. J.; Cooper, A. I. *J. Am. Chem. Soc.* **2013**, *135* (25), 9307-9310.
131. Hasell, T.; Schmidtmann, M.; Cooper, A. I. *J. Am. Chem. Soc.* **2011**, *133* (38), 14920-14923.
132. Mitra, T.; Jelfs, K. E.; Schmidtmann, M.; Ahmed, A.; Chong, S. Y.; Adams, D. J.; Cooper, A. I. *Nat. Chem.* **2013**, *5* (4), 276-281.
133. Chen, L.; Reiss, P. S.; Chong, S. Y.; Holden, D.; Jelfs, K. E.; Hasell, T.; Little, M. A.; Kewley, A.; Briggs, M. E.; Stephenson, A. *Nat. Mater.* **2014**, *13* (10), 954-960.
134. Liu, J.; Thallapally, P. K.; McGrail, B. P.; Brown, D. R.; Liu, J. *Chem. Soc. Rev.* **2012**, *41* (6), 2308-2322.
135. Murray, L. J.; Dincă, M.; Long, J. R. *Chem. Soc. Rev.* **2009**, *38* (5), 1294-1314.
136. Lee, J.; Farha, O. K.; Roberts, J.; Scheidt, K. A.; Nguyen, S. T.; Hupp, J. T. *Chem. Soc. Rev.* **2009**, *38* (5), 1450-1459.
137. Kim, K. *Nat. Chem.* **2009**, *1* (8), 603-604.
138. Inokuma, Y.; Yoshioka, S.; Ariyoshi, J.; Arai, T.; Hitora, Y.; Takada, K.; Matsunaga, S.; Rissanen, K.; Fujita, M. *Nature* **2013**, *495* (7442), 461-466.
139. Inokuma, Y.; Yoshioka, S.; Ariyoshi, J.; Arai, T.; Fujita, M. *Nat. Protoc.* **2014**, *9* (2), 246-252.
140. Hoshino, M.; Khutia, A.; Xing, H.; Inokuma, Y.; Fujita, M. *IUCrJ* **2016**, *3* (2), 139-151.
141. Alberti, G.; Casciola, M.; Palombari, R.; Peraio, A. *Solid State Ion.* **1992**, *58* (3-4), 339-344.
142. Sadakiyo, M.; Yamada, T.; Kitagawa, H. *J. Am. Chem. Soc.* **2009**, *131* (29), 9906-9907.
143. Taylor, J. M.; Dawson, K. W.; Shimizu, G. K. *J. Am. Chem. Soc.* **2013**, *135* (4), 1193-1196.



144. Kreuer, K.-D. *Chem. Mater.* **1996**, 8 (3), 610-641.
145. Rogers, S.; Ubbelohde, A. *Trans. Faraday Soc.* **1950**, 46, 1051-1061.
146. Liang, X.; Zhang, F.; Feng, W.; Zou, X.; Zhao, C.; Na, H.; Liu, C.; Sun, F.; Zhu, G. *Chem. Sci.* **2013**, 4 (3), 983-992.
147. Hassanali, A.; Giberti, F.; Cuny, J.; Kühne, T. D.; Parrinello, M. *Proc. Natl. Acad. Sci. U. S. A.* **2013**, 110 (34), 13723-13728.
148. Josberger, E. E.; Hassanzadeh, P.; Deng, Y.; Sohn, J.; Rego, M. J.; Amemiya, C. T.; Rolandi, M. *Sci. Adv.* **2016**, 2 (5).
149. Kreuer, K. *Annu. Rev. Mater. Sci.* **2003**, 33 (1), 333-359.
150. Watanabe, S.; Kido, J. *Chem. Lett.* **2007**, 36 (5), 590-591.
151. Li, Z. a.; Ye, S.; Liu, Y.; Yu, G.; Wu, W.; Qin, J.; Li, Z. *J. Phys. Chem. B* **2010**, 114 (28), 9101-9108.
152. Dilthey, W.; Schommer, W.; Trösken, O. *Eur. J. Inorg. Chem.* **1933**, 66 (11), 1627-1628.
153. Dilthey, W.; Schommer, W.; Höschen, W.; Die-richs, H. *Eur. J. Inorg. Chem.* **1935**, 68 (6), 1159-1162.
154. Geissman, T.; Mallatt, R. *J. Am. Chem. Soc.* **1939**, 61 (7), 1788-1790.
155. Grummitt, O.; Fick, J. *J. Chem. Educ.* **1950**, 27 (10), 538.
156. Fieser, L. F. *Org. Synth.* **1966**, 44-44.
157. Chio, K. S.; Park, M. K.; Han, B. H. *J. Chem. Res., Synop.* **1998**, (9), 518-519.
158. Yong, L.; Butenschön, H. *Chem. Commun.* **2002**, (23), 2852-2853.
159. Gust, D. *J. Am. Chem. Soc.* **1977**, 99 (21), 6980-6982.
160. Pepermans, H.; Willem, R.; Gielen, M.; Hoogzand, C. *J. Org. Chem.* **1986**, 51 (3), 301-306.
161. Pisula, W.; Feng, X.; Müllen, K. *Chem. Mater.* **2010**, 23 (3), 554-567.
162. Vij, V.; Bhalla, V.; Kumar, M. *Chem. Rev.* **2016**, 116 (16), 9565-9627.
163. Roll, M. F.; Kampf, J. W.; Laine, R. M. *Macromolecules* **2011**, 44 (9), 3425-3435.
164. Gagnon, E.; Rochefort, A.; Métivaud, V.; Wuest, J. D. *Org. Lett.* **2009**, 12 (2), 380-383.
165. Maly, K. E.; Gagnon, E.; Maris, T.; Wuest, J. D. *J. Am. Chem. Soc.* **2007**, 129 (14), 4306-4322.
166. Kobayashi, K.; Shirasaka, T.; Horn, E.; Furukawa, N. *Tetrahedron Lett.* **2000**, 41 (1), 89-93.

167. Kobayashi, K.; Shirasaka, T.; Sato, A.; Horn, E.; Furukawa, N. *Angew. Chem. Int. Ed. Engl.* **1999**, *38* (23), 3483-3486.
168. Kobayashi, K.; Sato, A.; Sakamoto, S.; Yamaguchi, K. *J. Am. Chem. Soc.* **2003**, *125* (10), 3035-3045.



## ***Chapter 2***

# ***Multivalent Hexaphenylbenzene-Based Supramolecular Sponges for Molecular Entrapping***



## Chapter-2

### Multivalent Hexaphenylbenzene-Based Supramolecular Sponges for Molecular Entrapping

#### 2.1 Introduction:

According to supramolecular chemistry, the state of a system can be regulated by mixing of different components that are having very strong interaction with each other resulting in the formation of super molecules. The physical properties of super molecules are entirely different from their original discrete molecules.<sup>1-3</sup> There are many types of supermolecules, among which host-guest systems have gained much interest because of their potential applications in ferro-electric,<sup>4-5</sup> catalysis,<sup>6</sup> drug delivery,<sup>7</sup> sensing,<sup>8-9</sup> gas storage<sup>10-12</sup> and isomers separation,<sup>13</sup> etc. On the other hand, molecular-recognition of the host-guest molecules using multivalent interactions has become an important component of supramolecular synthesis. The characteristic of multivalency is useful for molecules to be harnessed into functional materials through non-covalent forces. The host-guest systems can be classified according to their topologies into two types: intramolecular and extramolecular host-guest aggregates.<sup>14</sup> In intramolecular systems (cavitate), cavity is already inherent in their molecular structure, as seen in calixarenes,<sup>15-18</sup> pillararenes,<sup>19</sup> cucurbiturils<sup>20-21</sup> and shape-persistent organic cage compounds<sup>22</sup>. In contrast, extramolecular inclusion (adducts) arises purely based on aggregation through non-covalent forces such as charge transfer and directional H-bond, etc., and it is not inherent to the isolated molecular geometry of the host.<sup>23-25</sup> Although the intra-, extra- and mixed intra-extramolecular host-guest systems are well explored in the formation of inclusion complexes in their solid state using various host templates, a single host template by changing the H-bond donor in its multivalent places is still a rarity. It is possible to show such a system to uptake wide range of guest molecules through non covalent forces (supramolecular sponge) by choosing the host template which can exhibit supramolecular isomerism in its solid state. To design such a host molecule that could act as supramolecular sponges, the following structural features should be considered: 1) easily modifiable multivalent functional groups, 2) backbone rigidity with aromatic residues, and 3) non-covalent forces such as hydrogen bond, van der Waals force, etc.

## 2.2 Objective of the present work

Envisaging supramolecular spongy nature of hexaphenylbenzene (HPB) *via* cooperative interplay of back bone rigidity, non covalent forces and multivalency, we aimed to study the entrapping of various guest molecules by using single crystal X-ray diffraction technique.

Our aim was to synthesize a rationally designed new class of axially substituted multivalent hexaphenylbenzene derivatives (HPB) which could exhibit supramolecular isomerism in the solid-state, *via* the co-operative interplay of multivalency, noncovalent forces and backbone rigidity of HPB with respect to guests (supramolecular sponge). Further, we also focused on studying the guest entrapping ability of this system by varying H-bond donor in the each arm (multivalent places) of the HPB using single crystal X-ray diffraction technique.

## 2.3 Structural features of supramolecular sponge

In the propeller-shaped HPB, the central benzene ring is connected to six phenyl rings aligned perpendicularly, which is already known to show supramolecular isomerism in its solid state.<sup>26</sup> The highly substituted HPB featuring twelve functional groups are evenly projected in opposite planes, with respect to the central benzene ring, assuming a characteristic double basket shape (Fig. 2.01).

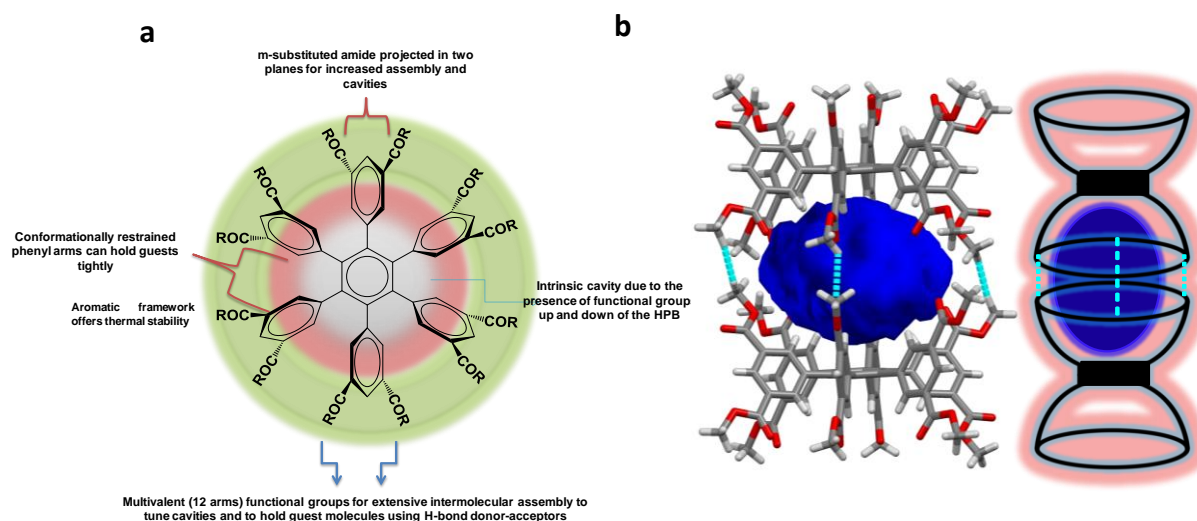
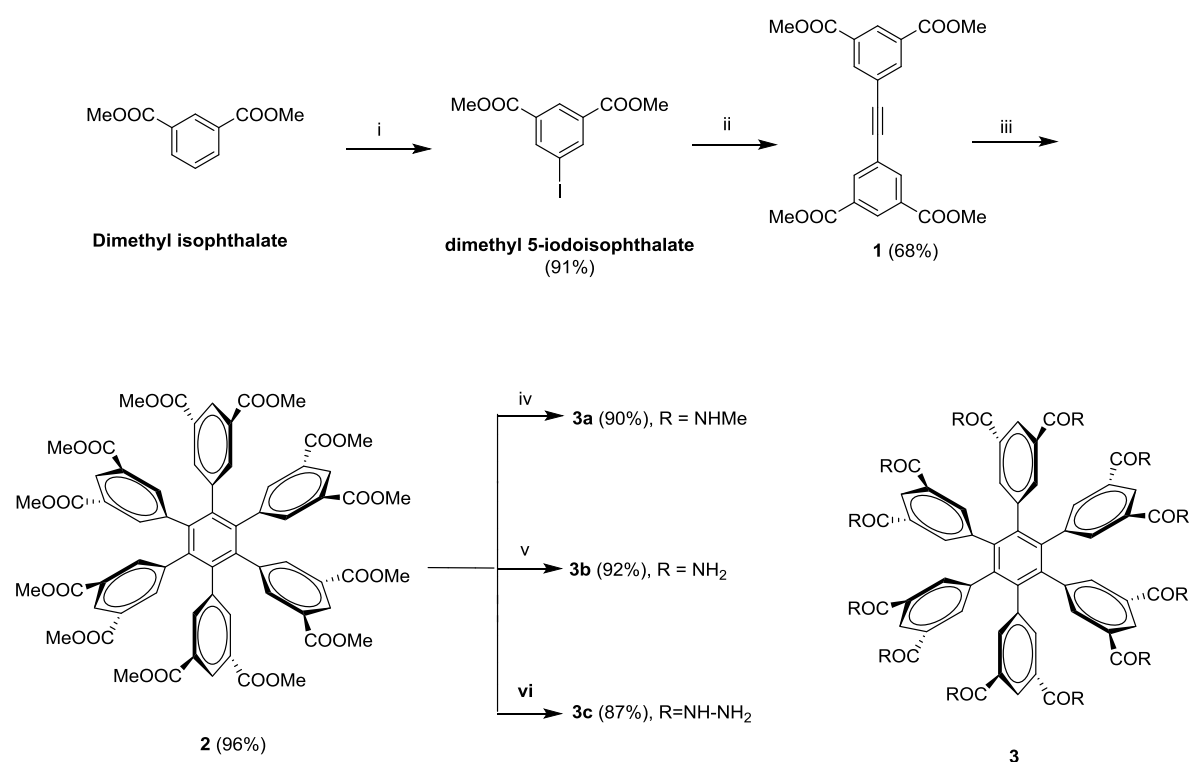


**Fig. 2.01:** a) Structural characteristics of multivalent hexaphenylbenzene (HPB)-based supramolecular sponge; b) 12-Armed HPB-based supramolecular sponge showing intrinsic cavity (blue colour) with the feature of double basket model.

## 2.4 Results and discussions

### 2.4.1 Synthesis

The HPB ester **2**, required for the formation of **3a** and **3b**, could be readily synthesized from the  $\text{Co}_2(\text{CO})_8$ -mediated trimerization of the tolane tetra ester **1**. This could be prepared efficiently in an one-pot sequential Sonogashira coupling between dimethyl-5-iodoisophthalate and trimethylsilylacetylene. The amides **3a**, **3b** and **3c** were obtained by the efficient amidation of the ester **2** under solvothermal conditions at 80 °C using methyl amine, ammonia and hydrazine hydrate, respectively (Scheme 2.01).



**Scheme 2.01: Reagents and Conditions:** i) NaIO<sub>4</sub>, I<sub>2</sub>, H<sub>2</sub>SO<sub>4</sub>, rt, 12 h; ii) PdCl<sub>2</sub>(PPh<sub>3</sub>)<sub>2</sub>, TMSA, CuI, Et<sub>3</sub>N, TBAF, THF, rt, 12 h; iii) Co<sub>2</sub>(CO)<sub>8</sub>, dioxane, reflux, 6 h; iv) methanolic methylamine, dioxane, steel bomb, 80 °C, 12 h; v) methanolic ammonia, dioxane, steel bomb, 80 °C, 12 h; vi) methanol, dioxane, hydrazine (35 wt. % in H<sub>2</sub>O), steel bomb, 80 °C, 12 h.

#### 2.4.2 Crystal growth methods used for preparation of inclusion crystals

Inclusion of guest molecules in multivalent-HPB was done in two methods.

##### A. Slow Evaporation method:

To a borosilicate vial containing compound in solution, suitable guest molecules were added either neat or as a solution (1-2 mL). Then, the vial was capped and slightly heated to dissolve the compound (homogenous solution). Further, the vial was set aside to allow crystals to form, which usually occurs on a timescale of several minutes to weeks.

##### B. Solvothermal method:

In this case, during the course of the reaction, compounds were crystallized while converting compound **2** to **3b** and **3c** under solvothermal conditions. In a typical condition

100 mg of compound **2** was suspended in a mixture of interested guest molecules and 35 ml dry methanolic ammonia (saturated solution). The mixture was heated slowly to 80 °C in stainless steel covered teflon-lined autoclave and constant the temperature was maintained for 12 h. Then, the reaction mixture was cooled slowly to room temperature to give inclusion crystals as colorless blocks or plates.

### 2.4.3 Investigations of Crystal structures:

#### 2.4.3.1 Inclusion of guest molecules in HPB(COOMe)<sub>12</sub>

The HPB ester **2** [HPB(COOMe)<sub>12</sub>] could be readily crystallized from solvents/solutions such as dichloromethane and a mixture of dichloromethane-guests (DCM-guests). Analysis of the crystal structure revealed that there were no inclusion of guest molecules when **2** was crystallized from dichloromethane alone, whereas the crystals obtained from a mixture of DCM and guests showed inclusion of guests in the cavity formed by the assistance of phenyl rings and the ester groups. This structural observation suggested that the intrinsic porosity in **2** is guest dependent and that a mere presence of phenyl rings and multiple ester groups appended on a rigid template are sufficient enough to endow **2** with efficient molecular sponge-like capability as like *cavitand* (Fig. 2.01 a, b).

**Table. 2.1:** Summary - Inclusion complexes of HPB(COOMe)<sub>12</sub>

S.No	Inclusion Crystal	Guest molecules used for crystallization	Guest molecules found in the crystal	Crystallization Condition
1	HPB(COOMe) <sub>12</sub>	DCM	-	Method- A
2	DMSO@HPB(COOMe) <sub>12</sub>	DCM, DMSO	DMSO	Method- A
3	DMF@HPB(COOMe) <sub>12</sub>	DCM, DMF	DMF	Method- A
4	Pyridine@HPB(COOMe) <sub>12</sub>	DCM, Pyridine	Pyridine	Method- A
5	12-Crown@HPB(COOMe) <sub>12</sub>	DCM, 12-Crown	12-Crown	Method- A
6	Benzene@HPB(COOMe) <sub>12</sub>	DCM, Benzene	Benzene	Method- A
7	Toluene@HPB(COOMe) <sub>12</sub>	DCM, Toluene	Toluene	Method- A



8	Aniline@HPB(COOMe) <sub>12</sub>	DCM, Aniline	Aniline	Method- A
9	N-methylaniline@HPB(COOMe) <sub>12</sub>	DCM, N-methylaniline	N-methylaniline	Method- A
10	Salicylaldehyde@HPB(COOMe) <sub>12</sub>	DCM, Salicylaldehyde	Salicylaldehyde	Method- A
11	<i>p</i> -Chlorobenzene@HPB(COOMe) <sub>12</sub>	DCM, <i>p</i> -Chlorobenzene	<i>p</i> - Chlorobenzene	Method- A
12	(±) Styreneoxide@HPB(COOMe) <sub>12</sub>	DCM, (±) Styreneoxide	(±) Styreneoxide	Method- A

*Note:* All the hosts and guests are mentioned in the following manner: Guest.guest@**Host**

Furthermore compound **2** was able to trap many guest molecules inside the cavity through C-H and CO of the two adjacent molecules of **2** with assistance of C-H of the phenyl rings which is perpendicular to the central benzene (Table 2.1). There were C-H $\cdots$ pi, C-H $\cdots$ O, C-H $\cdots$ N interactions observed when the host molecule **2** itself was crystallized (HPB (COOMe)<sub>12</sub> in DCM, space group, *P 21/c*) (Fig. 2.02k).

In general, similar kinds of interactions were also found while **2** was entrapping a series of non-polar and polar aprotic guests (Fig. 2.02 a-j). By utilizing this property (*cavitand*) of the ester functionalized supramolecular sponge **2**, guest molecules such as dimethyl formamide, dimethyl sulphoxide, [12]-crown ether, benzene, toluene, pyridine, aniline, N-methyl aniline, chlorobenzene and salicylaldehyde were trapped in the crystal structure of **2** (Fig. 2.02a-j). The space groups of the crystals are *P-1*, *P-1*, *P-1*, *P 21/c*, *P -1*, *P -1*, *P 21/c*, *Cc*, *P1* and *P-1* respectively. In the crystal structure of the cavities, the guest molecules are organized in an inverted manner. Furthermore, racemic mixture of styrene oxide was used as a guest and crystallized, following the above mentioned condition. The space group of the crystal was found to be *P-1*. Opposite enantiomers of the styrene oxides were seen in upper and lower rim of the HPB(COOMe)<sub>12</sub>. It has been observed that all *cavities* showed a 1:2 host-guest ratio except for [12]-crown ether@**HPB(COOMe)**<sub>12</sub> (1:1).

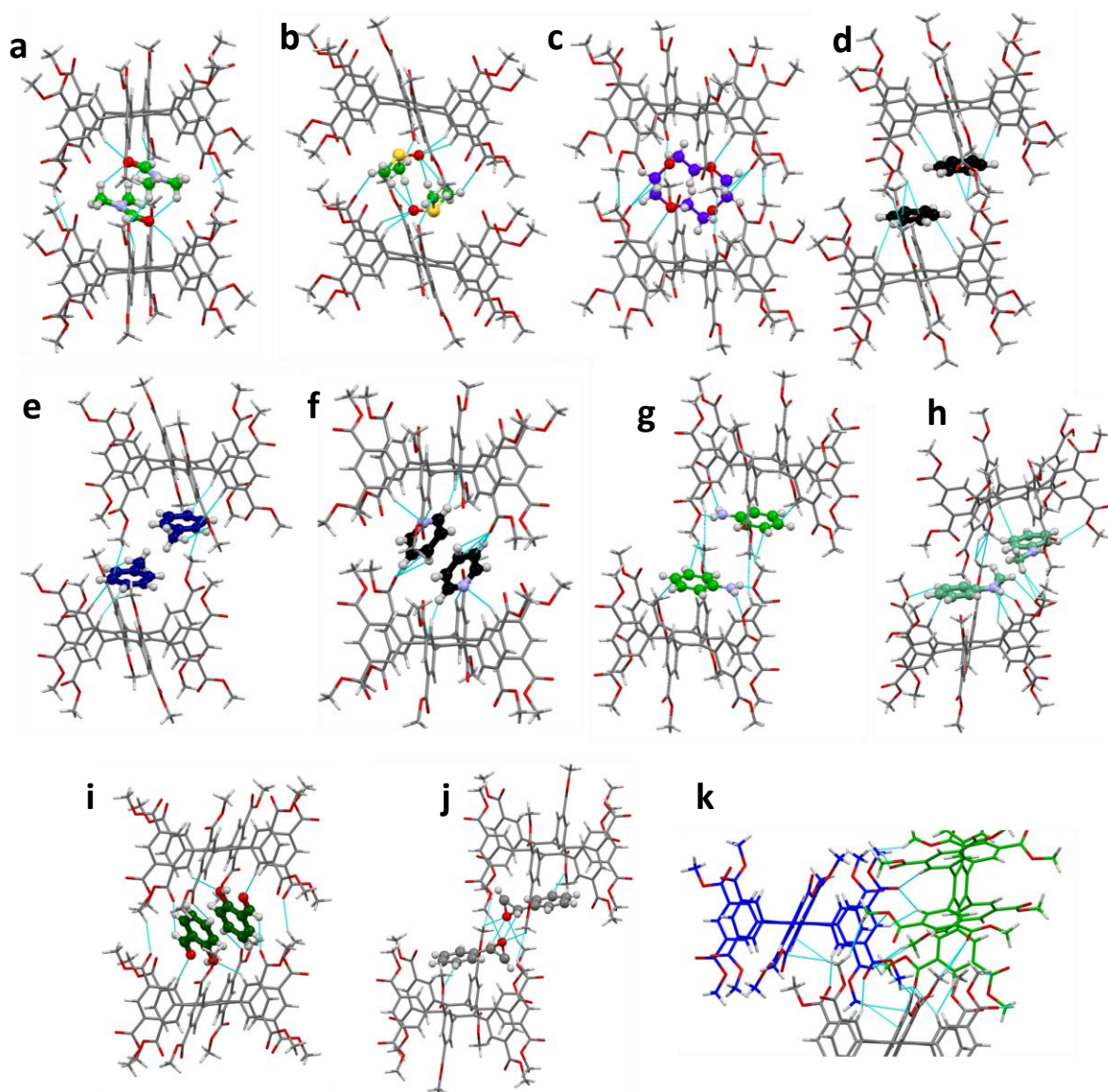


**Fig. 2.02:** Formation of various HPB based multivalent supramolecular sponge-cavities.

a) DMF@HPB(COOMe)<sub>12</sub>; b) DMSO@HPB(COOMe)<sub>12</sub>; c) [12]-crown ether@ HPB(COOMe)<sub>12</sub>; d) Benzene@HPB(COOMe)<sub>12</sub>; e) Toluene@HPB(COOMe)<sub>12</sub>; f) Pyridine@HPB(COOMe)<sub>12</sub>; g) Aniline@HPB(COOMe)<sub>12</sub>; h) N-methylaniline@HPB(COOMe)<sub>12</sub>; i) Salicylaldehyde@HPB(COOMe)<sub>12</sub>; j) (+/-)Styrene oxide@HPB(COOMe)<sub>12</sub>; k) penetration of ester functional groups and showing CH-O interaction in **2**.

### 2.4.3.2 Inclusion of guest molecules in HPB(CONHMe)<sub>12</sub>

The crystals of methylamide **3a** showed inclusion of good number of guest molecules. The guest molecules (water and acetone) were trapped in between 2D sheets formed through the self-assembly of host molecules in the respective crystals Acetone.H<sub>2</sub>O@HPB(CONHMe)<sub>12</sub> (space group: *P-1*) and H<sub>2</sub>O@HPB(CONHMe)<sub>12</sub> (space group: *P-1*) (Fig. 2.03a and 2.03d) (Table. 2.2). It is noteworthy to mention that most of the guest molecules were located in the cavities created by intermolecular assembly of the hosts, though the intrinsic cavities within the molecules (Fig. 2.03b-c and 2.03e-f). These observations imply that the secondary amide **3a** which is not having much change in the inclusion property, except 2D sheet formation through H-bond.

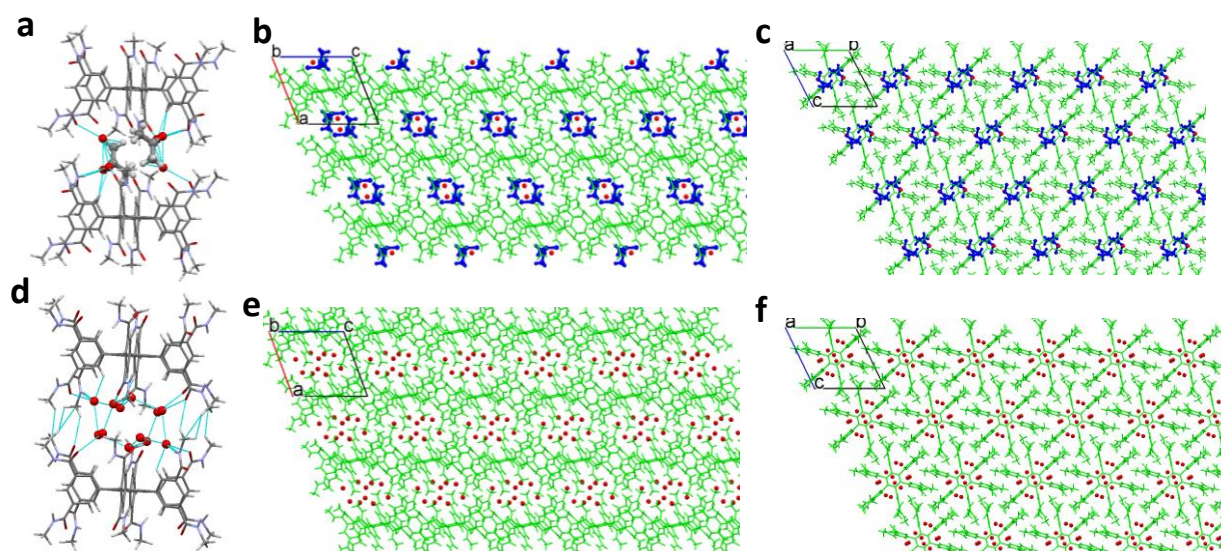


**Fig. 2.03: Crystal structure of methylamide **3a**.** a) Guest molecules acetone and water are trapped in the intrinsic cavity formed by **3a**; b) trapped guest molecules (water, acetone) seen between 2D sheet of **3a** in H<sub>2</sub>O@HPB(CONHMe)<sub>12</sub> (*b*-view); c) trapped guest molecules (water and acetone) between the 2D sheet of **3a** in Acetone.H<sub>2</sub>O@HPB(CONHMe)<sub>12</sub> (*a*-view); d) guest molecule water trapped in the intrinsic cavity formed by **3a**; e) trapped guest molecules (water) between the 2D sheet of **3a** in H<sub>2</sub>O@HPB(CONHMe)<sub>12</sub> (*b*-view) f) trapped guest molecule (water) between the 2D sheet of **3a** in H<sub>2</sub>O@HPB(CONHMe)<sub>12</sub> (*a*-view). *Note:* For clarity, host is shown in pale green color. Similarly, guests are shown in blue (acetone) and red (water) color.

**Table 2.2:** Summary of inclusion complexes of supramolecular sponge **HPB(CONHMe)<sub>12</sub>**

S.No	Inclusion Crystal	Guest molecules used for crystallization	Guest molecules found in the crystal	Crystallization Condition
1	Acetone.H <sub>2</sub> O@ <b>HPB(CONHMe)<sub>12</sub></b>	Acetone,H <sub>2</sub> O	Acetone,H <sub>2</sub> O	Method- A
2	H <sub>2</sub> O@ <b>HPB(CONHMe)<sub>12</sub></b>	H <sub>2</sub> O	H <sub>2</sub> O	Method- A

### 2.4.3.3 Entrapping of guest molecules in **HPB(CONH<sub>2</sub>)<sub>12</sub>**

The primary amide derivative **3b** has plenty of hydrogen bond donor-acceptor sites in its structure and that undergoes extensive self-assembly (aggregation) to become insoluble in many of the common organic solvent systems at ambient conditions. Fortunately, **3b** dissolved in hot DMSO from which it quickly crystallized. These observations suggested that the presence of strong intermolecular hydrogen bonding facilitates the formation of crystals of **3b** DMSO@**HPB(CONH<sub>2</sub>)<sub>12</sub>** (space group: *P-1*) with the inclusion of large number of DMSO as guest molecules in their crystal lattice. Some of the dimethyl sulfoxide guest molecules were accommodated in the intrinsic cavities of **3b** and rest of them held by the H-bonded arms as extrinsic guests (Fig. 2.04a, b). Likewise, **3b** captures large number of many other guest molecules (Table. 2.3) such as: DMSO-H<sub>2</sub>O (space group: *P-1*, Fig. 2.04c), N,N-dimethyl formamide (space group: *P-1*, DMF, Fig. 2.04d), N-methyl-2-pyrrolidone (space group: *P-1*, NMP, Fig. 2.04e), formic acid (space group: *P-1*, HCO<sub>2</sub>H, Fig. 2.04f) and N,N-dimethylformamide hydrogen bromide complex (space group: *P 21/n*, DMF.HBr, Fig. 2.04g).



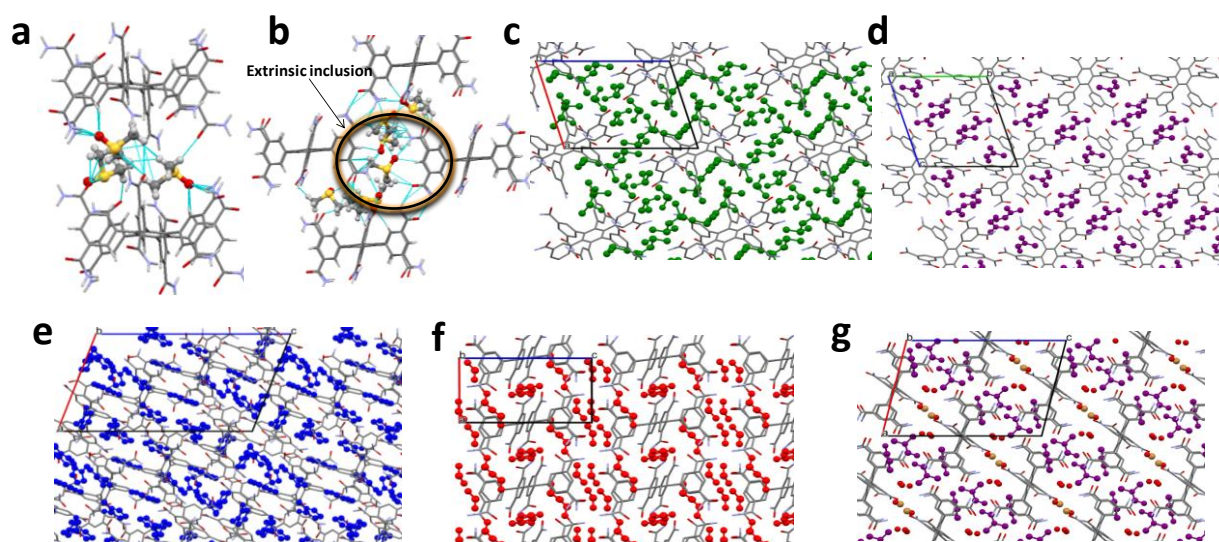


**Fig. 2.04:** Crystal structure of compound **3b** with the inclusion of various guest molecules. a) intrinsic inclusion of DMSO in DMSO@HPB(CONH<sub>2</sub>)<sub>12</sub>; b) extrinsic inclusion of DMSO in DMSO@HPB(CONH<sub>2</sub>)<sub>12</sub>; c) DMSO.H<sub>2</sub>O@HPB (CONH<sub>2</sub>)<sub>12</sub>; d) DMF@HPB(CONH<sub>2</sub>)<sub>12</sub>; e) NMP@HPB(CONH<sub>2</sub>)<sub>12</sub>; f) HCOOH@HPB(CONH<sub>2</sub>)<sub>12</sub>; g) DMF.HBr@HPB(CONH<sub>2</sub>)<sub>12</sub>. *Note:* for clarity, hydrogen atoms have been removed from the host and guests. The guest molecules DMSO, NMP, DMF and formic acid are shown in green, blue, purple and red color, respectively. Rest of the guest and host molecules atoms are shown in CPK color.

**Table 2.3:** Summary - Inclusion complexes of supramolecular sponge HPB(CONH<sub>2</sub>)<sub>12</sub>.

S.No	Inclusion Crystal	Guest molecules used for crystallization	Guest molecules found in the crystal	Crystallization Conditions
1	DMSO@HPB(CONH <sub>2</sub> ) <sub>12</sub>	DMSO	DMSO	Method- A
2	DMSO.H <sub>2</sub> O@HPB(CONH <sub>2</sub> ) <sub>12</sub>	DMSO	DMSO, H <sub>2</sub> O	Method- A (open vial)
3	DMF@ HPB(CONH <sub>2</sub> ) <sub>12</sub>	DMF, H <sub>2</sub> O	DMF	Method- A
4	NMP@HPB(CONH <sub>2</sub> ) <sub>12</sub>	NMP, H <sub>2</sub> O	NMP	Method- A
5	HCOOH.H <sub>2</sub> O@ HPB(CONH <sub>2</sub> ) <sub>12</sub>	HCOOH	HCOOH, H <sub>2</sub> O	Method- A
6	DMF.HBr@ HPB(CONH <sub>2</sub> ) <sub>12</sub>	DMF, H <sub>2</sub> O $\alpha$ -Bromoisobutyryl bromide	DMF, HBr	Method- A

7	DMSO.MeOH.C <sub>2</sub> H <sub>5</sub> OH. Hexane@ <b>HPB(CONH<sub>2</sub>)<sub>12</sub></b>	DMSO, C <sub>2</sub> H <sub>5</sub> OH,  Hexane, MeOH, NH <sub>3</sub>	DMSO, MeOH, C <sub>2</sub> H <sub>5</sub> OH,  Hexane	Method- B
8	MeOH.Dioxane.NH <sub>3</sub> @ <b>HPB(CONH<sub>2</sub>)<sub>12</sub></b>	MeOH, Dioxane, NH <sub>3</sub>	MeOH, Dioxane, NH <sub>3</sub>  (Type-1)	Method- B
9	MeOH.NH <sub>3</sub> @ <b>HPB(CONH<sub>2</sub>)<sub>12</sub></b>	MeOH, Dioxane, NH <sub>3</sub>	MeOH ,NH <sub>3</sub>  (Type-2)	Method- B
10	MeOH.Dioxane.NH <sub>3</sub> @ <b>HPB(CONH<sub>2</sub>)<sub>12</sub></b>	MeOH, Dioxane, NH <sub>3</sub>	MeOH, hexane, NH <sub>3</sub>  (Type-3)	Method- B
11	MeOH.Urotropine.NH <sub>3</sub> , aminomethyleneimine.Cl <sup>-</sup> @ <b>HPB(CONH<sub>2</sub>)<sub>12</sub></b>	MeOH, NH <sub>3</sub> , DCM	MeOH, Urotropine, NH <sub>3</sub> , aminomethyleneimi- -ne, chloride ion	Method- B

#### 2.4.4 Channelization of guest molecules in the crystal lattice

Another interesting property of compound **3b** is the ability to create two types of voids in the crystal due to the presence of hydrophobic (HPB intrinsic cavity) and hydrophilic (CONH<sub>2</sub> functional group, extrinsic cavity) regions in its structure, aiding in compartmentalization of polar and non-polar guest molecule in the respective voids of the sponge. This property was found when compound **3b** was crystallized under solvothermal method with a mixture of polar and non-polar solvents such as ammonia, DMSO, ethanol, methanol and hexane (space group: *P 21/c*). Analysis of the crystal structure revealed that the polar and non-polar guest molecules trapped in the HPB network were compartmentalized according to their polarity (ammonia). The polar guest molecules such as DMSO, MeOH and C<sub>2</sub>H<sub>5</sub>OH are trapped in the extrinsic cavity (hydrophobic) formed through the assistance of multivalent-hydrogen bonds whereas, non-polar guest molecules are trapped in the intrinsic cavity - formed through backbone rigidity of HPB, as shown in Fig. 2.05a.

### 2.4.5 Ammonia inclusion studies of $\text{HPB}(\text{CONH})_{12}$

The inclusion of gas molecules in single crystal structures of discrete organic molecular materials is well known in the literature. However, most of them are formed from intrinsic hosts like calixarene, carcerands, etc. Remarkably, in an unprecedented, way the twelve armed HPB system is able to trap ammonia in its crystal lattice of **3b**. These crystals of **3b** were prepared under hydrothermal conditions, in the course of the reaction while converting **2** to **3b**. This experiment has been repeatedly standardized using a mixture of highly saturated methanolic ammonia and dioxane in stainless steel with covered autoclave at 80-90 °C to obtain **3b** as block-shaped crystals. A suitable single crystals were mounted for the data collection and the crystal structure revealed the presence of three types of crystals, one with ammonia, methanol and dioxane as guests (type-1, space group:  $P4_32_1$ ,  $\text{MeOH.Dioxane.NH}_3@ \text{HPB}(\text{CONH}_2)_{12}$ ), second with ammonia, methanol as guest (type-2, space group:  $P2_1/c$ ,  $\text{MeOH.NH}_3@ \text{HPB}(\text{CONH}_2)_{12}$ ) and other with ammonia, methanol, hexane as a guests (type-3, space group:  $P 2_1/c$ ,  $\text{MeOH.Hexane.NH}_3@ \text{HPB}(\text{CONH}_2)_{12}$ ) in the crystal lattice of **3b** (Fig. 2.05b-d)



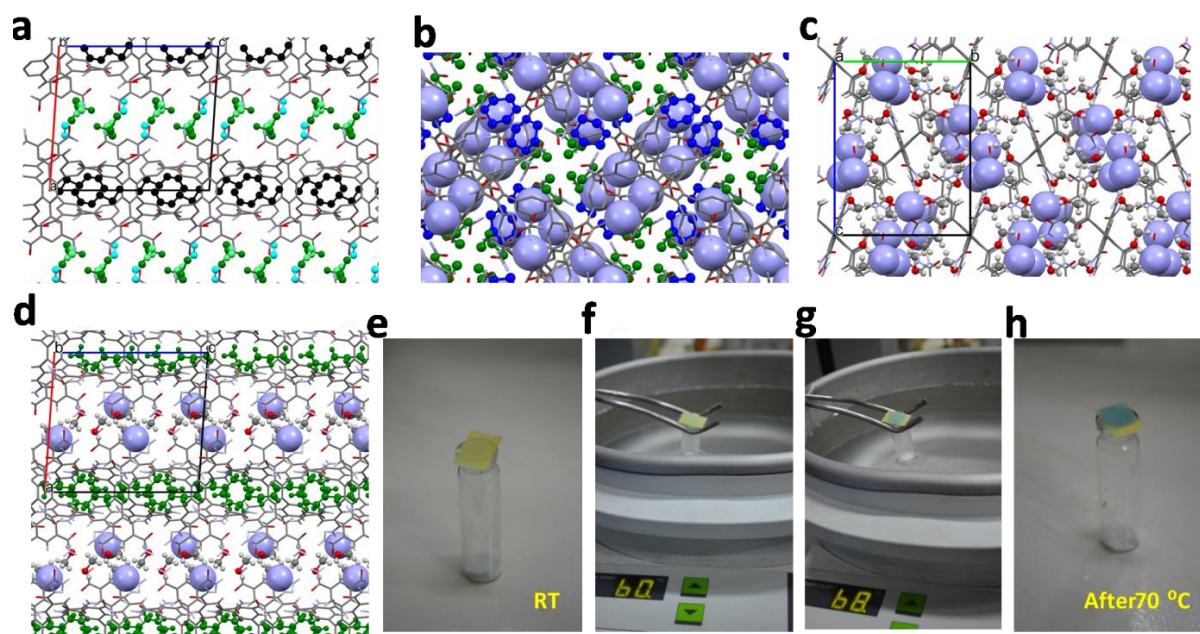


**Fig. 2.05:** a) Polarity-dependent channelization of guest molecules such as methanol (light blue), ethanol (light green), DMSO (green), hexane (black) in compound **3b** (DMSO.MeOH. C<sub>2</sub>H<sub>5</sub>OH.Hexane@HPB(CONH<sub>2</sub>)<sub>12</sub>); b) trapped ammonia (violet colored spacefill), dioxane (blue colored ball&stick) and methanol (green colored ball&stick) in the crystal lattice of compound **3b** (type-1); c) trapped ammonia (violet colored spacefill) and methanol (ball&stick) in the crystal lattice of compound **3b** (type-2); d) trapped ammonia (violet colored spacefill), hexane (green colored ball&stick) and methanol (ball&stick) in the crystal lattice of compound **3b** (type-3); e) mixer of crumbled crystals type-1, type-2 and type-3 are showing pH paper color test, negligible color change at RT; f) slight blue color at 60°C; g) blue color changes at 68°C; h) intense blue color on or above 70°C.

It is well-known that ammonia exists as gas at ambient temperature due to lack of hydrogen bonding acceptor sites. However, when the external molecules provide suitable hydrogen bonding acceptor sites, the ammonia molecules may get entrapped within the lattice of the complex. The same concept is used here to trap ammonia in the crystal lattice of **3b**, wherein the twelve arms of the HPB are involved in the formation of cavities as well as to trap the guest molecules, through non covalent forces. The twelve arms of the HPB are symmetrically arranged in such a way that if guest molecules would try to escape from one of the arms, the other arms may readily catch hold of them in the crystal lattice. Crystals were seen to be unstable under ambient conditions since they crumble slowly and emit ammonia. The escaping ammonia bubbles could be seen under a microscope. However, crystals have been found to be stable in the methanolic ammonia mother liquor and to a certain extent in silicone oil. Crystals also quickly crumbled when

suspended in solvents such as methanol. It is noteworthy that the crumbled crystals do not release ammonia significantly at ambient conditions, as evident from a negative pH paper test (Fig. 2.05e). pH paper test: mixture of crumbled crystals of type-1, type-2 and type-3 was taken in a glass vial and on top of that, a water dipped pH paper was kept and it was slowly warmed from room temperature to 70 °C. The color of pH paper was gradually turned into bluish green (Fig. 2.06) indicating the slow release of ammonia from the crystal lattice upon heating.

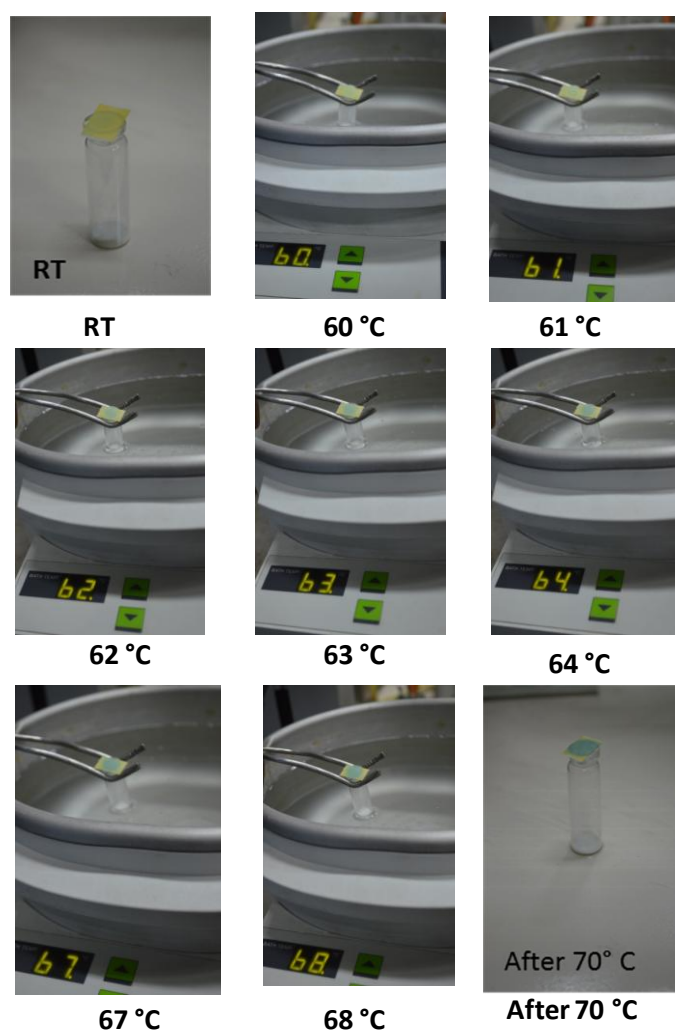


**Fig. 2.06:** pH paper test: a) Gradual release of ammonia from crumbled crystals of type-1, type-2 and type-3 at different temperatures.

This experiment suggested that the bound ammonia was having strong interaction in the crystal lattice with host molecules under ambient conditions. Nevertheless, upon heating, ammonia was released from the system due to the destruction of intermolecular

interactions between host-guest and guest-guest molecules. Moreover, the presence of umbrella type mode band at  $1015\text{ cm}^{-1}$  and broadening of the IR band about  $3100\text{-}3500\text{ cm}^{-1}$  in fresh crystals of mixer of type-1 to type-3, when compared with sample heated at  $40\text{ }^{\circ}\text{C}$  for 24h, supports the presence of ammonia in the system (Fig. 2.08). Further, the weight loss about 8% at the temperature range  $30\text{-}90\text{ }^{\circ}\text{C}$  in thermogravimetric analysis (TGA) is attributed to slow release of ammonia and other guest molecules. This clearly indicates that the guest holding ability of compound **3b** is temperature-dependent (Fig. 2.07). Furthermore, as an example, superposition of the X-ray crystal structure of  $\text{MeOH.Dioxane.NH}_3\text{@HPB}(\text{CONH}_2)_{12}$  with DFT optimized structure were compared and the result supported the favourability of the system. The framework and guest molecules were fully relaxed in the DFT optimization. The atoms of the  $\text{HPB}(\text{CONH}_2)_{12}$  framework were fixed to the experimental X-ray positions.

#### 2.4.6 Evidences for the presence of ammonia as a guest in the crystal of $\text{MeOH.Dioxane.NH}_3\text{@HPB}(\text{CONH}_2)_{12}$

##### 2.4.6.1 Thermogravimetric Analysis (TGA)

Thermogravimetric analysis (TGA) was conducted to determine the weight loss upon increasing temperature at constant rate. The crystals were removed from mother liquor and TGA was recorded. The weight loss of crystals showed 8% below  $250\text{ }^{\circ}\text{C}$  (Fig. 2.07) corresponding to gradual loss of guest molecules such as ammonia, hexane, dioxane, methanol. The weight loss observed at above  $350\text{ }^{\circ}\text{C}$  was due to the decomposition of the compound **3b**. The gradual weight loss of crystals (in temperature range  $30\text{-}120\text{ }^{\circ}\text{C}$ ) is attributed to the loss of guest molecules from the crystal structure. The gradual weight loss due to slow escaping of guest molecules imply that the number of guest molecules interacted with the host molecules are temperature and time dependent.

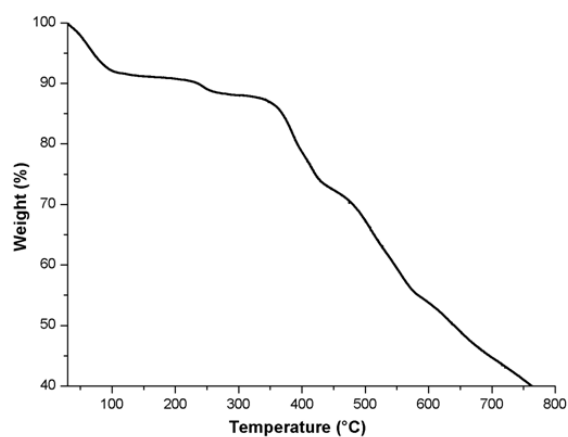


**Fig. 2.07:** TGA [open pan] of crystals of mixture of type-1, type-2 and type-3.

#### 2.4.6.2 Infrared analysis (IR)

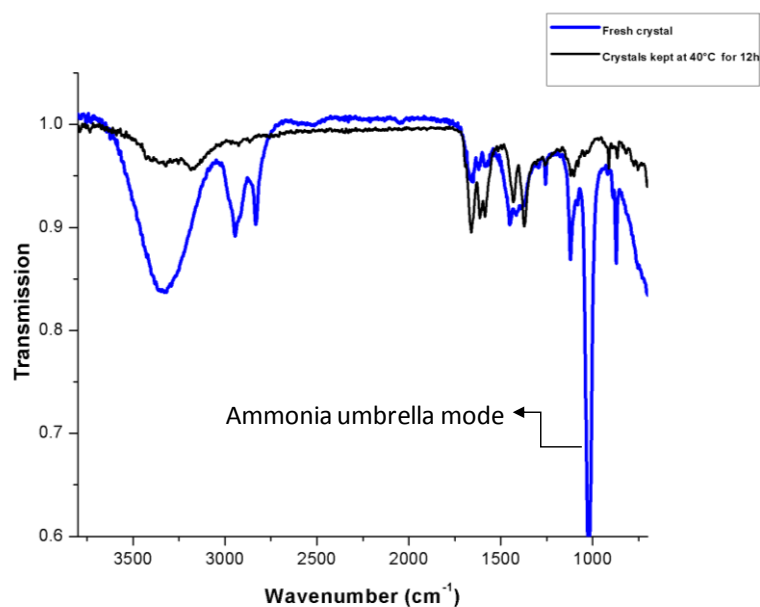


**Fig. 2.08:** IR [AT IR] of crystals, Fresh sample (blue) and warmed at 40°C (black) for 12h.

IR spectrum of fresh samples shows (Fig. 2.08) an umbrella mode (1015 cm<sup>-1</sup>) absorption which is not found in the case of heated sample. This is attributed to the presence of ammonia in the fresh sample and negligible amount of ammonia in the warmed sample. The relative broadening of the fresh sample is possibly due to the

dynamic motion and escape of kinetically trapped ammonia and other guest molecules. The gradual weight loss is attributed to the instability of the crystals under ambient conditions and is found to be nearly 8% (at temperature range 30- 120° C). This is because the guest molecules have gradually escaped upon preparing the sample for TGA analysis.

#### 2.4.6.3 Surface Characterization of HPB(CONH<sub>2</sub>)<sub>12</sub>

In order to determine the morphology and porous nature of crumbled crystal of HPB(CONH<sub>2</sub>)<sub>12</sub> SEM was used in our study.

##### Scanning electron microscope(SEM)

Crumbled crystal sample was analyzed on a FEI make SEM system of Quanta 200 3D series (dual beam ESEM) bearing tungsten filament as the electron source and was operated at 10 kV. The SEM image (Fig. 2.09) shows the clubbed scale like particles in surface of the solid, which reveals the escaping of low volatile guest molecules from the crystal and thus possibly crystal crumbling into small pieces.

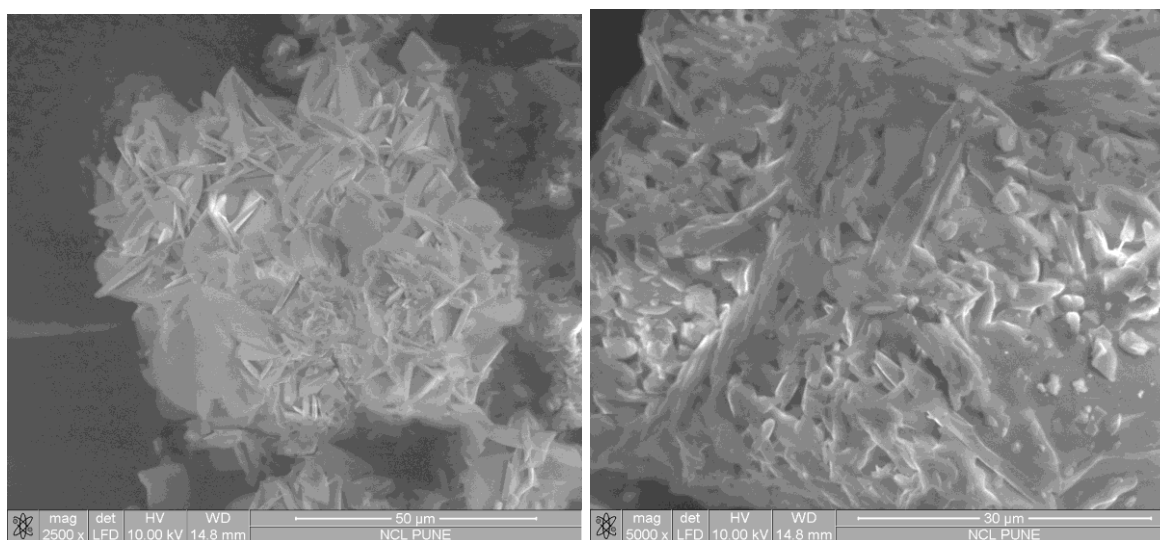


**Fig. 2.09:** Representative SEM images of crumbled sample (mixture of type-1, type-2 and type-3). The clubbed scale like particles is attributed to the escape of low volatile guest molecules which leads to the breakage of crystal into small pieces of scale like units.



### 2.4.7 Trapping of reaction intermediates: Mechanical investigation of urotropine decomposition

The ability of **HPB(CONH<sub>2</sub>)<sub>12</sub>** (**3b**) to entrap several guest molecules has motivated us to investigate the reaction mechanism for the decomposition of urotropine in basic pH under hydrothermal condition. Although literature precedence on the decomposition mechanism of urotropine in the solution state is plenty,<sup>27</sup> evidences are seldom provided – particularly by single crystal studies. It has already been shown that the reaction of ammonia with dichloromethane could give urotropine and ammonium chloride (Fig. 2.10c).<sup>28-29</sup> Further, the formation of 2-azaallenium ion is previously studied by the decomposition of urotropine under acidic and basic pH.<sup>27, 30</sup> Upon replacing dioxane with DCM in the conversion of compound **2** to **3b**, we have found the presence of urotropine along with 2-azaallenium (CH<sub>2</sub>=N<sup>+</sup>=CH<sub>2</sub>) intermediate bearing chloride (Cl<sup>-</sup>) counter ion, ammonia and methanol in the crystal lattice (space group: *P*-1, Fig. 2.10a-b).

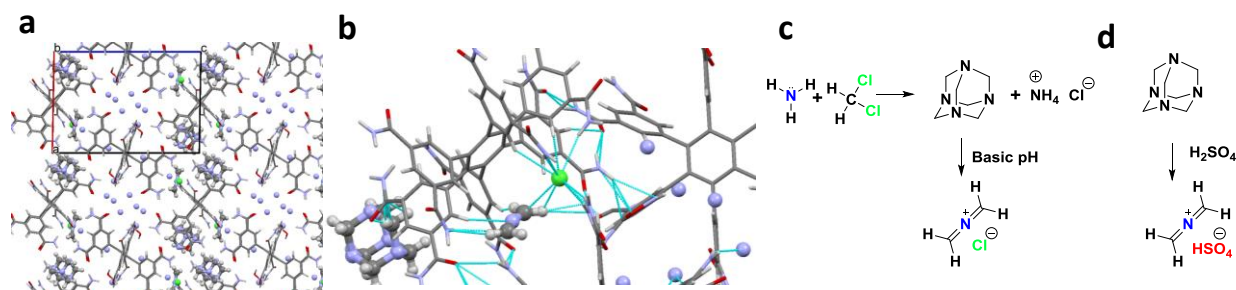


**Fig. 2.10:** a) Trapped ammonia, methanol, urotropine, 2-azaallenium with counter ion chloride in the crystal lattice of compound **3b** (MeOH.Urotropine.NH<sub>3</sub>.2-azaallenium.Cl<sup>-</sup>@**HPB(CONH<sub>2</sub>)<sub>12</sub>**); b) 2-azaallenium ion is having short contact with counter ion and hosts **3b**, Note: all atom colors are shown in standard CPK, guests are shown in ball and stick; c) Formation of urotropine and ammonium chloride by reaction of DCM and ammonia and followed by decomposition urotropine under basic pH yields chloride ion stabilized 2-azaallenium (present work); d) decomposition of urotropine in the aqueous H<sub>2</sub>SO<sub>4</sub> yields HSO<sub>4</sub><sup>-</sup> ion stabilized 2-azaallenium (previous work, solid state NMR studies).

It should be emphasized that 2-azaallenium is believed to be an equilibrium structure of one of the intermediates which is formed in the decomposition of urotropine at basic pH (Fig. 2.10c).<sup>30</sup> This is first time that 2-azaallenium intermediate has been characterized using single crystal X-ray structure. It is noteworthy that this intermediate has been proposed to be involved in a several reactions, including the aminomethylation of tannins.<sup>27, 30-31</sup> 2-Azaallenium intermediate has only been characterized, so far, through

spectroscopic techniques such as NMR by the stabilization of counter ion sulphate (Fig. 2.10d).<sup>27</sup> Further, DFT energy minimised model of MeOH.Urotropine.NH<sub>3</sub>.2-azaallenium.Cl<sup>-</sup>@HPB(CONH<sub>2</sub>)<sub>12</sub> supports the favourability of the system.

Next, we increased the number of hydrogen bonding donors to three by converting all the ester groups which are present in **2** to hydrazide (CONHNH<sub>2</sub>). The spongy nature of **3a** was investigated in two conditions: in first case, water, dioxane and methanol was used as solvent systems (hydrothermal) and in the second case, only water was used as a guest (space group: *P-1* and *C 2/c*, respectively, Table. 2.4). The obtained crystal structure of both the cases showed the presence of guest in the intrinsic cavities of HPB. But, very few water molecules were found in the extrinsic cavities of the crystals. Therefore, increment of H-donors in the HPB twist back and showed increment in the intrinsic inclusion property (Fig. 2.11).

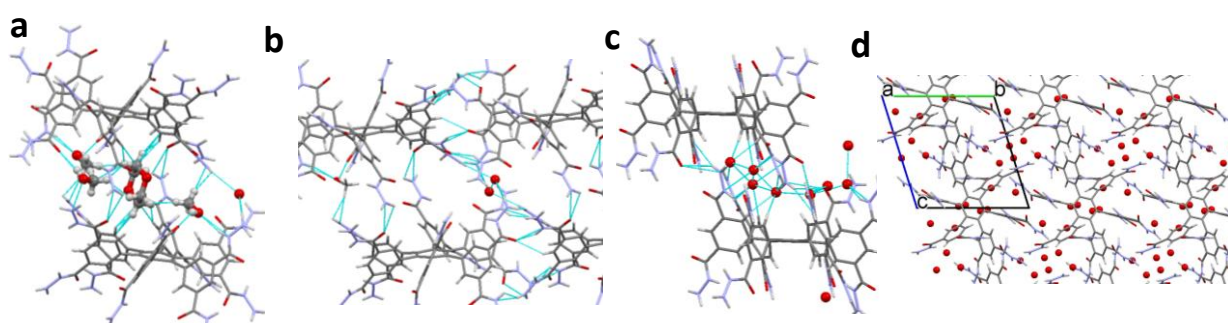


**Fig. 2.11:** a) Presence of guest molecules dioxane and methanol in the intrinsic cavity of **3c**; b) water molecules were trapped in the extrinsic place formed by intermolecular H-bonds; c) presence of water guest molecules in the intrinsic cavity of **3c**; d) water molecules are accommodated in intrinsic and extrinsic places of crystal structure of **3c**.

**Table 2.4:** Summary - Inclusion complexes of supramolecular sponge HPB(CONH<sub>2</sub>)<sub>12</sub>

S.No	Inclusion Crystal	Guest molecules used for crystallization	Guest molecules found in the crystal	Crystallization Condition
1	Dioxane.Methanol.H <sub>2</sub> O@ HPB(CONH <sub>2</sub> ) <sub>12</sub>	Hydrazine, Dioxane, Methanol, H <sub>2</sub> O	Dioxane, Methanol, H <sub>2</sub> O	Method- B
2	H <sub>2</sub> O@ HPB(CONH <sub>2</sub> ) <sub>12</sub>	H <sub>2</sub> O	H <sub>2</sub> O	Method- A



#### 2.4.8 DFT Optimization of MeOH.Dioxane.NH<sub>3</sub>@HPB(CONH<sub>2</sub>)<sub>12</sub> and MeOH.Urotropine.NH<sub>3</sub>.2-azaallenium.Cl<sup>-</sup>@ HPB(CONH<sub>2</sub>)<sub>12</sub>

##### Details of DFT calculations

All the calculations in this study have been performed with density functional theory (DFT), with the aid of Turbomole 6.4 suite of programs,<sup>32</sup> using the PBE functional.<sup>33</sup> The TZVP<sup>34</sup> basis set has been employed. The resolution of identity (RI),<sup>35</sup> along with the multipole accelerated resolution of identity (marij)<sup>36</sup> approximations have been employed for an accurate and efficient treatment of the electronic Coulomb term in the DFT calculations. The values are reported in  $\Delta E$  values, with the temperature at 298.15 K.

Full quantum chemical calculations were done with density functional theory (DFT) at the PBE/TZVP level of theory in order to gain further understanding of the system. Specifically, the type of binding and the interaction between the host (HPB) and the guest molecules (ammonia) in the presence of explicit methanol, dioxane, as well as the urotropine molecules with the intermediate has been investigated. The Fig. 2.12a and Fig. 2.12b show the superposition of the X-ray structure of complex-1 (MeOH.Dioxane.NH<sub>3</sub>@HPB (CONH<sub>2</sub>)<sub>12</sub>) and complex-2 (MeOH.Urotropine.NH<sub>3</sub>.2-azaallenium.Cl<sup>-</sup>@HPB(CONH<sub>2</sub>)<sub>12</sub>), respectively, with the DFT optimized structures. In both the cases, the geometry optimizations were initiated from the experimental X-ray crystal structures. Both the host and NH<sub>3</sub> positions were determined from X-ray were found to be in good agreement with the DFT optimized structures (Fig. 2.13 & 2.14). The DFT calculated binding energies of complex **1** and complex **2** are thermodynamically highly stable, with the  $\Delta E$  of binding found to be -100.5 kcal/mol and -177.8 kcal/mol respectively. These values suggest that the formation of complexes-**1** and complex-**2** are highly favorable reactions. This is because both the complexes are stabilized by the presence of a strong hydrogen-bonding network.

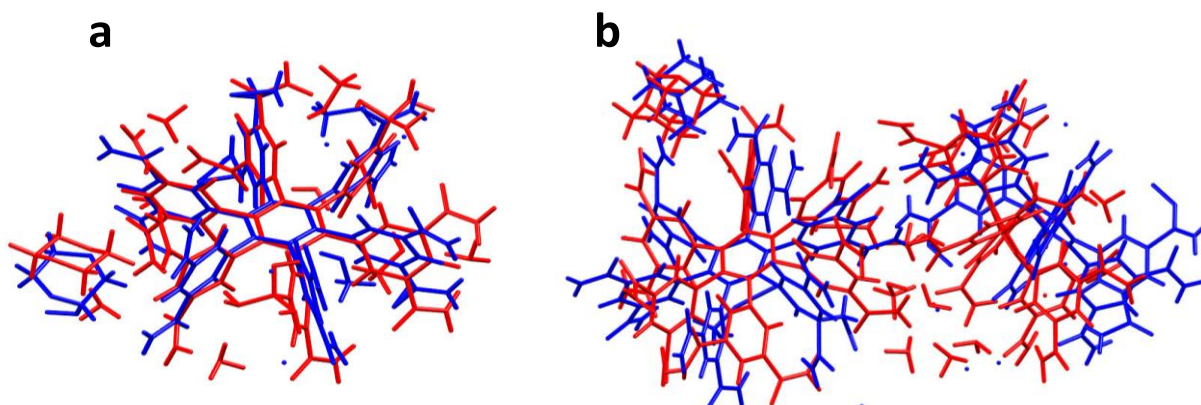


**Fig. 2.12:** a) Superposition of the X-ray structure (blue) of MeOH.Dioxane.NH<sub>3</sub>@HPB(CONH<sub>2</sub>)<sub>12</sub>, and b) MeOH.Urotropine.NH<sub>3</sub>.2-azaallenium.Cl@HPB(CONH<sub>2</sub>)<sub>12</sub> with DFT optimized structures (red). The framework and guest molecules are fully relaxed in the DFT optimization. The heavy atoms of the framework in b are fixed to the experimental X-ray positions.

A perusal of the structures makes it clear that the NH<sub>3</sub> molecules are trapped in the central framework by the strong hydrogen bonding network. Two types of hydrogen-bonding (donor and acceptor) are present in both the complexes with respect to the central host molecule: (i) the carbonyl oxygen interacts with the hydrogen of NH<sub>3</sub>, and (ii) the hydrogen of the amide interacts with the nitrogen of the NH<sub>3</sub>. The hydrogen-bond distance ranges from 1.8 Å to 2.2 Å for both the complexes. The bond angles range from 157° to 177° in complex-1, while a comparatively lower bond angle (145° to 170°) has been observed in case of complex 2. The C=N bond length (1.25 Å) and the C-N-C bond angle (171.6°) of the intermediate (CH<sub>2</sub>=N<sup>+</sup>=CH<sub>2</sub>) present in the complex-2 agree well with the corresponding X-ray crystal data.

1. The cartesian coordinates of the optimized geometry of complex-1 (Dioxane.NH<sub>3</sub>@HPB(CONH<sub>2</sub>)<sub>12</sub>) are provided below.

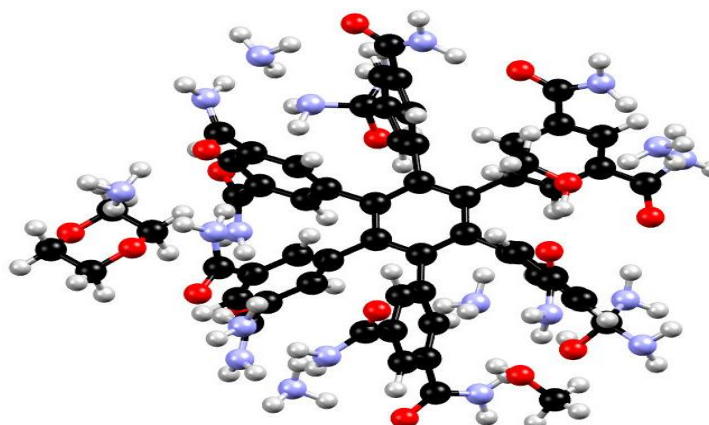


**Fig. 2.13:** DFT optimized structure of MeOH.Dioxane.NH<sub>3</sub>@HPB(CONH<sub>2</sub>)<sub>12</sub>

2. The cartesian coordinates of the optimized geometry of complex-2 (MeOH.Urotropine.NH<sub>3</sub>.2-azaallenium.Cl<sup>-</sup>@HPB(CONH<sub>2</sub>)<sub>12</sub>) are provided below.

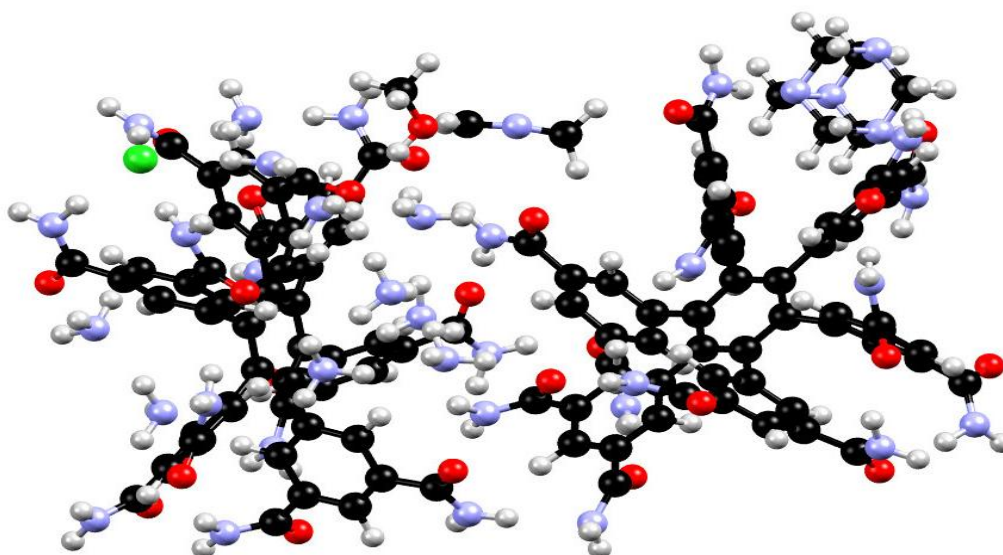
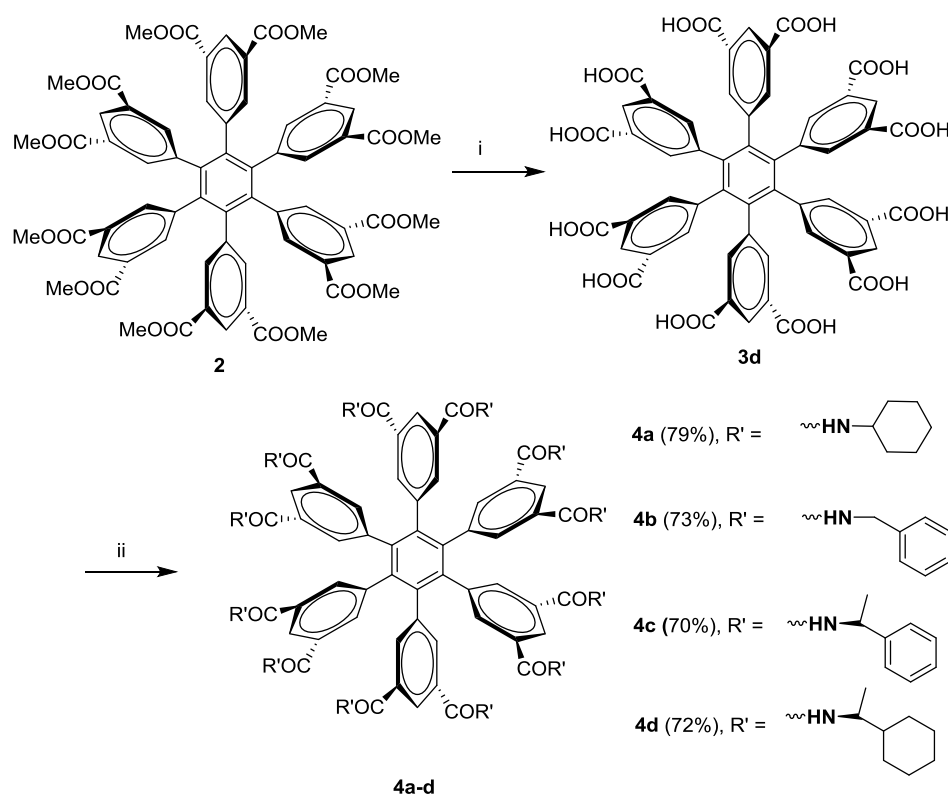


**Fig. 2.14:** DFT optimized structure of MeOH.Urotropine.NH<sub>3</sub>.2-azaallenium.Cl<sup>-</sup>@HPB(CONH<sub>2</sub>)<sub>12</sub>.

### 2.4.9 An attempt to discriminate the chiral molecules using multivalent supramolecular sponges

Encouraged by the previous results, we have extended our investigation to the chiral discrimination of guest molecules using chiral groups incorporated multi-armed supramolecular sponges. Incorporation of chiral groups were initially performed by the trans etherification of HPB (COOMe)<sub>12</sub> using menthol and borneol as alcoholic counterpart. Unfortunately both the products were highly soluble in most of the non-polar solvents and didn't show any crystalline nature. So we changed our strategy to prepare chiral amides. In contrast to methylamine, the direct amidation of HPB(COOMe)<sub>12</sub> could not be performed for chiral amines. Therefore, first we have converted HPB(COOMe)<sub>12</sub> into its corresponding carboxylic acid (HPB(COOH)<sub>12</sub>), and then transformed them in to various chiral groups attached HPB (HPB(COR\*)<sub>12</sub>) by following an acid-amine coupling strategy using HBTU as a coupling reagent (Scheme 2.02). Usage of other coupling reagents like DCC and EDC ended with various mixtures of products.



**Scheme 2.02: Reagents and conditions:** i) a) aqueous dioxane, KOH, 120 °C (Teflon lined stainless steel autoclave), 12 h, b) Con. HCl, water; ii) R'-H, HBTU, DIEA, DMSO, rt, 12h.

Initial standardization of the coupling reaction was performed using cyclohexylamine as an amine counterpart, wherein we could obtain 79% yield of amide **4a**. The material was recrystallized from methanol to understand the extended structural architecture of the system. X-crystal structure of **4a** as shown in Fig. 2.15b reveals that it has a double basket-like structure (space group: *P-1*).

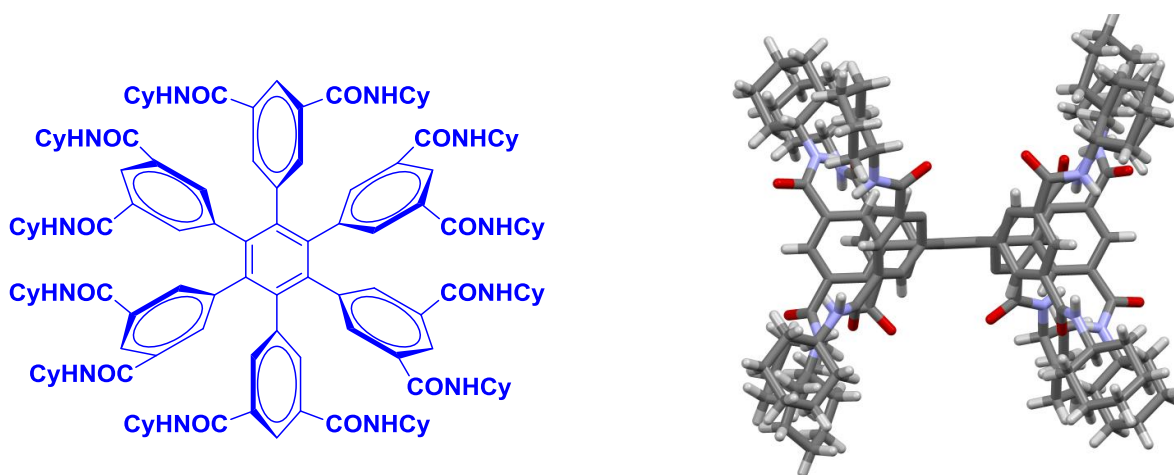


**Fig. 2.15:** a) Chemical structure of HPB(CONHCy)<sub>12</sub>. b) X-crystal structure of HPB(CONHCy)<sub>12</sub>.

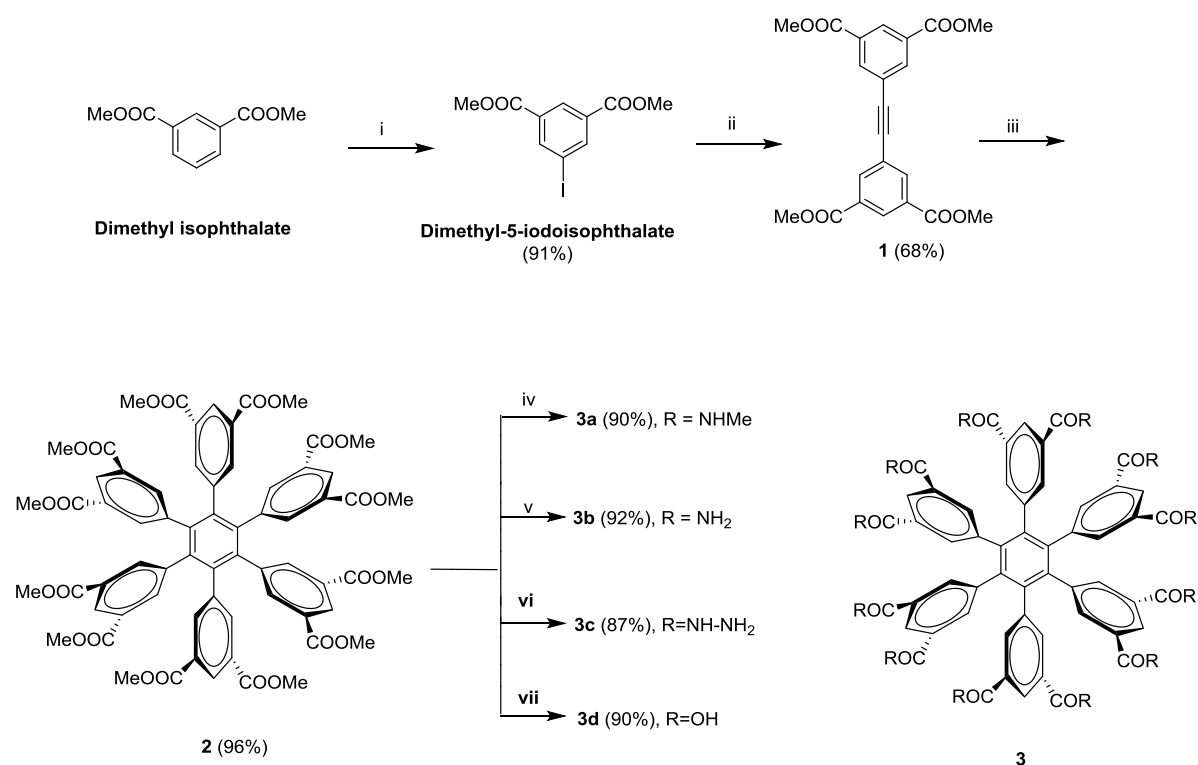
Further, HPB(CONHCH<sub>2</sub>C<sub>6</sub>H<sub>5</sub>)<sub>12</sub> (**4b**) was prepared in a similar manner of the above mentioned reaction procedure using benzylamine as an amine counterpart to examine the reaction versatility. The yield of the reaction was found to be 73%. Then, chiral amines (*S*)-(-)- $\alpha$ -methylbenzylamine and (*S*)-(+)- $\alpha$ -methylcyclohexanemethylamine were treated to obtain amides **4c** and **4d** respectively. **4c** is readily soluble in dichloromethane chloroform and hot ethanol. The optical rotation value is:  $[\alpha]_{\text{D}}^{24}$ : +18.4° (*c* = 0.77). The **4c** was recrystallised from ethanol. Due to poor quality data, we could not obtain completely solved X-crystal structure of **4c**. **4c** was tested for chiral discrimination with racemic small molecules such as  $\alpha$ -methylbenzylamine, 2-iodobutane, menthol, 2-butanol and 2-ethylcyclohexylmine. None of the above cases provide good quality crystals. **4d** is also readily soluble in dichloromethane, chloroform and hot ethanol. However, **4d** didn't show any crystalline nature. The chiral discrimination of the racemic mixtures in various solvents systems using **4c** and **4d** is under process in our lab.

## 2.5 Conclusion

In conclusion, we have shown rationally designed giant supramolecular sponges **2**, **3a**, **3b** and **3c** to uptake diverse guest molecules. Multivalency without hydrogen-bonding sites in the rigid core of the HPB ester **2** shows *cavitand* formation for the inclusion of various guest molecules including salicylaldehyde, aniline, N-methyl aniline, 12-crown ether and racemic styrene oxide. All the guest molecules of the *cavitands* (**2**, **3a**, **3b**, **3c**) were having C-H--pi, C-H--O, C-H--N interactions with 3'- C-H of the HPB. However, the gradual increase of complementary hydrogen bonding sites increased the extrinsic voids due to the cooperative interplay of directionality of hydrogen bond and backbone rigidity of HPB in **3a** and **3b**. As a result, the exemplary material **3b** resulted in an enhanced extrinsic inclusion property through the formation of 3D network by the assistance of backbone rigidity of HPB and multi-arms with hydrogen bonding sites. The arms which are freed from the network formation got involved in the capturing of the guest molecules in the hybrid voids. But, when the H-bond donors was increased to three (**3c**), the property was slightly modified to intrinsic. It was also demonstrated that the molecular sponge **3b** is able to channelize guest molecules based on their polarity. In addition, the reaction mechanism for the decomposition of urotropine could be investigated by trapping the reaction intermediate within the crystal lattice of the host molecule. Remarkably, compound **3b** has been shown to be capable of holding ammonia in its single crystal lattice. Further, the spongy nature of the HPB derivatives was demonstrated through the inclusion of many guest molecules in the crystal lattice of the HPB and they were well characterized with single crystal XRD. The findings suggest that this modified supramolecular sponge can be used to store low volatile small molecules and gases such as methane, ammonia and CO<sub>2</sub>, etc. Furthermore, the spongy and high crystalline nature of these systems with heavy atoms can be utilized to get the crystal structure of challenging substances such as reaction intermediates, liquid and pasty natural products, etc., which is our future interest.

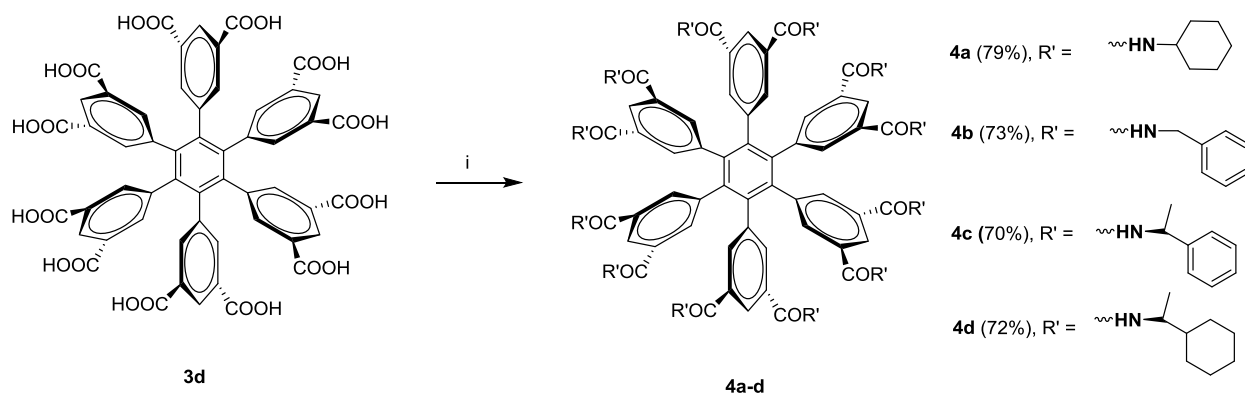
## 2.6 Experimental section

## Scheme 2.03: Synthesis of compounds 2, 3a-d and 4a-d.



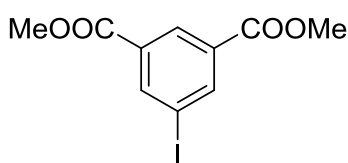
**Reagents and conditions:** i) NaIO<sub>4</sub>, I<sub>2</sub>, H<sub>2</sub>SO<sub>4</sub>, rt, 12 h; ii) PdCl<sub>2</sub>(PPh<sub>3</sub>)<sub>2</sub>, TMSA, CuI, Et<sub>3</sub>N, TBAF, THF, rt, 12 h; iii) Co<sub>2</sub>(CO)<sub>8</sub>, dioxane, reflux, 6 h; iv) methanolic methylamine, dioxane, steel bomb, 80 °C, 12 h; v) methanolic ammonia, dioxane, steel bomb, 80 °C, 12 h; vi) methanol, dioxane, hydrazine in 35 wt. % in H<sub>2</sub>O, steel bomb, 80 °C, 12 h; vii a) aqueous dioxane, KOH, 120 °C (teflon lined stainless steel autoclave), 12 h, b) con. HCl, water.





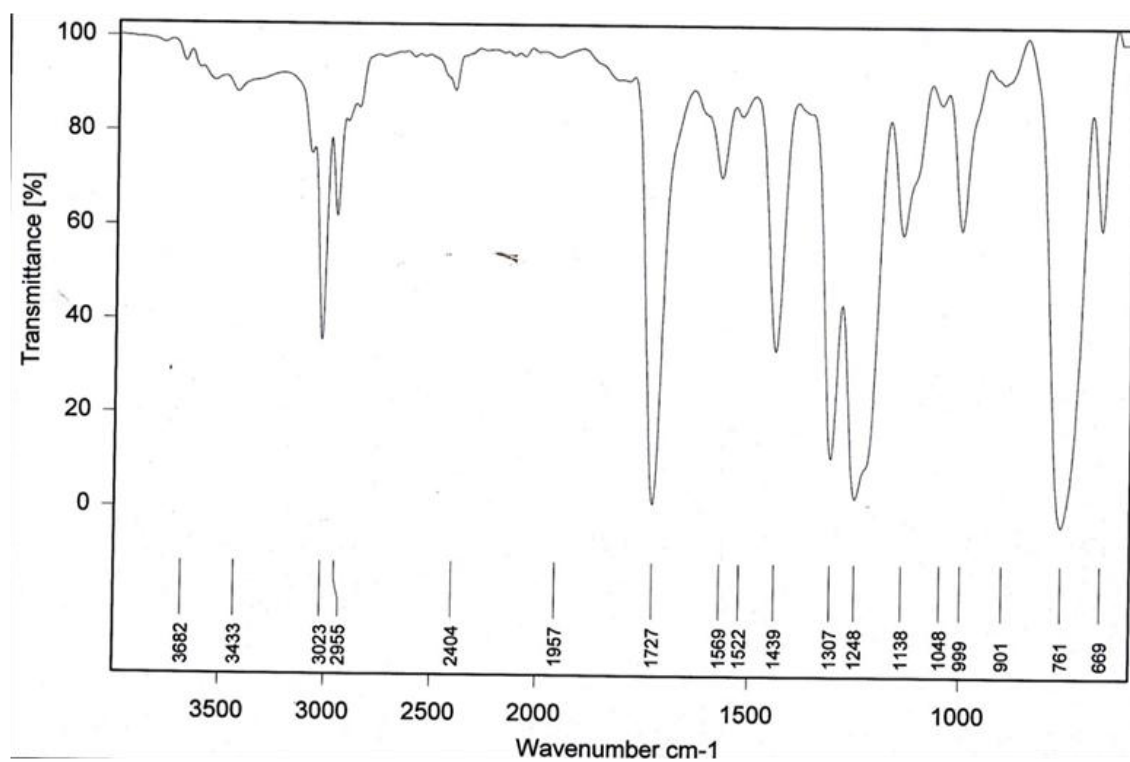
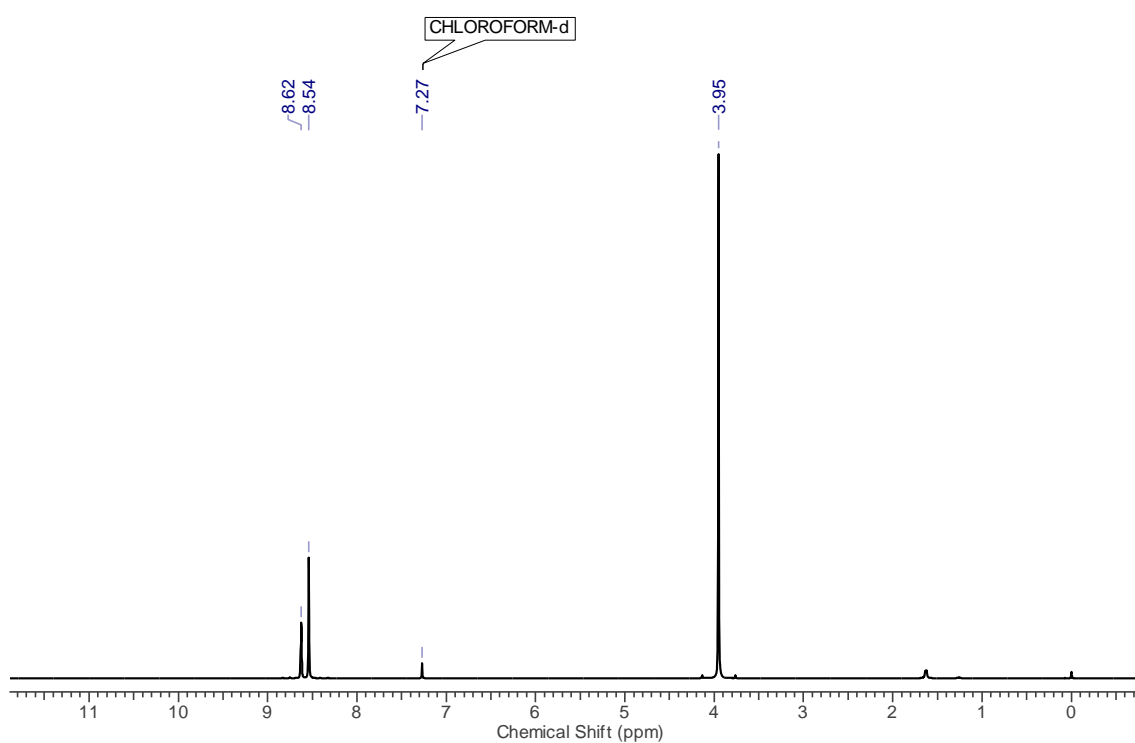
**Reagents and conditions:** (i) R'-H, HBTU, DIEA, DMSO, rt, 12h.

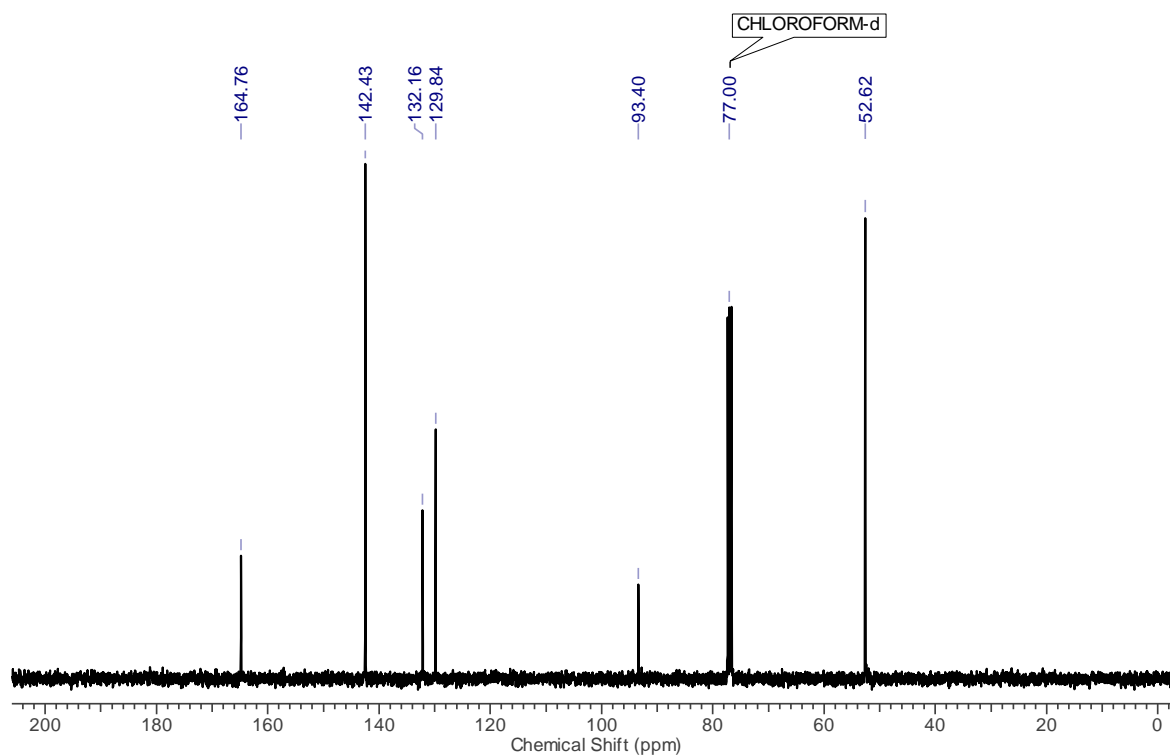
### Dimethyl-5-iodoisophthalate



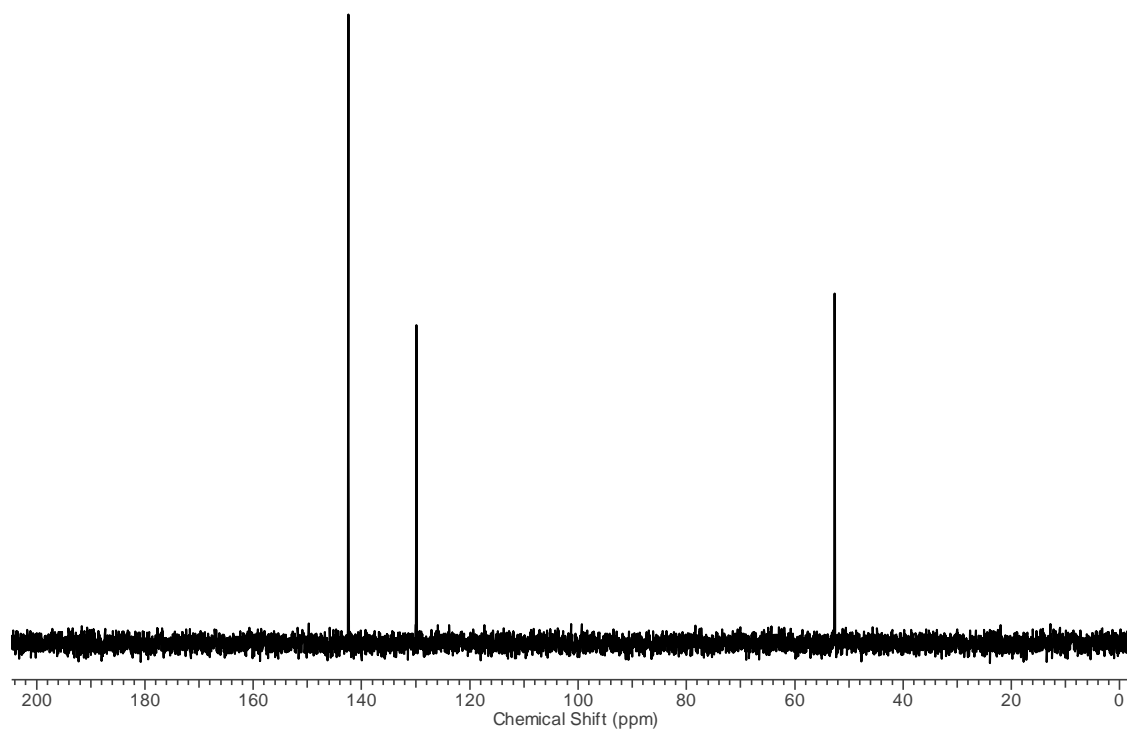
Dimethyl-5-iodoisophthalate was prepared by following a slightly modified procedure of the previous report.<sup>37</sup>

Iodine (18.29 g, 72 mmol) was added to a stirred solution of sodium periodate (8.8 g, 41 mmol) in 110 mL 96% sulfuric acid at 36 °C under argon atmosphere. The resulting mixture was stirred for 30 minutes. To this mixture was added dimethyl isophthalate (20 g, 103 mmol) and stirring was continued for 12 h. After completion of the reaction, the reaction mixture was poured into conical flask containing crushed ice and dichloromethane (DCM). The organic layer was then separated and the aqueous layer repeatedly washed with dichloromethane. The collected organic layers were carefully washed with sodium bicarbonate, sodium thiosulfate and brine, respectively. The combined organic layers were collected and dried over anhydrous sodium sulfate followed by evaporation to afford compound Dimethyl-5-iodoisophthalate as colorless crystalline material (30 g, 91 %) which was used without further purification for the next step. mp: 99-101 °C; TLC (Ethyl acetate:pet ether, 5:95 v/v):  $R_f = 0.3$ ; IR (CHCl<sub>3</sub>) cm<sup>-1</sup>: 3023, 2955, 1727 (C=O), 1569; <sup>1</sup>H NMR (CDCl<sub>3</sub>, 400 MHz)  $\delta$ : 8.62 (s, 1H), 8.54 (s, 2H), 3.95 (s, 6H); <sup>13</sup>C NMR (CDCl<sub>3</sub>, 100 MHz)  $\delta$ : 164.76, 142.43, 132.16, 129.84, 93.40, 52.62.

IR spectrum of **Dimethyl-5-iodoisophthalate**<sup>1</sup>H NMR spectrum of **Dimethyl-5-iodoisophthalate** (CDCl<sub>3</sub>, 400 MHz, 298 K)



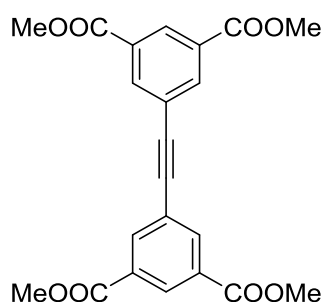
$^{13}\text{C}$  NMR spectrum of **Dimethyl-5-iodoisophthalate** ( $\text{CDCl}_3$ , 100 MHz, 298 K)



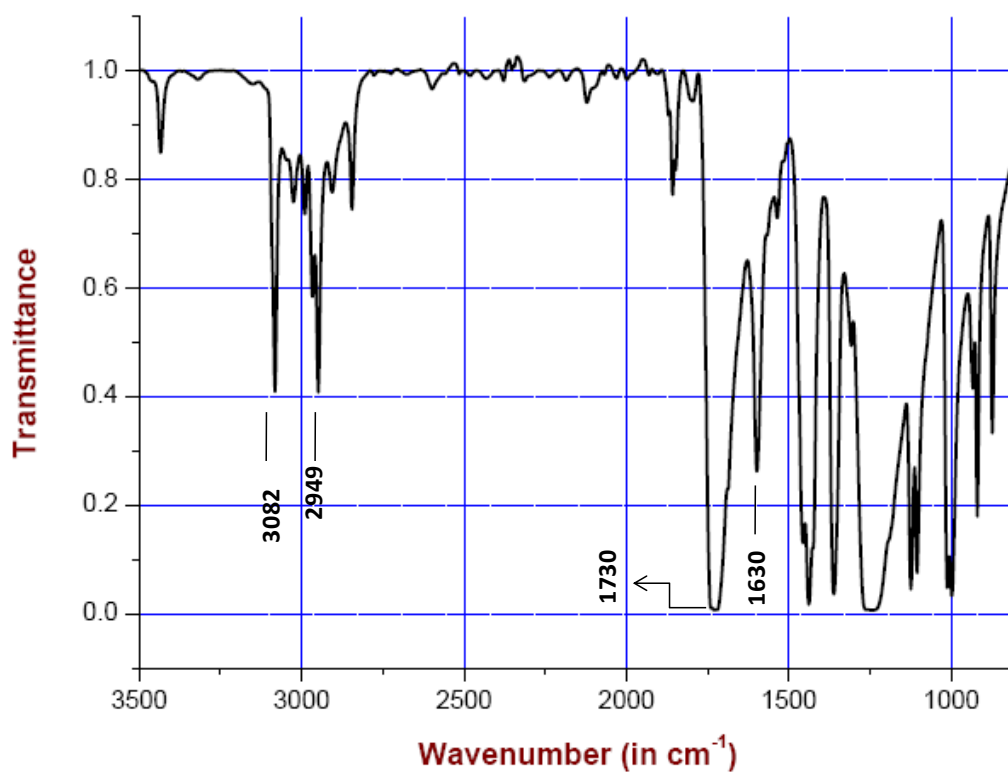
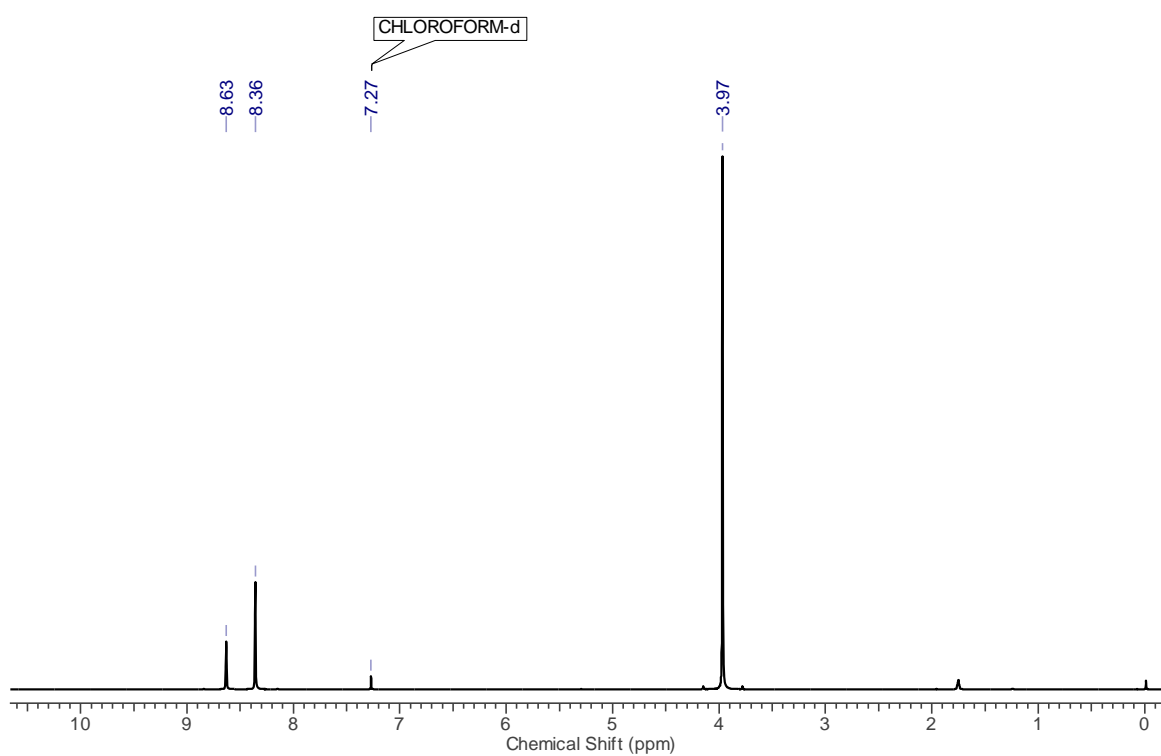
DEPT 135 spectrum of **Dimethyl-5-iodoisophthalate** ( $\text{CDCl}_3$ , 100 MHz, 298 K)

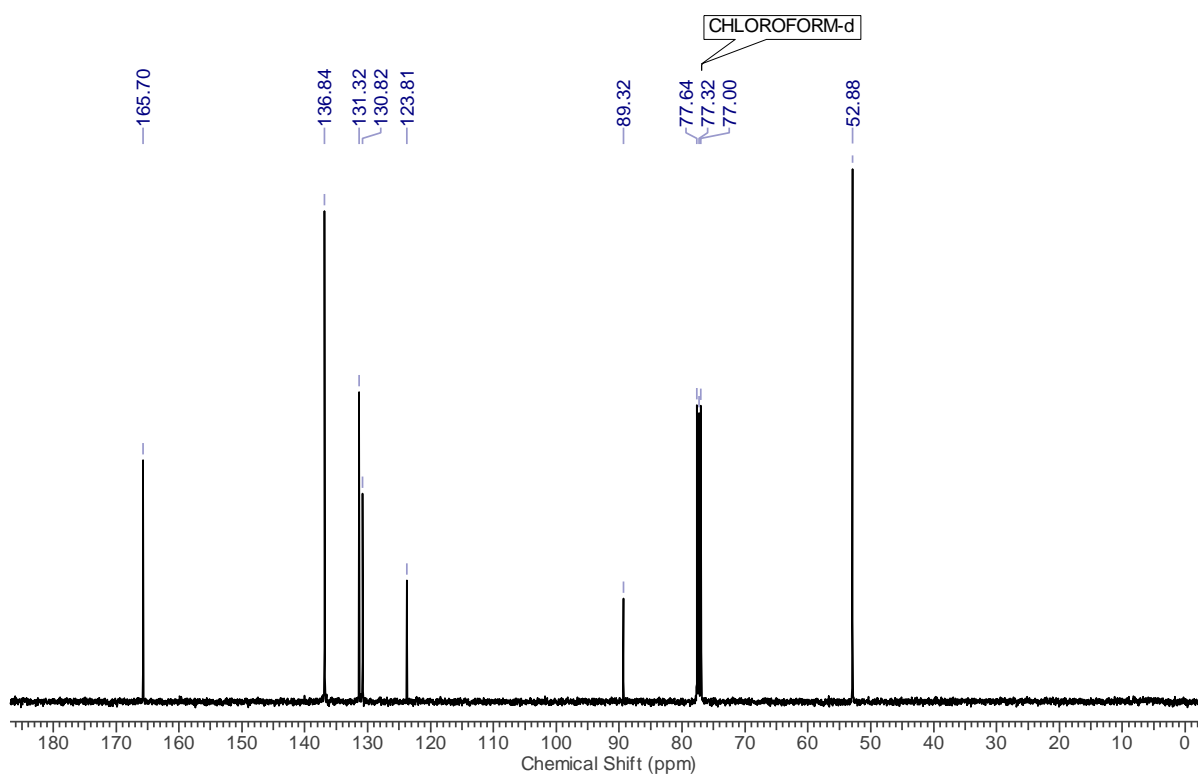
**Compound 1**

One pot sequential Sonagashira coupling:

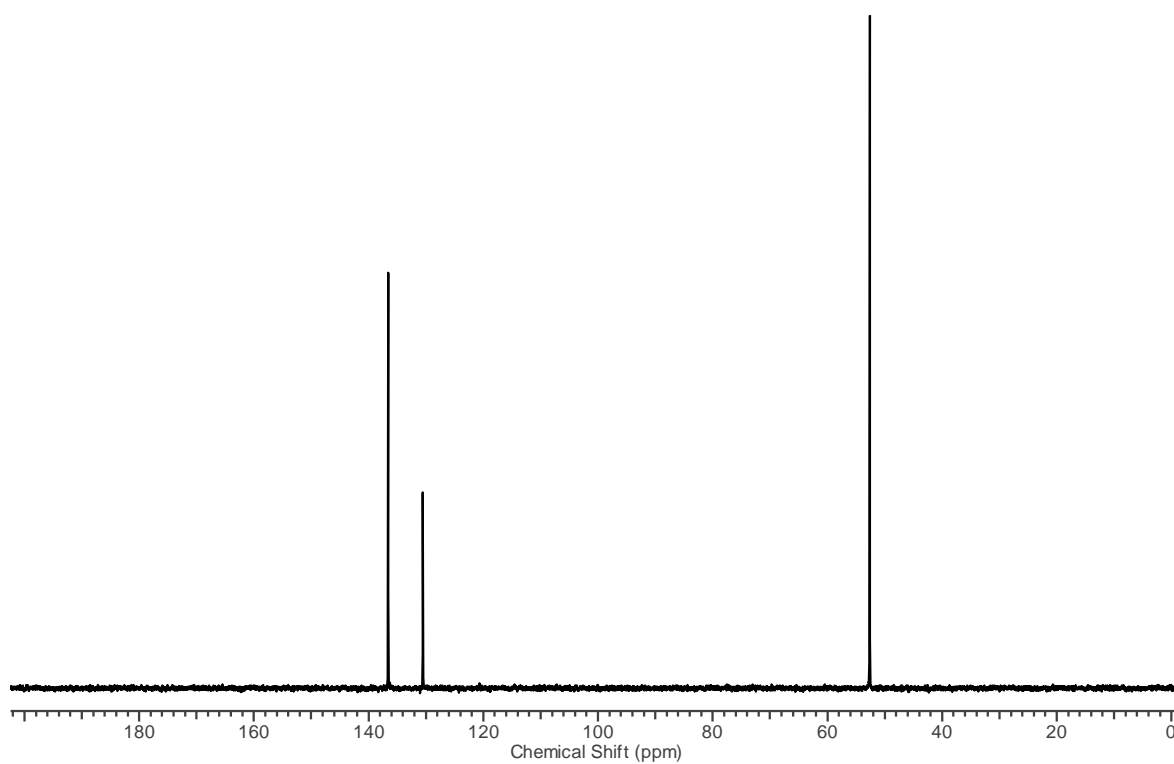


To a magnetically stirred mixture of dimethyl-5-iodoisophthalate (10 g, 31.21 mmol),  $\text{PdCl}_2(\text{PPh}_3)_2$  (1.53 g, 2.18 mmol) and  $\text{CuI}$  (0.594 g, 3.12 mmol) in dry degassed THF (50.00 mL) TMSA (2.2 mL, 15.60 mmol) and dry triethylamine (17.5 mL, 124.8 mmol) were added under an inert atmosphere. The solution was stirred at room temperature for 3 h to form one terminal aryl coupled and the other terminal TMSA protected product (monitored by TLC). Then TBAF (8.97 g, 34 mmol) 0.3 M in THF was added drop wise for 3 h and further the reaction mixture was stirred at room temperature for 12 h. After completion of the reaction, the mixture was diluted with ethyl acetate and filtered through celite. The filtrate was washed with water followed by brine. The combined organic layers were dried over anhydrous  $\text{Na}_2\text{SO}_4$  and concentrated *in vacuo* to give pale brown solid which was further subjected to fractional crystallisation using DCM to afford expected product as block-shaped thick crystals in good yield. (4.35 g, 68%). mp:193-195 °C; TLC (ethyl acetate:pet ether, 20:80 v/v):  $R_f = 0.4$ ; IR (KBr)  $\text{cm}^{-1}$ : 3082, 2949, 1861, 1730 (C=O), 1630 (Ar);  $^1\text{H}$  NMR ( $\text{CDCl}_3$ , 400 MHz)  $\delta$ : 8.63 (s, 2H), 8.36 (s, 4H), 3.97 (s, 12H);  $^{13}\text{C}$  NMR ( $\text{CDCl}_3$ , 100 MHz)  $\delta$ : 165.70, 136.84, 131.32, 130.82, 123.81, 89.32, 52.88; MALDI-MS (m/z):  $[\text{M}+\text{K}]^+$  449.1736. Elemental analysis calculated for  $\text{C}_{22}\text{H}_{18}\text{O}_8$ : C, 64.39; H, 4.42. Found: C, 64.42; H, 4.41.

IR spectrum of compound **1**<sup>1</sup>H NMR spectrum of compound **1** (CDCl<sub>3</sub>, 400 MHz, 298 K)



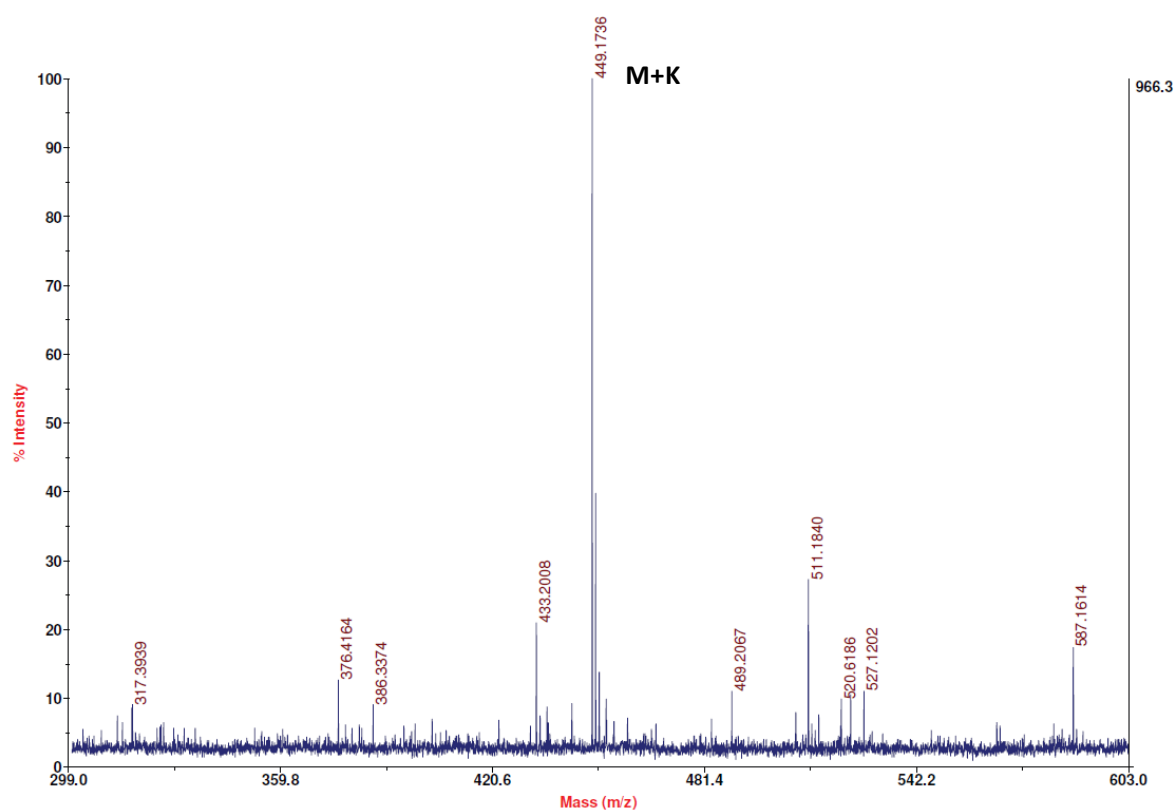
$^{13}\text{C}$  NMR spectrum of compound **1** ( $\text{CDCl}_3$ , 100 MHz, 298 K)



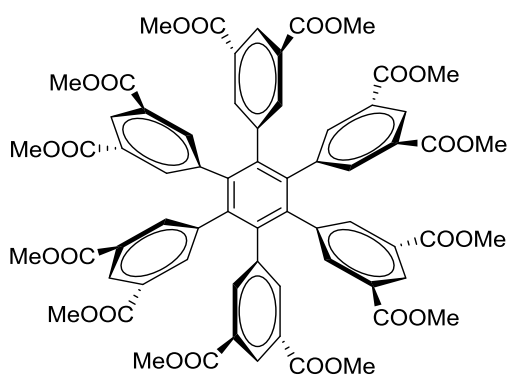
DEPT 135 spectrum of compound **1** ( $\text{CDCl}_3$ , 100 MHz, 298 K)

AB Sciex TOF/TOF™ Series Explorer™ 72085

TOF/TOF™ Reflector Spec #1 [BP = 449.2, 966]

MS (MALDI-TOF) of compound **1**

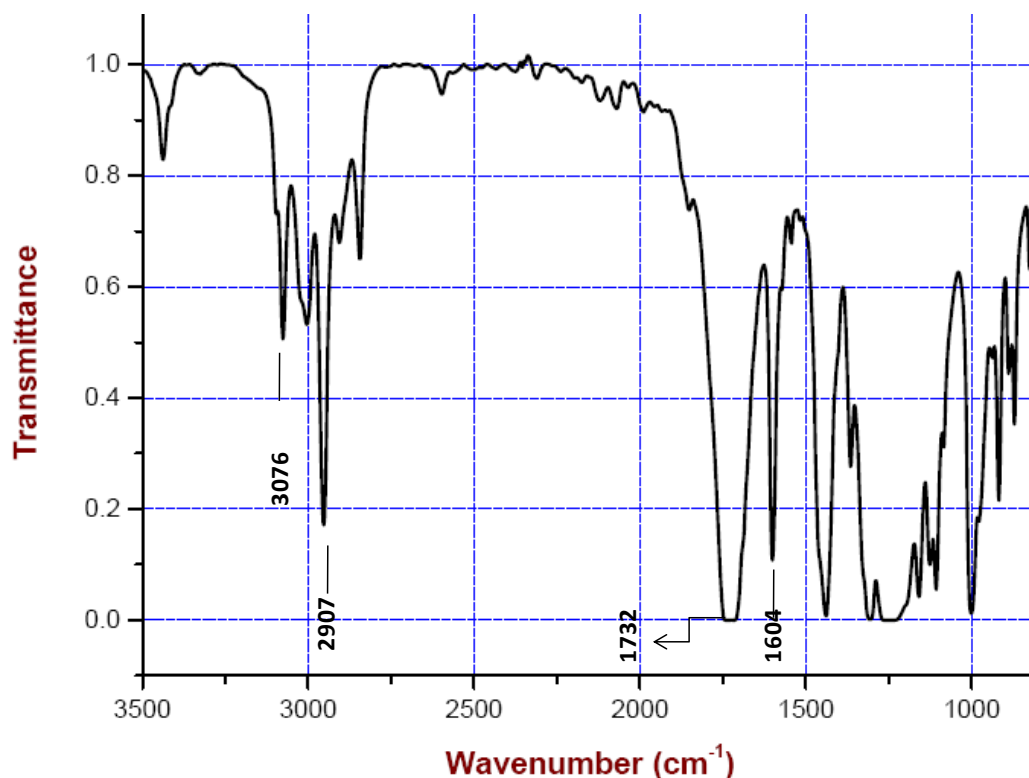
## Compound 2



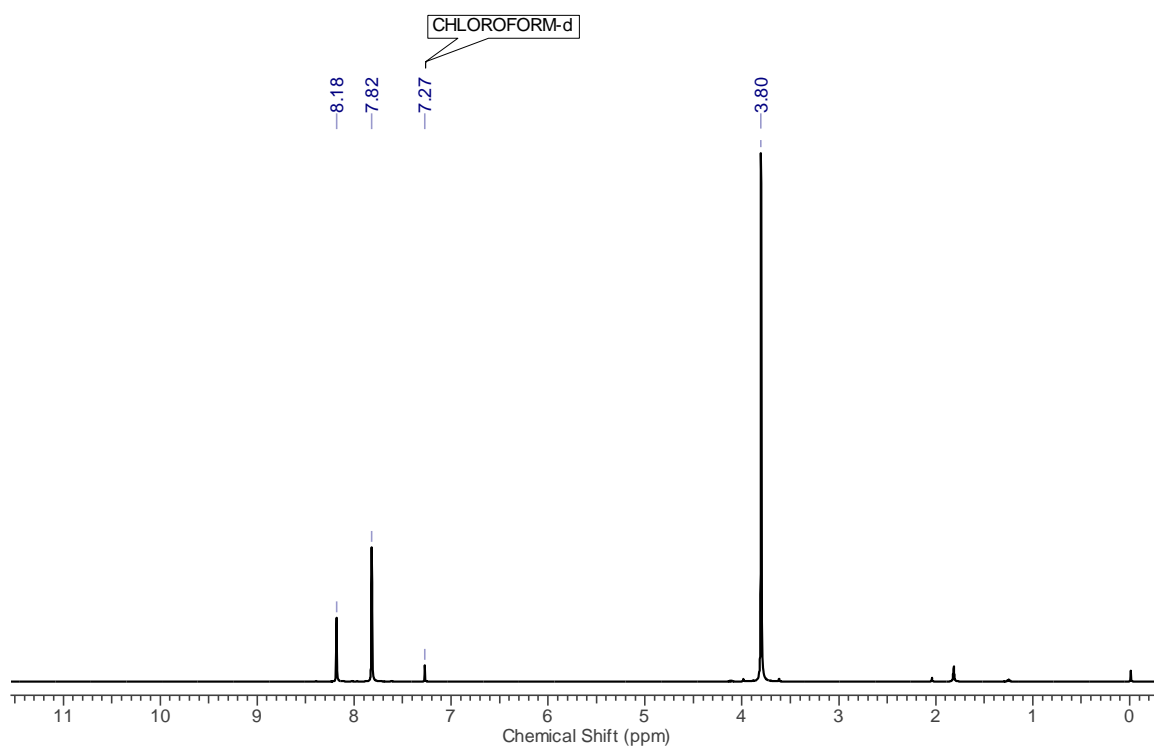
Compound **1** (2.5 g, 6.09 mmol) was dissolved in dry 1,4-dioxane (150 ml) under argon atmosphere and dicobaltoctacarbonyl (0.208 g, 0.609 mmol) was added. The resulting mixture was refluxed for 6 h. After completion of the reaction monitored by TLC, dioxane was removed under reduced pressure. The obtained residue was dissolved in DCM and filtered through celite®, the filtrate was further evacuated to give compound **2** as a



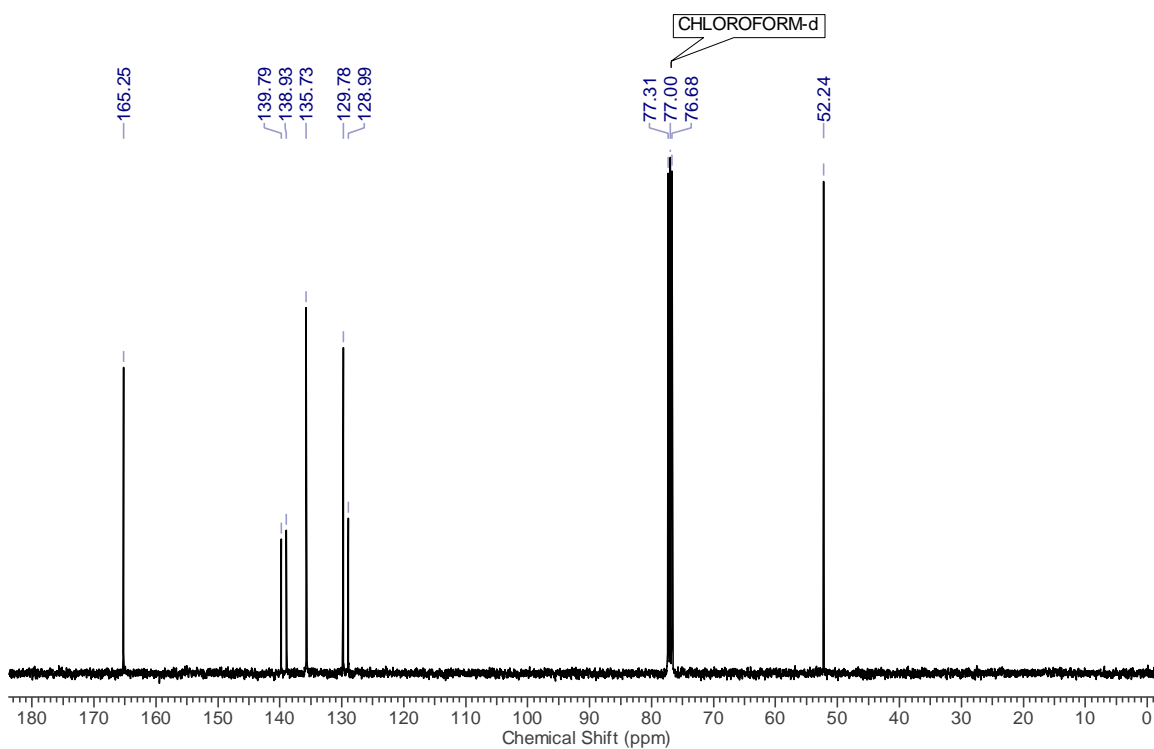
colorless solid (2.4 g, 96 %). mp: 345-347 °C; TLC (ethyl acetate/pet ether, 70:30 v/v):  $R_f = 0.5$ ; IR (KBr)  $\text{cm}^{-1}$ : 3076, 3002, 2907, 2844, 1732 (C=O), 1604 (Ar);  $^1\text{H-NMR}$  (400 MHz,  $\text{CDCl}_3$ )  $\delta$ : 8.18 (t, 6H), 7.82 (d, 12H), 3.80 (s, 36H);  $^{13}\text{C NMR}$  (100 MHz,  $\text{CDCl}_3$ )  $\delta$ : 165.25, 139.79, 138.93, 135.73, 129.78, 128.99, 52.24; HRMS ( $m/z$ ): calcd for  $\text{C}_{66}\text{H}_{55}\text{O}_{24}$   $[\text{M}+\text{H}]^+$  1231.3078, found 1231.3137.



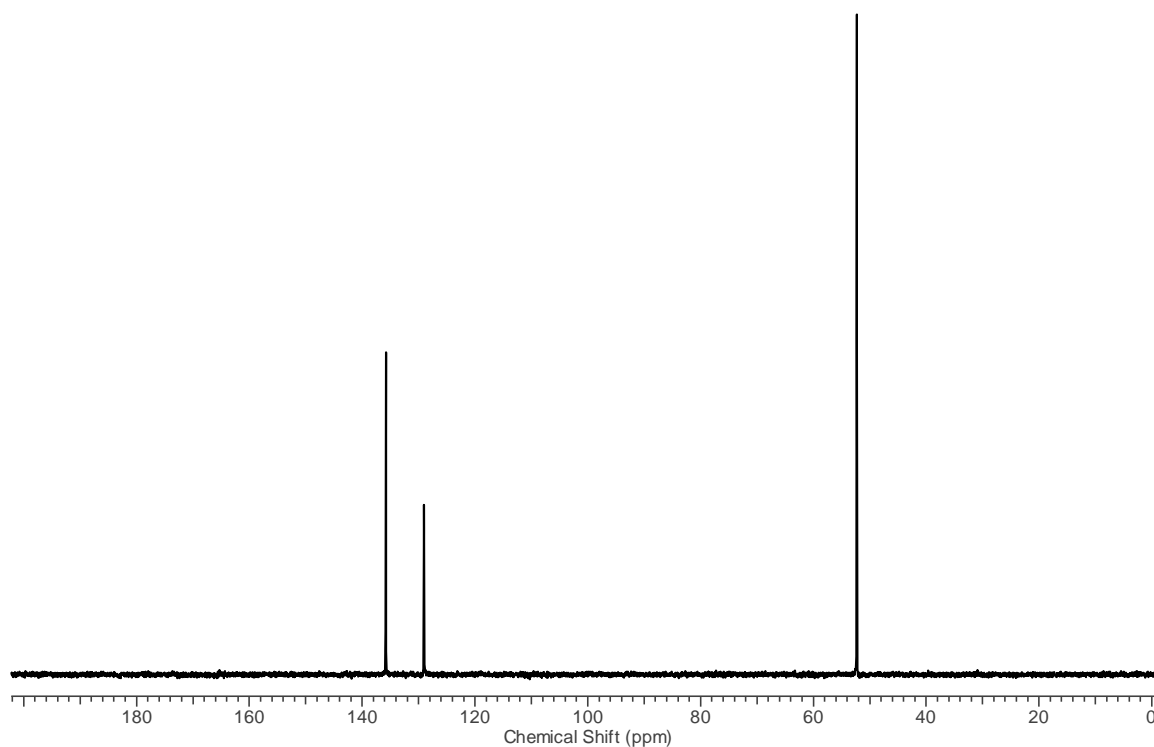
IR spectrum of compound 2



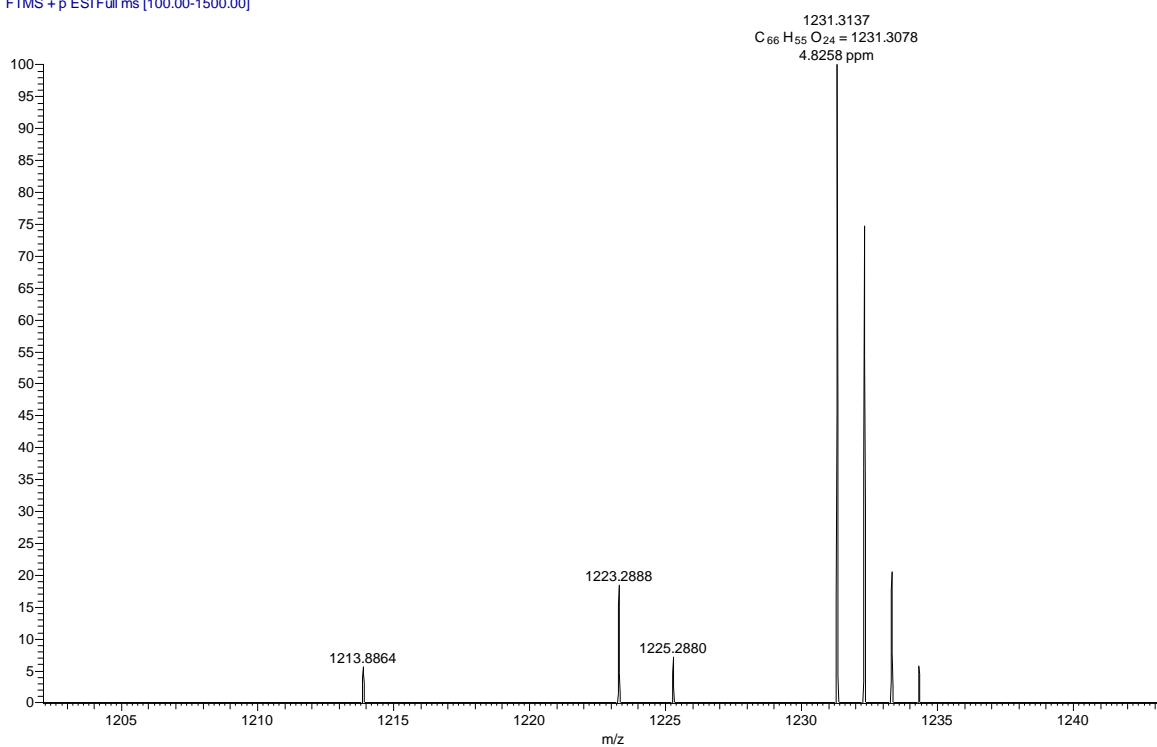
$^1\text{H}$  NMR spectrum of compound **2** ( $\text{CDCl}_3$ , 400 MHz, 298 K)

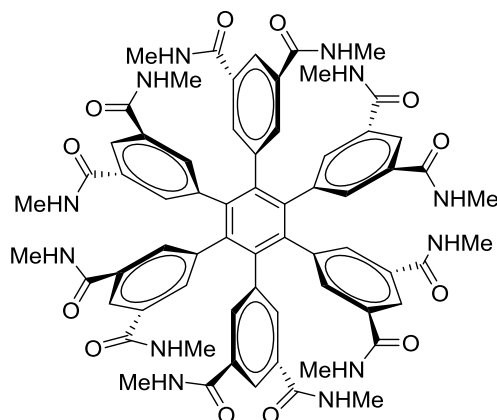


$^{13}\text{C}$  NMR spectrum of compound **2** ( $\text{CDCl}_3$ , 100 MHz, 298 K)

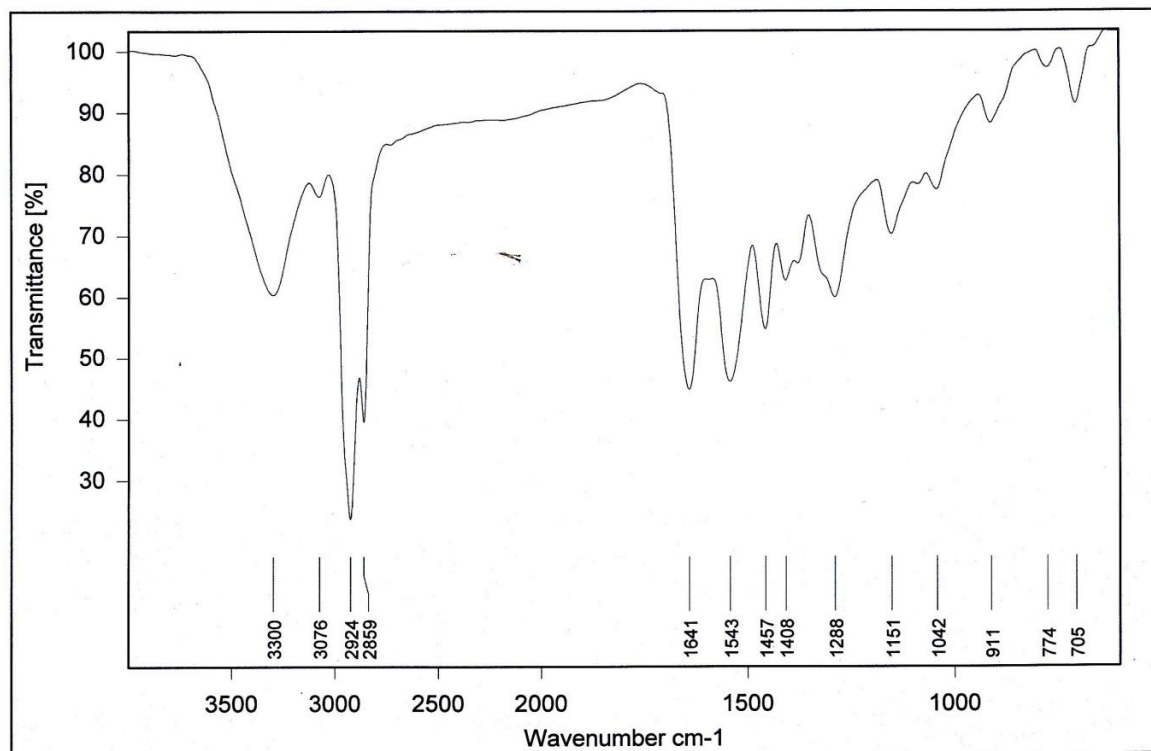
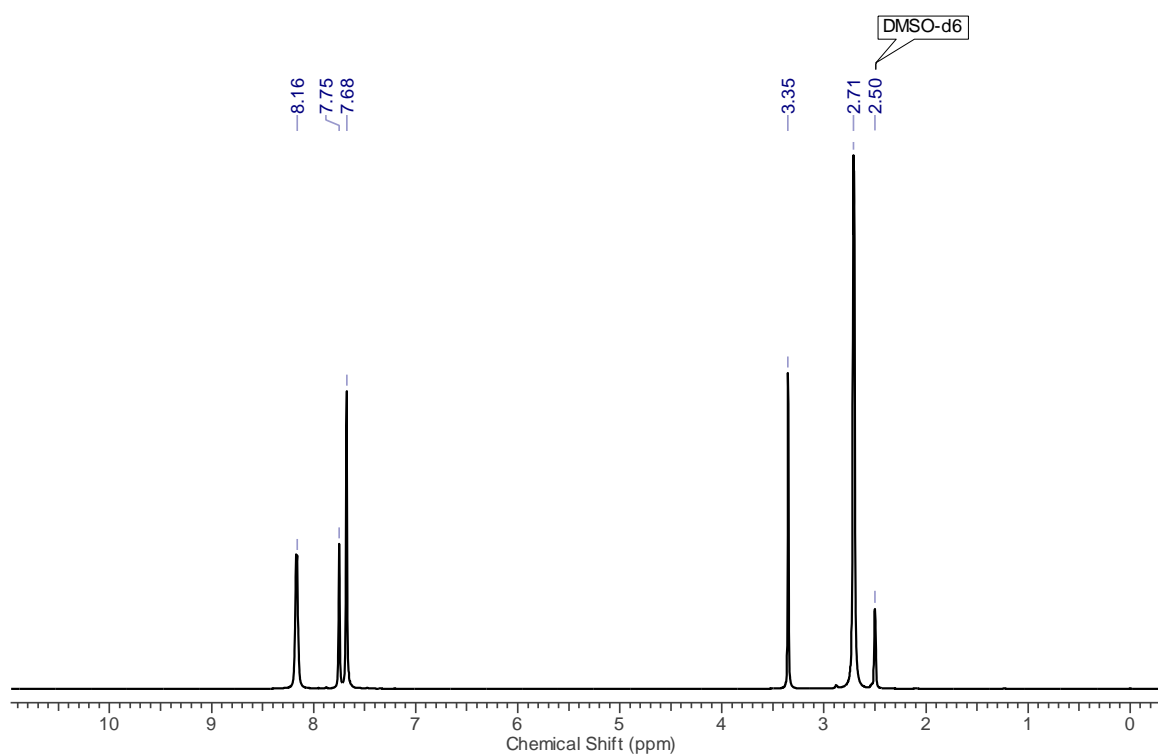
DEPT 135 spectrum of compound **2** (CDCl<sub>3</sub>, 100 MHz, 298 K)

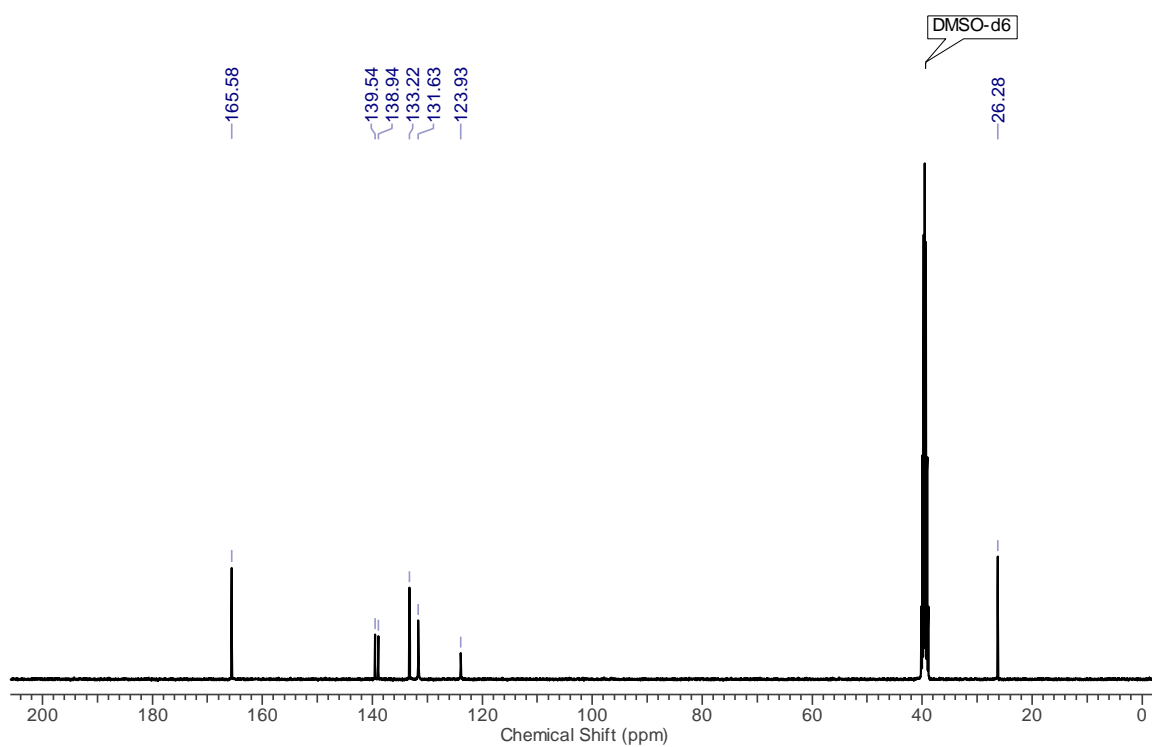
HPB-COOME #197 RT: 0.88 AV: 1 NL: 1.42E6  
T: FTMS + p ESI Full ms [100.00-1500.00]

HRMS of compound **2**

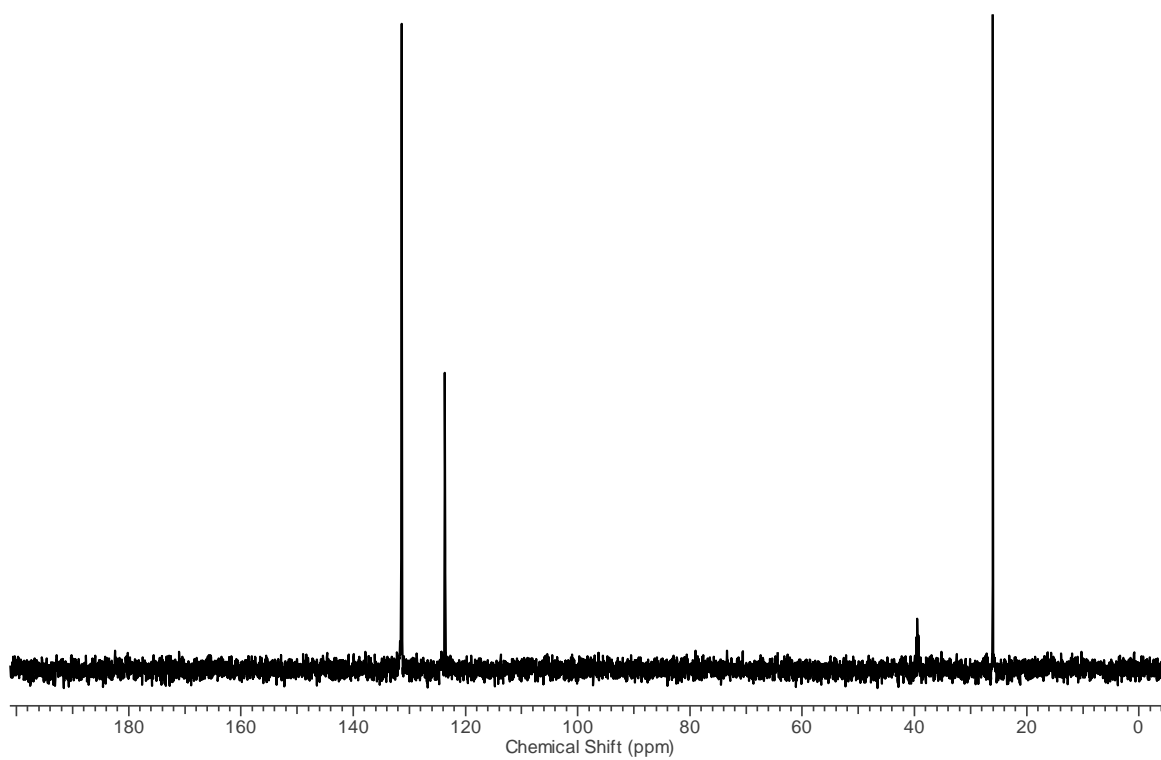
**Compound 3a**

0.1 g (0.0812 mmol) of compound **2** was suspended in a mixture of 2 mL dioxane and 30 mL dry methanolic-methylamine at room temperature. The mixture was heated to 80 °C in stainless steel covered teflon-lined autoclave and further the heating was maintained at the same temperature for 12 h. Then the reaction mixture was slowly cooled to room temperature to obtain compound **3a** as colorless crystals in quantitative yield (0.09 g, 90%). m.p >350 °C (decomposes). IR (CHCl<sub>3</sub>) cm<sup>-1</sup>: 3300, 3076, 2924, 2859, 1641 (C=O), 1543, 1457; <sup>1</sup>H-NMR (400 MHz, DMSO-d<sub>6</sub>) δ: 8.16(q, 12H), 7.75(s, 6H), 7.68(s, 12H), 2.71(d, 36H); <sup>13</sup>C NMR (100 MHz, DMSO-d<sub>6</sub>) δ: 165.58, 139.54, 138.94, 133.22, 131.63, 123.93, 26.28; MALDI-MS (m/z): [M+Na]<sup>+</sup>, [M+K]<sup>+</sup> 1241.0850, 1257.0382. HRMS (m/z): calcd for C<sub>66</sub>H<sub>67</sub>N<sub>12</sub>O<sub>12</sub> [M+H]<sup>+</sup> 1219.4996, found 1219.5054.

IR spectrum of compound **3a**<sup>1</sup>H NMR spectrum of compound **3a** (DMSO-d<sub>6</sub>, 400 MHz, 298 K)

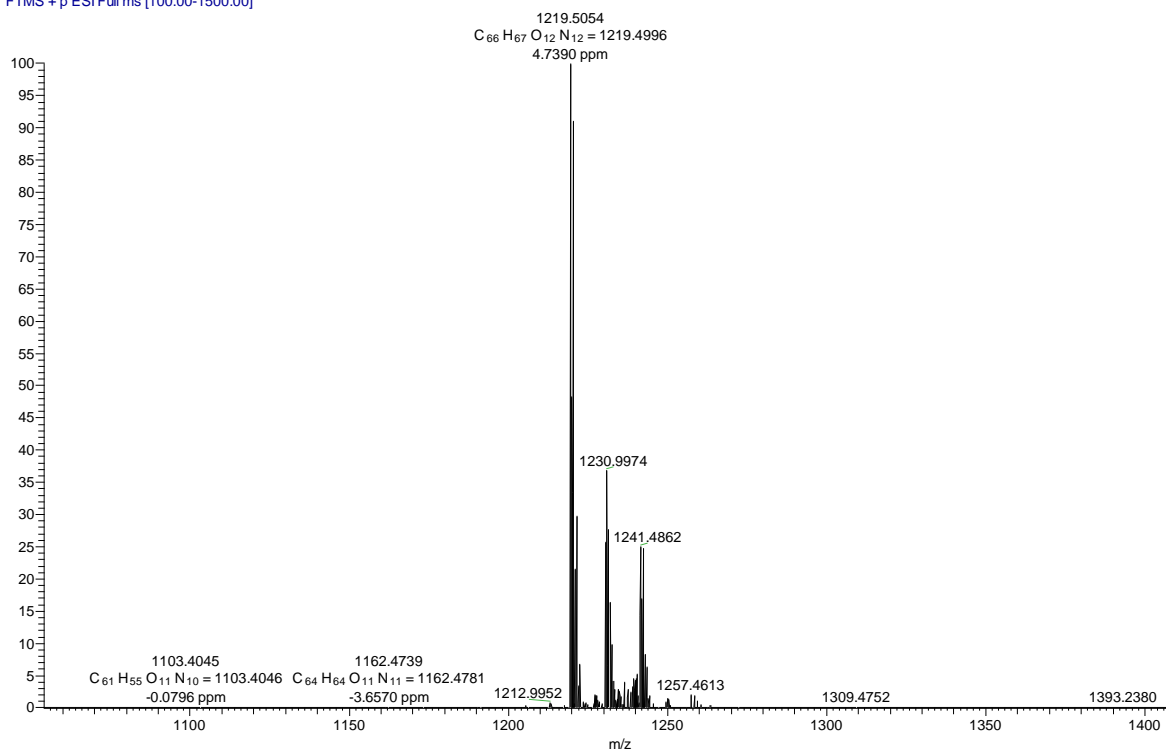


$^{13}\text{C}$  spectrum of compound **3a** ( $\text{DMSO-}d_6$ , 100 MHz, 298 K)



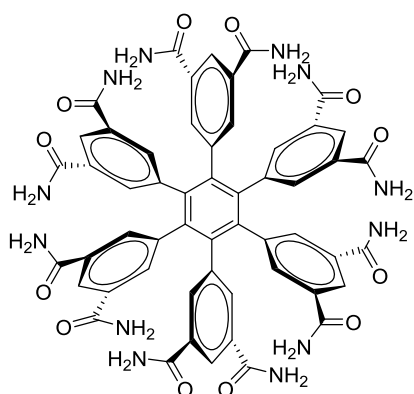
DEPT 135 spectrum of compound **3a** ( $\text{DMSO-}d_6$ , 100 MHz, 298 K)

HPB-COMHME #105 RT: 0.47 AV: 1 NL: 2.11E8  
T: FTMS + p ESI Full ms [100.00-1500.00]



HRMS of compound **3a**

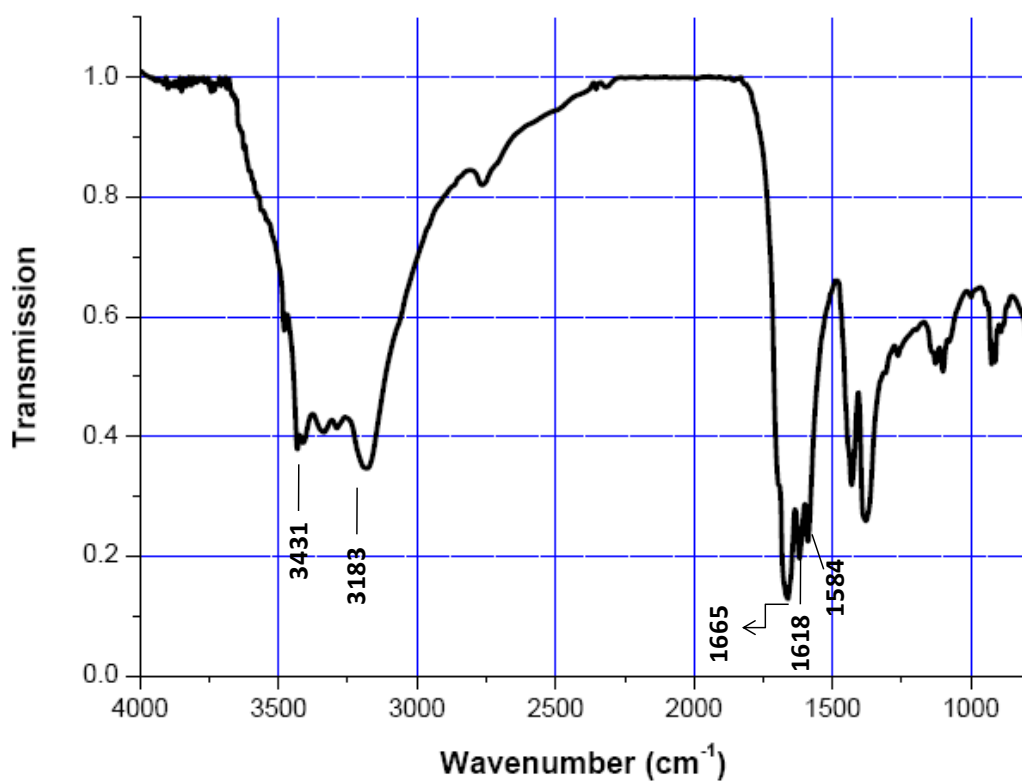
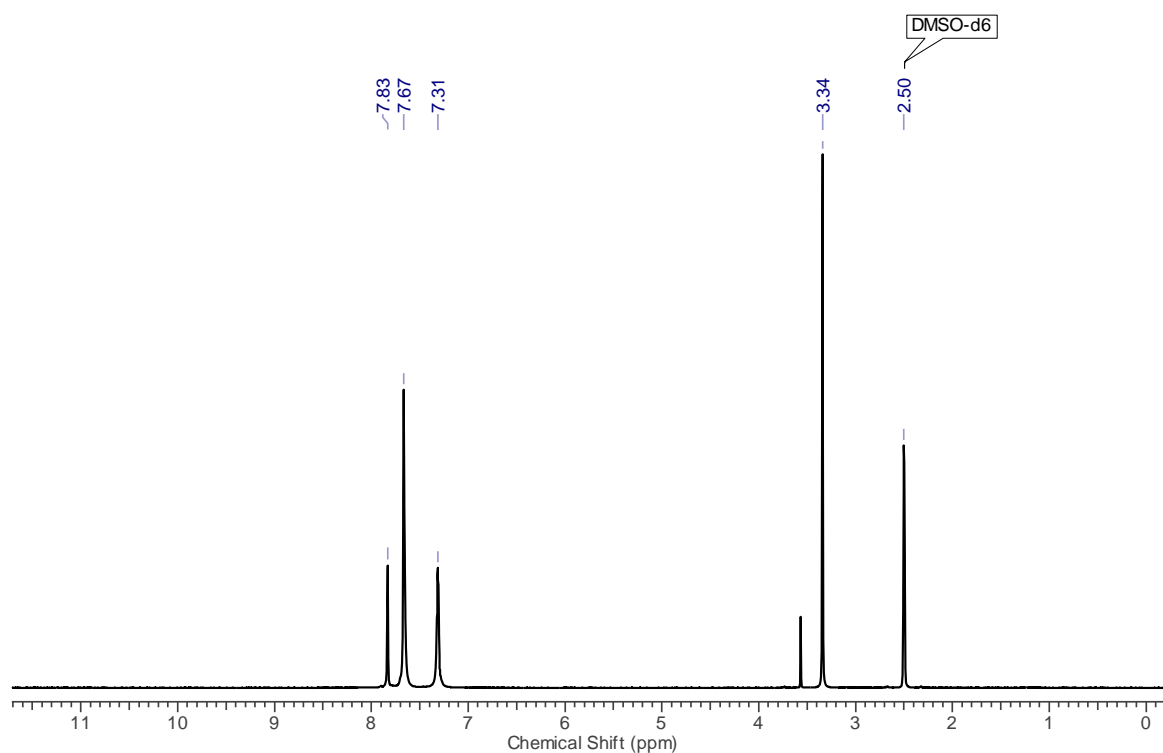
### Compound **3b**

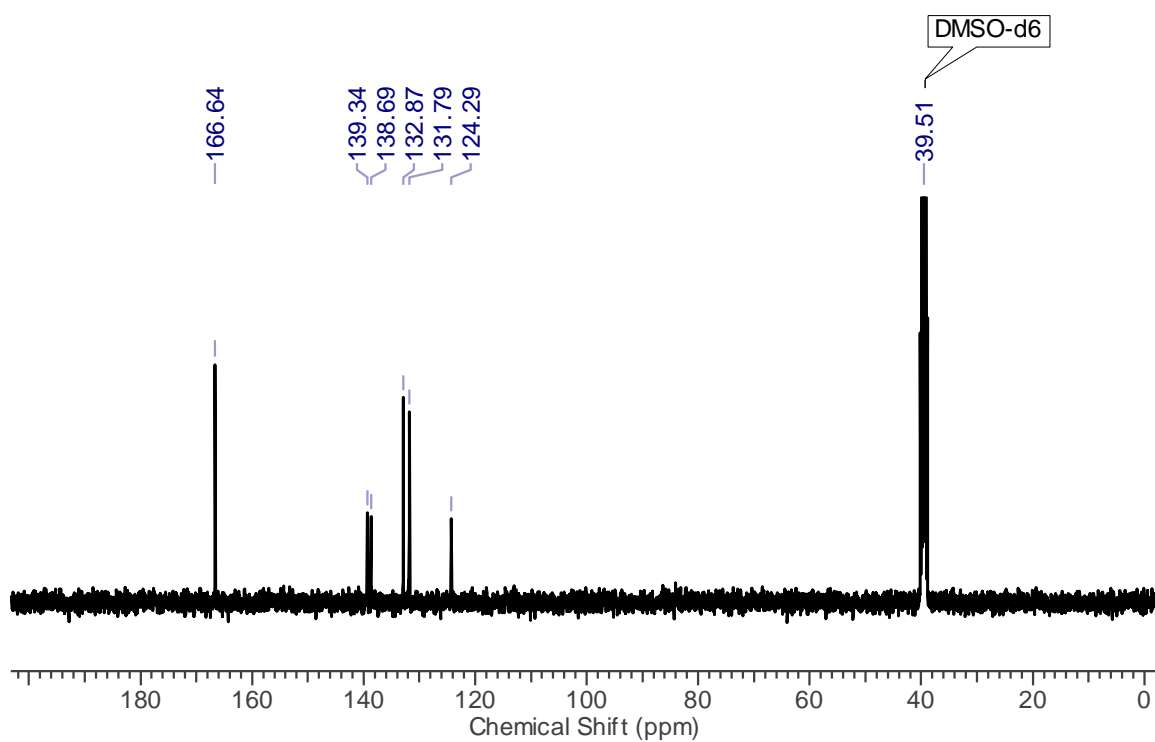


Compound **3b** was synthesized from **2**, following the procedure for **3a**. 0.1 g (0.0812 mmol) of compound **2**, dry methanolic ammonia (35 mL). Yield: 0.079 g (92%). Suitable crystal was subjected for single crystal X-ray diffraction. mp: >350 °C (decomposes); IR (KBr)  $\text{cm}^{-1}$ : 3431, 3183, 1665 (C=O), 1618, 1584;  $^1\text{H-NMR}$  (400 MHz, DMSO- $d_6$ )  $\delta$ : 7.83 (s, 6H), 7.67(s, 24H [12H of Ar, 12H of  $\text{NH}_2$ ]), 7.31(s, 12H);  $^{13}\text{C}$

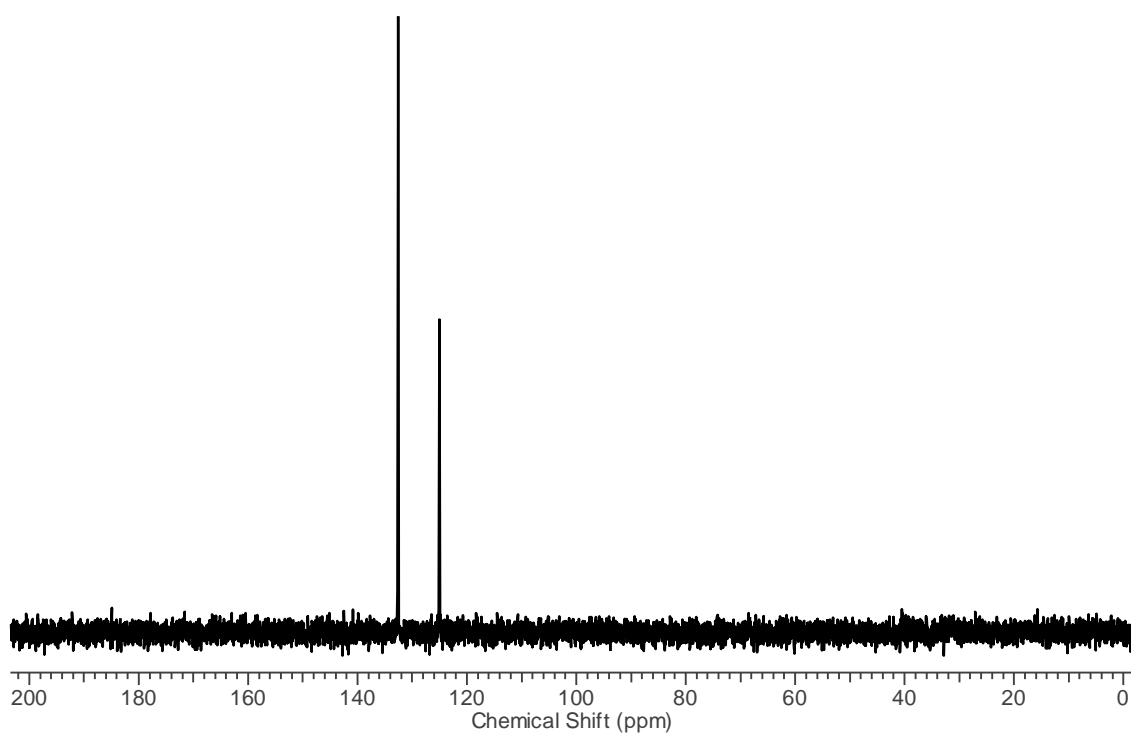
NMR (100 MHz,  $\text{CDCl}_3$ )  $\delta$ : 166.64, 139.34, 138.69, 132.87, 131.79, 124.29; MALDI-MS (m/z):  $[\text{M}+\text{Na}]^+$ ,  $[\text{M}+\text{K}]^+$  found 1073.0458, 1088.0322.



IR spectrum of compound **3b** $^1\text{H}$  NMR spectrum of compound **3b** (DMSO- $d_6$ , 400 MHz, 296.8 K)



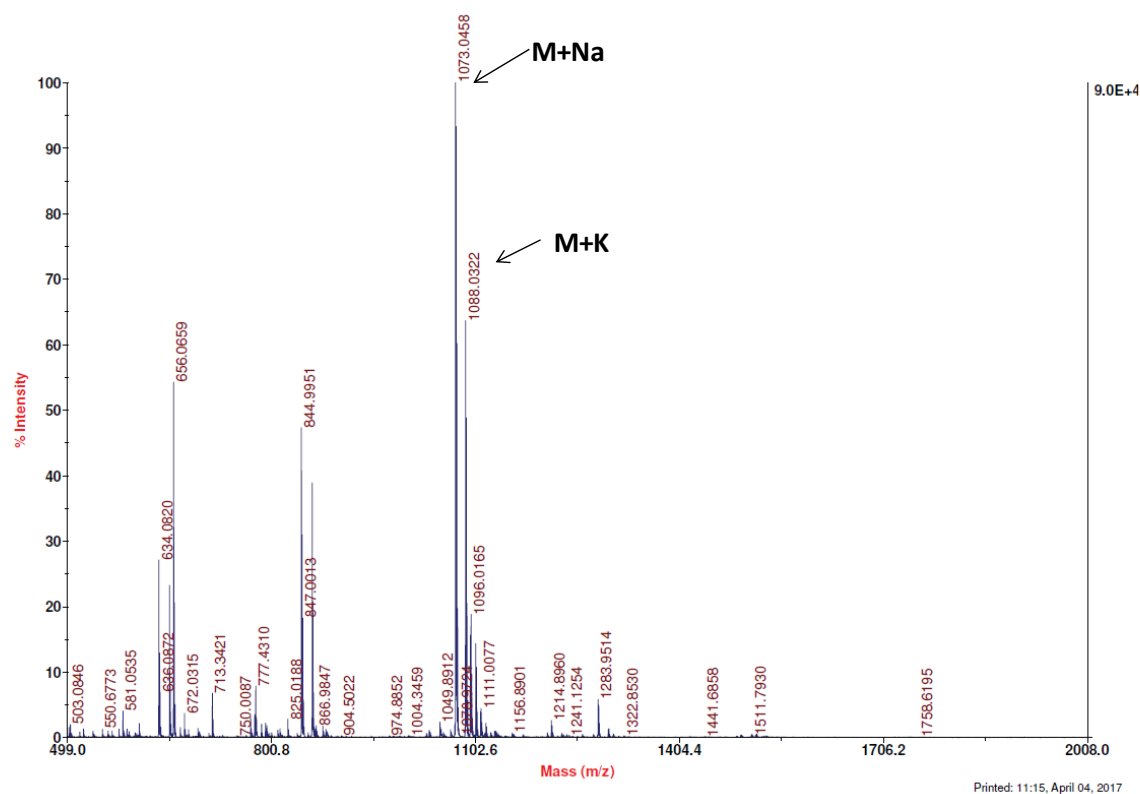
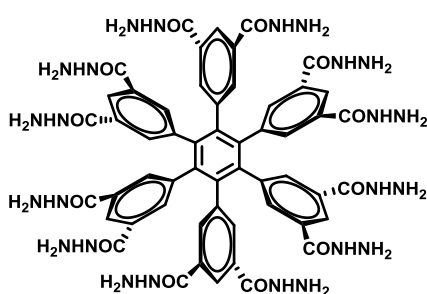
$^{13}\text{C}$  NMR spectrum of compound **3b** (DMSO- $d_6$ , 100 MHz, 343 K)



DEPT 135 spectrum of compound **3b** (DMSO- $d_6$ , 100 MHz, 343 K)

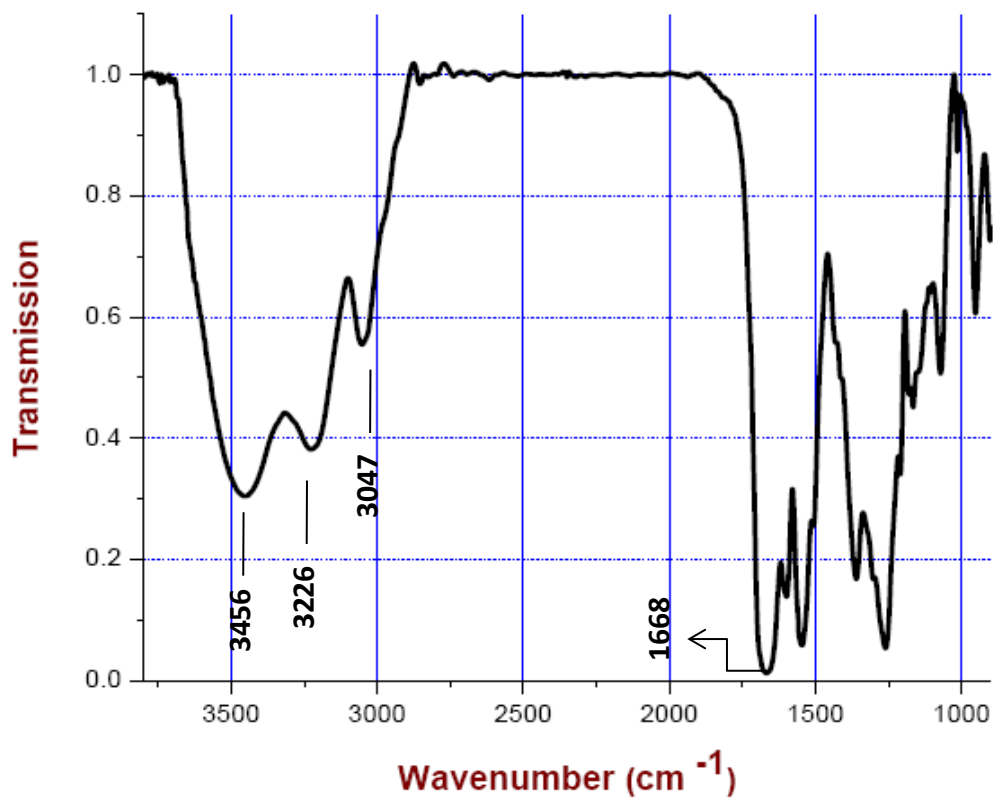
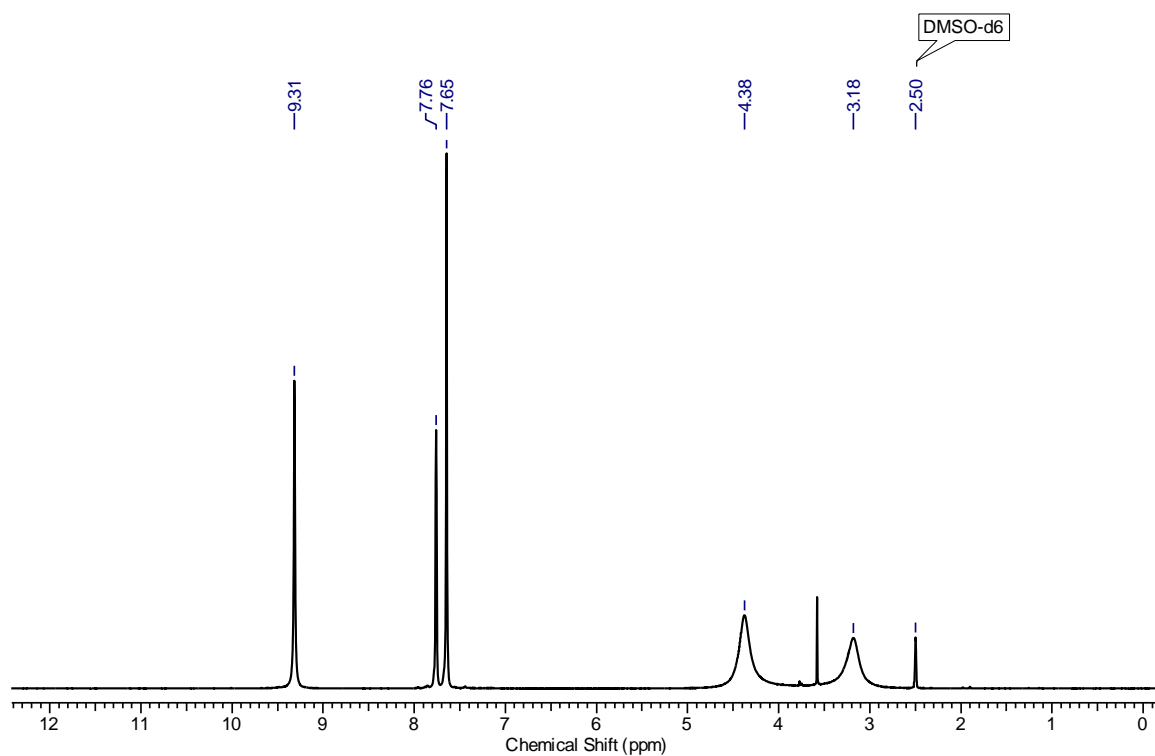
AB Sciex TOF/TOF™ Series Explorer™ 72085

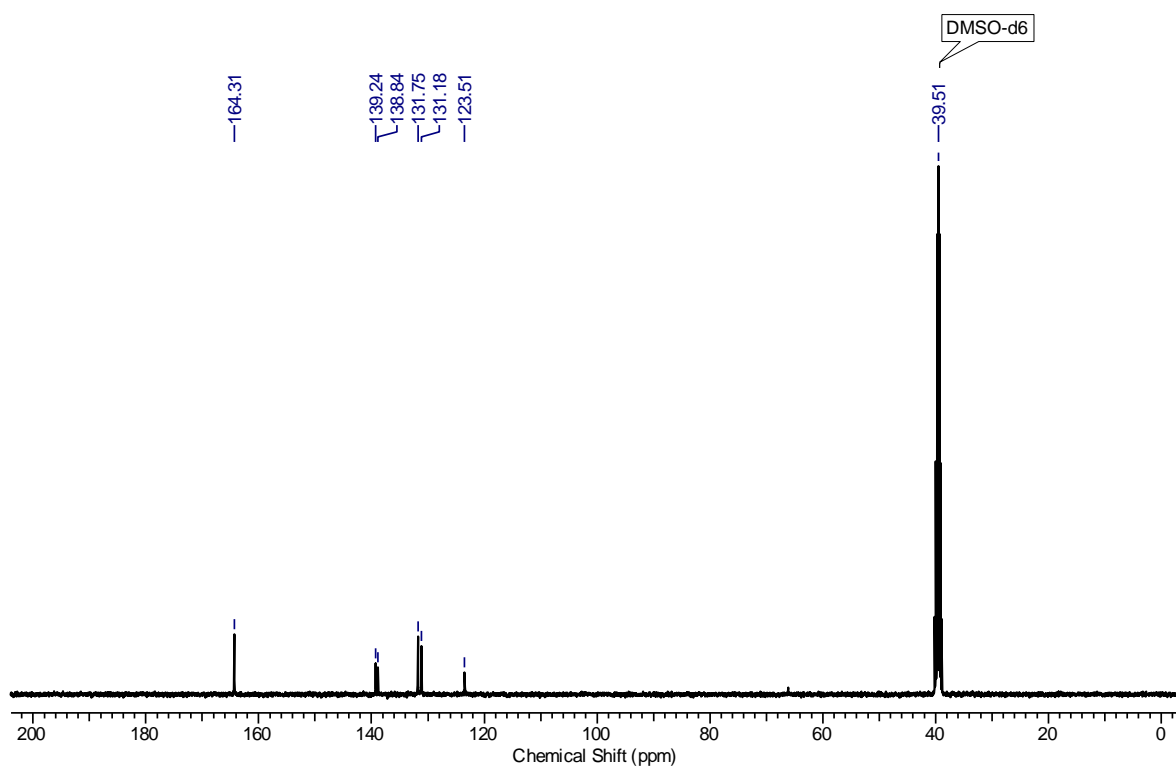
TOF/TOF™ Reflector Spec #1[BP = 1073.0, 90438]

MS (MALDI-TOF) of compound **3b**Compound **3c**

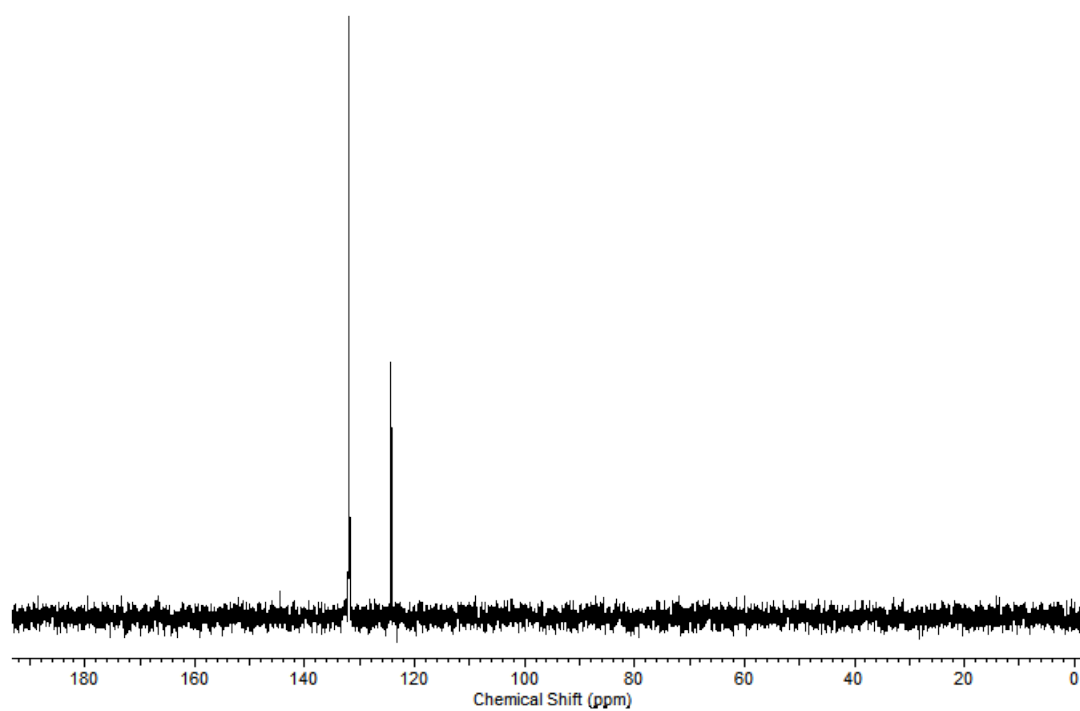
0.1 g of compound **2** was suspended in a mixture of 1 mL dioxane, 2 mL hydrazine in 35 wt. % in H<sub>2</sub>O and 30 mL of methanol. The mixture was heated slowly to 80 °C in stainless steel covered with teflon-lined autoclave and maintained at the same temperature for 12 h. Then the

reaction mixture was cooled to room temperature to get compound **3c** as colorless crystals. Yield: 0.087 g(87%). mp: >400°C (decomposes); IR (KBr) cm<sup>-1</sup>: 3456, 3226, 3047, 1668, 1542, 1359, 1257; <sup>1</sup>H-NMR (400 MHz, DMSO-d<sub>6</sub>) δ: 9.31(s, 12H), 7.76(s, 6H), 7.65(s, 12H), 4.38(bs, 24H); <sup>13</sup>C-NMR (100 MHz, DMSO-d<sub>6</sub>) δ: 164.31, 139.24, 138.84, 131.75, 131.18, 123.51; HRMS (*m/z*): calcd for C<sub>54</sub>H<sub>55</sub>N<sub>24</sub>O<sub>12</sub> [M+H]<sup>+</sup> 1231.4426, found 1231.4403.

IR spectrum of compound **3c** $^1\text{H}$  NMR spectrum of compound **3c** (DMSO-*d*<sub>6</sub>, 400MHz, 298 K)

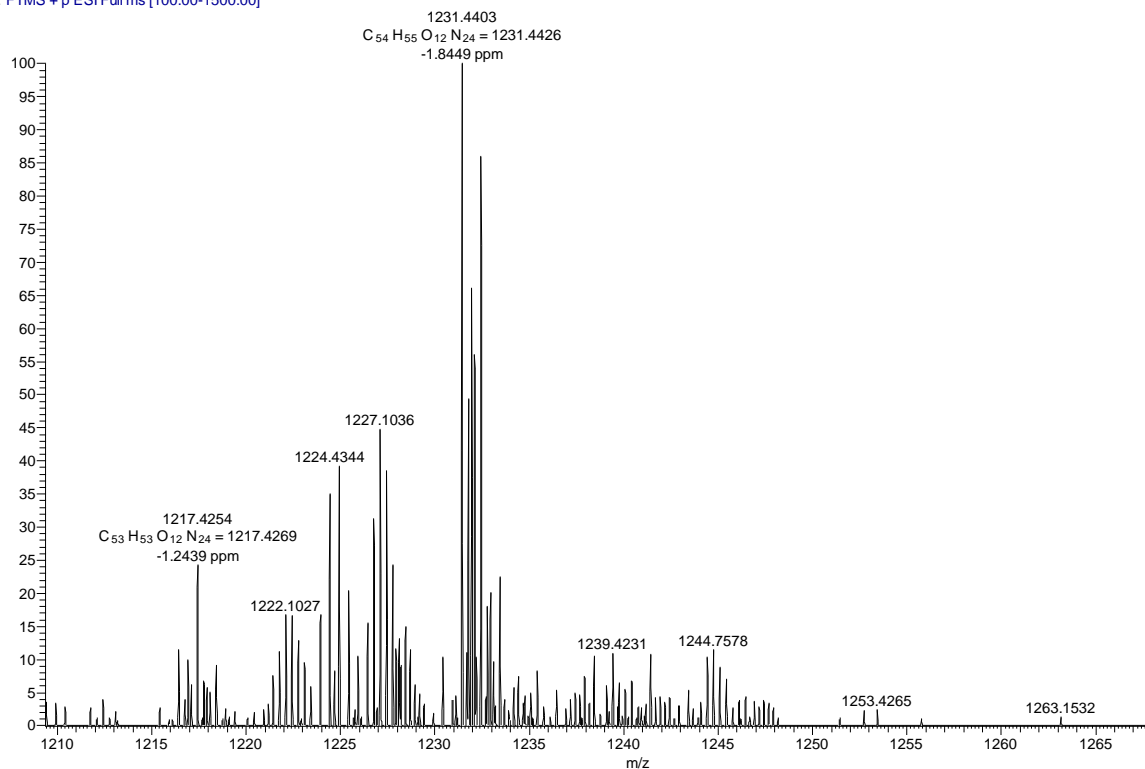


$^{13}\text{C}$  NMR spectrum of compound **3c** (DMSO-*d*<sub>6</sub>, 100MHz, 298 K)

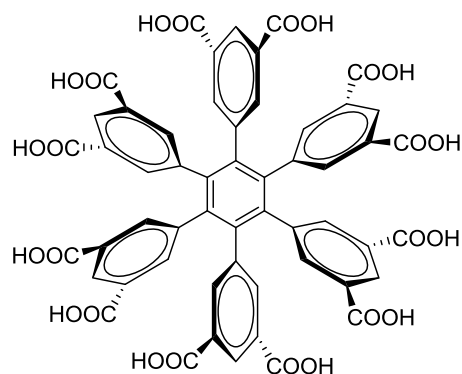


DEPT 135 spectrum of compound **3c** (DMSO-*d*<sub>6</sub>, 100MHz, 298 K)

HPB-CONHMH2 #95 RT: 0.42 AV: 1 NL: 3.38E7  
T: FTMS + p ESI Full ms [100.00-1500.00]

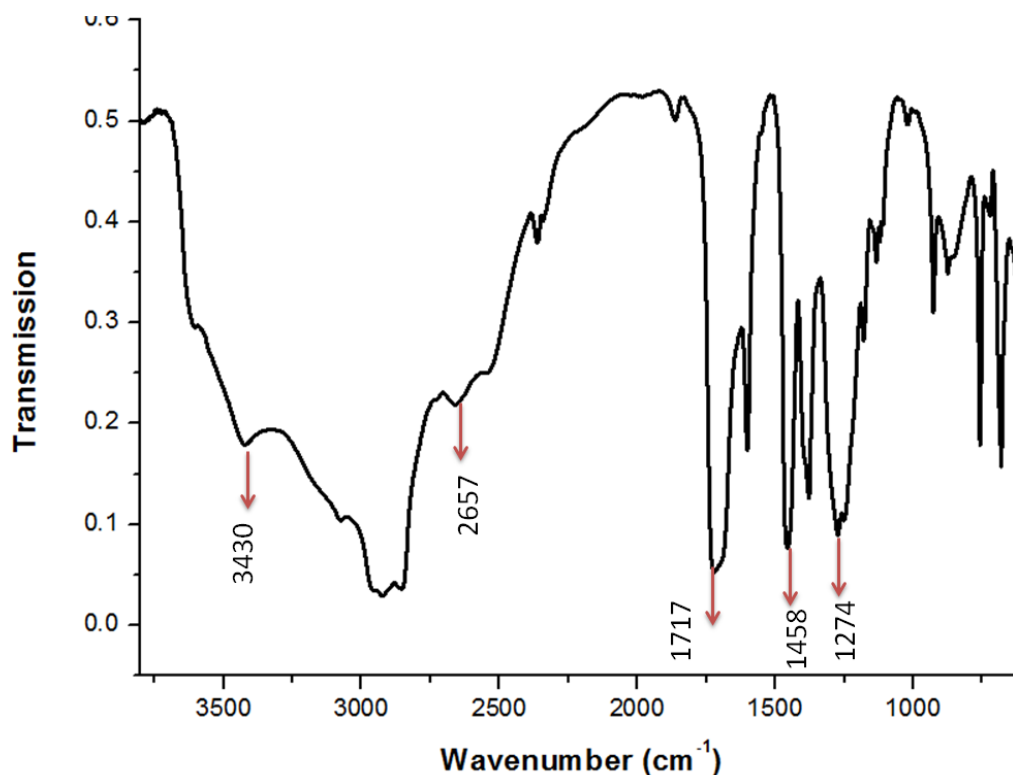


### Compound **3d**



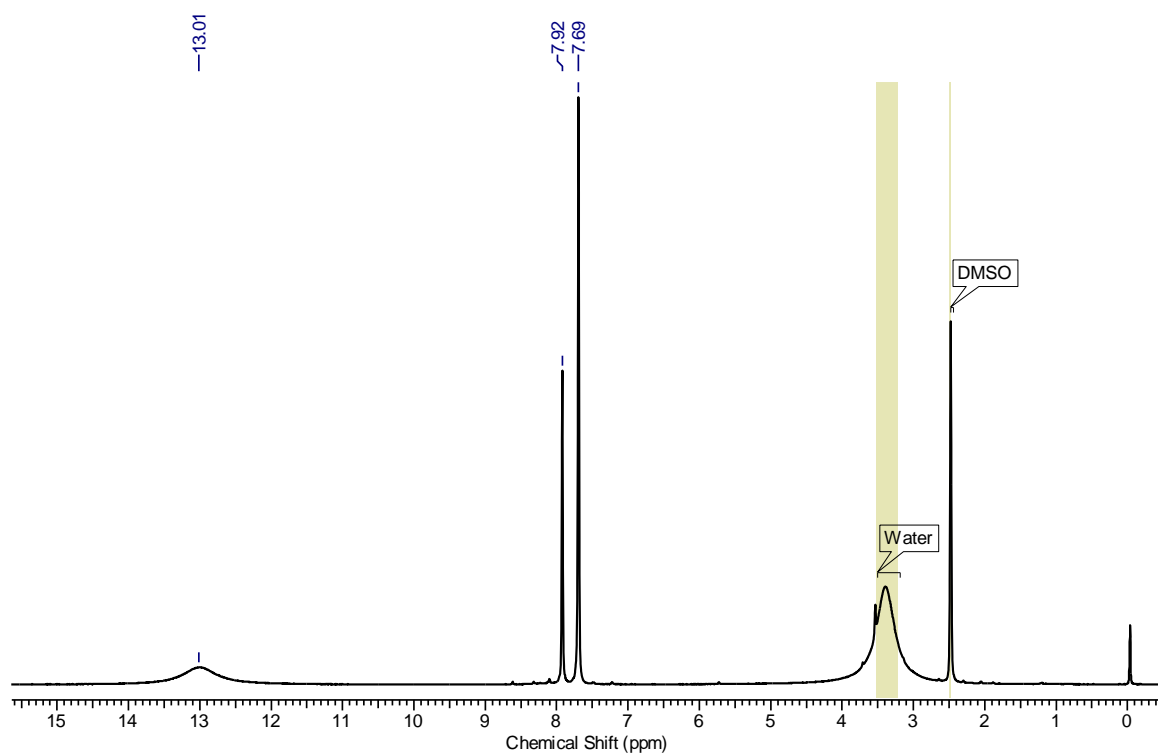
compound **2** (5 g, 4.06 mmol) and KOH (6.83 g, 121.839 mmol) were suspended in aqueous dioxane (dioxane : water, 30 mL :20 mL). The mixture was heated to 120 °C in stainless steel covered with teflon-lined autoclave and heating was maintained at the same temperature for 24 h. Then, the reaction mixture was slowly cooled to room temperature and ice-chilled water was added until the entire mixture became a clear homogeneous solution. The aqueous solution was acidified with concentrated aqueous hydrochloric acid to precipitate the solid. The solid was filtered over a Buchner funnel and washed with

water several times. The wet solid was then dried in air at 60 °C overnight and then dried over P<sub>2</sub>O<sub>5</sub> to obtain white colored solid. Yield: 3.9 g (90 %). mp: >350 °C, decomposes; IR (nujol) (cm<sup>-1</sup>): 3430, 2657, 1717, 1458, 1274; <sup>1</sup>H NMR (400MHz, DMSO-*d*<sub>6</sub>) δ: 13.00 (br. s., 12H), 7.92 (br. s., 6H), 7.69 (br. s., 12H); <sup>13</sup>C NMR (101MHz, DMSO-*d*<sub>6</sub>) δ: 166.0, 139.8, 138.8, 135.8, 130.1, 127.7; MALDI-TOF/TOF: 1084.9149 [M+Na]<sup>+</sup>.

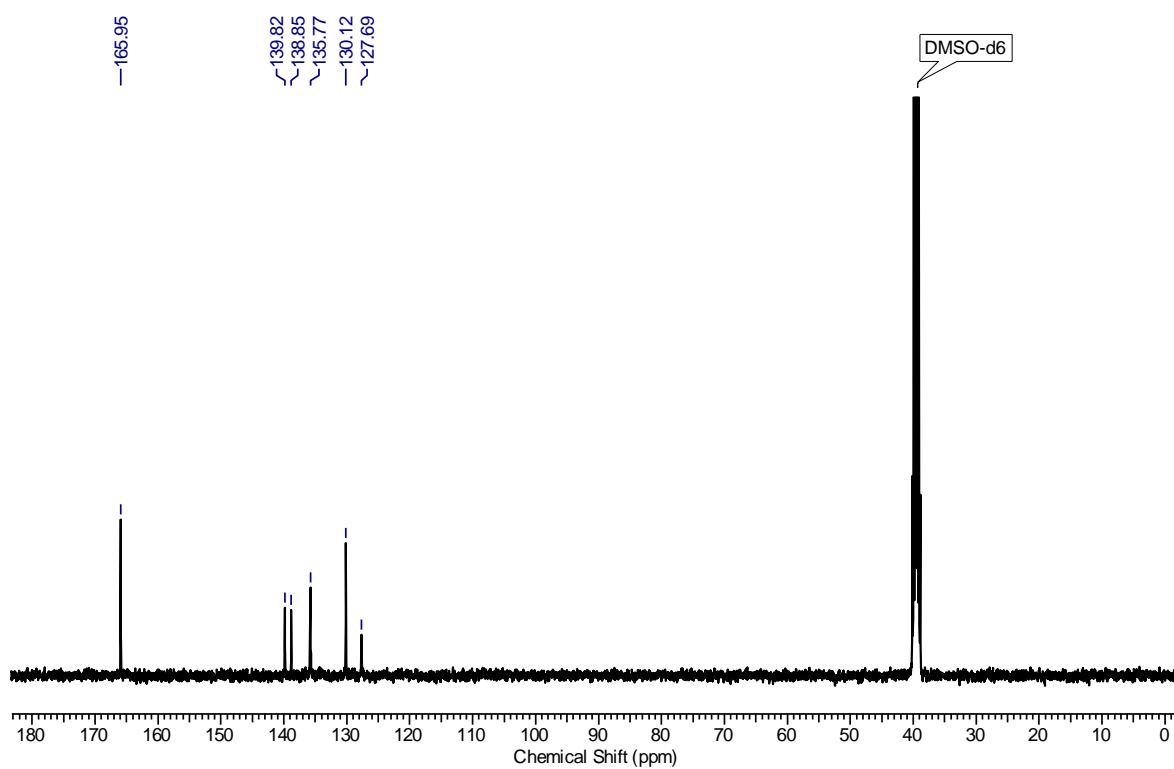


IR spectrum of compound **3d**

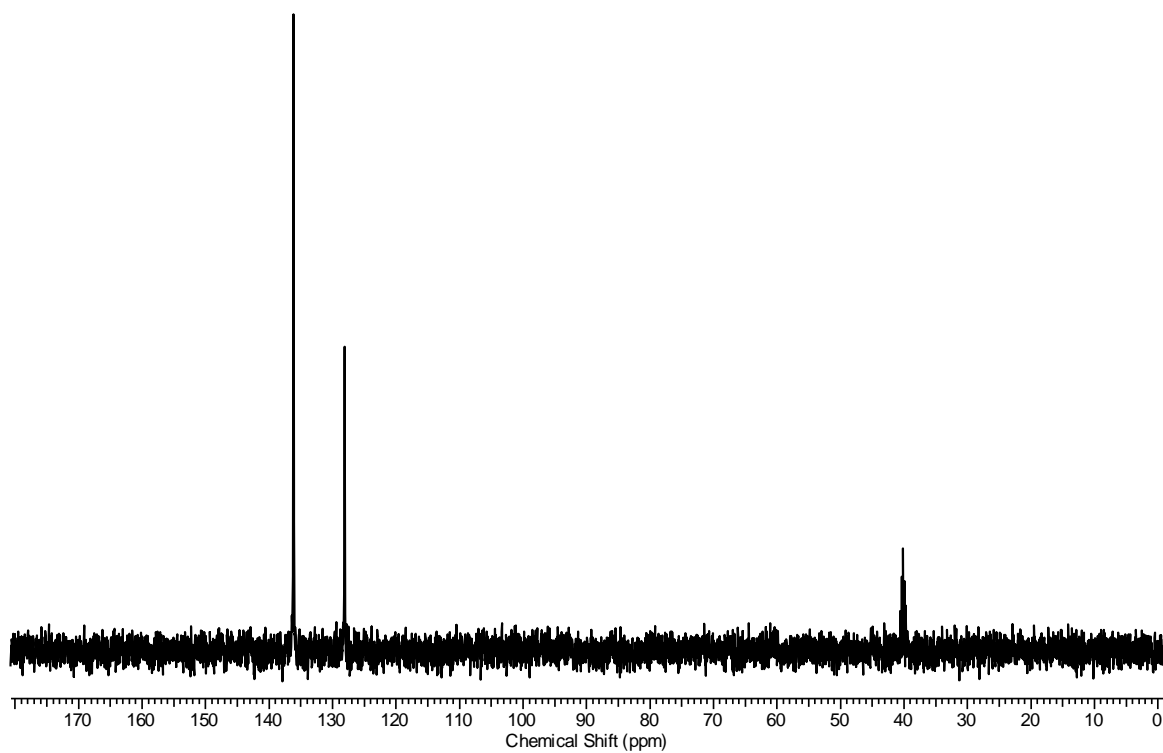




$^1\text{H}$  NMR spectrum of compound **3d** (DMSO- $d_6$ , 400MHz, 298 K)



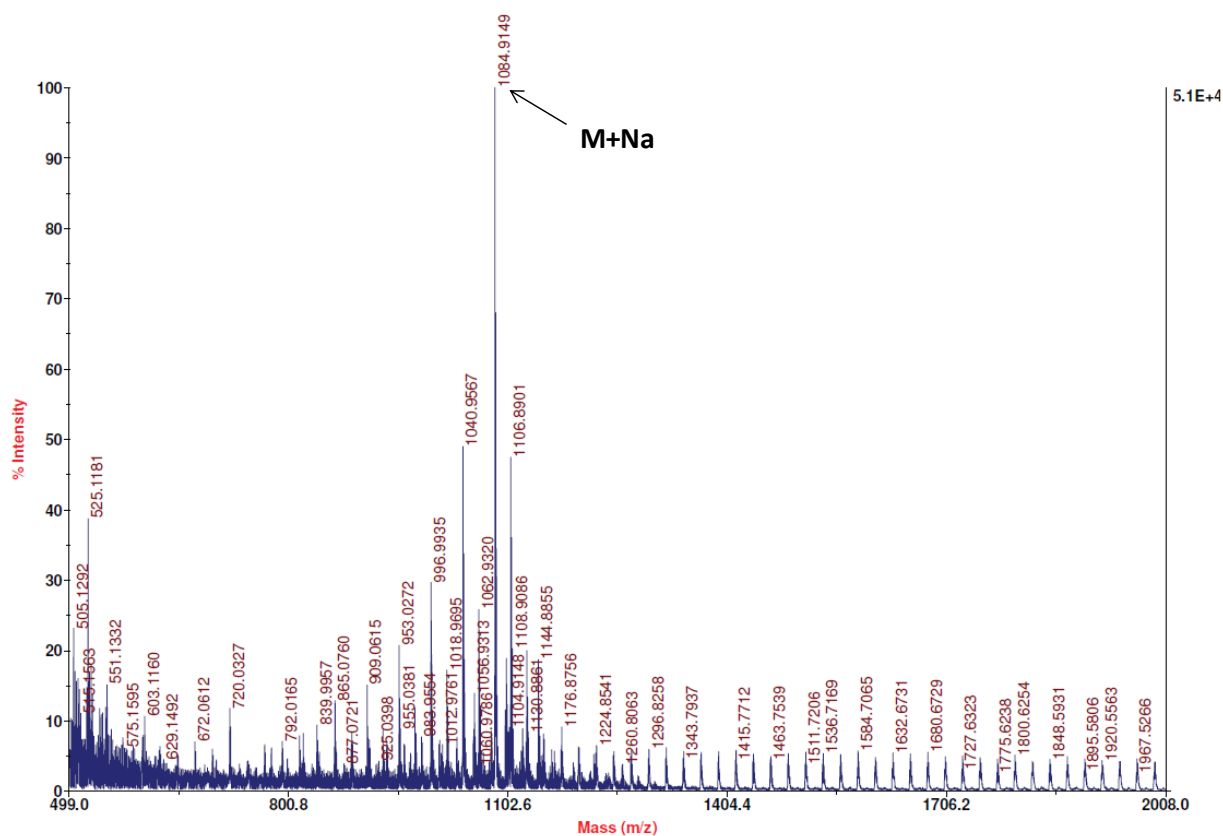
$^{13}\text{C}$  NMR spectrum of compound **3d** (DMSO- $d_6$ , 100 MHz, 343 K)



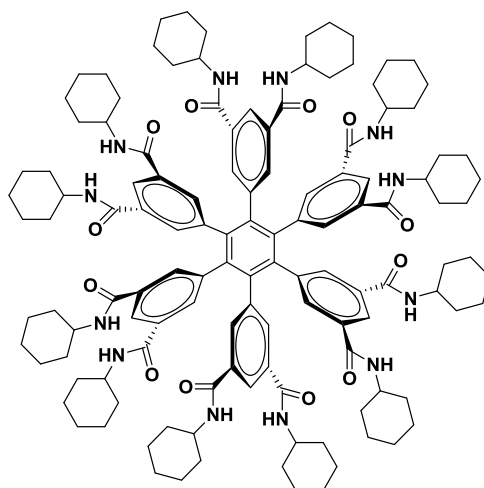
DEPT 135 spectrum of compound **3d** (DMSO-*d*<sub>6</sub>, 100MHz, 298 K)

AB Sciex TOF/TOF™ Series Explorer™ 72085

TOF/TOF™ Reflector Spec #1[BP = 1084.9, 50599]

MS (MALDI-TOF) of compound **3d**

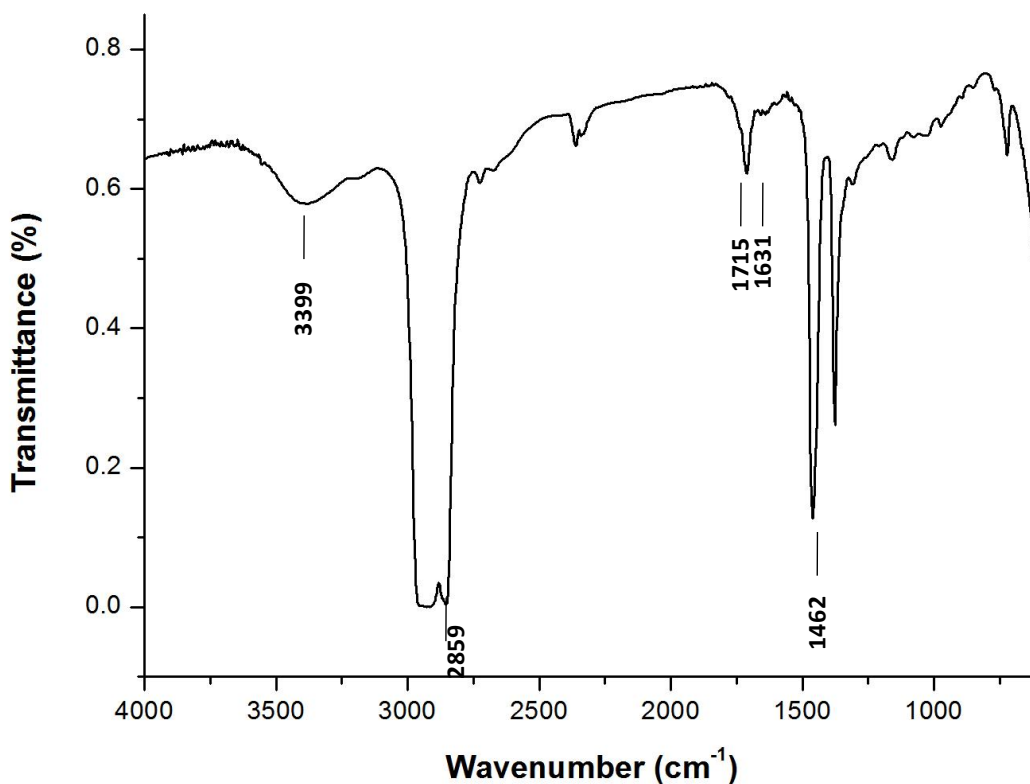
### Compound **4a**



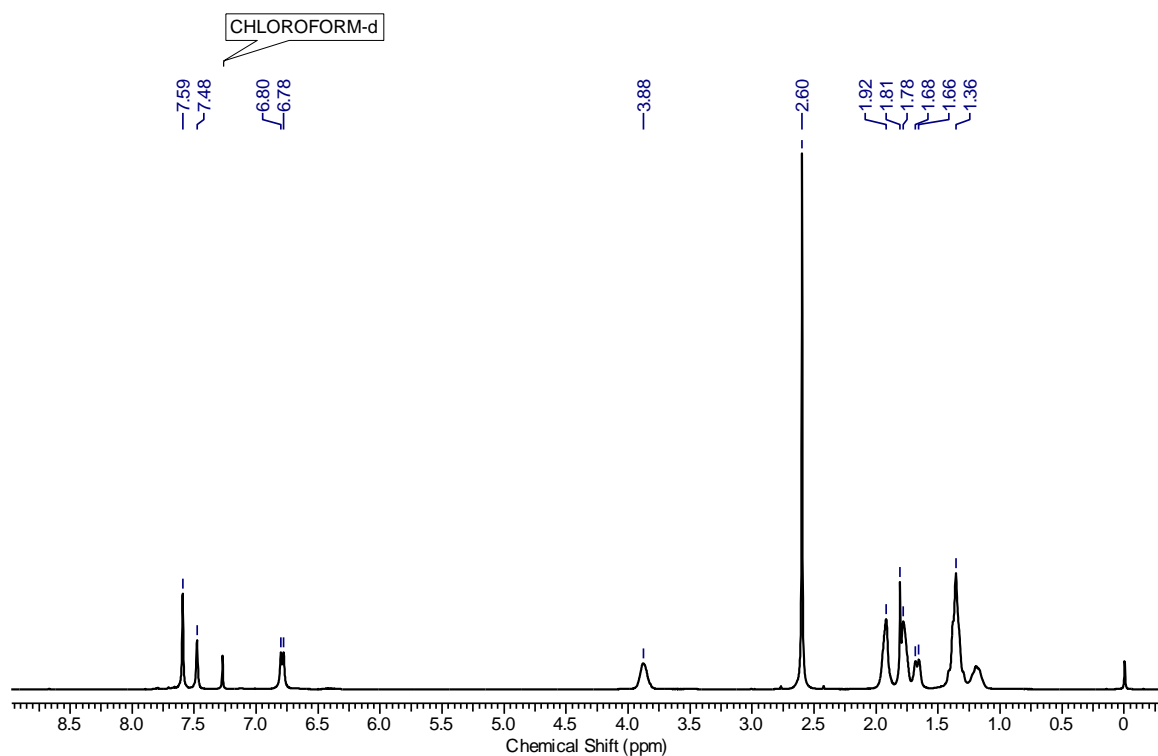
To a suspension of **3d** (0.06 g, 0.0565 mmol) and DIEA (0.177 mL, 1.01 mmol) in DMSO (3 mL) HBTU (0.385, 1.01 mmol) was added and the mixture was stirred at room temperature for 5 minutes to form clear solution. Then, cyclohexylamine (0.098 mL,

1.01 mmol) was added and stirring was continued for 12 h. After completion of the reaction, the reaction mixture was diluted with ice-chilled water and thrice extracted with dichloromethane. The combined organic phases were dried over sodium sulfate and evaporated *in vacuo*. The residue obtained was purified by column chromatography (eluent: AcOEt/ PET ether, 50:50 v/v,  $R_f = 0.5$ ) to afford **4a** (0.091 g, 79%) as a fluffy white solid.

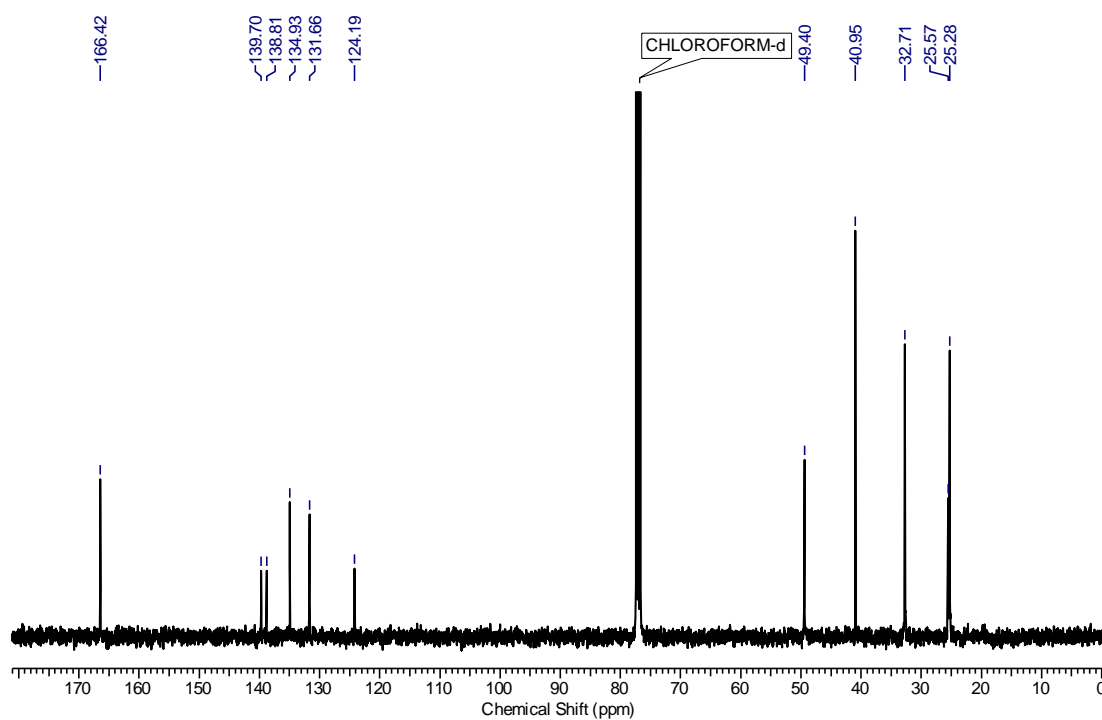
mp: 310 °C; IR (Nujol) ( $\text{cm}^{-1}$ ): 3399, 2859, 1715, 1631, 1462;  $^1\text{H-NMR}$  (400MHz,  $\text{CDCl}_3$ )  $\delta$ : 7.59 (s, 12H), 7.48 (s, 6H), 6.79 (d,  $J = 7.9$  Hz, 12H), 3.88 (br. s., 12H), 1.92 (br. s., 24H), 1.83 - 1.73 (m, 24H), 1.67 (d,  $J = 11.0$  Hz, 12H), 1.36 (br. s., 48H), 1.19 (br. s., 12H);  $^{13}\text{C-NMR}$  (101MHz,  $\text{CDCl}_3$ )  $\delta$ : 166.4, 139.7, 138.8, 134.9, 131.7, 124.2, 49.4, 40.9, 32.7, 25.6, 25.3; MALDI-TOF/TOF: 2057.8196  $[\text{M}+\text{Na}]^+$ , 2074.2876  $[\text{M}+\text{K}]^+$ ; Elemental analysis calculated for  $\text{C}_{126}\text{H}_{162}\text{N}_{12}\text{O}_{12}$ : C, 74.3; H, 8.02; N, 8.25. Found: C, 74.9; H, 8.09; N, 8.10.



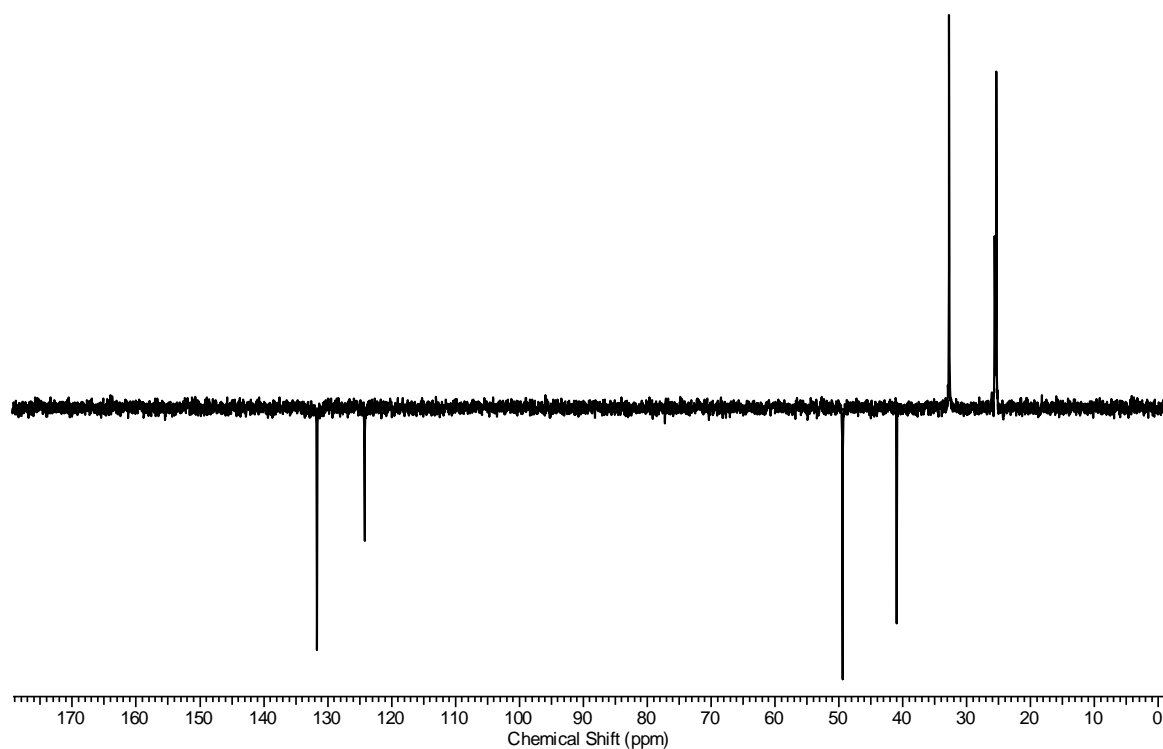
IR spectrum of compound **4a**



$^1\text{H}$  NMR spectrum of compound **4a** ( $\text{CDCl}_3$ , 400MHz, 298 K). Note: Peak at  $\delta=2.60$  corresponding to DMSO (compound **4a** recrystallized from DMSO and then NMR was recorded).



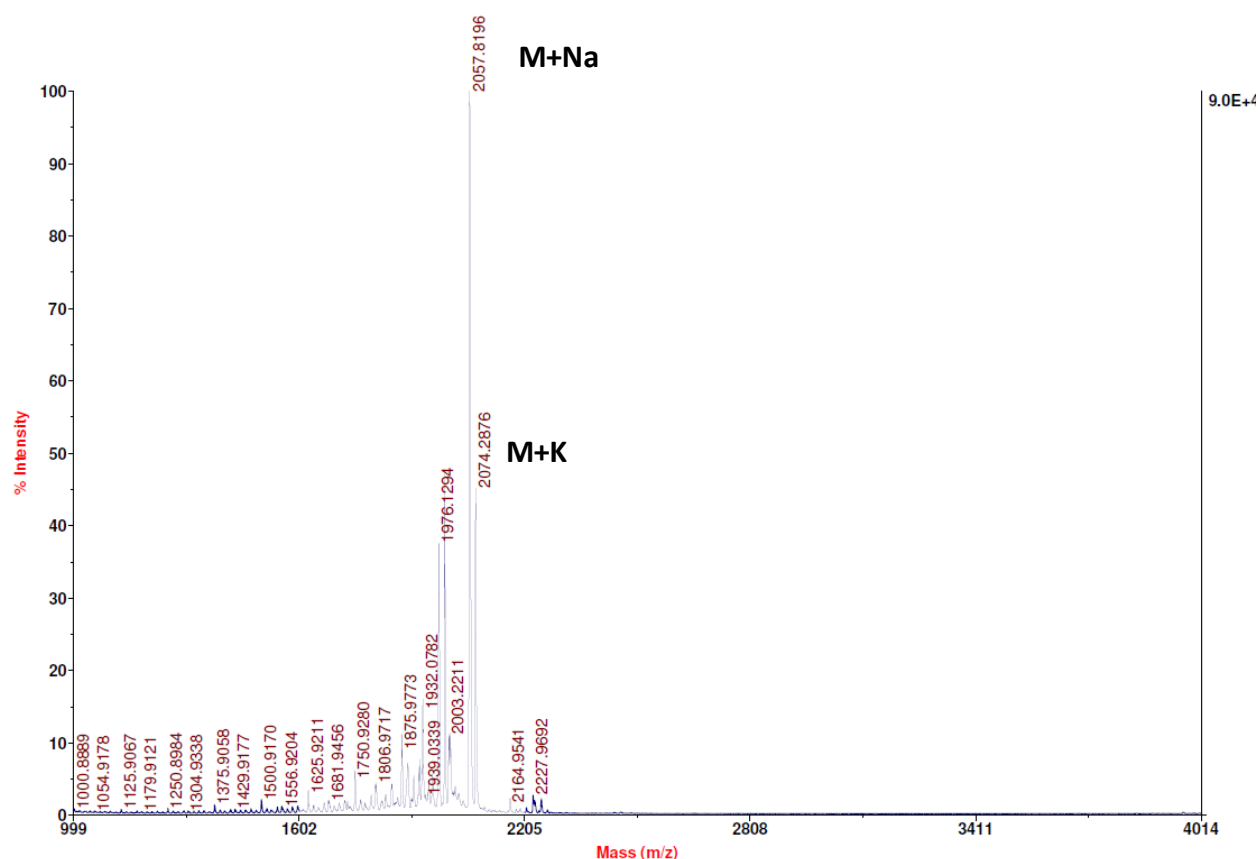
$^{13}\text{C}$  NMR spectrum of compound **4a** ( $\text{CDCl}_3$ , 100 MHz, 343 K). Note: Peak at  $\delta=40.95$  corresponding to DMSO (compound **4a** recrystallized from DMSO and then NMR was recorded).



DEPT 135 spectrum of compound **4a** ( $\text{CDCl}_3$ , 100MHz, 298 K). *Note:* Peak at  $\delta=40.95$  corresponding to DMSO (compound **4a** recrystallised from DMSO and then NMR was recorded).

AB Sciex TOF/TOF™ Series Explorer™ 72085

TOF/TOF™ Reflector Spec #1[BP = 2058.2, 89945]

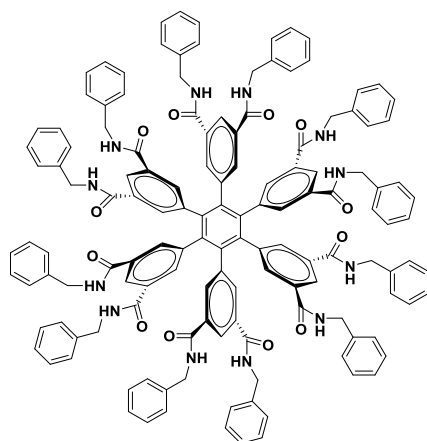


V:\2017\DR GJ SANJAYAN\30-3-2017\HPB (CY)12.4.T2D

Printed: 20:10, March 30, 2017

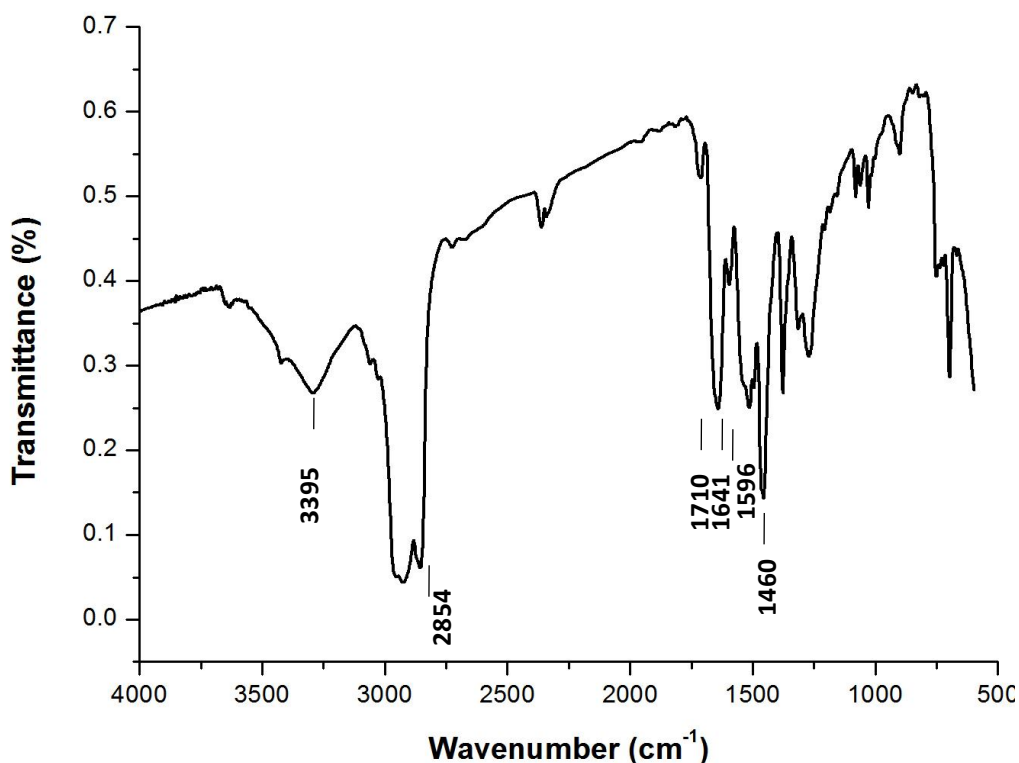
MS (MALDI-TOF) of compound **4a**

### Compound **4b**



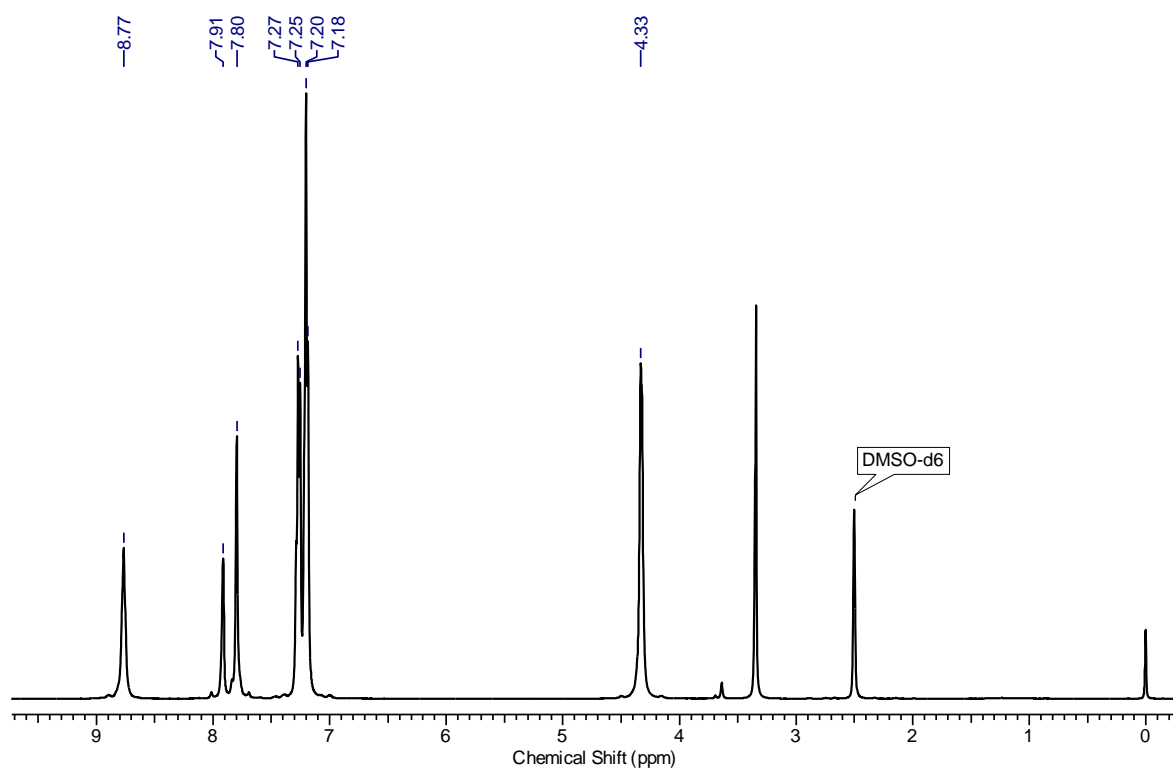
To a suspension of **3d** (0.06 g, 0.0565 mmol) and DIEA (0.177 mL, 1.01 mmol) in DMSO (3 mL) HBTU (0.385, 1.01 mmol) was added and the mixture was stirred at room

temperature for 5 minutes to form clear solution. Then, benzylamine (0.11 mL, 1.01 mmol) was added and stirring was continued for 12 h. After completion of the reaction, the reaction mixture was diluted with ice-chilled water and thrice extracted with ethylacetate. The combined organic phases were dried over sodium sulfate and evaporated *in vacuo*. The residue obtained was purified by column chromatography (eluent: AcOEt/PET ether, 70:30 v/v,  $R_f=0.5$ ) to afford **4b** (0.088 g, 73%) as a white solid. mp:172-174 °C; IR (*Nujol*)  $\text{cm}^{-1}$ : 3395, 2854, 1710, 1641, 1596, 1460;  $^1\text{H}$  NMR (400MHz, DMSO- $d_6$ )  $\delta$ : 8.77 (br. s., 12H), 7.91 (br. s., 6H), 7.80 (br. s., 12H), 7.33 - 7.12 (m, 60H), 4.33 (br. s., 24 H);  $^{13}\text{C}$  NMR (101MHz, DMSO- $d_6$ )  $\delta$ : 165.3, 139.6, 139.2, 139.0, 133.3, 132.0, 128.3, 127.0, 126.7, 124.4, 42.6; MALDI-TOF/TOF: 2153.9270 ( $\text{M}+\text{Na}$ ) $^+$ , 2170.4648 ( $\text{M}+\text{K}$ ) $^+$ ; Elemental analysis calculated for  $\text{C}_{138}\text{H}_{114}\text{N}_{12}\text{O}_{12}$ : C, 77.73; H, 5.39; N, 7.88. Found: C, 77.79; H, 5.44; N, 7.82.

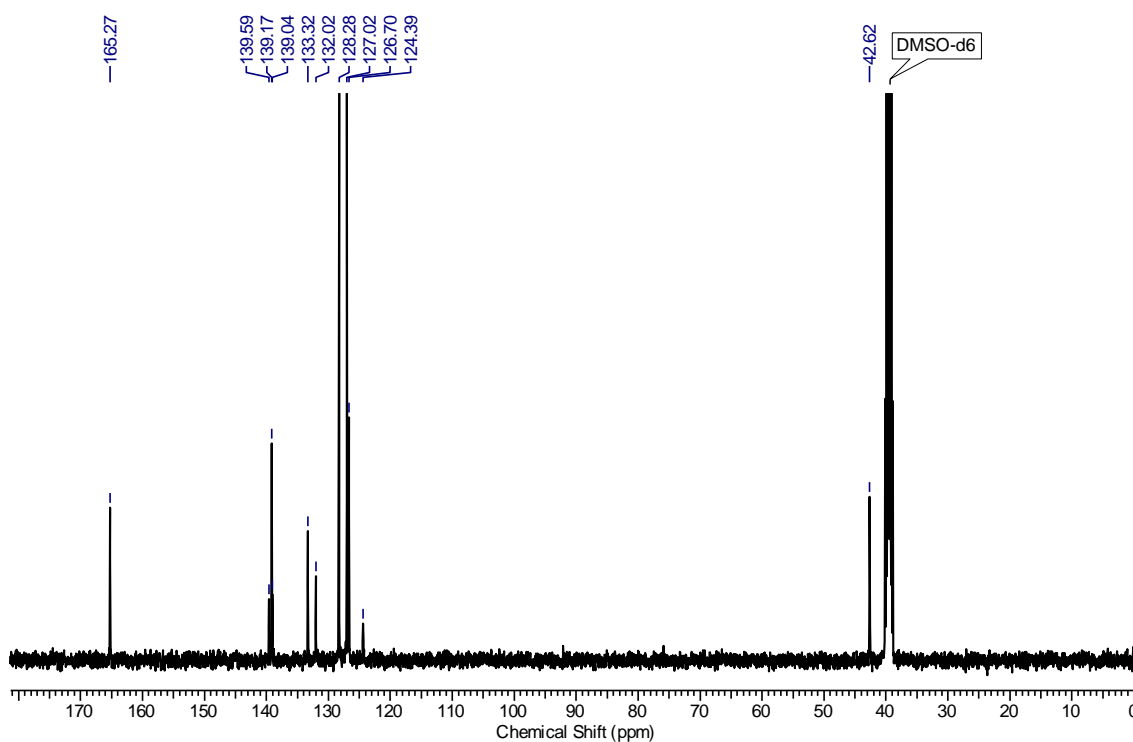


IR spectrum of compound **4b**

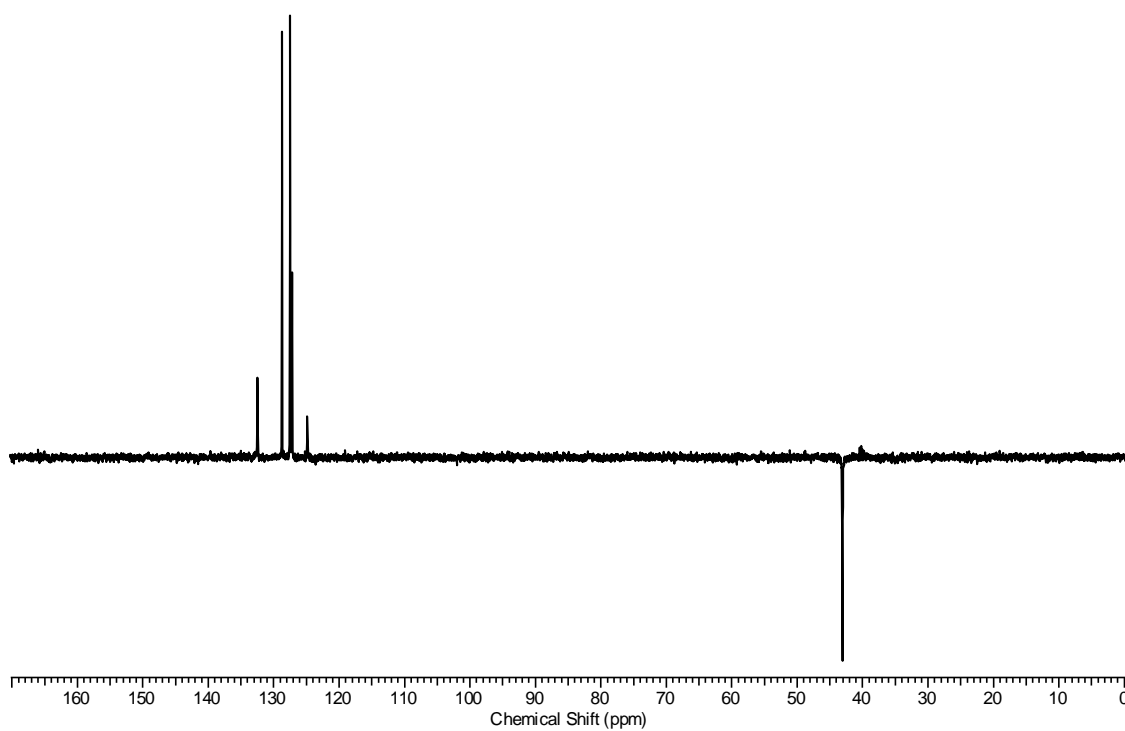




<sup>1</sup>H NMR spectrum of compound **4b** (DMSO-*d*<sub>6</sub>, 400MHz, 298 K)

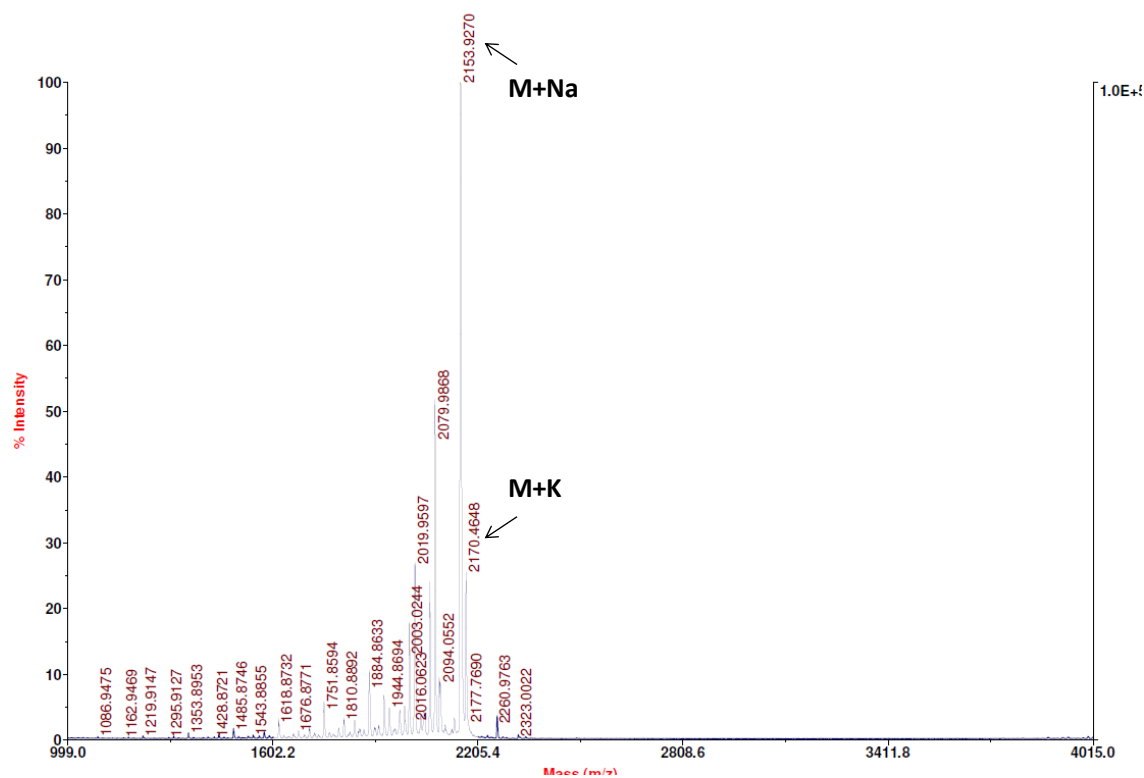


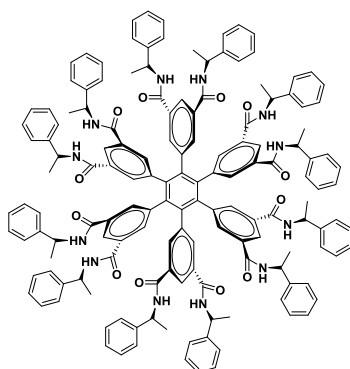
<sup>13</sup>C NMR spectrum of compound **4b** (DMSO-*d*<sub>6</sub>, 100 MHz, 343 K)

DEPT 135 spectrum of compound **4b** (DMSO-*d*<sub>6</sub>, 100MHz, 298 K)

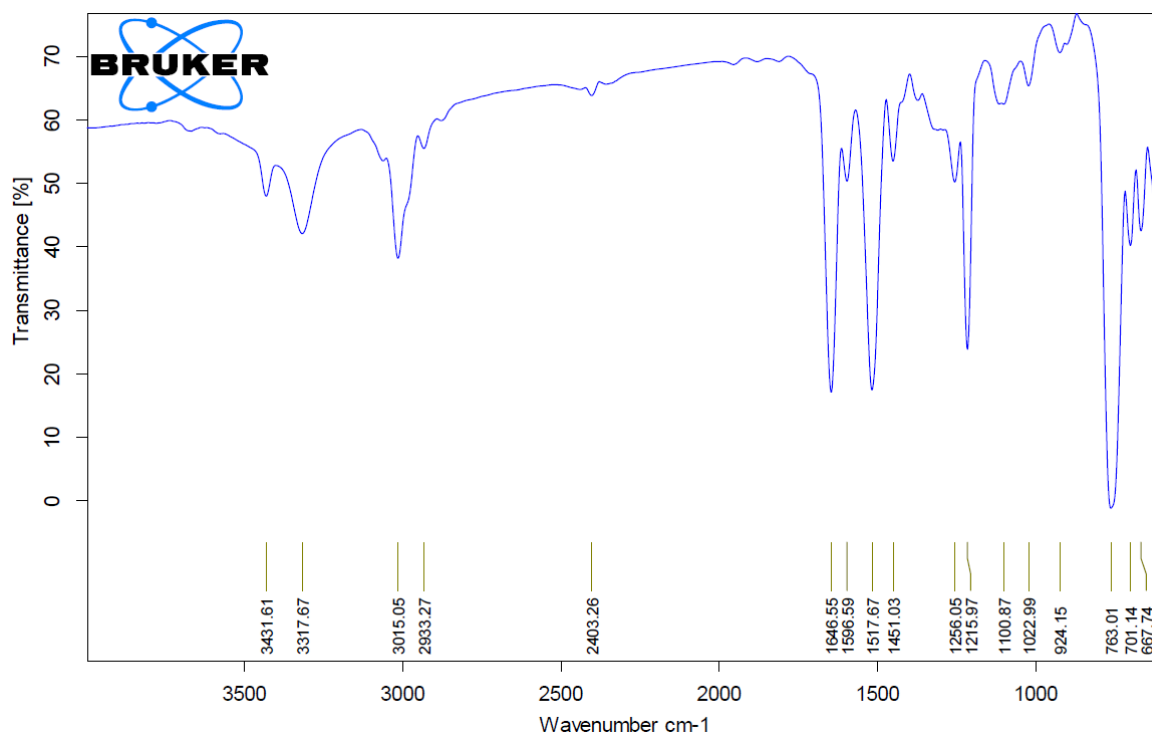
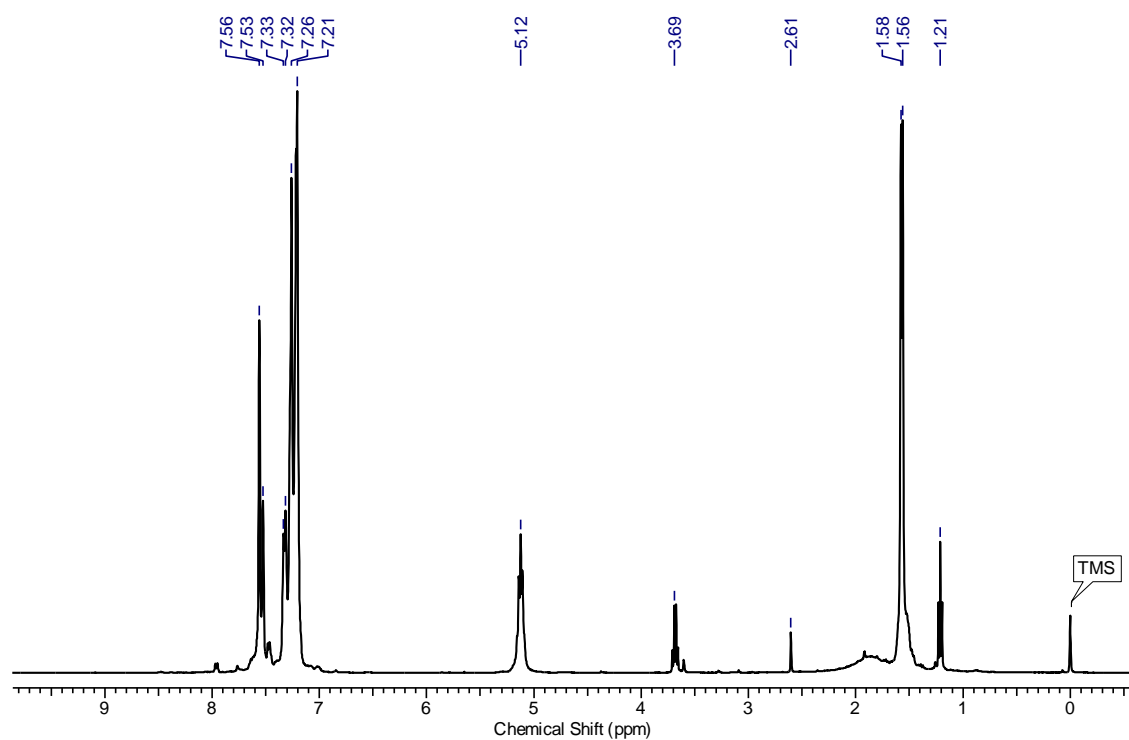
AB Sciex TOF/TOF™ Series Explorer™ 72085

TOF/TOF™ Reflector Spec #1[BP = 2154.4, 99972]

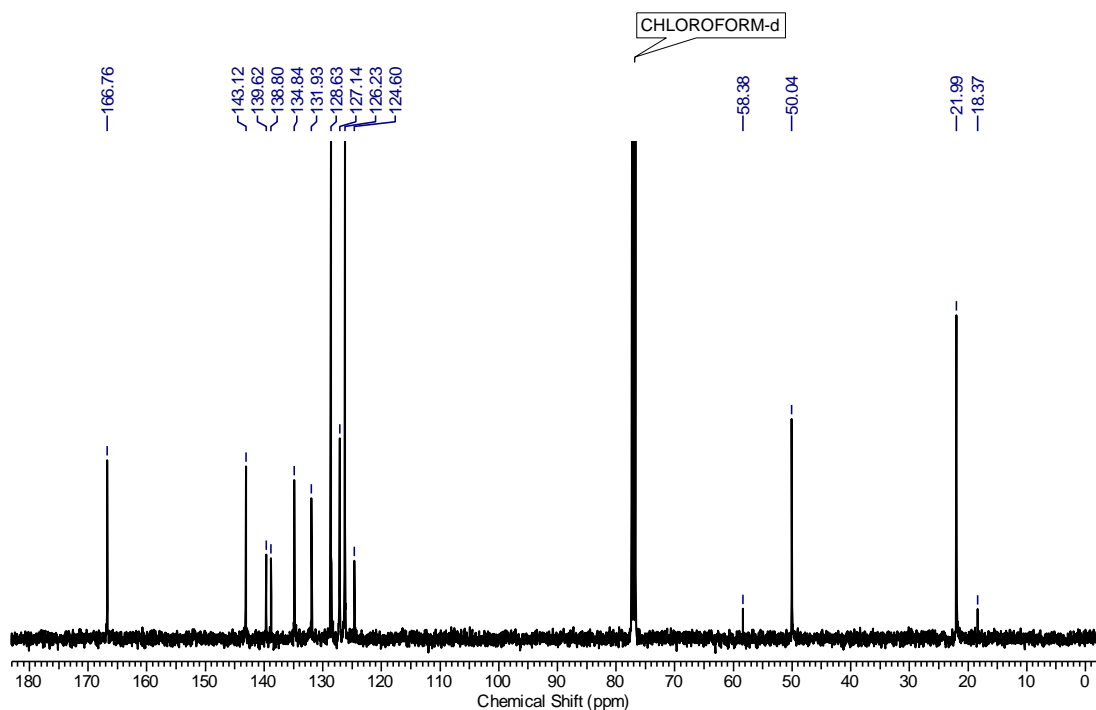
MS (MALDI-TOF) of compound **4b**

**Compound 4c**

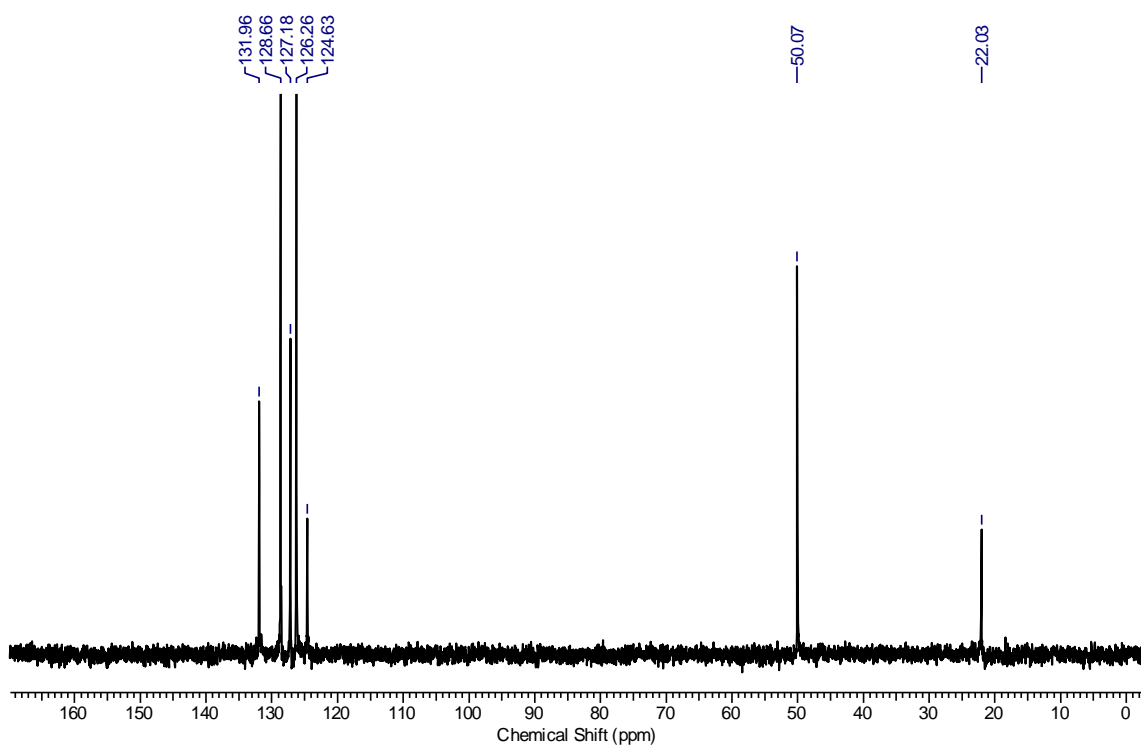
To a suspension of **3d** (0.2 g, 0.188 mmol) and DIEA (0.6 mL, 3.38 mmol) in DMSO (4 mL) HBTU (1.50 g, 3.38 mmol) was added and the mixture was stirred at room temperature for 5 minutes to form clear solution. Then (*S*)-(-)- $\alpha$ -methylbenzylamine (0.43 mL, 3.38 mmol) was added and stirring was continued for 12 h. After completion of the reaction, the reaction mixture was diluted with ice-chilled water and thrice extracted with DCM. The combined organic phases were dried over sodium sulfate and evaporated *in vacuo*. The residue obtained was further recrystallised using absolute ethanol to get amide **4c** as colorless crystals. Yield : 0.31 g (70 %). mp: 265-267 °C; TLC (ethyl acetate/pet ether, 50:50 v/v):  $R_f = 0.5$ ;  $[\alpha]_D^{24}$ : +18.4° ( $c = 0.77$ ,  $\text{CHCl}_3$ ); IR ( $\text{CHCl}_3$ )  $\text{cm}^{-1}$ : 3461, 3317, 3015, 2933, 1646, 1596, 1517, 1451, 1215, 763;  $^1\text{H-NMR}$  (400MHz,  $\text{CDCl}_3$ )  $\delta$ : 7.56 (s, 12H), 7.53 (br. s., 6H), 7.32 (d,  $J = 7.3$  Hz, 12H), 7.29 - 7.19 (m, 60H), 5.12 (br. s., 12H), 1.58 (d, 36H);  $^{13}\text{C NMR}$  (101MHz,  $\text{CDCl}_3$ )  $\delta$ : 166.8, 143.1, 139.6, 138.8, 134.8, 131.9, 128.6, 127.1, 126.2, 124.6, 50.0, 22.0; MALDI-TOF/TOF: 2321.9221  $[\text{M}+\text{Na}]^+$ , 2338.3105  $[\text{M}+\text{K}]^+$ ; Elemental analysis calculated for  $\text{C}_{150}\text{H}_{138}\text{N}_{12}\text{O}_{12}$ : C, 78.3; H, 6.05; N, 7.31. Found: C, 78.28; H, 6.09; N, 7.39.

IR spectrum of compound **4c**

<sup>1</sup>H NMR spectrum of compound **4c** (CDCl<sub>3</sub>, 400MHz, 298 K). *Note:* Peak at  $\delta=2.61$  and 1.21 corresponding to ethanol (compound **4c** crecrystallised from ethanol and then NMR was recorded).



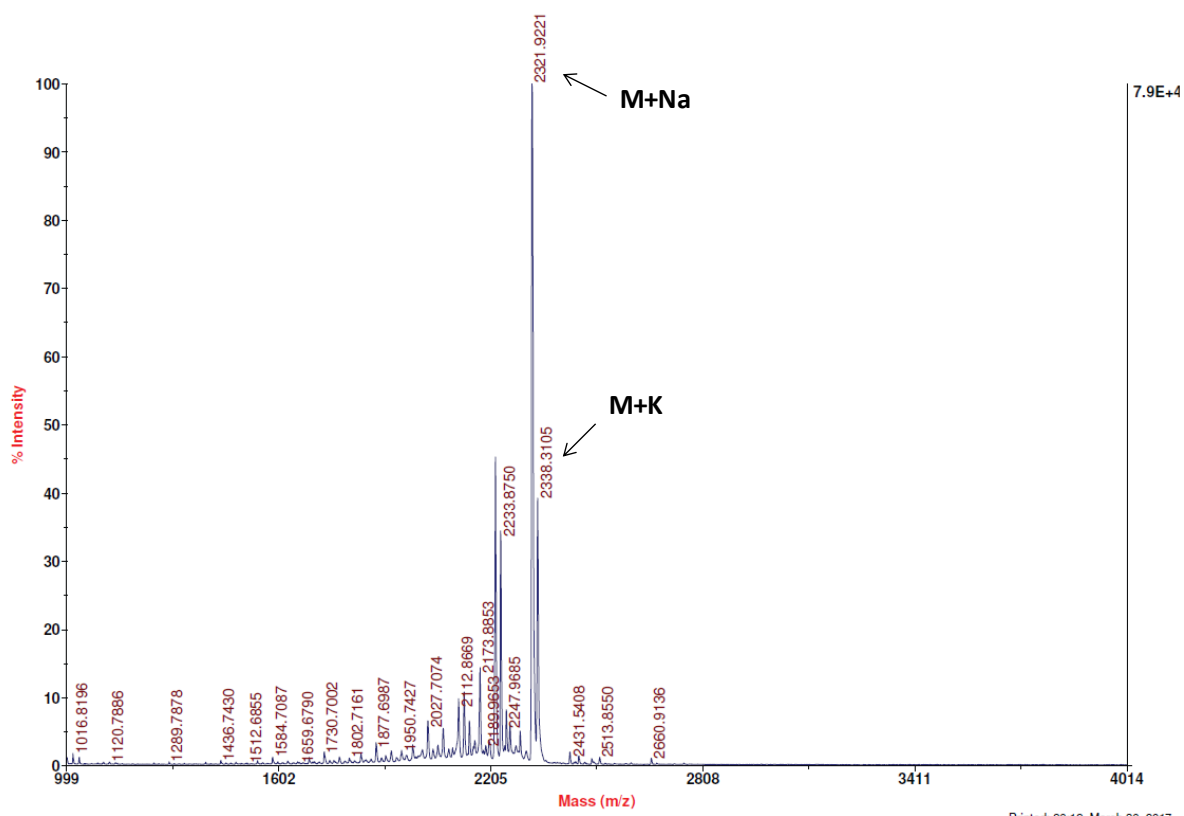
<sup>13</sup>C-NMR spectrum of compound **4c** (CDCl<sub>3</sub>, 100 MHz, 343 K). Note: Peak at  $\delta=58.38$  and 18.37 corresponding to ethanol (compound **4c** recrystallised from ethanol and then NMR was recorded).



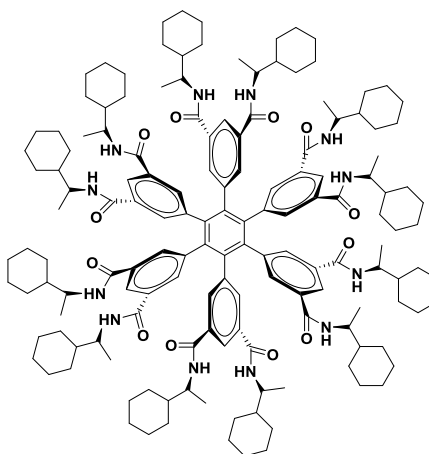
DEPT 135 spectrum of compound **4c** (CDCl<sub>3</sub>, 100MHz, 298 K)

AB Sciex TOF/TOF™ Series Explorer™ 72085

TOF/TOF™ Reflector Spec #1[BP = 2322.2, 79162]

MS (MALDI-TOF) of compound **4c**

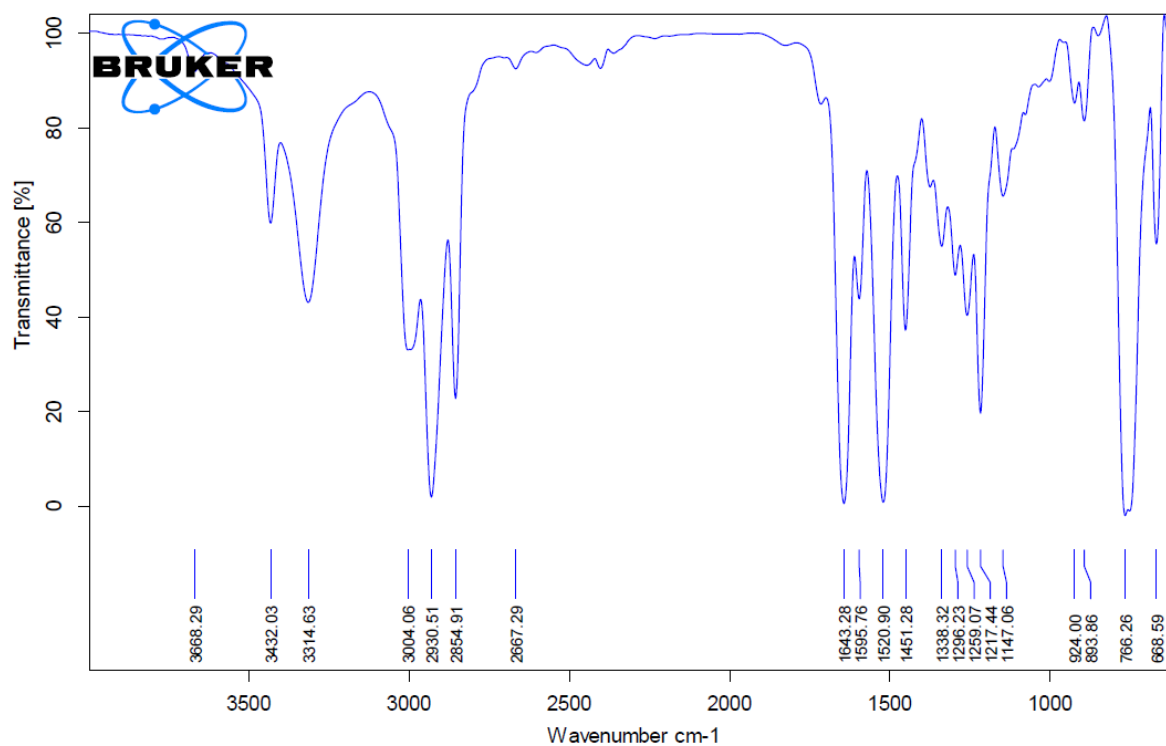
### Compound **4d**



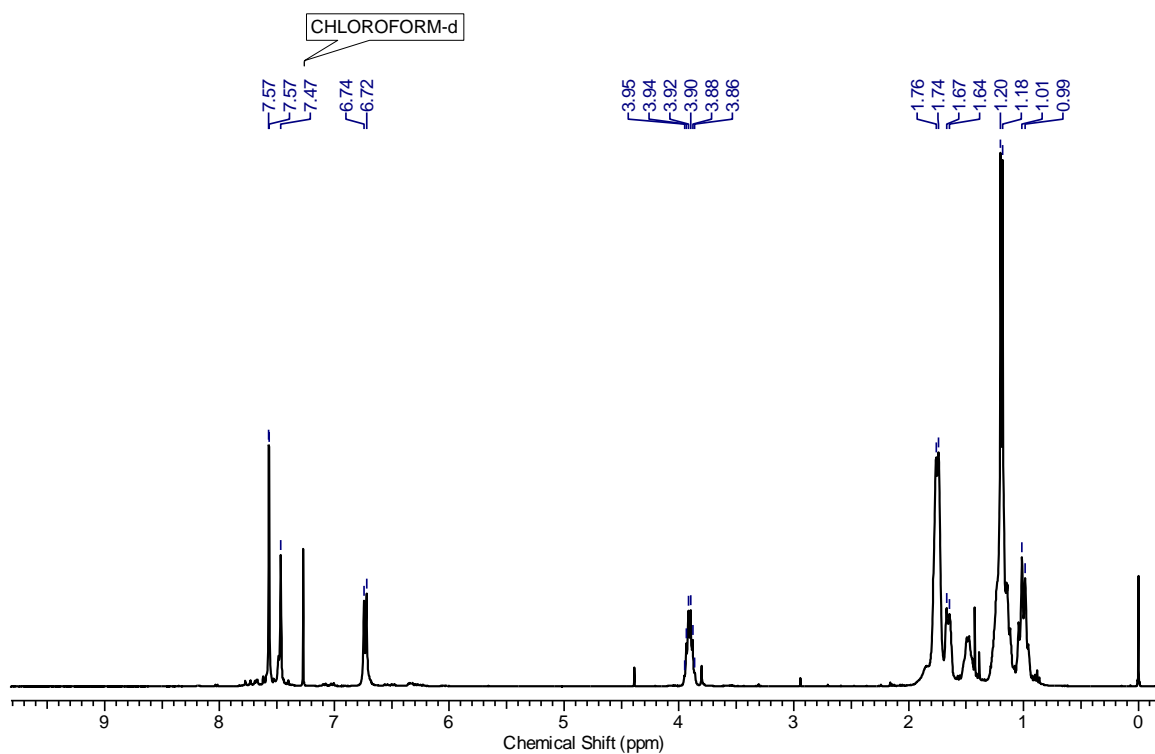
Compound **4d** was synthesized, following the procedure for **4a**, using compound **3d** (0.1 g, 0.094 mmol), DIEA (0.29 mL, 1.69 mmol), HBTU (0.75 g, 1.69 mmol), (*S*)-(+)-1-

Cyclohexylethylamine (0.25 mL, 1.69 mmol) and DMSO (4 mL). Column chromatographic purification (eluent: AcOEt/ pet. ether, 30/70 v/v,  $R_f = 0.6$ ) of the residue afforded **4d** as a white solid. Yield: 0.161 g (72%).

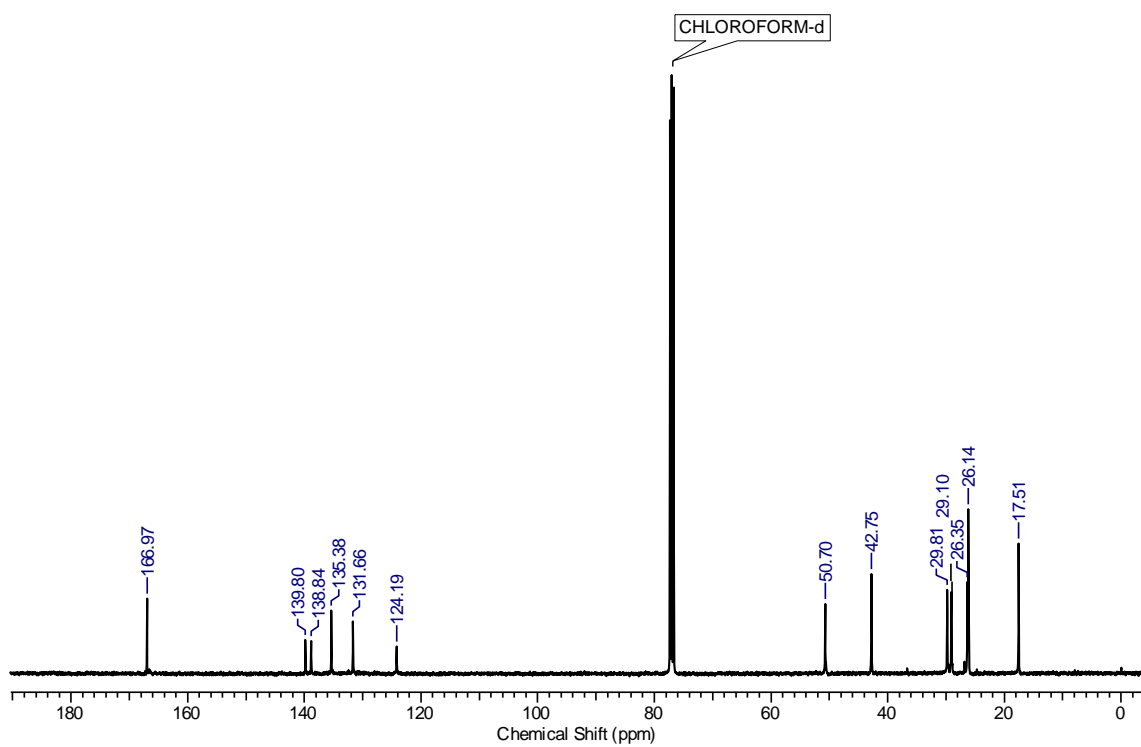
mp: 185-187 °C;  $[\alpha]_D^{23}$ : +82.2° (c = 0.1, CHCl<sub>3</sub>); IR (CHCl<sub>3</sub>) cm<sup>-1</sup>: 3668, 3432, 3314, 3004, 2930, 2854, 2667, 1643, 1595, 1520, 1451, 1338, 1296, 1259, 924, 893, 766, 668; <sup>1</sup>H-NMR (400MHz, CDCl<sub>3</sub>) δ: 7.57 (d, *J* = 1.4 Hz, 12H), 7.47 (s, 6H), 6.73 (d, *J* = 8.7 Hz, 12H), 3.96 - 3.86 (m, 12H), 1.75 (d, *J* = 8.2 Hz, 60H), 1.66 (d, *J* = 11.0 Hz, 12H), 1.19 (d, *J* = 6.9 Hz, 60H), 1.06 - 0.95 (m, 36H); <sup>13</sup>C-NMR (101MHz, CDCl<sub>3</sub>) δ: 167.0, 139.8, 138.8, 135.4, 131.7, 124.2, 50.7, 42.8, 29.8, 29.1, 26.4, 26.1, 17.5; MALDI-TOF/TOF: 2394.3000 [M+Na]<sup>+</sup>, 2410.9954 [M+K]<sup>+</sup>; Elemental analysis calculated for C<sub>150</sub>H<sub>210</sub>N<sub>12</sub>O<sub>12</sub>: C, 75.91; H, 8.92; N, 7.08. Found: C, 75.95; H, 8.95; N, 7.10.



IR spectrum of compound **4d**

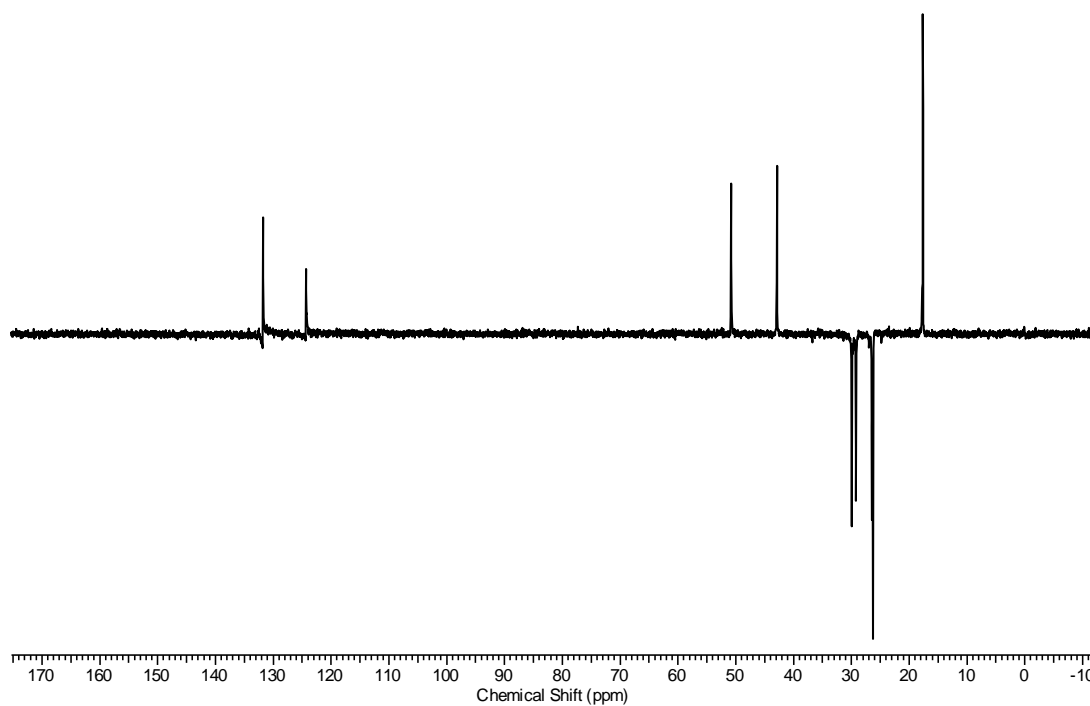


<sup>1</sup>H NMR spectrum of compound **4d** (CDCl<sub>3</sub>, 400MHz, 298 K).



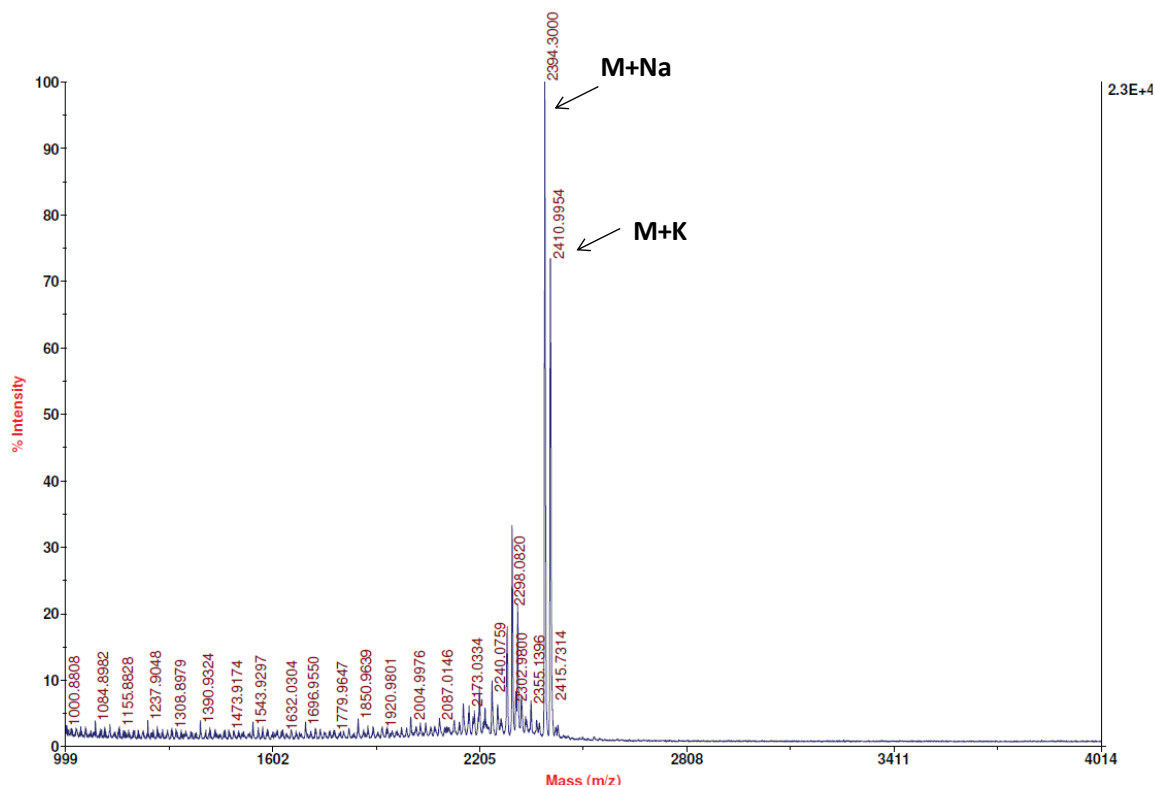
<sup>13</sup>C-NMR spectrum of compound **4d** (CDCl<sub>3</sub>, 100 MHz, 343 K).



DEPT 135 spectrum of compound **4d** ( $\text{CDCl}_3$ , 100MHz, 298 K)

AB Sciex TOF/TOF™ Series Explorer™ 72085

TOF/TOF™ Reflector Spec #1[BP = 2394.2, 23233]

MS (MALDI-TOF) of compound **4d**

## 2.7 X-ray Crystallography:

X-ray intensity data measurements of crystals (+/-)Styreneoxide@**HPB(COOMe)**<sub>12</sub> and **HPB(CONH- $\alpha$ -methylbenzylamine)**<sub>12</sub> were carried out on a Bruker D8-VENT-URE Kappa Duo PHOTON II CPAD diffractometer equipped with Incoatech multilayer mirrors optics. The intensity measurements were carried out with copper micro-focus sealed tube diffraction source ( $\text{CuK}_{\alpha} = 1.54178 \text{ \AA}$ ) at 100(2) K temperature. The X-ray generator was operated at 50 kV and 1.1 mA. A preliminary set of cell constants and an orientation matrix were calculated from three sets of 40 frames. Data were collected with  $\omega$  scan width of  $0.5^{\circ}$  at different settings of  $\varphi$  and  $2\theta$  keeping the sample-to-detector distance fixed at 5.00 cm. The X-ray data collection was monitored by APEX3 program (Bruker, 2016).<sup>38</sup> On the other hand X-ray intensity data measurements of crystals DMF@**HPB(COOMe)**<sub>12</sub>, DMSO@**HPB(COOMe)**<sub>12</sub>, [12]-crown-ether@**HPB(COOMe)**<sub>12</sub>, Benzene@**HPB(COOMe)**<sub>12</sub>, Pyridine@**HPB(COOMe)**<sub>12</sub>, Aniline@**HPB(COOMe)**<sub>12</sub>, N-methylaniline@**HPB(COOMe)**<sub>12</sub>, Salicylaldehyde@**HPB(COOMe)**<sub>12</sub>, **HPB(COOMe)**<sub>12</sub>, Acetone.H<sub>2</sub>O@**HPB(CONHMe)**<sub>12</sub>, DMSO@**HPB(CONH<sub>2</sub>)**<sub>12</sub>, DMSO.H<sub>2</sub>O@**HPB(CONH<sub>2</sub>)**<sub>12</sub>, NMP@**HPB(CONH<sub>2</sub>)**<sub>12</sub>, DMF@**HPB(CONH<sub>2</sub>)**<sub>12</sub>, HCOOH@**HPB(CONH<sub>2</sub>)**<sub>12</sub>, DMF.HBr@**HPB(CONH<sub>2</sub>)**<sub>12</sub>, DMSO.MeOH.C<sub>2</sub>H<sub>5</sub>OH.Hexane@**HPB(CONH<sub>2</sub>)**<sub>12</sub>, MeOH.Dioxane.NH<sub>3</sub>@**HPB(CONH<sub>2</sub>)**<sub>12</sub>, MeOH.NH<sub>3</sub>@**HPB(CONH<sub>2</sub>)**<sub>12</sub>, MeOH.Hexane.NH<sub>3</sub>@**HPB(CONH<sub>2</sub>)**<sub>12</sub>, Dioxane.Methanol.H<sub>2</sub>O@**HPB(CONHNH<sub>2</sub>)**<sub>12</sub> and H<sub>2</sub>O@**HPB(CONHNH<sub>2</sub>)**<sub>12</sub> were carried out on a Bruker SMART APEX II CCD diffractometer with graphite monochromatized ( $\text{MoK}_{\alpha} = 0.71073 \text{ \AA}$ ) radiation. The X-ray generator was operated at 50 kV and 30 mA. A preliminary set of cell constants and an orientation matrix were calculated from three sets of 36 frames. Data were collected with  $\omega$  scan width of  $0.5^{\circ}$  at different settings of  $\varphi$  and  $2\theta$  keeping the sample-to-detector distance fixed at 5.00 cm. The X-ray data collection was monitored by APEX2 program (Bruker, 2006).<sup>39</sup> H<sub>2</sub>O@ **HPB(CONHMe)**<sub>12</sub> and Toluene@**HPB(COOMe)**<sub>12</sub> data were collected in Bruker APEX II Cu source. (+/-)Styreneoxide@**HPB(COOMe)**<sub>12</sub> and **HPB(CONH- $\alpha$ -methylbenzylamine)**<sub>12</sub> data were collected in Bruker APEX III Cu/Mo source. All the data were corrected for Lorentzian, polarization and absorption effects using SAINT and SADABS programs (Bruker, 2016). SHELX-97 was used for structure solution and full matrix least-squares refinement on  $F^2$ .<sup>40,41</sup> All the

hydrogen atoms were placed in geometrically idealized position and constrained to ride on the parent atoms.

## 2.8 References

1. Lehn, J.-M.; Sanders, J. *Angew. Chem. Int. Ed. Engl.* **1995**, *34* (22), 2563.
2. Lehn, J. M. *Angew. Chem. Int. Ed. Engl.* **1988**, *27* (1), 89-112.
3. Lehn, J.-M., *Supramolecular chemistry*. Vch, Weinheim: **1995**; Vol. 1.
4. Horiuchi, S.; Tokura, Y. *Nat. Mater* **2008**, *7* (5), 357-366.
5. Tayi, A. S.; Shveyd, A. K.; Sue, A. C.-H.; Szarko, J. M.; Rolczynski, B. S.; Cao, D.; Kennedy, T. J.; Sarjeant, A. A.; Stern, C. L.; Paxton, W. F. *Nature* **2012**, *488* (7412), 485-489.
6. Endo, K.; Koike, T.; Sawaki, T.; Hayashida, O.; Masuda, H.; Aoyama, Y. *J. Am. Chem. Soc.* **1997**, *119* (18), 4117-4122.
7. Ma, X.; Zhao, Y. *Chem. Rev.* **2014**, *115* (15), 7794-7839.
8. Ooyama, Y.; Nagano, S.; Okamura, M.; Yoshida, K. *Eur. J. Org. Chem.* **2008**, (35), 5899-5906.
9. Fei, Z.; Kocher, N.; Mohrschladt, C. J.; Ihmels, H.; Stalke, D. *Angew. Chem. Int. Ed. Engl.* **2003**, *42* (7), 783-787.
10. Atwood, J. L.; Barbour, L. J.; Jerga, A. *Science* **2002**, *296* (5577), 2367-2369.
11. Msayib, K. J.; Book, D.; Budd, P. M.; Chaukura, N.; Harris, K. D.; Helliwell, M.; Tedds, S.; Walton, A.; Warren, J. E.; Xu, M. *Angew. Chem. Int. Ed.* **2009**, *121* (18), 3323-3327.
12. Sozzani, P.; Bracco, S.; Comotti, A.; Ferretti, L.; Simonutti, R. *Angew. Chem. Int. Ed.* **2005**, *44* (12), 1816-1820.
13. Mahata, G.; Roy, S.; Biradha, K. *Chem. Commun.* **2011**, *47* (23), 6614-6616.
14. Weber, E.; Josel, H.-P. *J Incl Phenom Macrocycl Chem.* **1983**, *1* (1), 79-85.
15. Tian, J.; Thallapally, P. K.; McGrail, B. P. *CrystEngComm.* **2012**, *14* (6), 1909-1919.
16. Dalgarno, S. J.; Thallapally, P. K.; Barbour, L. J.; Atwood, J. L. *Chem. Soc. Rev.* **2007**, *36* (2), 236-245.
17. Thallapally, P. K.; McGrail, B. P.; Atwood, J. L.; Gaeta, C.; Tedesco, C.; Neri, P. *Chem. Mater.* **2007**, *19* (14), 3355-3357.
18. Atwood, J. L.; Barbour, L. J.; Jerga, A.; Schottel, B. L. *Science* **2002**, *298* (5595), 1000-1002.
19. Tan, L. L.; Li, H.; Tao, Y.; Zhang, S. X. A.; Wang, B.; Yang, Y. W. *Adv. Mater.* **2014**, *26* (41), 7027-7031.

20. Barrow, S. J.; Kasera, S.; Rowland, M. J.; del Barrio, J.; Scherman, O. A. *Chem. Rev* **2015**, *115* (22), 12320-12406.
21. Lim, S.; Kim, H.; Selvapalam, N.; Kim, K. J.; Cho, S. J.; Seo, G.; Kim, K. *Angew. Chem. Int. Ed.* **2008**, *120* (18), 3400-3403.
22. Tozawa, T.; Jones, J. T.; Swamy, S. I.; Jiang, S.; Adams, D. J.; Shakespeare, S.; Clowes, R.; Bradshaw, D.; Hasell, T.; Chong, S. Y. *Nat. Mater.* **2009**, *8* (12), 973-978.
23. Barrer, R. M.; Shanson, V. H. *J. Chem. Soc., Chem. Commun.* **1976**, (9), 333-334.
24. Mastalerz, M.; Oppel, I. M. *Angew. Chem. Int. Ed. Engl.* **2012**, *51* (21), 5252-5255.
25. Natarajan, R.; Bridgland, L.; Sirikulakajorn, A.; Lee, J.-H.; Haddow, M. F.; Magro, G.; Ali, B.; Narayanan, S.; Strickland, P.; Charmant, J. P. *J. Am. Chem. Soc.* **2013**, *135* (45), 16912-16925.
26. Kobayashi, K.; Sato, A.; Sakamoto, S.; Yamaguchi, K. *J. Am. Chem. Soc.* **2003**, *125* (10), 3035-3045.
27. Kamoun, C.; Pizzi, A.; Zanetti, M. *J. Appl. Polym. Sci.* **2003**, *90* (1), 203-214.
28. Carter, C. B.; Coxe, A. E., Process of producing hexamethylenetetramine. Google Patents: 1924.
29. Carter, C. B., Production of hexamethylenetetramine and ammonium chloride. Google Patents: 1925.
30. Arbenz, A.; Averous, L. *Green Chem.* **2015**, *17* (5), 2626-2646.
31. Pichelin, F.; Nakatani, M.; Pizzi, A.; Wieland, S. *Forest. Prod. J.* **2006**, *56* (5), 31.
32. Ahlrichs, R.; Bär, M.; Häser, M.; Horn, H.; Kölmel, C. *Chem. Phys. Lett.* **1989**, *162* (3), 165-169.
33. Perdew, J. P.; Burke, K.; Ernzerhof, M. *Phys. Rev. Lett.* **1996**, *77* (18), 3865.
34. Schäfer, A.; Huber, C.; Ahlrichs, R. *J. Chem. Phys.* **1994**, *100* (8), 5829-5835.
35. Eichkorn, K.; Treutler, O.; Öhm, H.; Häser, M.; Ahlrichs, R. *Chem. Phys. Lett.* **1995**, *240* (4), 283-290.
36. Sierka, M.; Hogeckamp, A.; Ahlrichs, R. *J. Chem. Phys.* **2003**, *118* (20), 9136-9148.
37. Kraszkiewicz, L.; Sosnowski, M.; Skulski, L. *Synthesis* **2006**, *2006* (07), 1195-1199.

38. Bruker (2016). APEX3, SAINT and SADABS. Bruker AXS Inc., Madison, Wisconsin, USA.
39. Bruker (2006). APEX3, SAINT and SADABS. Bruker AXS Inc., Madison, Wisconsin, USA.
40. Sheldrick, G. M. *Acta Crystallogr.*, **2008**, A64, 112.
41. Farrugia, L. J. *J. Appl. Cryst.* **1997**, 30, 565–565.



## ***Chapter 3***

### ***Section-A***

# ***High Proton Conductivity Exhibited by a Twelve-Armed Hexaphenylbenzene-based Supramolecular Sponge***





## Chapter-3

### Section-A

## High Proton Conductivity Exhibited by a Twelve-Armed Hexaphenylbenzene-based Supramolecular Sponge

### 3.1 Proton (H<sup>+</sup>) conductivity

Proton (H<sup>+</sup>) conductivity (PC) is an important phenomena found naturally in many of the biochemical pathways such as ATP oxidative phosphorylation in mitochondria, HCVN1 voltage-gated proton channel and light-activated proton pumping in bacteriorhodopsin etc.<sup>1-3</sup> Furthermore, this phenomenon plays a vital role in fuel cell<sup>4</sup> and electro-sensor applications,<sup>5</sup> due to which proton conducting materials have got immense attention in the field of material science.<sup>6-11</sup> Consequently, in order to develop proton conducting materials, researchers have performed extensive studies on a variety of materials with various structures over the past decade.<sup>12-19</sup> Among them, the well known the commercially available organic proton-exchange membrane (PEM) materials are sulfonated fluoropolymers such as Nafion and its derivatives.<sup>20-22</sup> Their proton conductivity (PC) is in the order of 10<sup>-1</sup> S/cm which makes it suitable PEM material in the field of electrochemistry.<sup>22</sup> Furthermore, the polymeric porous materials such as metal organic frameworks (MOFs)<sup>23-26</sup> and covalent organic frameworks (COFs)<sup>18, 27-29</sup> have also been investigated as possible candidates for proton-conducting applications in recent years. The growing competitors of polymeric materials in gas adsorption and storage are discrete organic molecular materials. They are emerging candidates for the proton conductivity as well. For instance, Mullen *et al.* showed high proton conductivity in crystalline non-porous hexakis(p-phosphonatophenyl)benzene up to 2.5 X 10<sup>-2</sup> Scm<sup>-1</sup> at room temperature, and 95% RH (relative humidity).<sup>14</sup> Kim *et al.* reported proton conductivity in acid-water hydrogen bond network containing cucurbituril-based materials which were recrystallised from mineral acids (Fig 3.01).<sup>30</sup> The high anisotropic conductivity of the single crystal material was 4.3 X 10<sup>-2</sup> Scm<sup>-1</sup> at 298 K (98 % RH). Cooper and co-workers showed 3D-proton conductivity in porous molecular cages with the conductivity range up to 10<sup>-3</sup> S cm<sup>-1</sup> at 95% RH and 303 K.<sup>31</sup> Recently, Gosh *et al.* showed proton conductivity in the order of 10<sup>-2</sup> S cm<sup>-1</sup> in porous 2D hydrogen bonded organic frame work (HOF) materials based on arene sulfonates and guanidinium cations.<sup>32</sup> In addition to the above mentioned studies, novel materials have always been welcomed by the research community to bring out the high proton conducting materials.

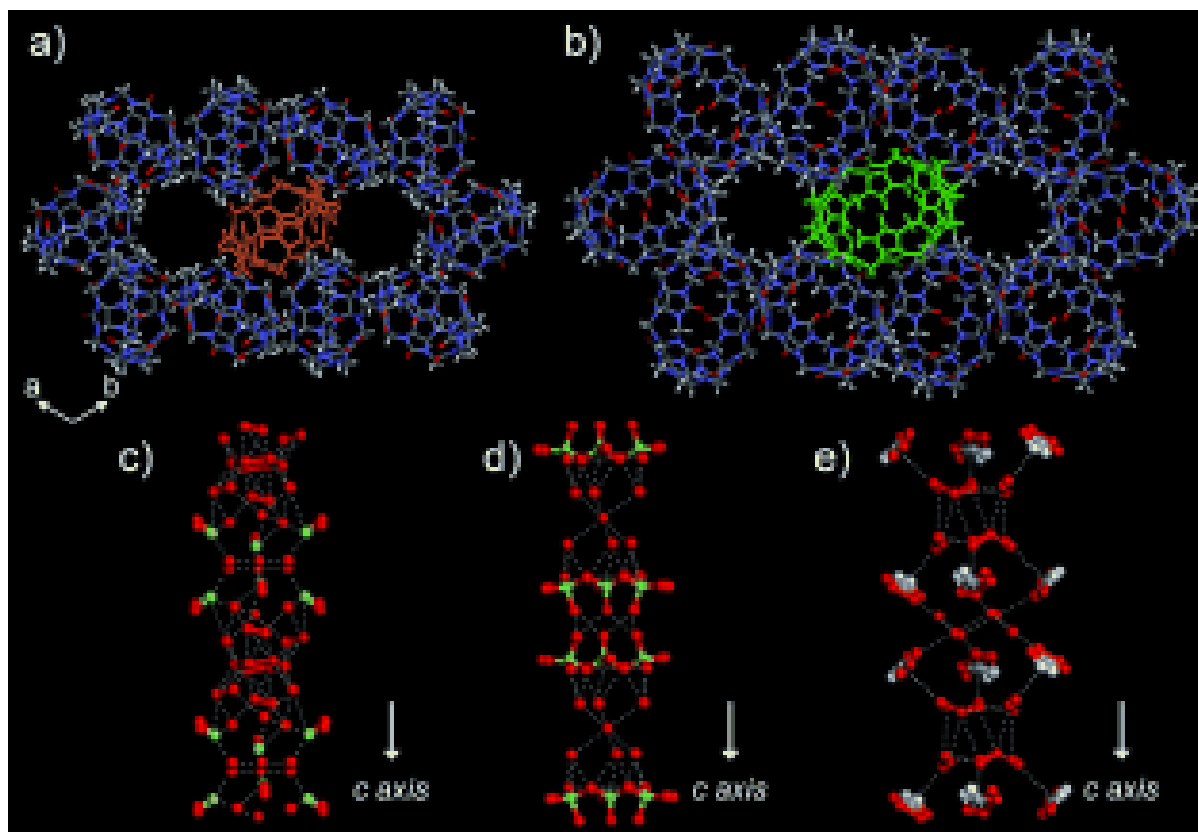


**Fig. 3.01:** a) X-ray crystal structures of porous CB[6] viewed down the *c* axis. b) X-ray crystal structure of porous CB[8] viewed down the *c* axis. c) water–HCl array in the 1D channel of CB[6]; d) water–H<sub>2</sub>SO<sub>4</sub> array in the 1D channel of CB[6]; e) water–HCO<sub>2</sub>H array in the 1D channel of CB[8]. Reproduced with permission from ref.30 Copyright 2011 John Wiley and Sons.

### 3.2 Objective of the present work

In the previous chapter, we have thoroughly studied the supramolecular sponge property of 12-armed HPB-based materials such as HPB(COOMe)<sub>12</sub>, HPB(CONH<sub>2</sub>)<sub>12</sub>, HPB(CONHNH<sub>2</sub>)<sub>12</sub> and HPB(CONHR)<sub>12</sub>. It was our observation that in all the cases, the presence of double bowl-shaped backbone and multivalency leads to uptake of guest molecules in their solid state pores. Therefore, we have envisaged that carboxylic acid derivative **HPB(COOH)<sub>12</sub>** (compound **5d** in chapter-2) (Fig.3.02), would behave like its other derivatives and hence we decided to use this material for proton conductivity applications by up taking water molecules (Fig 3.02). The main reason is, under humid conditions, these materials could form extended hydrogen bonded network, which is very much required for the solid state proton conduction.

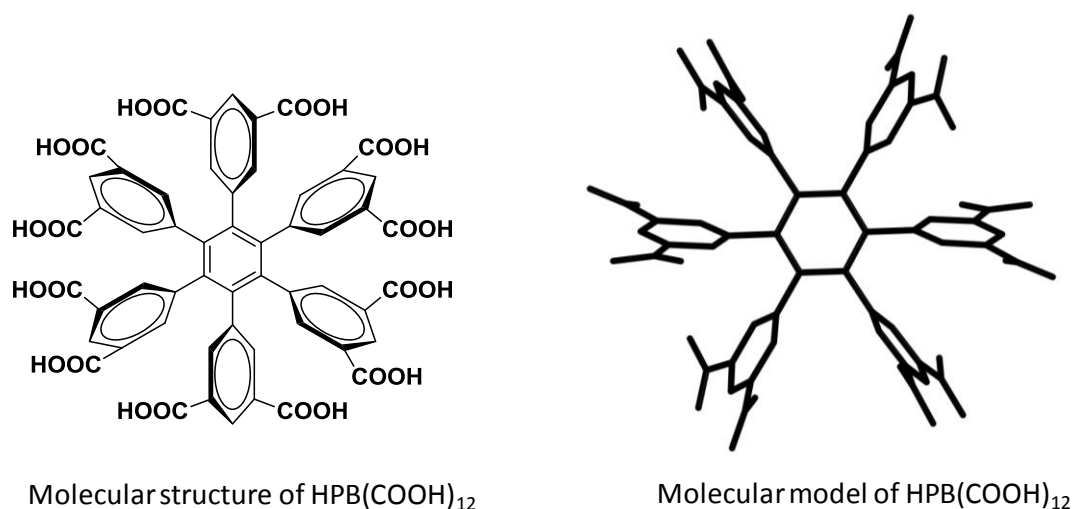
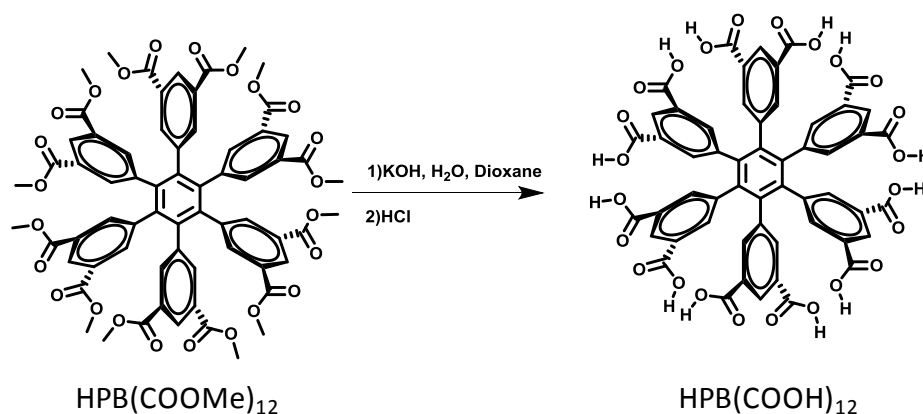


**Fig. 3.02:** Molecular structure and molecular model of HPB(COOH)<sub>12</sub>

### 3.3 Synthesis and characterization



**Scheme 3.01:** Synthesis of HPB(COOH)<sub>12</sub> from HPB(COOH)<sub>12</sub>.

As mentioned in the chapter-2, HPB(COOH)<sub>12</sub> (**3d**) was synthesized from the base hydrolysis of HPB(COOMe)<sub>12</sub> under hydrothermal condition using aqueous dioxane as a solvent followed by neutralization with concentrated HCl (Scheme 3.01). The obtained material was insoluble in common organic solvent systems and soluble in hot DMSO indicating the presence of strong intermolecular forces. Further, the material was well characterized by IR, NMR and MASS to confirm the complete conversion and homogeneity of the system (Experimental section 2.6). The IR broad band seen at 2947 cm<sup>-1</sup> indicates the dense intermolecular H-bond interactions and the sharp band at 1714 cm<sup>-1</sup> is corresponding to the carbonyl of carboxylic acid (Fig.3.03a). The weight loss at about 10% in a thermogravimetric analysis of HPB(COOH)<sub>12</sub> revealed the loss of residual guest molecules and its decomposition temperatures above 300° C suggested the high

thermal stability of the material (Fig.3.03b). Further, powder X-ray diffraction pattern of the material clearly showed the presence of moderate crystalline nature of HPB(COOH)<sub>12</sub> (Fig.3.04).

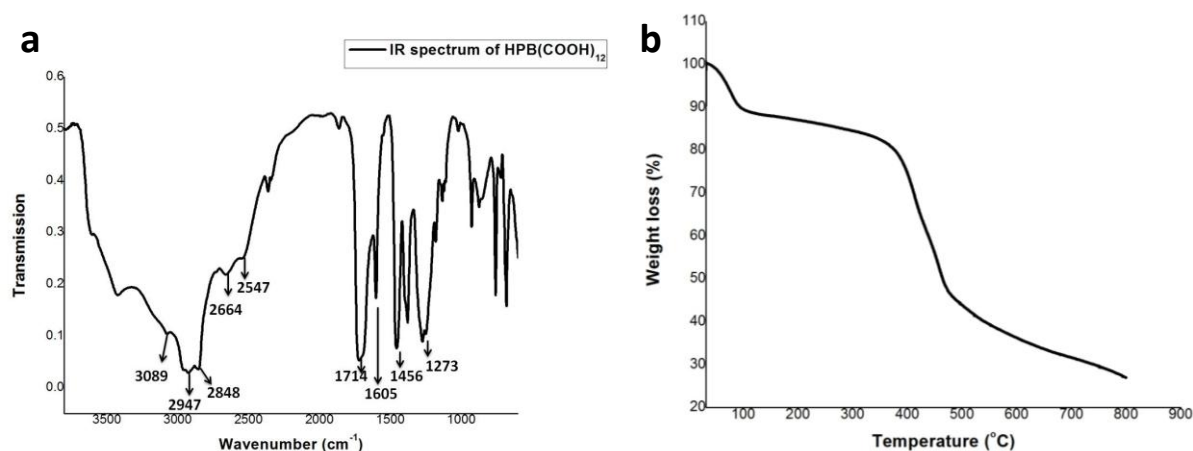


**Fig. 3.03:** a) IR spectrum of HPB(COOH)<sub>12</sub> showing the intermolecular H-bonding (about 3000 cm<sup>-1</sup>) and carbonyl of the carboxylic acid (1714 cm<sup>-1</sup>). b) Thermogravimetric analysis plot of HPB(COOH)<sub>12</sub> showing the thermal stability above 350 °C.

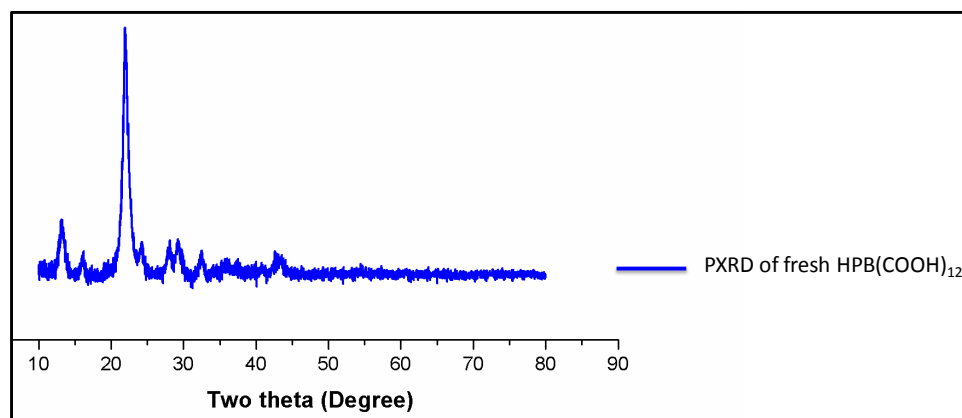


**Fig. 3.04:** Powder X-ray diffraction pattern of fresh HPB(COOH)<sub>12</sub>.

Nitrogen gas adsorption experiment revealed the moderate uptake of N<sub>2</sub>, 98 cc/g at 77 K with distorted type II isotherm,<sup>33</sup> which is comparable to many of the reported organic porous materials. The corresponding N<sub>2</sub> adsorption experiment BET surface area was 114.5 m<sup>2</sup>g<sup>-1</sup>. A similar experiment was conducted for CO<sub>2</sub> as well, wherein the uptake of gas was 30.9 cc/g. These adsorption experiments (Fig. 3.05) revealed the porous nature of the H-bonded molecular solid HPB(COOH)<sub>12</sub>. Based on the adsorption and other spectroscopic characterizations, H-bonded porous channels are possible in the HPB(COOH)<sub>12</sub> and the schematic representation of the material has been shown in Fig.

3.06. The structural features, guest uptaking supramolecular spongy nature and thermal stability of HPB(COOH)<sub>12</sub> has encouraged us to investigate its proton conductivity.

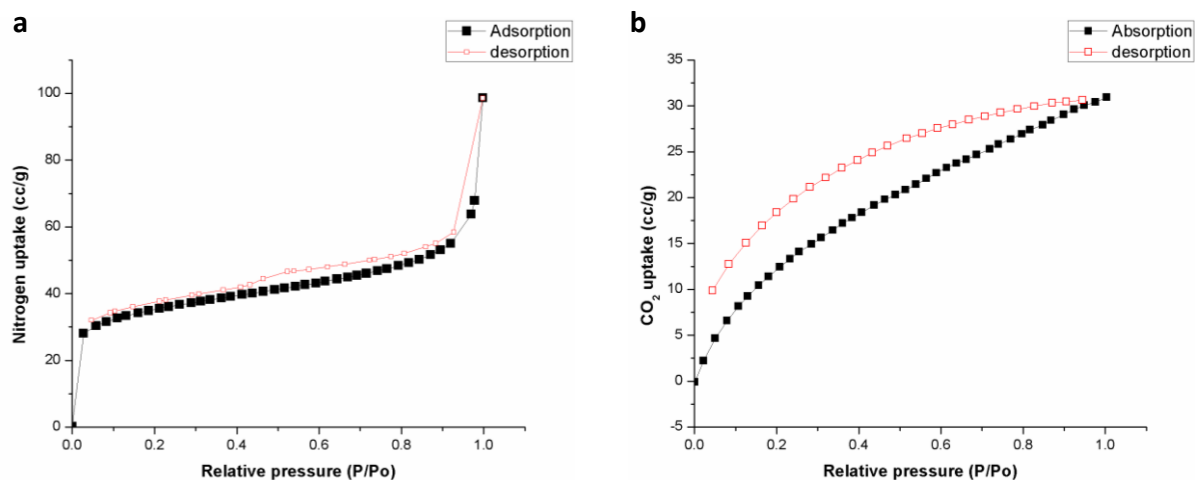


**Fig. 3.05:** a) Nitrogen isotherm of HPB(COOH)<sub>12</sub> performed at 77K. b) CO<sub>2</sub> isotherm of HPB(COOH)<sub>12</sub> performed at 273K.

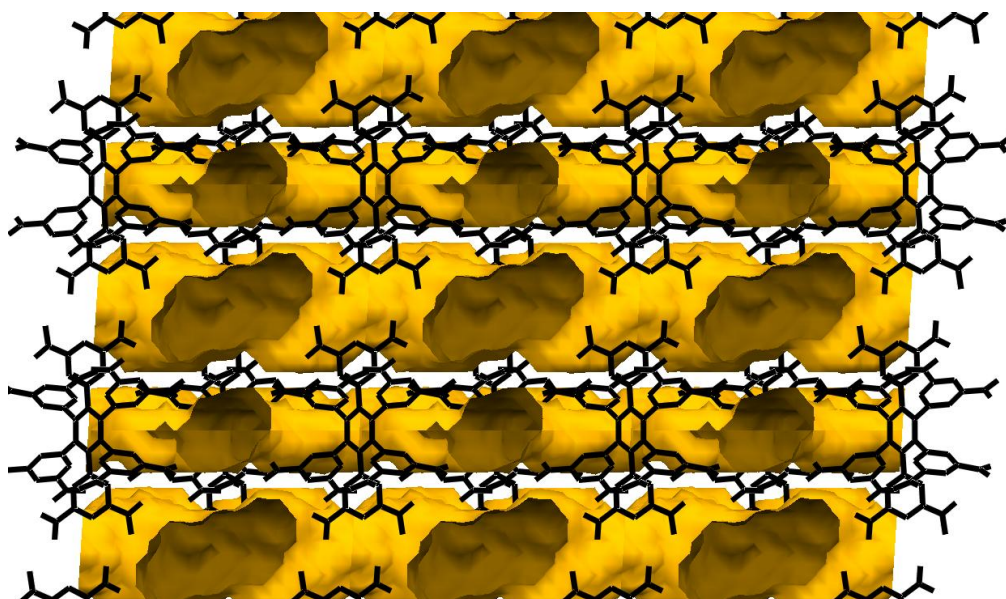


**Fig. 3.06:** Schematic representation of possible channels in the HPB(COOH)<sub>12</sub>

### 3.4 Proton conductivity studies

Proton conduction studies of this material were performed using electrochemical impedance spectroscopy, wherein sample was pelletized and then analyzed under controlled humidity and temperatures. The systematic experiments were performed by a gradual increment of humidity at constant temperature and *vice-versa*. The results of these experiments show that this material has scattered proton conduction at low temperature

and low humid conditions. In contrast, when the temperature had reached 60 °C and 60% RH conductivity was somewhat stabilized at approximately  $3.0 \times 10^{-5} \text{ Scm}^{-1}$  (Fig. 3.07). Further, increase in relative humidity in regular intervals by keeping the temperature at 60 °C, proton conductivity was seen gradually increasing and finally reached to highest value of  $3.2 \times 10^{-2} \text{ Scm}^{-1}$  at 95%, RH (Fig. 3.07). This value is about three fold lesser than the state-of-the-art material Nafion ( $10^{-1} \text{ Scm}^{-1}$ ).

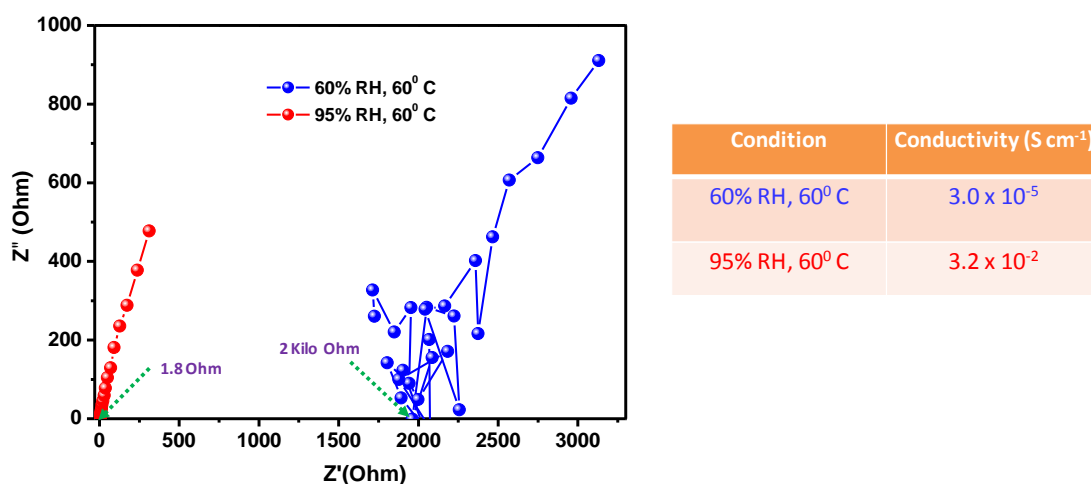


**Fig. 3.07:** Nyquist plot of humidity dependent proton conductivity of HPB(COOH)<sub>12</sub> at 60 °C.

Moreover, this is the highest proton conducting value reported for an organic homomolecular material without any inclusion of acidic guests. In Table. 3.1, we have compared our values with many other porous materials, such as HOFS, MOFs and cages.

**Table. 3.1:** Comparison of proton conductivity of HPB(COOH)<sub>12</sub> with various proton conducting materials.

Compounds	Conductivity (S cm <sup>-1</sup> )	Conditions	Reference
<b>HPB(COOH)<sub>12</sub></b>	<b><math>3.2 \times 10^{-2}</math></b>	<b>60 °C, 95% RH</b>	<b>This work</b>
Mn(dhbq)(H <sub>2</sub> O) <sub>2</sub>	$3.5 \times 10^{-9}$	25 °C, 60% RH	<i>Chem. Lett.</i> , <b>2009</b> , 38, 654-655
[NH(prol) <sub>3</sub> ][MnCr(ox) <sub>3</sub> ]·2H <sub>2</sub> O	$2.0 \times 10^{-6}$	25 °C, 65% RH	<i>J. Am. Chem. Soc.</i> , <b>2009</b> , 131, 13516-13522.
(NH <sub>4</sub> ) <sub>4</sub> [MnCr <sub>2</sub> (ox) <sub>6</sub> ]·4H <sub>2</sub> O	$3.0 \times 10^{-5}$	22 °C, 69% R.H	<i>J. Am. Chem. Soc.</i> , <b>2010</b> , 132, 6620–6621.
Me-FeCr	$0.8 \times 10^{-4}$	25 °C, 65% RH	<i>J. Am. Chem. Soc.</i> <b>2012</b> , 134, 5472-5475.

Cu-TCPP nano-sheet	$3.9 \times 10^{-3}$	25 °C, 98% RH	<i>J. Am. Chem. Soc.</i> <b>2013</b> , <i>135</i> , 7438-7441.
PCMOF-5	$4 \times 10^{-3}$	62 °C, 98% RH	<i>J. Am. Chem. Soc.</i> <b>2013</b> , <i>135</i> , 1193-1196.
im@TPB-DMTP-COF	$1.79 \times 10^{-3}$	100 °C, anhydrous	<i>Nat. Mater.</i> <i>15</i> , 722–726 (2016)
trz@TPB-DMTP-COF	$7.0 \times 10^{-4}$	100 °C, anhydrous	<i>Nat. Mater.</i> <i>15</i> , 722–726 (2016)
CB[6]·1.2H <sub>2</sub> SO <sub>4</sub> ·6.4H <sub>2</sub> O (Organic material)	$1.3 \times 10^{-3}$	25 °C, 98% RH	<i>Angew. Chem. Int. Ed.</i> , <b>2011</b> , <i>34</i> , 7870-7873.
CB[6]·1.1 HCl·11.3H <sub>2</sub> O (Organic material)	$1.1 \times 10^{-3}$	25 °C, 98% RH	<i>Angew. Chem. Int. Ed.</i> , <b>2011</b> , <i>34</i> , 7870-7873.
HOF-GS-11	$1.8 \times 10^{-2}$	30 °C, 95% RH	<i>Angew. Chem. Int. Ed.</i> <b>2016</b> , <i>55</i> , 10667-10671
HOF-GS-10	$7.5 \times 10^{-3}$	30 °C, 95% RH	<i>Angew. Chem. Int. Ed.</i> <b>2016</b> , <i>55</i> , 10667-10671
PCF-1-SO <sub>3</sub> H	$2.6 \times 10^{-2}$	30 °C, 95% RH	<i>J. Mater. Chem. A</i> , 2017, <i>5</i> , 13659

The comparisons of IR and NMR spectra obtained before and after proton conductivity of the materials revealed that there was no change in the signals (Fig. 3.08 & Fig. 3.09a). The PXRD for before and after proton conductivity of the materials was compared (Fig. 3.10); the results showed there was no change in the pattern. This result indicates the stability of post proton conducting material, which is very necessary for the materials application in PEM.

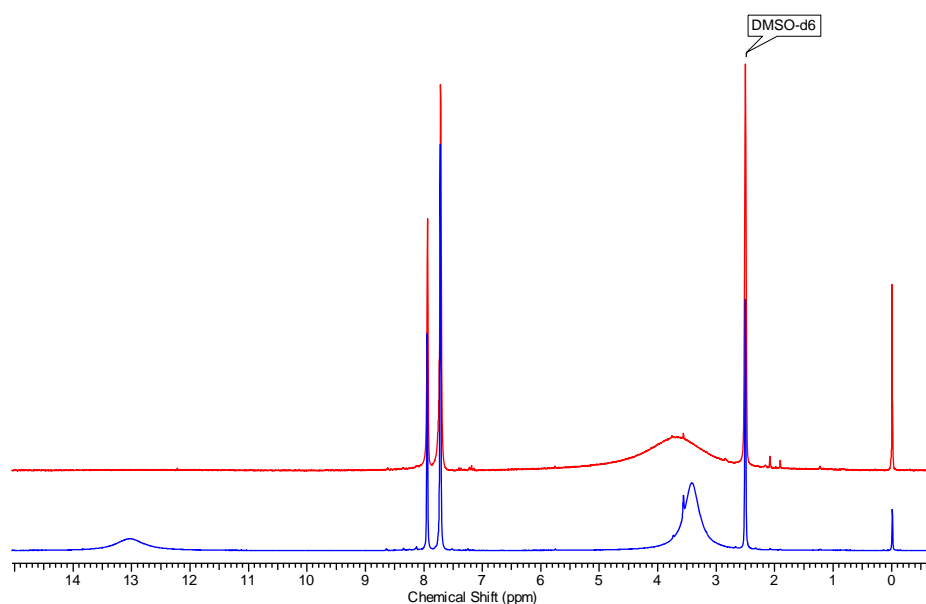


**Fig. 3.08:** <sup>1</sup>H-NMR of HPB(COOH)<sub>12</sub> before (blue) and after (red) proton conductivity (60 °C, 95% RH).



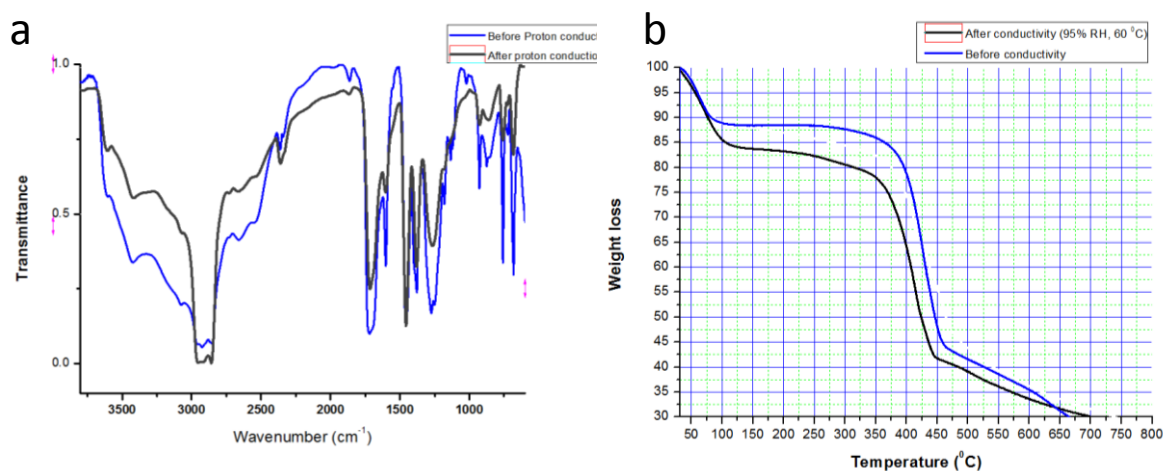


**Fig. 3.09:** a) Infrared spectrum of HPB(COOH)<sub>12</sub> before (blue) and after (black) proton conductivity (60 °C, 95% RH). b) Thermo gravimetric analysis of HPB(COOH)<sub>12</sub> before (blue) and after (black) proton conductivity (60 °C, 95% RH).

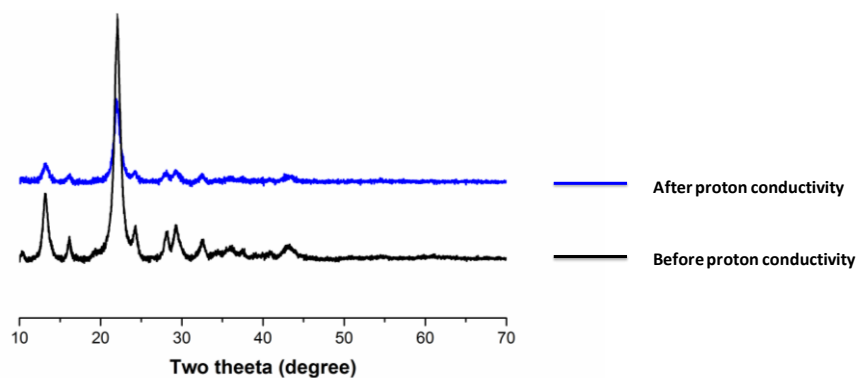
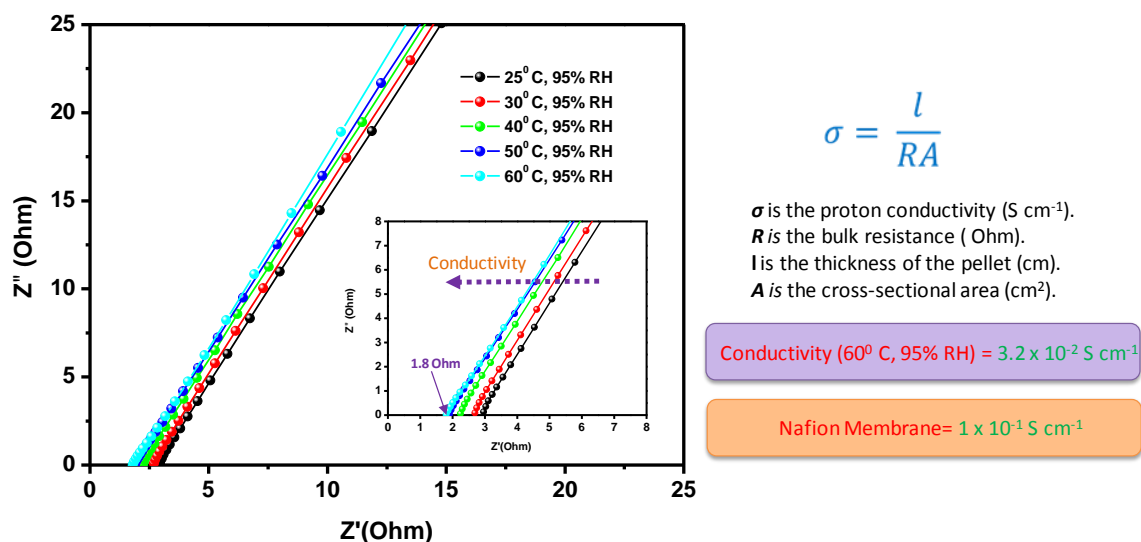


**Fig. 3.10:** PXRD patterns of HPB(COOH)<sub>12</sub> before (black) and after (blue) proton conductivity (60 °C, 95% RH).

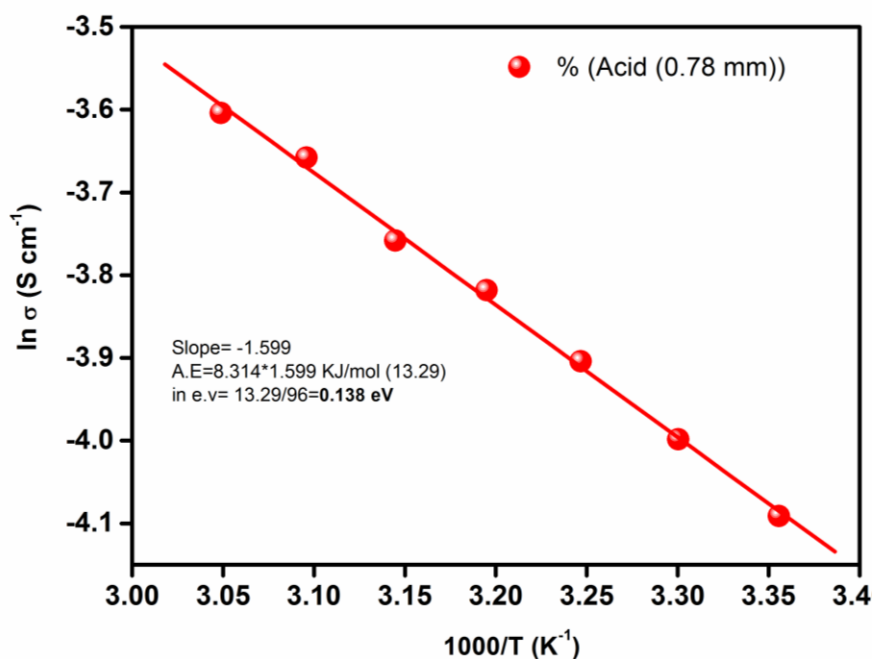
TGA of the post PC measurement material showed approximately 17% weight loss up to 150 °C which could be attributed to the loss of entrapped water molecules (Fig. 3.09b). Upon increasing the temperature above 80 °C, the proton conductivity was decreased. This clearly indicates the significant of role played by water in the proton conducting pathway of the material. The reproducibility of the material was consistent in the order of more than five times. It is very important to ascertain the mechanism of proton conduction for PEM fuel cell applications. Hence, we have calculated the activation energy ( $E_a$ ) value by performing temperature dependent PC measurement at 95% RH (Fig.3.11 & Fig. 3.12). The determined activation energy for the proton conduction was found to be 0.138 eV. This lower activation energy value authenticates the proton conduction mechanism to be Grotthuss type and the value is comparable with lowest activation energy reported for Grotthuss type mechanism (Table. 3.2). Further, proton conductivity measurement of the material was performed in D<sub>2</sub>O under identical

conditions, wherein it was found that the conductivity of D<sub>2</sub>O measurement was lesser than the water (Fig. 3.13). This observation supports the Grotthuss type mechanism. Due to the lesser weight, the proton can be easily conducted than the deuterium (the mass of the proton is little lesser than that of deuterium).

Nyquist Plot : Temperature Dependent @ 95% RH



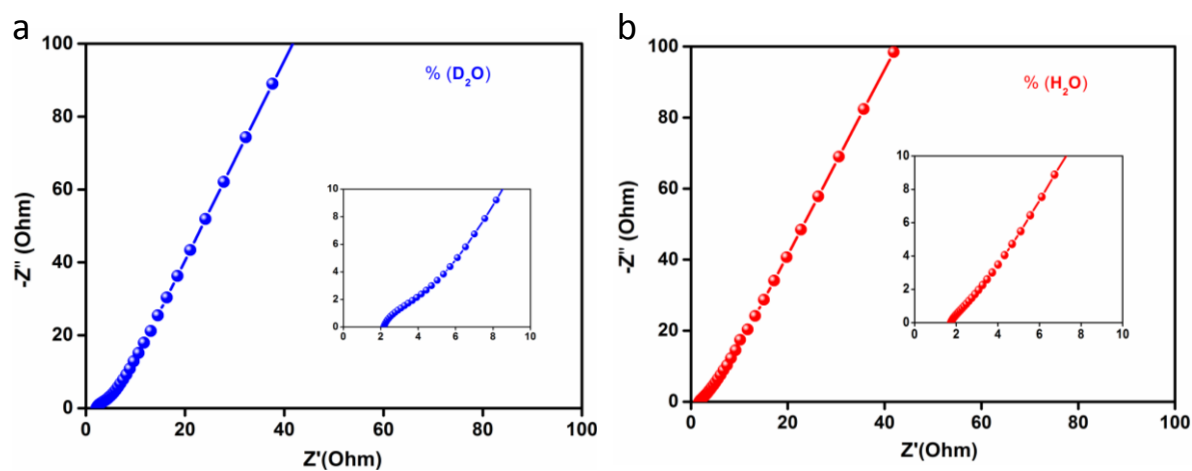
**Fig. 3.11:** Nyquist plot of temperature dependent proton conductivity of HPB(COOH)<sub>12</sub> at 95%.



**Fig. 3.12:** Arrhenius plot for proton conduction of HPB(COOH)<sub>12</sub> at 95% RH.

**Table 3.2:** Activation energy of HPB(COOH)<sub>12</sub> along with some other known proton conducting materials materials with very low activation energies.

Compounds	E <sub>a</sub> (eV)	References
<b>HPB(COOH)<sub>12</sub></b>	<b>0.138</b>	<b>This work</b>
HPF2-100	0.10	<i>Adv. Mater. Interfaces</i> 2015, 2, 1500301
PCMOF-5	0.16	<i>J. Am. Chem. Soc.</i> <b>2013</b> , 135, 1193-1196.
TfOH@MIL-101	0.18	<i>ACS Appl. Mater. Interfaces</i> <b>2014</b> , 6, 5161-5167
PCF-1-SO <sub>3</sub> H	0.19	<i>J. Mater. Chem. A</i> , 2017, 5, 13659
PCF-1	0.18	<i>J. Mater. Chem. A</i> , 2017, 5, 13659
HOF-GS-11	0.13	<i>Angew. Chem. Int. Ed.</i> <b>2016</b> , 55,10667-10671
HOF-GS-10	0.489	<i>Angew. Chem. Int. Ed.</i> <b>2016</b> , 55,10667-10671

**Fig. 3.13:** a) Nyquist plot of proton conductivity of HPB(COOH)<sub>12</sub> in 99% RH (D<sub>2</sub>O) at 60 °C. b) Nyquist plot of proton conductivity of HPB(COOH)<sub>12</sub> in 99% RH (H<sub>2</sub>O) at 60 °C.

### 3.4.1 The role of supramolecular sponge nature in the proton conduction of HPB(COOH)<sub>12</sub>.

We speculated that this material could conduct proton in two path ways A and B (Fig. 3.14).

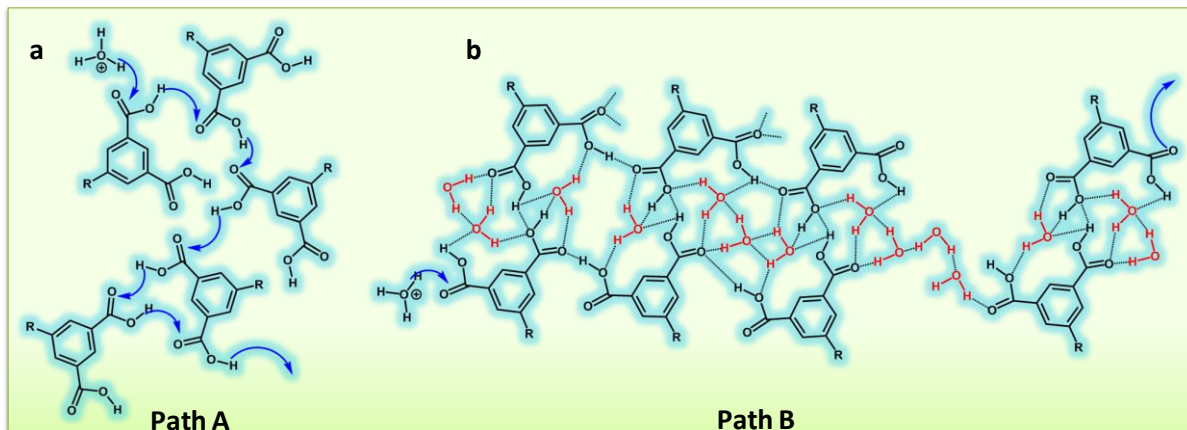


**Fig. 3.14:** a) Possible proton conducting path ways of supramolecular sponge HPB(COOH)<sub>12</sub>.

In path A, very less number of water molecules are enough to initiate the conduction and rest of the proton conduction could happen through hydrogen bonded network of the carboxylic acids. While in Path B, proton conduction could happen only after reaching the entrapment of the water molecules in optimum numbers for the formation of hydrogen bonded network for the easy conduction of protons (supramolecular spongy action). In this path way, both carboxylic acid group and water molecules were cooperatively involved in the H-bond network formation, and it could follow lower energy path way. All the experimental evidence like scattered/poor conduction under lower humid condition (even at higher temperature), lower activation energy are not in favor of path A. On the contrary, high RH value, high proton conduction (above 60%), lower activation energy are suggesting that the path B could be a better fitting path way. At optimum temperature and humidity, it is possible for water molecules to jointly form an extended H-bonding network with host molecule HPB(COOH)<sub>12</sub>. But, at lower temperature and humidity, they could not form such H-bond networks sufficiently for the effective proton conduction. The temperatures above 80 °C, water molecules could try to escape as gases owing to breakage of H-bonding and as a result, the proton conductivity gets reduced to  $5 \times 10^{-3} \text{ Scm}^{-1}$  (Fig. 3.15). Moreover, tolane tetra carboxylic acid **2** was prepared from tolane tetra ester **1** by following the reported procedure<sup>34</sup> (Scheme 3.02) and its proton conductivity was performed under similar

conditions of HPB(COOH)<sub>12</sub>. The proton conductivity of **2** is scattered (Fig. 3.16) even at high temperature and high humidity conditions which clearly indicates the high proton conductivity of HPB(COOH)<sub>12</sub> arising from its spongy nature.

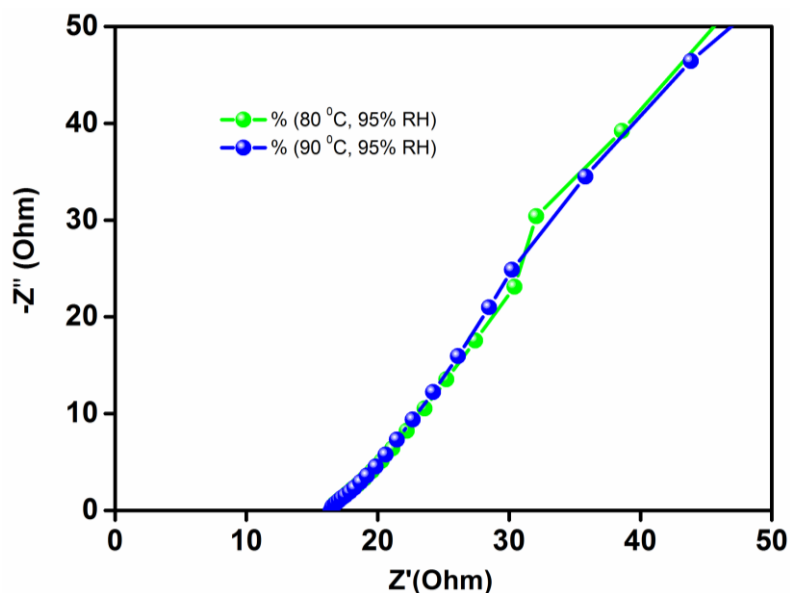
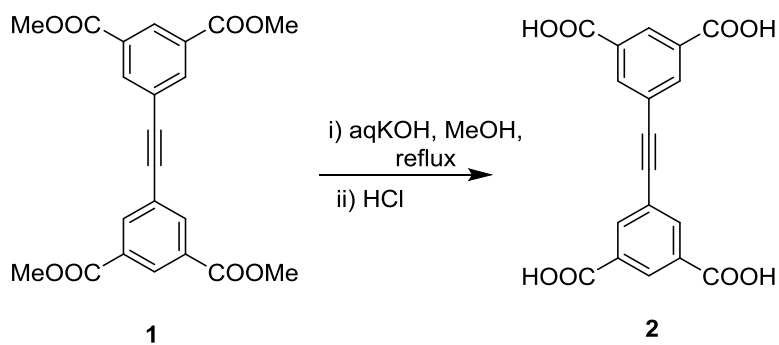


**Fig. 3.15:** Nyquist plot for proton conductivity of HPB(COOH)<sub>12</sub> at 80 °C and 90 °C, 95% RH.



**Scheme 3.02** Synthesis of tolane tetra carboxylic acid (**2**)

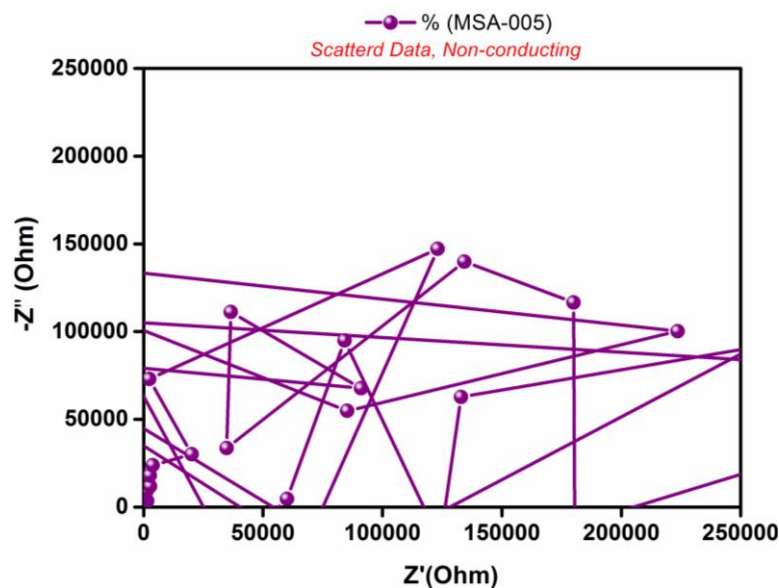


**Fig. 3.16:** Nyquist plot for proton conductivity of  $\text{Ar}(\text{COOH})_4$  (**2**) at 60 °C, 95% RH.

### 3.4.2 Reversal of temperature in proton conductivity of $\text{HPB}(\text{COOH})_{12}$

It is noteworthy that consistency of proton conductivity upon reversing the temperature is important in fuel cell applications. Therefore, reverse proton conductivity was performed by gradual reduction of temperature which was almost consistent with the forward ones (Fig. 3.17). In this experiment, we first recorded proton conductivity of  $\text{HPB}(\text{COOH})_{12}$  by increasing temperature from 25 °C to 60 °C at 95% RH. Then, same experiment was continued and proton conductivity was measured by decreasing the temperature from 60 °C to 25 °C at 95% RH. While reversing the temperature, slight reduction of resistance was observed.

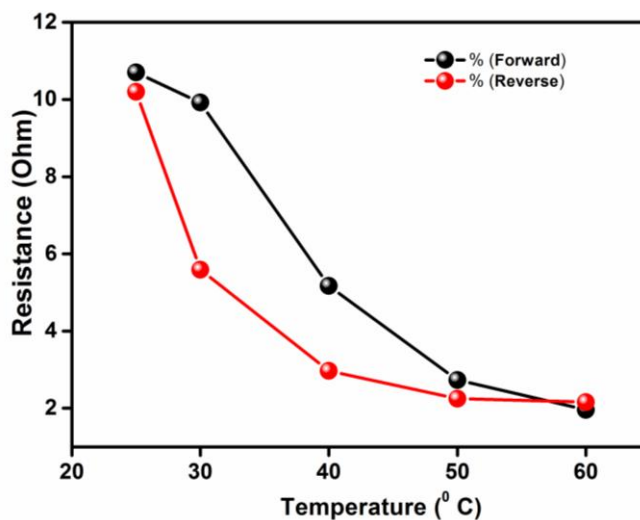
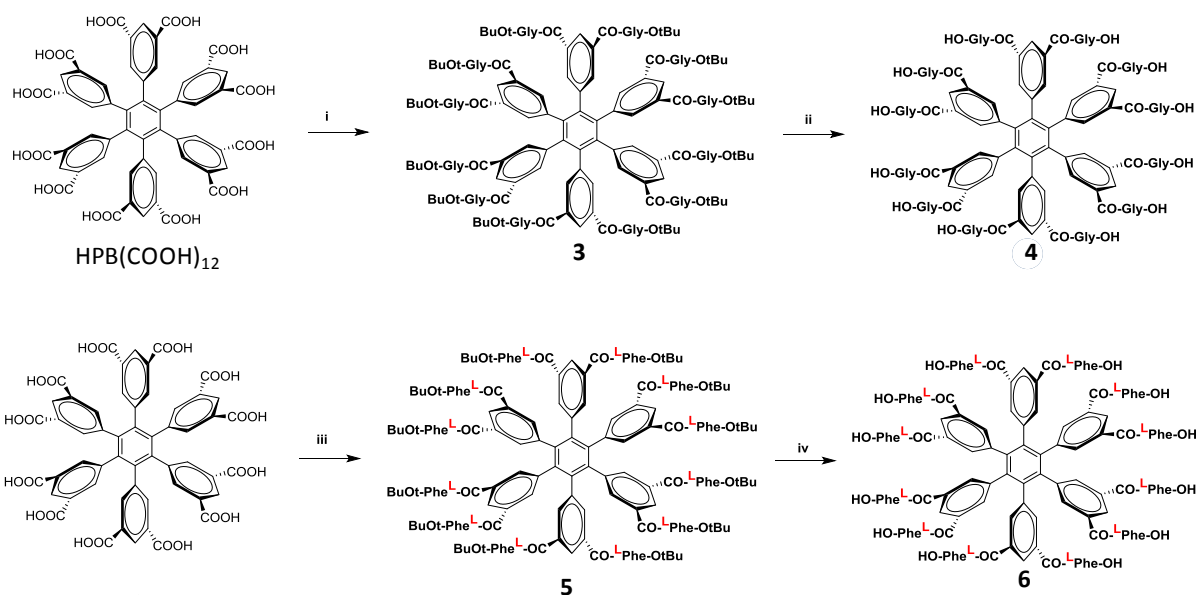


**Fig. 3.17:** Resistance of  $\text{HPB}(\text{COOH})_{12}$  upon temperature forward and reversal.

### 3.5 An attempt for the synthesis, characterizations and proton conductivity applications of amino acid coupled extended systems.

Motivated with these results, we have prepared the extended derivatives of HPB(CONHGly-OH)<sub>12</sub> (**4**) and HPB(CONH<sup>L</sup>Phe-OH)<sub>12</sub> (**6**) by reacting *t*-butyl ester of corresponding amino acids with HPB(COOH)<sub>12</sub> and followed by deprotection of *t*-butyl ester using DCM-TFA (Scheme 3.03). The coupling of amino acids with HPB(COOH)<sub>12</sub> was performed with slightly modified procedure of chapter-1. The compounds **4** and **6** were characterized by IR, NMR, MASS.



**Scheme 3.03:** Reagents and conditions: (i) glycine *tert*-butyl ester hydrochloride, HBTU, DIEA, DMSO, rt, 12h; ii) TFA:DCM (3:1), rt, 4h; iii) L-phenylalanine methyl ester hydrochloride, HBTU, DIEA, DMSO, rt, 12h; iv) TFA:DCM (3:1), rt, 4h.

HPB(CONHGly-OH)<sub>12</sub> is readily soluble in water. Therefore, we could not proceed further for proton conductivity measurements. The compound HPB(CONHPhe-OH)<sub>12</sub> was not readily soluble in water. So we have attempted to make a pellet for studying PC measurements, but unfortunately, we could not pelletize the material owing to its amorphous-sticky nature.

### 3.6 Conclusion

We described a porous organic molecular material which was literally behaving as a supramolecular sponge to uptake water molecules into their cavities, as a result of which it showed highest proton conductivities in the order of  $10^{-2}$  S/cm at 60 °C, 95% RH. This conductivity is about only three-fold lesser than the state-of-the-art proton-conducting polymer Nafion and much higher than many of the reported MOF, COF materials so far. Moreover, this is a unique report wherein powdered homo-molecular H-bonded porous material showed unprecedented conductivity without any inclusion of acid guests. Temperature, humidity dependent proton conductivity studies, and isotopic experiments clearly revealed that the proton transport mechanism is through low-energy-barrier Grotthuss hopping mechanism. The reversibility, reproducibility of the proton conduction studies, PXRD, TGA and other analytical characteristic revealed that the physical and chemical stability of this material. The synthesis of 12-armed HPB derivatives such as HPB(CONHGly-OH)<sub>12</sub> and HPB(CONHPhe-OH)<sub>12</sub> was achieved using peptide coupling strategy but their PC measurement could not be accomplished, owing to their solubility and amorphous-sticky nature. Further improvement of HPB-based proton conducting materials and their fuel cell applications are ongoing research in our lab.

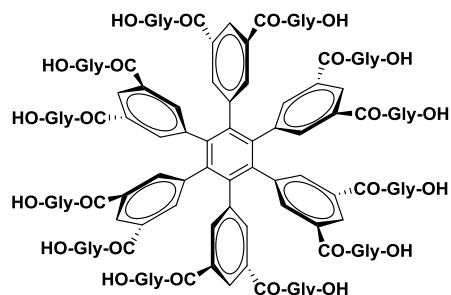


### 3.7 Experimental section:

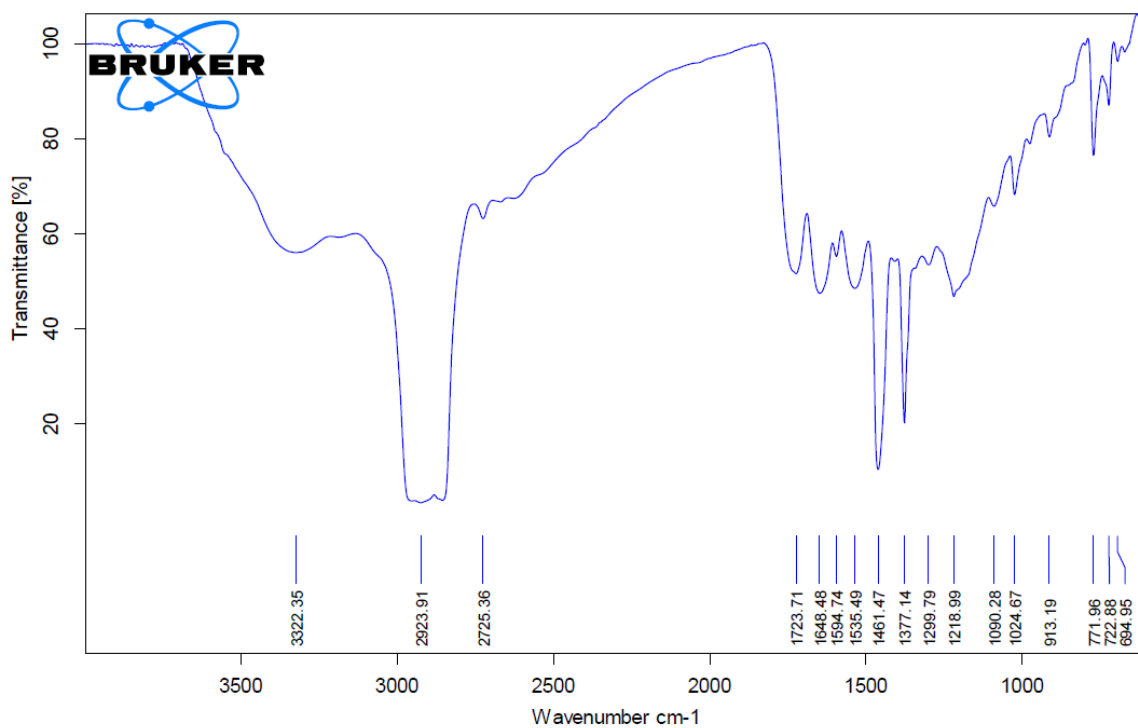
#### Synthesis

Synthesis of **HPB(COOH)<sub>12</sub>** is mentioned in the chapter-2.

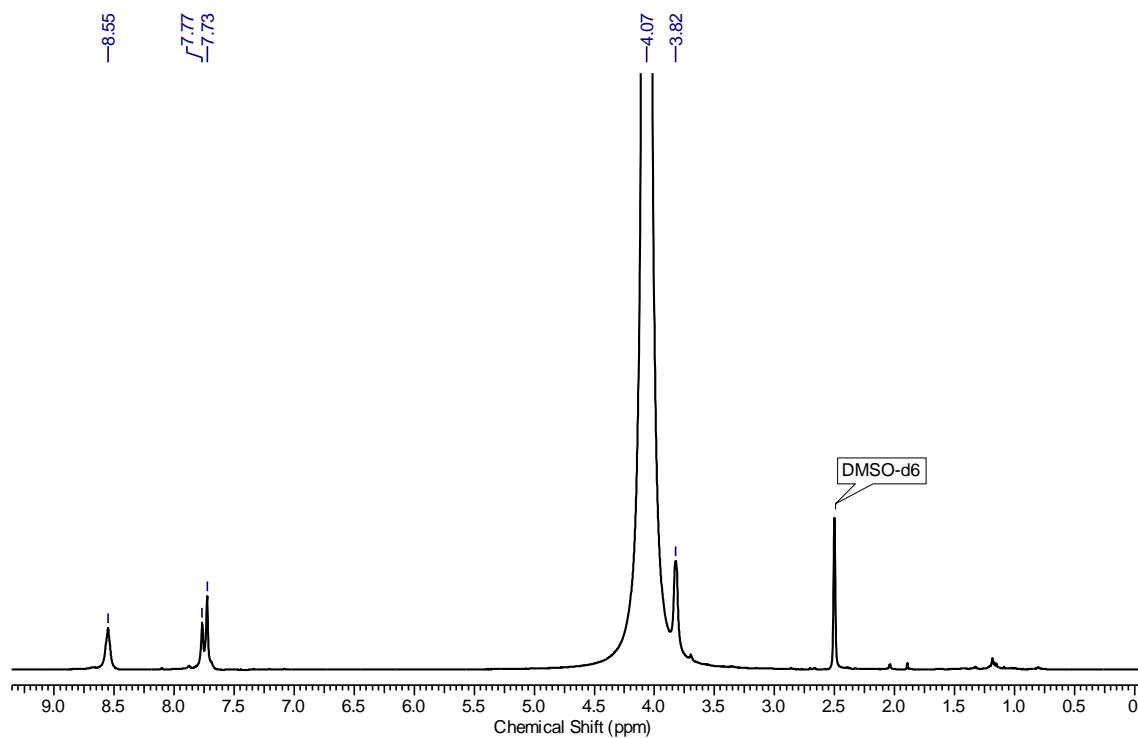
#### Compound 4

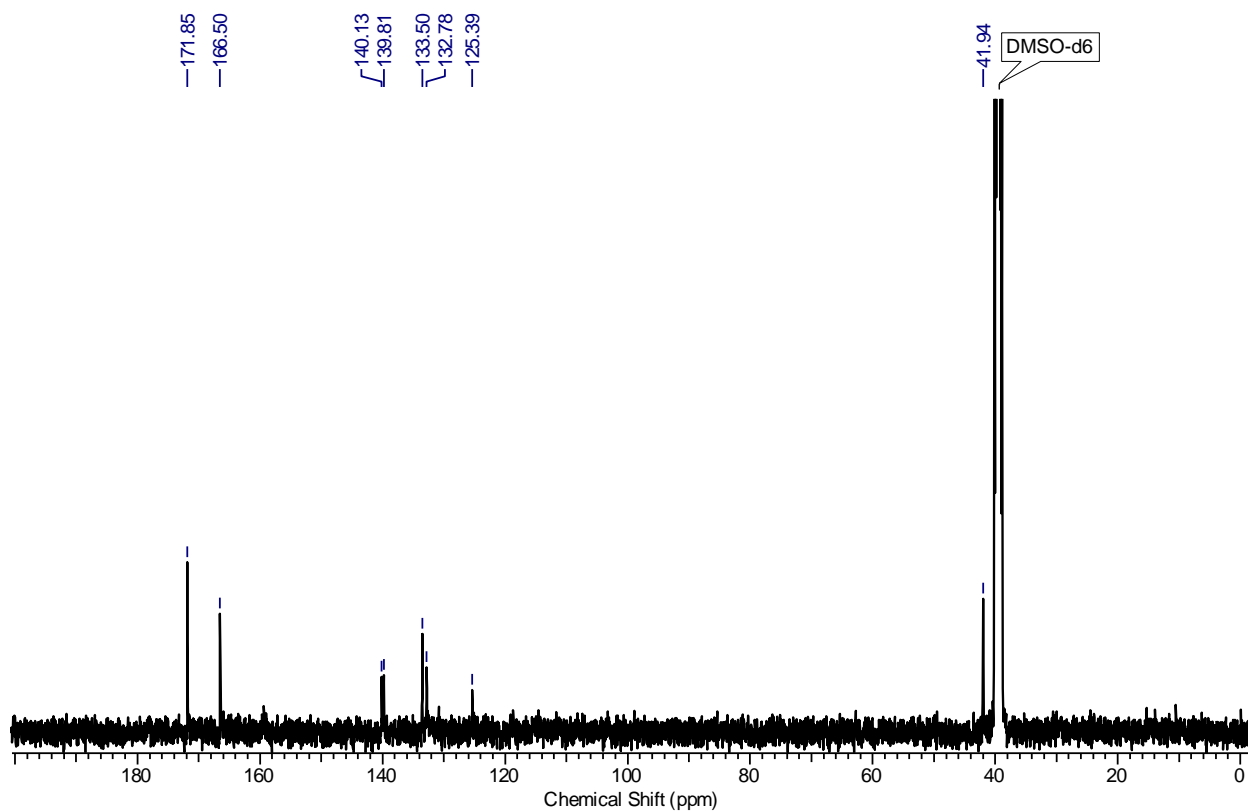


To a suspension of **HPB(COOH)<sub>12</sub>** (0.05 g, 0.04708 mmol) and DIEA (0.328 mL, 1.88 mmol) in DMSO (4 mL) was added HBTU (0.321 g, 0.847 mmol) and the mixture was stirred at room temperature for 5 minutes to form clear solution. Then glycine *tert*-butyl ester hydrochloride (0.1420 g, 0.847 mmol) was added and stirring was continued for 12 h. After completion of the reaction, the reaction mixture was diluted with ice-chilled water and thrice extracted with DCM. The combined organic phases were dried over sodium sulfate and evaporated *in vacuo*. The crude product was purified by column chromatography (eluent: AcOEt/ pet. ether, 60/40 v/v,  $R_f = 0.6$ ) to furnish **3** as a fluffy white solid. The material obtained was further subjected to deprotect the *t*-butyl groups using TFA: DCM (3 mL: 1 mL, 3:1) at room temperature for 4 h. After complete deprotection (monitored by TLC), the reaction mixture was evacuated *in vacuo*. The residue obtained was treated with dry diethyl ether and then filtered over a Buchner funnel and washed with diethyl ether several times to get **4** as white colored solid. Yield: 68%. mp: 234-236 °C; IR (nujol)  $\text{cm}^{-1}$ : 3322, 2923, 2725, 1723, 1648, 1594, 1535, 1461, 1377, 1299, 1218, 1090, 913, 771, 722, 694;  $^1\text{H-NMR}$  (400MHz, DMSO- $d_6$ )  $\delta$ : 8.55 (s, 12H), 7.77 (s, 6H), 7.73 (s, 12H), 3.82 (s, 24H);  $^{13}\text{C-NMR}$  (101MHz, DMSO- $d_6$ )  $\delta$ : 171.9, 166.5, 140.1, 139.8, 133.5, 132.8, 125.4, 41.9; MALDI-TOF/TOF: 1769.3600  $[\text{M}+\text{Na}]^+$ .

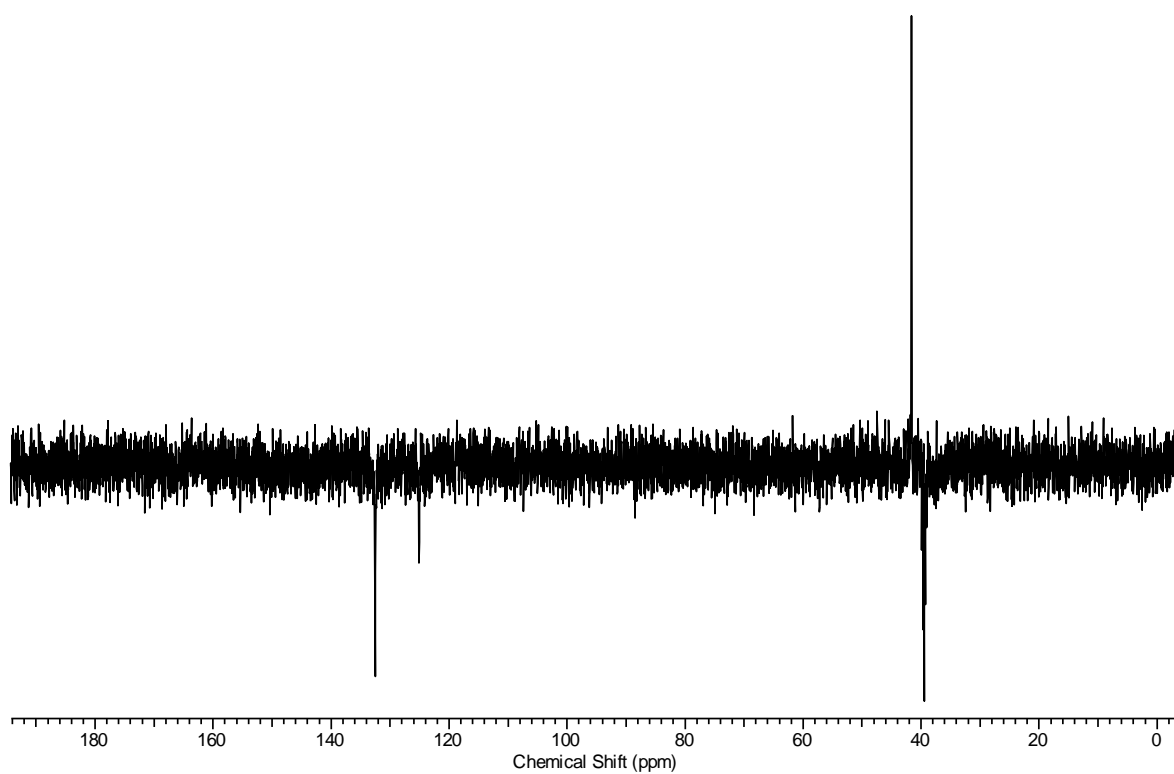


IR spectrum of compound 4

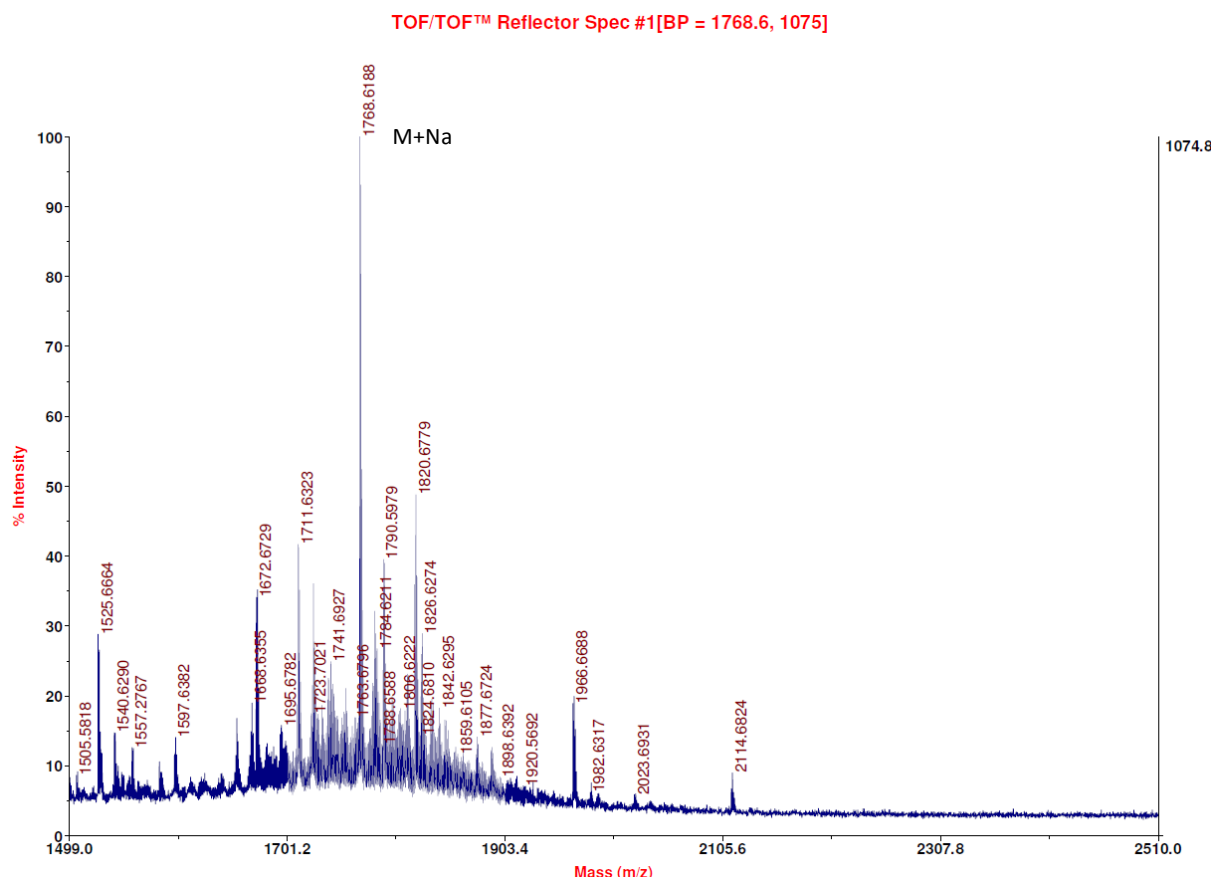
 $^1\text{H}$  NMR spectrum of compound 4 ( $\text{DMSO-}d_6$ , 400 MHz, 298 K)



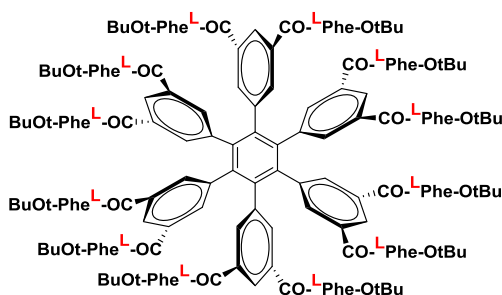
$^{13}\text{C}$  NMR spectrum of compound **4** (DMSO-*d*<sub>6</sub>, 100 MHz, 298 K)



DEPT 135 spectrum of compound **4** (DMSO-*d*<sub>6</sub>, 100 MHz, 298 K)

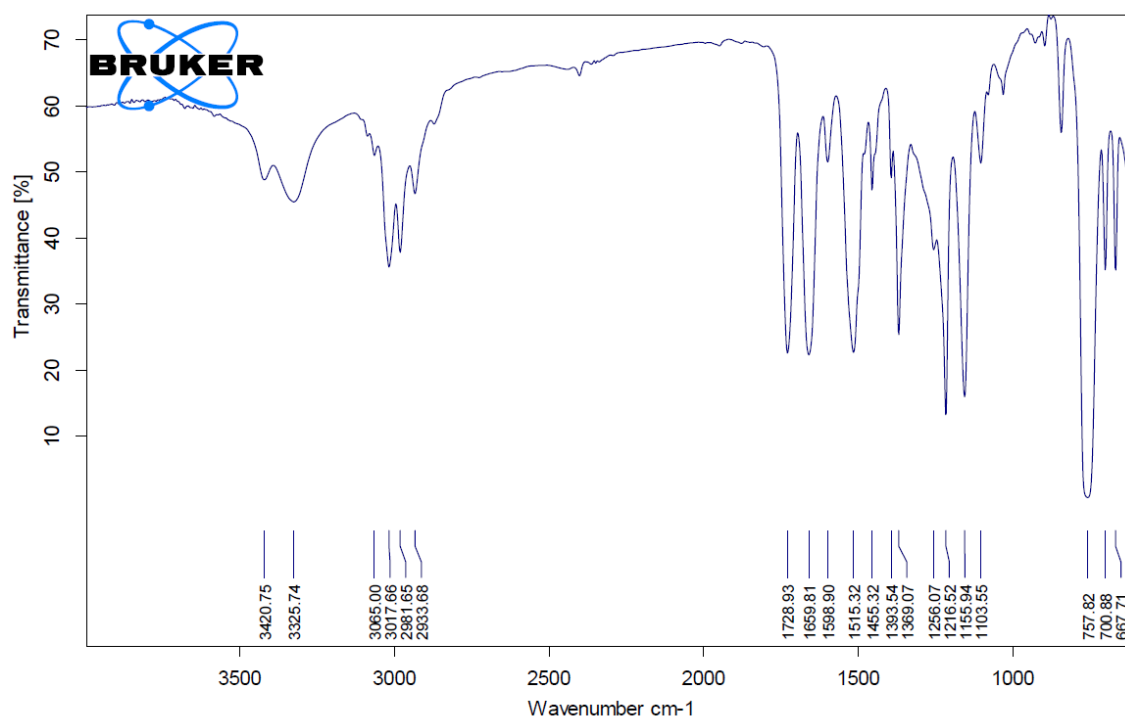


### Compound **5**

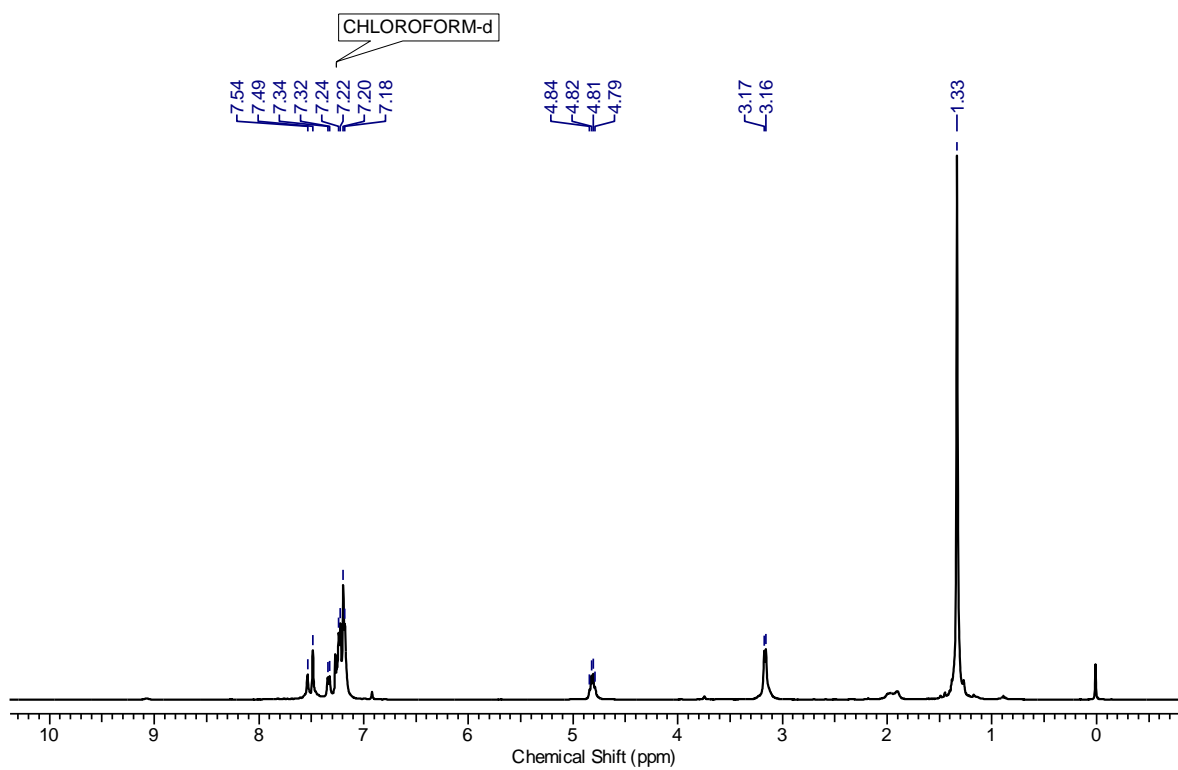


Compound **5** was synthesized, following the procedure for **4**, using compound HPB(COOH)<sub>12</sub> (0.2 g, 0.188 mmol), DIEA (1.12 mL, 6.4 mmol), DMSO (7 mL), HBTU (1.21 g, 3.2 mmol), L-phenylalanine *tert*-butyl ester hydrochloride (0.73 g, 2.82 mmol). The crude product was purified by column chromatography (eluent: AcOEt/ pet. ether, 60/40 v/v, R<sub>f</sub>= 0.6) to furnish **5** as a fluffy white solid. Yield: 0.48 g (73 %). mp: 178-180 °C; TLC (ethyl acetate/pet ether, 40:60 v/v): R<sub>f</sub> = 0.5; [α]<sub>D</sub><sup>23</sup>: -35.1° (c = 0.1, CHCl<sub>3</sub>); IR

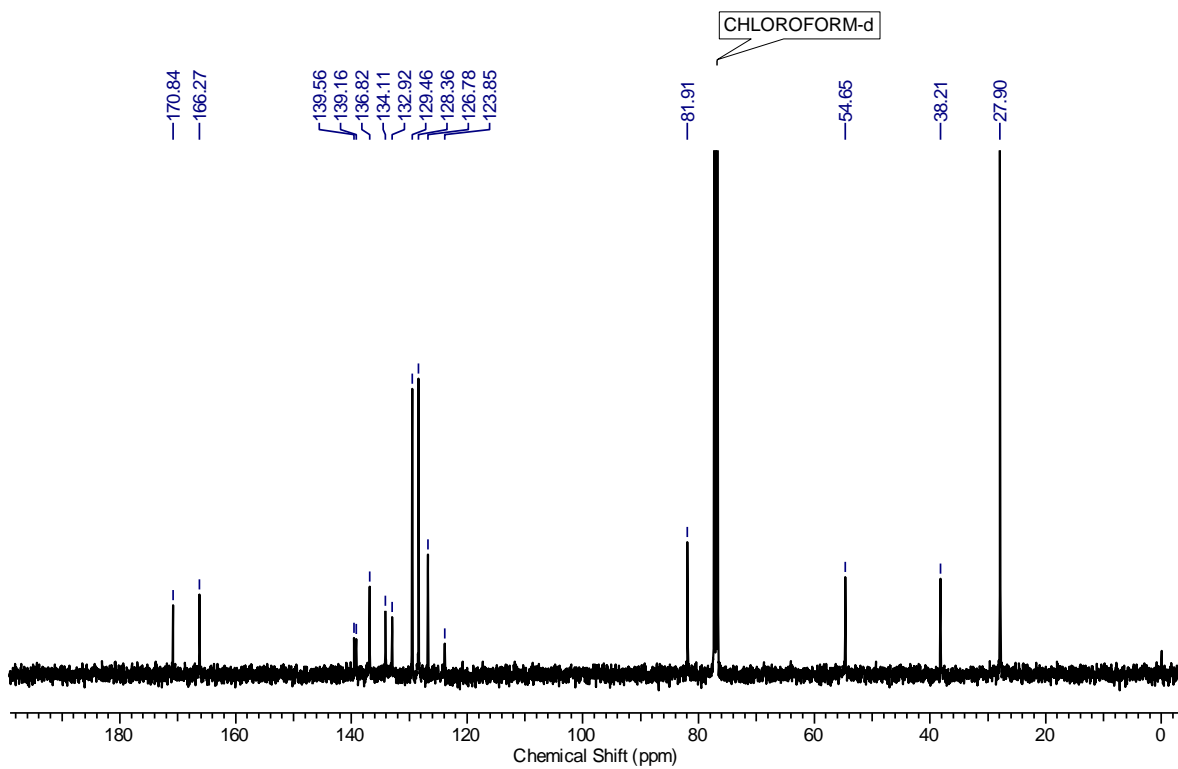
(CHCl<sub>3</sub>) cm<sup>-1</sup>: 3420, 3325, 3065, 3017, 2981, 2933, 1728, 1659, 1598, 1515, 1455, 1393, 1369, 1256, 1216, 1155, 1103, 757, 700, 667; <sup>1</sup>H-NMR (400MHz, CDCl<sub>3</sub>) δ: 7.54 (br. s., 6H), 7.49 (s, 12H), 7.33 (d, *J* = 7.9 Hz, 12H), 7.21 (m, 60 H), 4.82 (q, *J* = 7.1 Hz, 12H), 3.17 (d, *J* = 6.7 Hz, 24H), 1.33 (s, 108H); <sup>13</sup>C-NMR (101MHz, CDCl<sub>3</sub>) δ: 70.8, 166.3, 139.6, 139.2, 136.8, 134.1, 132.9, 129.5, 128.4, 126.8, 123.9, 81.9, 54.6, 38.2, 27.9; MALDI-TOF/TOF: 3521.7063 [M+Na]<sup>+</sup>, all t-butyl deprotected acid 2850.2949 [M+Na]<sup>+</sup>; Elemental analysis calculated for C<sub>210</sub>H<sub>234</sub>N<sub>12</sub>O<sub>36</sub>: C, 72.02; H, 6.73; N, 4.80. Found: C, 72.06; H, 6.67; N, 4.83.



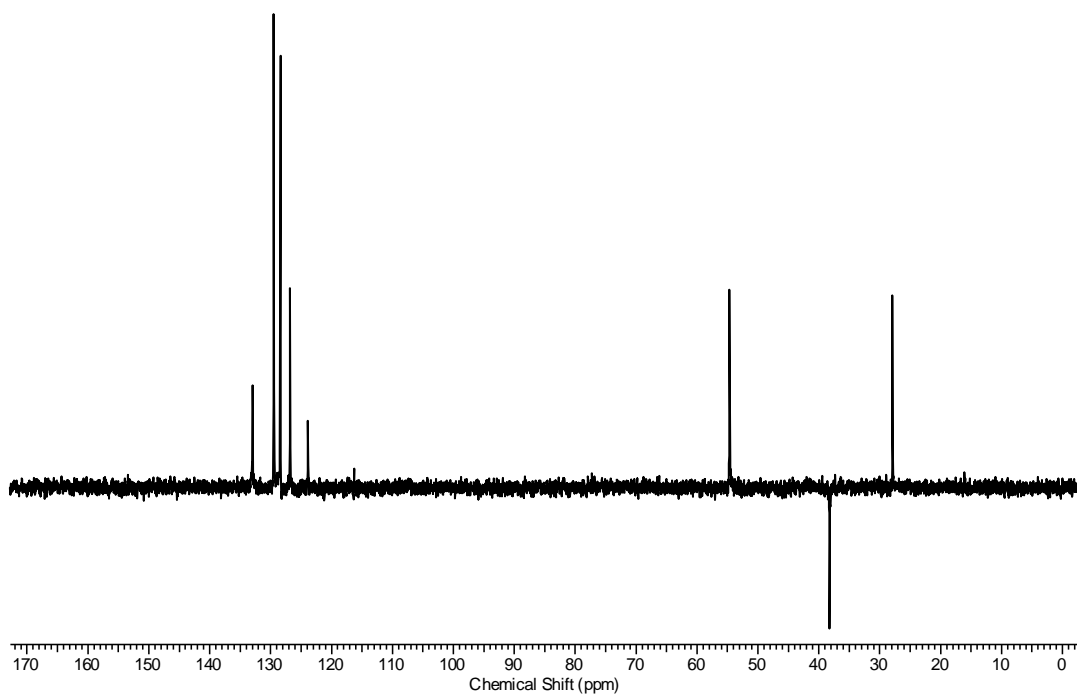
IR spectrum of compound 5



$^1\text{H}$  NMR spectrum of compound **5** ( $\text{CDCl}_3$ , 400 MHz, 298 K)

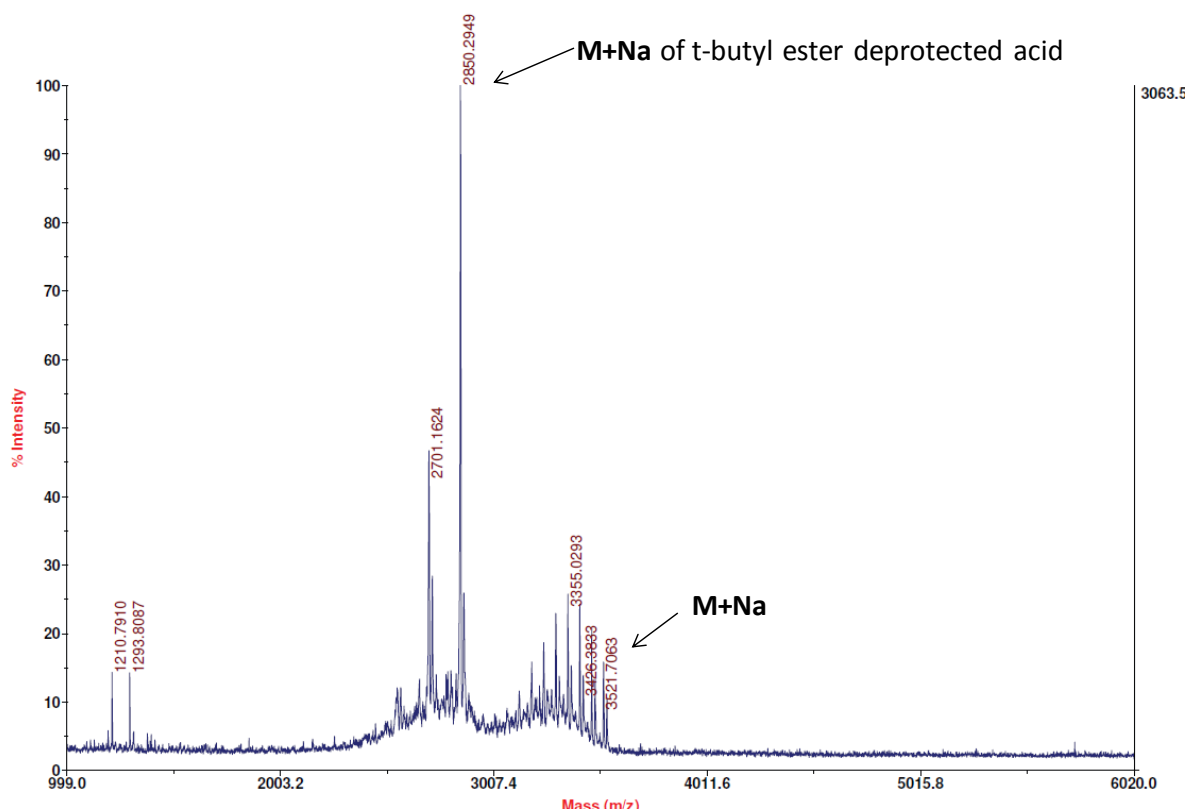


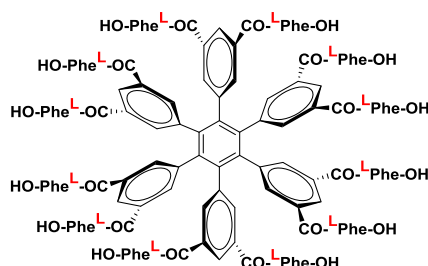
$^{13}\text{C}$  NMR spectrum of compound **5** ( $\text{CDCl}_3$ , 100 MHz, 298 K)

DEPT 135 spectrum of compound **5** (CDCl<sub>3</sub>, 100 MHz, 298 K)

AB Sciex TOF/TOF™ Series Explorer™ 72085

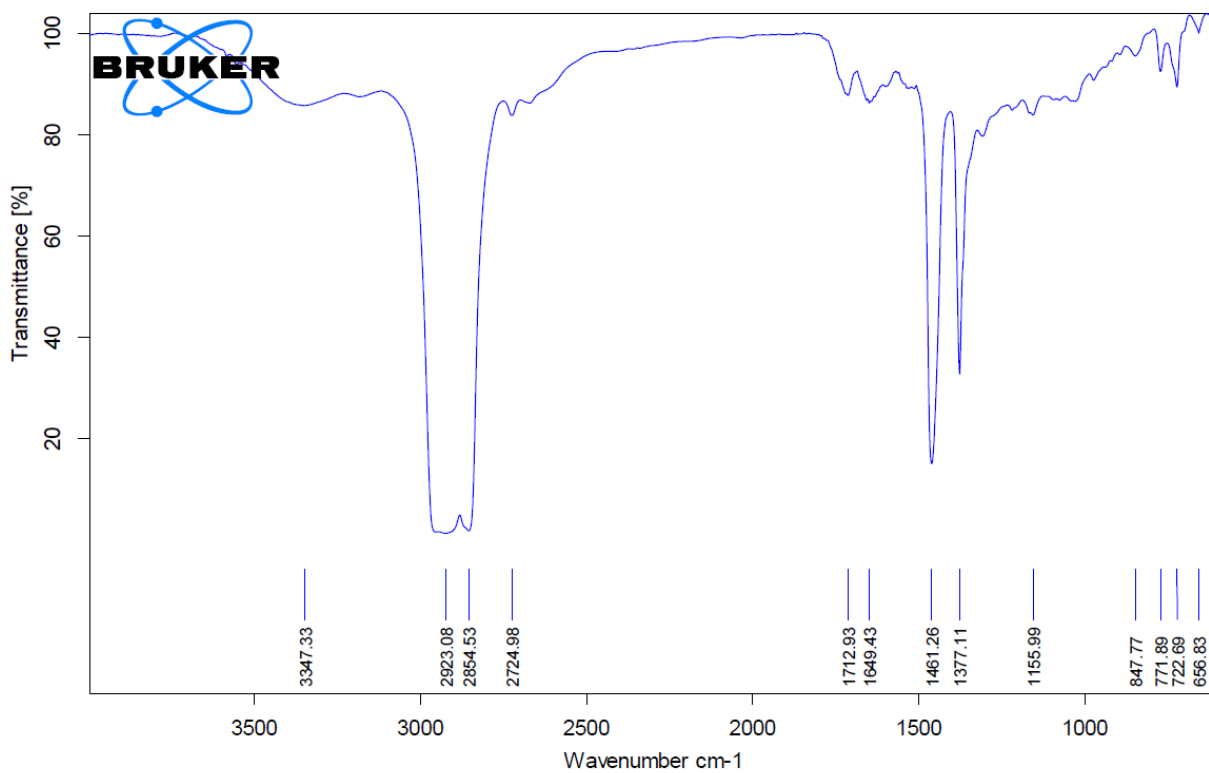
TOF/TOF™ Reflector Spec #1[BP = 2850.4, 3064]

MS (MALDI-TOF) of compound **5**

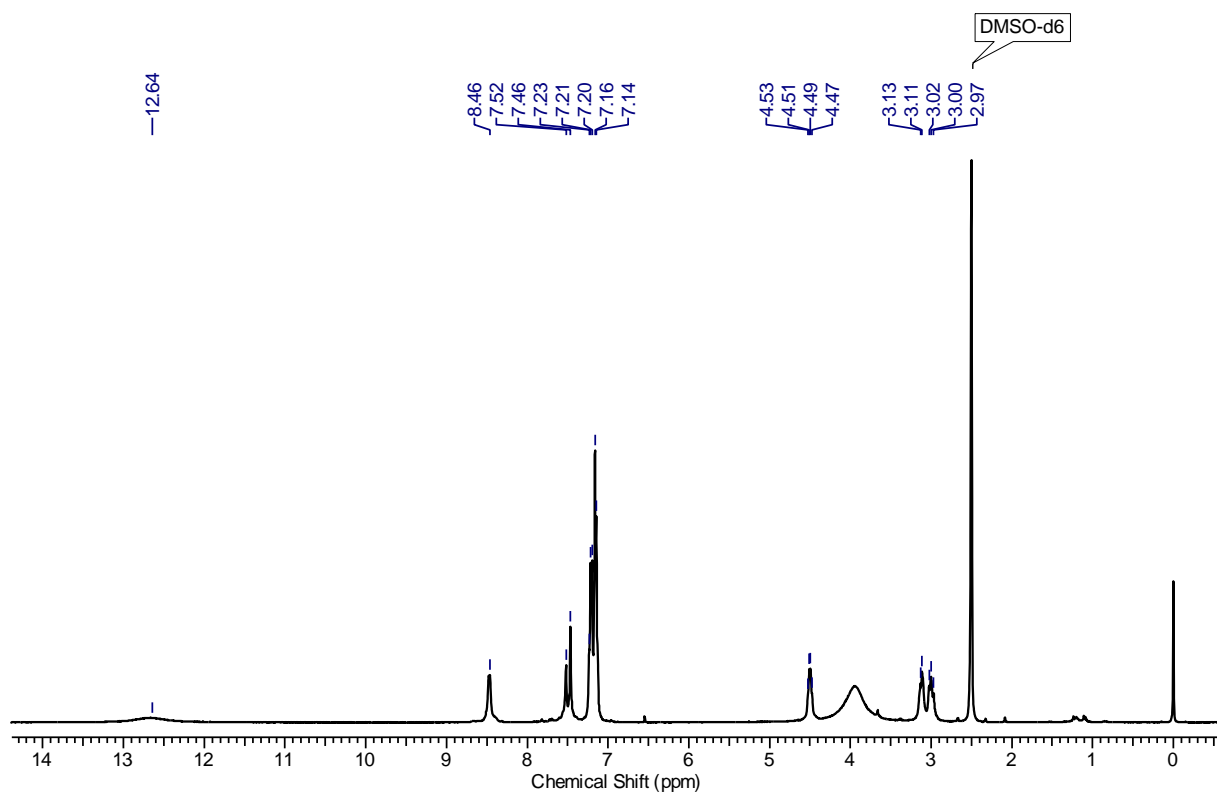
**Compound 6**

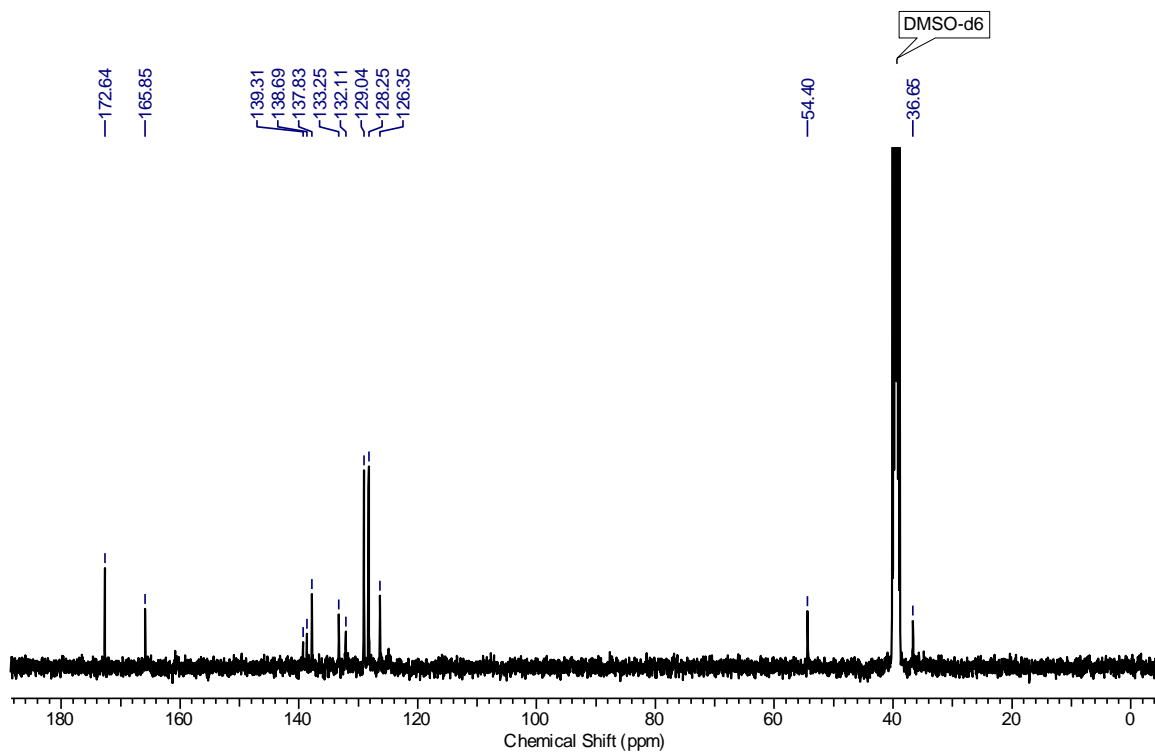
To a 3:1 mixture of TFA and DCM (10 mL), **5** (0.4 g) was added at room temperature. After stirring for 4 h., the reaction mixture was stripped off the volatiles under reduced pressure. The residue obtained was treated with dry diethyl ether and then filtered over a Buchner funnel and washed with diethyl ether several times to get **6** as white colored solid. Yield: 0.31 g (96%). mp: 186-188 °C;  $[\alpha]_D^{24}$ : -260.3° (c = 0.1, CHCl<sub>3</sub>); IR (nujol) cm<sup>-1</sup>: 3347, 2923, 1712, 1649, 1461, 1377, 1155, 847, 771, 722, 656; <sup>1</sup>H-NMR (400MHz, DMSO-d<sub>6</sub>) δ: 12.64 (br. s., 12H), 8.46 (br. s., 12H), 7.52 (br. s., 6H), 7.46 (br. s., 12H), 7.26 - 7.10 (m, 60H), 4.55 - 4.45 (m, 12H), 3.20 - 2.92 (m, 24H); <sup>13</sup>C NMR (101MHz, DMSO-d<sub>6</sub>) δ: 172.6, 165.8, 139.3, 138.7, 137.8, 133.3, 132.1, 129.0, 128.3, 126.4, 54.4, 36.7; MALDI-TOF/TOF: 2825.9 [M+Na]<sup>+</sup>, 2847.3.



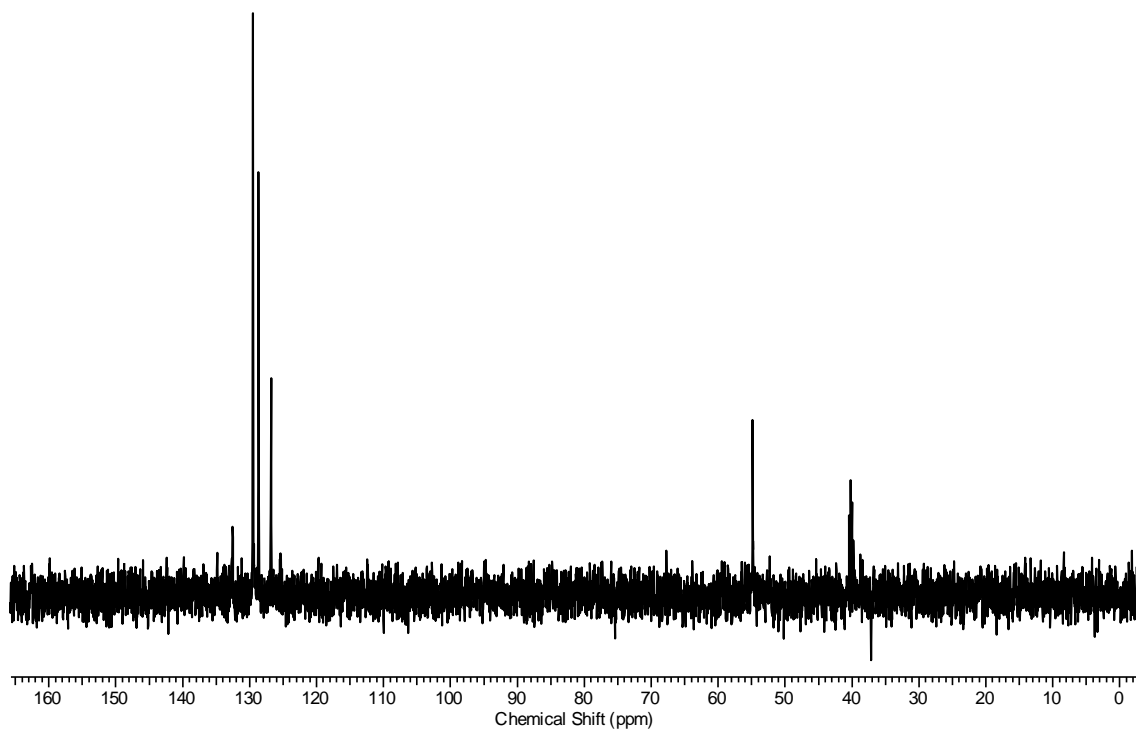


IR spectrum of compound 6

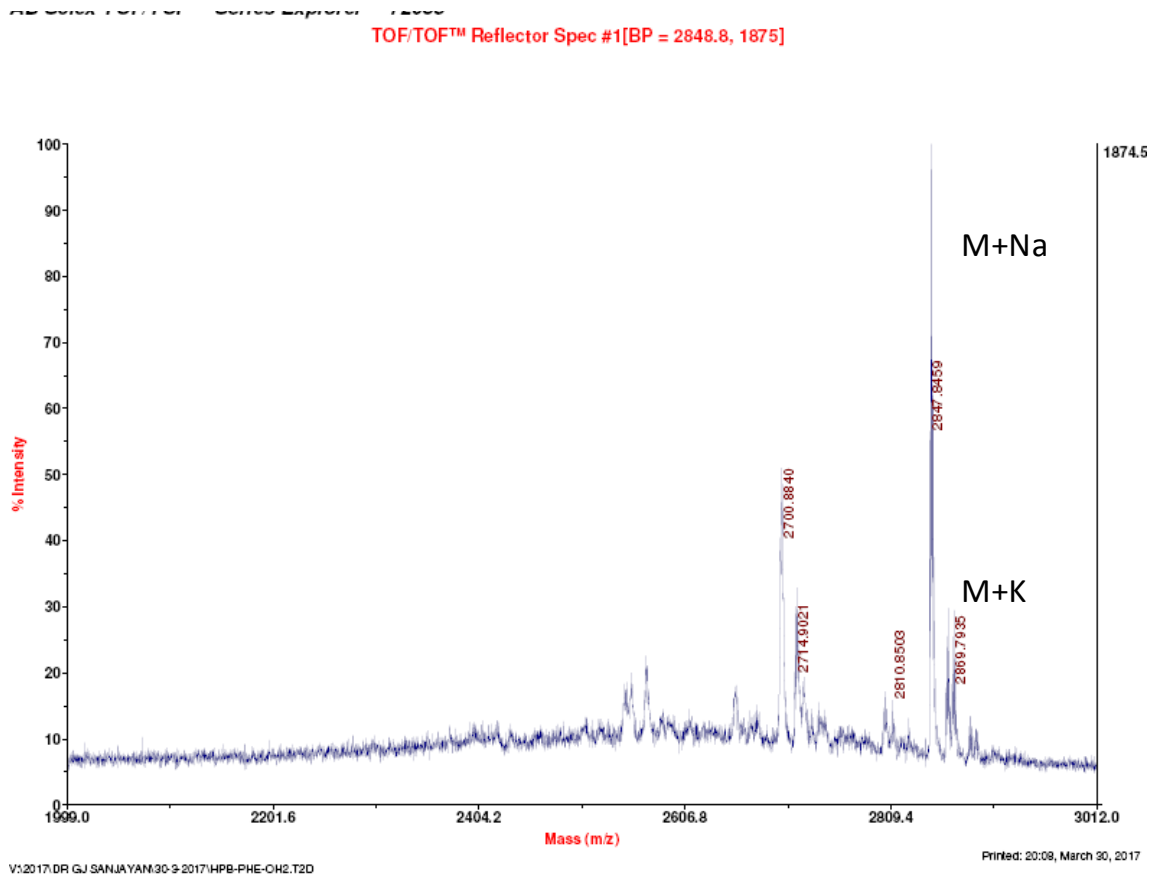
<sup>1</sup>H NMR spectrum of compound 6 (DMSO-*d*<sub>6</sub>, 400 MHz, 298 K)



$^{13}\text{C}$  NMR spectrum of compound **6** (DMSO-*d*<sub>6</sub>, 100 MHz, 298 K)



DEPT 135 spectrum of compound **6** (DMSO-*d*<sub>6</sub>, 100 MHz, 298 K)

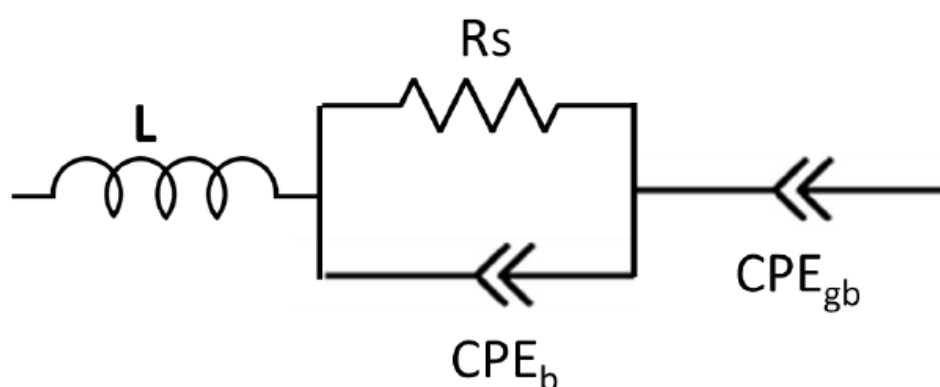
MS (MALDI-TOF) of compound **6**

**Gas adsorption:**

Nitrogen adsorption isotherms analyses were performed on Quantachrome Quadrasorb automatic volumetric instrument at 77 K using liquid N<sub>2</sub> bath. Before going for gas adsorption treatment, samples were degassed at 100 °C for 12 h under vacuum. Surface areas were calculated using Brunauer-Emmett-Teller (BET) model applied between P/P<sub>0</sub> values of 0.05. CO<sub>2</sub> adsorption measurements were performed at 273 K on Quantachrome Quadrasorb automatic volumetric instrument.

**Proton conductivity measurements:**

Impedance Analysis: Impedance analyses of the samples were carried out in BioLogic VMP-3. Measurements were done in a two-electrode assembly using stainless steel discs as electrode and samples were kept in between them in the form of solid pellets. The complete cell assembly was kept in Espec environmental test chamber for controlling the relative humidity and temperature. We have used the frequency range for the measurement from 10<sup>6</sup> to 0.1 Hz against the open circuit potential with sinus amplitude of 10 mV. All the EIS data were fitted using a EC-Lab Software V10.19 by equivalent circuit as shown below, where L is inductance (H), R<sub>s</sub> is the bulk resistance (Ω) of the pellet, CPE<sub>b</sub> and CPE<sub>gb</sub> are the non-ideal capacitance for bulk and non-ideal capacitance for grain boundary (F.S<sup>a-1</sup>). Further, R<sub>s</sub> is used to calculate the conductivity of the sample by considering the area and thickness of the sample.



### 3.8 References

1. Wraight, C. A. *Biochim. Biophys. Acta (BBA)-Bioenergetics* **2006**, 1757 (8), 886-912.
2. Nagle, J.; Mille, M.; Morowitz, H. *J. Chem. Phys.* **1980**, 72 (7), 3959-3971.
3. Capasso, M.; DeCoursey, T. E.; Dyer, M. J. *Trends Cell Biol* **2011**, 21 (1), 20-28.
4. Steele, B. C.; Heinzl, A. *Nature* **2001**, 414 (6861), 345-352.
5. Jensen, J.; Kleitz, M., *Solid State Protonic Conductors I: For Fuel Cells and Sensors*. Univ Pr of Southern Denmark: 1982; Vol. 1.
6. Zhong, C.; Deng, Y.; Roudsari, A. F.; Kapetanovic, A.; Anantram, M.; Rolandi, M. *Nat. Commun.* **2011**, 2, 476.
7. Kreuer, K.-D. *Chem. Mater.* **1996**, 8 (3), 610-641.
8. Kreuer, K.-D.; Paddison, S. J.; Spohr, E.; Schuster, M. *Chem. Rev.* **2004**, 104 (10), 4637-4678.
9. Knauth, P.; Di Vona, M. L., *Solid state proton conductors: properties and applications in fuel cells*. John Wiley & Sons: 2012.
10. Shimizu, G. K.; Taylor, J. M.; Kim, S. *Science* **2013**, 341 (6144), 354-355.
11. Josberger, E. E.; Hassanzadeh, P.; Deng, Y.; Sohn, J.; Rego, M. J.; Amemiya, C. T.; Rolandi, M. *Sci. Adv.* **2016**, 2 (5), e1600112.
12. Yakiyama, Y.; Lee, G. R.; Kim, S. Y.; Matsushita, Y.; Morita, Y.; Park, M. J.; Kawano, M. *Chem. Commun.* **2015**, 51 (31), 6828-6831.
13. Liang, X.; Zhang, F.; Feng, W.; Zou, X.; Zhao, C.; Na, H.; Liu, C.; Sun, F.; Zhu, G. *Chem. Sci* **2013**, 4 (3), 983-992.
14. Jiménez-García, L.; Kaltbeitzel, A.; Pisula, W.; Gutmann, J. S.; Klapper, M.; Müllen, K. *Angew. Chem. Int. Ed. Engl.* **2009**, 48 (52), 9951-9953.
15. Kreuer, K.; Fuchs, A.; Ise, M.; Spaeth, M.; Maier, J. *Electrochimica Acta* **1998**, 43 (10), 1281-1288.
16. Kreuer, K. *J. Membr. Sci.* **2001**, 185 (1), 29-39.
17. Bazaga-García, M.; Colodrero, R. M.; Papadaki, M.; Garczarek, P.; Zoń, J.; Olivera-Pastor, P.; Losilla, E. R.; León-Reina, L.; Aranda, M. A.; Choquesillo-Lazarte, D. *J. Am. Chem. Soc.* **2014**, 136 (15), 5731-5739.
18. Xu, H.; Tao, S.; Jiang, D. *Nat. Mater* **2016**, 15 (7), 722-726.
19. Yoon, M.; Suh, K.; Natarajan, S.; Kim, K. *Angew. Chem. Int. Ed. Engl.* **2013**, 52 (10), 2688-2700.

20. Yang, Y.; Shi, Z.; Holdcroft, S. *Macromolecules* **2004**, *37* (5), 1678-1681.
21. Shi, Z.; Holdcroft, S. *Macromolecules* **2005**, *38* (10), 4193-4201.
22. Mauritz, K. A.; Moore, R. B. *Chem. Rev.* **2004**, *104* (10), 4535-4586.
23. Yamada, T.; Sadakiyo, M.; Shigematsu, A.; Kitagawa, H. *Bull. Chem. Soc. Jpn.* **2015**, *89* (1), 1-10.
24. Hurd, J. A.; Vaidhyanathan, R.; Thangadurai, V.; Ratcliffe, C. I.; Moudrakovski, I. L.; Shimizu, G. K. *Nat. Chem.* **2009**, *1* (9), 705-710.
25. Jeong, N. C.; Samanta, B.; Lee, C. Y.; Farha, O. K.; Hupp, J. T. *J. Am. Chem. Soc.* **2011**, *134* (1), 51-54.
26. Furukawa, H.; Cordova, K. E.; O'Keeffe, M.; Yaghi, O. M. *Science* **2013**, *341* (6149), 1230444.
27. Chandra, S.; Kundu, T.; Kandambeth, S.; BabaRao, R.; Marathe, Y.; Kunjir, S. M.; Banerjee, R. *J. Am. Chem. Soc.* **2014**, *136* (18), 6570-6573.
28. Ma, H.; Liu, B.; Li, B.; Zhang, L.; Li, Y.-G.; Tan, H.-Q.; Zang, H.-Y.; Zhu, G. *J. Am. Chem. Soc.* **2016**, *138* (18), 5897-5903.
29. Chandra, S.; Kundu, T.; Dey, K.; Addicoat, M.; Heine, T.; Banerjee, R. *Chem. Mater.* **2016**, *28* (5), 1489-1494.
30. Yoon, M.; Suh, K.; Kim, H.; Kim, Y.; Selvapalam, N.; Kim, K. *Angew. Chem. Int. Ed.* **2011**, *123* (34), 8016-8019.
31. Liu, M.; Chen, L.; Lewis, S.; Chong, S. Y.; Little, M. A.; Hasell, T.; Aldous, I. M.; Brown, C. M.; Smith, M. W.; Morrison, C. A.; Hardwick, L. J.; Cooper, A. I. *Nat Commun.* **2016**, *7*, 12750.
32. Karmakar, A.; Illathvalappil, R.; Anothumakkool, B.; Sen, A.; Samanta, P.; Desai, A. V.; Kurungot, S.; Ghosh, S. K. *Angew. Chem. Int. Ed.* **2016**, *128* (36), 10825-10829.
33. Gómez-Gualdrón, D. A.; Moghadam, P. Z.; Hupp, J. T.; Farha, O. K.; Snurr, R. Q. *J. Am. Chem. Soc.* **2016**, *138* (1), 215-224.
34. Hausdorf, S.; Seichter, W.; Weber, E.; Mertens, F. O. R. L. *Dalton Trans.* **2009**, (7), 1107-1113.



***Chapter 3***

***Section-B***

***Three Dimensional Metal-Organic Polymers of  
Multivalent Hexaphenylbenzene***





## Chapter-3

### Section-B

#### Three Dimensional Metal-Organic Polymers of Multivalent Hexaphenylbenzene

### 3.9 Introduction

Metal-organic frameworks (MOF) are one of the interesting materials of supramolecular chemistry owing to their broad range of applications in material and biomedical sciences. Particularly, its potential applications in gas adsorption, separation and, storage,<sup>1-2</sup> sensors,<sup>3-4</sup> magnetism,<sup>5</sup> catalysis,<sup>6-7</sup> medicinal-dental materials,<sup>8-10</sup> and chiral separations,<sup>11-12</sup> have been well explored in literature. For the synthesis of these above mentioned materials, surplus number of organic linkers was used. Most commonly used linkers were used carboxylates, sulphonates, phosphates, imidazoles and polypyridyls.<sup>13-15</sup> Recently, there has been considerable attention in the usage of multicarboxylate organic linkers in the MOF synthesis due to their unique structural features (higher connectivity than metals ions) and intrinsic properties. For instance, Furukawa *et al.* reported synthesis and selective carbon dioxide capturing of several metal-organic frame works using a hexatopic ligand **A** (Fig. 3.18).<sup>16</sup> Mircea Dinca and co-workers have synthesized a rigid metal organic framework using octatopic ligand **B** (Fig 3.18).<sup>17</sup> Mohamed Eddaoudi and co-workers have synthesized the extended nanocages using a multivalent ligands **C** and **D**, wherein it is claimed that their material had shown highest porosity and gas storage than other MOFS (Fig. 3.18).<sup>18</sup> Zhou *et al* reported a highly porous and robust (3,3,4)-connected metal–organic framework which was constructed using a 90° bridging-angle embedded in an octacarboxylate ligand (carbazole based ligand) **E** (Fig. 3.18).<sup>19</sup> Jian Zhang *et al.* demonstrated the synthesis of a “pillar-free”, highly porous metalloporphyrinic framework **F** exhibiting an eclipsed porphyrin arrays. This was constructed using an octacarboxylate ligand connected with paddlewheel secondary building units (Fig. 3.18).<sup>20</sup>

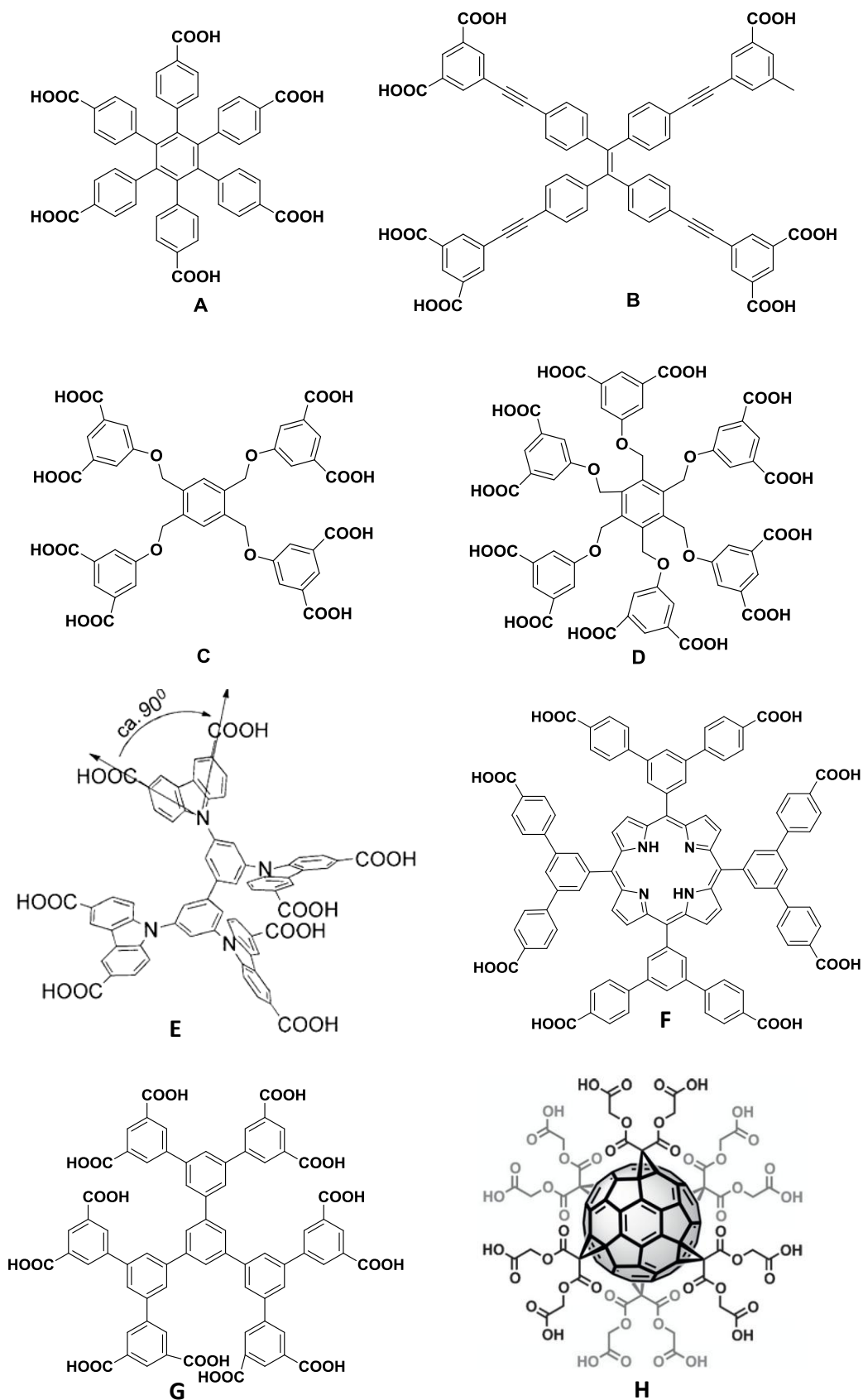


**Fig. 3.18:** Multicarboxylate organic linkers **A-H** involved in various MOF synthesis. (Fig. 3.18 H is adapted from ref: 19)

Although thousands of MOF's were reported in the literature, only three of the dodecatopic ligands have been used for the synthesis of MOF's till now. Guangshan Zhu and co-workers synthesized a MOF using dendritic aromatic 12-carboxyl ligand **G** (Fig. 3.18).<sup>21</sup> Florian Beuerle and co-workers reported three dimensional MOF's using fullerene-based dodecatopic linkers **H** (Fig. 3.18).<sup>22</sup> Mohamed Eddaoudi and co-workers have constructed the extended nanocages using the dodecatopic ligand **D** (Fig. 3.18).<sup>18</sup> On the other side, MOF synthesized from s-block elements have received large attention due to their relatively less density, strong bonding interactions, flexibility, nontoxic, cost effective, etc.<sup>23-24</sup>

### 3.10 Objective of the present work

In view of importance of multi carboxylate linkers and the rarity of s-block elements in MOF synthesis, we have anticipated that these combinations of two could provide some interesting structural architectures with unprecedented potential applications. Therefore, we planned to prepare metal organic frame works using dodecatopic ligand  $\text{HPB}(\text{COOH})_{12}$  (Fig. 3.19) and sodium, potassium metal cations to obtain highly compact water coordinated frame work for proton conductivity applications.

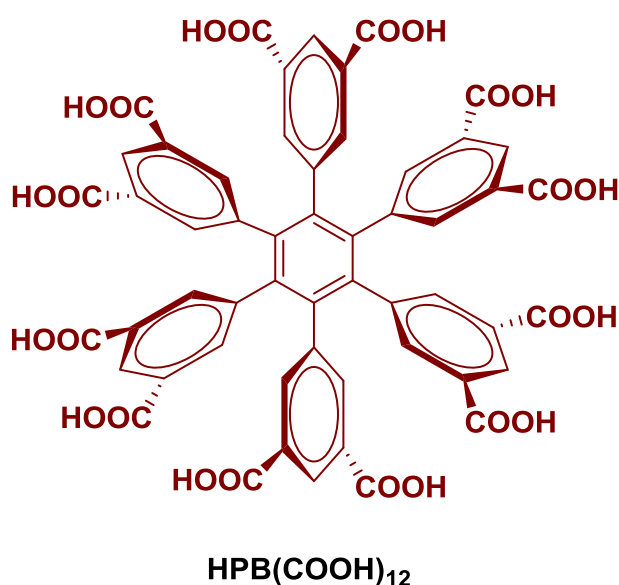


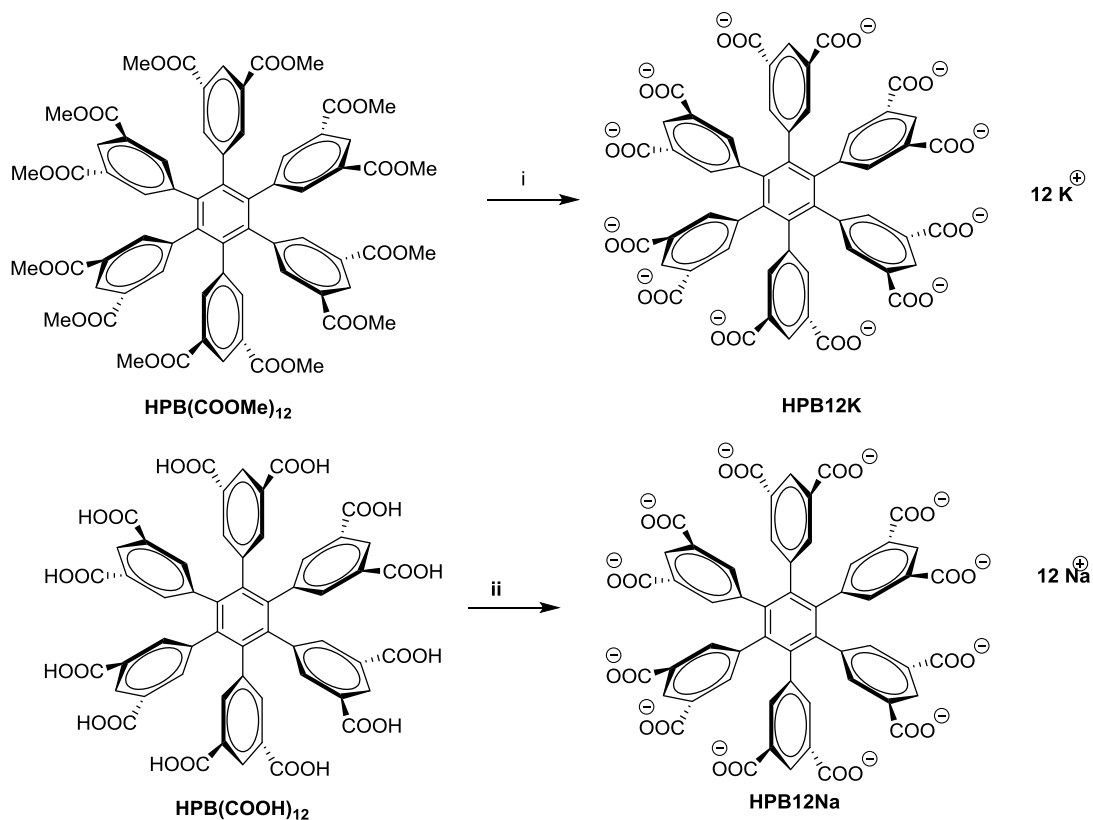
**Fig. 3.19:** Chemical structure of dodecatopic ligand  $\text{HPB}(\text{COOH})_{12}$ .

### 3.11 Synthesis and characterization:

Synthesis of dodecatopic ligand **HPB(COOH)<sub>12</sub>** is mentioned in chapter-2

#### Synthesis of **HPB12K** and **HPB12Na**:

MOF-**HPB12K** was prepared by direct hydrolysis of **HPB(COOMe)<sub>12</sub>** using aqueous potassium hydroxide, methanol and dioxane at 120 °C (Scheme 3.04). After 12h, the reaction vessel was opened, wherein it was found to have two layers. The bottom layer was separated carefully and kept it at 60 °C for a week in order to obtain block shaped crystal of **HPB12K**. The crystal suitable for single crystal XRD was directly taken from the reaction vial and used for analysis. This analysis revealed that the **HPB12K** fallen on *P-1* space group. Following the similar procedure, we could not obtain crystals of sodium metal organic polymer. However, aqueous sodium hydroxide treatment of **HPB(COOH)<sub>12</sub>** provided a neutralized solution and yielded **HPB12Na** in a couple of week upon crystallization by the addition of few drops of anti solvent dimethyl formamide (Scheme 3.04). Then, the suitable single crystal was mounted for the data collection and the space group was found to be *C2/c*.



**Scheme 3.04:** Synthesis of metal-organic polymers **HPB12K** and **HPB12Na**. Reagents and conditions: (i) a) aqueous dioxane, KOH, 120 °C (teflon lined stainless steel autoclave), 12 h; ii) H<sub>2</sub>O, NaOH, DMF, rt, 7-14 days.

The homogeneity of the bulk samples **HPB12K** and **HPB12Na** were verified by the powder X-ray diffraction (PXRD). The slight positional shift and intensity variation in the power XRD was seen due to the temperature difference in the data collection of SXRD and PXRD (Fig. 3.20 & 3.21).

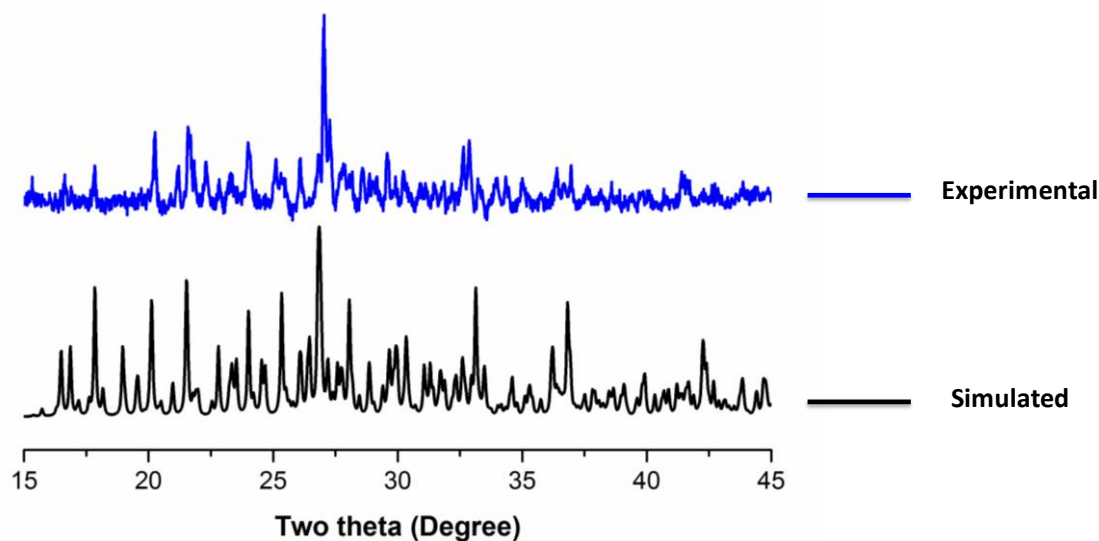


**Fig. 3.20:** Comparison of experimental (blue) and simulated (black) PXRD (from the single crystal structure) patterns of **HPB12K**.

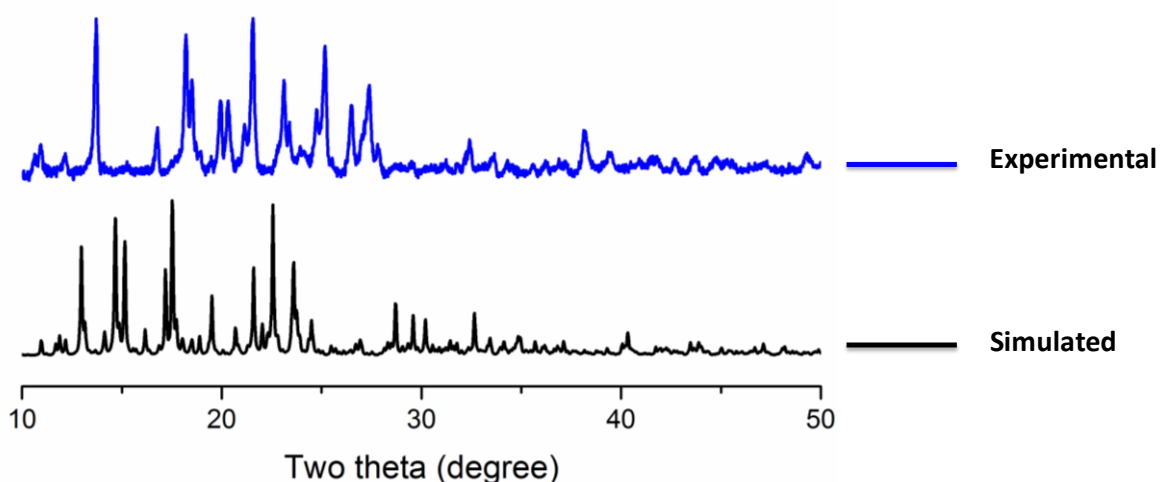


**Fig. 3.21:** Comparison of experimental (blue) and simulated (black) PXRD (from the single crystal structure) patterns of **HPB12Na**.

Thermo gravimetric analysis (TGA) was used to verify the thermal stability of metal-organic polymer. The TGA of the crystal was performed under nitrogen atmosphere and the analysis revealed that the **HPB12K** was stable up to 550 °C (Fig. 3.22a). An initial

weight loss about 17% (below 150 °C) in the TGA of **HPB12K** was accounted for the loss of solvent molecules. Similarly, the TGA of **HPB12Na** has showed weight loss of about 10% for temperatures below 120° C which could be attributed to the loss of entrapped solvent molecules (Fig. 3.22b). The material was decomposed at 250 °C. These observations were revealed that these materials are thermally stable and useful for proton conductivity studies.

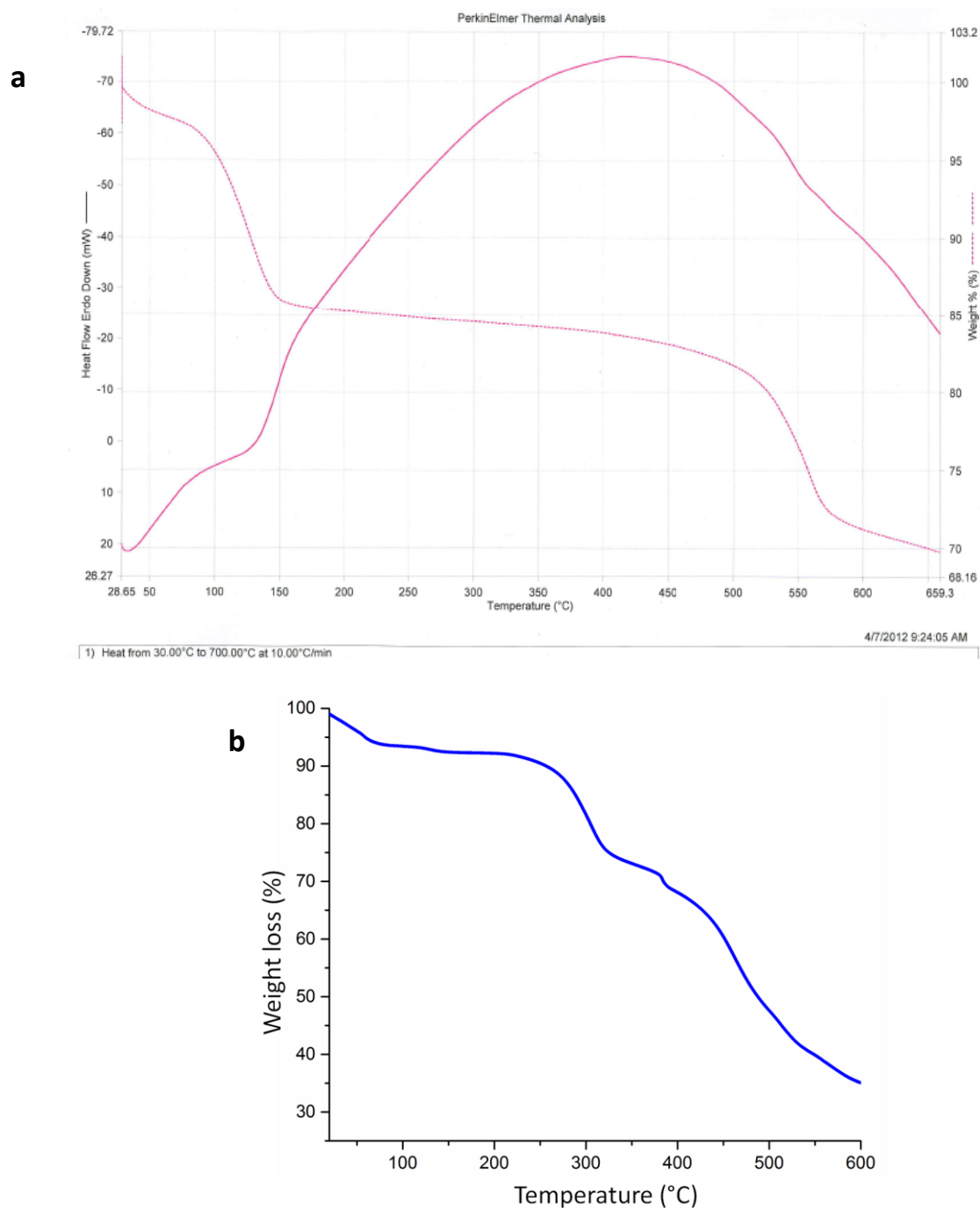


**Fig. 3.22:** TGA data of metal-organic polymers. a) **HPB12K** heated to 700 °C at the rate of 10 °C /min. b) **HPB12Na** heated to 500 °C at the rate of 10 °C /min.

### 3.12 Single crystal X-ray studies

The crystal structure of compound **HPB12K** consists of a three-dimensional framework K ions, HPB(COOH)<sub>12</sub> ligands, HCOOH, trapped water, and coordinated water molecules as shown in Fig. 3.23. X-crystal structure-asymmetric unit consists of six potassium atoms, half of HPB(COOH)<sub>12</sub> ligand, one formic acid, five coordinated water molecules, one free water molecule and one linear triatomic molecule.

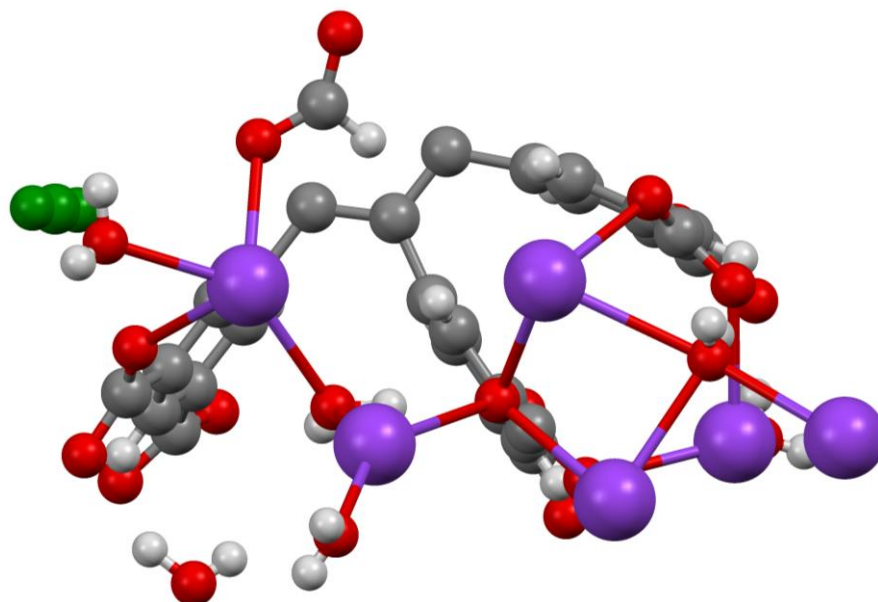


**Fig. 3.23:** X-ray crystal structure-asymmetric unit (*a*-view) of HPBK showing six atoms, half of HPB(COOH)<sub>12</sub> ligand, one formic acid, five coordinated water molecules, one free water molecule and one linear triatomic molecule (green). *Note:* except triatomic molecule, rests of the all atoms are showed as per CPK model.

The X-ray crystal structure has shown two surprising findings: i) existence of formates as linkers in the structure and ii) presence of linear triatomic molecules. These two chemical species were not added in the reaction vessel and must have been formed during the course of the reaction. Formic acid could have formed from methanol which was initially added in the reaction vessel. We have also observed that under similar reaction conditions, alkyne triple bond was reduced to its corresponding hydrocarbon analogue. While refining the crystal structure, the linear triatomic molecule was having good fitting with CO<sub>2</sub>, but the bond lengths were not matching. Therefore, the triatomic molecule could be disordered water molecules.



X-ray crystal structure of **HPB12K** had showed three dimensional networks in its structure. The connectivity between the metal and ligand was highly dense due to which the crystal structure had not shown any voids in the crystal lattice. The structural rigidity of HPB could have created some voids in the crystal lattice, but those were occupied by water and triatomic molecules (green ring in Fig. 3.24a). Further, the crystal axis-*a* view (Fig. 3.24a) has revealed that metal cations and ligands were connected with each other to form two dimensional sheet like architectures. Crystal axis-*b* view (Fig. 3.24b) was showing the connection between the 2D layers by potassium ion. As a result axis-*b* view resembled like pillars, wherein HPB moieties were connected by metal cations.

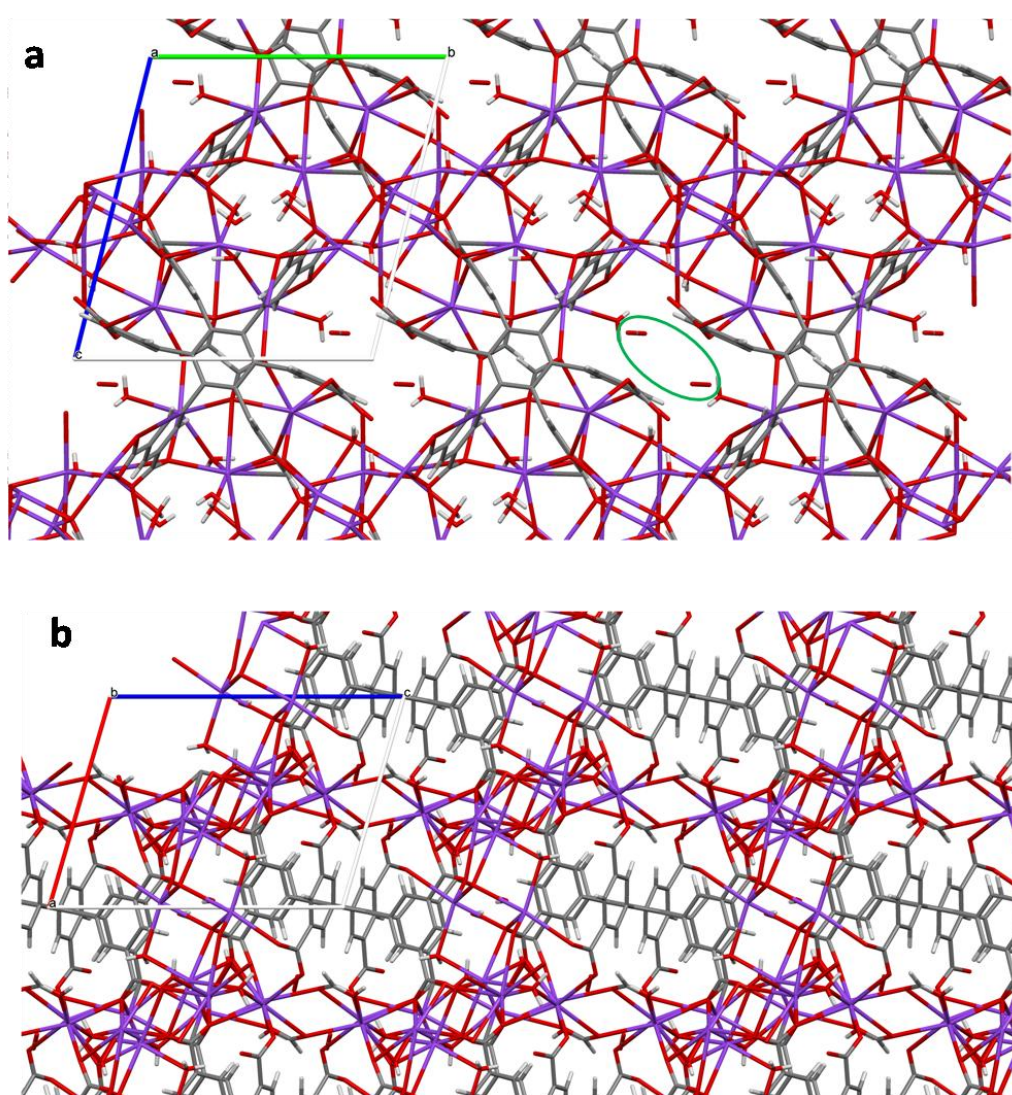


**Fig. 3.24:** a) X-ray crystal structure of **HPB12K** *a*-view showing the connectivity between the ligand and potassium metal cation. b) X-ray crystal structure of **HPB12K** *b*-view showing the formation of pillared structure by the linking of HPB moieties and potassium cation.

The X-ray crystal structure of **HPB12Na** showed lots of trapped water molecules and dimethylformamide in its crystal lattice (space group:  $C 2/c$ , Fig. 3.25).

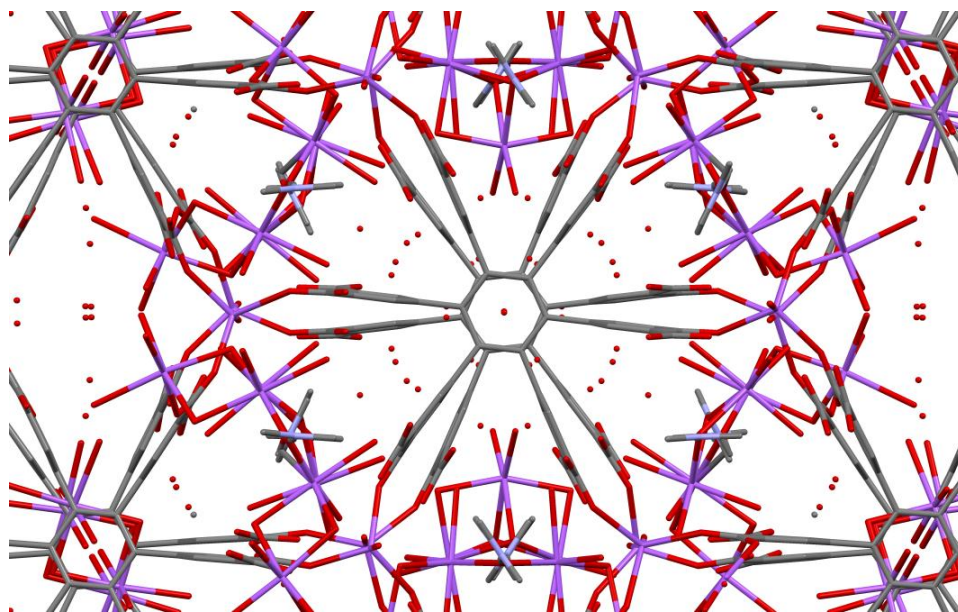


**Fig. 3.25:** X-ray crystal structure (*c*-view) of **HPB12Na** showing the trapped guest molecules (DMF, water) in the crystal lattice.

### 3.13 Conclusion:

Two new metal organic polymers have been synthesized using s-block metal ions (potassium, sodium) and **HPB(COOMe)<sub>12</sub>** and/or **HPB(COOH)<sub>12</sub>** as building blocks. These compounds were characterized by thermo gravimetric analysis, infrared spectroscopy and PXRD. The X-ray crystal structure of **HPB12K** was solved and the structure was a three-dimensional framework consisting of HPB moiety, formic acid and potassium cation. Formic acid was formed during the course of the reaction while converting from **HPB(COOMe)<sub>12</sub>** to **HPB(COOH)<sub>12</sub>** and it was incorporated in the framework. The X-ray crystal structure of **HPB12Na** has shown the presence of a large number of DMF and water molecules in its three dimensional frame works.

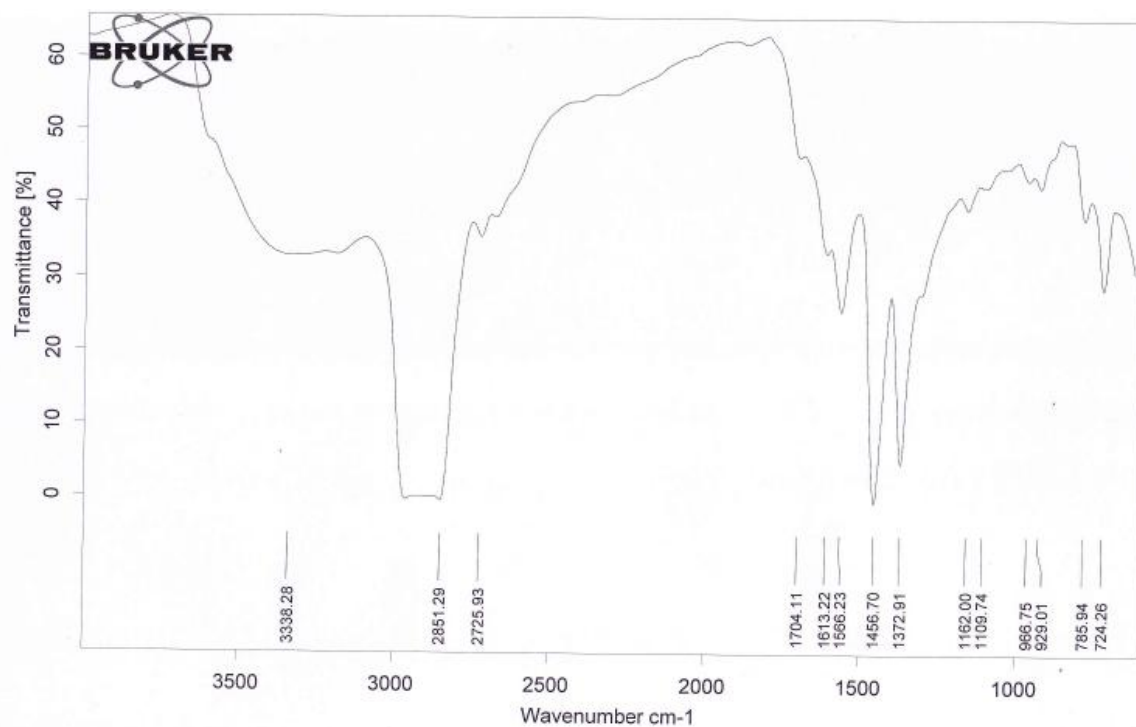
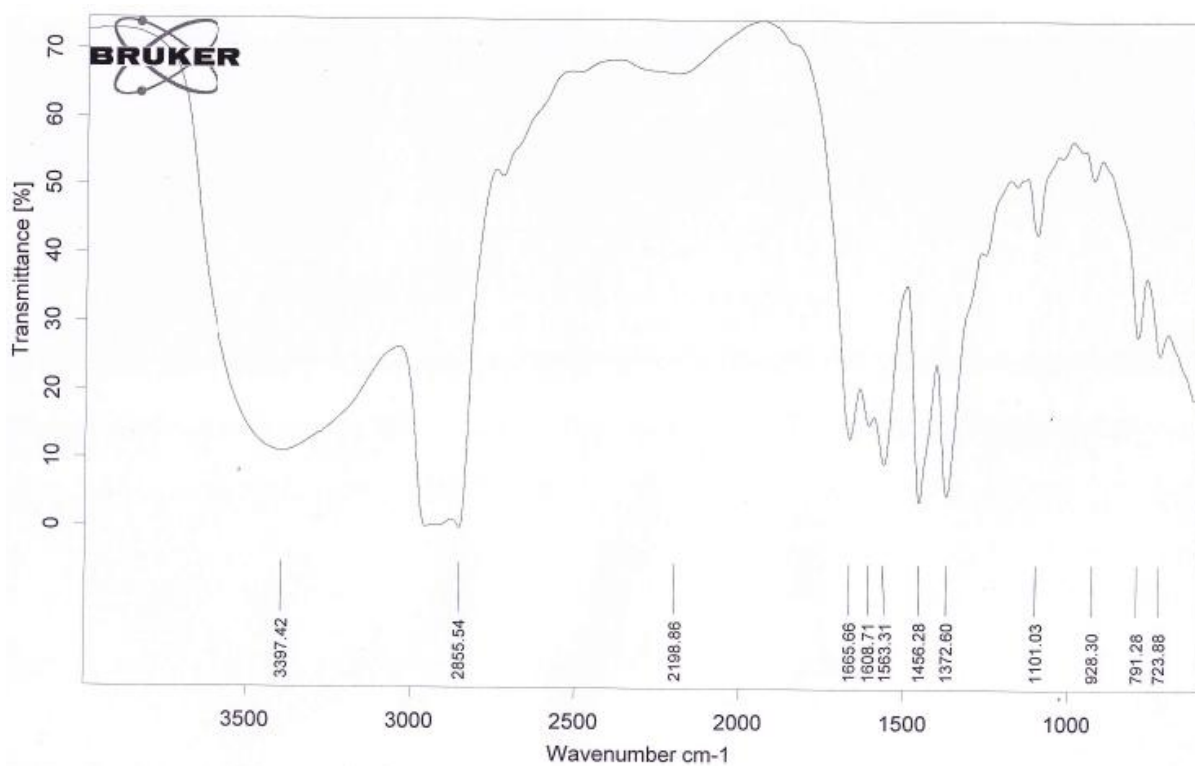
### 3.14 Experimental section

#### Metal-organic polymer-HPB12K

**HPB(COOMe)<sub>12</sub>** (5 g, 4.06 mmol) and KOH (6.83 g, 121.839 mmol ) were suspended in aqueous dioxane (dioxane : water, 30 mL : 20 mL). The mixture was heated to 120 °C in stainless steel covered teflon-lined autoclave and the heating was maintained at the same temperature for 24 h. Then, the reaction mixture was slowly cooled down to room temperature to get two layers. The bottom layer was carefully separated and was kept at 70 °C for 7-14 days to obtain HPB-K (**11**) as colorless crystals. The crystal suitable for X-ray crystallography was removed directly from the sample vial to obtain crystal structure of the **HPB12K**.

#### Metal-organic polymer-HPB12Na.

**HPB(COOH)<sub>12</sub>** (0.2 g, 0.188 mmol) was suspended in water (0.5 mL) and dissolved by the addition of aqueous NaOH (0.09g, 2.25 mmol in 0.5ml). The clear solution was filtered through Whatmann filter and then DMF was slowly diffused until it was slight turbid. After that, the reaction mixture was heated and kept without disturbance at room temperature for 7-14 days to obtain **HPB12Na** as colorless crystals.

IR spectrum of **HPB12K**IR spectrum of **HPB12Na**

### 3.15 X-ray Crystallography:

#### Single crystal X-ray diffraction studies

X-ray intensity data measurements of **HPB12Na** was carried out on a Bruker D8 VENTURE Kappa Duo PHOTON II CPAD diffractometer equipped with Incoatech multilayer mirrors optics. The intensity measurements were carried out with Cu micro-focus sealed tube diffraction source ( $\text{CuK}_{\alpha} = 1.54178 \text{ \AA}$ ) at 100(2) K temperature. The X-ray generator was operated at 50 kV and 1.1 mA. A preliminary set of cell constants and an orientation matrix were calculated from three sets of 40 frames. Data were collected with  $\omega$  scan width of  $0.5^{\circ}$  at different settings of  $\varphi$  and  $2\theta$  keeping the sample-to-detector distance fixed at 5.00 cm. The X-ray data collection was monitored by APEX3 program (Bruker, 2016).<sup>25</sup> On the other hand X-ray intensity data measurements of **HPB12K** was carried out on a Bruker SMART APEX II CCD diffractometer with graphite monochromatized ( $\text{MoK}_{\alpha} = 0.71073 \text{ \AA}$ ) radiation at 100(2) K. The X-ray generator was operated at 50 kV and 30 mA. A preliminary set of cell constants and an orientation matrix were calculated from three sets of 36 frames. Data were collected with  $\omega$  scan width of  $0.5^{\circ}$  at different settings of  $\varphi$  and  $2\theta$  keeping the sample-to-detector distance fixed at 5.00 cm. The X-ray data collection was monitored by APEX2 program (Bruker, 2006).<sup>26</sup> All the data were corrected for Lorentzian, polarization and absorption effects using SAINT and SADABS programs (Bruker, 2016). SHELX-97 was used for structure solution and full matrix least-squares refinement on  $F^2$ .<sup>27,28</sup> All the hydrogen atoms were placed in geometrically idealized position and constrained to ride on the parent atoms.



### 3.16 References

1. Jiang, H.-L.; Xu, Q. *Chem. Commun.* **2011**, 47 (12), 3351-3370.
2. Schröder, M., *Functional metal-organic frameworks: gas storage, separation and catalysis*. Springer: 2010; Vol. 293.
3. Liu, D.; Lu, K.; Poon, C.; Lin, W. *Inorg. Chem.* **2013**, 53 (4), 1916-1924.
4. Manos, M. J.; Moushi, E. E.; Papaefstathiou, G. S.; Tasiopoulos, A. J. *Cryst. Growth Des.* **2012**, 12 (11), 5471-5480.
5. Lago, A. B.; Carballo, R.; Fabelo, O.; Fernández-Hermida, N.; Lloret, F.; Vázquez-López, E. M. *CrystEngComm.* **2013**, 15 (48), 10550-10562.
6. Yoon, M.; Srirambalaji, R.; Kim, K. *Chem. Rev.* **2011**, 112 (2), 1196-1231.
7. Gu, Z. Y.; Park, J.; Raiff, A.; Wei, Z.; Zhou, H. C. *ChemCatChem* **2014**, 6 (1), 67-75.
8. Sun, C.-Y.; Qin, C.; Wang, X.-L.; Su, Z.-M. *Expert Opin. Drug Deliv.* **2013**, 10 (1), 89-101.
9. Baimpos, T.; Shrestha, B. R.; Hu, Q.; Genchev, G.; Valtiner, M. *J. Phys. Chem.C* **2015**, 119 (29), 16769-16776.
10. Demadis, K. D.; Paspalaki, M.; Theodorou, J. *Ind. Eng. Chem. Res.* **2011**, 50 (9), 5873-5876.
11. Dong, D.-P.; Li, J.; Sun, Z.-G.; Zheng, X.-F.; Chen, H.; Meng, L.; Zhu, Y.-Y.; Zhao, Y.; Zhang, J. *Inorg. Chem. Commun.* **2007**, 10 (9), 1109-1112.
12. Nickerl, G.; Henschel, A.; Grünker, R.; Gedrich, K.; Kaskel, S. *Chem. Ing. Tech.* **2011**, 83 (1-2), 90-103.
13. Du, D.-Y.; Qin, J.-S.; Li, S.-L.; Su, Z.-M.; Lan, Y.-Q. *Chem. Soc. Rev* **2014**, 43 (13), 4615-4632.
14. Chen, T.-H.; Popov, I.; Kaveevivitchai, W.; Miljanić, O. S. *Chem. Mater.* **2014**, 26 (15), 4322-4325.
15. Liu, R.; Yu, T.; Shi, Z.; Wang, Z. *Int. J. Nanomed.* **2016**, 11, 1187.
16. Nguyen, P. T.; Nguyen, H. T.; Pham, H. Q.; Kim, J.; Cordova, K. E.; Furukawa, H. *Inorg. Chem* **2015**, 54 (20), 10065-10072.
17. Shustova, N. B.; Cozzolino, A. F.; Dincă, M. *J. Am. Chem. Soc.* **2012**, 134 (48), 19596-19599.
18. Eubank, J. F.; Mouttaki, H.; Cairns, A. J.; Belmabkhout, Y.; Wojtas, L.; Luebke, R.; Alkordi, M.; Eddaoudi, M. *J. Am. Chem. Soc.* **2011**, 133 (36), 14204-14207.

19. Lu, W.; Yuan, D.; Makal, T. A.; Li, J. R.; Zhou, H. C. *Angew. Chem. Int. Ed. Engl.* **2012**, *51* (7), 1580-1584.
20. Johnson, J. A.; Lin, Q.; Wu, L.-C.; Obaidi, N.; Olson, Z. L.; Reeson, T. C.; Chen, Y.-S.; Zhang, J. *Chem. Commun.* **2013**, *49* (27), 2828-2830.
21. He, H.; Sun, F.; Jia, J.; Bian, Z.; Zhao, N.; Qiu, X.; Gao, L.; Zhu, G. *Cryst. Growth Des.* **2014**, *14* (9), 4258-4261.
22. Kraft, A.; Roth, P.; Schmidt, D.; Stangl, J.; Müller-Buschbaum, K.; Beuerle, F. *Chem. Eur. J.* **2016**, *22* (17), 5982-5987.
23. Snurr, R. Q.; Hupp, J. T.; Nguyen, S. T. *AIChE Journal* **2004**, *50* (6), 1090-1095.
24. D'Alessandro, D. M.; Smit, B.; Long, J. R. *Angew. Chem. Int. Ed. Engl.* **2010**, *49* (35), 6058-6082.
25. Bruker (2016). *APEX3, SAINT and SADABS*. Bruker AXS Inc., Madison, Wisconsin, USA.
26. Bruker (2006). *APEX3, SAINT and SADABS*. Bruker AXS Inc., Madison, Wisconsin, USA.
27. G. M. Sheldrick, *Acta Crystallogr.*, **2008**, *A64*, 112.
28. L. J. Farrugia, *J. Appl. Cryst.* **1997**, *30*, 565-565.





***Chapter 3***

***Section-C***

***Synthesis of HPB-based Template Assembled  
Synthetic Proteins***



## Chapter-3

### SECTION-C: Synthesis of HPB-based Template Assembled Synthetic Proteins

**3.17 Introduction:** Proteins are macromolecules that constitutes as one of the major building units of cells. They are very essential for the life of any living species.<sup>1-3</sup> They consist of one or more long chains of amino acid residues or poly peptides.<sup>4-6</sup> It has to be noted that proteins are involved in vast array of biological functions such as DNA replication,<sup>7-9</sup> catalyzing metabolic reactions,<sup>10-11</sup> transporting molecules from one location of the organism to the other location<sup>12-13</sup> and so on. The structures and functions of the proteins are dictated by the nucleotide sequence of specific genes.<sup>14-16</sup> For long, there have been scientific communities involved in the study of protein folding and the factors that affecting it.<sup>17-19</sup> Since Emil Fischer attempted the synthesis of polypeptide chain, the design and synthesis of proteins have progressed significantly till to date.<sup>20-22</sup> William De-Grado was one of the pioneers in *de novo* protein design who made significant contribution in this field.<sup>23-24</sup> Afterwards, the template assembled synthetic proteins (TASPs) were initiated by Mutter and Vulleumies.<sup>25-26</sup> In TASPs, proteins were tethered into rigid scaffolds which could alter the protein folding as well as their secondary and tertiary structure.<sup>27-29</sup> These TASPs have been widely used in enzyme mimicking and protein-protein interactions.<sup>30-31</sup> Several rigid scaffolds or templates have been used to construct the TASPs in the literature. Mutter *et al.* assembled the TASPs by tethering of four unordered peptide strands on cyclic or acyclic peptide-based rigid templates.<sup>25-26, 32-33</sup> The resultant structure of the TASP had shown four-helix bundles on the peptide-based template (Fig. 3.26).<sup>26, 34-35</sup>

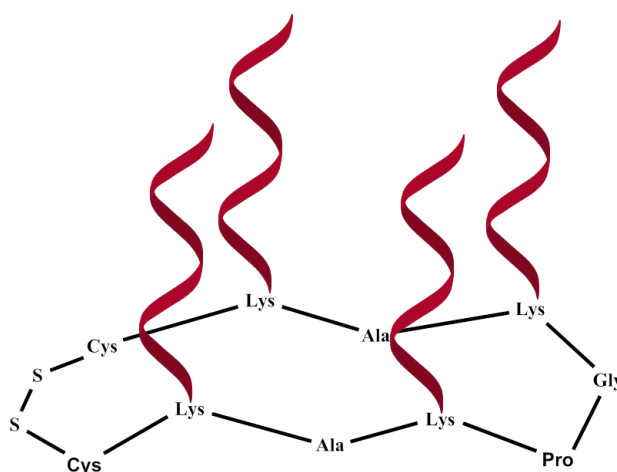


**Fig. 3.26:** The structure of cyclic peptide-based template used for designing of TASPs by Mutter and co-workers.

Haehnel *et al.* reported a library of combinatorial species by assembling small proteins on a cyclic decapeptide-template.<sup>36</sup> Fairlie *et al.* showed synthetic four-helix bundles using a series of aromatic scaffolds and a cyclic octapeptide and they found that the size, shape and directionality of the rigid templates are extremely important for designing of TASP.<sup>29</sup> Further, carbohydrates,<sup>37</sup> several aromatic ring-based templates<sup>38</sup> and porphyrin rings<sup>39</sup> were also used for the construction of TASPs.

The vase shaped rigid molecules called as cavitands were also used as scaffolds in TASP chemistry (Fig. 3.27) in which four functional arms were employed for protein tethering.<sup>40-41</sup> These peptide-attached-cavitands are commonly referred to as caviteins. The term cavitein (cavitand+ protein) was coined by Sherman (1995). Recently, his research group had reported an X-ray crystal structure of cavitein Q4.<sup>42</sup> Another interesting scaffold used for the synthesis of TASPs was polyhedral oligomeric silsesquioxanes (POSS) in which total eight peptide attachable arms were present in its structure (Fig. 3.28).<sup>43-46</sup> However, more than eight peptide attachable multivalent templates are still rare in the literature.

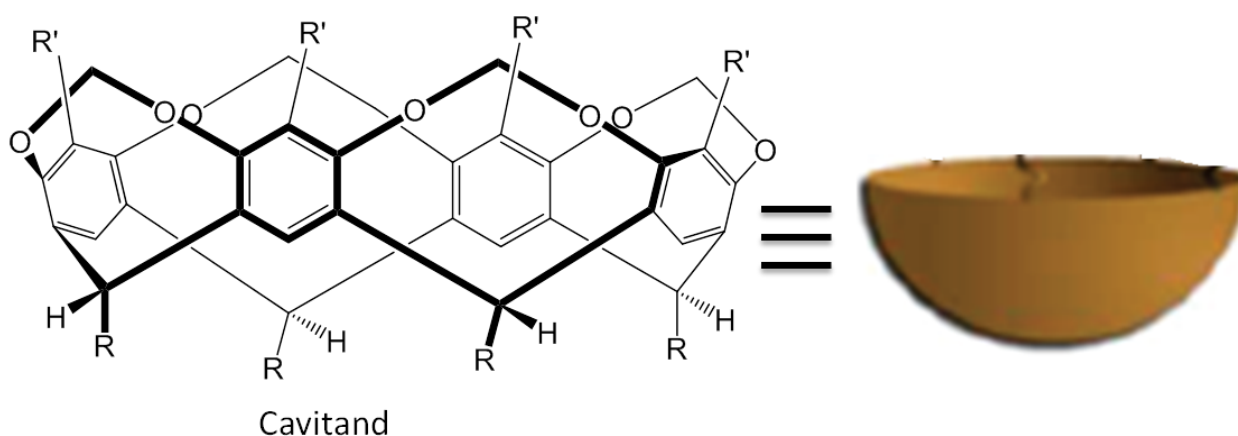
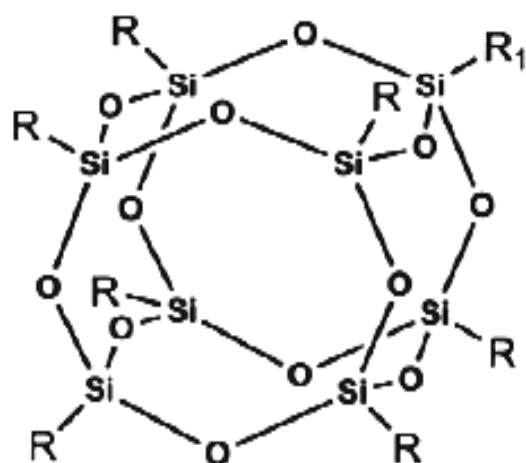


**Fig. 3.27:** The structure of [4]-cavitand template showing four peptide attachable sites (R).<sup>47</sup>



R = Peptide attachable site

### POSS

**Fig. 3.28:** The structure of polyhedral oligomeric silsesquioxanes template showing eight peptide attachable sites (R).<sup>46</sup>

#### 3.18 Objective of the present work:

Considering the above mentioned importance of TASP and the lack of novel multivalent scaffolds for the peptide attachments, we envisaged axially substituted double basket-shaped hexaphenyl benzene could serve as a good platform for constructing TASP (Fig. 3.29). Therefore, we have attempted to tether small peptide units on the axial arms of HPB(COOH)<sub>12</sub> using a simple peptide coupling strategy.

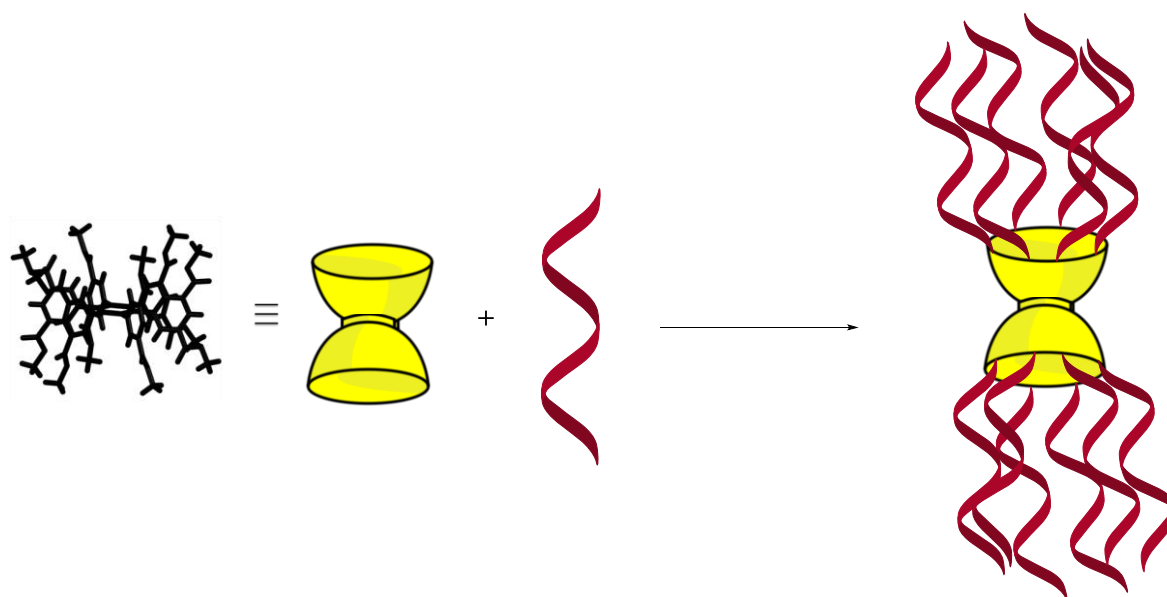
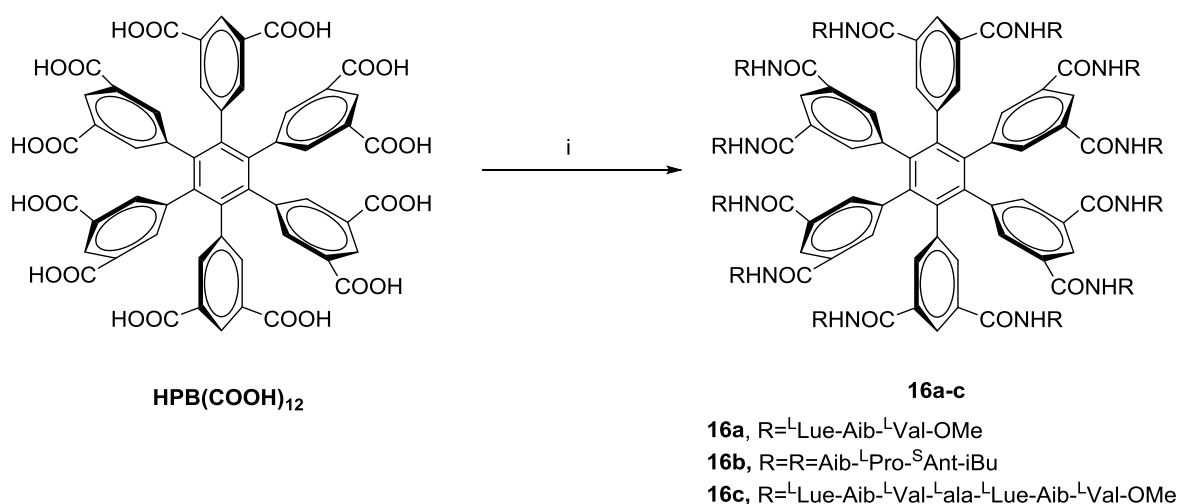


**Fig. 3.29:** Schematic representation of double basket-shaped axially substituted HPB-based TASP formation.

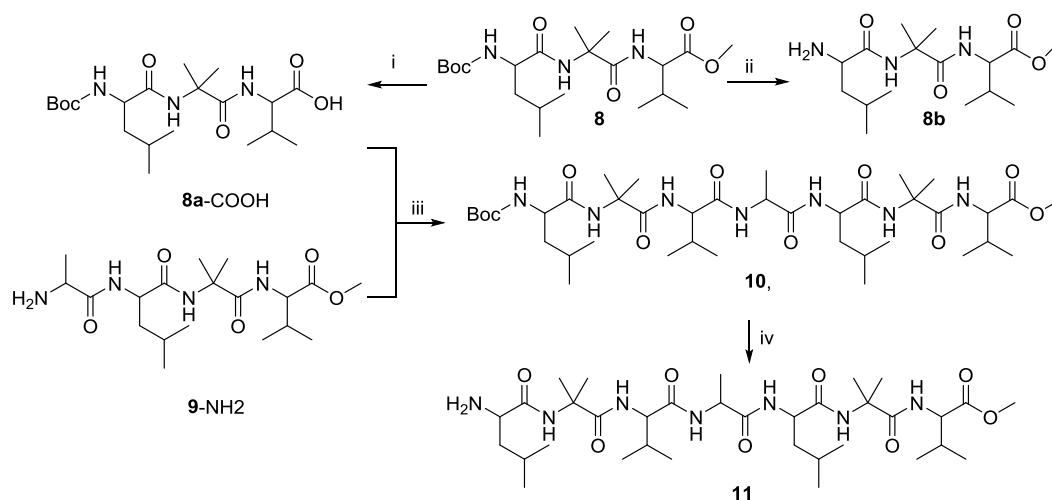
### 3.19 Result and discussion:

#### Synthesis:

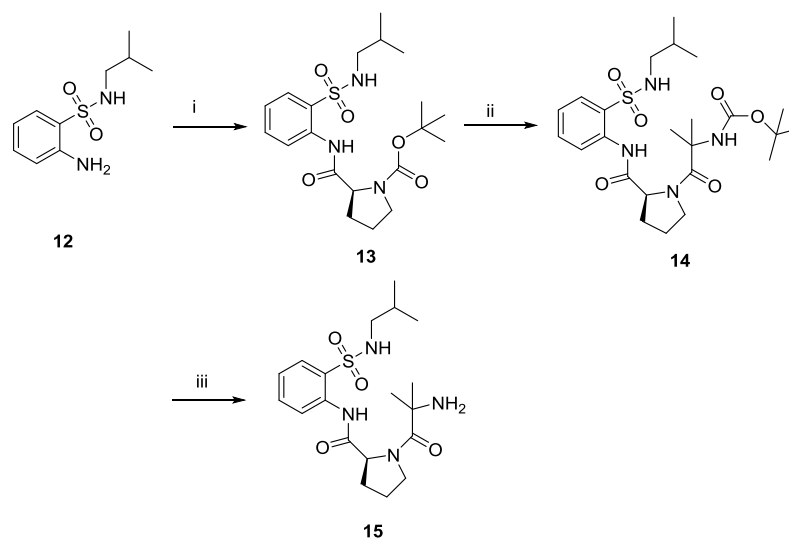
The reaction of **HPB(COOH)<sub>12</sub>** with free amines of the peptide chains (**8b** and **15**) were performed under conventional solution-phase using HBTU or BOP as a coupling reagents in a single step (Scheme 3.05). Due to insolubility of **HPB(COOH)<sub>12</sub>**, the reactions were conducted using polar aprotic solvents like dimethyl sulfoxide (DMSO) or dimethylformamide (DMF). The yields of the HPB-based TASP **16a** and **16b** were found to be 60-80%. Peptide counterparts **8b** (NH<sub>2</sub>-<sup>L</sup>Leu-Aib-<sup>L</sup>Val-OMe) and **11** (NH<sub>2</sub>-<sup>L</sup>Leu-Aib-<sup>L</sup>Val-<sup>L</sup>Ala-<sup>L</sup>Leu-Aib-<sup>L</sup>Val-OMe) were synthesized using solution-phase methods as per the reported procedures (Scheme 3.06).<sup>48-50</sup> Peptide counterparts **14** (Boc-Aib-<sup>L</sup>Pro-<sup>S</sup>Ant-iBu) and **15** (NH<sub>2</sub>-Aib-<sup>L</sup>Pro-<sup>S</sup>Ant-iBu) were synthesized with slight modification from the reported procedures (Scheme 3.07).<sup>51-52</sup> Compounds **16a** and **16b** were completely soluble in chloroform and were characterized by IR and <sup>1</sup>H NMR, <sup>13</sup>C NMR spectroscopy. The broad signals were seen in the <sup>1</sup>H NMR of compound **16a** and **16b** revealing the macromolecular nature of the substances. Mass spectrometry (MALDI-MS) analysis of **16a** showed [**16a** + Na]<sup>+</sup> an ion peak at *m/z* = 4818.3970 [M+Na]<sup>+</sup>, is consistent with a macromolecule structure that was composed of twelve units of **8b** and one unit of **HPB(COOH)<sub>12</sub>** with a formula C<sub>246</sub>H<sub>378</sub>N<sub>36</sub>O<sub>60</sub> (Fig. 3.32). Similarly, mass spectrometry (MALDI-MS) of compound **16b** showed [**16b** + K]<sup>+</sup> an ion peak at 5810.2129 [M+K]<sup>+</sup>, which was corresponding to the molecular structure of **16b** with a formula C<sub>282</sub>H<sub>366</sub>N<sub>48</sub>O<sub>60</sub>S<sub>12</sub> (Fig. 3.32).



**Scheme 3.05:** Reagents and conditions: BOP/HBTU, free amine of peptide, DIEA, DMSO, rt, 12 h.



**Scheme 3.06:** Reagents and conditions: i) LiOH, H<sub>2</sub>O, MeOH. (ii) TFA: CH<sub>2</sub>Cl<sub>2</sub> (1:1), 0 °C to rt. ii) EDC, HOBt, DIPEA, DMF, rt, 24h. iii) dioxane.HCl.



**Scheme 3.07:** Reagents and conditions: i) Boc-L-Pro-OH, EtOCOC<sub>2</sub>Cl, Et<sub>3</sub>N, THF, reflux, 16 h. (ii) (a) TFA:DCM (1:1), rt, 2 h, (b) Boc-Aib-OH, HBTU, DIEA, CH<sub>3</sub>CN, rt, 12 h. (iii) TFA:DCM (1:1), rt, 2 h.

While recording the mass spectra of the **16a** and **16b**, we have observed the solvent dependent (methanol and dichloromethane) mass peaks in the spectra. Compounds **16a** and **16b** were dissolved in methanol and were spotted on the MALDI plate for mass analysis. The recorded mass spectra have showed [M+methanol] peak (Fig. 3.30) & (Fig. 3.31). On the contrary, compounds **16a** and **16b** dissolved in DCM and their recorded mass spectra have showed only either [M+Na] or [M+K] peak. This could be due to the strongly bound solvent molecules inside the cavities of **16a** and **16b**.



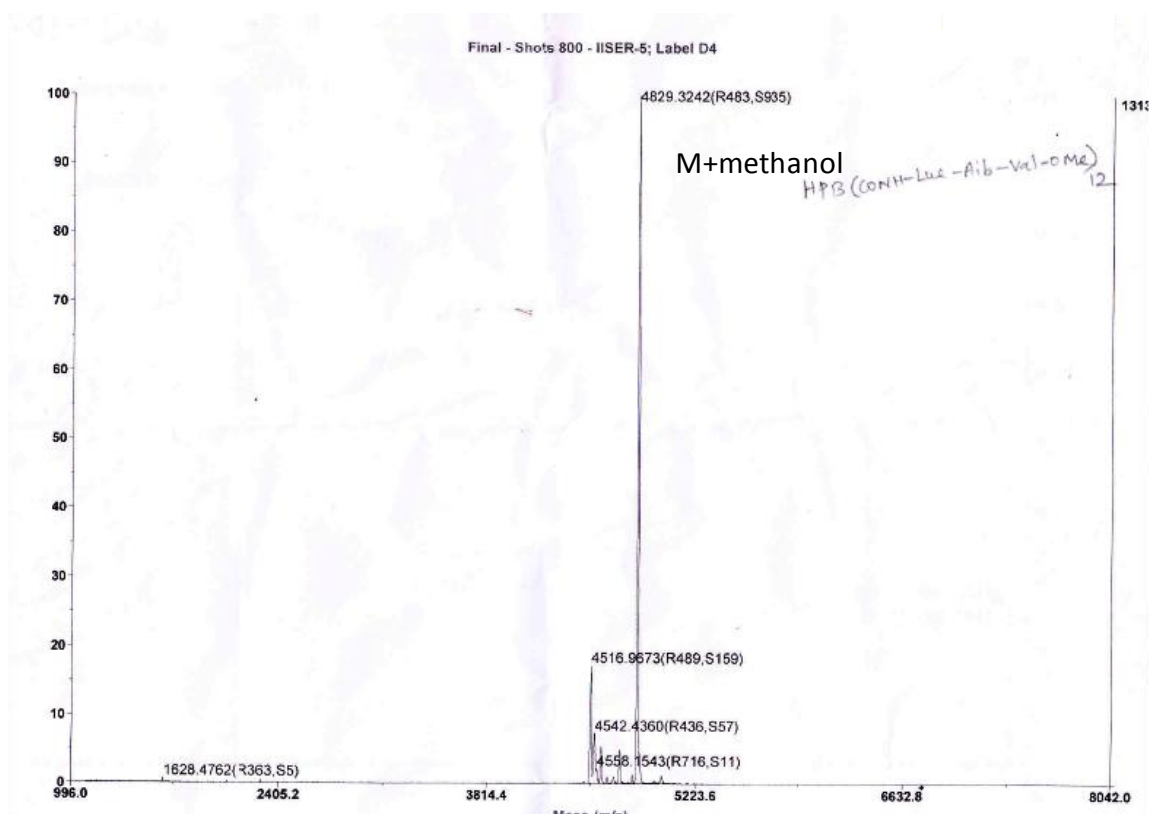


**Fig. 3.30:** MALDI-mass spectrum of **16a** (spotted in methanol)

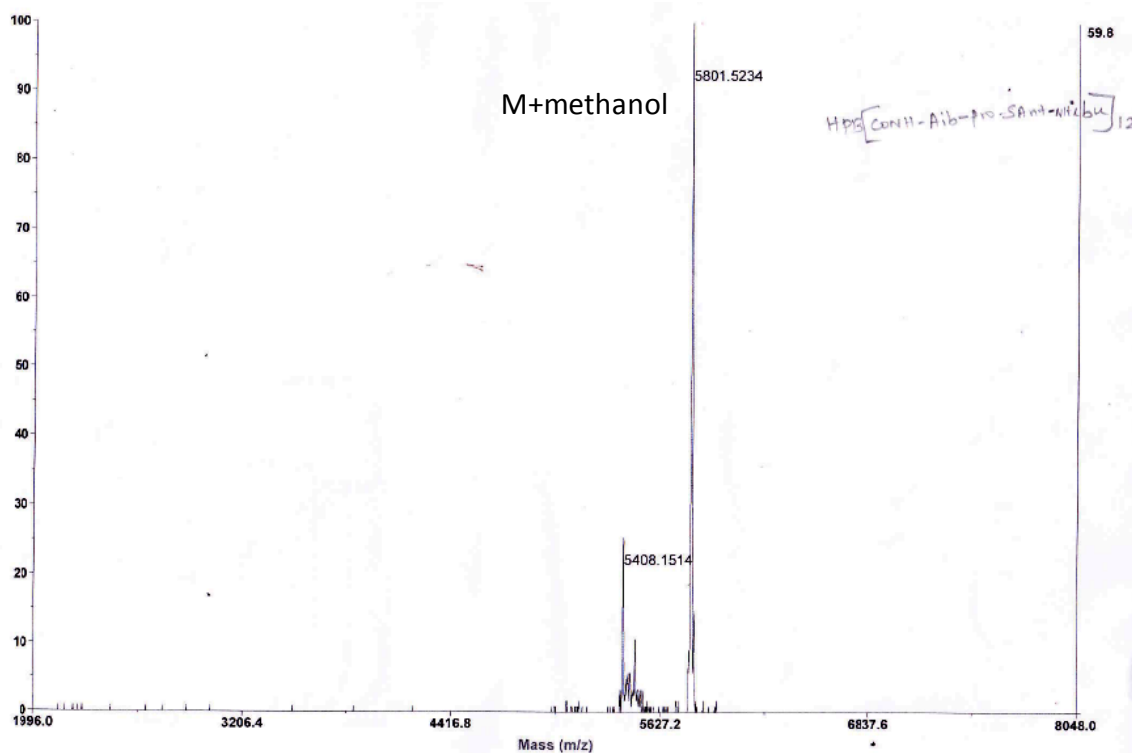


**Fig. 3.31:** MALDI-mass spectrum of **16b** (spotted in methanol)

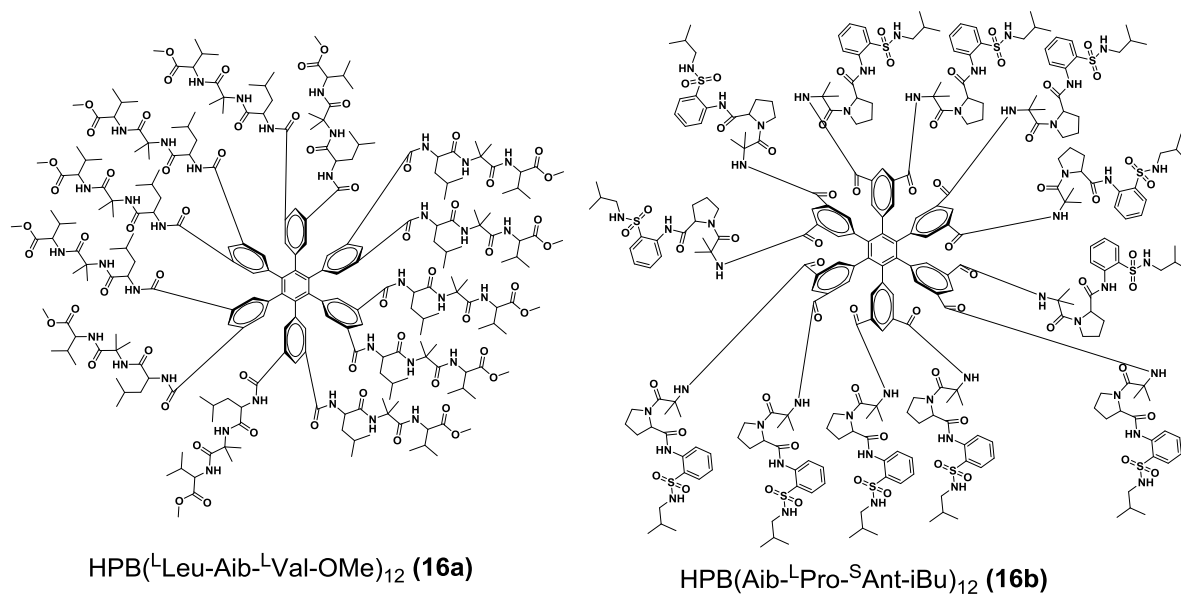


**Fig. 3.32:** Molecular structures of TASPs **16a** and **16b**.

Further, these results have motivated us to incorporate heptapeptide **11** using the above mentioned condition. Though, we could not separate the components of the reaction mixture using column chromatography, the mass spectrometry analysis (MALDI-Mass) of reaction mixture showed the presence of expected product **16c** mass ( $M + Na$ , 9244.2627) with other impurity peaks (Fig. 3.33). Purification of **16c** and tethering of other biologically important peptides are currently pursued in our lab.

Compound **16a** was recrystallised from hot ethanol and a crystal that was suitable for X-ray crystallography was removed directly from the sample vial in order to obtain crystal data. The initial data collection had revealed that the unit cell was larger one (cell volume approximately  $36000 \text{ \AA}^3$ ). Similarly, the compound **16b** was crystallized from aqueous DMSO and single crystal data analysis had revealed that the unit cell size was large. Unfortunately, in both the cases we could not solve the crystal structure due to phase problem. Then, we have also tried to get the crystal structure of **16b** using heavy atom method using sulfur atoms which were present in its structure.

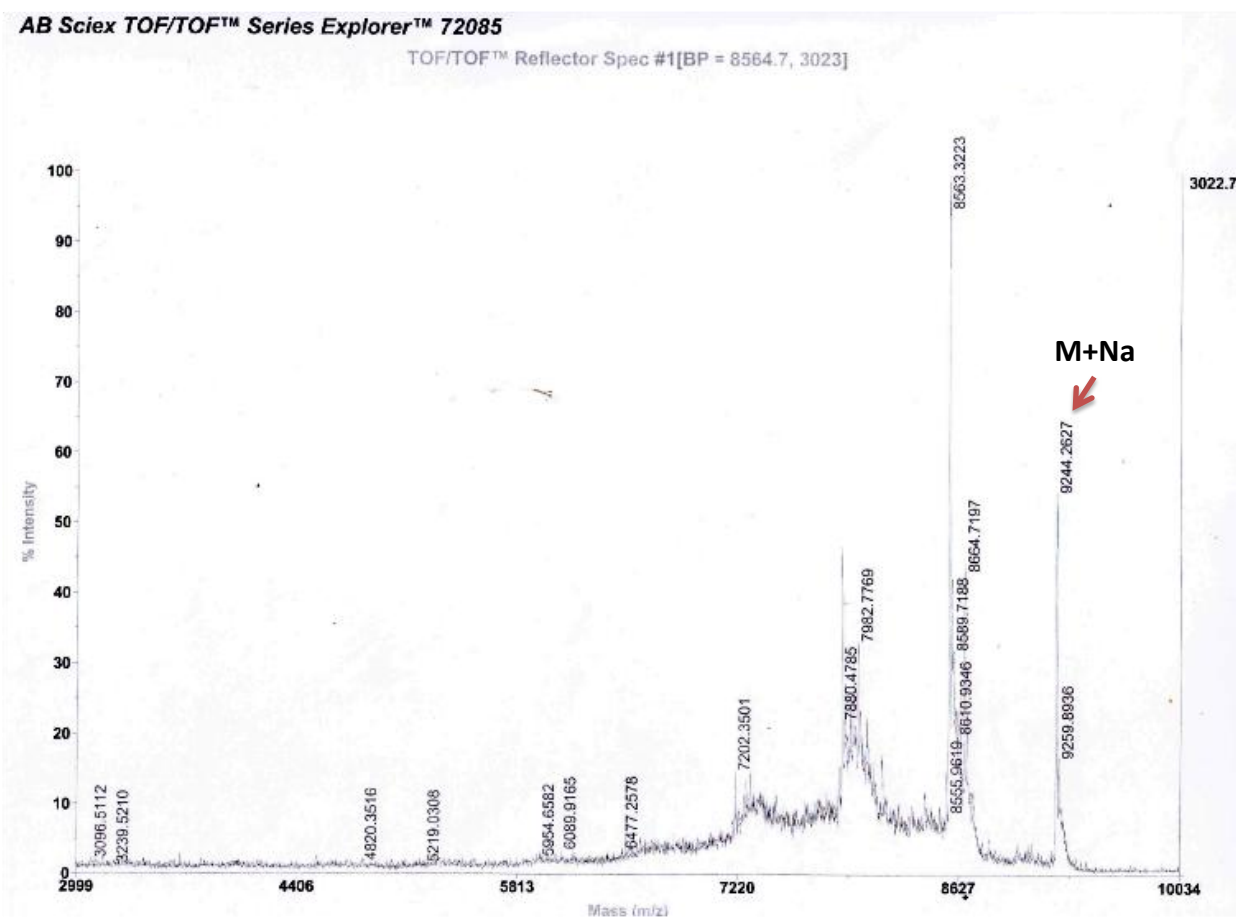


**Fig. 3.33:** MALDI-mass spectrum of **16c** (HPB(<sup>L</sup>Leu-Aib-<sup>L</sup>Val-<sup>L</sup>Ala-<sup>L</sup>Leu-Aib-<sup>L</sup>Val-OMe)<sub>12</sub>).

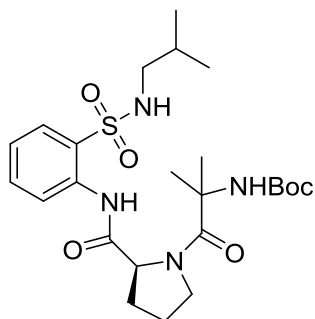
### 3.20 Conclusion

In summary, we have successfully demonstrated the tethering of peptides on axially substituted HPB-based template (**HPB(COOH)**<sub>12</sub>). Then, the synthesized template assembled proteins were characterized by IR, <sup>1</sup>H-NMR, <sup>13</sup>C-NMR and mass spectrometry. Interestingly, TASP **16a** HPB(<sup>L</sup>Leu-Aib-<sup>L</sup>Val-OMe)<sub>12</sub> and **16b** (HPB(Aib-<sup>L</sup>Pro-<sup>S</sup>Ant-iBu)<sub>12</sub> showed [M+methanol] mass peaks in the mass spectrometry analysis, which could have arisen due to the presence of trapped methanol in the cavities of **16a** and **16b**. Then, the synthesis of **16c** HPB(<sup>L</sup>Leu-Aib-<sup>L</sup>Val-<sup>L</sup>Ala-<sup>L</sup>Leu-Aib-<sup>L</sup>Val-OMe)<sub>12</sub> was performed which could not be purified under conventional column chromatographic method. Attempts were also made to get the crystal structure of **16a** and **16b**, but they failed due to phase problem. These synthesised macromolecules may have some potential applications in the biomedical field due to their novel structural architectures.

### 3.21 Experimental procedures:

Compounds **8**, **8a**, **8b**, **11** and **13** were prepared by following the reported procedures.<sup>31</sup>, 50-52

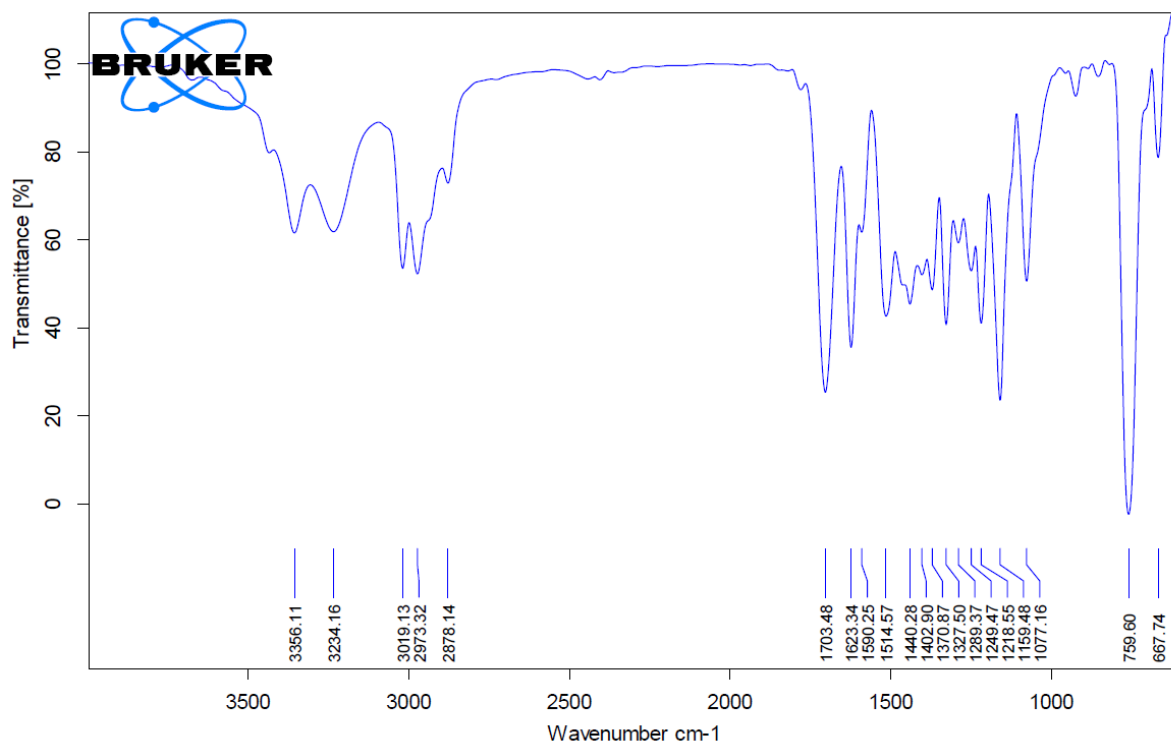
#### Compound 14:



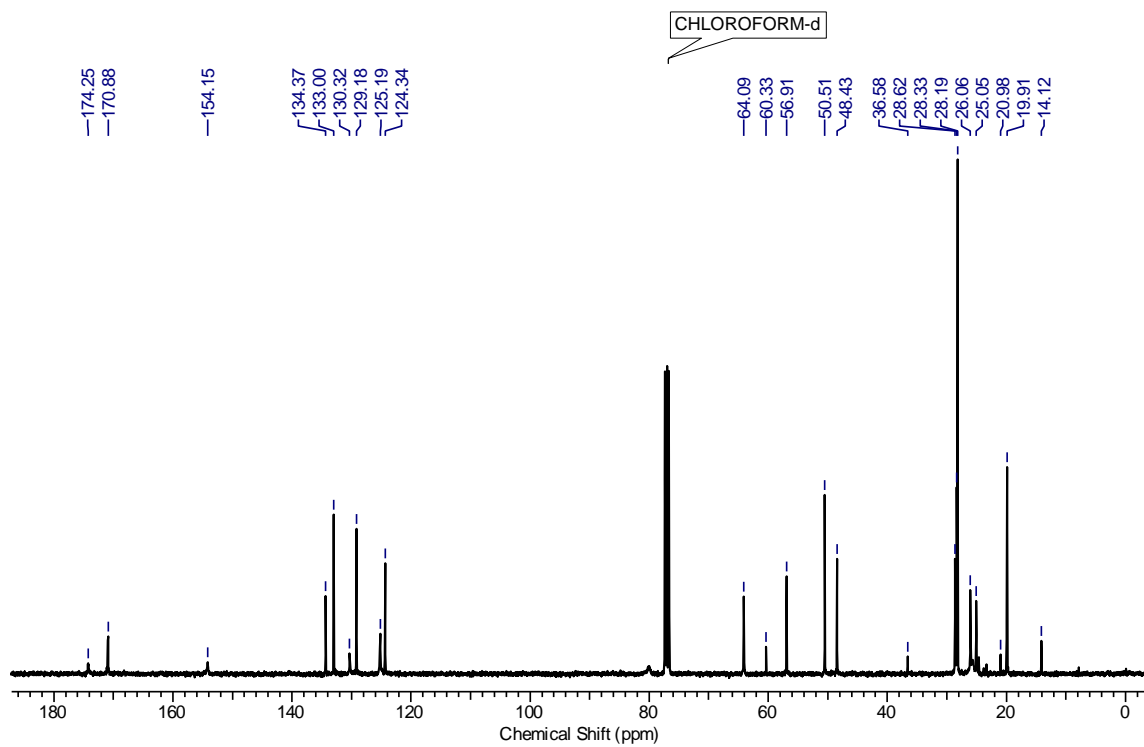
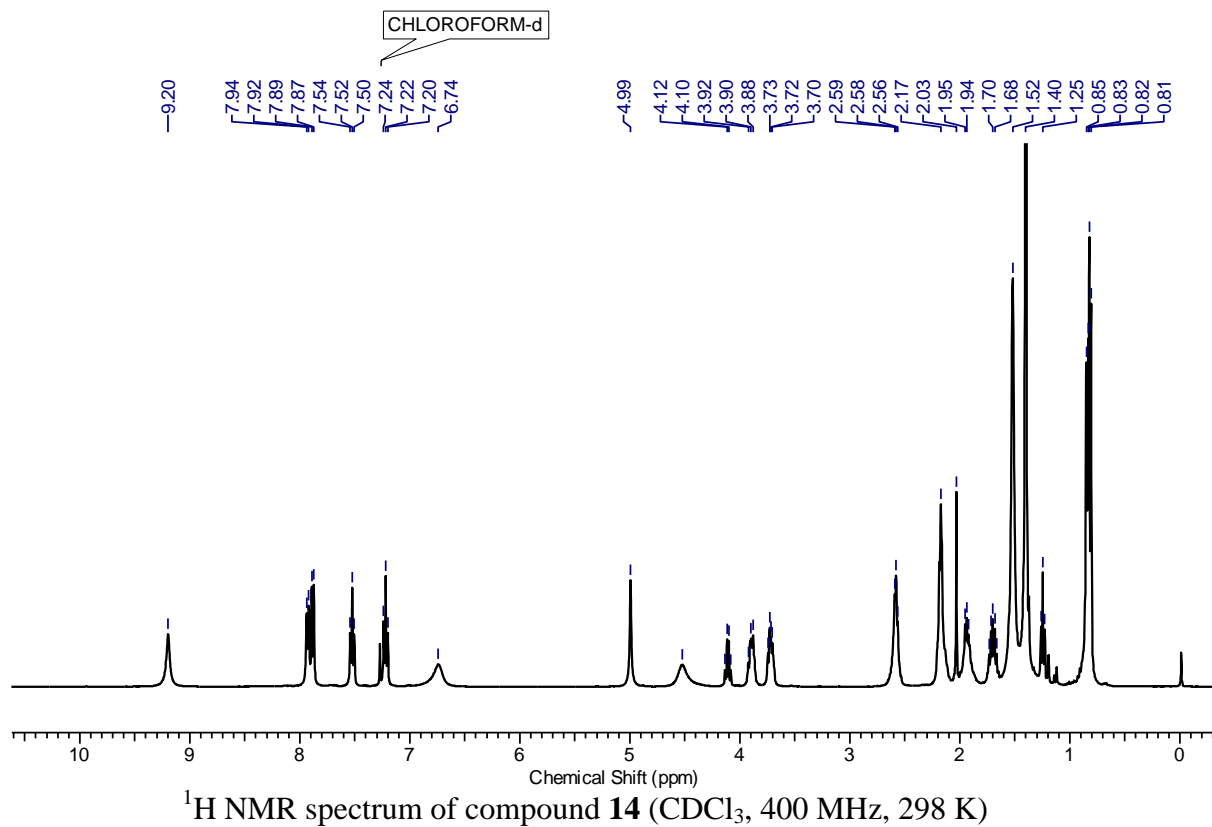
Compound **13** (0.7 g, 1.64 mmol) was subjected to *t*-Boc deprotection using TFA (8 mL) in DCM (8 mL). The reaction mixture was evaporated and the residue was neutralized with NaHCO<sub>3</sub> solution, followed by extraction using DCM (3 x 50 mL) and evaporation to yield the free amine.

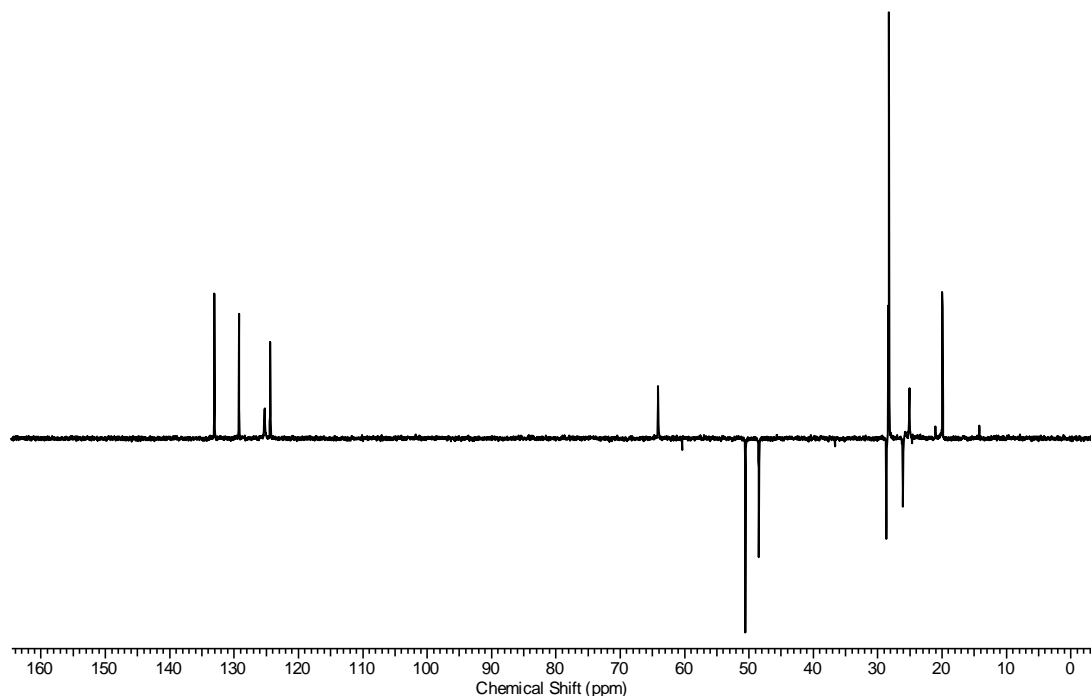
To a suspension of Boc-Aib-OH (0.367 g, 1.80 mmol) and DIEA (0.348 mL, 1.97 mmol) in dry ACN (15 mL), HBTU (0.686 g, 1.80 mmol) was added and then the mixture was stirred at room temperature for 5 minutes to form a clear solution. Then free amine (in 5 mL ACN) which was prepared earlier (<sup>L</sup>Pro-<sup>S</sup>Ant-iBu) (0.535 g, 1.64 mmol) was added through syringe and stirring was continued for 12 h. Then, the reaction mixture was evaporated on rota vapor and residue was diluted with dichloromethane (50 mL) and the organic layer was washed with saturated solutions of NaHCO<sub>3</sub> (30 mL), KHSO<sub>4</sub> (20 mL) and water (30 mL), sequentially. The organic layer was dried over anhydrous sodium sulphate. The clear solution obtained was evaporated under reduced pressure to get crude product which was chromatographed (ethyl acetate/pet. ether, 50/50, R<sub>f</sub>= 0.4) to afford **1** as a white solid. Yield: 0.62 g (74%). mp: 78-80 °C; IR (CHCl<sub>3</sub>) cm<sup>-1</sup>: 3356, 3234, 3019, 2973, 2878, 1703, 1623, 1590, 1514, 1440, 1402, 1370, 1327, 1289, 1249, 1218, 1159, 1077, 759, 667; <sup>1</sup>H-NMR (400MHz, CDCl<sub>3</sub>) δ: 9.20 (s, 1H), 7.90 (dd, *J* = 7.9, 18.9 Hz, 2H), 7.52 (t, *J* = 7.3 Hz, 1H), 7.22 (t, *J* = 7.6 Hz, 1H), 6.74 (s, 1H), 4.99 (br. s., 1H), 4.52 (s, 1H), 3.96 - 3.83 (m, 1H), 3.80 - 3.65 (m, 1H), 2.67 - 2.50 (m, 2H), 2.18 (m, 3H), 2.03 (s, 1H), 1.99 - 1.86 (m, 2H), 1.78 - 1.63 (m, 2H), 1.52 (br. s., 3H), 1.44 - 1.36 (m, 9H), 0.83 (dd, *J* = 6.7, 10.4 Hz, 6H); <sup>13</sup>C-NMR (101MHz, CDCl<sub>3</sub>) δ = 174.3, 170.9, 154.1,

134.4, 133.0, 130.3, 129.2, 125.2, 124.3, 64.1, 60.3, 56.9, 50.5, 48.4, 36.6, 28.6, 28.3, 28.1, 26.1, 25.0, 19.9, 19.8, 14.1; MALDI-TOF-MS: 533.2379  $[M+Na]^+$ , 549.1960  $[M+K]^+$ ; Elemental analysis calculated for  $C_{24}H_{38}N_4O_6S$ : C, 56.45; H, 7.50; N, 10.97; Found: C, 56.82; H, 7.80; N, 10.64.



IR spectrum of compound 14

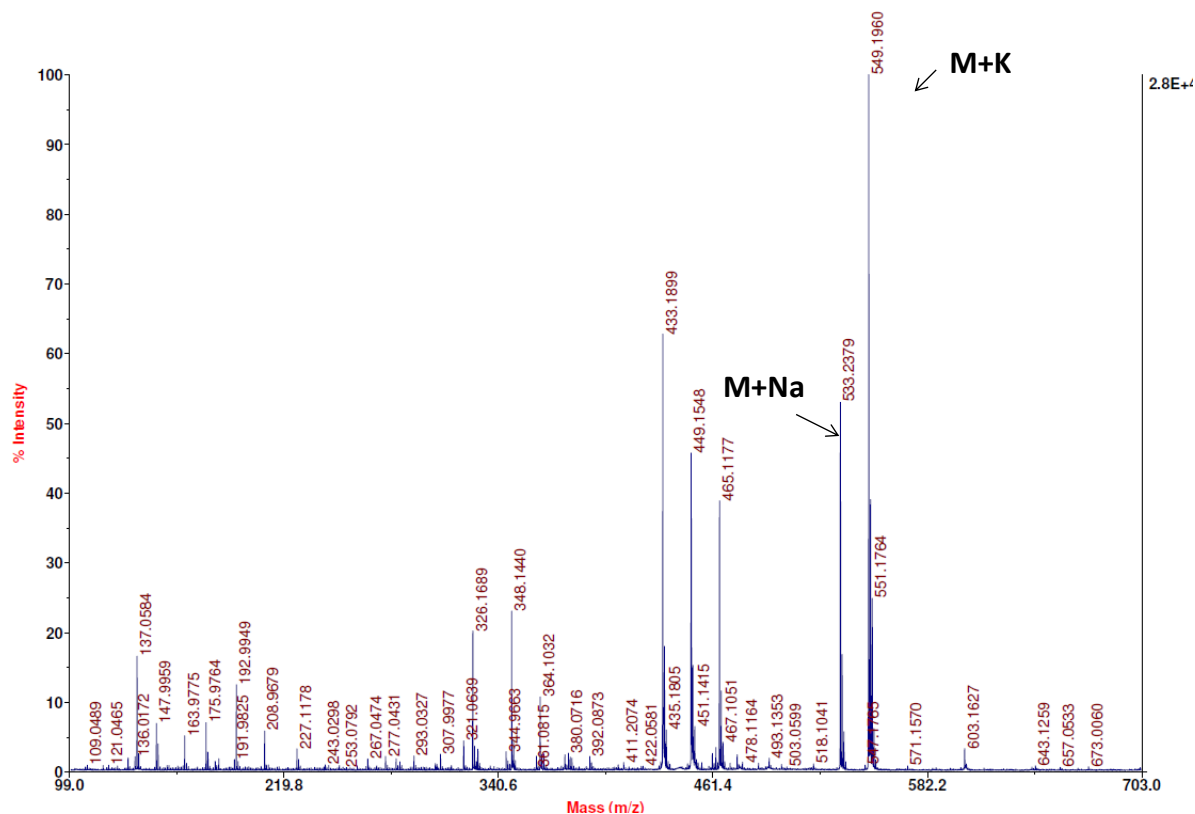




DEPT 135 spectrum of compound **14** (CDCl<sub>3</sub>, 100 MHz, 298 K)

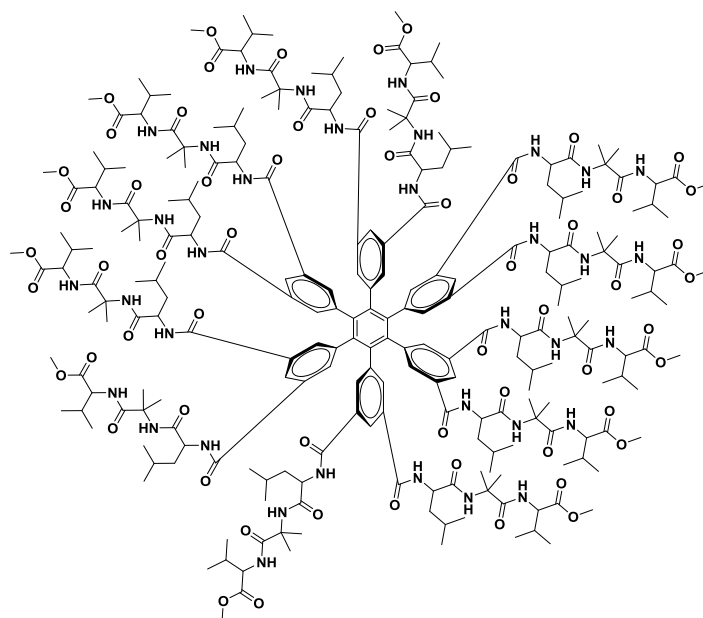
AB Sciex TOF/TOF™ Series Explorer™ 72085

TOF/TOF™ Reflector Spec #1[BP = 549.2, 28136]



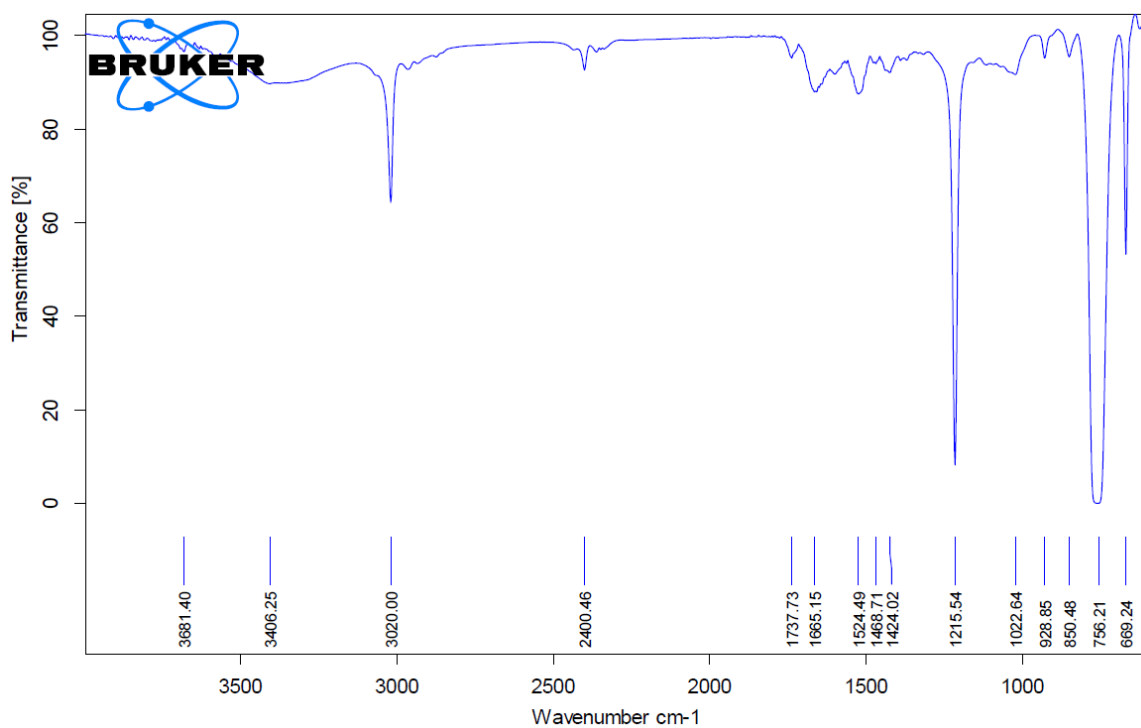
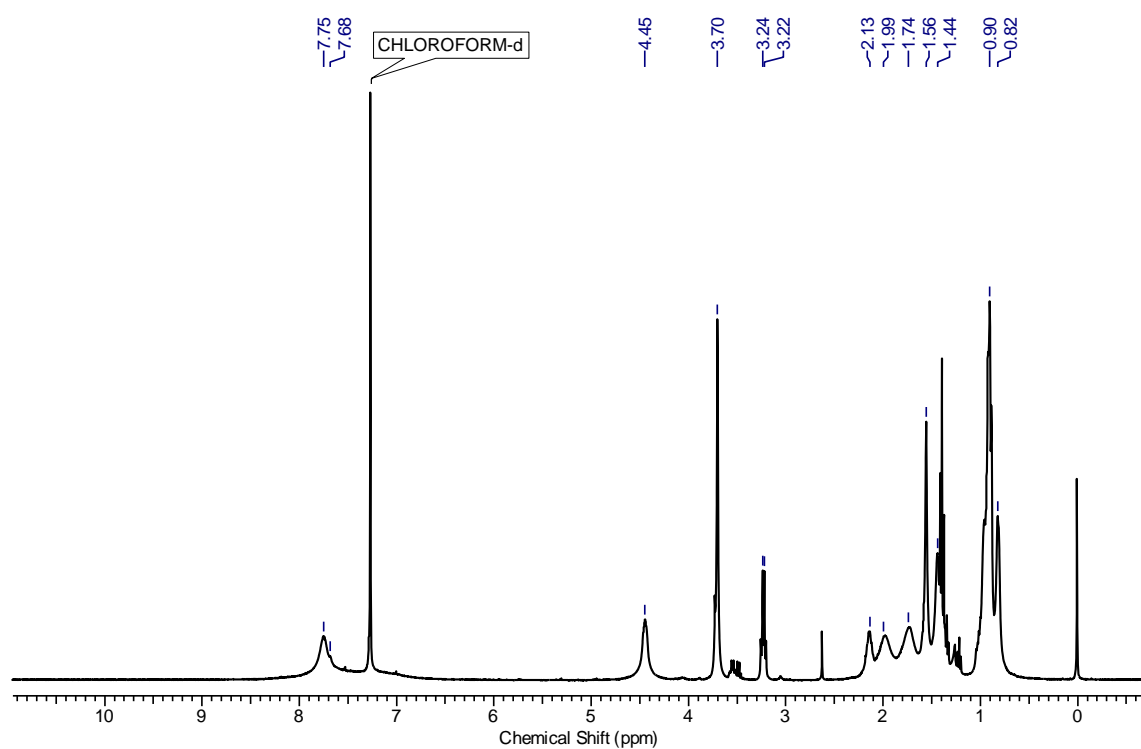
MS (MALDI-TOF) of compound **14**

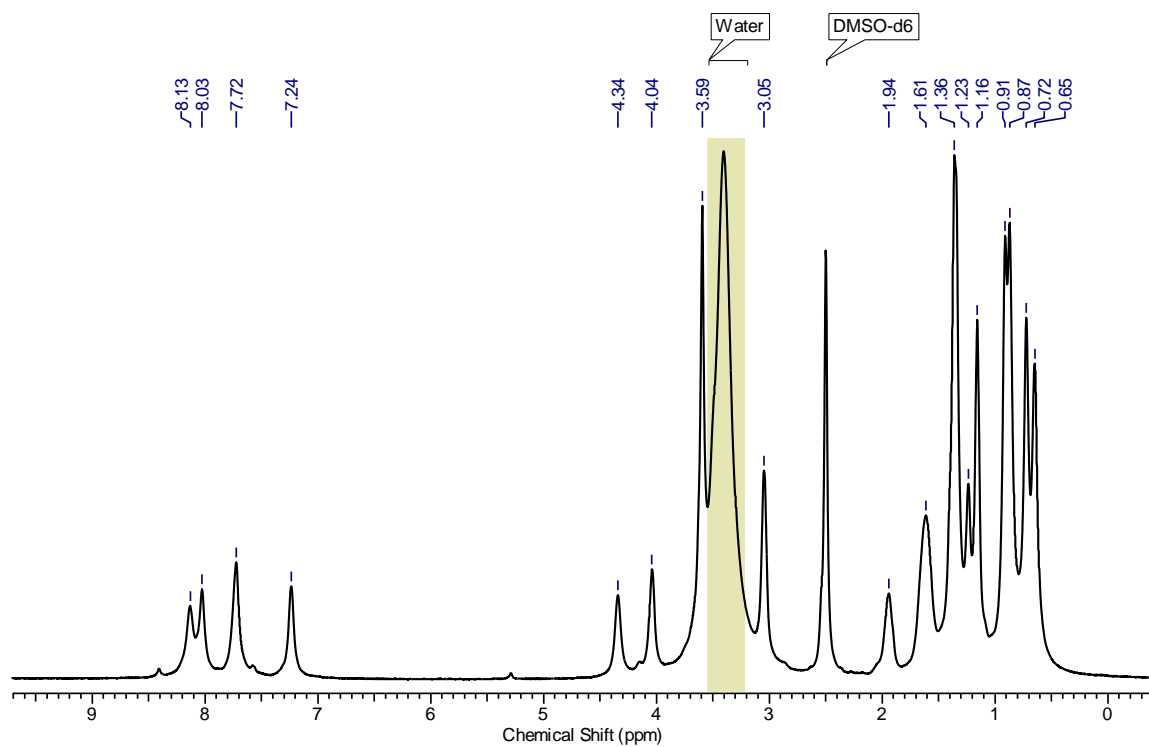


**Compound 16a**

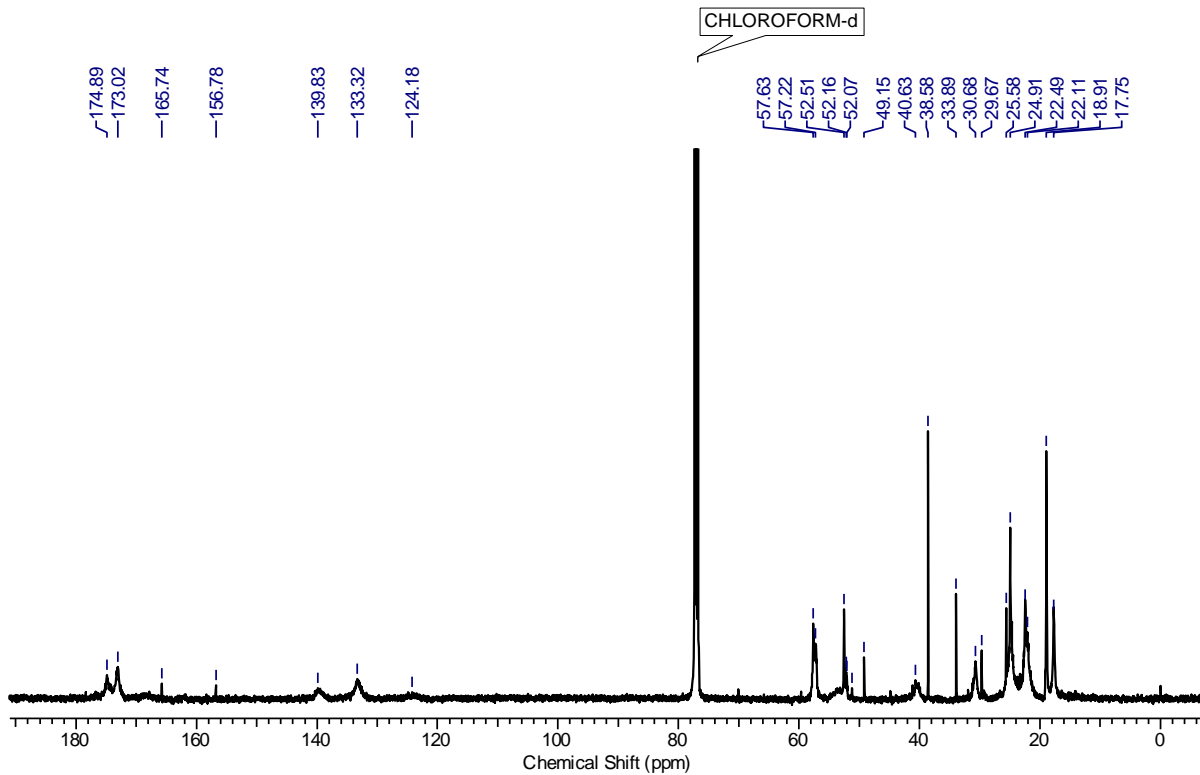
Compound **8** (0.22 g, 0.51 mmol) was subjected to *t*-Boc deprotection using dioxane in HCl (5 mL). The reaction mixture was evaporated and the residue was neutralized with NaHCO<sub>3</sub> solution, followed by extraction using DCM (3 x 50 mL) and was evaporated to yield the free amine (0.144 g, 72%).

To a suspension of **HPB(COOH)**<sub>12</sub> (0.01 g, 0.0094 mmol) and DIEA (0.03 mL, 0.17 mmol) in DMSO (2 mL), BOP (0.074 g, 0.17 mmol) was added and the mixture was stirred at room temperature for 5 minutes to form a clear solution. Then **8b** (0.055 g, 0.17 mmol) in DCM (2 mL) was added and stirring was continued for 12 h. After completion of the reaction, the reaction mixture was diluted with ice-chilled water and thrice extracted with DCM. The combined organic phases were dried over sodium sulfate and evaporated *in vacuo*. Then, the crude product was purified by column chromatography (eluent: MeOH/DCM, 5/95 v/v, R<sub>f</sub> = 0.4) to furnish **16a** as a fluffy white solid. mp: 173-175 °C; [α]<sub>D</sub><sup>23</sup> = -16.6°, C=0.1, 23° C; IR (CHCl<sub>3</sub>) cm<sup>-1</sup>: 3681, 3406, 3020, 2400, 1737, 1665, 1524, 1468, 1424, 1215, 1022, 928, 850, 756, 669; <sup>1</sup>H-NMR (400MHz, CDCl<sub>3</sub>) δ: 8.20 - 6.94 (m, 54H), 4.46 (br. s., 12H), 3.77 - 3.66 (m, 36H), 3.24 (q, *J* = 7.3 Hz, 12H), 2.22 - 2.11 (m, 12H), 2.07 - 1.93 (m, 12H), 1.75 (br. s., 36H), 1.57 (br. s., 36H), 1.45 (br. s., 24H), 1.02 - 0.80 (m, 144 H); <sup>13</sup>C-NMR (126 MHz, CDCl<sub>3</sub>) δ: 174.9, 173.2, 165.7, 156.8, 139.7, 133.3, 70.2, 59.6, 57.6, 57.2, 52.5, 52.2, 52.1, 52.0, 51.2, 49.2, 44.8, 41.1, 40.5, 40.0, 38.6, 33.9, 31.2, 30.8, 29.7, 25.6, 24.8, 23.7, 23.3, 22.4, 22.1, 21.9, 21.5, 18.9, 17.7; MALDI-TOF/TOF: 4818.3970 [M+Na]<sup>+</sup>.

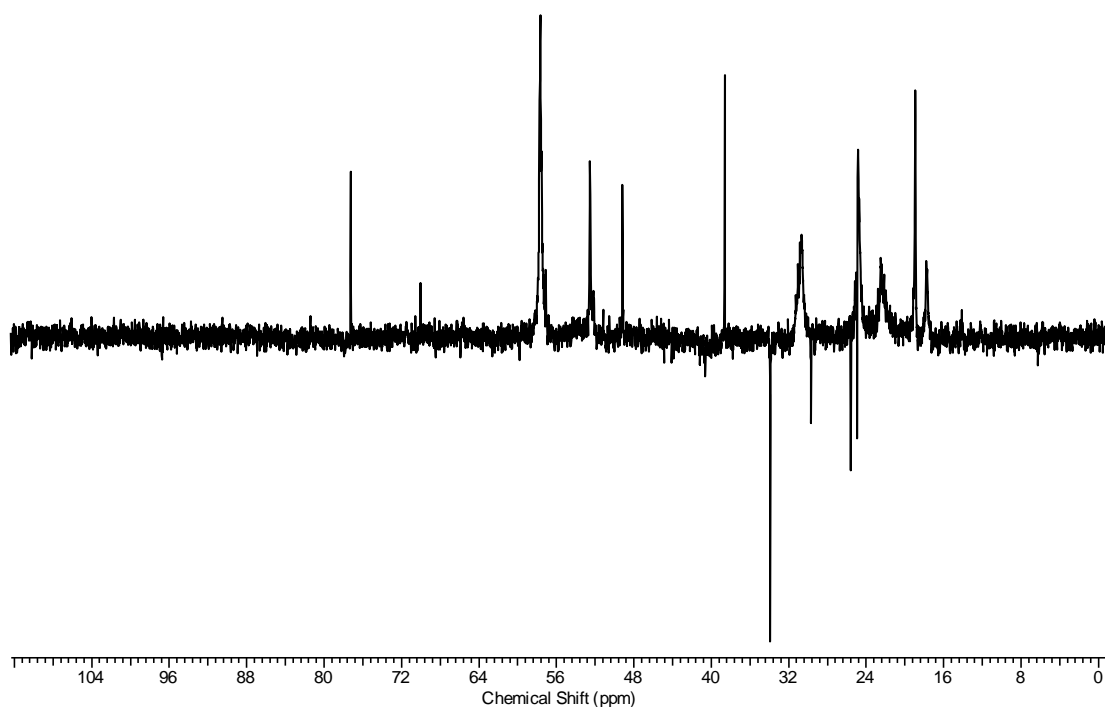
IR spectrum of compound **16a** $^1\text{H}$  NMR spectrum of compound **16a** ( $\text{CDCl}_3$ , 400 MHz, 298 K)



<sup>1</sup>H NMR spectrum of compound **16a** (DMSO-*d*<sub>6</sub>, 500 MHz, 298 K)

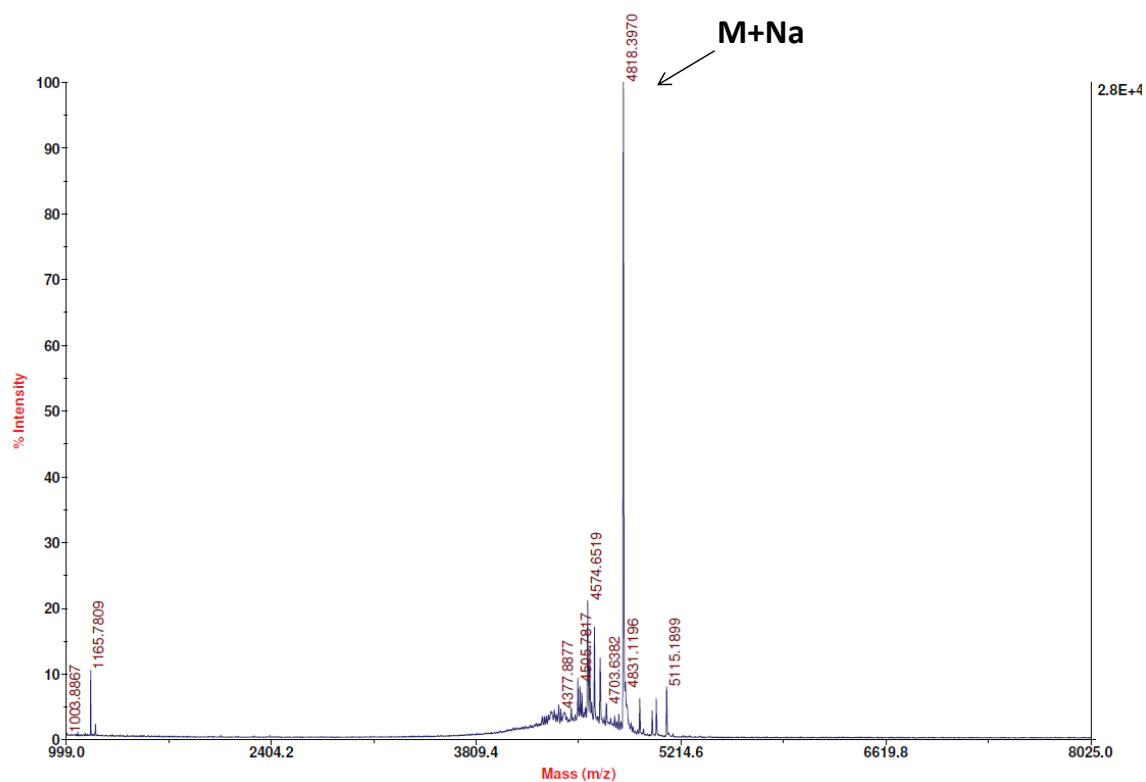


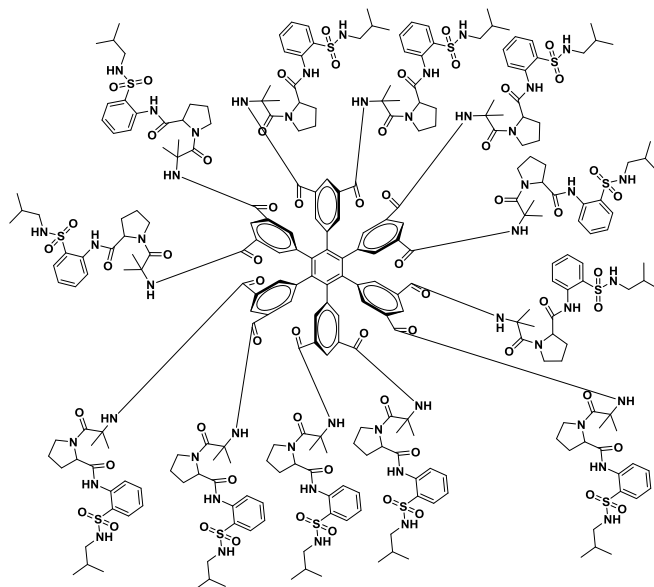
<sup>13</sup>C NMR spectrum of compound **16a** (CDCl<sub>3</sub>, 126 MHz, 298 K)

DEPT 135 spectrum of compound **16a** (CDCl<sub>3</sub>, 100 MHz, 298 K)

AB Sciex TOF/TOF™ Series Explorer™ 72085

TOF/TOF™ Reflector Spec #1[BP = 4818.8, 27777]

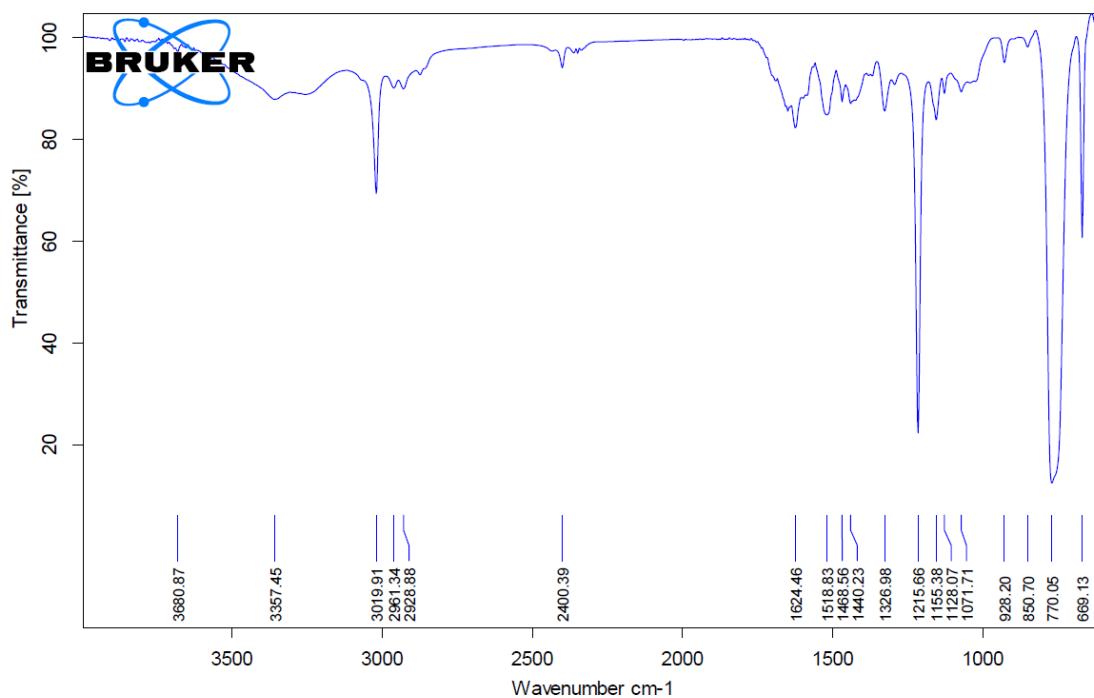
MS (MALDI-TOF) of compound **16a**

**Compound 16b:**

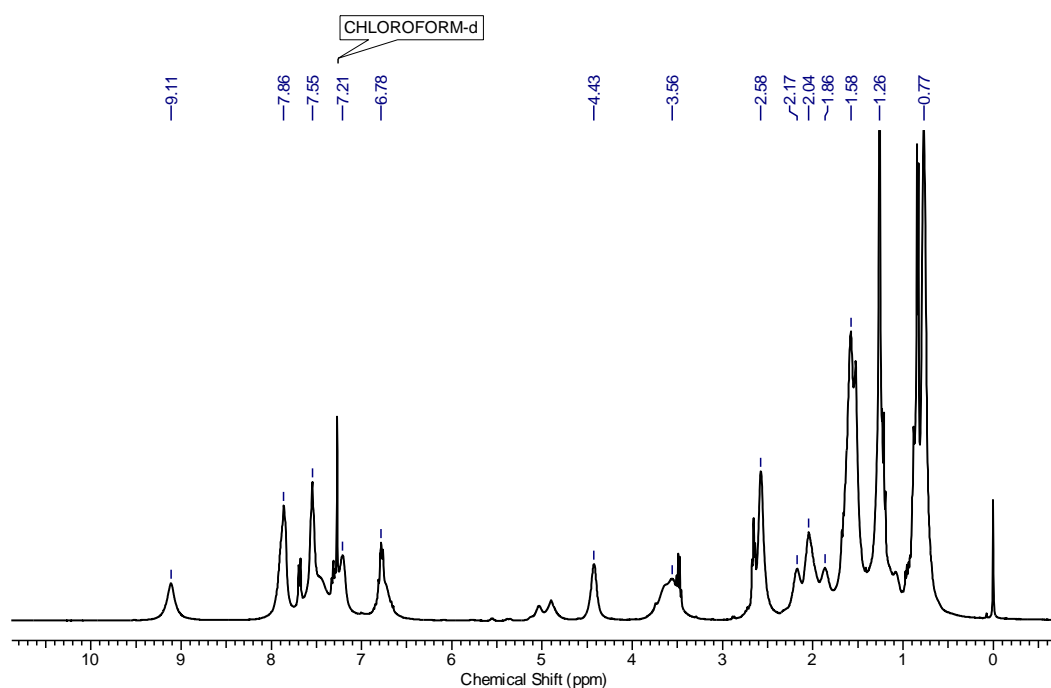
Compound **14** (1 g, 1.95 mmol) was subjected to *t*-Boc deprotection using TFA (7 mL) in DCM (7 mL). The reaction mixture was evaporated and the residue was neutralized with NaHCO<sub>3</sub> solution, followed by extraction using DCM (3 x 60 mL) and was evaporated to yield the free amine **15**.

To a suspension of **HPB(COOH)**<sub>12</sub> (0.130 g, 0.122 mmol) and DIEA (0.383 mL, 2.20 mmol) in DMSO (6 mL), HBTU (0.696 g, 1.83 mmol) was added and the mixture was stirred at room temperature for 5 minutes to form a clear solution. Then **15** (0.75 g, 1.83 mmol) in ACN (2 mL) was added and the stirring was continued for 12 h. After completion of the reaction, the reaction mixture was diluted with ice-chilled water and thrice extracted with DCM. The combined organic phases were dried over sodium sulfate and evaporated *in vacuo*. The crude product was purified by column chromatography (eluent: MeOH/CHCl<sub>3</sub>, 5/95 v/v, R<sub>f</sub>= 0.5) to furnish **16b** as a fluffy white solid. Yield: 0.47 g (67%). mp: 193-195 °C; [α]<sub>D</sub><sup>23</sup> = - 83°, C=0.1, 23° C; IR (CHCl<sub>3</sub>) cm<sup>-1</sup>: 3680, 3357, 3019, 2961, 2928, 2400, 1624, 1518, 1468, 1440, 1326, 1215, 1155, 1128, 1071, 928, 770, 669; <sup>1</sup>H-NMR (400MHz, CDCl<sub>3</sub>) δ: 9.11 (br. s., 12H), 7.86 (br. s., 24H), 7.61 - 7.16 (m, 54H), 6.79 (br. s., 12H), 4.43 (br. s., 12H), 3.80 - 3.53 (m, 24H), 2.58 (br. s., 24H), 2.28 - 1.95 (m, 36H), 1.86 (br. s., 12H), 1.58 (br. s., 48H), 1.26 (br. s., 36H), 0.77 (br. s., 72H); <sup>13</sup>C-NMR (176MHz, CDCl<sub>3</sub>) δ = 173.2, 171.0, 166.3, 145.0, 139.5, 134.4, 134.0, 133.3, 130.4, 129.5, 129.2, 125.7, 124.8, 121.4, 118.6, 117.6, 115.5, 65.8, 65.7, 64.0, 57.7, 50.6, 50.5, 49.1, 48.7, 39.4, 39.3, 39.0, 37.4, 37.4, 37.3, 37.0, 36.6, 34.3, 33.6,

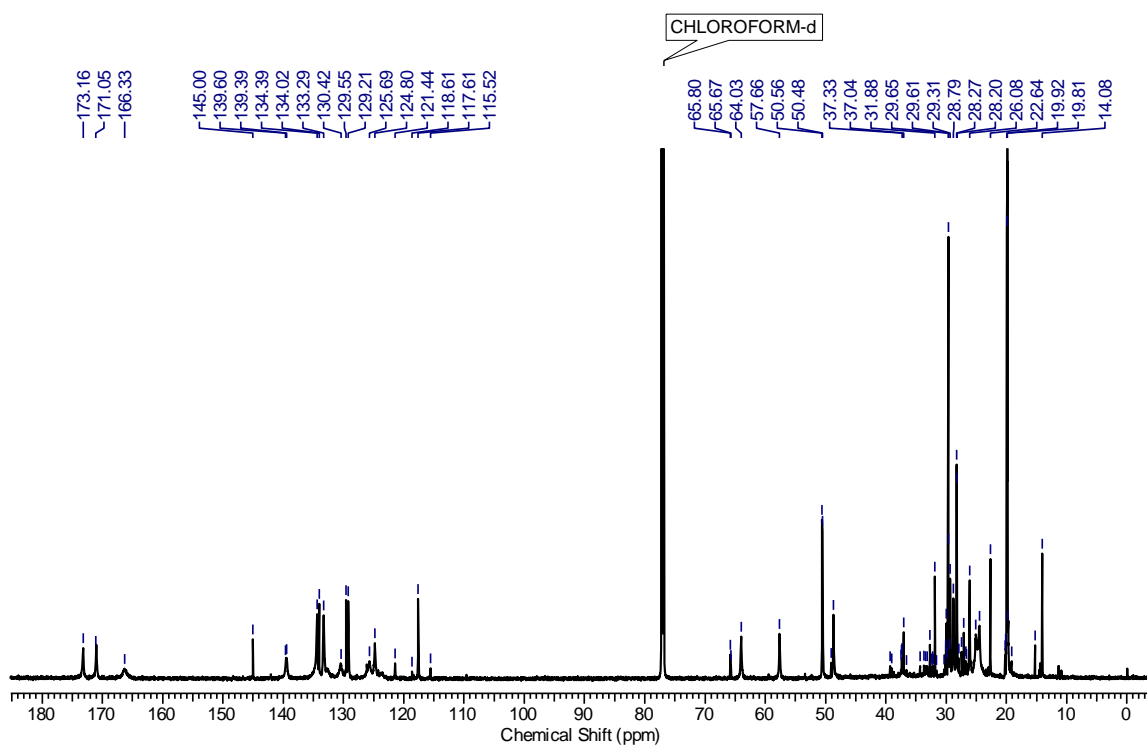
33.4, 33.2, 32.7, 32.4, 32.3, 32.2, 32.1, 31.9, 31.6, 30.3, 30.1, 30.0, 29.9, 29.6, 29.6, 29.5, 29.4, 29.3, 28.8, 28.3, 28.2, 27.9, 27.4, 27.4, 27.0, 26.7, 26.6, 26.1, 25.1, 24.4, 22.6, 20.2, 20.1, 19.9, 19.9, 19.8, 19.7, 19.1, 15.2, 14.1; MALDI-TOF: 5810.2129 [M+K]<sup>+</sup>.



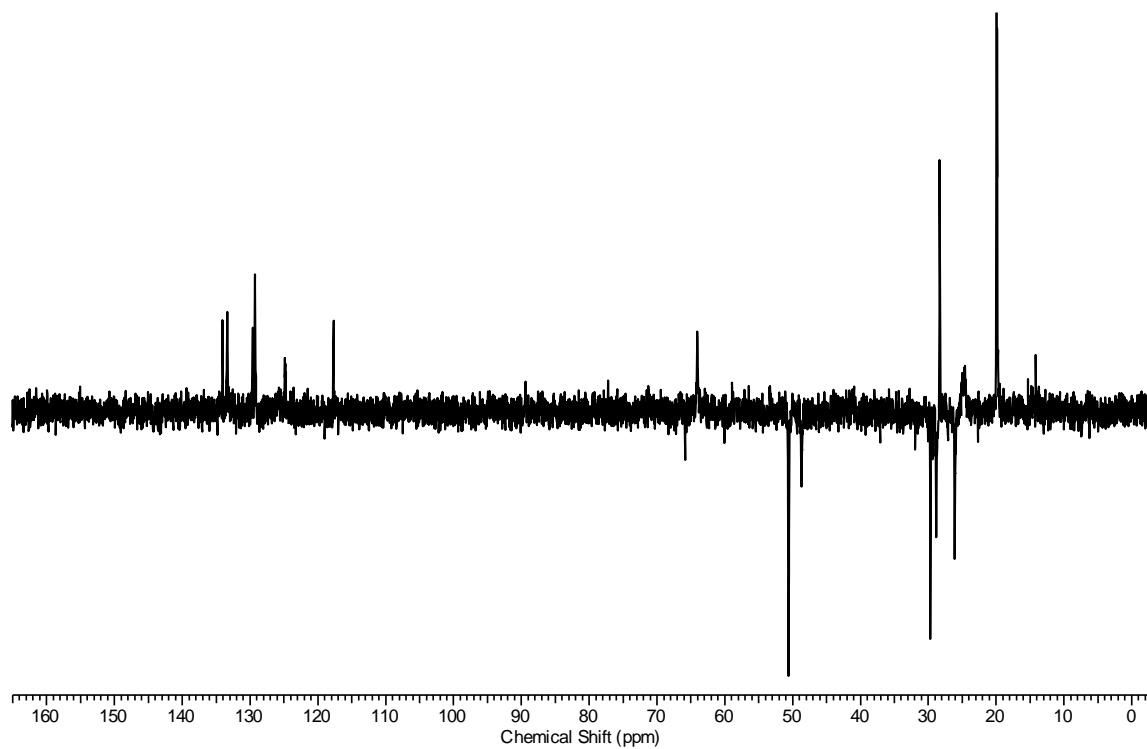
IR spectrum of compound **16b**



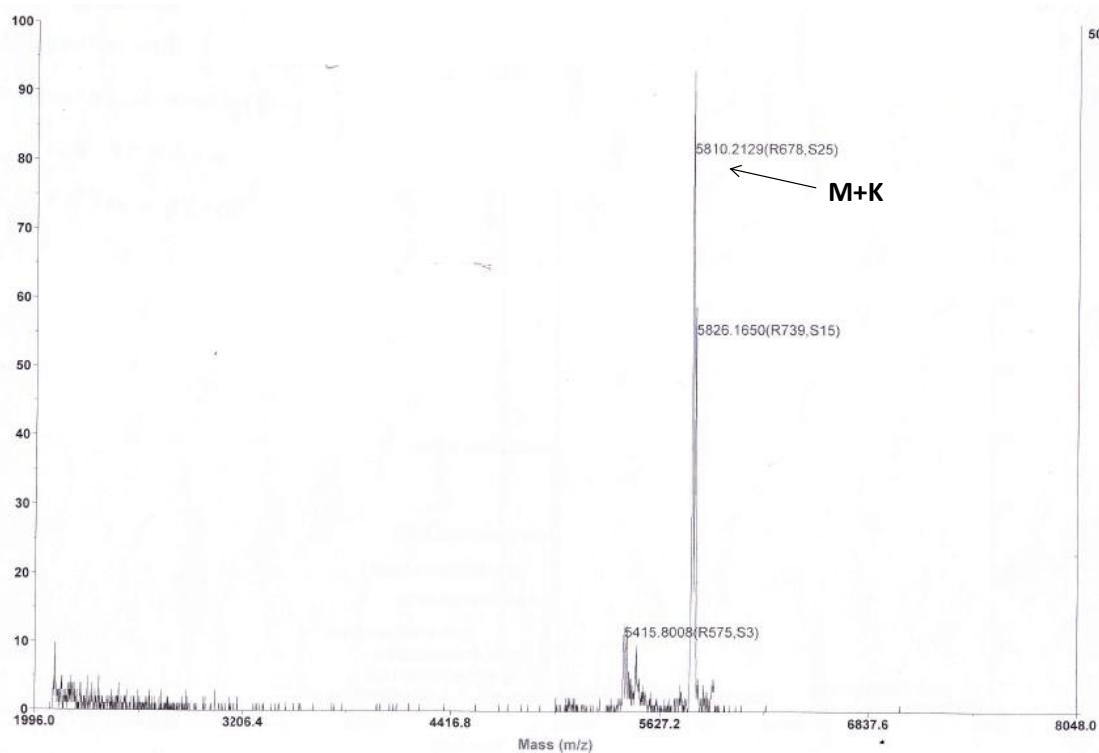
<sup>1</sup>H NMR spectrum of compound **16b** (CDCl<sub>3</sub>, 700 MHz, 298 K)



$^{13}\text{C}$  NMR spectrum of compound **16b** ( $\text{CDCl}_3$ , 126 MHz, 298 K)



DEPT 135 spectrum of compound **16b** ( $\text{CDCl}_3$ , 100 MHz, 298 K)



(MALDI-TOF) of compound **16b**

### Compound **16c**:

Compound **16c** was synthesized following the procedure for **16a**, using **11** and **HPB(COOH)<sub>12</sub>**.



### 3.22 References

1. Eisenberg, D. *Annu. Rev. Biochem* **1984**, 53 (1), 595-623.
2. Saudek, V.; Atkinson, R. A.; Pelton, J. T. *Biochem.* **1991**, 30 (30), 7369-7372.
3. Hendrick, J. P.; Hartl, F.-U. *Annu. Rev. Biochem* **1993**, 62 (1), 349-384.
4. Nelson, D. L.; Cox, M. M.; Lehninger, A. L., *Principles of Biochem.*. 2005; Vol. 1, p 2.
5. Gutteridge, A.; Thornton, J. M. *Trends Biochem. Sci* **2005**, 30 (11), 622-629.
6. Lodish, H.; Berk, A.; Zipursky, S. L.; Matsudaira, P.; Baltimore, D.; Darnell, J. *National Center for Biotechnology Information's Bookshelf* **2000**.
7. Alberts, B.; Johnson, A.; Lewis, J.; Raff, M.; Roberts, K.; Walter, P., *Molecular Biology of the Cell* (Garland Science, New York, 2002). 1997.
8. Alberts, B.; Bray, D.; Hopkin, K.; Johnson, A.; Lewis, J.; Raff, M.; Roberts, K.; Walter, P., *Essential cell biology*. Garland Science: 2013.
9. Yuan, S. M.; Clarke, N. D. *Proteins: Struct., Funct., Bioinf.* **1998**, 30 (2), 136-143.
10. Kamerlin, S. C.; Warshel, A. *Proteins: Struct., Funct., Bioinf.* **2010**, 78 (6), 1339-1375.
11. Koshland, D. *Proceedings of the National Academy of Sciences* **1958**, 44 (2), 98-104.
12. Lodish, H.; Berk, A.; Zipursky, S.; Matsudaira, P.; Baltimore, D.; Darnell, J. *Mol. Cell. Biol.* **2000**, 4.
13. Chevalier-Larsen, E.; Holzbaaur, E. L. *Biochim. Biophys. Acta.* **2006**, 1762 (11), 1094-1108.
14. Shu, J.-J. *BioSystems* **2017**, 151, 21-26.
15. Crick, F. *What Mad Pursuit: A Personal View of Scientific Discovery* **1988**, 89-101.
16. Turanov, A. A.; Lobanov, A. V.; Fomenko, D. E.; Morrison, H. G.; Sogin, M. L.; Klobutcher, L. A.; Hatfield, D. L.; Gladyshev, V. N. *Science* **2009**, 323 (5911), 259-261.
17. Dill, K. A.; MacCallum, J. L. *Science* **2012**, 338 (6110), 1042-1046.
18. Rose, G. D.; Wolfenden, R. *Annu. Rev. Biophys. Biomol. Struct.* **1993**, 22 (1), 381-415.

19. Prabhakaran, P.; Kale, S. S.; Puranik, V. G.; Rajamohanan, P.; Chetina, O.; Howard, J. A.; Hofmann, H.-J. r.; Sanjayan, G. J. *J. Am. Chem. Soc.* **2008**, *130* (52), 17743-17754.
20. Schneider, J. P.; Kelly, J. W. *Chem. Rev.* **1995**, *95* (6), 2169-2187.
21. Sadowsky, J. D.; Schmitt, M. A.; Lee, H.-S.; Umezawa, N.; Wang, S.; Tomita, Y.; Gellman, S. H. *J. Am. Chem. Soc.* **2005**, *127* (34), 11966-11968.
22. Fruton, J. S. *Molecules and life.* **1972**.
23. DeGrado, W. F.; Wasserman, Z. R.; Lear, J. D. In *Protein Desing, a Minimalist Approach*, JSTOR: 1989.
24. Regan, L.; DeGrado, W. F. *Science* **1988**, *241* (4868), 976-978.
25. Mutter, M.; Vuilleumier, S. *Angew. Chem. Int. Ed. Engl.* **1989**, *28* (5), 535-554.
26. Mutter, M.; Altmann, E.; Altmann, K. H.; Hersperger, R.; Koziej, P.; Nebel, K.; Tuchsecherer, G.; Vuilleumier, S.; Gremlich, H. U.; Müller, K. *Helv. Chim. Acta.* **1988**, *71* (4), 835-847.
27. Li, W. W.; Hellwig, P.; Ritter, M.; Haehnel, W. *Chem. Eur. J.* **2006**, *12* (27), 7236-7245.
28. Akerfeldt, K. S.; Kim, R. M.; Camac, D.; Groves, J. T.; Lear, J. D.; DeGrado, W. F. *J. Am. Chem. Soc.* **1992**, *114* (24), 9656-9657.
29. Wong, A. K.; Jacobsen, M. P.; Winzor, D. J.; Fairlie, D. P. *J. Am. Chem. Soc.* **1998**, *120* (16), 3836-3841.
30. Shogren-Knaak, M. A.; Alaimo, P. J.; Shokat, K. M. *Annu. Rev. Cell Dev. Biol.* **2001**, *17* (1), 405-433.
31. Karle, I. L.; Flippen-Anderson, J. L.; Uma, K.; Balaram, P. *Biopolymers* **1993**, *33* (5), 827-837.
32. Tuchscherer, G.; Dömer, B.; Sila, U.; Kamber, B.; Mutter, M. *Tetrahedron* **1993**, *49* (17), 3559-3575.
33. Mutter, M. *Trends Biochem. Sci* **1988**, *13* (7), 260-265.
34. Floegel, R.; Mutter, M. *Biopolymers* **1992**, *32* (10), 1283-1310.
35. Mutter, M. *Angew. Chem. Int. Ed. Engl.* **1985**, *24* (8), 639-653.
36. Haehnel, W. *Molec. Divers.* **2004**, *8* (3), 219-229.
37. Tofteng, A. P.; Hansen, T. H.; Brask, J.; Nielsen, J.; Thulstrup, P. W.; Jensen, K. *J. Org. Biomol. Chem* **2007**, *5* (14), 2225-2233.
38. Khew, S. T.; Tong, Y. W. *Biochem.* **2008**, *47* (2), 585-596.

39. Sasaki, T.; Kaiser, E. T. *J. Am. Chem. Soc.* **1989**, *111* (1), 380-381.
40. Gibb, B. C.; Mezo, A. R.; Sherman, J. C. *Tetrahedron Lett.* **1995**, *36* (42), 7587-7590.
41. Mezo, A. R.; Sherman, J. C. *J. Am. Chem. Soc.* **1999**, *121* (39), 8983-8994.
42. Freeman, J. O.; Lee, W. C.; Murphy, M. E.; Sherman, J. C. *J. Am. Chem. Soc.* **2009**, *131* (21), 7421-7429.
43. Kuo, S.-W.; Lee, H.-F.; Huang, W.-J.; Jeong, K.-U.; Chang, F.-C. *Macromolecules* **2009**, *42* (5), 1619-1626.
44. Haldar, U.; Pan, A.; Mukherjee, I.; De, P. *Polym. Chem.* **2016**, *7* (40), 6231-6240.
45. Haldar, U.; Saha, B.; Azmeera, V.; De, P. *Polym. Sci., Part A: Polym. Chem.* **2016**, *54* (22), 3643-3651.
46. Fabritz, S.; Heyl, D.; Bagutski, V.; Empting, M.; Rikowski, E.; Frauendorf, H.; Balog, I.; Fessner, W.-D.; Schneider, J. J.; Avrutina, O. *Org. Biomol. Chem* **2010**, *8* (9), 2212-2218.
47. Cram, D. J.; Karbach, S.; Kim, H. E.; Knobler, C. B.; Maverick, E. F.; Ericson, J. L.; Helgeson, R. C. *J. Am. Chem. Soc.* **1988**, *110* (7), 2229-2237.
48. Karle, I. L.; Flippen-Anderson, J. L.; Uma, K.; Balaram, P. *Proteins: Struct., Funct., Bioinf.* **1990**, *7* (1), 62-73.
49. Ling, R.; Yoshida, M.; Mariano, P. S. *J. Org. Chem.* **1996**, *61* (13), 4439-4449.
50. Banerjee, A.; Datta, S.; Pramanik, A.; Shamala, N.; Balaram, P. *J. Am. Chem. Soc.* **1996**, *118* (40), 9477-9483.
51. Jedhe, G. S.; Vijayadas, K. N.; Kotmale, A. S.; Sangtani, E.; Shinde, D. R.; Gonnade, R. G.; Rajamohanan, P. R.; Sanjayan, G. J. *RSC Adv.* **2016**, *6* (42), 35328-35331.
52. Kale, S. S.; Priya, G.; Kotmale, A. S.; Gawade, R. L.; Puranik, V. G.; Rajamohanan, P.; Sanjayan, G. J. *Chem. Commun.* **2013**, *49* (22), 2222-2224.

# ***Chapter 4***

## ***Effect of Gem-Dimethyl Groups in the Formation of Imine-Based Macrocycles and Cages***



## Chapter-4

### Effect of Gem-Dimethyl Groups in the Formation of Imine-Based Macrocycles and Cages

#### 4.1 Introduction: Imine-based macrocycles:

Imine bonds are one of the best linkages for the construction of large and robust organic architectures owing to their dynamic nature. Imine-based macrocycles have shown exceptional versatility in supramolecular chemistry.<sup>1-2</sup> They are among the first synthetic macrocyclic complexes to be synthesized. Further, Schiff base-linked macrocycles have displayed important role in the development of artificial macrocyclic chemistry (Fig. 4.01). Imine bond formation was first discovered in 1864 by Hugo Schiff, through the condensation of primary amines with carbonyl compounds.<sup>3</sup> Since early 1980's, imine-based macrocycles have attracted immense attention of supramolecular chemists.

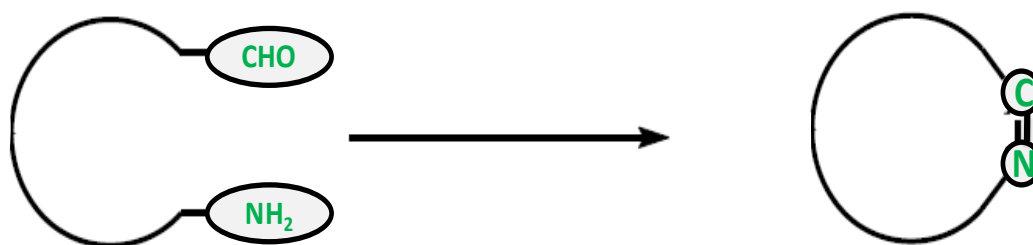


**Fig. 4.01:** Reaction of aldehyde and amine forming imine-based macrocycle.

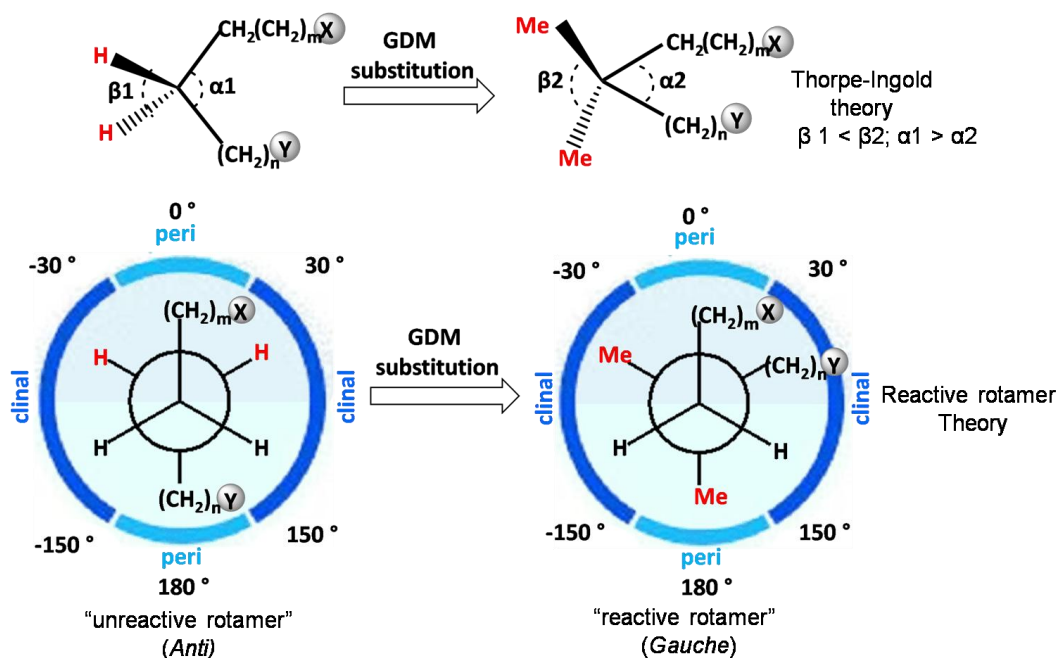
#### 4.1.1 Requirements of novel-strategies for the synthesis of imine-based organic macrocycles.

Currently, imine-based macrocycles and cages are considered as important classes of compounds owing to their fascinating structural architectures and properties. Hence, they find utility in numerous applications such as shape-selective chromatography phases,<sup>4-5</sup> gas adsorption/storage,<sup>6-8</sup> proton conductivity,<sup>9</sup> materials for molecular/ion sensing<sup>10-11</sup> and separation of sulfur hexafluorides.<sup>12</sup> In all the above-mentioned studies, the macrocyclic molecules were often prepared by the conventional method wherein precursors like acyclic, cyclic, vicinal, and rigid aromatic primary amines were reacted under high dilution conditions to avoid the presence of oligomeric side products.<sup>13</sup> It was

also shown that the properties of macrocycles could be tuned by ideal design strategies in choosing the building blocks. Cooper *et al.* (2015) reported first porous cages having liquid nature by utilizing crown-ether substituted vicinal cyclic amine precursors as an amine counterpart.<sup>14-15</sup> Lisowski *et al.* (2016) showed a direct synthesis of organic keto-enamine cages by ideal selection of aldehyde-synthon<sup>16</sup> and their similar types of cages have been shown to exhibit stability under acidic and basic conditions (2017).<sup>17</sup> Hence, robust strategies involving ideal building blocks would be always welcome to the synthesis of imine-based macrocycles.

#### 4.2 Gem-dimethyl effect and its advantages in macrocyclization chemistry.

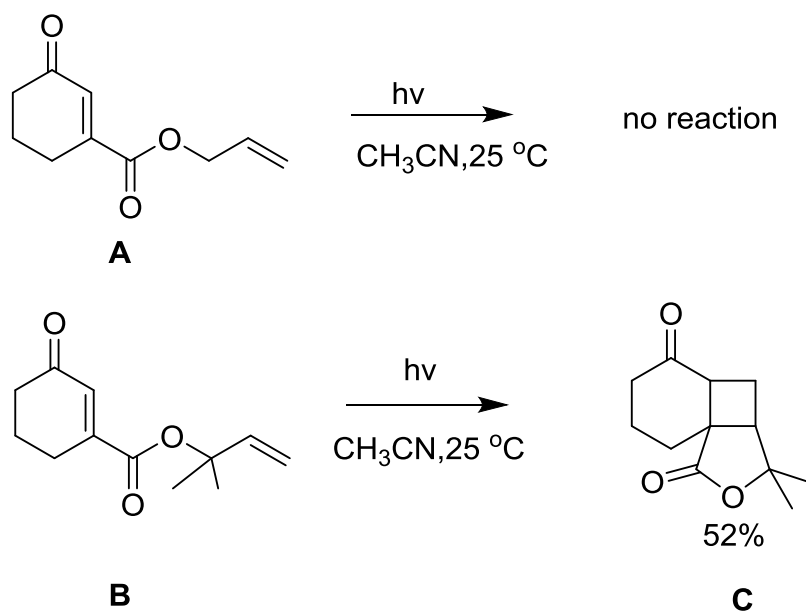
It has generally been observed that substitution of hydrogen atoms with methyl groups on the carbon connecting two reacting centers X and Y facilitates cyclization (*gem*-dimethyl effect or GDM effect). Several theories have been proposed to explain the effect of *gem*-dimethyl group on the acceleration of cyclization reactions, out of which Thorpe-Ingold and reactive rotamer theories are well-accepted. (Fig. 4.02).<sup>18</sup> According to Thorpe-Ingold theory, the presence of *gem*-dimethyl group reduces the internal angle ' $\alpha$ ' due to increase in the bond angle ' $\beta$ ' by mutual repulsion of methyl groups, thus facilitating the reactive end groups to come close by.<sup>19-20</sup> According to reactive rotamer theory, it is postulated that *gem*-dimethyl group increases the relative population of *gauche* conformation reactive rotamers and causes an increase in the ground state energy of the system, thereby facilitating the reactivity.<sup>21</sup>



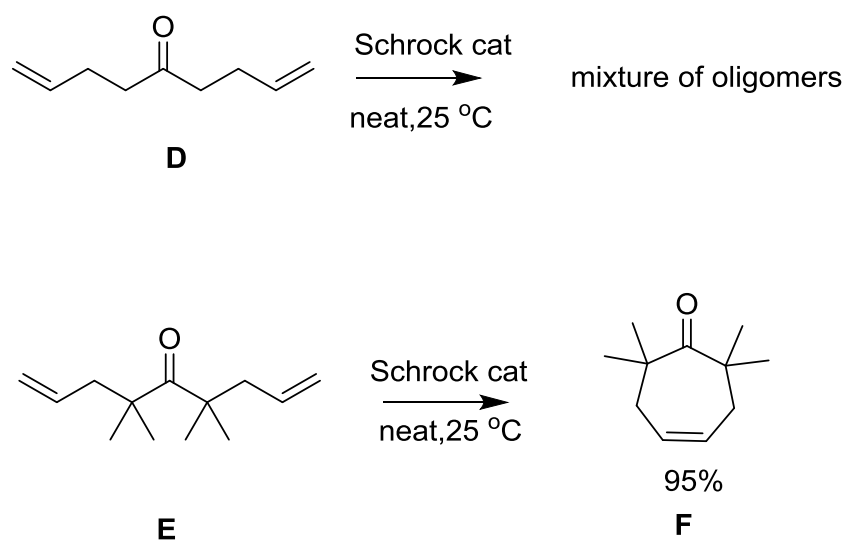
**Fig. 4.02:** Schematic representation of *gem*-dimethyl (GDM) effect explained by Thorpe-Ingold (top) and reactive rotameric (bottom) theories on cyclization reactions. *Note:* X and Y are reactive end groups.

Thus, the *gem*-dimethyl group substitution plays a noticeable influence in the construction of covalent and non-covalent cyclic architectures through inter/intramolecular cyclization reactions. For instance, Meijer *et al.* showed non-covalent macrocycle formation using the *gem*-dimethyl effect in a quadruple hydrogen bonding system.<sup>22</sup> Pete *et al.* photo-chemically studied the effect of *gem*-dimethyl groups on the chain of allyl ester **A**, wherein, they have found that the ester containing *gem*-dimethyl group **B** showed photochemical cyclisation with 85% yield and no cyclisation was found in **A** (without *gem*-dimethyl group) (Fig. 4.03).<sup>23</sup> Forbes *et al.* have reported ring closer olefin metathesis reaction in the absence of solvent with 95% yield using *gem*-dimethyl effect as a platform.<sup>24</sup> Further, they have compared ring closing metathesis of olefins in the absence of GDM as in **D** and presence of GDM as in **E**. The results have shown formation of oligomers in the absence of GDM (Fig. 4.04). It was noted that this ring closer metathesis reaction was reversible.



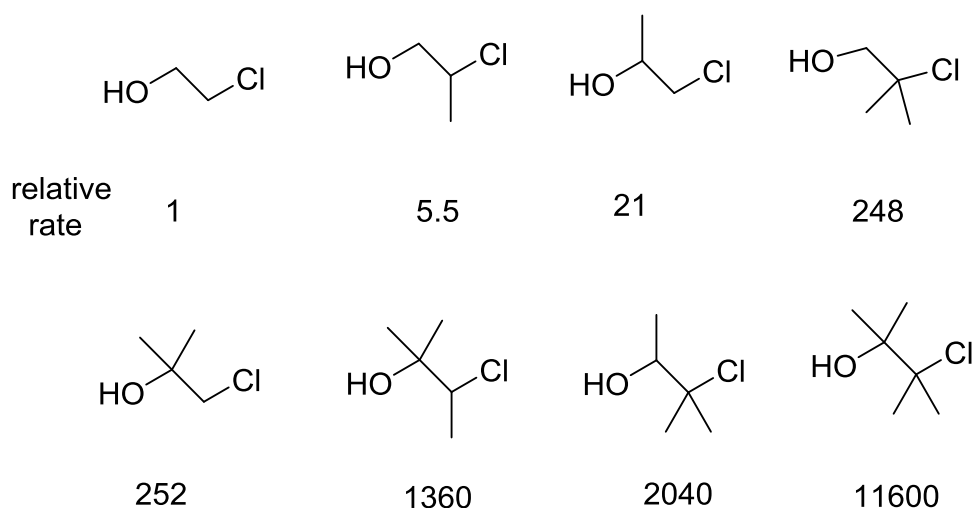


**Fig. 4.03:** Photochemical reaction of allyl esters with and without *gem*-dimethyl group.



**Fig. 4.04:** Olefin ring closing metathesis reactions of olefins with and without *gem*-dimethyl group.

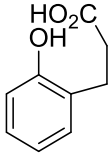
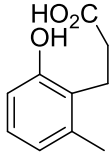
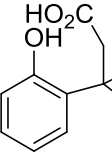
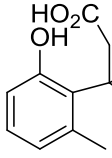
Nilsson *et al.* studied the effect of methyl groups in cyclization reactions of chlorohydrins, wherein they have found an increment of one Me group in the backbone increased the rate of reaction approximately five times. Similarly, an increase of reaction rate was observed for two Me groups 10 times, three Me groups 100 times and 4 Me groups 10000 times (Fig. 4.05).<sup>25</sup>



**Fig. 4.05:** Effect of methyl groups in rate of cyclization reactions of chlorohydrins.

Further, Cohen and Milstien studied the rate and equilibrium constants for the lactonization of various substituted hydrocoumarinic acids. Analysis of the kinetic data showed that the addition of a *gem*-dimethyl group on the carbon chain (**J**) resulted in a remarkable rate enhancement ( $>10^{10}$ ) than its parent acid (**G**) (Table 4.1).<sup>26-27</sup>



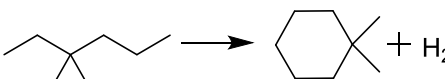
**Table. 4.1:** Rate and equilibrium constants for the lactonization of various methyl substituted hydrocoumarinic acids.

Various substituted hydrocoumarinic acids				
	<b>G</b>	<b>H</b>	<b>I</b>	<b>J</b>
$K_{H_3O^+}$ (mole <sup>-1</sup> s <sup>-1</sup> )	$5.9 \times 10^{-6}$	$5.9 \times 10^{-6}$	$2.6 \times 10^{-2}$	$3.0 \times 10^5$
$K_{rel}$	1	1	4400	$5.1 \times 10^{10}$
$K_{eq}$	0.0373	0.621	25.67	>99

Allinger and Zalkow in 1960 reported the first quantitative analysis of the thermodynamic factors of *gem*-dimethyl effect.<sup>28-29</sup> Owing to the substitution of methylene hydrogens with methyl groups, the equilibrium constants for the formation of the cyclohexanes were

improved by  $10^2$ - $10^3$  (Table 4.2). This marked effect of alkyl substituents is due to more favorable values of either enthalpy or entropy or both.

**Table 4.2:** Calculated equilibrium constants ( $K_{eq}$ ) and thermodynamic ( $\Delta G^\circ$ ,  $\Delta H^\circ$ ,  $\Delta S^\circ$ ) data for the cyclization of cyclohexanes from various methyl substituted hexanes at 25 °C.

	$\Delta G^\circ$ (kcal mole <sup>-1</sup> )	$\Delta H^\circ$ (kcal mole <sup>-1</sup> )	$\Delta S^\circ$ (cal °K <sup>-1</sup> )	$K_{eq}$
	7.65	10.53	9.66	$2.40 \times 10^{-7}$
	5.86	10.45	15.39	$4.96 \times 10^{-5}$
	5.23	9.35	13.85	$1.44 \times 10^{-4}$

*Gem*-dimethyl group substitution effect has seen profound utility in peptide science as well. For instance,  $\alpha$ -aminoisobutyric acid (Aib), a *gem*-dimethyl group-containing unnatural amino acid, is extensively used for the conformational rigidification of polypeptide chains.<sup>30-33</sup>

Further, the existence of the *gem*-dimethyl group is known to play a vital role in the stability of natural products such as terpenoids and many other cyclic systems.<sup>21, 34-36</sup> For instance, Bruice *et al.* observed the reduction in the rate of anhydride hydrolysis upon the substitution of *gem*-dimethyl group.<sup>21, 37</sup> Jung *et al.* studied the intramolecular Diels-Alder cycloaddition of 2-furfuryl methyl fumarates (Fig. 4.06).<sup>38</sup> The authors have designed a system that contain *gem*-dialkyl substitution and compared it with the cyclisation ability of the unsubstituted system. The results of the intramolecular Diels-Alder cycloaddition of the precursors **K-O** are summarized in Table 4.3. It is unambiguous that *gem*-dialkyl substitution on the tethering chain produced an enhancement of the rate of cyclization.

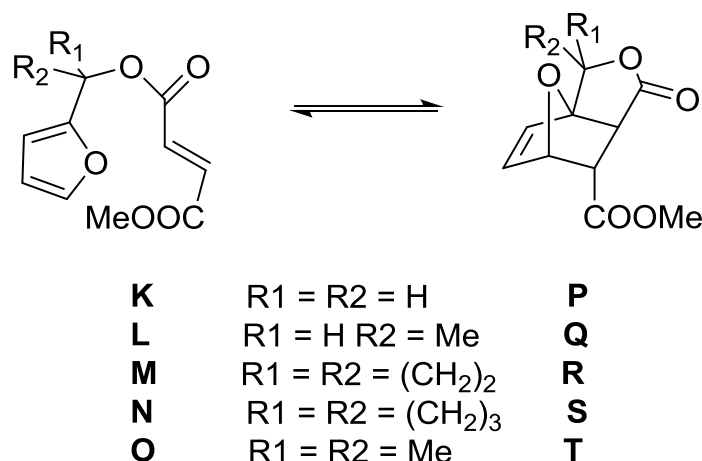


**Fig. 4.06:** Intramolecular Diels-Alder cycloaddition of various methyl substituted 2-furfuryl fumarates.

**Table. 4.3:** Kinetic parameters for the intramolecular Diels-Alder of the furfuryl fumarates **K-O** at 298 K in CD<sub>3</sub>CN.

Compound	$k_{298}$ (s <sup>-1</sup> )	$k_{rel}$	$E_{act}$ (kcal/mol)	$\Delta H^{\#}_{298}$ (kcal/mol)	$\Delta S^{\#}_{298}$ (cal/mol.deg)	$\Delta G^{\#}_{298}$ (kcal/mol)
<b>K</b>	$1.94 \times 10^{-7}$	1	20.5	19.8	-22.7	26.6
<b>L</b>	$1.62 \times 10^{-6}$	8.35	19.1	18.4	-23.2	25.3
<b>M</b>	$2.03 \times 10^{-6}$	10.5	17.9	17.3	-26.6	25.2
<b>N</b>	$4.03 \times 10^{-5}$	208	16.9	16.3	-23.9	23.4
<b>O</b>	$4.12 \times 10^{-4}$	2123	15.5	14.9	-24.0	22.1

Gellman *et al.* found that the nickel (II) was binding more effectively with *gem*-dimethyl substituted tetrathioether **W** than its unsubstituted analogue **U**, which clearly explained the profound effect of *gem*-dimethyl groups on the conformational preference of macrocyclic- backbone (Fig. 4.07).<sup>39</sup>

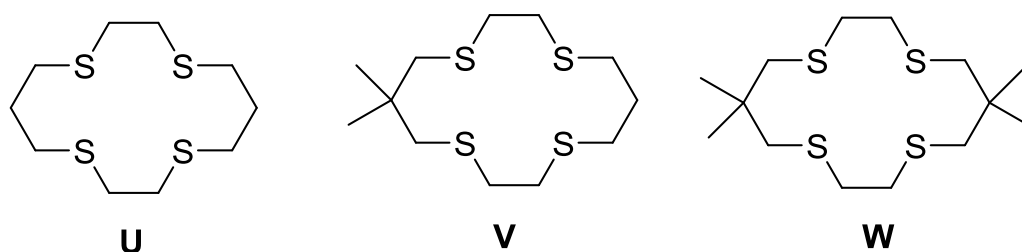


**Fig. 4.07:** Unsubstituted (U) and *gem*-dimethyl substituted tetrathioethers V and W which are used for nickel binding.

### 4.3 Objective of our present work

Considering all these aforementioned requirements of novel strategies to the synthesis of imine-based macrocycles and advantages of the presence of the *gem*-dimethyl group in cyclization reactions, we envisaged that the use of *gem*-dimethyl groups could increase the rate of imine-based macrocyclisation drastically (Fig. 4.08). Further, we anticipated that the *gem*-dimethyl group containing macrocycle/cages can have good thermal as well as chemical stabilities which are very much required for the material applications of macrocycles.

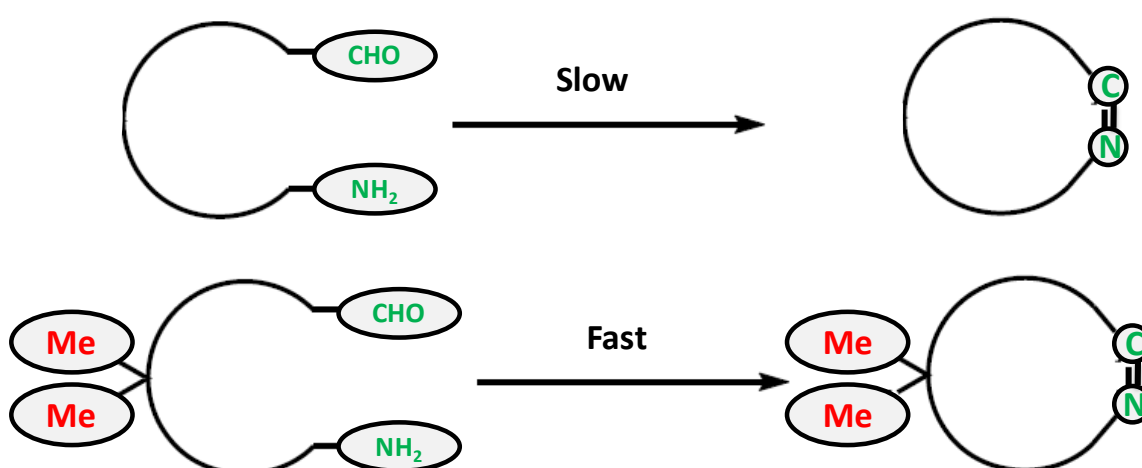
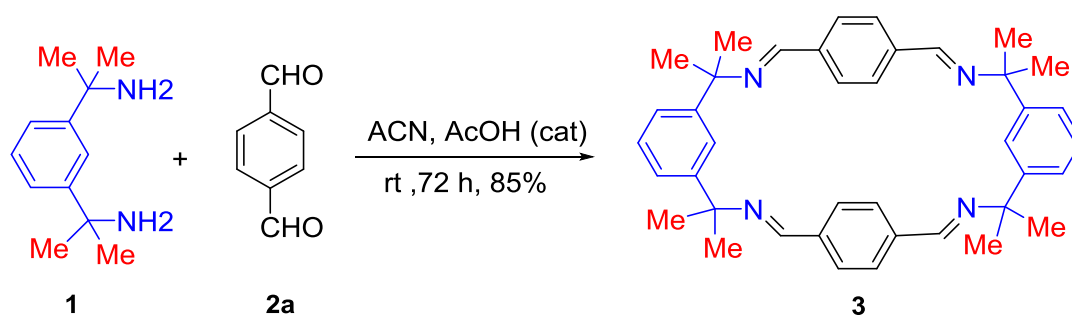


**Fig. 4.08:** Schematic representation of unsubstituted and *gem*-dimethyl substituted imine-based macrocycle formation.

## 4.4 Synthesis, results and discussion

### 4.4.1 Synthesis and characterization of [2+2] macrocycles using *gem*-dimethyl effect.

Commercially available/readily obtainable primary amines containing *gem*-dimethyl groups and aromatic aldehydes were chosen for macrocyclization. Relying on this concept, we first mixed *gem*-substituted *m*-xylylenediamine **1** and terephthalaldehyde **2a** in 1:1 ratio in acetonitrile (ACN) containing catalytic amount (20  $\mu$ l) of acetic acid, at ambient condition (Scheme 4.01).



**Scheme 4.01** Synthesis of [2+2] macrocycles using *gem*-dimethyl effect as a platform. The reaction of *gem*-dimethyl-substituted amine **1** with terephthalaldehyde **2a**, forming macrocycle **3**.

Over time, needle-shaped crystals were formed, in nearly quantitative yield, in the reaction vessel. These crystals were completely soluble in  $\text{CHCl}_3$  and were spectroscopically well characterized. Mass spectrometry showed  $[\mathbf{3} + \text{H}]^+$  ion peak at  $m/z = 581.3627$ , in agreement with a [2+2] cyclic structure composed of two units of **1** and two units of **2a** with the formula  $\text{C}_{40}\text{H}_{44}\text{N}_4$ . Single crystal X-ray diffraction analysis revealed that **3** crystallized in the monoclinic,  $P2_1/c$  space group. As depicted in Fig. 4.09, the approximate length and breadth of the macrocycles are 10.1 Å and 3.8 Å, respectively. Macrocycle **3** could be readily prepared in solvents like DCM and  $\text{CHCl}_3$  wherein, all the dynamic combinatorial libraries (DCL) of this system are soluble.

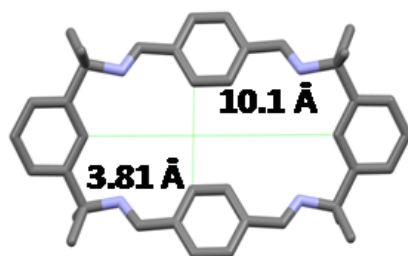
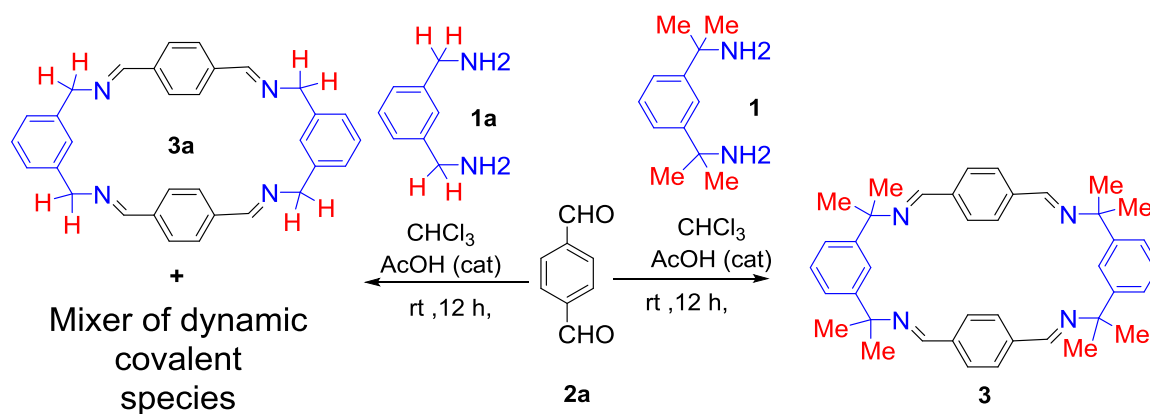


**Fig. 4.09:** X-ray crystal structure of [2+2] macrocycle **3** showing the length and breadth of the macrocycle to be 10.1 Å and 3.81 Å, respectively.

In order to demonstrate the role of *gem*-dimethyl effect in the imine-based macrocyclization, the *gem*-dimethyl substituted amine **1** and its corresponding unsubstituted amine analog **1a** were reacted separately with aldehyde **2a** (1 M concentration) in  $\text{CHCl}_3$  at ambient conditions (Scheme 4.02).



**Scheme 4.02** Comparison of macrocyclization with *gem*-dimethyl groups (**1**) and without *gem*-dimethyl groups (**1a**) in the amines with dialdehyde **2a** at high concentrations.

After 12 h,  $^1\text{H-NMR}$  was recorded for both the reaction mixtures. The results revealed the presence of macrocycle **3** exclusively in the reaction of **1** with **2a**, and a mixture of dynamic covalent species in the reaction of **1a** with **2a** (Fig. 4.10 & 4.11). In addition, macrocycle **3a** was prepared under reported high dilution procedure ( $2 \times 10^{-2} \text{ M}$ )<sup>40</sup>, and its  $^1\text{H-NMR}$  was compared with the DCL of high concentration reaction performed for macrocyclization of **3a** which suggested the presence of relatively less amount of **3a** in the DCL (Fig. 4.12 & 4.13).

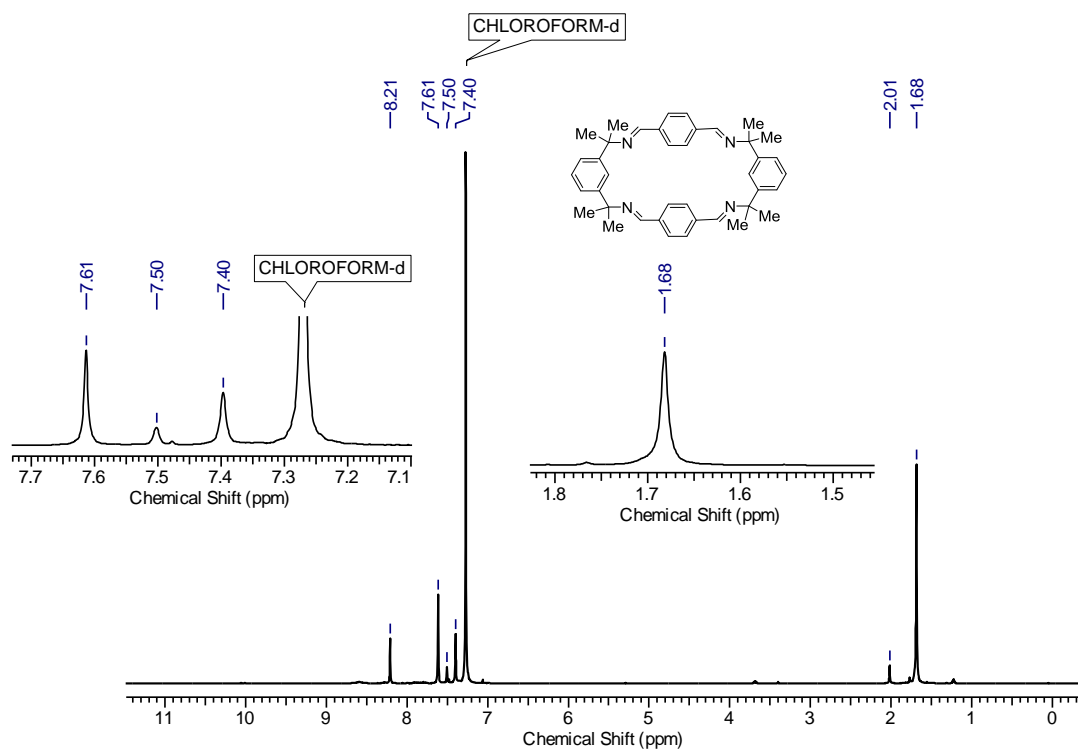


**Fig. 4.10:**  $^1\text{H}$  NMR spectrum recorded for direct reaction mixture of macrocyclization of **3** performed at 1 M concentration (in  $\text{CHCl}_3$ ) shows the presence of almost only, [2+2] macrocycle-**3**. *Note:* The peak at  $\delta=2.01$  corresponds to  $\text{CH}_3\text{COOH}$ .

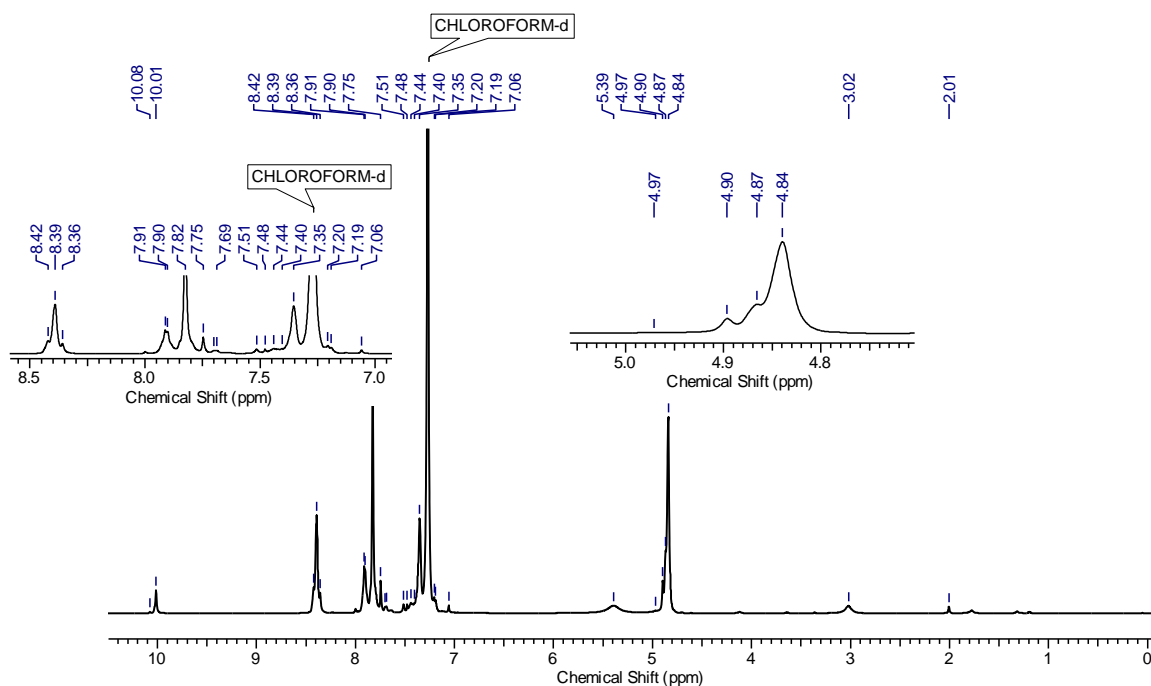


**Fig. 4.11:**  $^1\text{H}$  NMR spectrum of the direct reaction mixture of macrocycle-**3a** formation performed at 1 M concentrations (in  $\text{CHCl}_3$ ) shows the presence of various dynamic combinatorial libraries (DCL). *Note:* The peak at  $\delta=2.01$  corresponds to  $\text{CH}_3\text{COOH}$ .



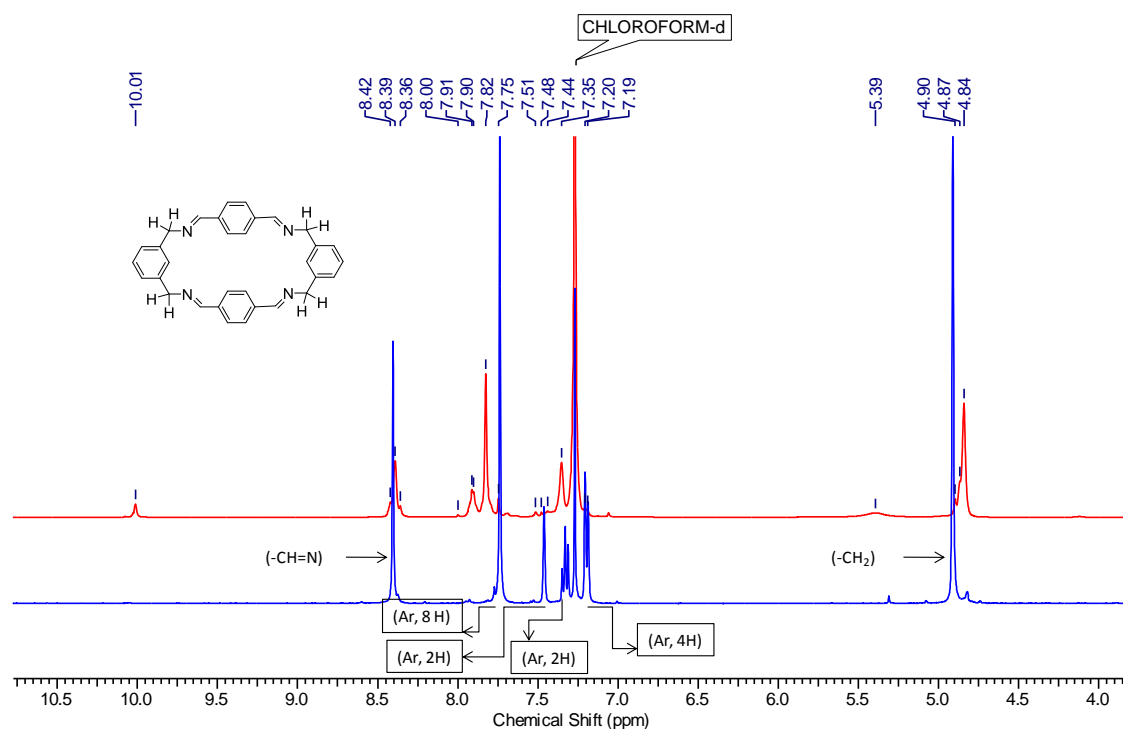


**Fig. 4.12:**  $^1\text{H}$  NMR spectrum comparison of pure macrocycle-**3a** (prepared under high dilution method) and the direct reaction mixture of macrocyclization performed for **3a** at 1 M concentration.

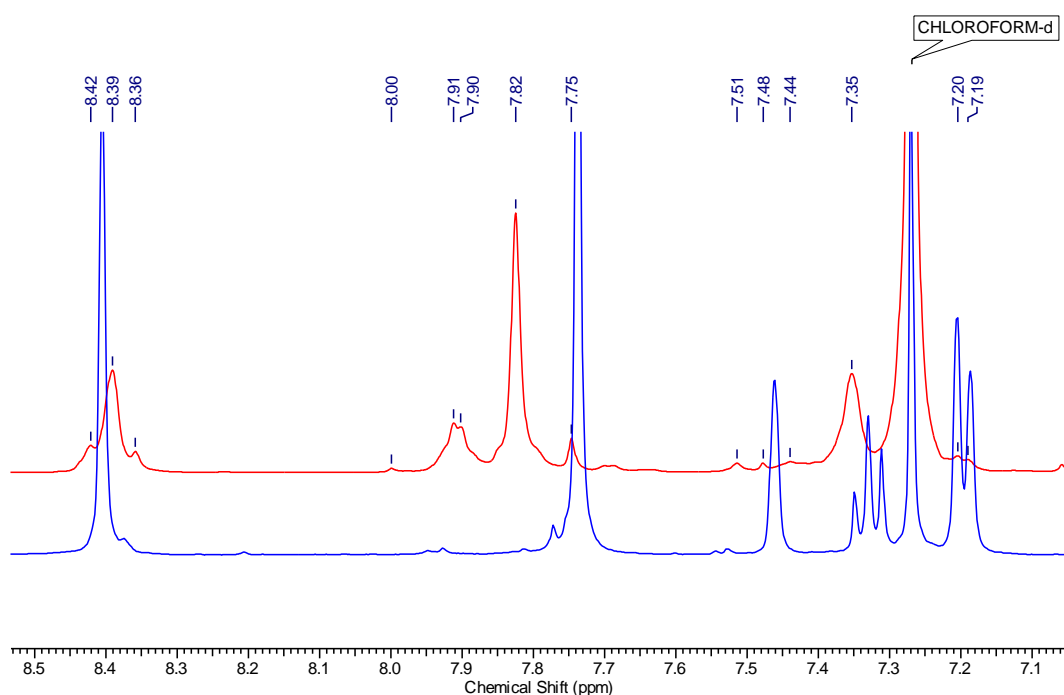


**Fig. 4.13:**  $^1\text{H}$  NMR spectrum comparison of pure macrocycle-**3a** (prepared under high dilution method) and the direct reaction mixture of macrocyclization performed for **3a** at 1 M. concentration (aromatic region expanded).

Similar observation was found in 0.09 M concentration as well. To a 20 mL glass vial, a solution of **2a** (0.049 g, 0.367 mmol in 4 mL  $\text{CHCl}_3$ ) was added instantly to **1a** (0.05 g, 0.367 mmol) without stirring at room temperature. While doing addition, immediate precipitate was observed (Fig. 4.14). After complete addition of **1a**, a catalytic amount of acetic acid (10  $\mu\text{L}$ ) was added (amount of precipitate rapidly increased) and the reaction mixture was kept undisturbed at room temperature for a week. Then, the reaction mixture with precipitate was evaporated under vacuum to obtain the residue and it was washed with diethyl ether for a couple of times to get a clear solid. Further, the material was characterized by IR, NMR, MALDI-MS.  $^1\text{H}$  NMR of pure macrocycle **3a** was compared with that of 1 M experiment; the result revealed the amount of macrocycle-**3a** was relatively better than 1 M case (Fig. 4.17).  $^1\text{H}$  NMR of the DMSO-*d*<sub>6</sub> soluble part of the substance was recorded and it showed clearly distinct oligomeric peaks (Fig. 4.16). Further, the presence of IR bands at 1702(C=O) and 1645(CH=N)  $\text{cm}^{-1}$  supported the existence of oligomers in the **3a** case (Fig. 4.15). MALDI-MS showed many peaks with a characteristic of various oligomers (Fig. 4.18).

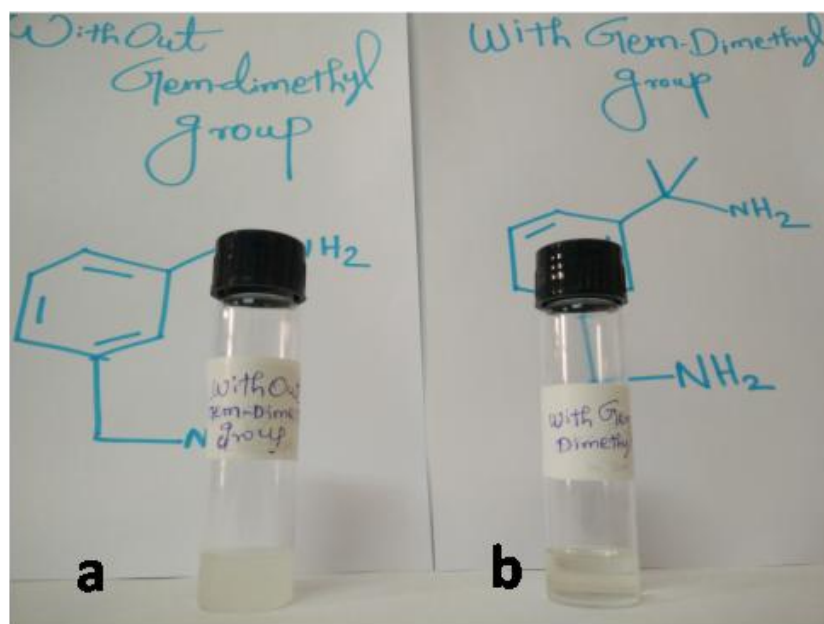


**Fig. 4.14:** Comparison of imine-based macrocyclization with and without *gem*-dimethyl groups (**1** and **1a** respectively) in the amine at 0.09 M concentration. After instant mixing of amines **1a** and **1** with dialdehyde **2a**, separately; a) instantly formed precipitate in macrocyclization of **3a**; b) clear solution formed in macrocyclization of **3**.

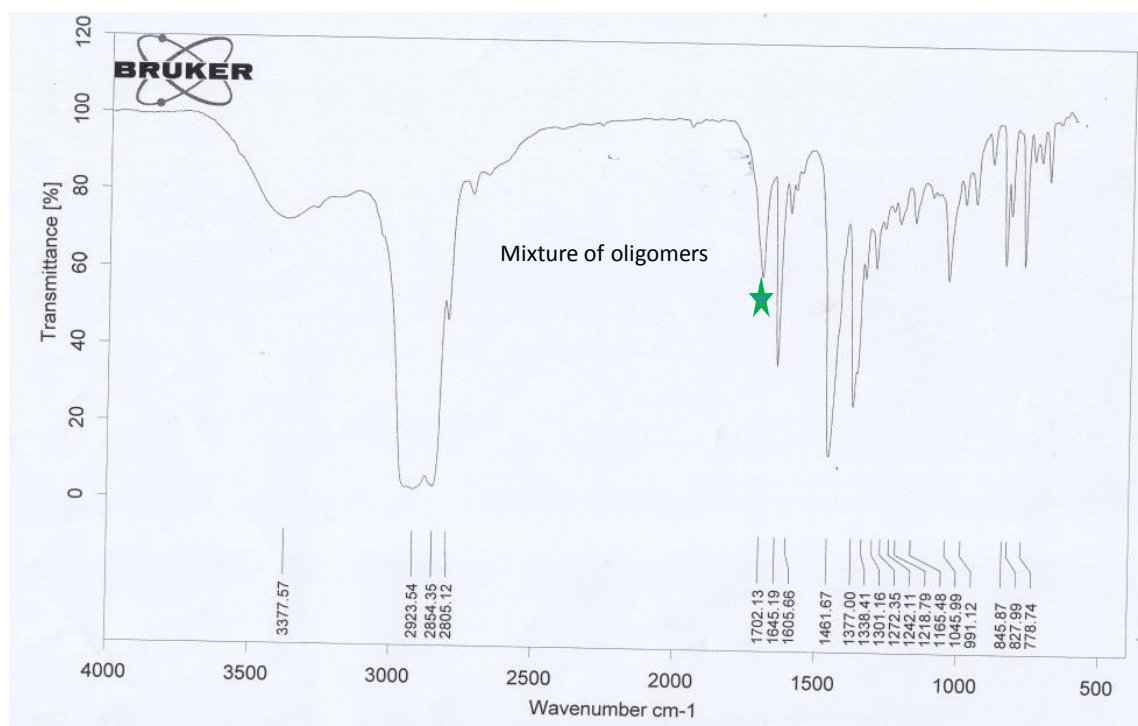


**Fig. 4.15:** IR spectrum of imine-based macrocyclization (at 0.09 M concentration) performed for **3a**.

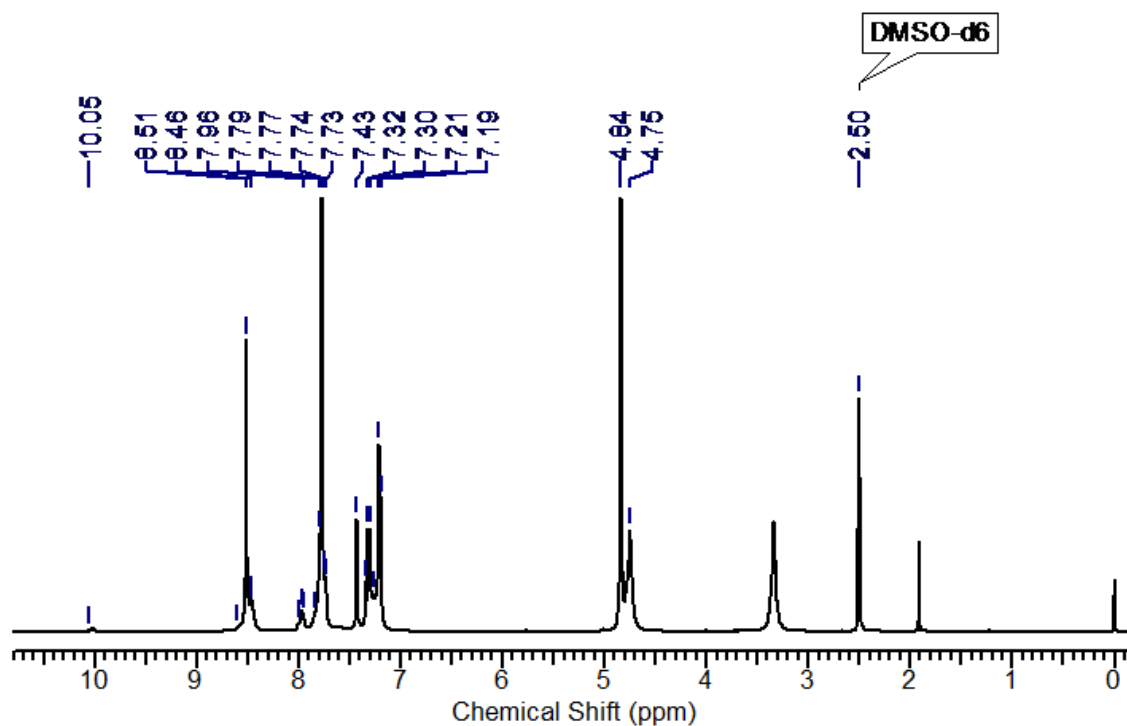


**Fig. 4.16:** <sup>1</sup>H NMR spectrum of imine-based macrocyclization performed for **3a** (at 0.09 M concentration) shows various DCL (DMSO-*d*<sup>6</sup>, 400 MHz, 298 K).

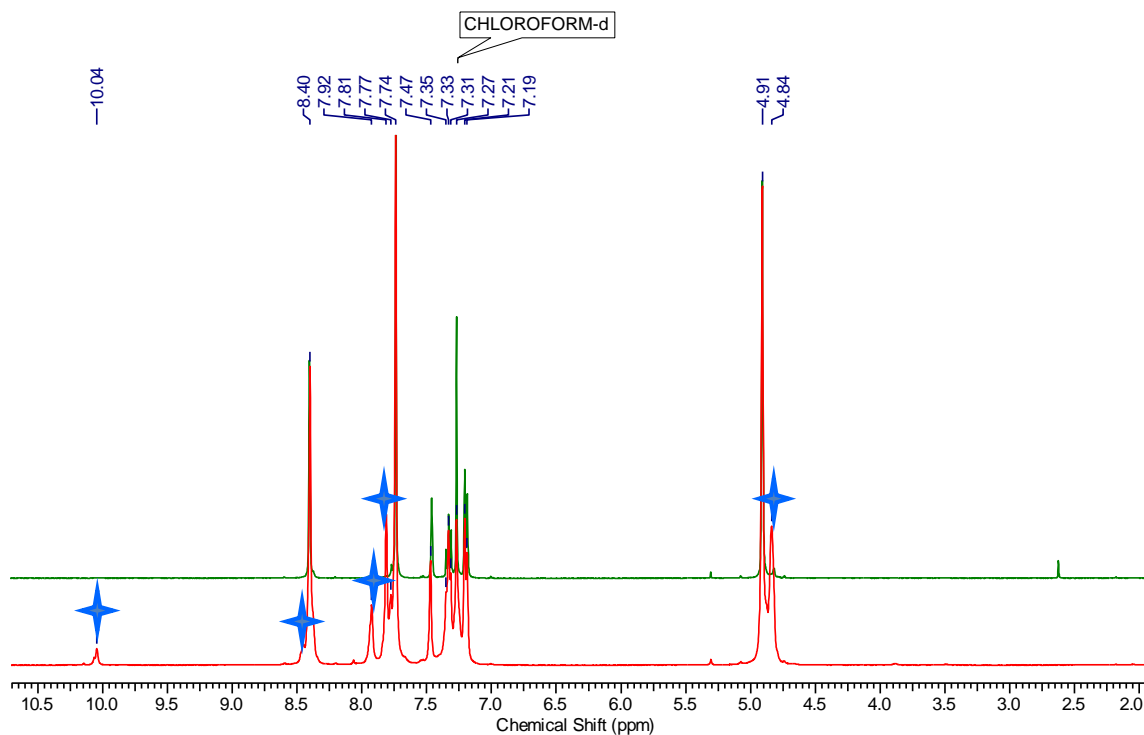


**Fig. 4.17:** Comparison of  $^1\text{H}$  NMR spectrum of imine-based macrocyclization performed for **3a** at 0.09 M (red) and pure-**3a** synthesized under high dilution (green) (additional peaks are indicated in blue stars which correspond to other DCL).

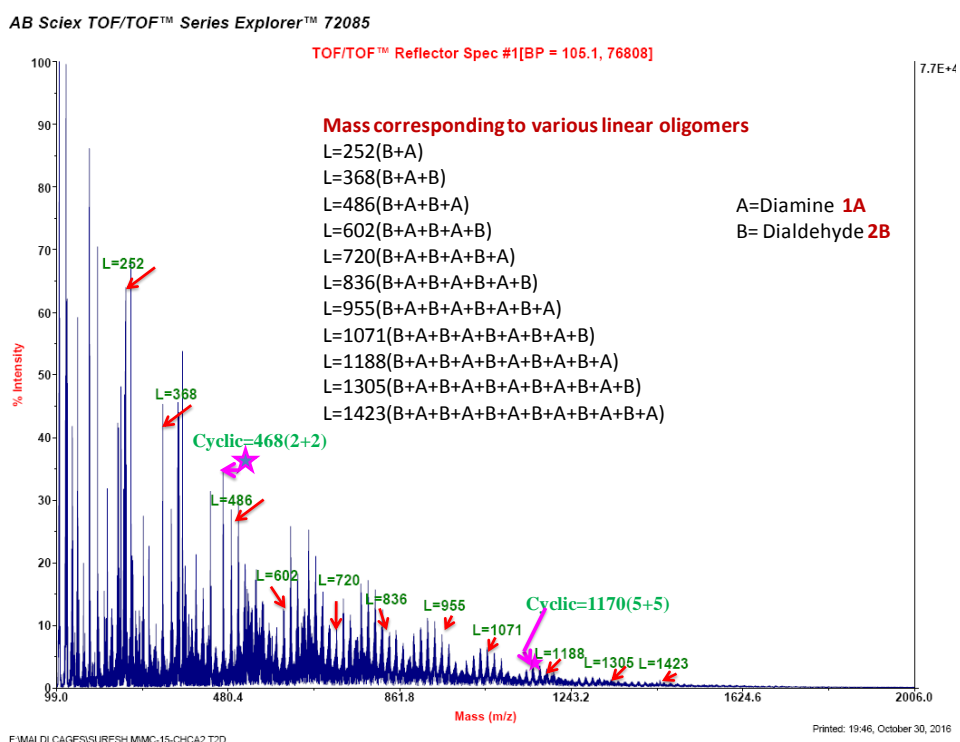
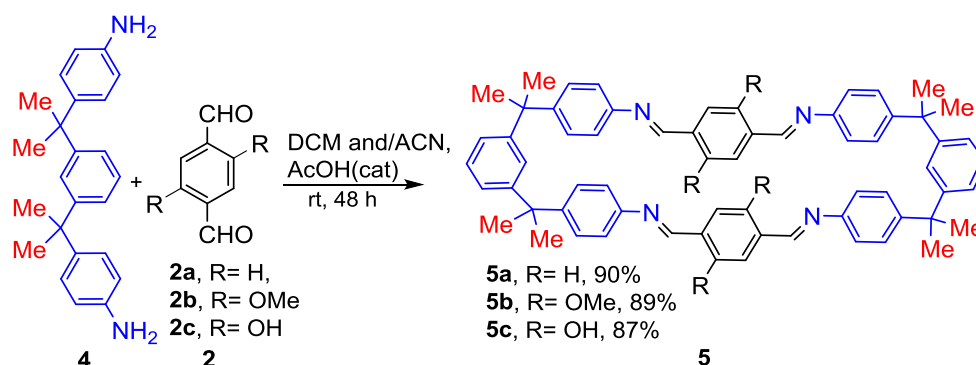


**Fig. 4.18:** MALDI-MS of mixture of oligomers found in imine-based macrocyclization (at 0.09 M concentration) performed for **3a**.

#### 4.4.2 Synthesis and characterization of elongated macrocycles using *gem*-dimethyl effect.

Encouraged with this finding, we next moved to investigate the possibility of macrocyclization using the elongated *gem*-dimethyl substituted amine **4** with the dialdehyde **2a**, under ambient condition in dichloromethane (Scheme 4.03), wherein the initially formed clear solution was concentrated after 48 h *in vacuo* and then the residue obtained was recrystallized from *o*-dichlorobenzene to afford crystalline macrocycle **5a** in 90% yield.



**Scheme 4.03** Synthesis of [2+2] macrocycles using *gem*-dimethyl effect as a platform. The reaction of *gem*-dimethyl-substituted amine **4** with terephthalaldehyde **2a-c**, forming macrocycles **5a-c**.

**5a** was characterized by IR and  $^1\text{H}$  NMR and  $^{13}\text{C}$  NMR spectroscopy. Mass spectrometry (MALDI-MS) showed  $[\mathbf{5a} + \text{H}]^+$  ion peak at  $m/z = 885.7652$ , consistent with a [2+2] macrocycle structure composed of two units of **4** and two units of **2a** with a formula  $\text{C}_{64}\text{H}_{60}\text{N}_4$ . Single crystal X-ray diffraction analysis showed that **5a** crystallized in the  $P2_1/c$  monoclinic space group. The approximate length and breadth of the macrocycle are 18.8 Å and 3.7 Å, respectively (Fig. 4.19). The centroid...centroid distance between the two central benzene rings is 3.7 Å, which is typical for parallel displaced  $\pi$ - $\pi$  stacking.

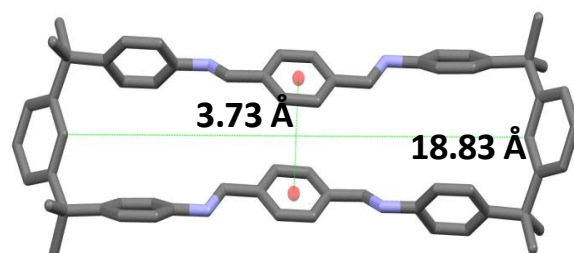


**Fig. 4.19:** a) X-ray crystal structure of phenyl ring extended [2+2] macrocycle **5a** showing the length and breadth of the macrocycle to be 18.83 Å and 3.73 Å, respectively.

The presence of a large number of intermolecular C-H $\cdots$  $\pi$  and  $\pi\cdots\pi$  interactions (Fig. 4.20) may presumably be the reason for the poor solubility of the substance in common organic solvents. Similarly, following above-mentioned reaction conditions, macrocycles **5b** and **5c** were synthesized by the reaction of amine **4** with aldehydes **2b** and **2c**, respectively (Scheme 4.03). In these cases, products were obtained as fiber like needle-shaped crystals (Fig. 4.21) insoluble in most of the common organic solvents.

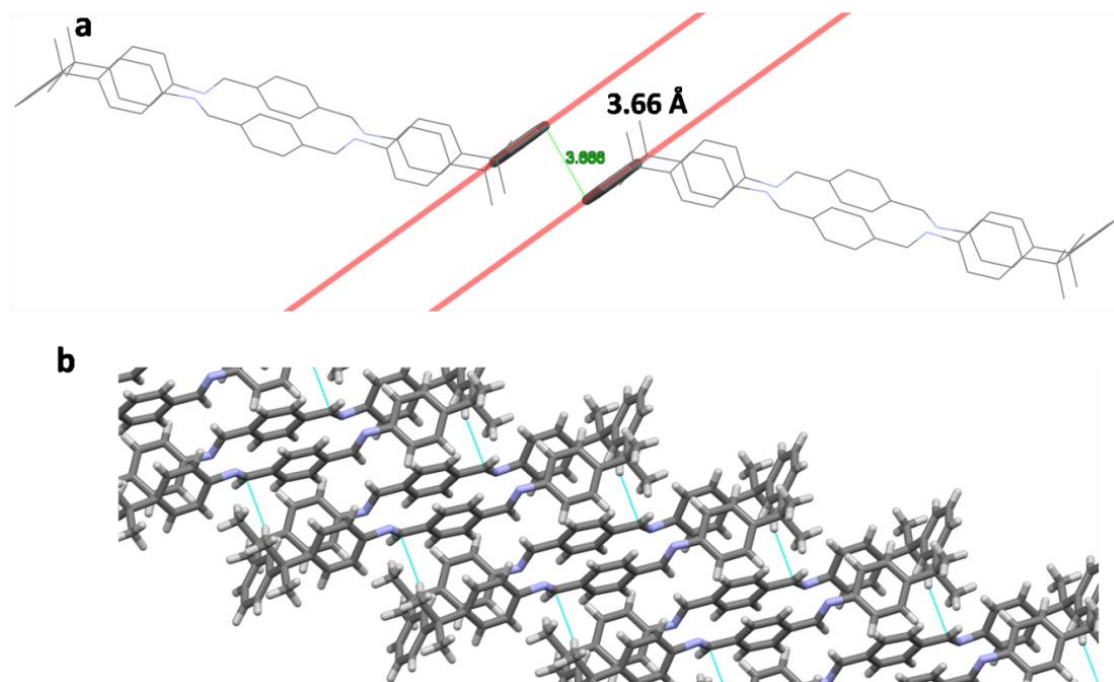


**Fig. 4.20: CH- $\pi$  and  $\pi$ - $\pi$  stacking interaction in the macrocycle-5a.** a) Terminal benzene ring of the macrocycle **5a** showing intermolecular parallel displaced  $\pi$ - $\pi$  stacking with the distance of 3.6 Å. b) X-ray crystal structure of macrocycle-**5a** showing continuous intermolecular CH- $\pi$  interactions. *Note:* The presence of a large number of continuous intermolecular CH- $\pi$  and  $\pi$ - $\pi$  stacking interactions is presumably the reason for the reduced solubility of macrocycle-**5a**.

The formation of [2+2] macrocycles **5b** and **5c** were confirmed by the presence of IR bands at 1624 and 1614  $\text{cm}^{-1}$  and MALDI,  $[\text{M} + \text{H}]^+$  ion peaks at  $m/z = 1005.40$  ( $\text{C}_{68}\text{H}_{68}\text{N}_4\text{O}_4$ ) and 949.34 ( $\text{C}_{64}\text{H}_{60}\text{N}_4\text{O}_4$ ), respectively. Despite several attempts, we could not obtain single crystal structures of **5b** and **5c** due to poor diffraction of the crystals. Powder XRD of these materials clearly suggested that they are highly crystalline (Fig. 4.22).



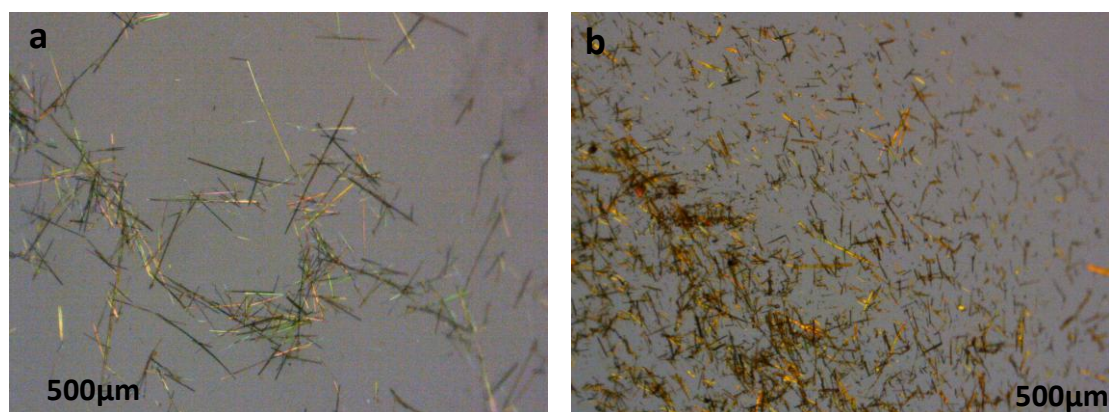


**Fig. 4.21:** a) Yellow colored crystals of macrocycle **5b**; b) Orange colored crystals of macrocycle **5c**.

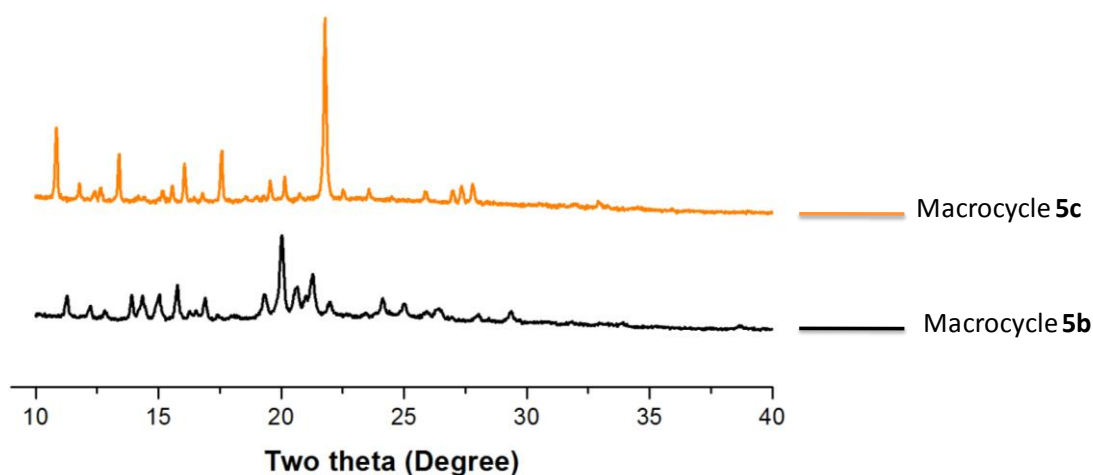
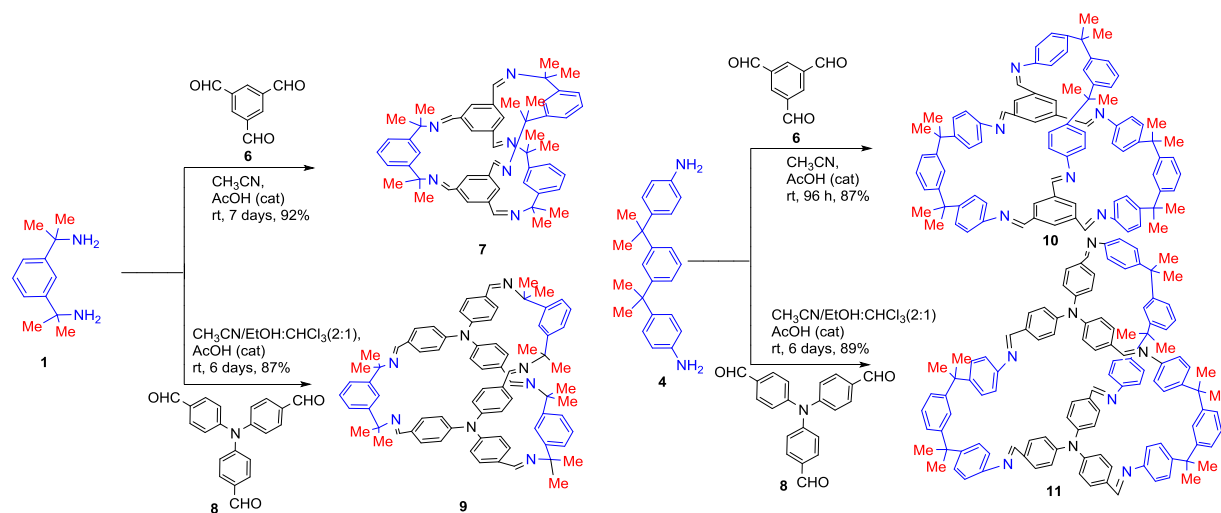


**Fig. 4.22:** Powder X-ray diffraction patterns for macrocycle **5b** (black) and **5c** (orange).

#### 4.4.3 Synthesis and characterization of macrobicycles/cages using *gem*-dimethyl effect.

Afterwards, we explored this strategy for cage formation as shown in Scheme 4.04. The trialdehyde **6** and *gem*-dimethyl-substituted diamine **1** were reacted in ACN at ambient conditions. The clear solution formed initially was preserved without disturbance at room temperature for **7** days to get colorless, block-shaped crystals of cage **7** in excellent yield. The successful formation of imine bond was justified by the presence of IR absorption band observed at  $1651\text{ cm}^{-1}$ . The material was readily soluble in chloroform and was fully characterized by IR,  $^1\text{H}$  NMR and  $^{13}\text{C}$

NMR spectroscopy. Mass spectrometry showed  $[7+H]^+$  ion peak at  $m/z = 793.4916$ , consistent with a [2+3] cage structure composed of two units of aldehyde **6** and three units of amine **1** with a formula  $C_{54}H_{60}N_6$ .



**Scheme 4.04** Synthesis of various [2+3] co-facial organic cages using *gem*-dimethyl effect as a platform. Reaction of *gem*-dimethylamines **1** and **4** with trialdehydes **6** and torsionally flexible **8**, to form cages **7**, **10** and **9**, **11**, respectively.

Single crystal X-ray diffraction analysis of **7** revealed that the molecules crystallized in the triclinic system with the space group *P*-1. Similarly, cage **10** was obtained by the reaction of trialdehyde **6** with phenyl ring extended *gem*-dimethyl-substituted diamine **4** in ACN. The formation of imine bond could be readily verified by the presence of IR absorption band observed at  $1627\text{ cm}^{-1}$ . The material was also fully characterized by  $^1\text{H}$  NMR and  $^{13}\text{C}$  NMR spectroscopy. Mass spectrometry showed  $[\mathbf{10}]^+$  ion peak at  $m/z = 1248.6787$ , ascribed for a [2+3] cage structure **10** with a formula  $C_{90}H_{84}N_6$ . Single crystal X-ray diffraction analysis of **10** revealed that the molecules are crystallized in the triclinic system with the space group *P*-1.

To extend our studies, we treated *gem*-dimethylamines **1** and **4** with torsionally flexible propeller-shaped aldehyde **8** to afford co-facial propeller-shaped cages **9** and **11**, respectively. These cages were synthesized following the conditions adopted for obtaining cage **7**, with slight modification. The formation of [2+3] cages were confirmed by the



presence of  $[M+H]^+$  peak at 1127.6372 ( $C_{78}H_{79}N_6$ ) in HRMS for **9** and MALDI-MS,  $[M]^+$  peak at 1584.0385 ( $C_{90}H_{84}N_6$ ) for **11**. Further, spectroscopic analyses such as IR and  $^1H$  NMR supported the [2+3] cage structure. Single crystal X-ray diffraction analysis revealed that **7** and **11** were crystallized in the monoclinic- $P2/c$  and trigonal- $P3_1$  space groups, respectively. Crystal structure of the cage **11** could not be obtained due to a large number of atoms in the single unit cell of the crystal with considerable disorder.

It is a general perception that imine-based macrocyclization reactions under high concentration lead to the formation of oligomeric side products (dynamic combinatorial library, DCL) which require high dilution conditions for self-correction to form thermodynamically stable products.<sup>1, 41-45</sup> On the contrary, following our strategy, we have shown the preferential formation of [2+2] macrocycles and [2+3] macrobicycles, even under high concentrations (based on aldehyde) by instant mixing of the aldehydes and amines at ambient conditions. The preparation of **3** and **5a** could be carried out without any difficulty, using 1.0 M and 0.6 M concentration in DCM/ $CHCl_3$ , respectively. For cages **10** and **9**, high concentration reactions were performed in 0.5 M and 0.12 M, respectively. Moreover,  $^1H$ -NMR recorded for the direct reaction mixture of the high concentration reactions performed for the formation of macrocycle-**3** and cage-**10** (after 12 h) revealed the exclusive existence of **3** and **10** in the corresponding reaction mixtures (Fig. 4.10 & 4.23). This finding clearly attests to the utility of the *gem*-dimethyl group effect in macrocyclization reactions.

#### 4.4.4 Effect of *gem*-dimethyl groups in reaction equilibrium of the imine-based macrocyclization (studied by using $^1H$ NMR)

In general, in order to study equilibrium of the dynamic covalent library (DCL), the reaction should be performed in a solvent, in which all the DCL components are soluble. Then, the reaction mixture can be analyzed directly by  $^1H$  NMR. Herein, macrocycles **3**, **10** and their DCL were completely soluble in  $CHCl_3$ . Therefore, the macrocyclization of **3** and **10** were taken as exemplary systems to study the effect of *gem*-dimethyl groups in the equilibrium of the imine-based macrocyclization. The macrocyclization reactions for the formation of **3** and **10** were conducted in  $CHCl_3$ , at high concentrations 1 M and 0.5 M, respectively. After 12 h, both the reaction mixtures were directly taken from the reaction vial and  $^1H$  NMR were recorded separately. The

results of the  $^1\text{H}$  NMR have undoubtedly revealed the presence of [2+2] macrocycle and [2+3] cage respectively (Fig. 4.10 & 4.23). In all the above mentioned cases, in order to maintain the high concentration while recording  $^1\text{H}$  NMR, 450  $\mu\text{l}$  of the reaction solution and 100  $\mu\text{l}$  of  $\text{CDCl}_3$  were used.

In the presence of *gem*-dimethyl groups in the dynamic combinatorial libraries (DCL), the increase in  $\Delta S^\circ$  or decrease in  $\Delta H^\circ$  or both in the system could highly thermodynamically favors the cyclization<sup>28-29</sup> and can make the equilibrium always move towards the macrocycle formation (almost negligible amount of starting materials and other species could be found). On the other hand, a similar experiment was conducted for the formation macrocycle-3a in  $\text{CHCl}_3$ , at 1 M concentration, wherein  $^1\text{H}$  NMR (Fig. 4.11) clearly showed the presence of many DCL components in the reaction mixture.

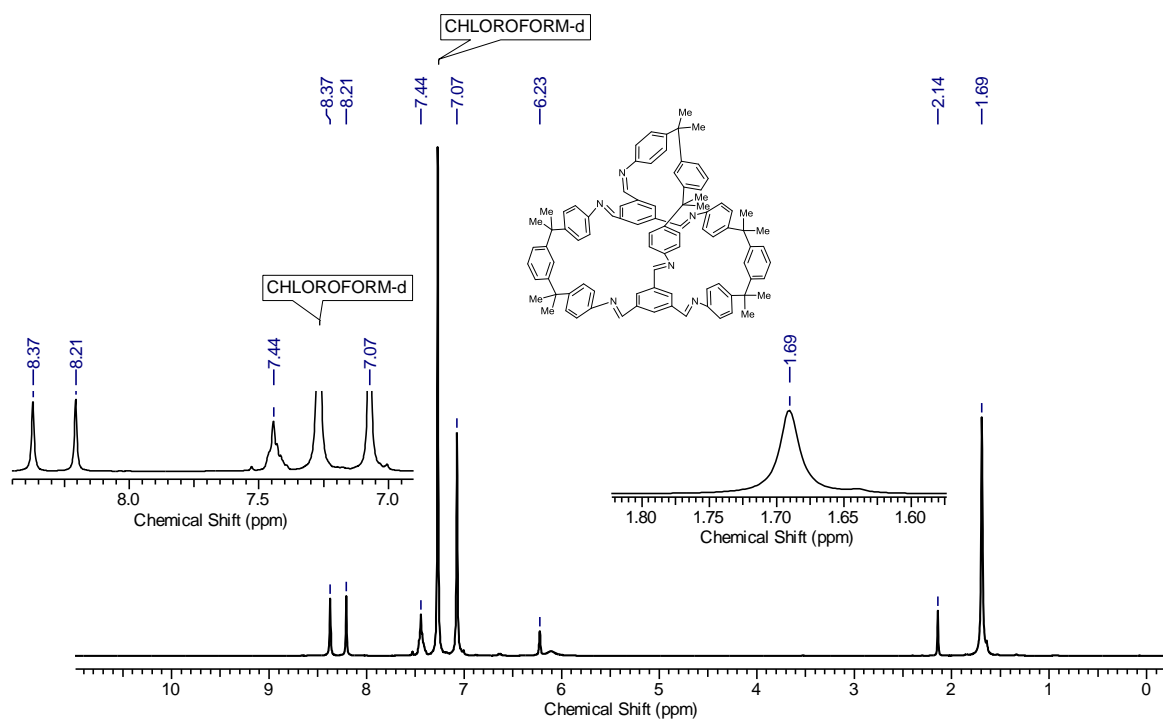


**Fig. 4.23:**  $^1\text{H}$  NMR spectrum of the direct reaction mixture of cage-10 formation performed at 1 M concentrations (in  $\text{CHCl}_3$ ) showing the presence of almost only, [2+3] cage-10. Note: The peak at  $\delta=2.14$  corresponds to  $\text{CH}_3\text{COOH}$ .

This could be the possible reason for the formation of macrocycles/cages under high concentrations as well as high yields over the unsubstituted classical ones. Further, there are several thermodynamic and kinetic factors which may inter-play the enhancement of the cyclization and their contribution may vary somewhat depending on the system being analyzed.

#### 4.4.5 Effect of *gem*-dimethyl groups in the stability of macrocycle.

In two open vials, 20 mg of macrocycle **3** and **3a** each were dissolved in CHCl<sub>3</sub> (2 ml) and kept separately without disturbance at ambient conditions. After 12 h, the maximum amount of solvent got evaporated and left some residue in both cases. The vial which contained macrocycle-**3** residue was completely soluble in CHCl<sub>3</sub> and there was no change in the pattern in <sup>1</sup>H NMR, whereas macrocycle-**3a** was not completely soluble in CHCl<sub>3</sub> and the soluble part of the <sup>1</sup>H NMR clearly suggested the presence of other DCL of **3a** and their derivatives (Fig. 4.24). This is possibly due to the easy hydrolysis of imine bond in the macrocycle-**3a**. On the contrary, hydrolysis was not happening in the case of **3** owing to the presence of *gem*-dimethyl groups. This behavior of the macrocycle-**3** is similar to the hydrolysis of the *gem*-dimethyl containing cyclic esters.<sup>21, 28, 35-36</sup>

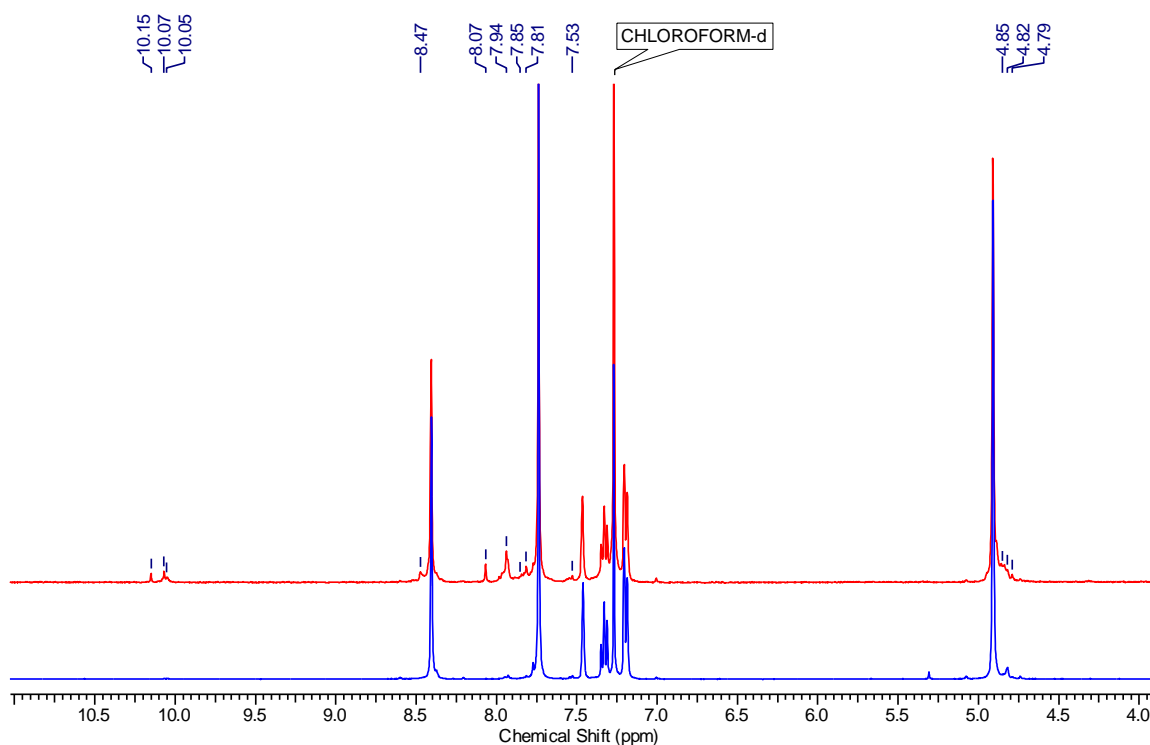


**Fig. 4.24:** <sup>1</sup>H NMR of macrocycle-**3a** before (bottom, blue) and after (top, red) 12 h kept in open vial at ambient condition.

#### 4.4.6 Thermogravimetric analysis of macrocycles/cages:

Thermogravimetric analysis (Fig. 4.25-4.26) of all synthesized macrocycles/cages (except **3**) showed decomposition temperature ~ 400 °C, which clearly indicated their high thermal stability. This observation is similar to the stability of other *gem*-dimethyl containing cyclic systems, which were proved experimentally as well as by computational studies.<sup>21, 35-36, 46</sup> Thermogravimetric analysis was carried out on NETSZCH TGA-DSC or METTLER TOLEDO, TGA/SDTA851e. The routine TGAs were done under N<sub>2</sub> gas flow (20ml or 50 ml/min) (purge + protective).

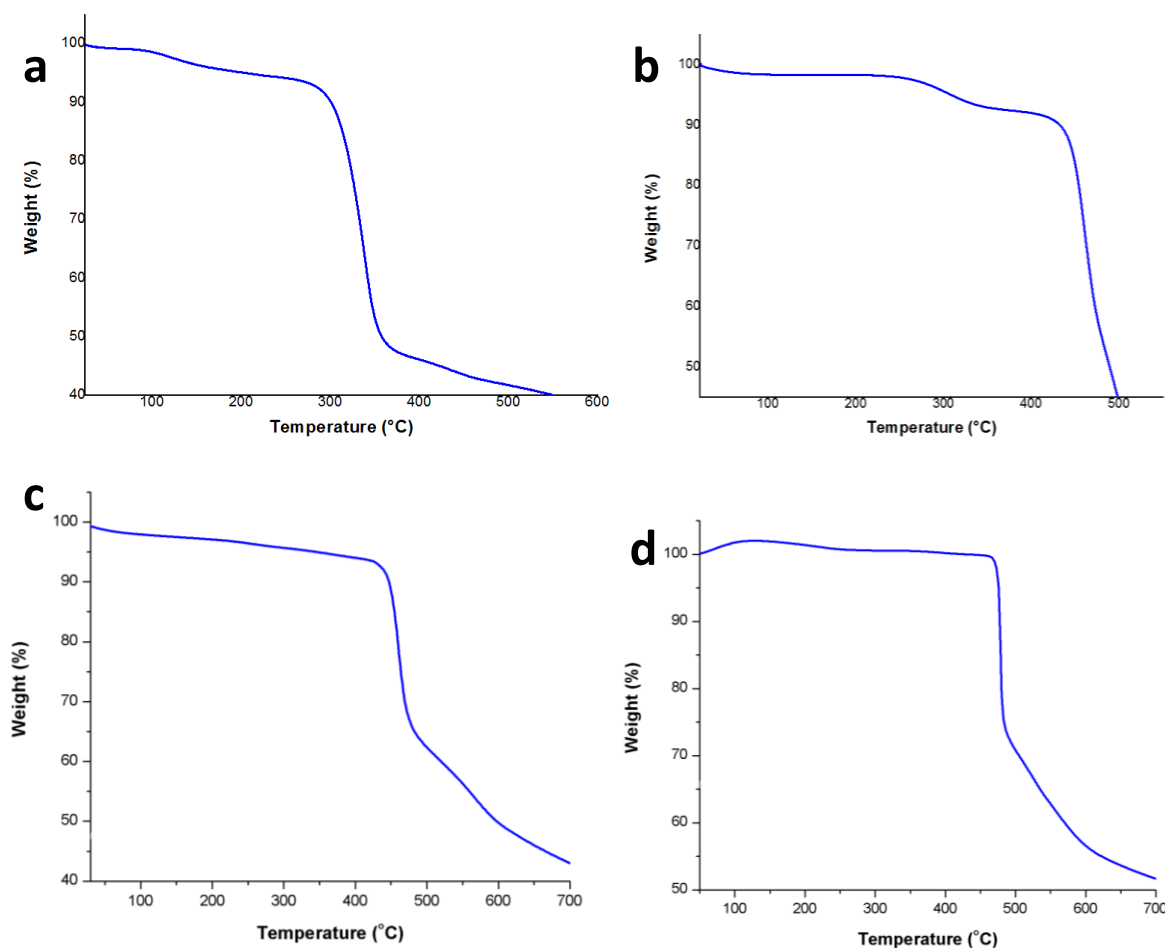


**Fig. 4.25:** TGA data of macrocycles. a) Macrocycle-**3** heated to 600 °C at the rate of 5 °C /min. b) Macrocycle-**5a** heated to 600 °C at the rate of 5 °C /min. c) Macrocycle-**5b** heated to 700 °C at the rate of 10 °C /min. d) Macrocycle-**5c** heated to 700 °C at the rate of 10 °C /min. *Note:* Except macrocycle-**3**, rest of the macrocycles showed decomposition temperature above 400 °C.

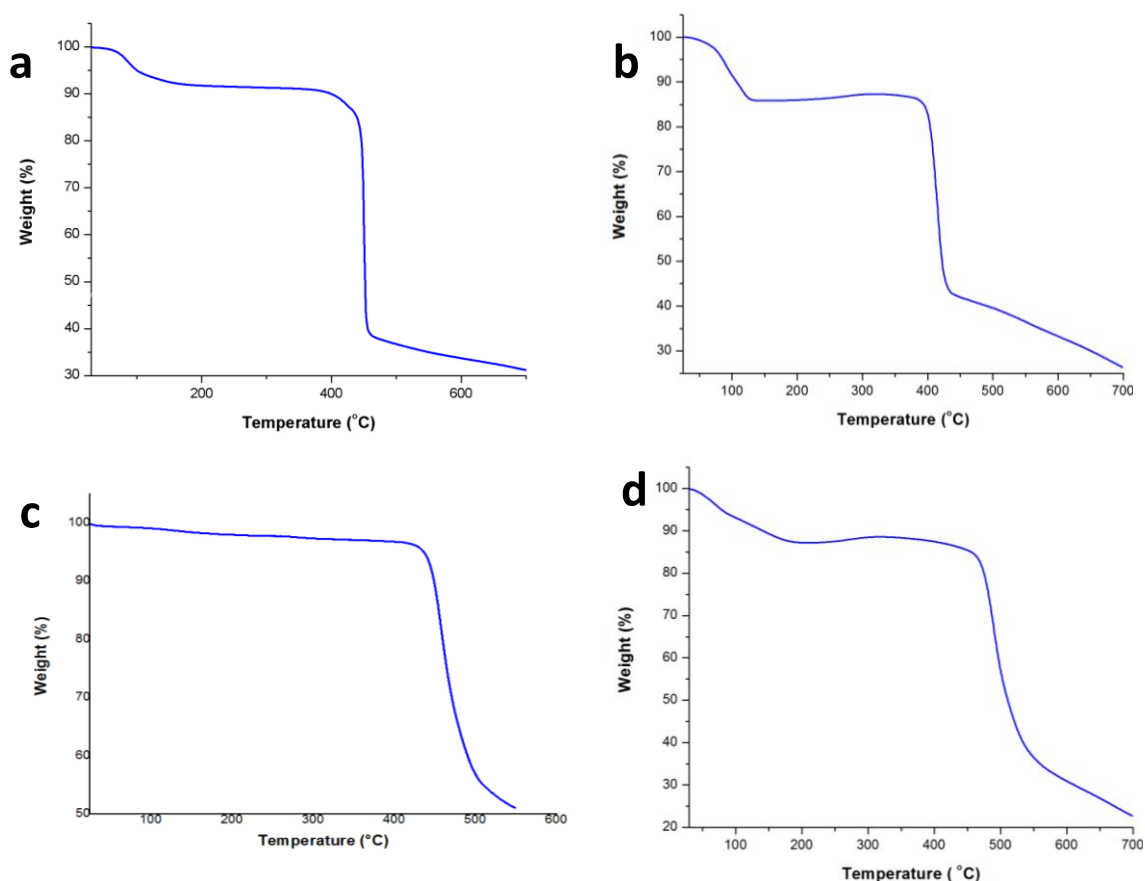


**Fig. 4.26:** TGA data of cages. a) Cage-7 heated to 700 °C at the rate of 10 °C /min. b) Cage-9 heated to 700 °C at the rate of 10 °C /min. c) Cage-10 heated to 600 °C at the rate of 5 °C /min. d) Cage-11 heated to 700 °C at the rate of 10 °C /min. *Note:* All the cages showed decomposition temperature above 400 °C.

#### 4.4.7 Single crystal X-ray studies and structural features of the cages

Single crystal structure of **7** showed two types of isomers found in the same unit cell; one with eclipsed central benzene rings and other with partially displaced structure (Fig. 4.27). The structure of cage **7** resemble a three-bladed fan-like architecture. The length of the wings is  $\sim 5.5$  to  $5.7$  Å (Fig. 4.28a). Further, analysis of the crystal structure showed that **7** has a compact structure with negligible intrinsic cavities and showed only small discontinuous extrinsic cavities, even after manual deletion of the solvent molecules (ACN) (Fig. 4.29). The distance between the central benzene rings of the cages is  $\sim 4.2$  to  $4.4$  Å which are not falling on the  $\pi$ - $\pi$  stacking range. On the other hand, the single crystal structure of **10** showed only one type of isomer. The central benzene rings facilitate the face-to-face alignment between them,

thereby generating parallel displaced  $\pi$ -stacking interactions (centroid...centroid distance = 3.778(2) Å) (Fig. 4.28b). The comparison of crystal structures **7** and **10** revealed that the extension of phenyl ring in **10** showed better flexibility to exhibit  $\pi$ - $\pi$  stacking and increased the length of the arms leading to the formation of voids in the lattice.

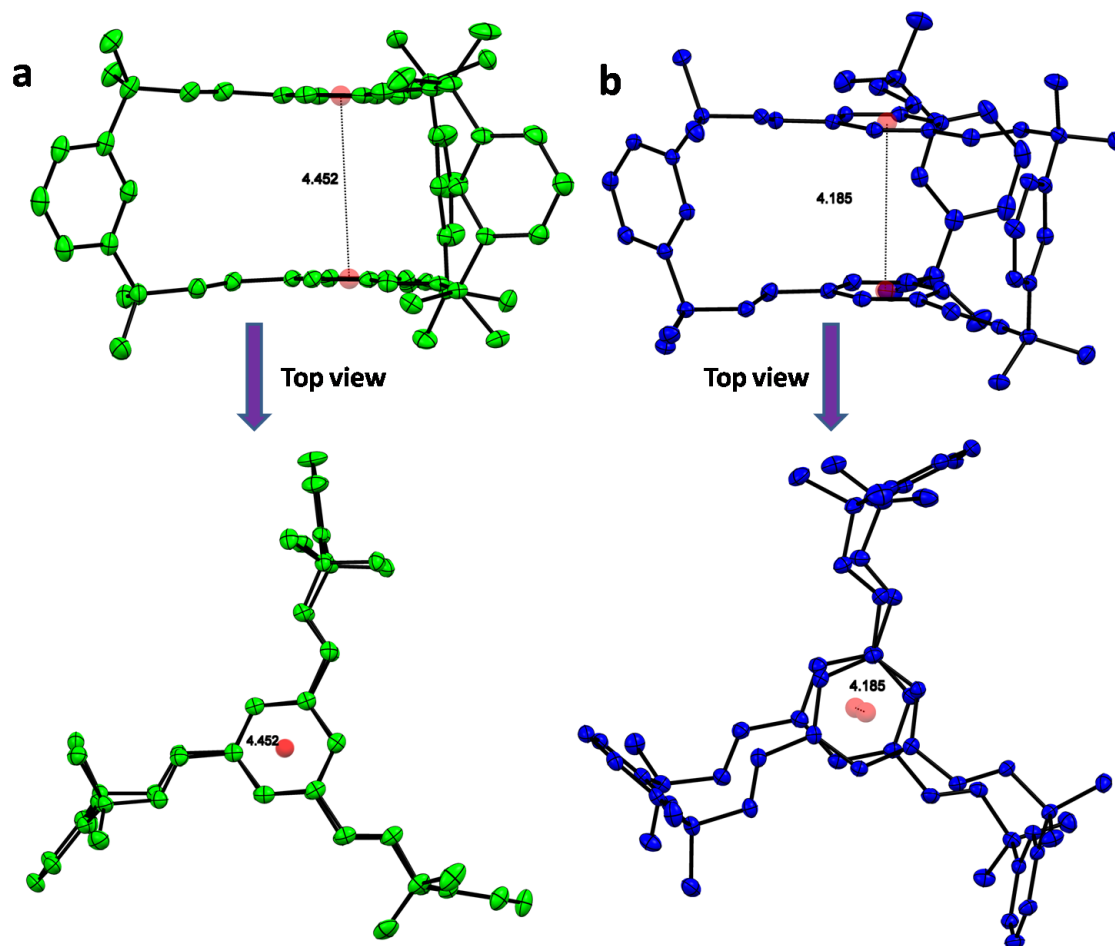


**Fig. 4.27:** Side and top views of the two types of isomers found in the unit cell of cage-7.

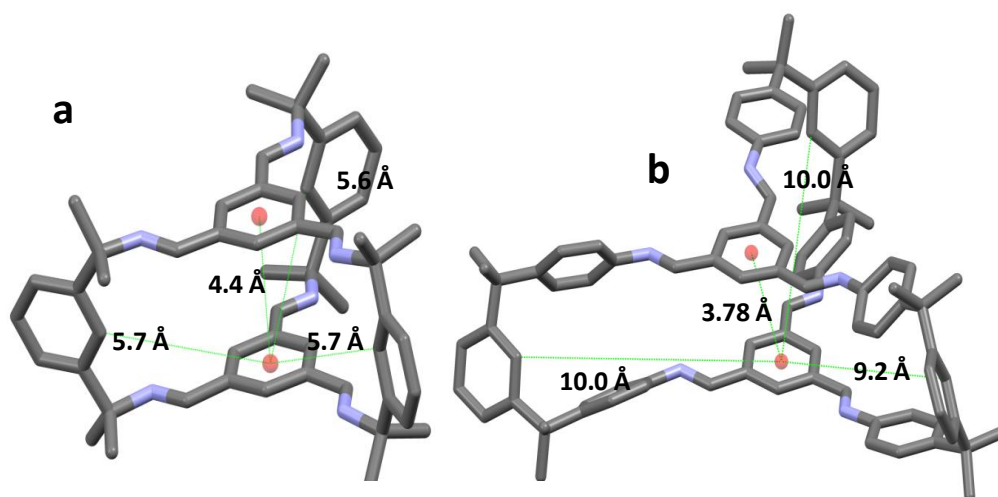


**Fig. 4.28:** a) Crystal structure of **7** showing the distance between the two central benzene rings to be 4.2 Å and length of the wings are ~ 5.7 Å. b) Crystal structure of **10** showing the distance between the two central benzene rings to be 3.78 Å and length of the wings are ~ 10 Å.

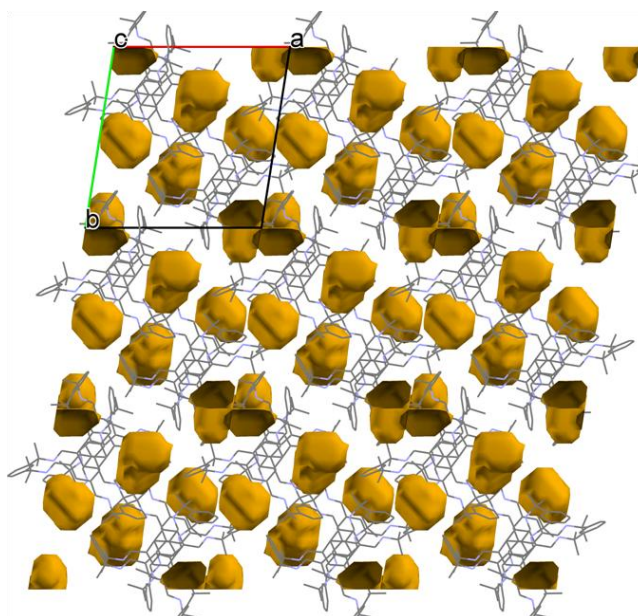


**Fig. 4.29:** Manual deletion of solvent molecules (ACN) from the crystal lattice of cage-**7** generates discontinuous extrinsic voids amounting to 262.13 Å<sup>3</sup> per unit cell (5.2% of the cell volume). *Note:* The voids are calculated using contact surface with the probe radius 2.0 Å.

Although the cage-**10** doesn't leave voids within its framework due to the face-to-face intramolecular  $\pi$ -stacking interactions, the successive association of six propeller-shaped cage molecules constitutes the hexagonal one-dimensional network comprising



open channels of approximate area  $11 \times 8 \text{ \AA}^2$  along the  $a$ -axis. Neighboring molecules in the hexagonal network are associated mostly through C-H...N, marginal CH... $\pi$  and other Van der Waals forces (Fig. 4.30a). The estimation of the voids created along the hexagonal network calculated using contact surface with the probe radius  $2.0 \text{ \AA}$  revealed voids amounting to  $507.18 \text{ \AA}^3$  per unit cell (12.9% of the cell volume) (Fig. 4.30). Moreover, there was no apparent loss of crystallinity when the material was degassed at  $120 \text{ }^\circ\text{C}$  under high vacuum for 12 h, which suggested that the crystal is stable under these conditions (Fig. 4.38). The 1-D channels present in crystals **10** have void diameter which is little larger than the kinetic diameter of many gasses (Fig. 4.31).

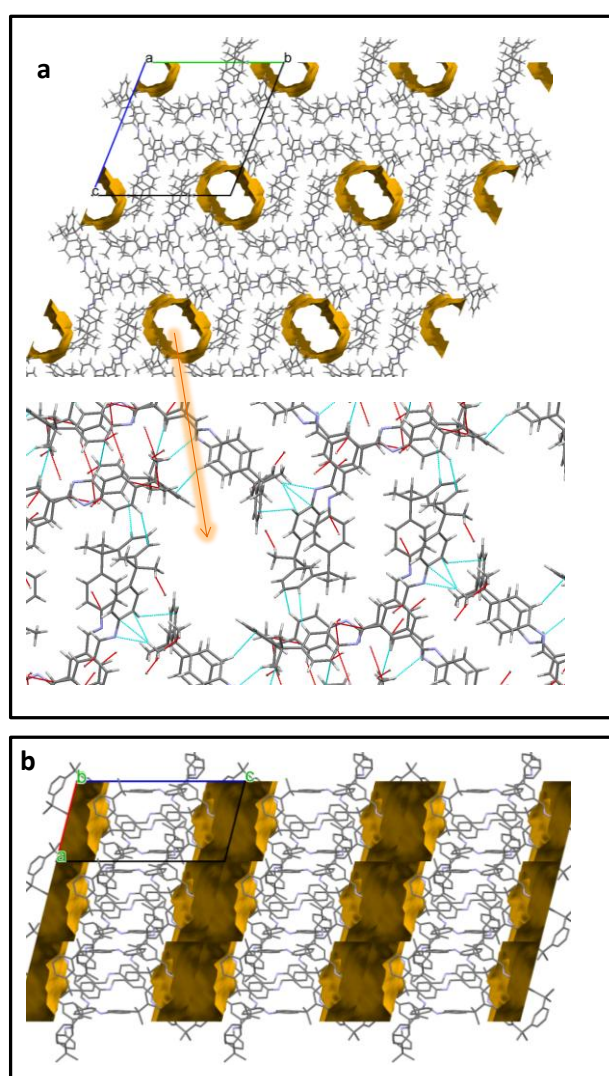


**Fig. 4.30:** a) The successive association (through C-H...N, marginal C-H... $\pi$  and other Van der Waals forces.) of six propeller-shaped cage **10** constitutes the hexagonal one-dimensional network along the  $a$ -axis. b) the voids generated along  $a$ -axis are calculated using contact surface with the probe radius  $2.0 \text{ \AA}$  revealing voids amounting to  $507.18 \text{ \AA}^3$  per unit cell (12.9% of the cell volume).

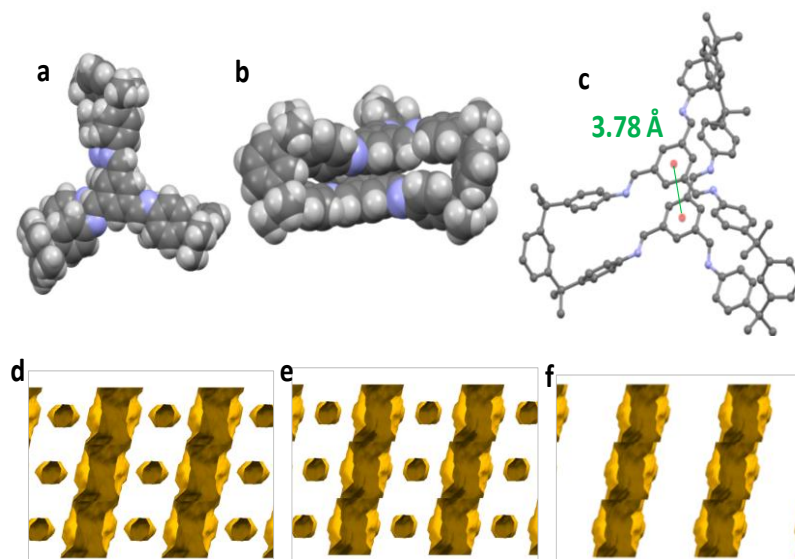


**Fig. 4.31:** a) Space-filling model of a three-bladed fan-like *pseudo* co-facial cage crystal structure of **10** viewed from the top. b) side view of the crystal structure of **10** shows negligible intrinsic voids (space-fill model). c) crystal structure of **7** (ball and stick model) shows the distance between the two central benzene rings to be 3.78 Å. d) connolly surfaces generated for hydrogen showing the channels/voids (probe radii: 1.42 Å), e) connolly surfaces generated for carbon dioxide showing the channels/voids (probe radii: 1.72 Å) and f) connolly surfaces generated for nitrogen showing the channels/voids (probe radii: 1.82 Å).

The single crystal structure of **9** showed two types of isomers in the same unit cell. In both isomers, the distance between the two central nitrogen atoms is  $\sim 4.9$  to  $5.3$  Å (Fig 4.32 & 4.33). The structures of **9** looks like two propeller-shaped architectures are connected by three linkers.

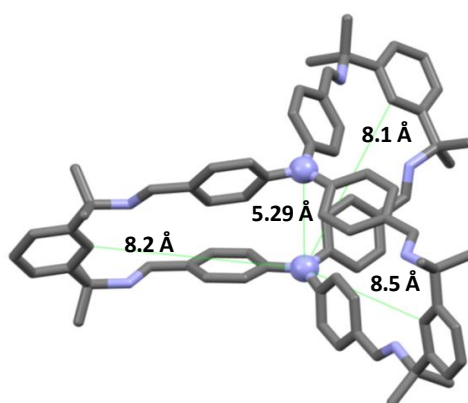


**Fig. 4.32:** Crystal structure of **9** showing the distance between the two central nitrogen atoms to be 5.29 Å and length of the wings are  $\sim 8.1$  to 8.5 Å. *Note:* X-ray crystal structures are showed in capped stick model.

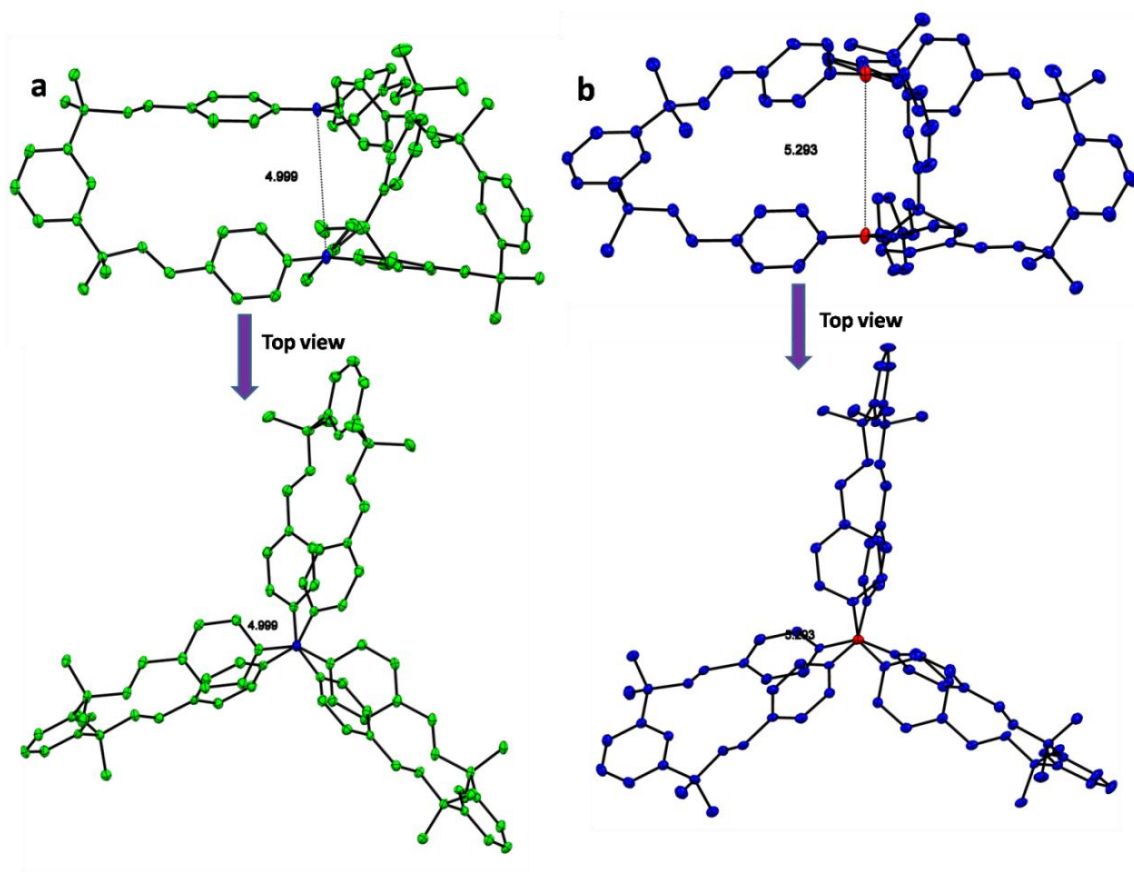


**Fig. 4.33:** Side and top views of the two types of isomers found in the unit cell of **cage-9**. a) isomer-1 showing the distance between the central nitrogen atoms (blue colored) is 4.99 Å. b) isomer-2 showing the distance between the central nitrogen atoms (red colored) is 5.293 Å.

#### 4.4.8 Powder X-ray diffraction (PXRD) studies of the macrocycles:

The homogeneity of the bulk sample of all the synthesized macrocycles were verified by comparing the experimental powder X-ray diffraction (PXRD) with a simulated PXRD pattern from single crystal X-ray diffraction data. Many of the overlays showed slight shifts in the peak positions of the experimental data with respect to the simulated data. This could be due to the temperature difference in intensity measurements. The experimental PXRD data was recorded at ambient temperature while the single crystal XRD data was collected at 100(2) K (Fig. 4.34-4.37). As a representative example, the powder X-ray diffraction patterns of **10** was recorded for the bulk sample as synthesized, simulated PXRD from the single crystal structure for **10** and after it was degassed at 120 °C under high vacuum for 24 h are compared. The analysis revealed that there was no change in the experimental PXRD data before and after

degassing at 120 °C under high vacuum for 24 h (Fig. 4.38). This suggested that the crystals are highly stable under these conditions.

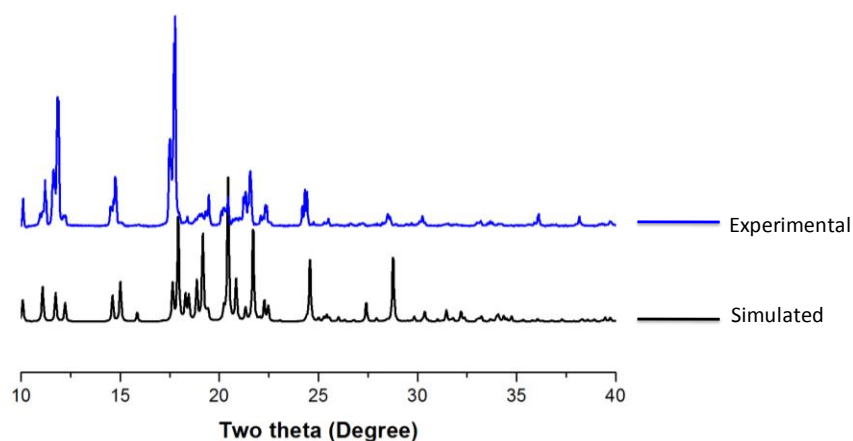


**Fig. 4.34:** Comparison of experimental (blue) and simulated (black) PXRD (from the single crystal structure) patterns of macrocycle **3**.

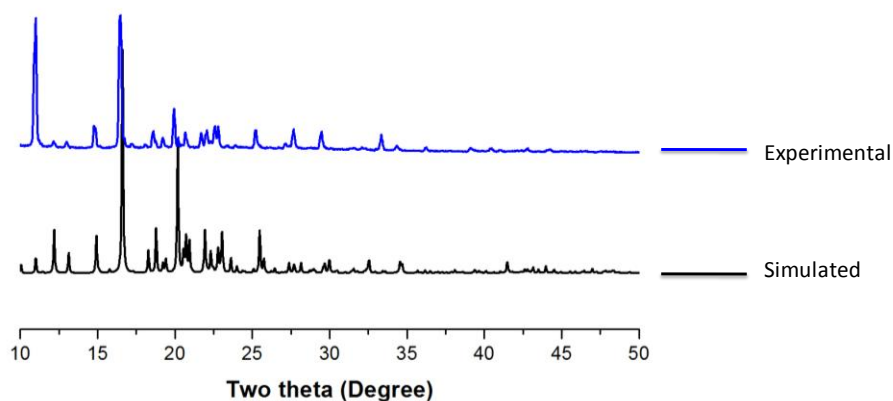


**Fig. 4.35:** Comparison of experimental (blue) and simulated (black) PXRD (from the single crystal structure) patterns of macrocycle **5a**.

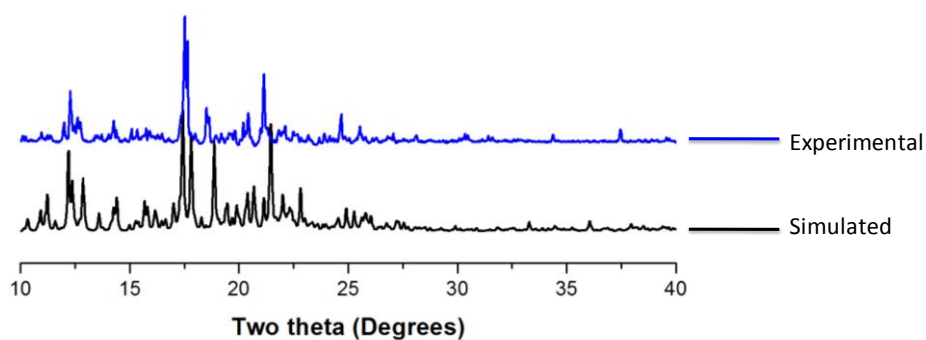


**Fig. 4.36:** Comparison of experimental (blue) and simulated (black) PXRD (from the single crystal structure) patterns of cage **7**.

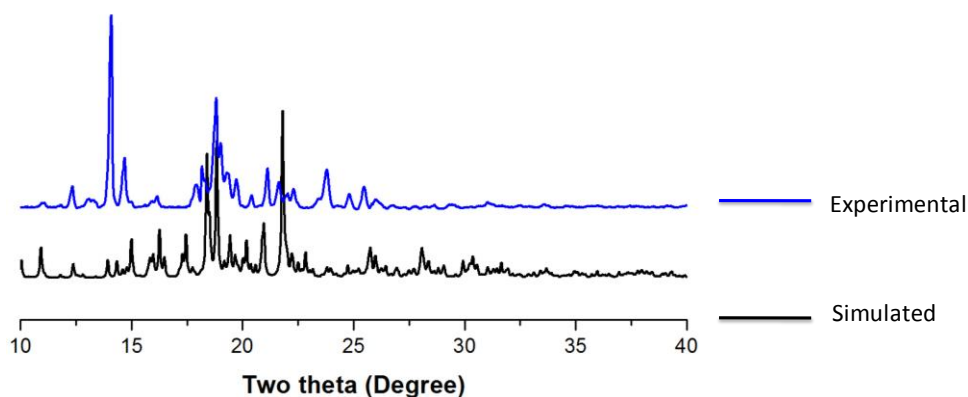


**Fig. 4.37:** Comparison of experimental (blue) and simulated (black) PXRD (from the single crystal structure) patterns of cage **9**.

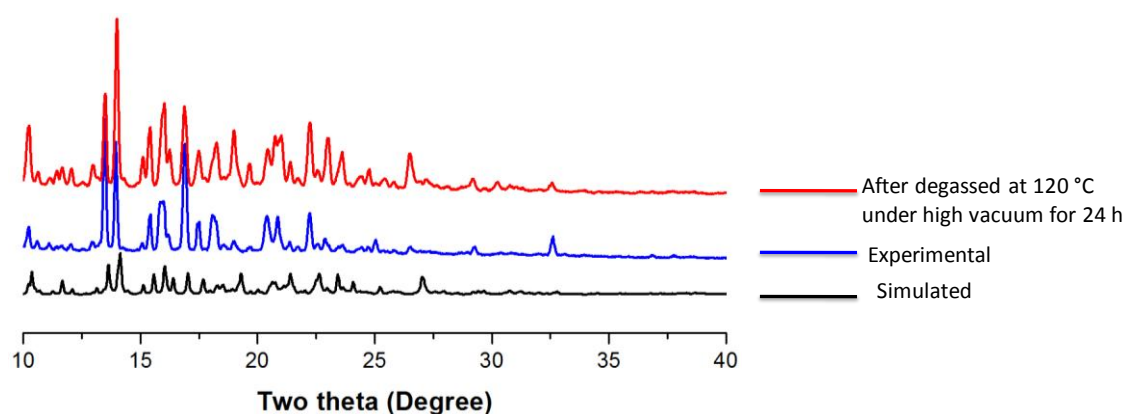


**Fig. 4.38:** Comparison of powder X-ray diffraction patterns for **10** recorded for the bulk sample as synthesized (middle, blue), simulated PXRD from the single crystal structure for **10** (bottom, black) and after degassed at 120 °C under high vacuum for 24 h (top, red). *Note* : The experimental PXRD data were collected at room temperature while the single crystal X-ray data that used to generate the simulated pattern were collected at 100 K.

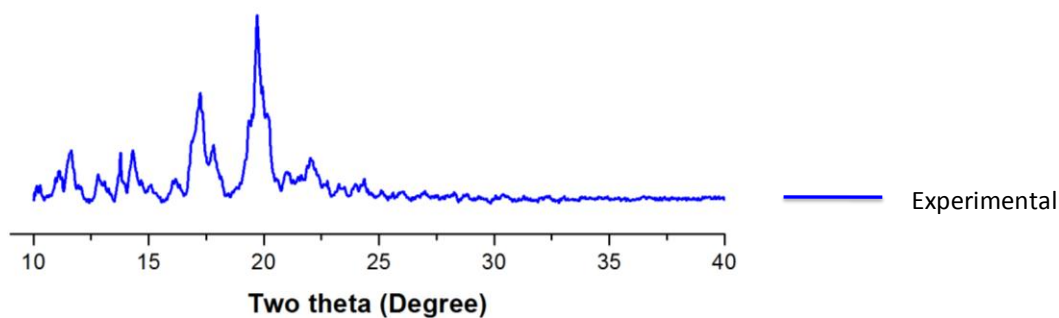


**Fig. 4.39:** Powder X-ray diffraction pattern of cage **11**.

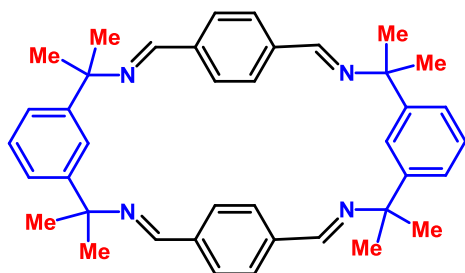
## 4.5 Conclusion

In conclusion, by using the *gem*-dimethyl group as a platform, we have demonstrated a selective and good-yielding alternative method to traditional macrocyclization. Utilizing this strategy, we have successfully obtained four new macrocycles and four propeller-shaped [2+3] cofacial organic cages by the dynamic imine bond formation of *gem*-dimethyl amines with various aldehydes - including torsionally flexible ones. Most of the synthesized molecular crystals of macrocycles and cages showed high thermal stability. It is noteworthy that this finding is in stark contrast to the general perception of conducting cyclization reactions under high dilution conditions. Based on our results, we believe that the use of *gem*-dimethyl effect in the formation of imine-based macrocyclic systems would result in the avoidance of the need for high-dilution methods and would enhance ease of isolation of pure thermally stable macrocycles – free from other DCL in high yields. Most importantly, this work would provide a key to rational designing of imine-based macrocycles with interesting structural architectures for various potential applications like gas storage and molecular recognition.



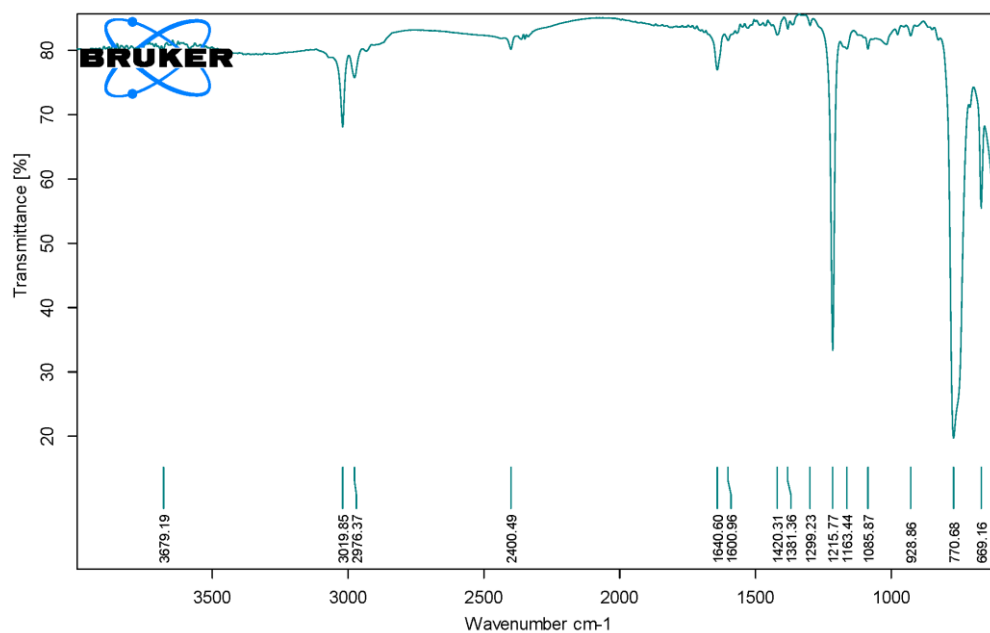
## 4.6 Experimental section

### Macrocycle 3.

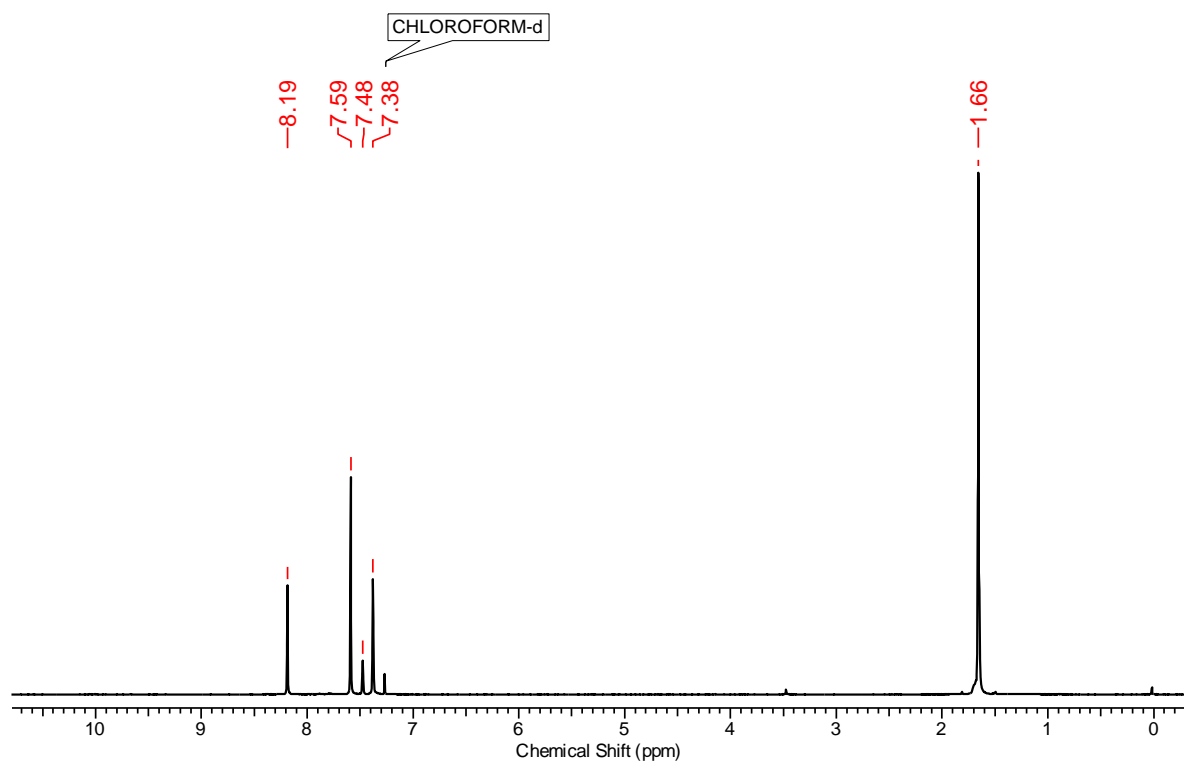


**Method A (under dilute condition):** A solution of **2a** (0.03 g, 0.22 mmol) in acetonitrile (ACN, 6 mL) was added slowly to a solution of **1** (0.043 g, 0.22 mmol) in ACN (6 mL) at room temperature. After complete addition of **2a**, a catalytic amount of acetic acid (20  $\mu$ l) was added and the reaction

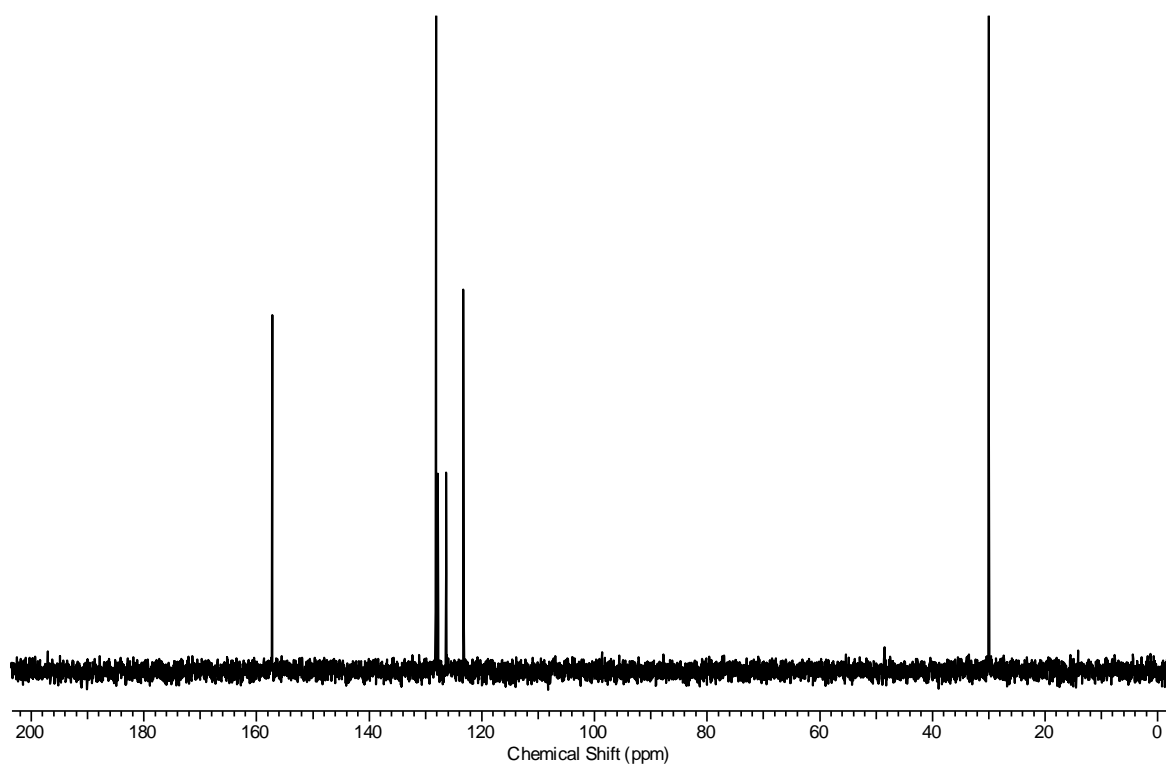
mixture was kept undisturbed at ambient temperature for 72 h to get colourless crystals. The crystals were filtered and then washed with ACN. The crystal suitable for X-ray crystallography was removed directly from the sample vial to obtain crystal structure of the macrocycle **3**. Yield: 0.055 g, 85%; m.p: 233-235  $^{\circ}$ C; IR ( $\text{CHCl}_3$ )  $\nu$  ( $\text{cm}^{-1}$ ): 3019 (m), 2976 (m), 1640 (CH=N), 1600 (Ar, C=C) (m), 1215;  $^1\text{H}$  NMR (400 MHz,  $\text{CDCl}_3$ )  $\delta$  (ppm): 8.19 (s, 4H), 7.59 (s, 8H), 7.48 (s, 2H), 7.38 (s, 6H), 1.66 (s, 24H);  $^{13}\text{C}$  NMR (100 MHz,  $\text{CDCl}_3$ )  $\delta$  (ppm): 157.2, 148.1, 138.3, 128.0, 127.7, 126.3, 123.2, 63.0, 29.9; HRMS ( $m/z$ ): calcd for  $\text{C}_{40}\text{H}_{45}\text{N}_4$   $[\text{M}+\text{H}]^+$  581.3639, found 581.3627.



IR spectrum of macrocycle **3**

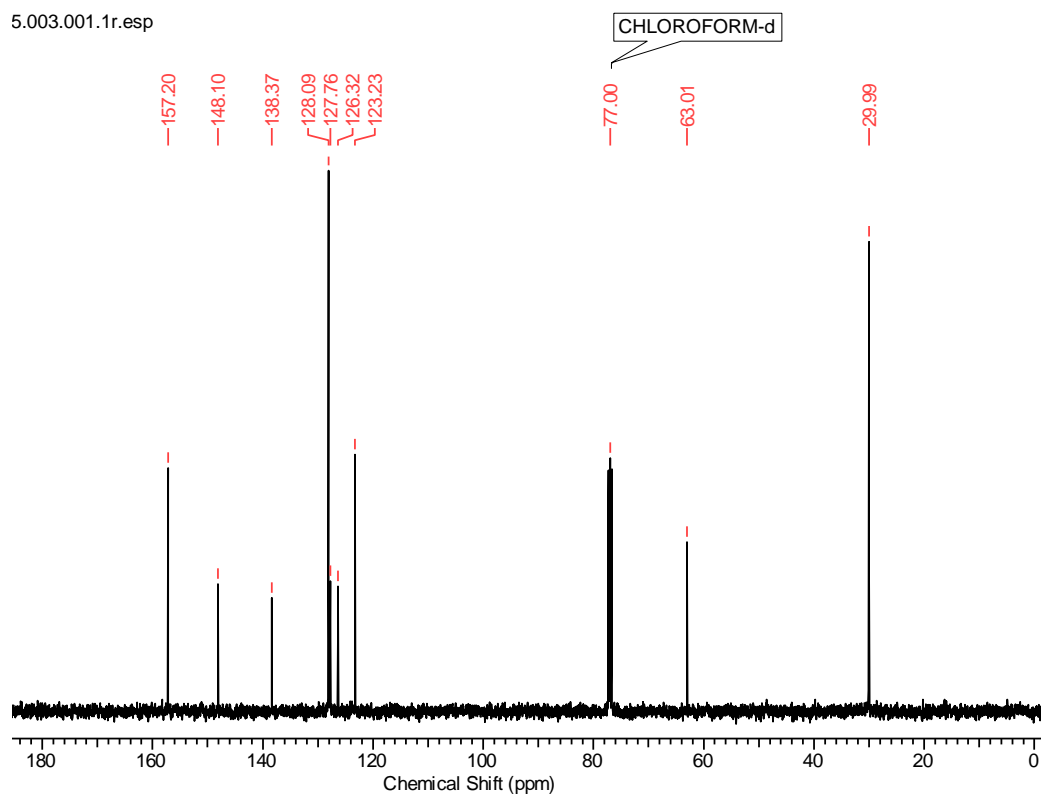


<sup>1</sup>H NMR spectrum of macrocycle **3** (CDCl<sub>3</sub>, 400 MHz, 298 K)



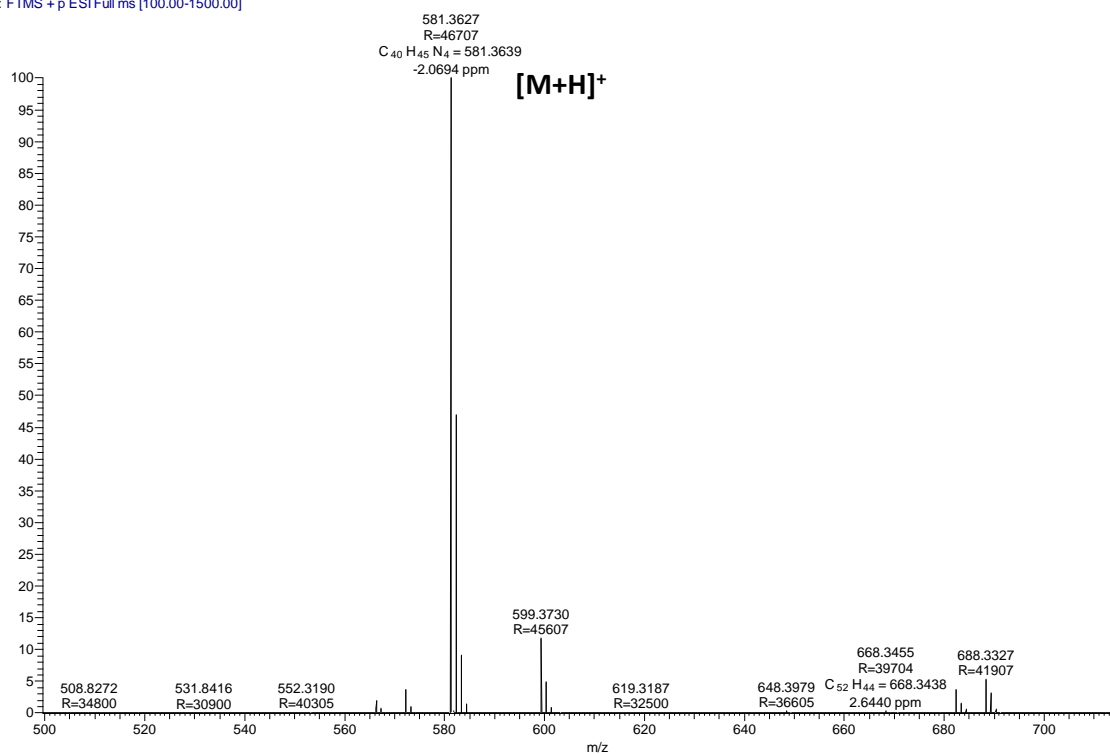
DEPT 135 spectrum of macrocycle **3** (CDCl<sub>3</sub>, 100 MHz, 298 K)



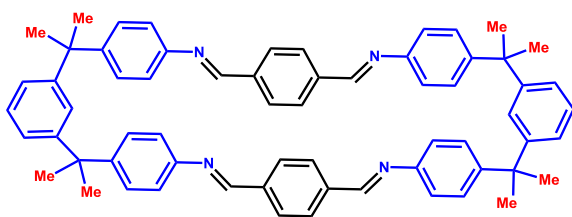


$^{13}\text{C}$  NMR spectrum of macrocycle **3** ( $\text{CDCl}_3$ , 100 MHz, 298 K)

19-B #140 RT: 0.62 AV: 1 NL: 1.38E8  
T: FTMS + p ESI Full ms [100.00-1500.00]



MS (HRMS) of macrocycle **3**

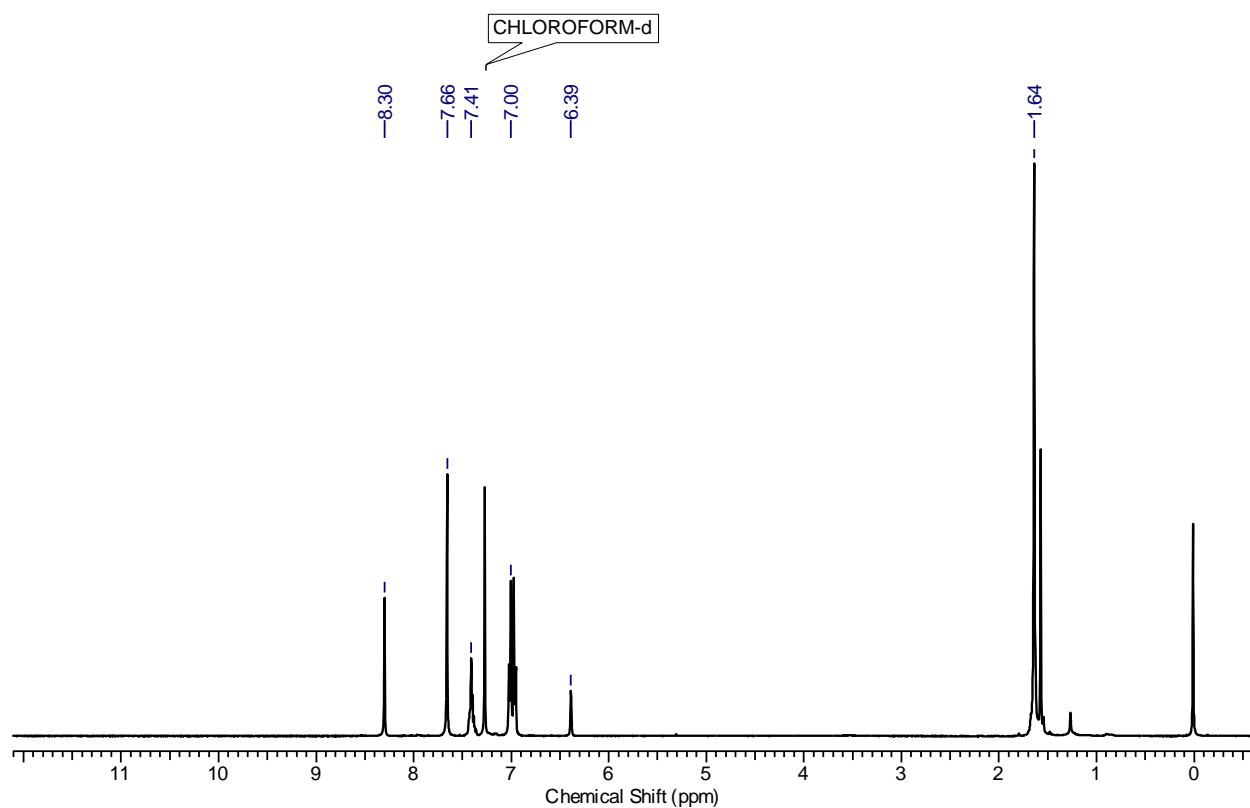
**Macrocycle 5a.**

A solution of **2a** (0.015 g, 0.111 mmol) in DCM (7 mL) was added drop wise to a solution of **4** (0.038 g, 0.111 mmol) taken in a 20 mL glass vial containing DCM (7 mL).

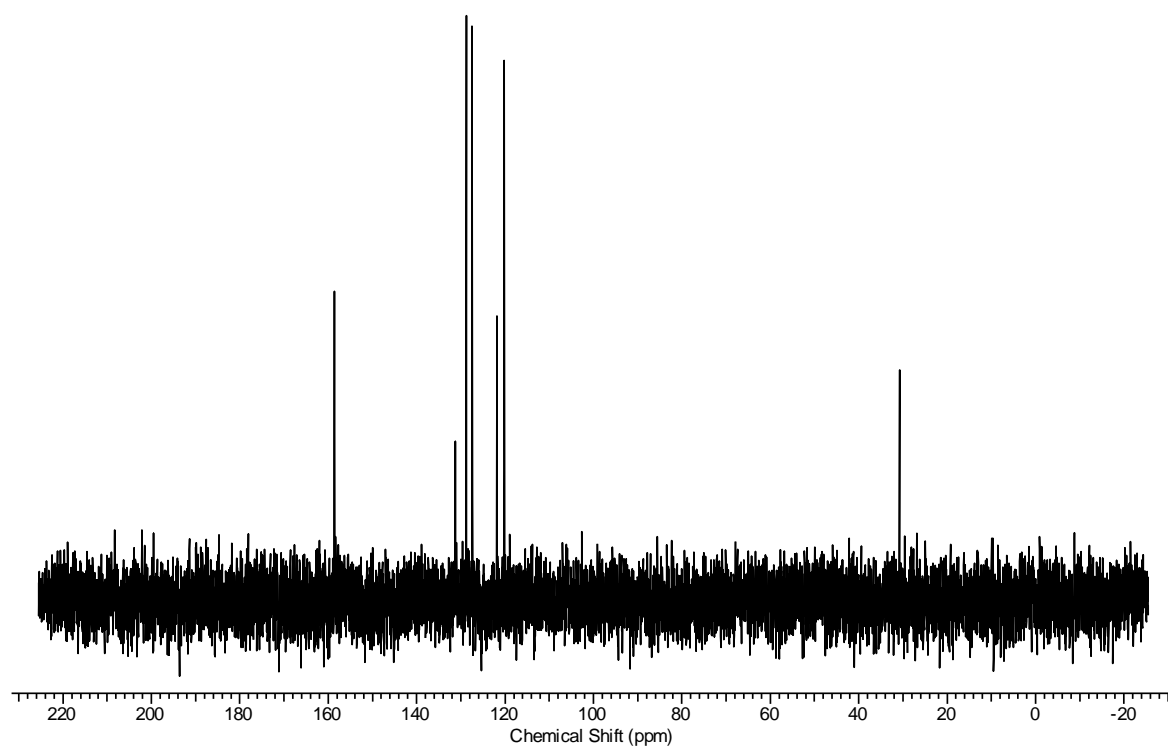
After complete addition of **2a**, a catalytic amount of acetic acid (20  $\mu$ l) was added and the reaction mixture was kept undisturbed at room temperature for 48 h to get a yellow coloured solution having some crystals. Then, the reaction mixture was concentrated *in vacuo* and the residue obtained was directly recrystallised from hot *o*-dichlorobenzene (3mL) to give pale yellow crystals. The crystals were filtered and washed with diethyl ether. Yield: 0.045 g, (90%); m.p: 294  $^{\circ}$ C; IR (Nujol,  $\nu$  (cm $^{-1}$ ) 2854, 1624 (CH=N), 1597 (Ar, C=C), 1377;  $^1$ H NMR (400 MHz, CDCl $_3$ )  $\delta$  (ppm): 8.30 (s, 4H), 7.66 (s, 8H), 7.45-7.36 (m, 6H), 7.04-6.93 (m, 16H), 6.39 (s, 2H), 1.64 (s, 24H);  $^{13}$ C NMR (100 MHz, CDCl $_3$ )  $\delta$  (ppm): 158.6, 150.3, 148.9, 131.2, 128.8, 127.4, 121.8, 120.1, 42.8, 30.7; MALDI-MS ( $m/z$ ): calcd for C $_{64}$ H $_{61}$ N $_4$  [M+H] $^+$  885.4896, found 885.7652.



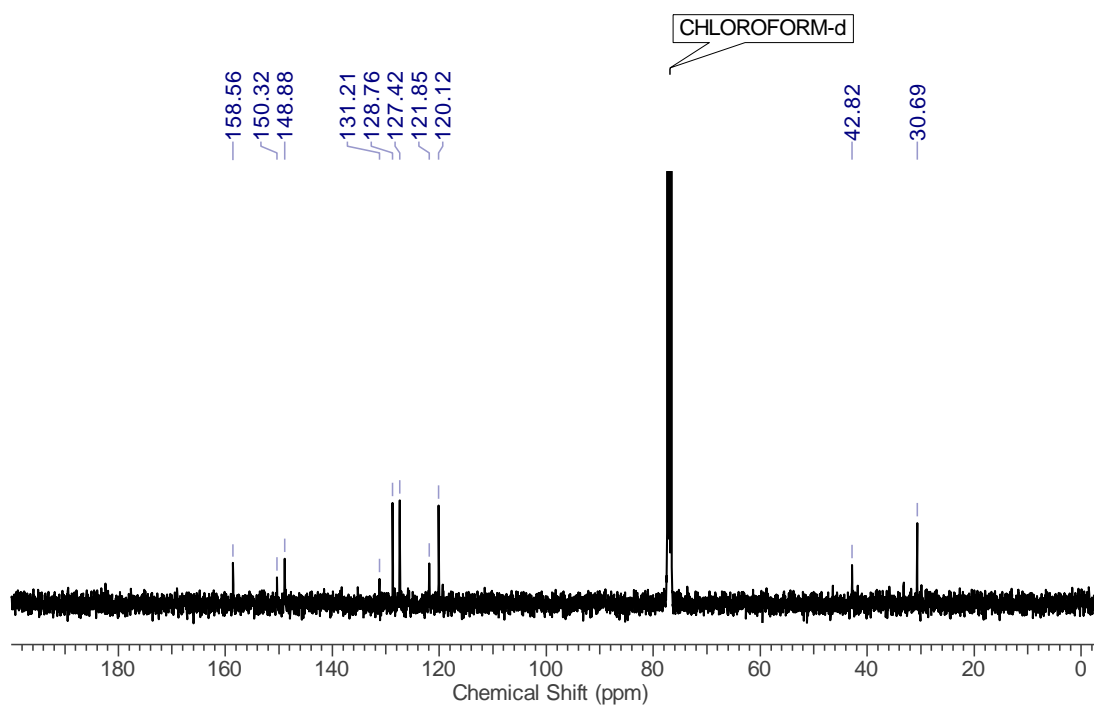
IR spectrum of macrocycle **5a**



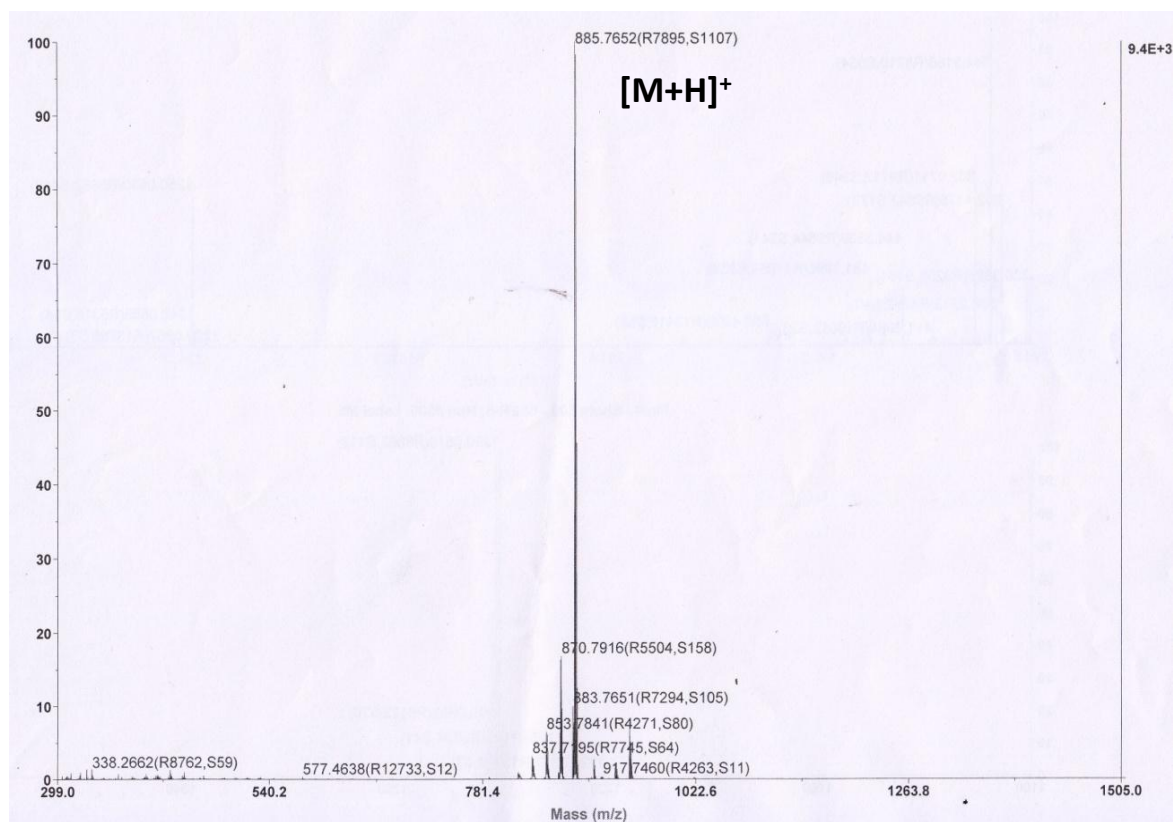
$^1\text{H}$  NMR spectrum of macrocycle **5a** ( $\text{CDCl}_3$ , 400 MHz, 298 K)



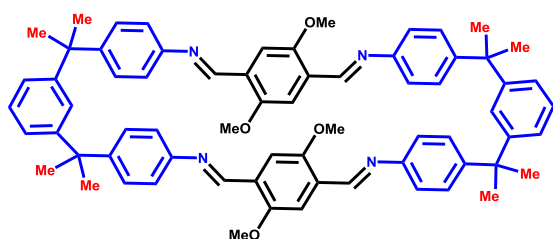
DEPT 135 spectrum of macrocycle **5a** ( $\text{CDCl}_3$ , 100 MHz, 298 K). *Note:* Concentrated NMR sample could not be obtained owing to the poor solubility of **5a** in  $\text{CDCl}_3$ .



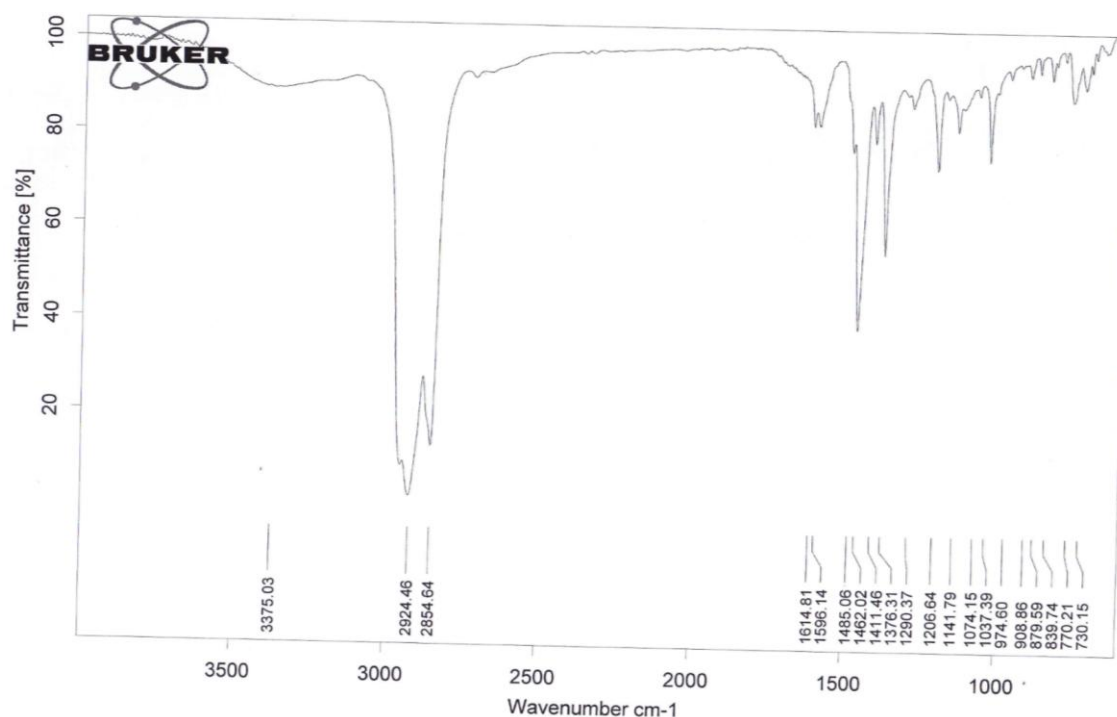
<sup>13</sup>C NMR spectrum of macrocycle **5a** (CDCl<sub>3</sub>, 100 MHz, 298 K). *Note:* Concentrated NMR sample could not be obtained owing to the poor solubility of **5a** in CDCl<sub>3</sub>.

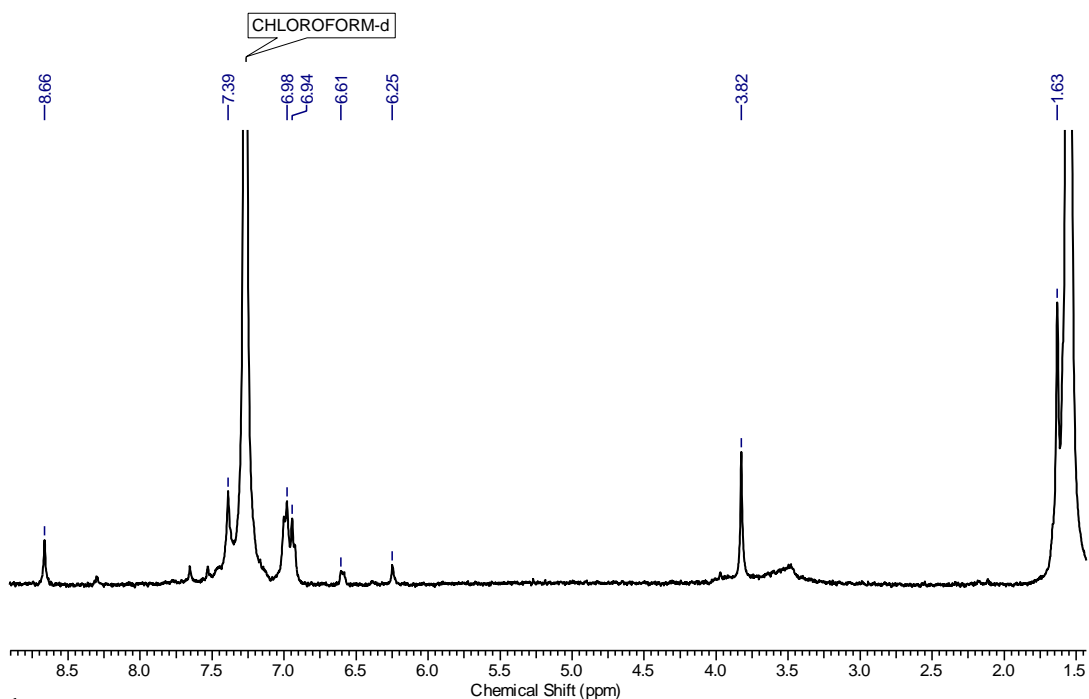


MALDI- MS of macrocycle **5a**

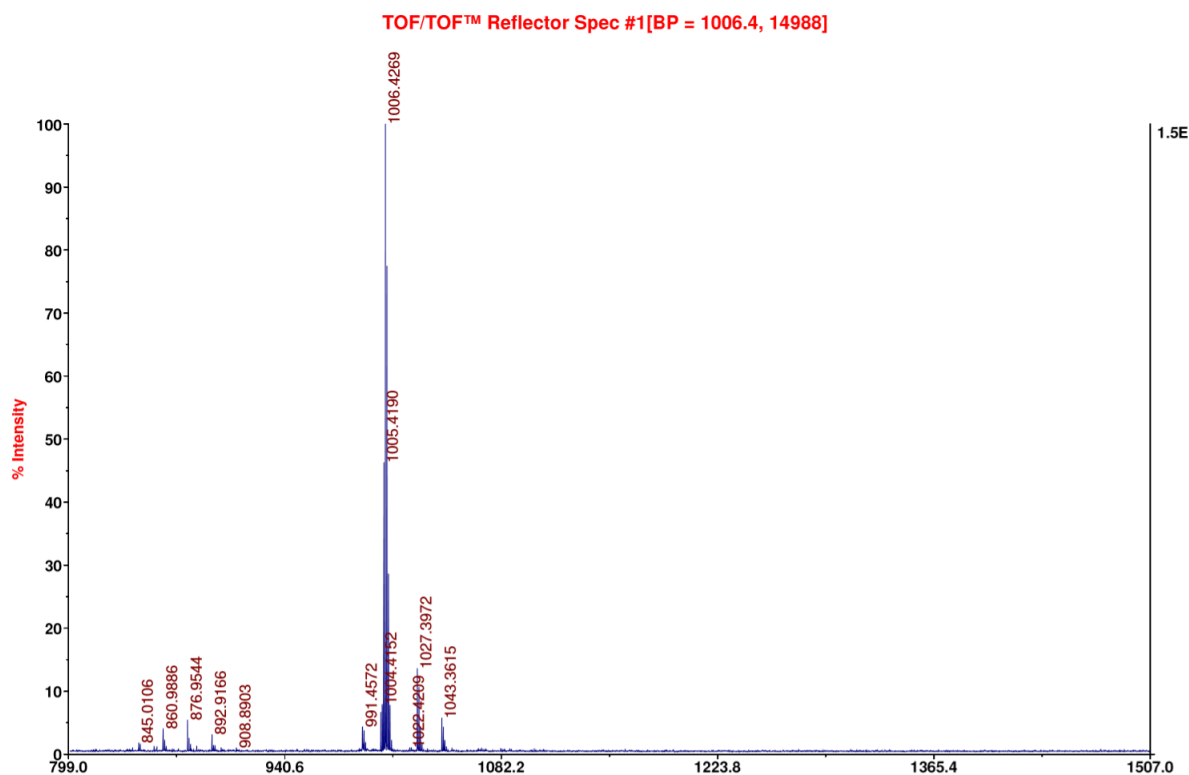
**Macrocycle 5b.**

A solution of 1,5-dimethoxyterephthalaldehyde (**2b**, 10 mg, 0.051 mmol) in ACN (2 mL) was added drop wise to a solution of *gem*-dimethylamine (**4**, 20 mg, 0.051 mmol) taken in a 4 mL glass vial containing DCM (2 mL). After complete addition of **2b**, a catalytic amount of acetic acid (5  $\mu$ l) was added and the reaction mixture was kept undisturbed at room temperature for 48 h to get a yellow coloured solution having some crystals. Then, the reaction mixture was concentrated *in vacuo* and the residue obtained was directly recrystallised from hot *o*-dichlorobenzene (2 mL) to give yellow coloured-needle shaped crystals. The crystals were filtered and washed with DCM. Yield: 0.023 g, (89%); m.p:  $>350$   $^{\circ}$ C; IR (Nujol,  $\nu$  ( $\text{cm}^{-1}$ )) 1624, 1596, 1485; Due to solubility issue, we could not obtain clear  $^1\text{H}$  NMR and  $^{13}\text{C}$  NMR of **5b**,  $^1\text{H}$  NMR (400 MHz,  $\text{CDCl}_3$ )  $\delta$  (ppm): 8.66 (s, CH=N, 4H), 7.39-6.25 (Ar, 28H), 3.82 (br. s,  $\text{OCH}_3$ , 12H), 1.63 (br. s,  $\text{CH}_3$ , 36H); MALDI- MS ( $m/z$ ):  $[\text{M}+\text{H}]^+$  1005.4190.

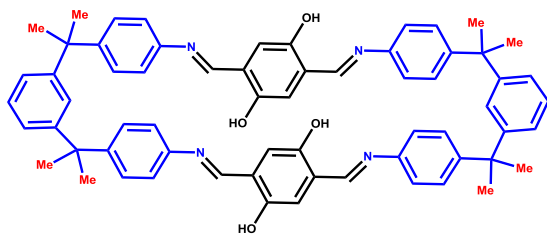
IR spectrum of macrocycle **5b**



$^1\text{H}$  NMR spectrum of macrocycle **5b** ( $\text{CDCl}_3$ , 400 MHz, 298 K). Note: Good quality NMR spectra could not be obtained owing to the poor solubility of **5b** in  $\text{CDCl}_3$ . The peak at  $\delta=1.5$  corresponds to  $\text{CDCl}_3$ -water.

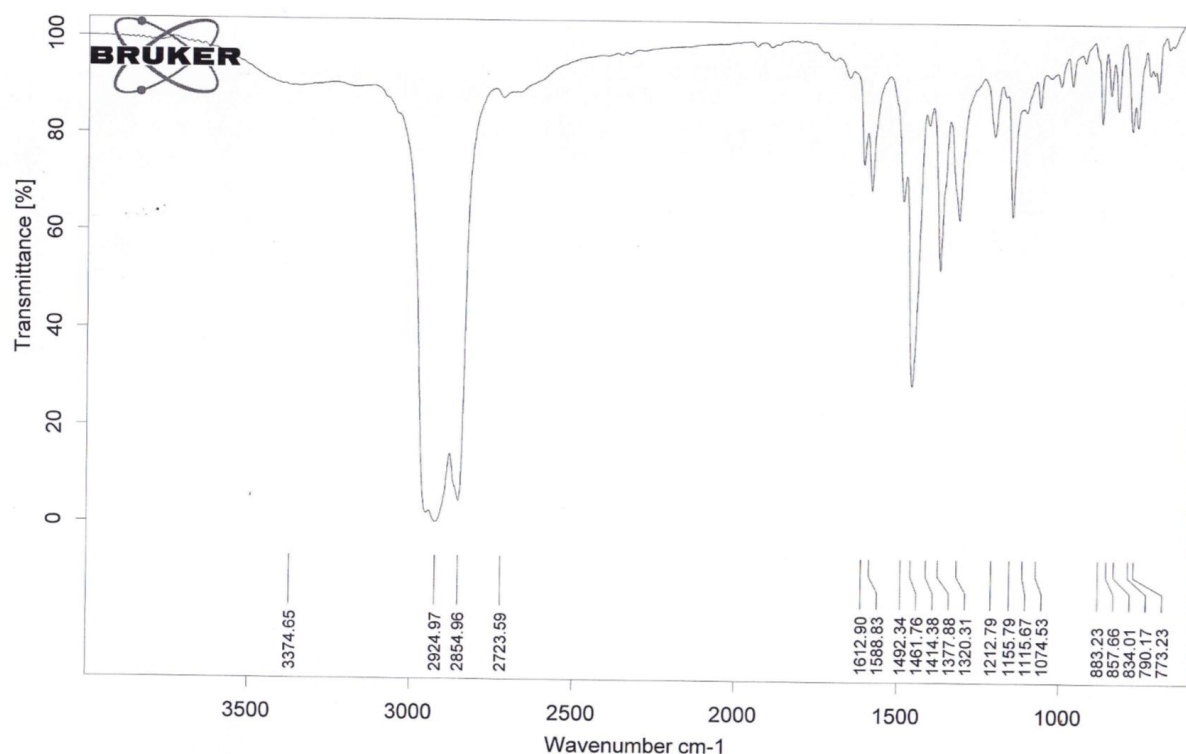


MALDI- MS of macrocycle **5b**

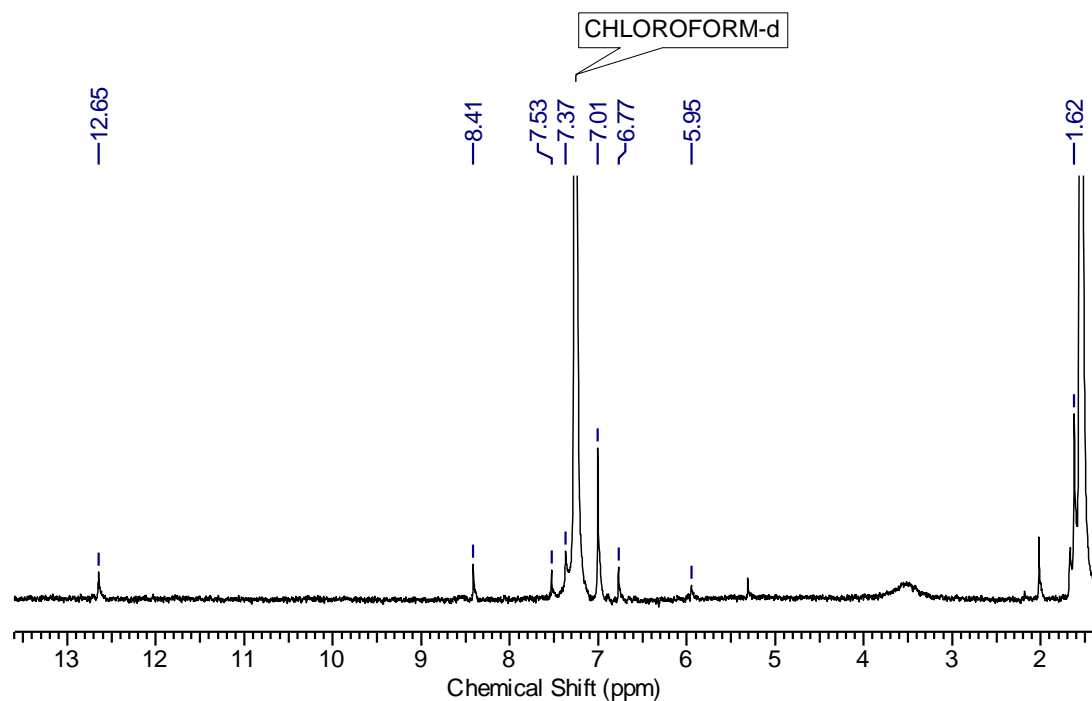
**Macrocycle 5c.**

The synthesis of **5c** was carried out by utilizing the same procedure of **5b**.

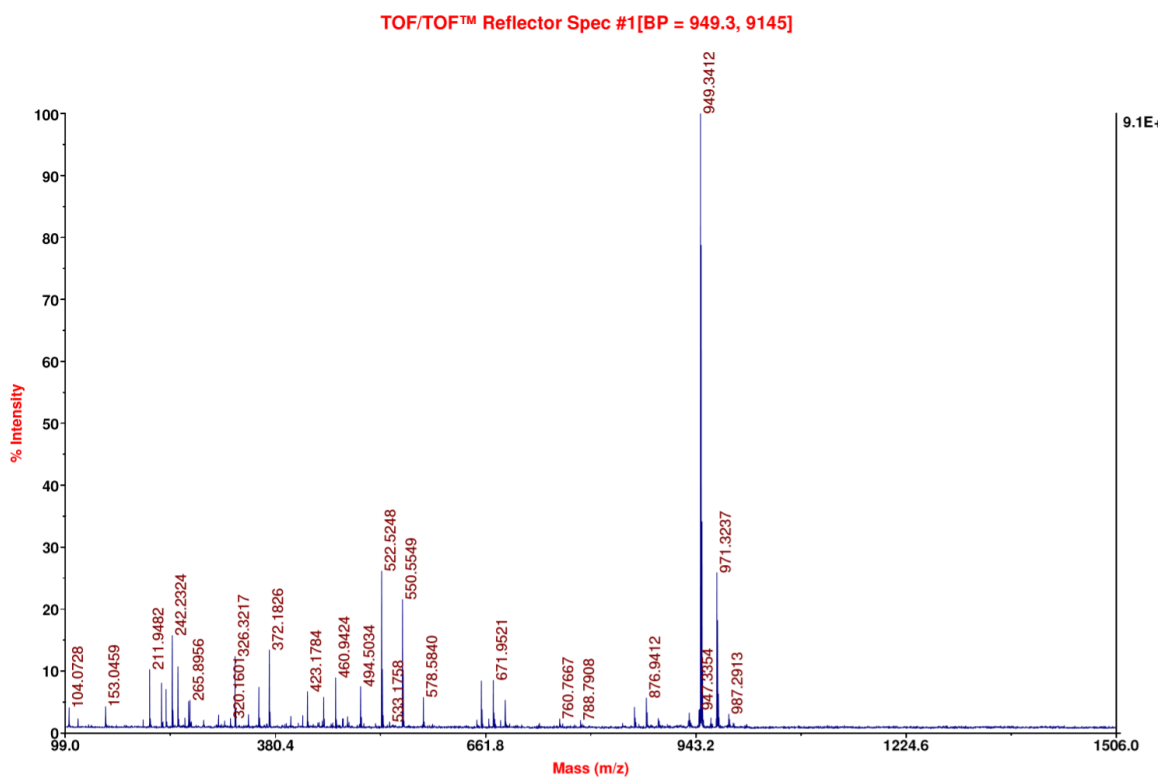
*Gem*-dimethylamine **4** (20 mg, 0.060 mmol), 2,5-dihydroxyterephthalaldehyde (**2c**, 10 mg, 0.06mmol), DCM (2 mL), ACN (2 mL), acetic acid (5  $\mu$ l). Orange coloured-needle shaped crystals. Yield: 0.025 g, (87%); m.p:  $>410$  °C; IR (Nujol,  $\nu$  (cm<sup>-1</sup>):1612, 1588, 1492; Due to solubility issue, we could not obtain clear <sup>1</sup>H NMR and <sup>13</sup>C NMR of **5c**, <sup>1</sup>H NMR (400 MHz, CDCl<sub>3</sub>)  $\delta$  (ppm): 12.65 (s, 4H), 8.41(s, CH=N, 4H), 7.54-5.9 (Ar, 28H), 1.62 (s, 36H); MALDI- MS ( $m/z$ ): [M+H]<sup>+</sup> is 949.34.



IR spectrum of macrocycle **5c**

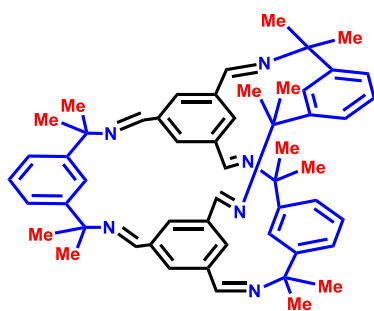


<sup>1</sup>H NMR spectrum of macrocycle **5c** (CDCl<sub>3</sub>, 400 MHz, 298 K). *Note:* Good quality NMR spectra could not be obtained owing to the poor solubility of **5b** in CDCl<sub>3</sub>. The solvent impurity peaks at  $\delta = 5.3$  and  $\delta = 1.5$  correspond to DCM and CDCl<sub>3</sub>-water, respectively.

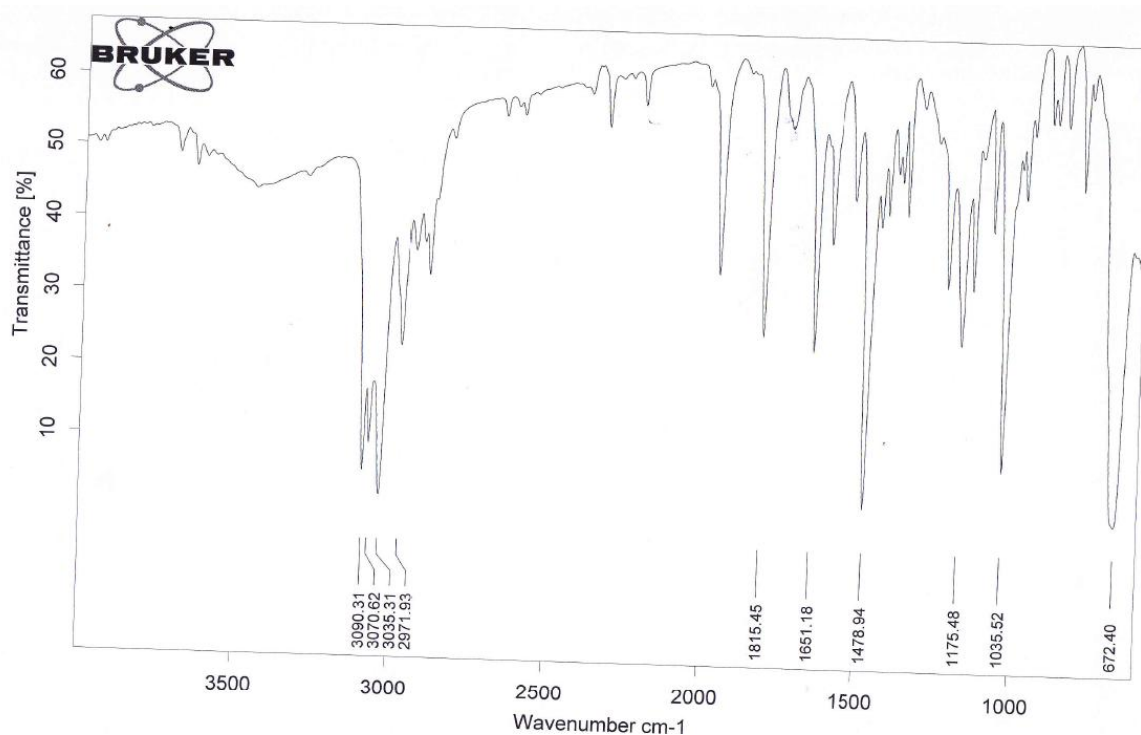


MALDI- MS of macrocycle **5c**

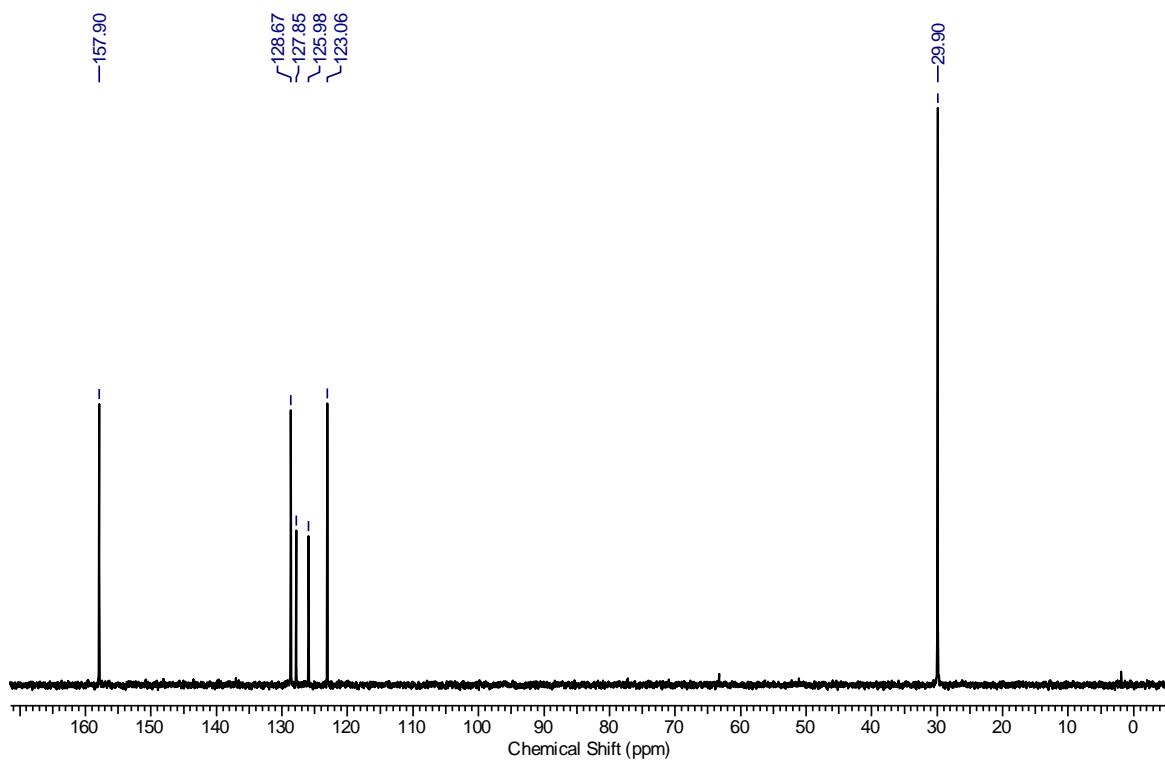
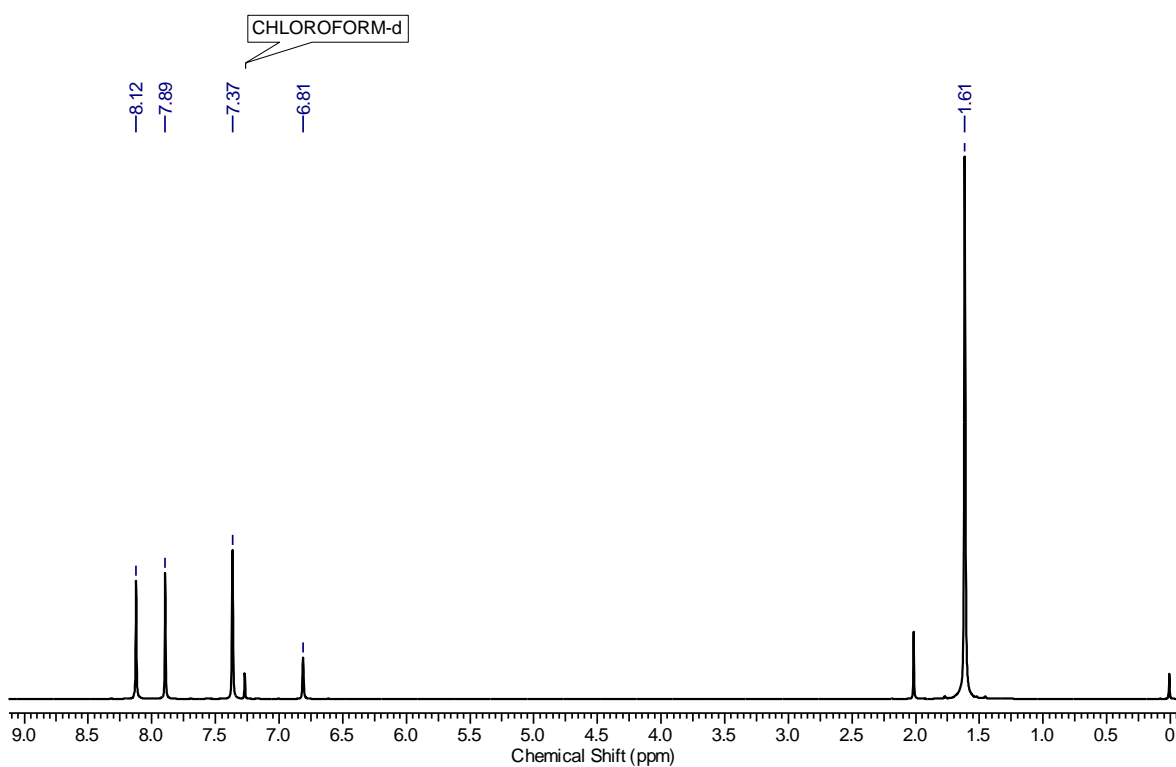


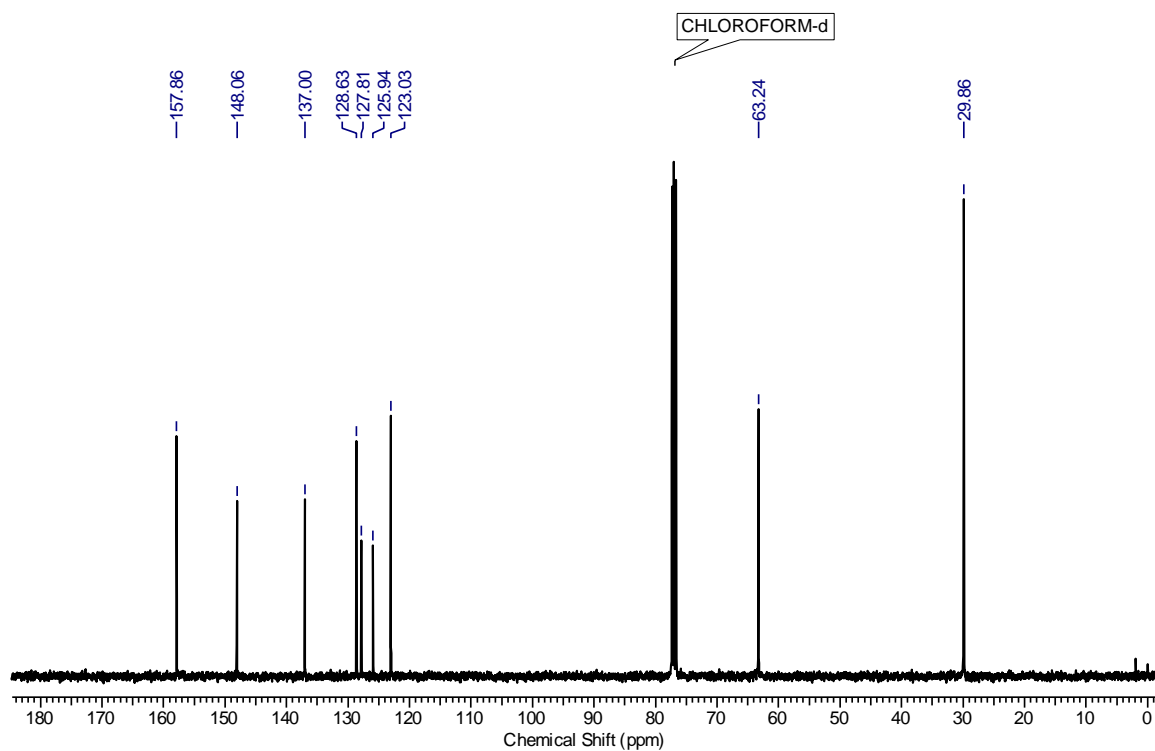
**Cage 7.**

A solution of **6** (0.030 g, 0.185 mmol) in ACN (7 mL) was added slowly to a solution of **1** (0.053 g, 0.277 mmol in 7 mL of ACN) taken in a 20 mL glass vial. After complete addition of **6**, a catalytic amount of acetic acid (50  $\mu$ l) was added and the reaction mixture was kept undisturbed at room temperature for 7 days to obtain colourless, block-shaped crystals. The crystals were filtered and then washed with ACN to remove impurities. The crystal suitable for X-ray crystallography was removed directly from the sample vial to obtain crystal structure of the product **7**. Yield: 0.068 g, (92%); m.p: >340  $^{\circ}$ C; IR (CHCl<sub>3</sub>,  $\nu$  (cm<sup>-1</sup>): 1651 (CH=N), 1478; <sup>1</sup>H NMR (400 MHz, CDCl<sub>3</sub>)  $\delta$  (ppm) : 8.12 (s, 6 H), 7.89 (s, 6 H), 7.37 (s, 9 H), 6.81 (s, 3 H), 1.61 (s, 36 H); <sup>13</sup>C NMR (100 MHz, CDCl<sub>3</sub>)  $\delta$  (ppm): 157.9, 148.1, 137.0, 128.6, 127.8, 125.9, 123.0, 63.2, 29.9; HRMS(*m/z*): calcd for C<sub>54</sub>H<sub>61</sub>N<sub>6</sub> [M+H]<sup>+</sup> 793.4952, found 793.4916.



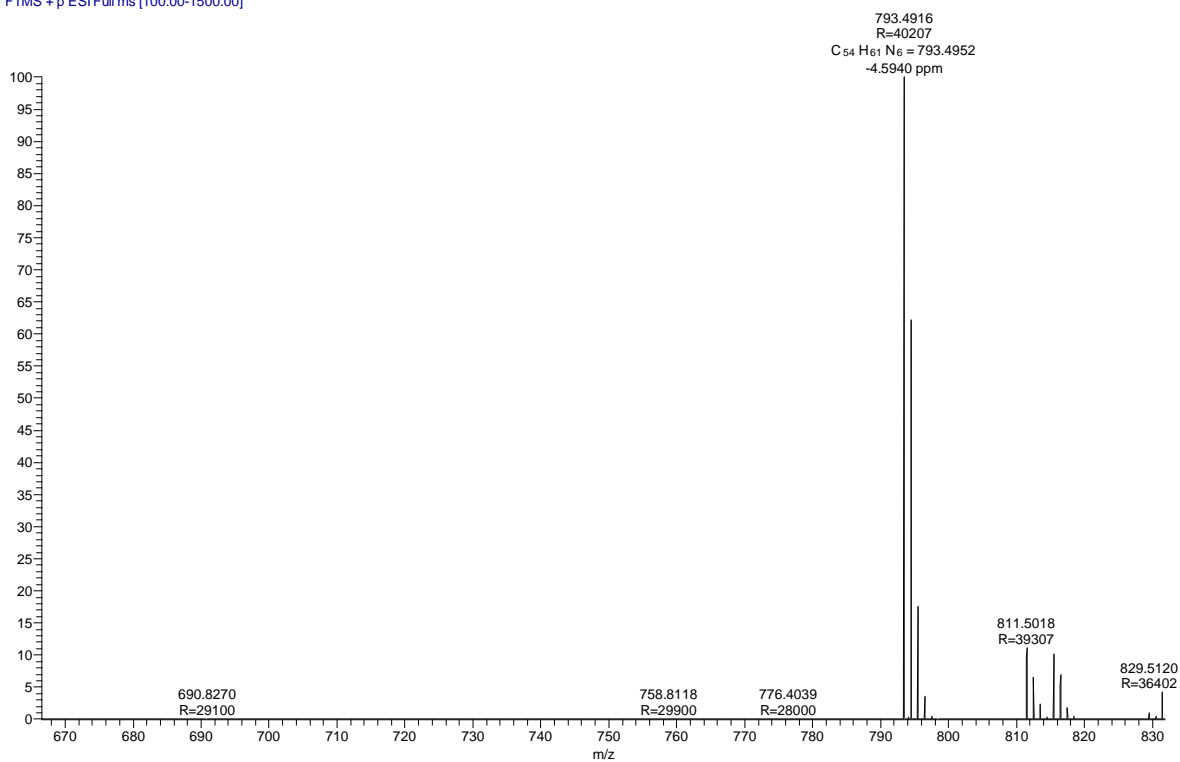
IR spectrum of cage 7



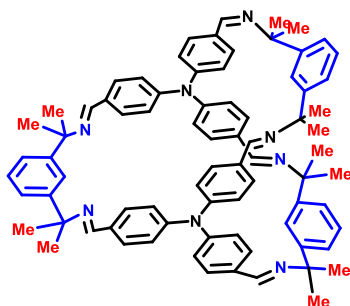


$^{13}\text{C}$  NMR spectrum of cage **7** ( $\text{CDCl}_3$ , 100 MHz, 298 K)

5\_170227154651 #203 RT: 0.90 AV: 1 NL: 5.76E8  
T: FTMS + p ESI Full ms [100.00-1500.00]



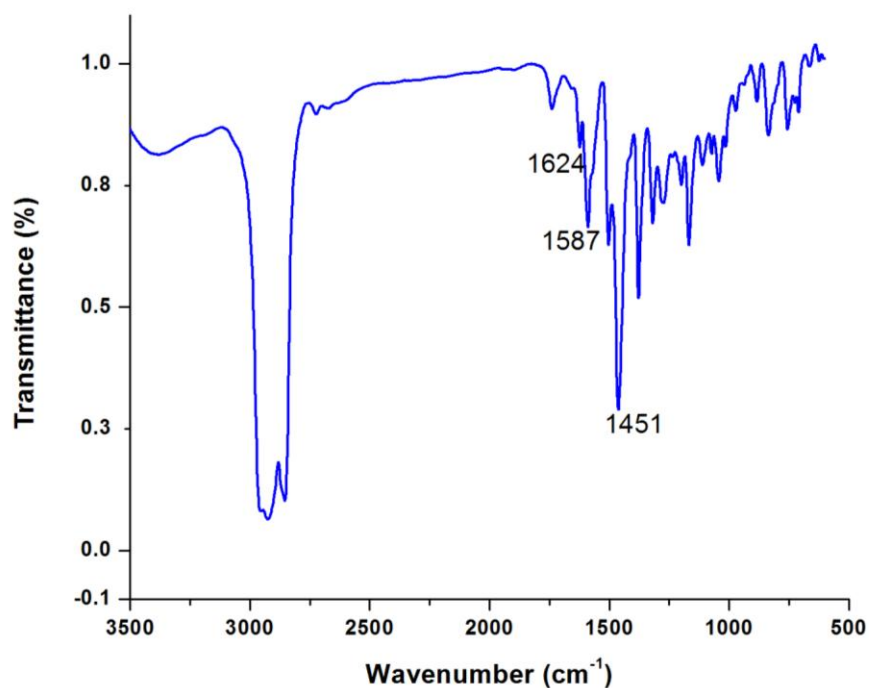
MS (HRMS) of cage **7**

**Cage 9.**

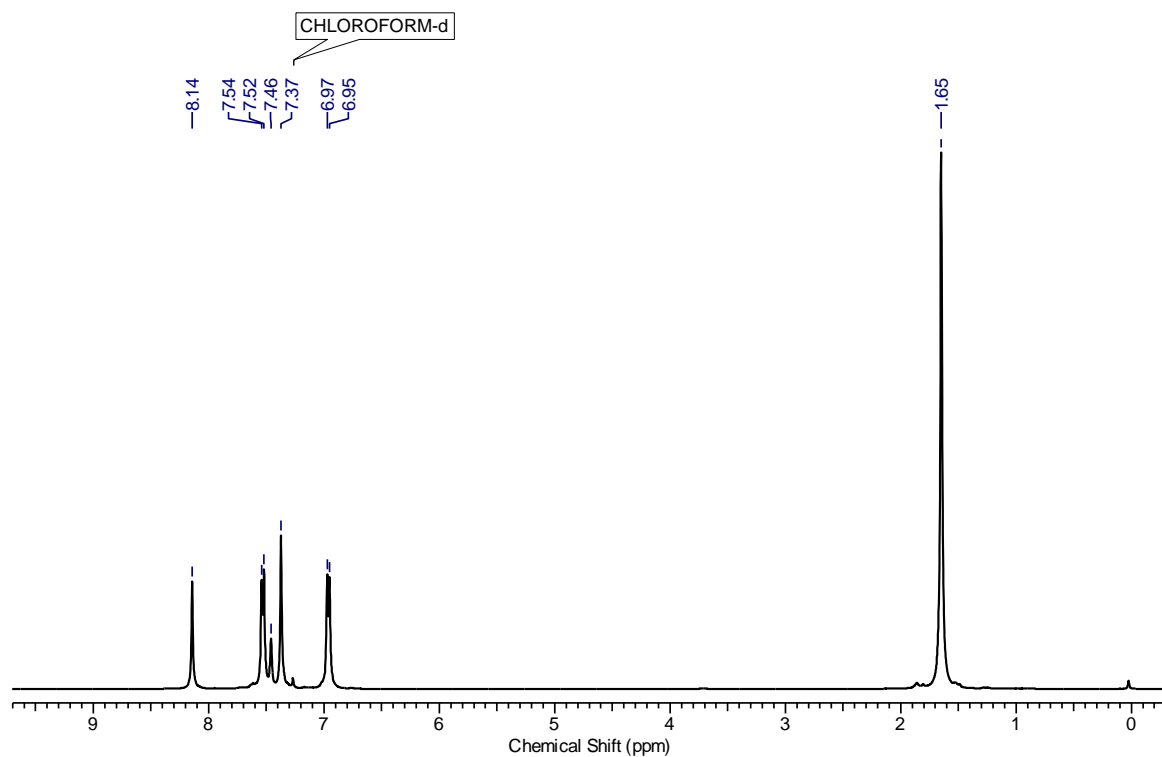
The synthesis of **9** was carried out by utilizing the same procedure of **7** using ACN as the solvent.

Gem-dimethylamine **1** (18.6 mg, 0.097 mmol), tris(4-formylphenyl)amine (**8**, 20 mg, 0.06mmol), ACN (10 mL), acetic acid (20  $\mu$ l). Pale-yellow coloured-needle shaped crystals.

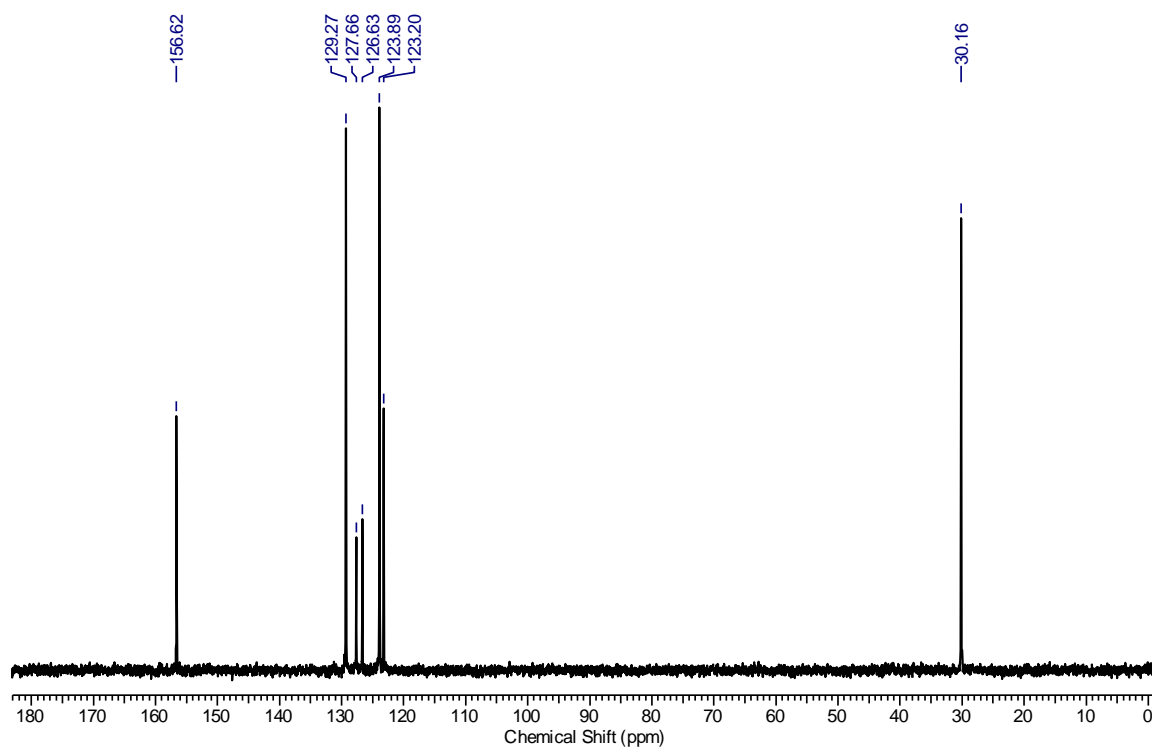
Yield: 0.030 g, (87%); m.p: >250 °C; IR (Nujol,  $\nu$  (cm<sup>-1</sup>): 1638 (CH=N), 1597; <sup>1</sup>H NMR (400 MHz, CDCl<sub>3</sub>)  $\delta$  (ppm) : 8.14 (s, 6H), 7.53 (d,  $J$  = 7.9 Hz, 12H), 7.46 (s, 3H), 7.37 (s, 9H), 6.96 (d,  $J$  = 7.9 Hz, 12H), 1.65 (s, 36H); <sup>13</sup>C NMR (100 MHz, CDCl<sub>3</sub>)  $\delta$  (ppm): 156.6, 148.3, 148.2, 132.0, 129.2, 127.6, 126.6, 123.8, 123.1, 62.7, 30.1; HRMS( $m/z$ ): calcd for C<sub>78</sub>H<sub>79</sub>N<sub>6</sub> [M+H]<sup>+</sup> 1127.6422, found 1127.6372.



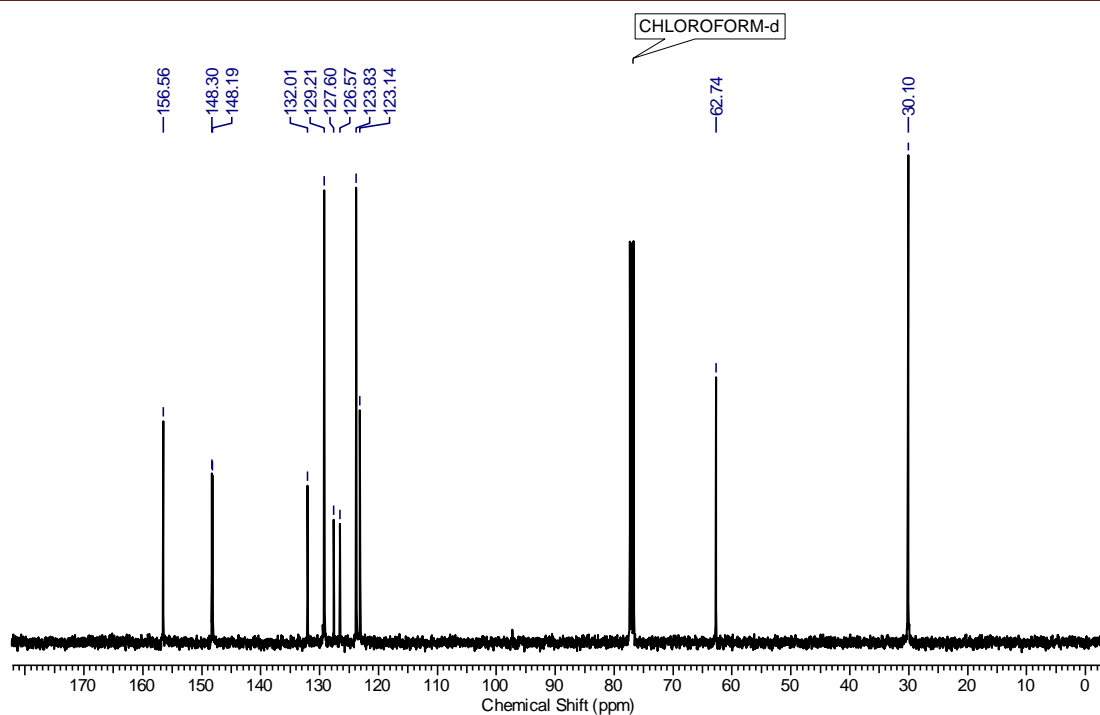
IR spectrum of cage **9**



$^1\text{H}$  NMR spectrum of cage **9** ( $\text{CDCl}_3$ , 400 MHz, 298 K)

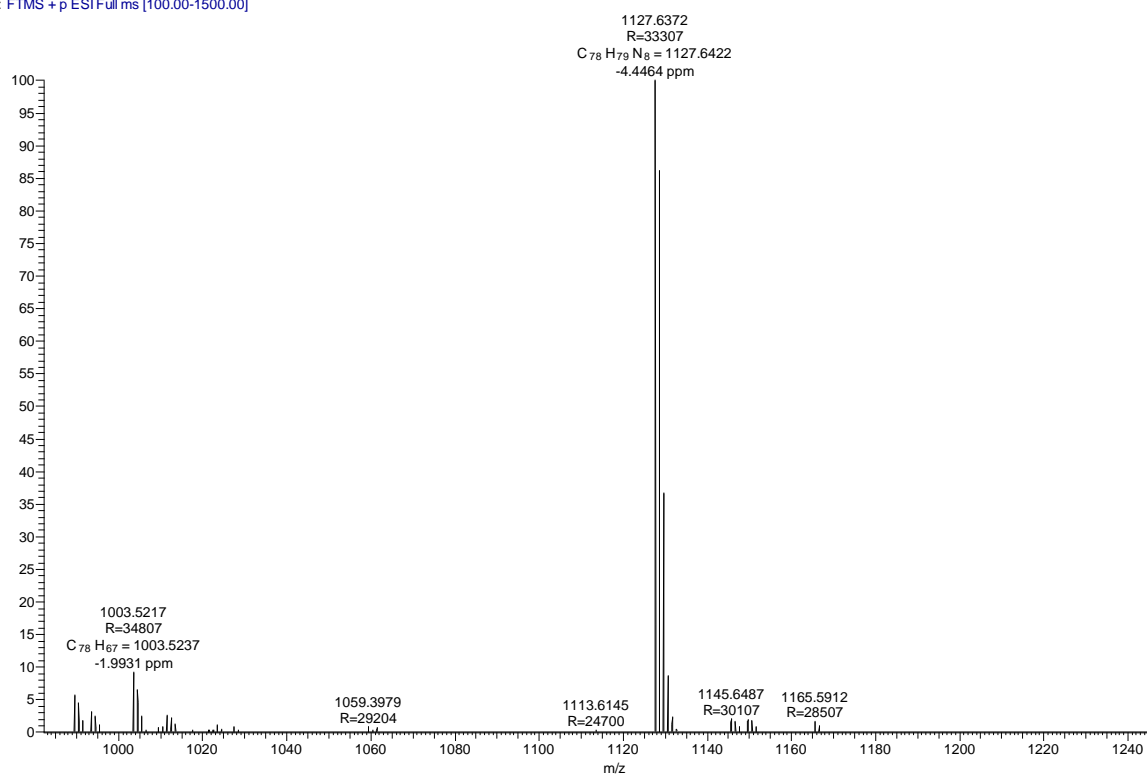


DEPT 135 spectrum of cage **9** ( $\text{CDCl}_3$ , 100 MHz, 298 K)



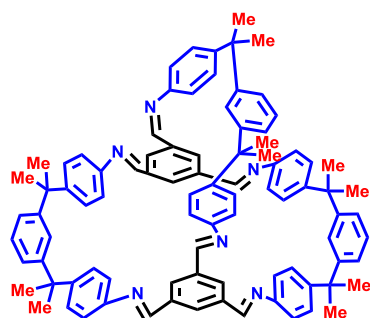
$^{13}\text{C}$  NMR spectrum of cage **9** ( $\text{CDCl}_3$ , 100 MHz, 298 K)

6\_170227154341 #103 RT: 0.46 AV: 1 NL: 4.24E7  
T: FTMS + p ESI Full ms [100.00-1500.00]



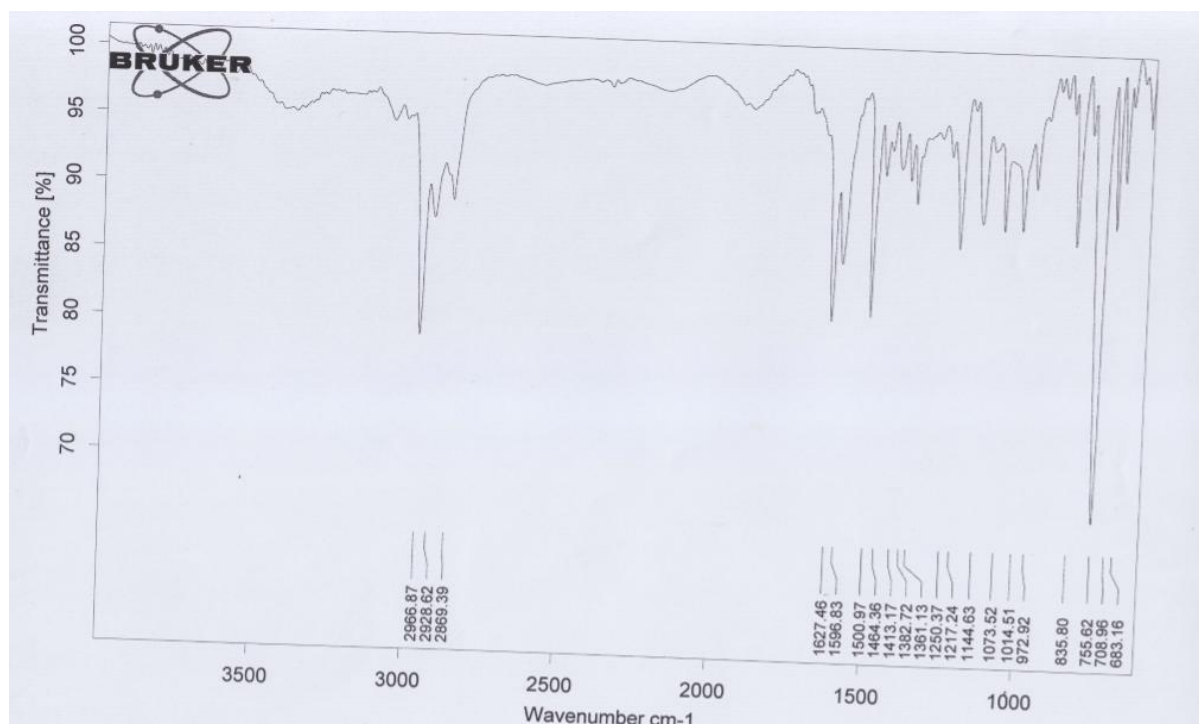
MS (HRMS) of cage **9**

## Cage 10.

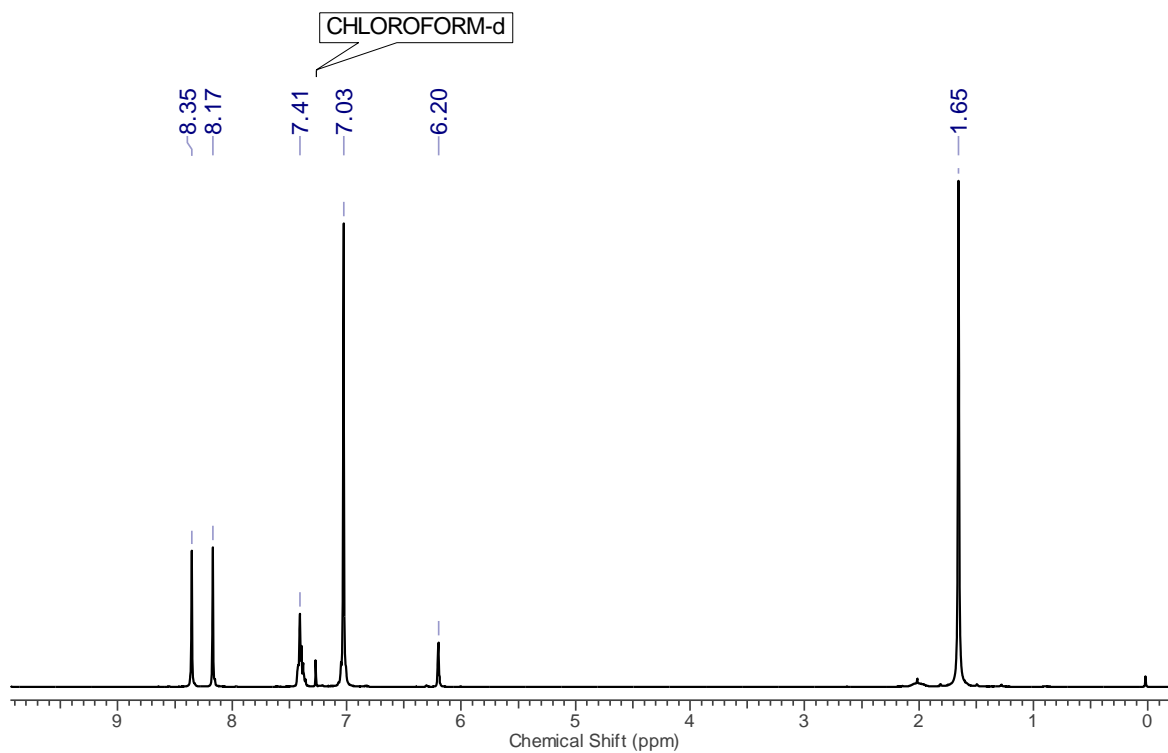


The synthesis of **10** was carried out by utilizing the same procedure of **7**.

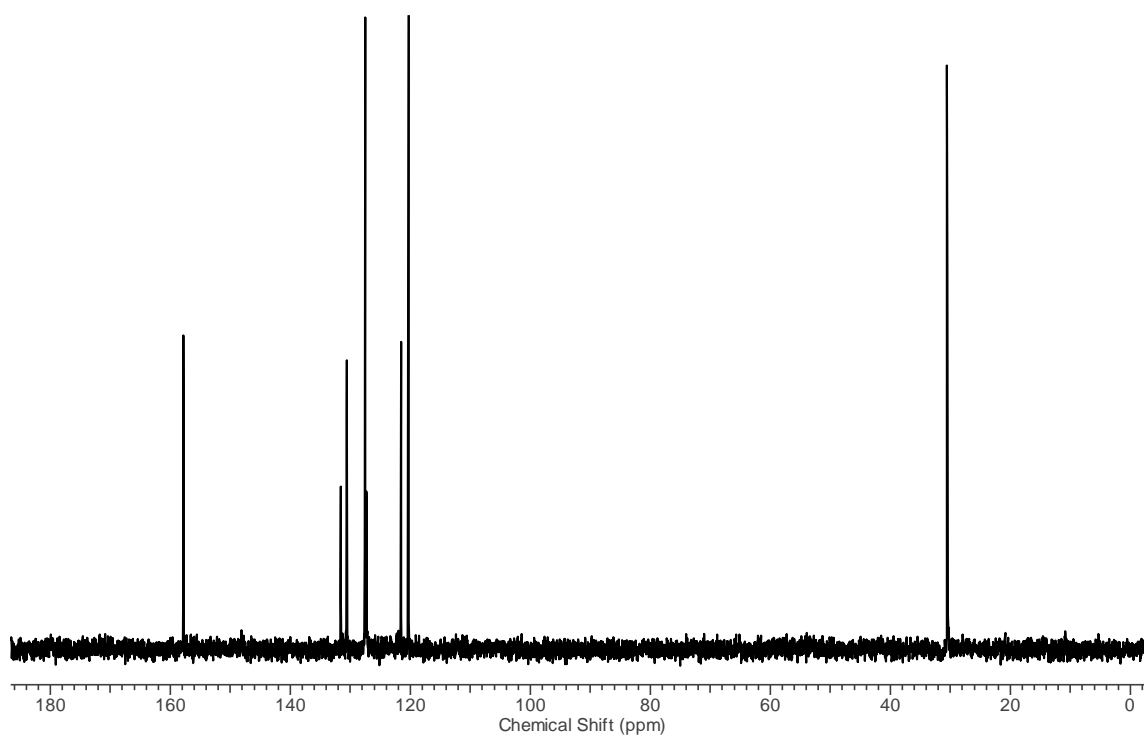
Benzene trialdehyde (**6**, 0.010 g, 0.061 mmol), *gem*-dimethylamine **4** (0.032 g, 0.092 mmol) ACN (14 mL), acetic acid (50  $\mu$ l). Pale yellow coloured, needle shaped crystals. The crystals were filtered and then washed with ACN. The crystal suitable for X-ray crystallography was removed directly from the sample vial to obtain crystal structure of the product **10**. Yield: 0.0336 g, (87%); m.p: 266-268  $^{\circ}$ C; IR ( $\text{CHCl}_3$ ,  $\nu$  ( $\text{cm}^{-1}$ ): 2966 (s), 2928, 2869, 1627 (CH=N), 1596 (Ar, C=C), 1500;  $^1\text{H}$  NMR (400 MHz,  $\text{CDCl}_3$ )  $\delta$  (ppm) : 8.35 (s, 6H), 8.17 (s, 6H), 7.45-7.35 (m, 9H), 7.03 (s, 24H), 6.20 (s, 3H), 1.65 (s, 36H);  $^{13}\text{C}$  NMR (100 MHz,  $\text{CDCl}_3$ )  $\delta$  (ppm): 157.7, 150.7, 149.1, 148.1, 137.1, 131.5, 130.6, 127.5, 127.2, 121.5, 120.3, 42.8, 30.5; HRMS( $m/z$ ): calcd for  $\text{C}_{90}\text{H}_{84}\text{N}_6$   $[\text{M}]^+$  1248.6752, found 1248.6787.



IR spectrum of cage **10**

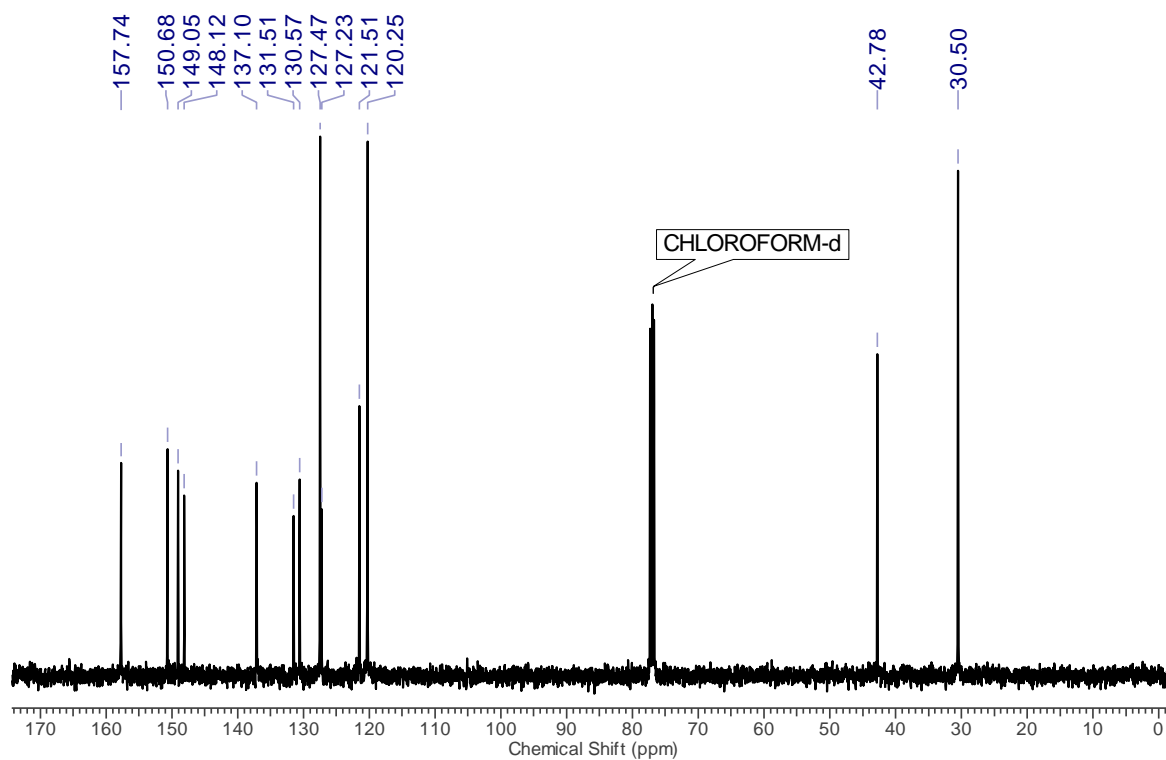


<sup>1</sup>H NMR spectrum of cage **10** (CDCl<sub>3</sub>, 400 MHz, 298 K)



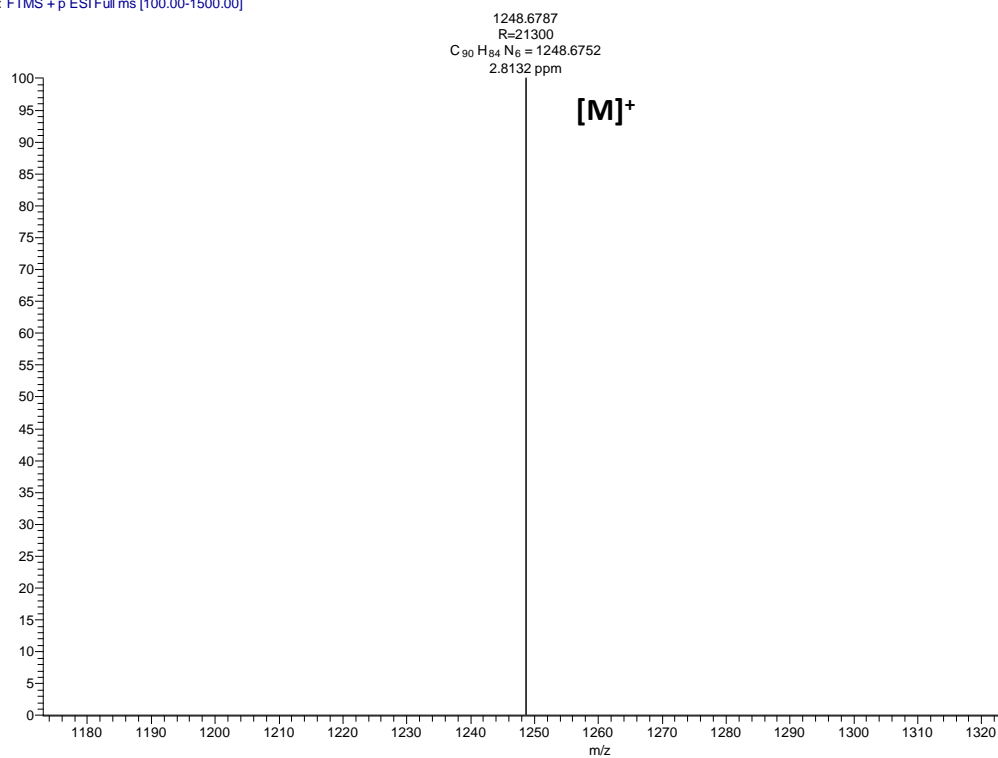
DEPT 135 spectrum of cage **10** (CDCl<sub>3</sub>, 100 MHz, 298 K)



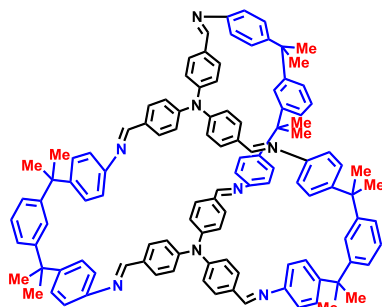


$^{13}\text{C}$  NMR spectrum of cage **10** ( $\text{CDCl}_3$ , 100 MHz, 298 K)

C-52\_160929123135 #256 RT: 1.14 AV: 1 NL: 3.07E4  
T: FTMS + p ESI Full ms [100.00-1500.00]



MS (HRMS) of cage **10**

**Cage 11.****Method 1 (Acetonitrile as a solvent):**

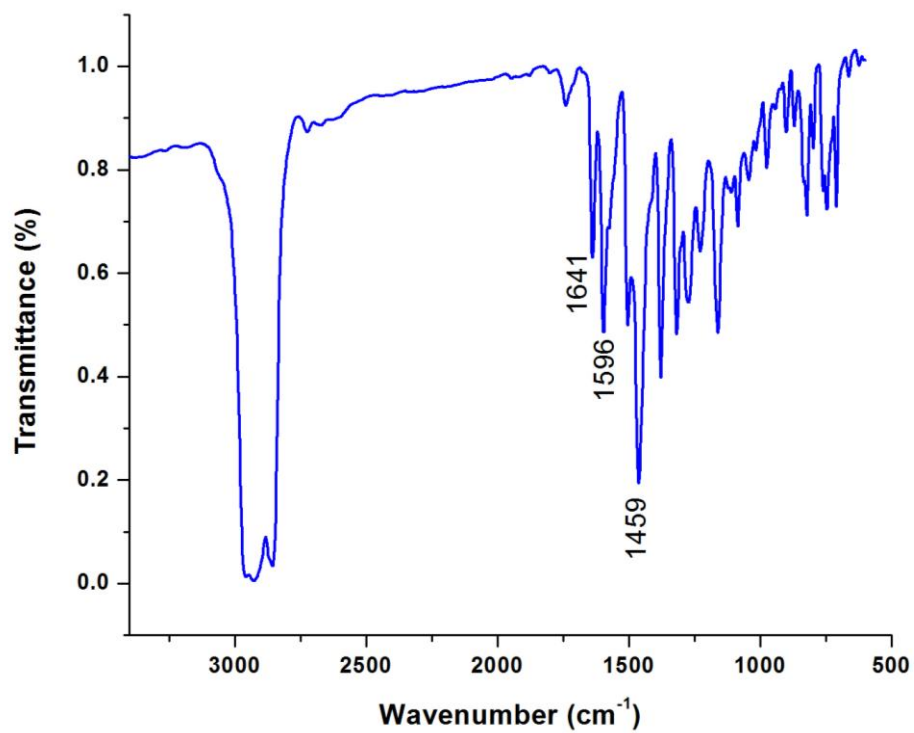
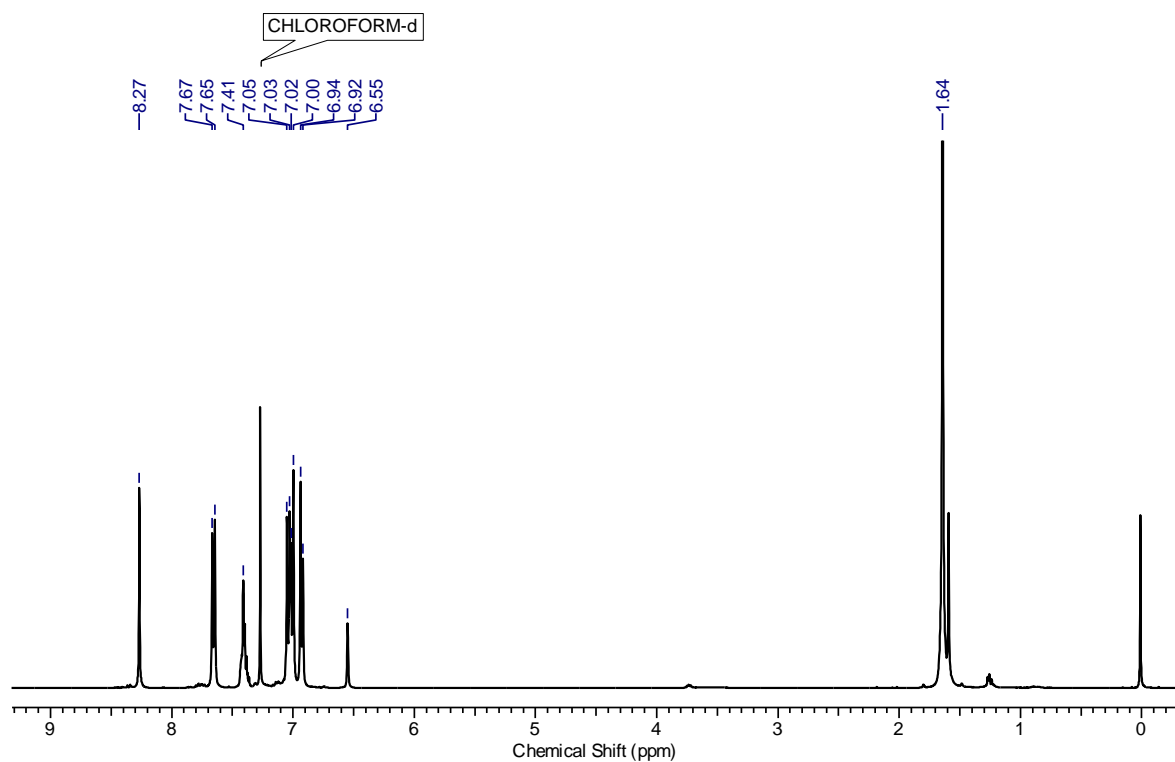
The synthesis of **11** was carried out by utilizing the same procedure of **7**.

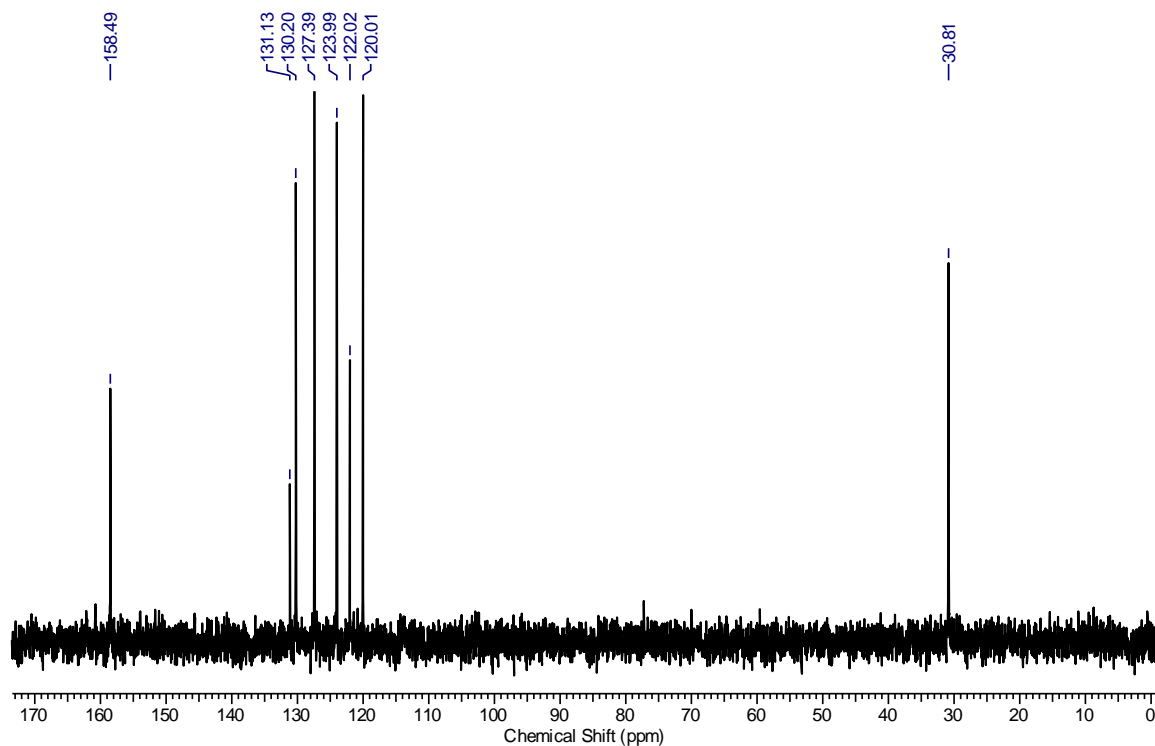
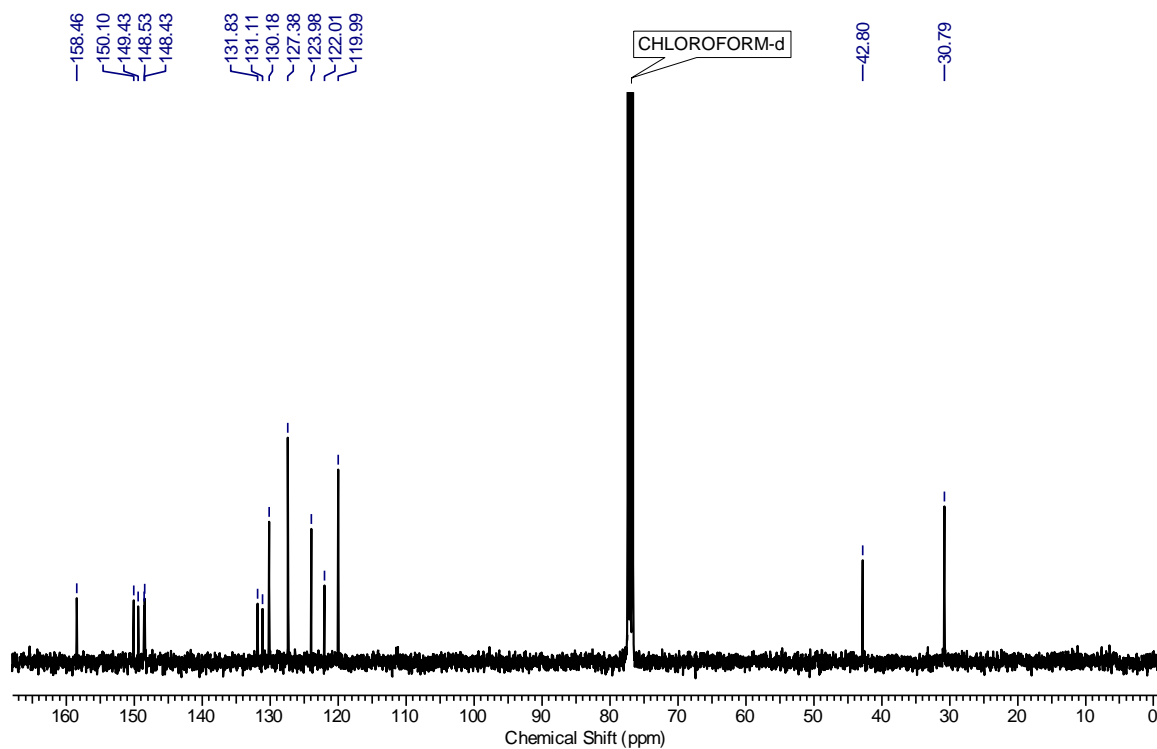
*Gem*-dimethylamine **4** (0.032g, 0.09 mmol), tris(4-formylphenyl)amine (**8**, 20 mg, 0.06mmol), ACN (14 mL), acetic acid (20  $\mu$ l). Pale yellow coloured, spongy-needle shaped crystals. The crystals were filtered and then recrystallised from ethanol/ $\text{CHCl}_3$  (2:1). Yield: 0.043 g, (89%); Above 350  $^\circ\text{C}$ , filmed; IR (Nujol,  $\nu$  ( $\text{cm}^{-1}$ )): 1636 (CH=N), 1595 (Ar, C=C);  $^1\text{H}$  NMR (400 MHz,  $\text{CDCl}_3$ )  $\delta$  (ppm) : 8.27 (s, 6H), 7.66 (d,  $J = 7.9$  Hz, 12H), 7.45 - 7.35 (m, 9H), 7.02 (dd,  $J = 8.5, 13.4$  Hz, 24H), 6.95 - 6.90 (m, 12H), 6.55 (s, 3H), 1.64 (s, 36H);  $^{13}\text{C}$  NMR (100 MHz,  $\text{CDCl}_3$ )  $\delta$  (ppm): 158.5, 150.1, 149.4, 148.5, 148.4, 131.8, 131.1, 130.2, 127.4, 124.0, 122.0, 120.0, 42.8, 30.8; MALDI-MS( $m/z$ ): calcd for  $\text{C}_{90}\text{H}_{84}\text{N}_6$   $[\text{M}]^+$  1583.8, found 1584.0385.

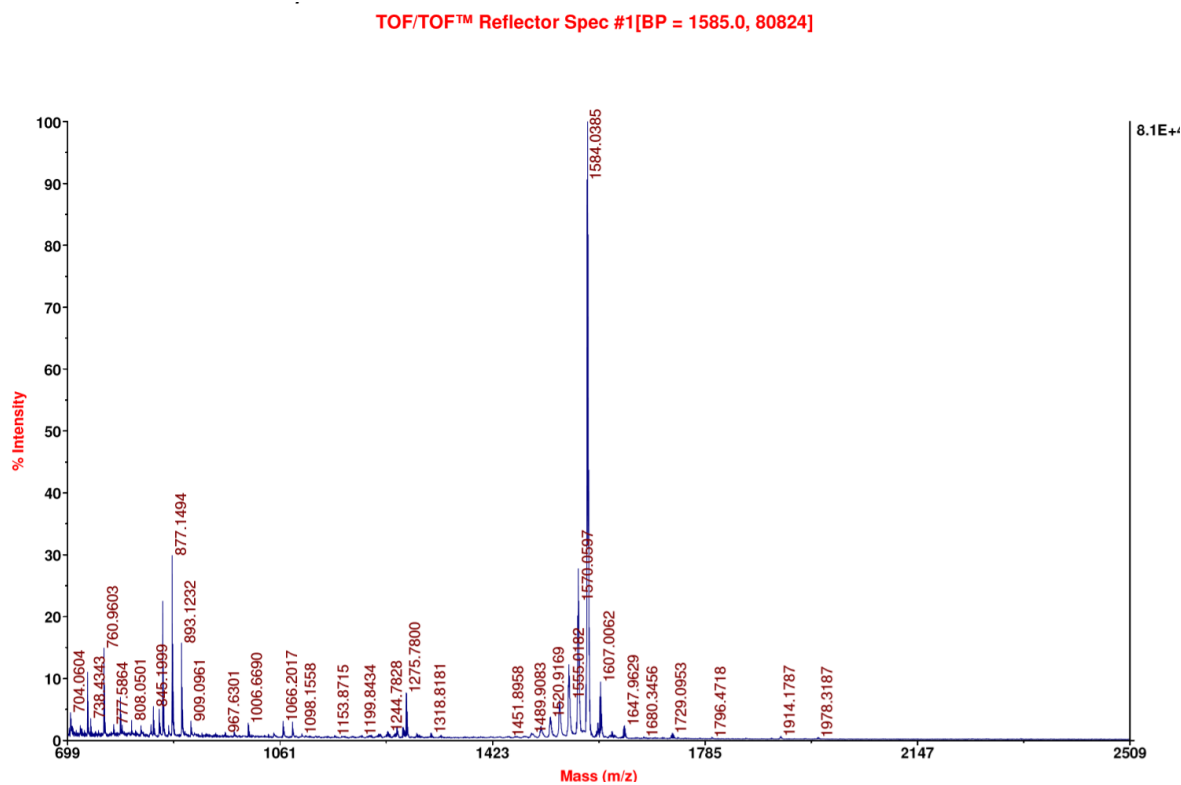
**Method 2 ( $\text{CHCl}_3$  as a solvent and ethanol as anti-solvent):**

Reaction was performed in 20ml glass vial containing a screw cap.

*gem*-dimethylamine (**4**, 0.032g, 0.09 mmol) was added to a solution of tris(4-formylphenyl)amine (**8**, 20 mg, 0.06mmol) in  $\text{CHCl}_3$  (7mL) at ambient temperature. The clear solution formed was kept without disturbance. After 24h, absolute ethanol (10ml) was added with slight shaking to get homogeneous solution. Then, the solution was kept without stirring for 7 days to obtain **11** as block shaped yellow crystals in good yields; 0.042 g (87%). *Note:* Anti solvent ethanol was added for the purpose of getting macrocycles/cages as good quality crystals.

IR spectrum of cage **11**<sup>1</sup>H NMR spectrum of cage **11** (CDCl<sub>3</sub>, 400 MHz, 298 K)

DEPT 135 spectrum of cage **11** ( $\text{CDCl}_3$ , 100 MHz, 298 K) $^{13}\text{C}$  NMR spectrum of cage **11** ( $\text{CDCl}_3$ , 100 MHz, 298 K)

MALDI- MS of cage **11**

## Macrocyclization under high concentrations.

### 1. Synthesis of macrocycle **3** in 1 M concentration:

To a 5 mL glass vial containing compound **2a** (0.136 g, 1.01mmol) and DCM (1 mL), **1** (0.199 mL, 1.01mmol) was added. The resultant clear solution was slowly hand-shaken for ~ 5-10 minutes, and then acetic acid (10  $\mu$ l) was added to catalyze the reaction. The vial was tightly capped and kept undisturbed, without stirring at ambient temperature. After 24 h, the cap was partially opened to allow slow evaporation of solvent, over time, to afford crystals of **3**. The crystals were filtered with the aid of ACN to obtain first crop. The filtrate was concentrated *in vacuo* and the residue obtained was triturated with ACN to get a second crop. The combined yield of the crystalline material was 0.240 g (81%).

### 2. Synthesis of macrocycle **5a** in 0.6 M concentration:

To a 5 mL glass vial containing compound **2a** (0.08g, 0.596 mmol) and DCM (1 mL), **4** (0.205 g, 0.596 mmol) was added. The resultant clear solution was slowly hand-shaken for ~ 5-10 minutes, and then acetic acid (10  $\mu$ l) was added to catalyze the reaction. The

vial was tightly capped and kept undisturbed, without stirring at ambient temperature. After 36 h, the solution containing crystals was evaporated under reduced pressure and the residue was directly recrystallised from *o*-dichlorobenzene to afford yellow coloured plate-like crystal of **5a**. 0.235 g (89%).

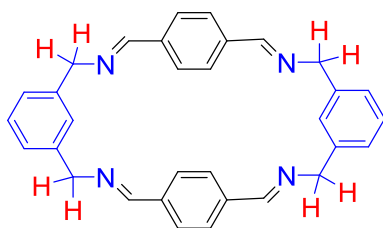
### 3. Synthesis of Cage 10 in 0.5 M concentration:

To a 5 mL glass vial containing compound **6** (0.0405 g, 0.2467 mmol) and DCM (0.5 mL), **4** (0.129g, 0.37 mmol) was added. The resultant clear solution was slowly hand-shaken for ~ 5-10 minutes, followed by addition of acetic acid (5  $\mu$ l). Then, the vial was tightly capped and kept without stirring at ambient temperature for 36 h. After that, two drops of ethanol was added and the initially formed precipitate was dissolved by gentle shaking of the vial. The solution thus obtained was kept without stirring for 3 days to obtain **10** as pale yellow coloured crystals. Yield: 0.140 g (90%)

### 4. Synthesis of Cage 9 in 0.12 M concentration:

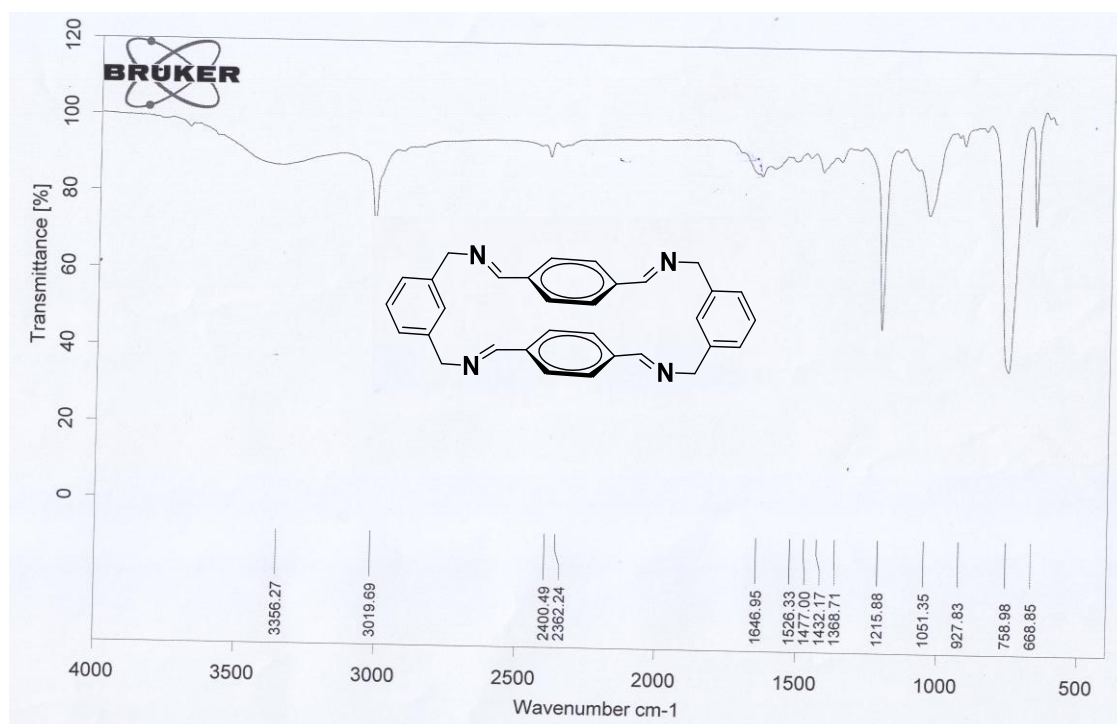
To a 5 mL glass vial containing compound **8** (0.040 g, 0.1214 mmol) in  $\text{CHCl}_3$  (1 mL), **1** (0.035 g, 0.182 mmol) was added. The resultant clear solution was slowly hand-shaken for ~ 5 minutes, followed by which acetic acid (5  $\mu$ l) was added to catalyze the reaction. Then, the vial was tightly capped and kept without stirring at ambient temperature for 36. After that, ethanol (2mL) was added and the initially formed precipitate was dissolved by gentle shaking of the vial. The solution thus obtained was kept without stirring for 3 days to obtain crystals of **9**. Yield: 0.056 g (82%). The crystal suitable for X-ray crystallography was removed directly from the sample vial to obtain crystal structure of the macrocycle **9**.

*Note:* Anti solvent ethanol was added for the purpose of getting macrocycles/cages as good quality crystals.

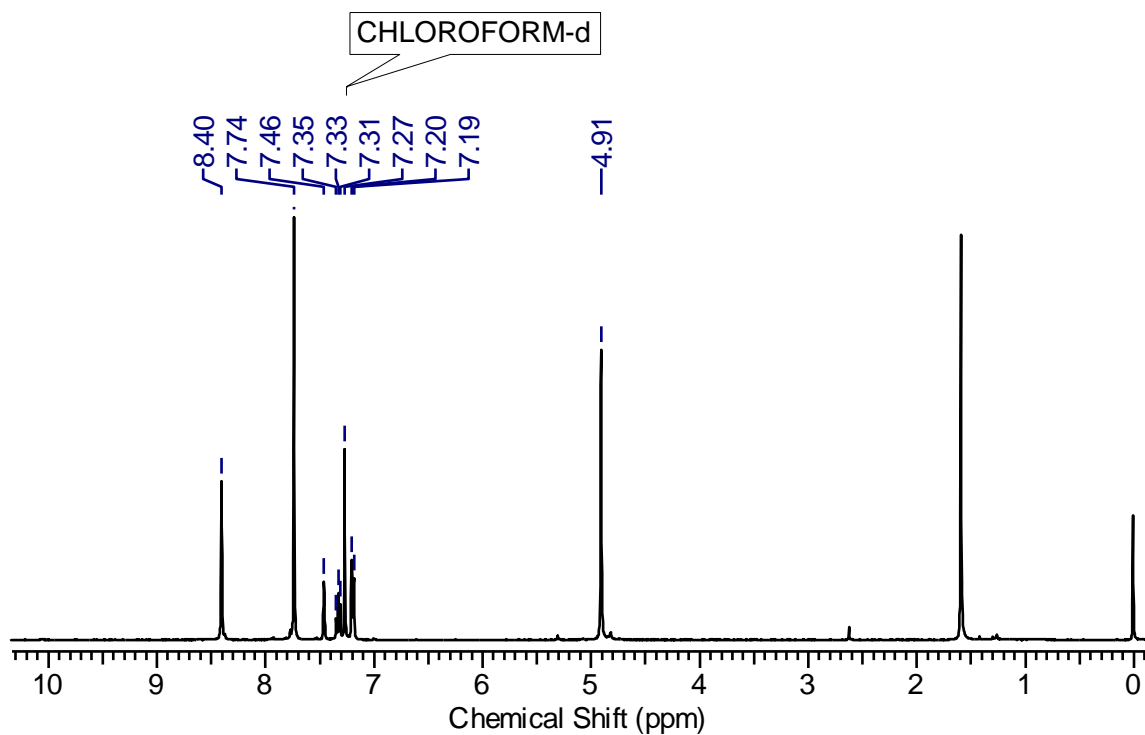
**Preparation of macrocycle 3a under high dilute condition.**

Macrocycle-**3a** was prepared by following the reported high dilution procedure<sup>40</sup> (0.02 M in ACN, 48 h ).

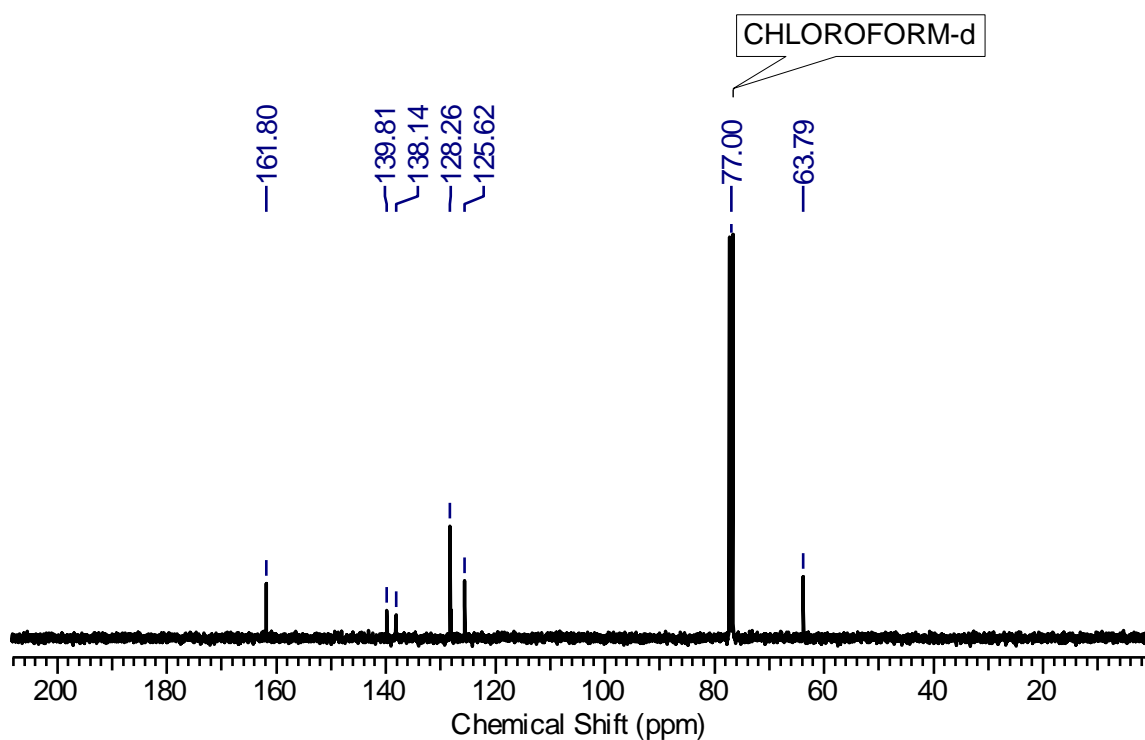
IR (CHCl<sub>3</sub>,  $\nu$ ): 1646(CH=N) cm<sup>-1</sup>; <sup>1</sup>H NMR (400MHz, CDCl<sub>3</sub>)  $\delta$ (ppm) : 8.40 (s, 4H), 7.74 (s, 8H), 7.19-7.46 (m, 8H), 4.91 (s, 8H); <sup>13</sup>C NMR (100MHz, CDCl<sub>3</sub>)  $\delta$ (ppm): 161.8, 139.81, 138.14, 128.26, 125.62, 63.79; MALDI-MS(m/z): calcd for C<sub>32</sub>H<sub>28</sub>N<sub>4</sub>, [M+H]<sup>+</sup>, [M+Na]<sup>+</sup>, [M+K]<sup>+</sup> 469.2314, 491.2212, 507.1951 found 469.1574, 491.1386, 507.1194.



IR spectrum of macrocycle **3a**



<sup>1</sup>H NMR spectrum of macrocycle **3a** (CDCl<sub>3</sub>, 400 MHz, 298 K)

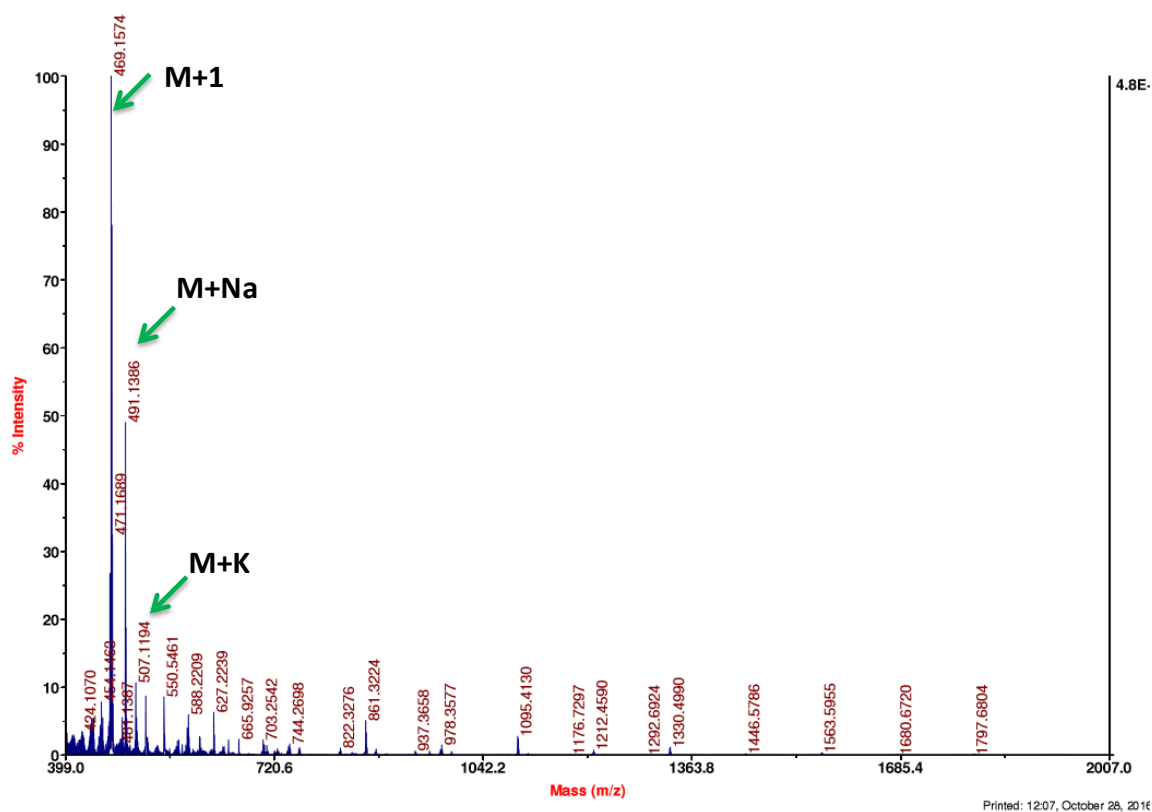


<sup>13</sup>C NMR spectrum of macrocycle **3a** (CDCl<sub>3</sub>, 100 MHz, 298 K)



AB Sciex TOF/TOF™ Series Explorer™ 72085

TOF/TOF™ Reflector Spec #1=&gt;AdvBC(32,0.5,0.1)=&gt;NR(2.00)[BP = 469.2, 48197]

MALDI-MS of macrocycle **3a**

## 4.7 X-ray Crystallography:

### Single crystal X-ray diffraction studies

X-ray intensity data measurements of macrocycles **7**, **9** and **10** were carried out on a Bruker D8 VENTURE Kappa Duo PHOTON II CPAD diffractometer equipped with Incoatech multilayer mirrors optics. The intensity measurements were carried out with Cu micro-focus sealed tube diffraction source ( $\text{CuK}\alpha = 1.54178 \text{ \AA}$ ) at 100(2) K temperature. The X-ray generator was operated at 50 kV and 1.1 mA. A preliminary set of cell constants and an orientation matrix were calculated from three sets of 40 frames. Data were collected with  $\omega$  scan width of  $0.5^\circ$  at different settings of  $\varphi$  and  $2\theta$  keeping the sample-to-detector distance fixed at 5.00 cm. The X-ray data collection was monitored by APEX3 program (Bruker, 2016).<sup>47</sup> On the other hand X-ray intensity data measurements of macrocycles **3** and **5a** were carried out on a Bruker SMART APEX II CCD diffractometer with graphite monochromatized ( $\text{MoK}\alpha =$

0.71073 Å) radiation at 100(2) K. The X-ray generator was operated at 50 kV and 30 mA. A preliminary set of cell constants and an orientation matrix were calculated from three sets of 36 frames. Data were collected with  $\omega$  scan width of  $0.5^\circ$  at different settings of  $\varphi$  and  $2\theta$  keeping the sample-to-detector distance fixed at 5.00 cm. The X-ray data collection was monitored by APEX2 program (Bruker, 2006).<sup>48</sup> All the data were corrected for Lorentzian, polarization and absorption effects using SAINT and SADABS programs (Bruker, 2016). SHELX-97 was used for structure solution and full matrix least-squares refinement on  $F^2$ .<sup>49,50</sup> All the hydrogen atoms were placed in geometrically idealized position and constrained to ride on the parent atoms. An ORTEP III<sup>3</sup> view of the compounds was drawn with 50% probability displacement ellipsoids and H atoms are shown as small spheres of arbitrary radii.

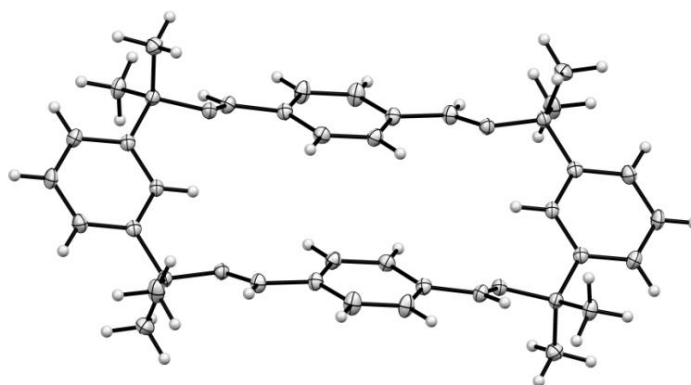


**Fig. 4.40:** ORTEP diagram of the macrocycle **3** (thermal ellipsoids are shown in 50% probability level).

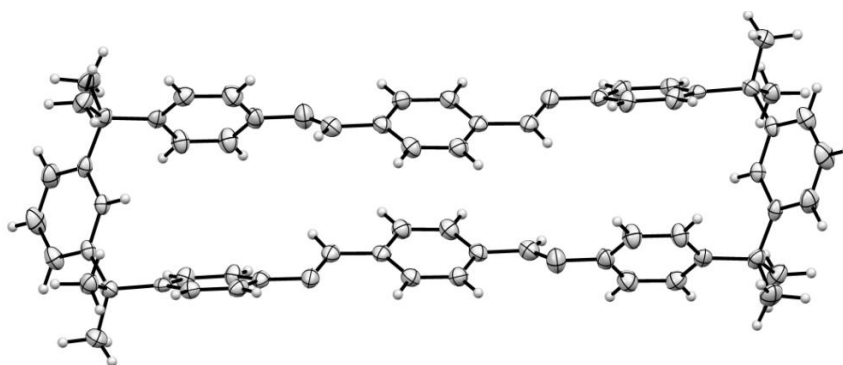


**Fig. 4.41:** ORTEP diagram of the macrocycle **5** (thermal ellipsoids are shown in 50% probability level).

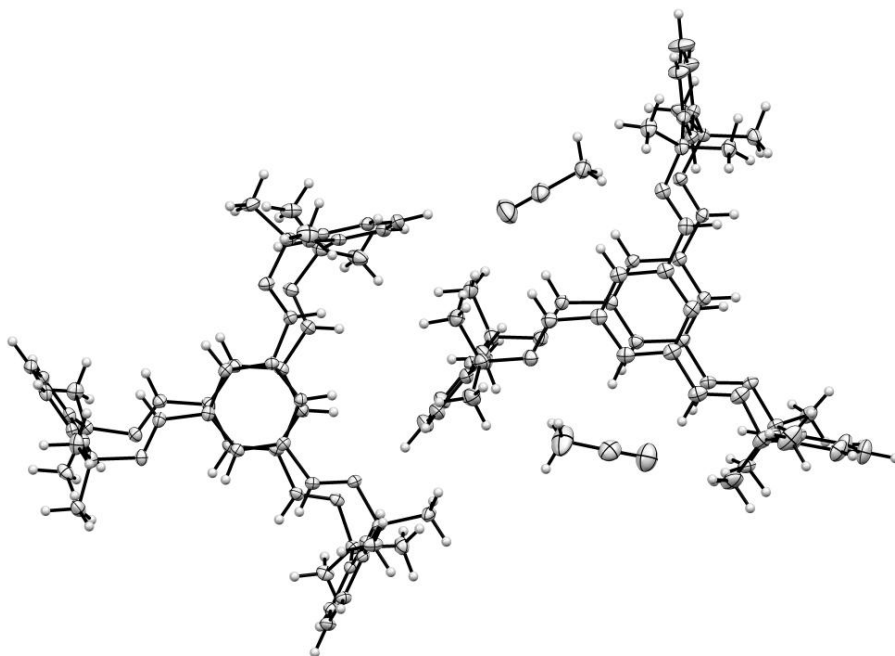


**Fig. 4.42:** ORTEP diagram of the two conformational isomers of macrocycle **7** with acetonitrile (thermal ellipsoids are shown in 50% probability level).

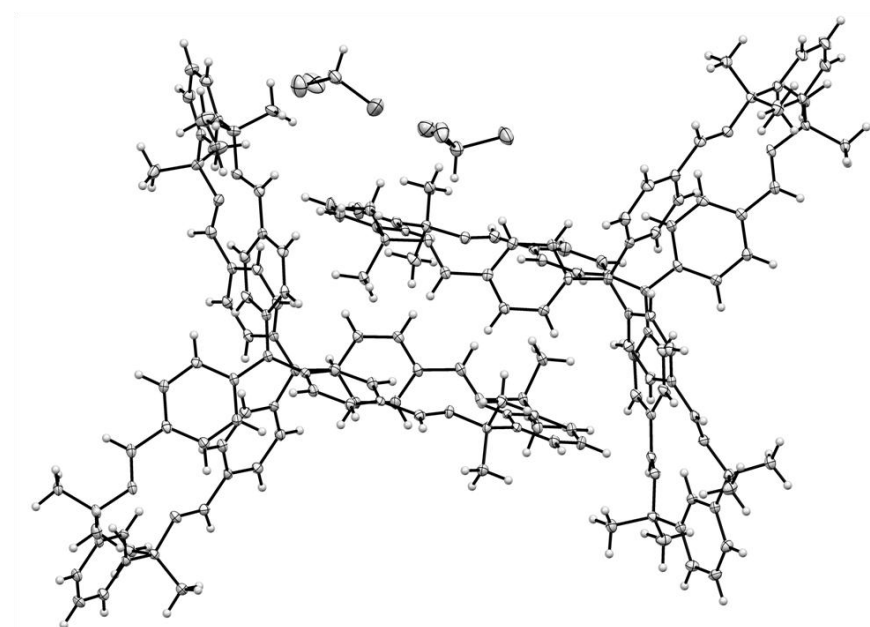


**Fig. 4.43:** ORTEP diagram of the two conformational isomers of macrocycle **9** with chloroform (thermal ellipsoids are shown in 50% probability level).

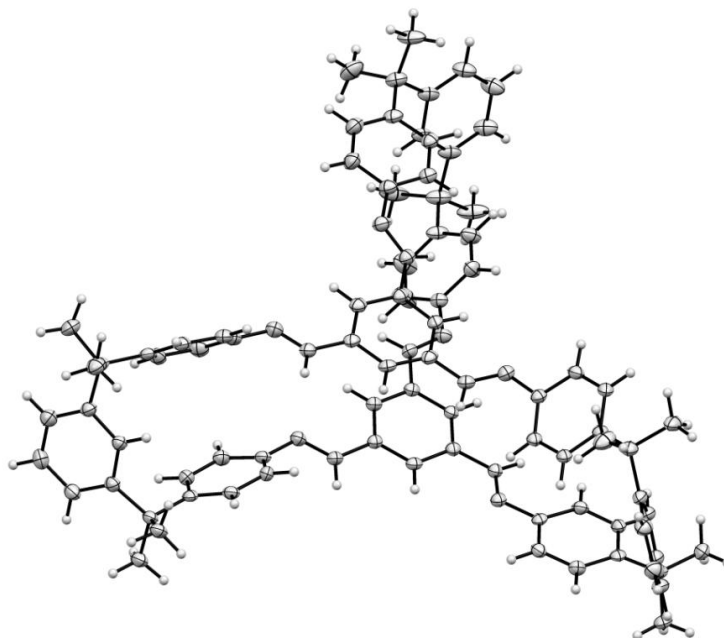


**Fig. 4.44:** ORTEP diagram of the macrocycle **10** (thermal ellipsoids are shown in 50% probability level).

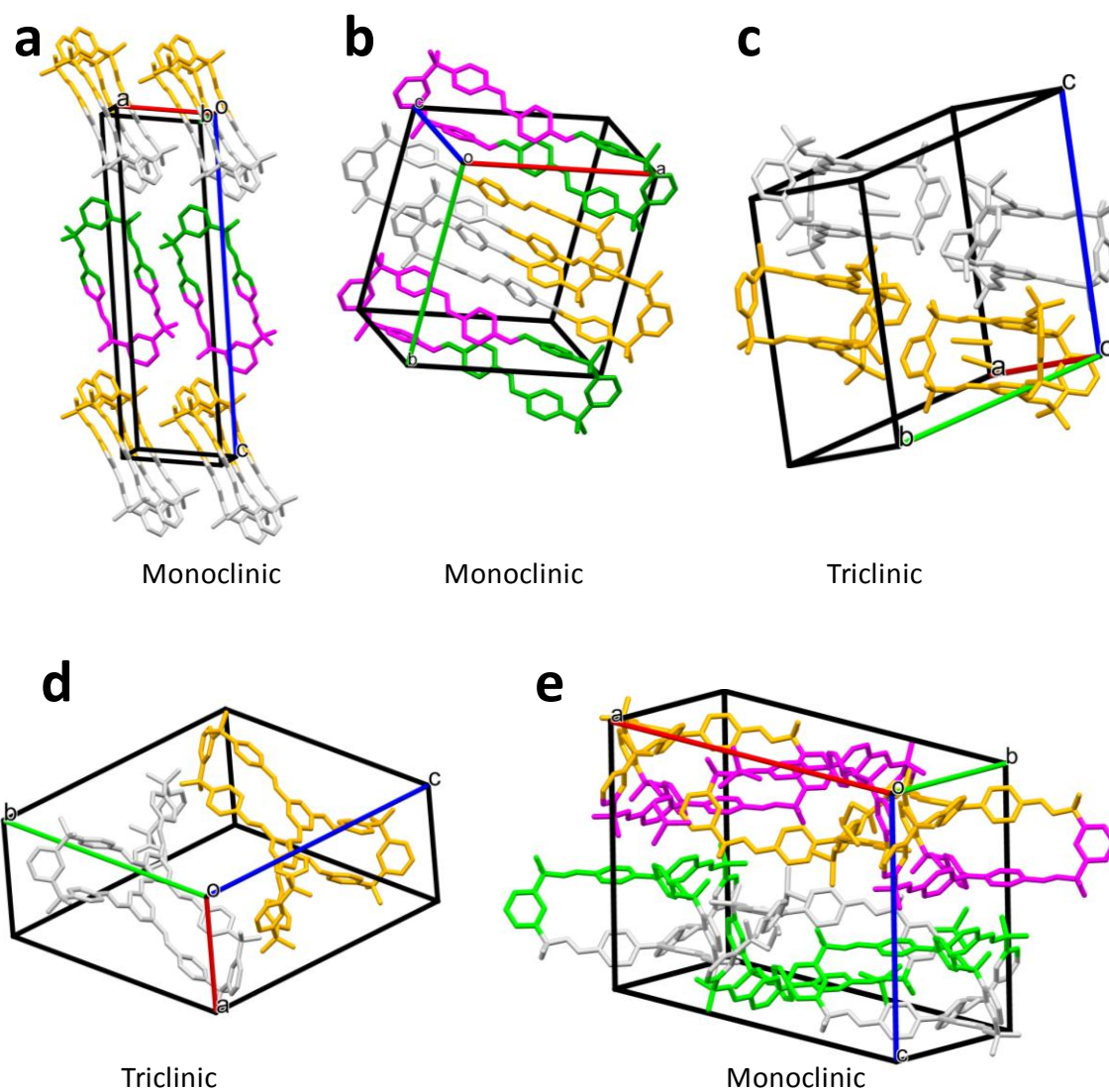


**Fig. 4.45:** Unit cells of macrocycle/cages with symmetry operation. a) Macrocycle-3, b) macrocycle-5a, c) cage-7, d) cage-10, e) cage-9.

#### 4.8 References

1. Borisova, N. E.; Reshetova, M. D.; Ustynyuk, Y. A. *Chem. Rev.* **2007**, *107* (1), 46-79.
2. Shanker, K.; Rohini, R.; Ravinder, V.; Reddy, P. M.; Ho, Y.-P. *Spectrochimica Acta Part A: Molecular and Biomolecular Spectroscopy* **2009**, *73* (1), 205-211.
3. Schiff, H. *Annali Di Chimica* **1864**, *131*, 118.
4. Mitra, T.; Jelfs, K. E.; Schmidtman, M.; Ahmed, A.; Chong, S. Y.; Adams, D. J.; Cooper, A. I. *Nat. Chem.* **2013**, *5* (4), 276-281.
5. Kewley, A.; Stephenson, A.; Chen, L.; Briggs, M. E.; Hasell, T.; Cooper, A. I. *Chem. Mater.* **2015**, *27* (9), 3207-3210.
6. Schneider, M. W.; Siegfried Hauswald, H.-J.; Stoll, R.; Mastalerz, M. *Chem. Commun.* **2012**, *48* (79), 9861-9863.
7. Jin, Y.; Yu, C.; Denman, R. J.; Zhang, W. *Chemical Society Reviews* **2013**, *42* (16), 6634-6654.
8. Jin, Y.; Voss, B. A.; Jin, A.; Long, H.; Noble, R. D.; Zhang, W. *J. Am. Chem. Soc.* **2011**, *133* (17), 6650-6658.
9. Liu, M.; Chen, L.; Lewis, S.; Chong, S. Y.; Little, M. A.; Hasell, T.; Aldous, I. M.; Brown, C. M.; Smith, M. W.; Morrison, C. A.; Hardwick, L. J.; Cooper, A. I. *Nat Commun* **2016**, *7*, 12750.
10. Brutschy, M.; Schneider, M. W.; Mastalerz, M.; Waldvogel, S. R. *Adv. Mater.* **2012**, *24* (45), 6049-6052.
11. Steinmetz, V.; Couty, F.; David, O. R. P. *Chem. Commun.* **2009**, (3), 343-345.
12. Hasell, T.; Miklitz, M.; Stephenson, A.; Little, M. A.; Chong, S. Y.; Clowes, R.; Chen, L.; Holden, D.; Tribello, G. A.; Jelfs, K. E.; Cooper, A. I. *J. Am. Chem. Soc.* **2016**, *138* (5), 1653-1659.
13. Hasell, T.; Cooper, A. I. *Nature Reviews Materials* **2016**, *1*, 16053.
14. Giri, N.; Del Pópolo, M. G.; Melaugh, G.; Greenaway, R. L.; Rätzke, K.; Koschine, T.; Pison, L.; Gomes, M. F. C.; Cooper, A. I.; James, S. L. *Nature* **2015**, *527* (7577), 216-220.
15. Greenaway, R. L.; Holden, D.; Eden, E. G. B.; Stephenson, A.; Yong, C. W.; Bennison, M. J.; Hasell, T.; Briggs, M. E.; James, S. L.; Cooper, A. I. *Chemical Science* **2017**.

16. Kieryk, P.; Janczak, J.; Panek, J.; Miklitz, M.; Lisowski, J. *Org. Lett.* **2016**, *18* (1), 12-15.
17. Bera, S.; Basu, A.; Tothadi, S.; Garai, B.; Banerjee, S.; Vanka, K.; Banerjee, R. *Angew. Chem. Int. Ed. Engl.* **2017**, *56* (8), 2123-2126.
18. Jung, M. E.; Piizzi, G. *Chem. Rev.* **2005**, *105* (5), 1735-1766.
19. Beesley, R. M.; Ingold, C. K.; Thorpe, J. F. *J. Chem. Soc. Trans.* **1915**, *107* (0), 1080-1106.
20. Ingold, C. K.; Sako, S.; Thorpe, J. F. *J. Chem. Soc. Trans.* **1922**, *121* (0), 1177-1198.
21. Bruice, T. C.; Pandit, U. K. *J. Am. Chem. Soc.* **1960**, *82* (22), 5858-5865.
22. Folmer, B. J. B.; Sijbesma, R. P.; Kooijman, H.; Spek, A. L.; Meijer, E. W. *J. Am. Chem. Soc.* **1999**, *121* (39), 9001-9007.
23. Pete, J.-P. *Chem. Commun.* **1998**, (2), 235-236.
24. Forbes, M. D. E.; Patton, J. T.; Myers, T. L.; Maynard, H. D.; Smith, D. W.; Schulz, G. R.; Wagener, K. B. *J. Am. Chem. Soc.* **1992**, *114* (27), 10978-10980.
25. Nilsson, H.; Smith, L. *Zeitschrift für Physikalische Chemie* **1933**, *166* (1), 136-146.
26. Milstien, S.; Cohen, L. A. *J. Am. Chem. Soc.* **1972**, *94* (26), 9158-9165.
27. Winans, R. E.; Wilcox Jr, C. F. *J. Am. Chem. Soc.* **1976**, *98* (14), 4281-4285.
28. ALLINGER, N. L.; ZALKOW, V. J. *Org. Chem.* **1960**, *25* (5), 701-704.
29. Jung, M. E.; Piizzi, G. *Chem. Rev.* **2005**, *105* (5), 1735-1766.
30. Toniolo, C.; Crisma, M.; Formaggio, F.; Peggion, C. *J. Pept. Sci.* **2001**, *60* (6), 396-419.
31. Karle, I. L.; Flippen-Anderson, J. L.; Gurunath, R.; Balaram, P. *Prot. Sci.* **1994**, *3* (9), 1547-1555.
32. Srinivas, D.; Gonnade, R.; Ravindranathan, S.; Sanjayan, G. J. *J. Org. Chem.* **2007**, *72* (18), 7022-7025.
33. Vijayalakshmi, S.; Rao, R. B.; Karle, I.; Balaram, P. *Biopolymers* **2000**, *53* (1), 84-98.
34. Ingold, C. K. *J. Chem. Soc. Trans.* **1921**, *119*, 951-970.
35. Smith, S. W.; Newman, M. S. *J. Am. Chem. Soc.* **1968**, *90* (5), 1253-1257.
36. Ringer, A. L.; Magers, D. H. *J. Org. Chem.* **2007**, *72* (7), 2533-2537.



37. Bruice, T. C.; Bradbury, W. C. *J. Am. Chem. Soc.* **1965**, *87* (21), 4838-4845.
38. Jung, M. E.; Gervay, J. *J. Am. Chem. Soc.* **1991**, *113* (1), 224-232.
39. Desper, J. M.; Gellman, S. H.; Wolf Jr, R. E.; Cooper, S. R. *J. Am. Chem. Soc.* **1991**, *113* (23), 8663-8671.
40. Chen, D.; Martell, A. E. *Tetrahedron* **1991**, *47* (34), 6895-6902.
41. Cram, D. *Science* **1988**, *240* (4853), 760-767.
42. Aguiari, A.; Bullita, E.; Casellato, U.; Guerriero, P.; Tamburini, S.; Vigato, P. A. *Inorg. Chim. Acta.* **1992**, *202* (2), 157-171.
43. Belowich, M. E.; Stoddart, J. F. *Chemical Society Reviews* **2012**, *41* (6), 2003-2024.
44. Mastalerz, M. *Angew. Chem. Int. Ed. Engl.* **2010**, *49* (30), 5042-5053.
45. Rue, N. M.; Sun, J.; Warmuth, R. *Israel Journal of Chemistry* **2011**, *51* (7), 743-768.
46. Ingold, C. K. *J. Chem. Soc. Trans.* **1921**, *119* (0), 305-329.
47. Bruker (2016). *APEX3, SAINT and SADABS*. Bruker AXS Inc., Madison, Wisconsin, USA.
48. Bruker (2006). *APEX3, SAINT and SADABS*. Bruker AXS Inc., Madison, Wisconsin, USA.
49. G. M. Sheldrick, *Acta Crystallogr.*, **2008**, *A64*, 112.
50. L. J. Farrugia, *J. Appl. Cryst.* **1997**, *30*, 565-565.





## ***Corrigendum***